Fifth ANZ Young Geotechnical Professionals Conference

Rotorua, New Zealand 2002

Proceedings of

The 5th Australia New Zealand Young Geotechnical Professionals Conference

Tony Davies
Andrew Linton
Phil Chapman
Peter Bosselmann
(Organising Committee)

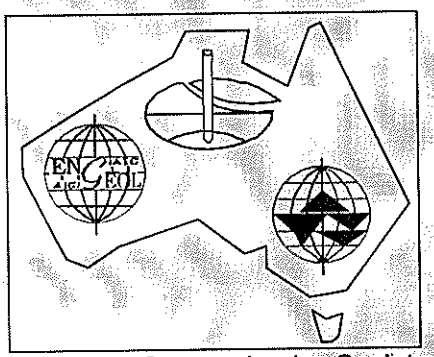

Australian Geomechanics Society

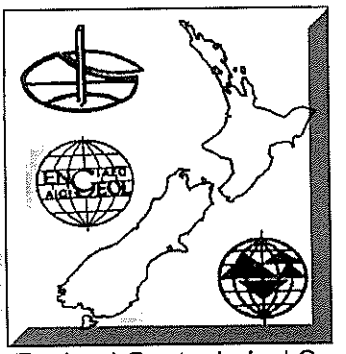

New Zealand Geotechnical Society

13 – 16 March 2002

Rotorua
New Zealand

ISBN 0-908960-41-7

Welcome

Welcome to the *Fifth Australia - New Zealand Young Geotechnical Professionals Conference,* Rotorua, NZ, 2002. Following on from previous successful conferences held in Sydney (1994), Auckland (1996), Melbourne (1998) and Perth (2000), this biannual event is a joint initiative of the Australian Geomechanics Society and the New Zealand Geotechnical Society.

The conference aims to provide a forum where the professional development of delegates is promoted through the sharing of experiences and ideas and meeting and networking with other young and more senior professionals and peers. The establishment of communication and understanding amongst the younger professionals is of benefit not only to those immediately involved, but also to the geotechnical community as a whole. An important by-product of the conference is the opportunity for all attendees to mix in a social atmosphere, further promoting the interaction of all involved.

Past conferences have noted the necessity for younger engineers to become more involved within the community, with particular reference to society matters. They have also highlighted the important role both research and practical applications have to the profession.

As with all previous YGP conferences, support of the geotechnical community is very important to ensure a successful end result. We would like to thank all companies and individuals that have assisted with the preparation of this conference. In particular, past and present committee members: Tony Davies, Phil Chapman, Peter Bosselmann, Jaime Bevin and Cherie Lee; who have contributed considerable time and effort in the past 14 months. Thanks also to all those involved in paper reviews on behalf of the delegates. Thanks to Contact Energy for their assistance in organising the site visit of the Wairakei Geothermal Power Station. Val Lee and Debbie Fellows of the AGS and NZGS have also been of great assistance in organising this event.

Keynote presenters and Senior mentors: Dr Warwick Prebble, Mr Max Ervin, Mr Garry Mostyn, Mr Guy Grocott, Mr Grant Murray, Prof. Mick Pender; without your valuable input the conference would lack much of what makes it such a success. The assistance of Dr Prebble in organising the field trip and volunteering to act as 'tour guide' was much appreciated and we look forward to a top-notch afternoon.

I wish all delegates an enjoyable and beneficial conference. Enjoy yourselves and make the most of the opportunity to meet those outside your normal circle of influence. I encourage you all to participate fully, in both the conference sessions and the social occasions. The organising committee members look forward to meeting you all, and joining you in an enjoyable and informative three days.

Andrew Linton
Chairman - Organising Committee

Organising Committee

Mr Andrew Linton
Mr Tony Davies
Mr Phil Chapman
Mr Peter Bosselmann

Senior Mentors

Mr Max Ervin
Mr Garry Mostyn
Mr Grant Murray
Mr Guy Grocott
Dr Warwick Prebble
Prof. Mick Pender

Special Thanks

Mr Jamie Bevin
Ms Cherie Lee
Mrs Robyn Adams
Mrs Lisa Stevenson-Reid

A senior geotechnical engineer independently reviewed all papers accepted for publication at this conference. Papers were reviewed to check technical accuracy, relevance and presentation.

THE ORGANISING COMMITTEE WOULD LIKE TO ACKNOWLEDGE THE GENEROUS FINANCIAL SUPPORT OBTAINED FROM THE CONFERENCE SPONSORS. WITHOUT THEIR CONTRIBUTION, THE CONFERENCE WOULD NOT HAVE BEEN POSSIBLE.

Douglas Partners

Practical, innovative and cost effective solutions

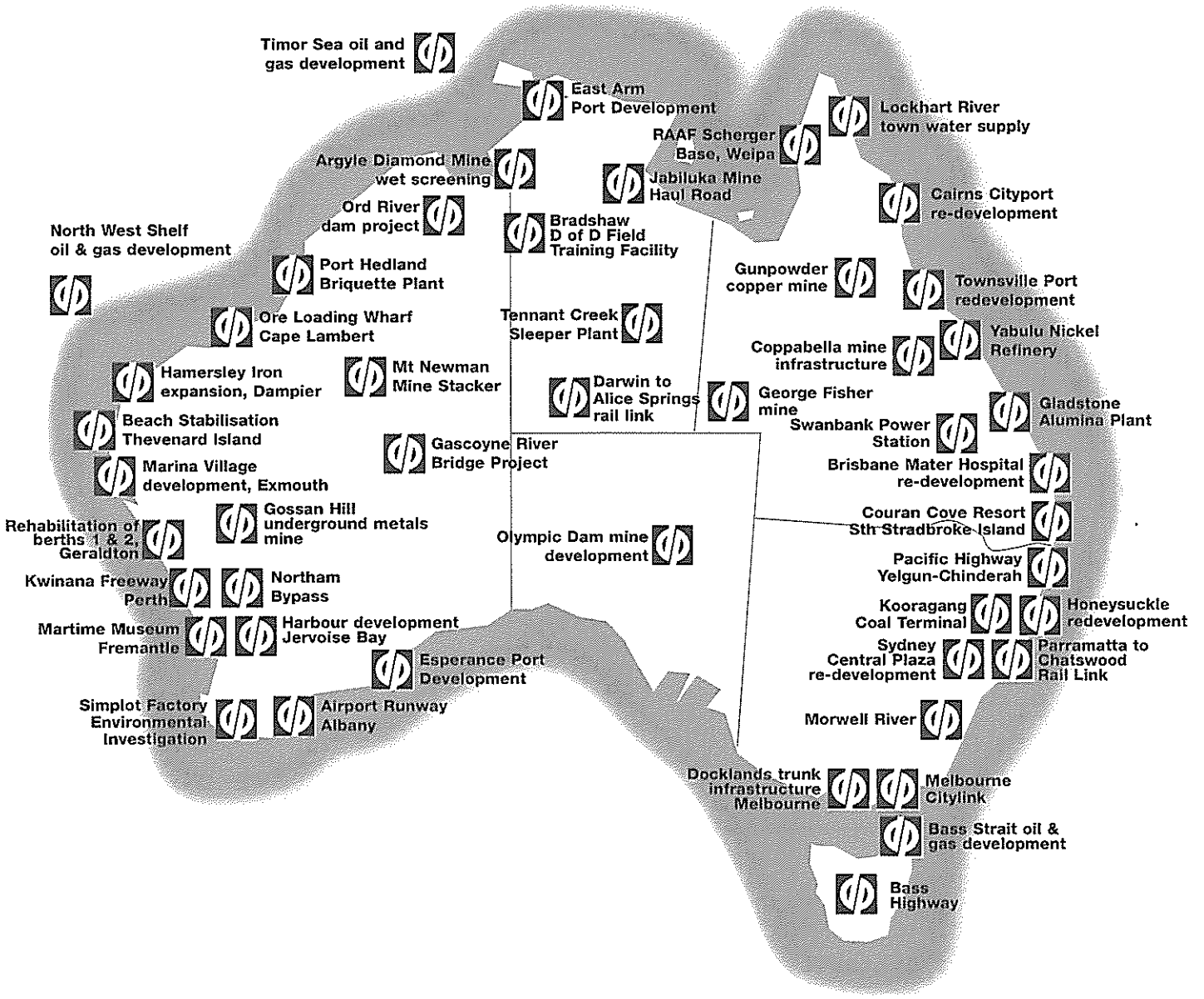

Douglas Partners' 35 years experience and 11 offices nationwide have made us the consultants of choice for a broad range of clients across Australia.

From geotechnical, environmental and groundwater engineering, to NATA registered laboratory testing and quality systems consulting, Douglas Partners has the skills and expertise to deliver. For more information visit www.douglaspartners.com.au

Douglas Partners

Geotechnics · Environment · Groundwater

BRISBANE
Alan Lee
Ph (07) 3237 8900
Fax (07) 3237 8999

CAIRNS
Dan Martin
Ph (07) 4055 1550
Fax (07) 4055 1774

CAMPBELLTOWN
Geoff McIntosh
Ph (02) 9820 3011
Fax (02) 9603 2217

DARWIN
Konrad Schultz
Ph (08) 8947 4400
Fax (08) 8947 4455

MELBOURNE
Peter McDonald
Ph (03) 9428 1831
Fax (03) 9428 7841

NEWCASTLE
John Harvey
Ph (02) 4960 9600
Fax (02) 4960 9601

PERTH
Charles Waterton
Ph (08) 9325 4774
Fax (08) 9325 4771

SYDNEY
Michael Thom
Ph (02) 9809 0666
Fax (02) 9809 4095

TOWNSVILLE
Ken Boddie
Ph (07) 4779 9866
Fax (07) 4725 1224

WOLLONGONG
Geoff McIntosh
Ph (02) 4271 1836
Fax (02) 4271 1897

WYONG
Ian Piper
Ph (02) 4351 1422
Fax (02) 4351 1410

Meritec

See what New Zealand's happiest employees are doing for lunch

Chances are, they're enjoying one of our 'brown bag sessions'. That's where everyone from engineers to support staff get together over lunch to hear interesting topics such as negotiating contracts or innovative investigation techniques. Although these sessions are optional, the turnout is impressive as it's all part of our flexible and friendly culture. It's also why we're one of the best places to work in New Zealand (Unlimited Magazine Jan 01).

Formerly Worley Consultants, our international, multi-disciplinary consultancy offers unique career opportunities for people with specialist skills in engineering, business and environmental fields.

With our award winning culture, career development focus and of course a competitive remuneration package, lunch at Meritec is a very tasty option indeed!

To find out more about us and what it is like to work here, visit us at:

www.meritec.org

Meritec Limited
47 George St, Newmarket
PO Box 4241, Auckland
Tel: +64 9 379 1200
Fax: +64 9 379 1201
meritec@meritec.org

ideas

NEVER BORING

Sinclair Knight Merz is a global technology consultancy currently employing over 3,000 people throughout the Asia Pacific region, Europe and South America. To continue our commitment to delivering technical and commercial solutions that create exceptional value, we are always looking for skilled and highly motivated professionals to join our company.

The sectors we cover are energy, infrastructure, mining, industrial, spatial, environmental, and buildings. Our services include technical consultancy, engineering design, specialist expertise, planning, feasibility and project and construction management.

Our reputation for engineering excellence, innovation and commitment to clients and staff is reflected by the numerous national and international awards that the company receives for its high profile projects. Current and recent projects include:

- Olympic Stadium - Stadium Australia
- Docklands Light Rail Development, London
- Olkaria Geothermal Project, Kenya
- Central Motorway Junction, Auckland
- Dublin Light Rail Project, Ireland
- Rewa Bridge, Fiji
- Yakin Oil & Gas Platform, Indonesia
- Eildon Hydro Power Station, Australia
- Auckland Integrated Catchment Studies

We have an exciting and challenging working environment and offer a focused employee development programme. Sinclair Knight Merz has an active policy of encouraging staff transfers between our international offices.

For more information please contact:
Grant Murray - telephone 09 913 8984.

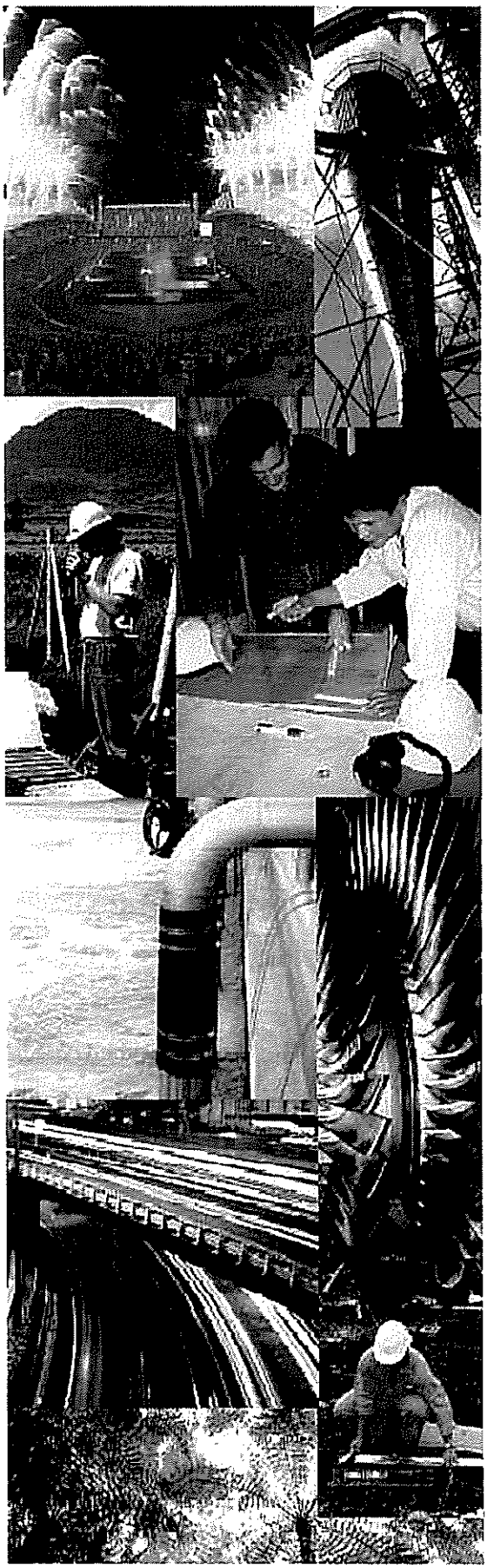

www.skmconsulting.com

SINCLAIR KNIGHT MERZ

DRILLWELL EXPLORATION

MEMBER OF NZDF NEW ZEALAND DRILLERS FEDERATION INC

Quality System
Quality Endorsed Company ISO9001

WORLD WIDE COVERAGE

ENVIRONMENTAL SURVEYS
- Sampling • Motoring Well Installation

GEOTECHNICAL DRILLING
- Site Investigation • Piezometer Networks • Instrumentation • Coring • Push Tubes
- SPT's • Shear Vane • Hydraulic Piston Samples • Core Orientation (Archway System)

WATER WELL DRILLING
- Town Supply • Domestic • Commercial • Farm • Irrigation
- Large Diameter Soak Holes

SPECIAL PROJECTS
- Barge • Underground • Confined Space • Helicopter Access
- Ground Stability Enhancement • Anchors • Mini Piles

SEISMIC SURVEYS
- Truck • Tractor • Heli Portable

EXPLORATION
- Geothermal • Gas • Oil • Gold
- Coal • Mineral (including wire line coring & RC drilling)

DRILLWELL EXPLORATION NZ LTD

9 Rawson Way, Takanini, Auckland, PO Box 75-360, Manurewa
Phone: 0-9-267 9100 Fax: 0-9-267 8100
Website: www.drillwell.co.nz Email: general@drillwell.co.nz

SOILS TESTING LABORATORY SERVICES

Having recently relocated to the Newmarket area, our soils testing laboratory has now reopened to continue providing quality service at competitive prices.

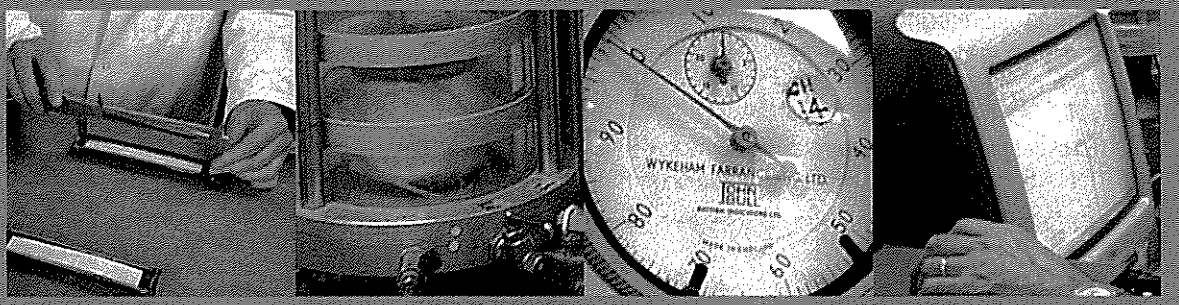

For an obligation free quote or to discuss your testing requirements, contact our Laboratory Manager **Barry Coker**

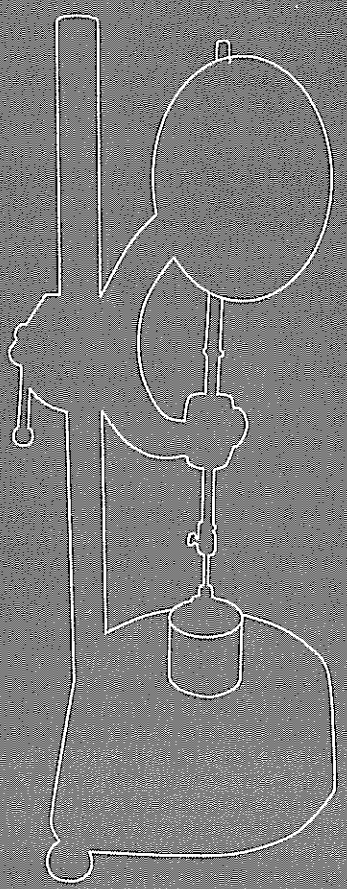

ph +64 0 523 5626
fax +64 9 523 5627
email contactus@fel-nz.com

or come in and see us at
216 Great South Road, Newmarket
(Patey Street entrance).

Registered since 1977 for more than 40 tests.

FOUNDATION ENGINEERING

CONTRACT LANDSCAPES LTD

FOUNDATION SPECIALIST'S

CONSTRUCTORS OF:

** FOUNDATIONS*
** RETAINING WALLS*
** DRIVEN & CONCRETE PILES*
** SLIP STABILISATION*
** TILT-UP PANELS*
** EXCAVATIONS*
** SITEWORKS*
** LANDSCAPING*
** CONTAMINATED WASTE DISPOSAL*

- CONTRACT LANDSCAPES PRIDES ITSELF AS BEING A PROGRESSIVE COMPANY OFFERING ITS CLIENTS A RANGE OF INNOVATIVE AND VERSATILE SERVICES THAT AID IN THE CONSTRCUTION OF A MULTITUDE OF CIVIL COMMERCIAL & DOMESTIC PROJECTS.

- WITH A DEPTH OF SKILL AND PLANT TO CALL ON, CONTRACT LANDSCAPES CAN OVERCOME MANY OF THE DIFFICULT AND UNFORSEEN SITUATIONS THAT CAN OCCUR IN THE MODERN CONSTRUCTION INDUSTRY.

- PLANT INCLUDES 13 T, 8T & 5T EXCAVATOR'S, PILE DRIVERS & DRILLING RIGS – 6 & 4 WH TRUCKS – 2 X BOBCAT'S & 50 STAFF.

PHONE THE FOLLOWING PEOPLE TO DISCUSS YOUR PROJECT:

TERRY DONNELLY	025 990654
ADAM BESSELL	021 905948
MARK LYNDON	021 808 020
OFFICE	09 483 4166

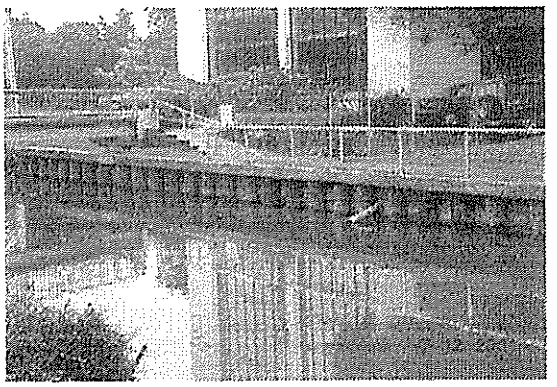

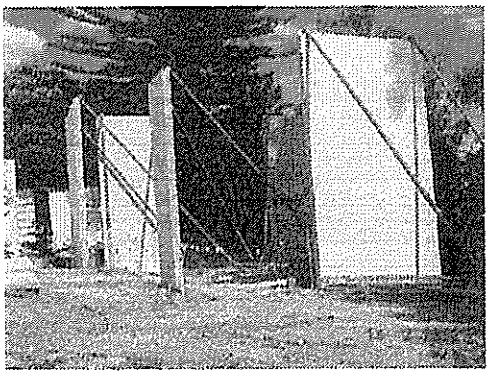

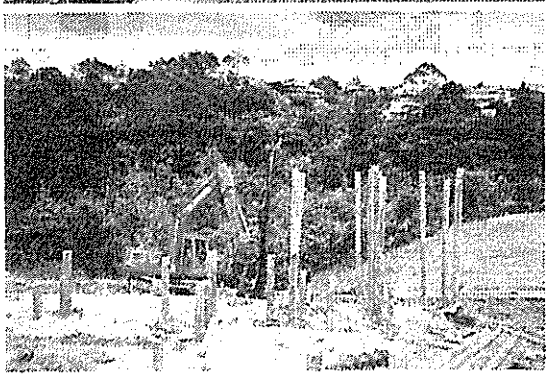

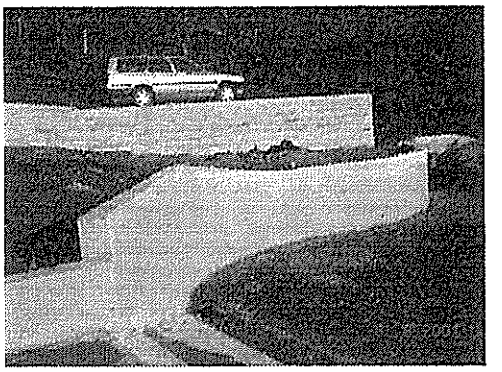

BRIAN PERRY CIVIL

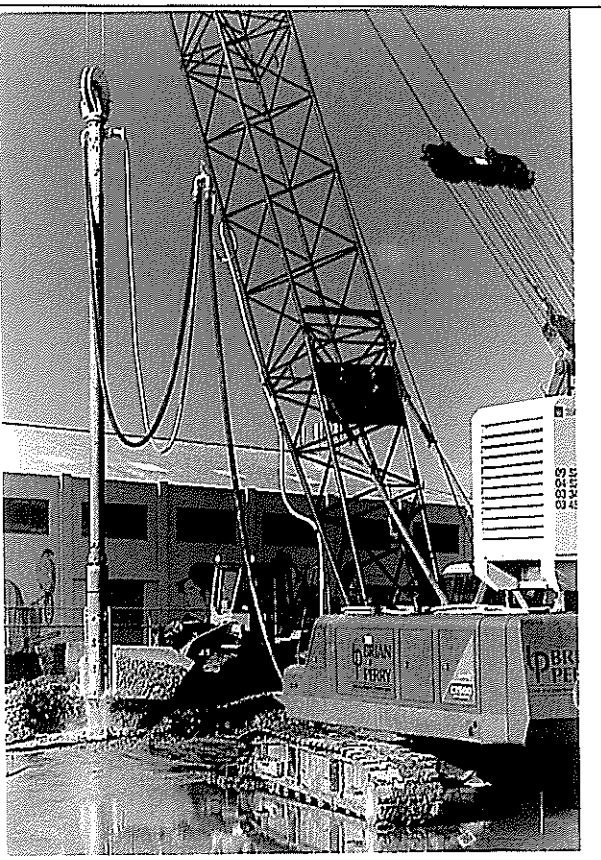

BRIAN PERRY CIVIL is New Zealand's leading foundation engineering Contractor with a strong reputation for performance, innovation and quality in demanding and high risk situations.

BRIAN PERRY CIVIL are specialists in all types of foundation works including bored and driven piles, temporary retention works, ground anchors, ground improvement, marine works, pressure grouting and pile load testing.

BRIAN PERRY CIVIL often work in joint ventures with specialist overseas experts to deliver the latest technology in foundation solution techniques utilizing our extensive range of modern piling equipment.

Contact one of our listed offices for further information.

Auckland:
3 Arthur Brown Place
PO Box 62 216
Mt Wellington
Ph: (09) 573 0690
Fax: (09) 573 0694

Hamilton:
Cnr Vickery & Daniel Sts
PO Box 10 068
Te Rapa, Hamilton
Ph: (07) 849 2879
Fax: (07) 849 4376

Wellington:
19 Tunnel Grove
Gracefield
PO Box 30 092 Lower Hutt
Ph (04) 568 9442
Fax: (04) 568 2547

HARRISON GRIERSON

Geotechnical Engineering

Harrison Grierson's Geotechnical Division has a very experienced team of geotechnical engineers and geologists working with the latest technology in computerised analysis, field investigations and laboratory testing.

Our design team works closely with professionals from other Harrison Grierson disciplines to ensure a total business solution is delivered to our clients.

Our services include:

- Hazard assessment
- Land suitability
- Earthworks design and control
- Foundation completion reports
- Foundation reports
- Failure investigation and remedy
- Slope stability
- Landfill and quarry management
- Expert evidence
- Engineering geology
- Housing

geolab

The Geotechnical division operates its own laboratory, Geolab, which in addition to undertaking soil testing for our land development clients, also carries out a wide range of specialised air and water testing for environmental engineering projects.

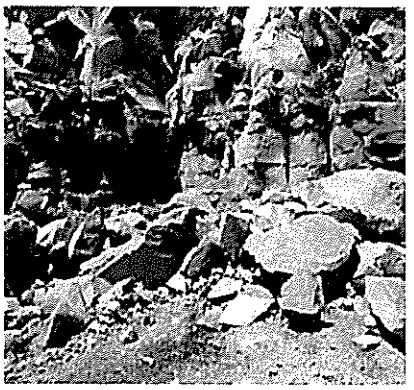

For further information please contact Phil Williams

e-mail p.williams@harrisongrierson.com

RILEY CONSULTANTS LTD
Engineers and Geologists

Riley Consultants Ltd - Specialists in Geotechnical, Civil and Water Resource Engineering

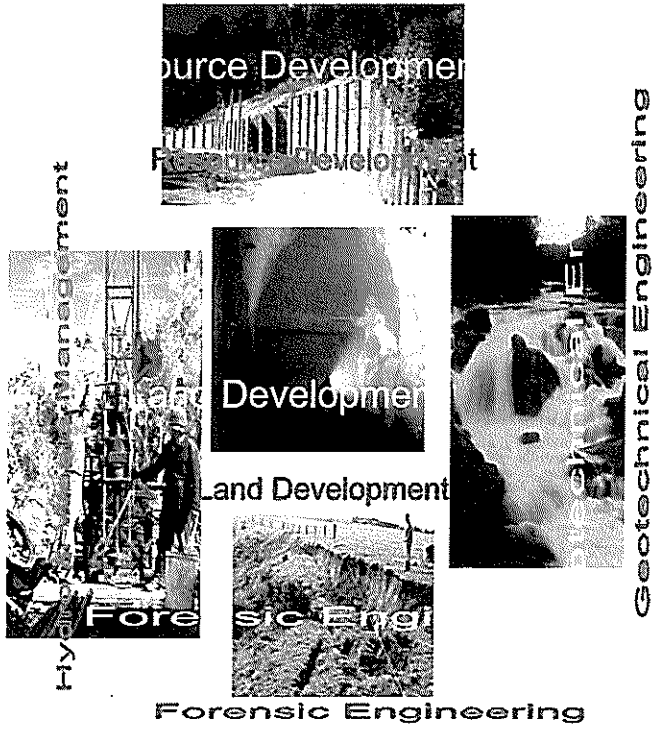

4 Fred Thomas Drive
TAKAPUNA, AUCKLAND
P O Box 100 253
North Shore Mail Centre
Ph 09 489 7872
Fax: 09 489 7873
Email: rileys@rcl.co.nz

79 Cambridge Terrace
P O Box 2281
CHRISTCHURCH
Ph: 03 379 4402
Fax: 03 379 4403
www.rcl.co.nz

Environmental Solutions

MACCAFERRI

Quality System Certified AS/NZS ISO 9002

GEOSYNTHETICS, RETAINING WALLS, REINFORCED SOILS, ROAD REINFORCEMENT, EROSION CONTROL, DRAINAGE, LANDSCAPING, CONTAINMENT SYSTEMS, HYDRAULIC STRUCTURES, COASTAL PROTECTION

Did you know MACCAFERRI Solutions include ?

☐ **RETAINING WALLS**
Anchor Wall – Vertica & Diamond Pro Segmental Blocks
Gabions - Mass & Semi Gravity

☐ **REINFORCED SOIL WALLS, SLOPES EMBANKMENTS**
Anchor Wall - Reinforced Segmental Block Walls
Fortrac Geogrids - Walls and Green Slopes
Terramesh Gabions - Walls and Green Slopes
Stabilenka - High Strength Wovens to 1000kN/m Basal Reinforcement

☐ **PAVEMENT REINFORCEMENT**
Enkagrid TRC - High modulus Sub-base Biaxial Geogrid Reinforcement with composite fabric separator
Enkagrid Max – P.P. subbase Biaxial Geogrid
Roadmesh – Asphalt Reinforcement Mesh
Hatelit - Asphalt & Slurry Geogrid Reinforcement
Bidim Sealmac - Chip Seal & Asphalt Sealing Fabrics
Bitac - Pavement Crack Bandage & Culvert Joints
Grass-Cel - Green Carpark Access & Overflow

☐ **DRAINAGE**
Megaflo - Road Edge, Turf & Landscape Drains
Enkadrain – Slopes and Basement Walls
Cordrain - Basement Wall Sheet Drainage
Plazadeck - Plaza & Roof Gardens
Colbonddrain - Wick Drains for Soil Consolidation

☐ **GEOTEXTILES**
Bidim - Non woven Needle-Punched Range for Separation, Drainage & Filtration
MacTex – Woven Geotextiles

☐ **EROSION CONTROL**
Gabions - Weirs & Hydraulic Control Structures
Reno Mattress - Channel & Scour Protection
Enkamat - Vegetal Root Reinforcement Mat
Biomac C - Coir Blankets for Revegetation
Biomac G – Grasstrike for Lawn Turf Care
Biomac W - Woolmulch Blankets for Revegetation
GreenLog – Bio Waterlogs With/Without Reinforcement
MacSac – Reusable MiniSac-gabion to replace Hay Bales
Silt Fence - Site Sediment Run-off Prevention
Rockfall - Safety Netting & Barrier Fences & Panels
Flexible Flumes – Discharge control down slopes
Dust Control – Earthworks, Roading & Stockpiles
FlexMac - Civil Emergency Flood & Military Barricades
Silt Curtains - Pre-fabricated Hydraulic Silt Curtains

☐ **COASTAL PROTECTION**
MacTube Sand Tubes - Coastal Protection & Embankment Reconstruction
MacTube Sediment Containers - Fabrics for Containment
C.O.P.E.D. - Coastal Protection Energy Dissipation Unit

☐ **CONTAINMENT SYSTEMS**
Bentofix - Geosynthetic Clay Liners (GCL)
Millennium – Flexible Polypropylene Geomembranes
Aeon – Elvaloy KEE Geomembranes
Enkadrain - Liner Drainage & Gas Collection

☐ **CUSTOMER SERVICES**
Product & Installation Specifications
Design Assistance & Environmental Detailing
Software Design Packages & Standard Drawings
Alternative Design Proposals
Recommended Installer Network
Product Usage Training & Site Visits
In-house Software Seminars & Design Workshops
Project Partnering / Joint Ventures

For further information please tick the relevant box and fax or E-mail to Maccaferri Fax No: (09) 6346492, (03) 3495004 E-mail sales@maccaferri.co.nz or christchurch@maccaferri.co.nz or Free phone 0800 60 60 20

Name : .....

Position : .....

Company : .....

Address : .....

EARTHTECH CONSULTING LTD

DIRECTORS: Philip Kelsey & Aidan Nelson
PO Box 721, Pukekohe, New Zealand
Ph: 64 9 2383669
Fax: 64 9 2381828

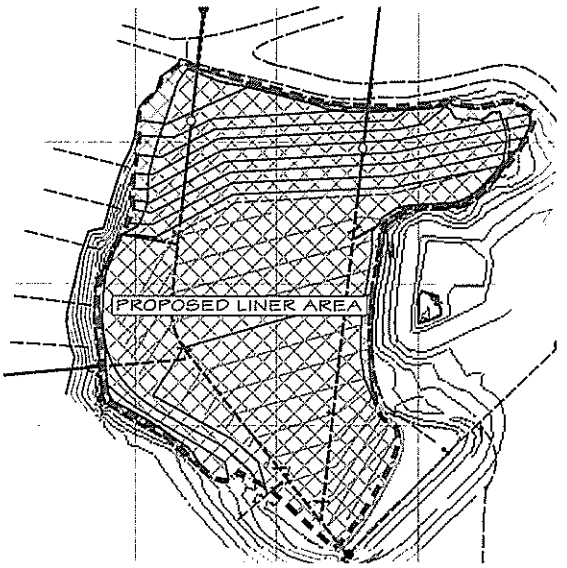

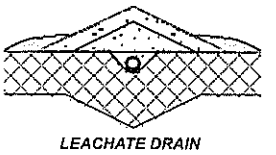

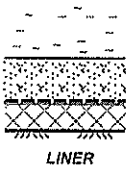

- GEOTECHNICAL ENGINEERING
- GROUNDWATER MODELLING
- ENGINEERING GEOLOGY
- CANAL DEVELOPMENT
- BRIDGE FOUNDATIONS
- LANDFILL DESIGN

Golder Associates

www.golder.com

Golder Associates is a world-wide group providing project services in earth, engineering, and environmental sciences to the industrial, construction and mining sectors, all levels of government, the legal profession, and private developers. Golder is oriented towards career development and is one of the world's largest employee-owned consultancies. We are pleased to support the 5th ANZ Young Geotechnical Professional Conference in Rotorua.

Golder Associates (NZ) Ltd
Level 1, 79 Cambridge Terrace
PO Box 2281
Christchurch
Ph: +64 3 377 5696
Fax: +64 3 377 9944
email: christchurch@golder.co.nz

BGL

BABBAGE GEOTECHNICAL LABORATORY

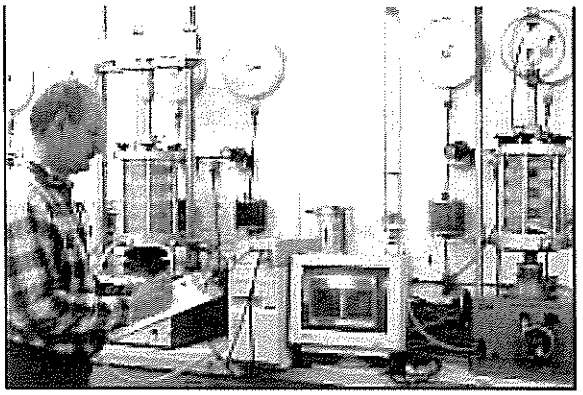

Triaxial testing underway with automated data acquisition using LabVIEW

BGL is an IANZ accredited Geotechnical Laboratory.

BGL offers the full range of Geotechnical Laboratory and Field Testing services.

Consolidation Tests

Soil Classification Tests

Permeability Tests

Triaxial Testing

Compaction Tests

Shear Box Testing

P O Box 2027, Auckland 1, Cnr Fanshawe & Halsey St's, Freemans Bay, Auckland, Ph (09) 367 4954, Fax (09) 377 0554, Email wec@babbage.co.nz

BGL is a Trading Division of Babbage Consultants Ltd

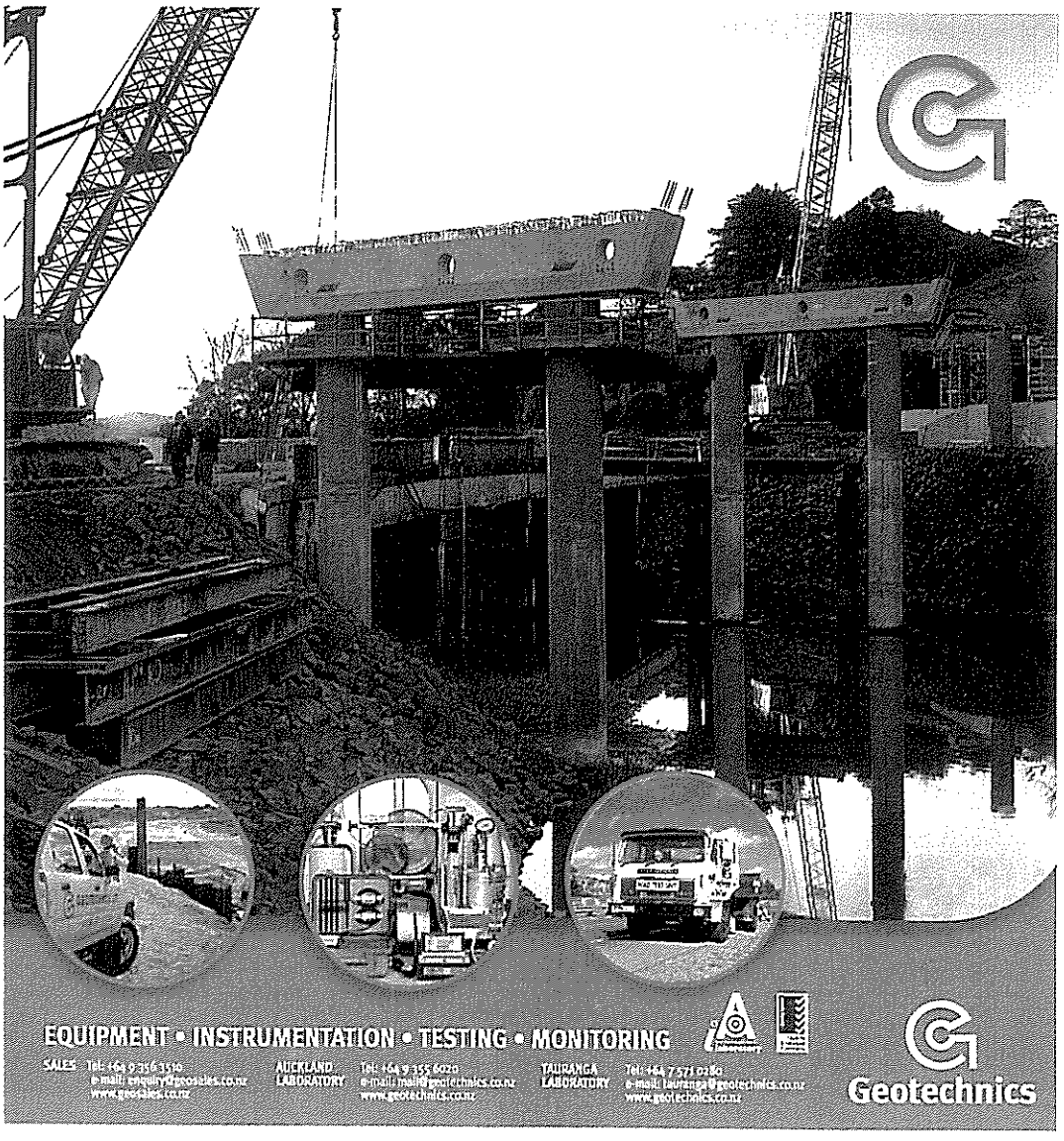

SUPERIOR REINFORCEMENT SYSTEMS

For over 20 years we have provided a specialist technical service and a wide variety of superior products to ensure ground stabilisation.

WALLS/SLOPES

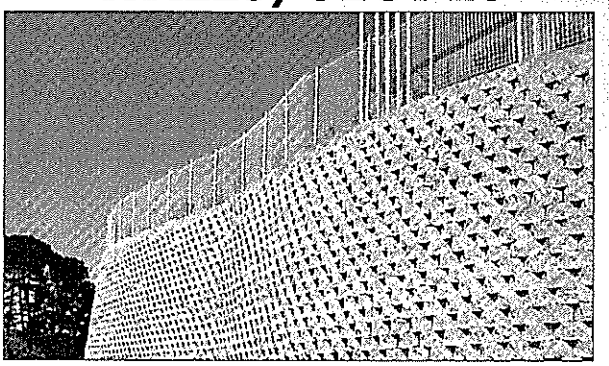

When the need is to hold the ground, we have a range of products for every situation from large scale hillside reinforcement to decorative retaining walls

DRAINAGE

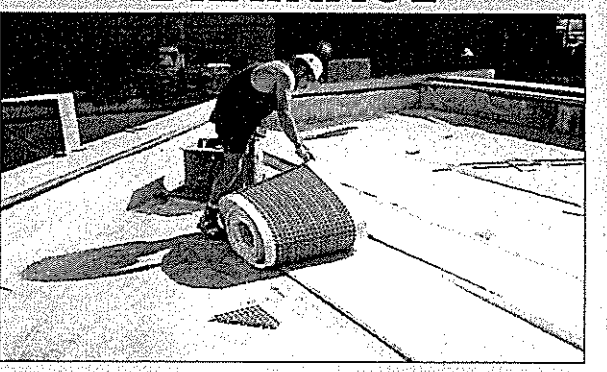

We specialise in a broad range of sophisticated drainage products which are economical and easy to install. The emphasis of these products is to be user friendly with features such as minimum excavation and backfill requirements in addition to high flow rates.

EROSION CONTROL

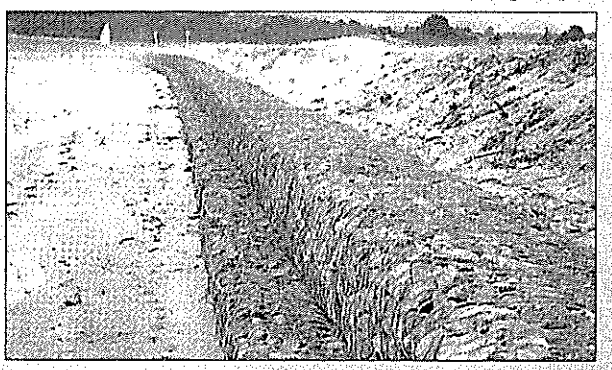

We have numerous products to achieve ground holding and erosion control - from biodegradable protection blankets and permanent grass reinfocement systems, to the rugged, heavy duty gabions.

ROADING

Our roading products are at the forefront of geosynthetic technology. These technically proven products are designed to extend the life of the road and increase the load bearing capacity.

FOR FURTHER INFORMATION CONTACT:

GROUND ENGINEERING LIMITED

FREEPOST 1439, AUCKLAND, FREEPHONE: 0800 659 000

AUCKLAND
Phone: 09 273 1065
Facsimile: 09 273 1066

WELLINGTON
Phone: 04 802 5114
Facsimile: 04 802 5116

CHRISTCHURCH
Phone: 03 349 2268
Facsimile: 03 349 3031

TABLE OF CONTENTS

Welcome

Sponsors

Table of Contents

GEOTECHNICAL PAPERS

Site Response in the Aburra Valley, Medellin, Columbia 1
Brian Adams

Probability and Sensitivity Analyses in Geotechnical Engineering 7
Karen Allan

A Three Dimensional Gravity Survey of the Pre-volcanic Topography in Epsom, Auckland 11
Dev Kumar Affleck

Geotechnical Aspects of the Wairau Storage Tank 17
Kevin Robert Anderson

Determination of the Structural Number of Pavements on Volcanic Subgrades 23
Rosslyn Bailey

Importance of Parameters Influencing the Filtration in Embankment Dams 29
Sharbaree Biswas

Geotechnical Instrumentation & Monitoring (Preload Performance) Kooragang Coal Terminal Stage 3 Expansion 37
Chris Bozinovski

Parametric Study of Embankments on Soft Soils Using a Creep Model 41
Hong Ngoc Bui

Slip Remediation in Onerahi Chaos (Northland Allocthon) 45
Murray Burt

Correlations for Gmax from the Seismic Cone Penetration Test (SCPT) 51
Terry Chang

Soil and Rock Property Relationships based on Test results from a Site Investigation in Waitemata Series Materials for the Central Motorway Junction Project in Auckland 57
Dean Coutts

Aspects of Low Angle Slope Instability in Tauranga Group Sediments 63
Steve Crook

Use of Cohesive Soil in Reinforced Earth Structures 69
Donald Craig Davidson

Centrifuge Modelling of Drag-in Plate Anchors 75
Sarah Elkhatib

Cyclic Loading Effects on the Secondary Consolidation of Clay 83
Brook Ewers

Geotechnical Site Characterization Using Surface Waves 89
Sebastiano Foti

Linden Bends - Stage IV, Great Western Highway, Road Widening & Realignment 95
Tony Gourlay

Combined Loading of Skirted Foundations 103
Susan Gourvenec

Quarrying - Modified Lava Flow Geology And Its Influence on the Effects of Groundwater Contamination 109
Peter Gringinger

Excavation Induced Vibrations in Sydney Sandstone 115
Gregory Albert Hackney

Bearing Capacity of a Strip Footing Subjected to an Inclined Load 121
Mohammed Hjiaj

Assessment of Existing Pile Foundations for Upgrading of Capacity 127
Sean Holt

Paleoearthquakes and Hazard of the Porters Pass Fault, Canterbury, New Zealand 135
Matthew Howard

Damage to Embankments Due to Liquefaction and Delayed Effects 141
Michael E Jacka

Earthquake Hazard Zoning within the City of Brisbane 147
Patrick Richard Kidd

Assessing Brine Leakage at a Solar Salt Works: An Engineering Geological Approach 155
Cameron Lines

Makara Road Carriageway Realignment - Case Study 163
Christopher Lyons

Mechanically Stabilised Embankment Construction Project Te Awa Recreational Reserve Pedestrian Access 169
David John Morton

The Influence of Clay Infill on the Shear Behaviour of a Rock Mass 177
Mathias Joseph Nagy

Case Study: A Piled Raft Foundation to Mitigate Liquefaction Induced Settlement of a Pipeline 185
Wataru Okada

Slope Failure in a Complex Volcanic Terrain, Opito Bay, Kaotunu Peninsula, Coromandel Peninsula 193
Steven Price

The seepage Modelling of Cosseys Dam Upgrade 199
Sandip Ranchhod

Mechanism Controlling the Cyclic Strength of Cemented Soil 205
Shambhu Sagar Sharma Acharya

Geotechnical Properties and Geothermal Instability of Kuirau Park, Rotorua 211
Marie Alice Slako

Predicting Long Term Seepage and Runoff from Tailings Storage Facilities to Facilitate Cost Effective and Timely Closure and Lease Surrender 219
Daniel Joseph Stolberg

Construction Monitoring of a Landfill Containment Bund on Soft Marine Sediment 225
Tony Wallis

Development of Efficient, High Moment Capacity Foundations 231
Phillip Geoffrey Watson

Lateral Spreading Assessment of Petrochemical Tanks Founded on Reclaimed Wellington Waterfront 239
Hadley Wick

Management of Creep Settlement in Dumped Rockfill by Surcharging 245
James C Willey

Piled Embankment Response via Simplified Methods 251
Sii Chung Wong

SH6 Nevis Bluff Rockfall and Risk Assessment, Central Otago, NZ 257
Philip Raymond Woodmansey

Site Response in the Aburrá Valley, Medellín, Colombia

Brian M Adams
URS New Zealand Limited, PO Box 4479, Christchurch, Brian_Adams@URSCorp.com

Medellín, Colombia's second largest city, is spread across the floor and sides of the 1200m deep and 15km wide Aburrá valley, which is set in the tectonically active central cordillera of the Northern Andes. The valley is covered by a variably thick layer of soft residual soils, debris-flow and alluvial deposits overlying a much stiffer bedrock. A 2-D elastic finite-element method is used to model seismic wave propagation within the valley and to investigate the variable nature of site response in Medellín. Site response is found to be highly dependent on multi-dimensional effects caused by local irregularities in the stratigraphy and topography. Amplification may be influenced strongly by sub-valley structures up to a few kilometers across, yet the influence of the valley as a whole is small.

1 INTRODUCTION

Non-uniform near-surface geology such as is found in sediment-filled basins often leads to serious multi-dimensional site effects such as focussing, basin resonance and edge effects. The city of Medellín is set in the deep Aburrá Valley in Colombia (Figure 1) which contains a 24-instrument network of accelerographs. Anomalously high levels of ground motion recorded at several of these stations indicate that the seismic response is probably dominated by multi-dimensional amplifications.

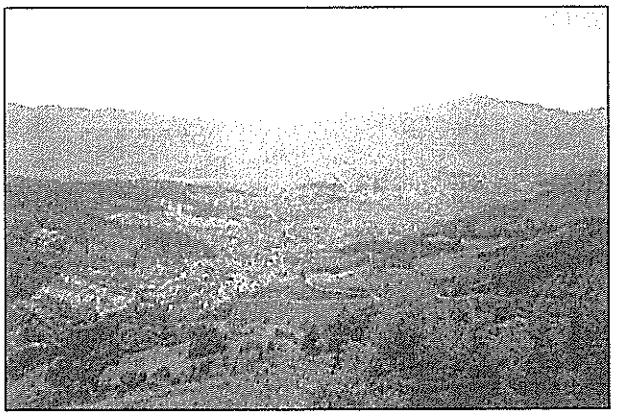

Figure 1. Medellín in the Aburrá valley.

Recent damaging earthquakes in Medellín (November 1979 and October 1992) sparked the start of a comprehensive study of earthquake risk in the city (Velásquez and Jaramillo, 1993; Hincapié et. al., 1993; Jaramillo and Ortega, 1993; GSM, 1997, 1999). It was noted that the damage distribution from the most recent earthquakes had been very erratic and concentrated in certain zones, indicating a very non-uniform shaking.

In this study two-dimensional elastic finite-element modelling techniques are used to investigate the seismic response across the width of the Aburrá Valley. A similar method was used in a study two-dimensional seismic response study of the much smaller Wellington-Hutt Valley basin in New Zealand (Adams et. al, 2000). This research was undertaken in attempt to determine if two-dimensional effects are likely to dominate the seismic response of the valley as a whole and to identify areas where multi-dimensional focussing or edge effects might generate locally high amplifications.

2 PHYSICAL SETTING

Colombia is located in the north-west corner of the South American continent near the boundary of the Nazca, Caribbean and South American tectonic plates (Figure 2). Frequent seismic events from both subduction and intraplate movement provide seismic risk to the area.

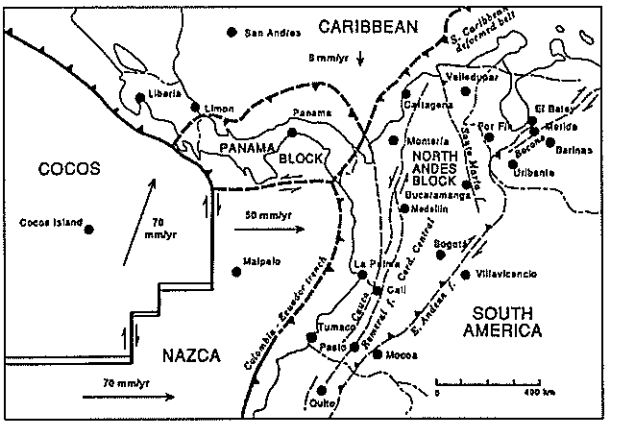

Figure 2. Tectonic plate interactions in Colombia (after Kellogg and Dixon, 1990).

Medellín, with a population of 1.8 million (June 1995), and an urban area of 110 km^2 is spread across the Aburrá Valley, a 1200 metre deep depression in the northern part of the Central Cordillera of the Northern Andes. The Aburrá Valley drains north to the Carribean Sea some 500km away. Medellín is located at an altitude of 1500 metres, while the surrounding rolling countryside of the cordillera lies at an altitude between 2600 and 2800 m.

2.1 Aburrá Valley Geology

There are several different types of basement rocks in the area, all of which are plutonic or metamorphic. The metamorphic rocks (gneiss and amphibolite) are the oldest and date back to the Cretaceous or possibly the lower Paleozoic, while the igneous stocks of dunite, gabbro, grano-diorite and diorite date back to the Cretaceous and have intruded into the gneiss and

amphibolites. The origin of the Aburrá valley is almost certainly associated with the north-south trending Romeral and Cauca fault systems of the Central Cordillera and Cauca Valley, and is possibly some form of extensional strike-slip duplex.

A variable depth of soft material exists above the basement rock within the valley. This soft covering may consist of one or any combination of residual soils, weathered non-consolidated debris flow deposits and alluvial deposits dating back to the quaternary. These soft units are on average 30 metres thick and may be as thick as 200 metres in places. The steepest and most elevated parts of the city generally coincide with basement rock with a residual soil covering. The slopes characterised by moderate inclinations (~10-30°) and elevations are often deposits of debris flows originating from higher and steeper slopes, while the flattest and lowest parts of the city are generally on alluvial deposits. Several outcropping hills form noticeable irregularities in the topography of the debris flows and alluvial deposits, indicating that the basement rock is highly irregular and capable of producing all manner of focussing and wave-path effects.

3 METHOD OF ANALYSIS

In this study a two-dimensional finite-element method is used to investigate the elastic seismic response of a typical cross-section through the Aburrá Valley.

3.1 Aburrá Valley Cross-Section and 2-D Model

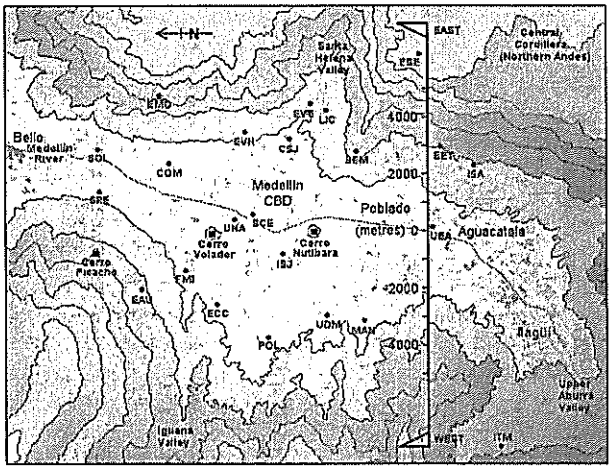

Figure 3. Topographic map of the Aburrá valley (contour interval 200m) showing the cross section line.

An east-west cross section has been taken though the southern end of the city as shown in Figure 3. The cross-section shown in Figure 4 extends for 9320 metres either side of the Medellín River. The lower semi-circular boundary of the model extends to a maximum depth of 1500 metres below the free surface in the centre of the valley. Using the mesh generator Triangle (Shewchuck, 1996), this geometry is used as the basis for constructing a fine mesh of triangular elements suitable for the finite element computation.

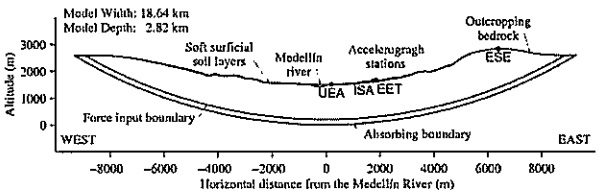

Figure 4. Geometry of the 2-D model

A total of twelve geological units are modelled; three basement rock types, and nine different near-surface soft sediments. Each of these units are assigned geotechnical properties (Table 1) on the basis of results from comprehensive borehole and laboratory testing (GSM, 1999).

Table 1. Eastic properties of soil and rock units

		Geological Unit	Bulk density ρ (kg/m^3)	Shear velocity V_s (m/s)	Shear modulus G (MPa)	Damping ratio ξ(%)
Basement rocks	SaM	Amphibolite	2650	2000	10,600	0
	SuM	Medellín Dunite	2650	2000	10,600	0
	SdA	Altavista Stock	2650	2000	10,600	0
Residual soils	KaM	Amphibolite Soil	1900	400	304	12
	KuM	Medellín Dunite Soil	1900	350	233	8
	KdA	Altavista Stock Soil	1700	250	106	4
Transported soils	Qal_1	Surface Alluvial	1500	150	34	7
	Qal_2	Deep Alluvial	1800	375	253	3
	Qfs	Soil of Debris Flows	1500	200	60	10
	Qfm	Mature Debris Flows	1600	250	100	7
	Qff	Fresh Debris Flows	1600	250	100	7
	Qfl	Artificial Fills	1500	150	34	7

The model assumes the soil and rock materials to be isotropic and homogeneous within each layer. Significant care has thus been taken to assign unit properties that are representative of the variable reality. Deposits within the model have an average depth of 32 metres, and a maximum of 94 metres. The central part of the valley contains a more complex succession of layering resulting from alluvial and debris flow deposition.

3.2 Finite Element Method

To model elastic SH wave propagation within our 2-D cross section of the valley, we use a software package called Archimedes (Bao et. al., 1998). The problem is one of two-dimensional elastic horizontally-polarised (SH) shear-wave propagation within a heterogeneous soft basin surrounded by a homogeneous half space of rock. Setting the cross section in the x-z plane, then the SH wave displacement field lies in the long-valley (y) direction. The anti-plane displacement field, $v(x,z,t)$, within each element is required to satisfy the wave equation.

$$\rho \frac{\partial^2 v}{\partial t^2} = G\left(\frac{\partial^2 v}{\partial x^2} + \frac{\partial^2 v}{\partial z^2}\right) \qquad [1]$$

Boundary conditions are imposed which require the continuity of force and displacement across each element, and the absence of tractions at the free surface. For equilibrium under an applied motion within the computational domain it is necessary to solve a system of ordinary differential equations of the form

$$[M]\frac{d^2v}{dt^2}+[C]\frac{dv}{dt}+[K]v = f(t) \qquad [2]$$

where [M], [C], and [K] are the mass, damping and stiffness matrices and $f(t)$ is the applied nodal force. Archimedes uses viscous Rayleigh damping within the model and a semi-circular viscous absorbing boundary around the lower extent of the model to simulate an infinitely large half-space. The input motion is a single vertically-propagating Ricker wavefront (Ricker, 1940) with a time-dependant displacement shown in Figure 5 and given by

$$v(t) = A\left[1-2\left(\omega_c t-3\sqrt{6}\right)^2\right] e^{-\left(\omega_c t-3\sqrt{6}\right)^2} \qquad [3]$$

where ω_c is the characteristic frequency and A is the wavelet amplitude. With a central frequency of 2.0 Hz, the Ricker pulse can be used to study frequencies up to 5.0 Hz.

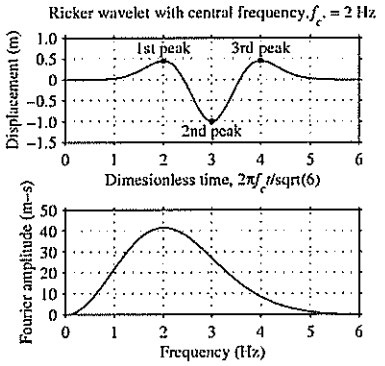

Figure 5. Displacement trace and spectral amplitude of a 2.0 Hz Ricker wavelet.

4 RESULTS

Figure 6 shows displacement seismograms computed across the surface of the Aburrá Valley The output shown is the displacement due to the vertical propagation of a horizontal SH wavefront with a central frequency, f_c, of 2.0 Hertz. Figure 7 shows a plot of Fourier spectral ratio (FSR) and is used to describe the frequency response across the surface of the valley

4.1 Amplification of the First Arrival

The plot in Figure 6 shows an amplified first arrival of the vertically propagating wavefront. The left-hand-most contoured ridge is the 1st (positive) peak of the Ricker displacement pulse arriving at the surface across the full width of the valley. It is followed closely by the 2nd (negative) and 3rd (positive) peaks. The wavefront is variably amplified and arrives at different times depending on both the topography, and the depth, geometry and material properties of any soft layers beneath.

4.2 Surface Wave Action

Figure 6 shows little evidence of significant surface wave action generated by the 2-D analysis. This is especially noticeable when compared to similar analyses of narrower basins with deep sediments such as the Lower Hutt (Adams et. al., 2000), where strong surface waves are generated at each edge of the valley. Weak surface waves, however, are generated at the edges of the deep alluvial dip in the centre of the plot, and at the edges of the debris-flow deposits between +1000 and +1800m. The former pair of surface waves cause amplification where they interfere constructively at –250m. On the whole, this model does not appear to be strongly affected by the presence of surface waves.

4.3 Vertical Wave Reflection and 1-D Resonance

In some parts of the valley, the SH wave appears to reflect up and down within the soft surface layers more strongly than at other locations. This can be seen on Figure 6 as a repeated pattern of wavefronts reaching the surface in a fashion that extends or stretches the shape of the initial arrival. The oscillations continue for longest in regions of thicker sediments.

4.4 Two-Dimensional Effects

Fourier spectral ratios shown in Figure 7 exhibit a pattern of peaks that reach a maximum of 18 at several locations. The strong spatial variability is clear evidence of two dimensional effects such as focussing, surface wave action and horizontal resonance. This variability occurs over the whole of the soft part of the valley. Within the alluvial dip to the west of UEA the spectral peaks show a clear pattern of two-dimensional resonance (Bard and Bouchon, 1985) such as was found in the Lower Hutt Valley (Adams et.al, 2000). The single peak at 1.15 Hz and triple peak at 1.65 Hz represent the 1st and 3rd horizontal resonant modes (respectively) of the 1st vertical resonant mode. The lower amplitude 5th and the 7th horizontal modes can also be seen at 2.10 Hz and 2.40 Hz respectively. At 3.15 Hz a further centrally located (x = 250m) peak indicates the onset of the 2nd vertical mode.

Two-dimensional resonance effects also occur in the thick layer of debris-flow and residual deposits between +300m and +3100m. Within this zone there appears to be a complex interaction of several resonance patterns of different size-scales. The largest of these is the full 2800-metre-width, which forms a (rather hypothetical) weak two-dimensional resonance pattern. Within this, the 1600-metre-width between +300m and +1900m forms a well-defined two-dimensional pattern.

On an even smaller scale, the small surficial debris flow deposits (Q_{fm}) at +2100m and +2600m generate small basin-resonances of their own. The horizontal resonance component within any of these patterns does not appear to be strong enough to generate a fully formed two-dimensional pattern; rather only the two-dimensional modes that coincide with the vertical resonance pattern are visibly amplified. At any point within the debris-flow deposits, it is difficult to determine how much of the response is due to resonance set up within the whole deposit or half the deposit, or whether it is just a very local effect.

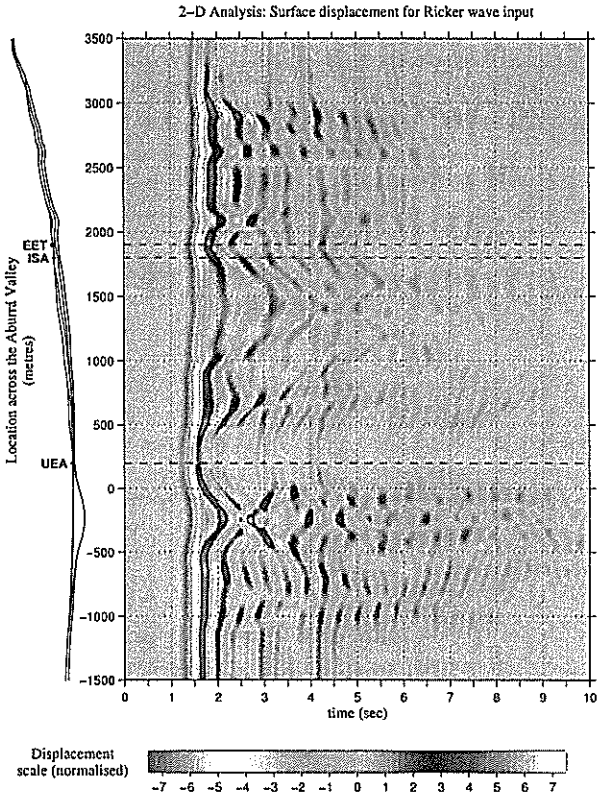

Figure 6. A displacement-time history at the surface of the model generated by a 2-D simulation.

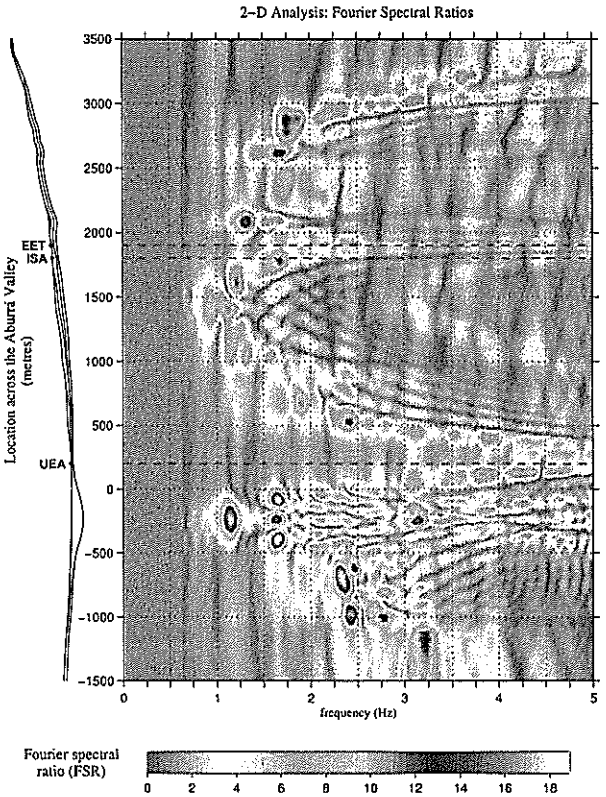

Figure 7. Fourier spectral ratios at the surface of the model generated by a 2-D simulation

5 DISCUSSION

The Aburrá Valley at Medellín appears to have a very complex seismic site response; a product, essentially, of its highly irregular near-surface geology. The variable yet thin covering of soil within such a large valley means that the response of the valley as a whole is less dominant than the response due to smaller-scale topographic and sub-surface features.

In modelling the Aburrá valley with two-dimensional methods, it has been shown that the seismic response at most locations is clearly due to a combination of one- two- and even three-dimensional effects. Multi-dimensional effects appear to exist on both small and large scales. Spatially variable and peaked amplifications of the first arrival of the Ricker wavelet is indicative of topographic and/or sub-surface stratigraphic focussing at many locations across the valley. Due to the relatively shallow depths of soil, this phenomenon is generally very local in nature. Another small-scale multi-dimensional effect observed in the Aburrá Valley model is strong horizontal resonance in small and well-defined soft deposits and topographic features.

On a slightly larger scale, multi-dimensional resonance within sub-basin structures and thick soil deposits appears to influence the response across much of the valley. There is clear evidence of strong two-dimensional amplification both within the alluvial dip in the centre of the valley, and debris-flow deposits on the eastern slope. Neither of these structures is particularly well constrained in the horizontal direction, and for that reason the higher mode horizontal resonances are not well developed. The net effect is a spatially-peaked and highly amplified pattern of resonance occurring at frequencies similar to those from the one-dimensional analysis.

For any given site within the Aburrá Valley, it is therefore essential to consider a significant volume of surrounding geology in order to predict the seismic response at that site. The results, however, show little influence from the overall large-scale dimensions of the valley. Rather, the structures within the valley on smaller scales from a few kilometres to a few metres wide appear to have the greatest influence on the results. These structures include well-defined dips and basins in the basement rock, localised thick depths of soft material that may act as resonators in the horizontal plane, and topographic features such as small side-valleys, gullies, banks, cliffs, sharp ridges and knolls. The incorporation of these features into a site-response model of the Aburrá Valley is crucial, while the incorporation of the whole valley is perhaps not quite so necessary.

The highly variable nature of the topography and near-surface geology exists in not only two, but all three spatial dimensions. Two-dimensional modelling has shown the nature and extent of the response due to the east-west horizontal dimensions of the valley and near-surface materials. As for the long-valley (north-south) dimension, the two-dimensional results have given an indication of its likely influence on the response. It appears that there will be little influence from the long-valley dimensions on a scale larger than 4-5km, yet on

a smaller scale of order less than 1-2km, there may be significant effect from side valleys, ridges and horizontally discontinuous deposits. Thus, although two-dimensional modelling has produced substantial insights into the problem, it is not an adequate way to completely characterise site response within the Aburrá Valley. A three-dimensional study is undoubtedly essential for a more realistic solution.

There are many different types of soft near-surface material, including residual soils, debris-flow deposits, alluvial deposits and artificial fills. The stratigraphy of these units is far from horizontal, with significant depths of soft material extending well up the sides of the valley. The boundaries between the geological units is sometimes very sharp (eg. between alluvial deposits and bedrock), but is more often gradational (eg. between residual soil and bedrock). Davis (1995) shows how the weathered transition zone between residual soil and basement rock may have the effect of flattening the amplitude spectrum, especially at high frequencies.

Seismic velocity data from borehole tests indicate that the shear-wave velocity often increases gradually with depth within layers of similar composition. Davis and Hunt (1994) indicate that by taking an average shear-wave velocity and modelling each layer as homogeneous, it is likely that amplification at the higher frequencies has been somewhat underestimated.

6. CONCLUSIONS

Although few conclusions can be made as to seismic site response for specific locations within the Aburrá Valley, this study has been highly successful in the sense that has identified the major contributors to seismic response.

- There is little evidence of a two-dimensional *whole*-valley response, and its effect does not appear to be dominant or even particularly important to the response at any given site. Although highly variable in nature and depth, the soft soil covering within the valley appears to be too thin compared to the overall dimensions of the valley to produce a significant whole-valley response pattern.
- The response at a given site appears to be highly dependant on an intricate combination of one- two- and even three-dimensional effects, which occur as a result of large- and small-scale features of the immediate and surrounding topography and near-surface soft soils. The most influential features are usually less than a few kilometres across.
- The anti-plane response is often influenced by weak two-dimensional patterns of resonance set up within poorly constrained soft units such as debris-flow deposits. At other sites that are more strongly defined and two-dimensional on a local scale – such as within the alluvial dip in the centre of the valley – strong horizontal resonant modes may be observed in the spectral response.
- While two-dimensional modelling has shown the role, scale and influence of horizontal effects within the valley, it is generally not an adequate characterisation for much of the Aburrá Valley. The extent to which soil deposits and topographic features in the cross-valley orientation influence the response leads us to expect the same in the long-valley direction, where the geology and topography are also highly irregular.

ACKNOWLEDGEMENTS

Thanks to Juan Diego Jaramillo and Luis Andrés Palacio (Ing. Civil, Universidad EAFIT, Medellin), Gloria Maria Estrada (Integrál SA, Medellin) and Diego Rondón (Consulting Geologist, Medellín) for both logistical and technical aspects of this study. Thanks also to Jacobo Beilak (Civil and Env. Engineering, Carnegie Mellon University, Pittsburgh, PA.) and Jifeng Xu (Lam Research Coorporation, Fremont, CA) for their support with the Archimedes computation; and to Rob Davis and John Berrill (Civil Eng., University of Canterbury) for their supervision and comments. This work was funded by the Earthquake Commission of New Zealand (EQC), the New Zealand Society for Earthquake Engineering, and the University of Canterbury.

REFERENCES

Adams, B.M.; Berrill, J.B.; Davis, R.O. and Taber, J.J. (2000). "Modeling Site Effects in the Lower Hutt Valley, New Zealand". *Proceedings of the 12th World Conference on Earthquake Engineering, Auckland, New Zealand.* Paper no. 2694.

Bao, H.; Bielak, J.; Ghattas, O.; Kallivokas, LF.; O'Hallaron, DR.; Shewchuk, JR. and Xu, J. (1998). "Large-Scale Simulation of Elastic Wave Propagation in Heterogeneous Media on Parallel Computers". *Computer Methods in Applied Mechanics and Engineering.* **152**: 85-102. Elsevier Science, S.A.

Bard, P.Y. and Bouchon, M. (1985). "The Two-Dimensional Resonance of Sediment-Filled Valleys". *Bull. Seism. Soc. Am.* **75**: 519-541.

Davis, R. (1995). "Effects of Weathering on Site Response". *Earthq. Eng. and Struct. Dyn.* **24**: 301-309.

Davis, R. and Hunt, B. (1994). "Amplification of Vertically Propagating SH Waves by Multiple Layers of Gibson Soils". *Intl. J. for Numerical and Analytical Methods in Geomechanics.* **18**: 205-212.

Groupo de Sismología de Medellín (1999). *"Instrumentación y Microzonificación Sísmica del Área Urbana de Medellín".* Informe para SIMPAD (Sistema Municipal de Prevención y Atención de Desastres) y Municipio de Medellín Secretaria Privada (in Spanish).

Groupo de Sismología de Medellín (1997). *"Instrumentación y Microzonificación Sísmica del*

Área Urbana de la Cuidad de Medellín". Informe Final (Versión detallado) con Adición CSA121 de Octubre1998. Contracto C112 para SIMPAD (in Spanish).

Hincapié, J.E.; Osorio, R.; Pineda, C.M. and Urrea D.P. (1993). "Hacia una Zonación Sismo-Geotécnica de Medellín". *Programa de Prevención Sísmica para Medellín, Segunda Etapa: Parte II*. PNUD, Alcaldía de Medellin. Universidad EAFIT (in Spanish).

Jaramillo, J.D. and Ortega, D.C. (1993). "Estudio del Riesgo Sísmico de Medellín". *Programa de Prevención Sísmica para Medellín, Segunda Etapa: Parte III*. PNUD, Alcaldía de Medellin. Universidad EAFIT (in Spanish).

Kellogg, J.N. and Dixon, T.H. (1990). "Central and South American GPS Geodesy – CASA UNO". *Geophysical Research Letters*. **17** (3): 195-198.

Ricker, N. (1940). "The Form and Nature of seismic Wavelets and the Structure of Seismograms". *Geophysics*. **5**: 348-366.

Shewchuck, J.R. (1996). "Triangle: Engineering a 2D Quality Mesh Generator and Delaunay Triangulator". *First Workshop on Applied Computational Geometry (Philidelphia, PA.)*. pp 124-133, ACM, May 1996.

Velásquez, E. and Jaramillo, J.D. (1993). "Estudio de la Amenaza Sísmica de Medellín". *Programa de Prevención Sísmica para Medellín, Segunda Etapa: Parte I*. PNUD, Alcaldía de Medellin. Universidad EAFIT (in Spanish).

Probability and Sensitivity Analyses for Geotechnical Engineering Applications

Karen Allan MIEAust CPEng, Golder Associates Pty Ltd, Brisbane

This paper presents a brief overview of four commercially available tools which can be used to perform probability and/or multiple scenario analyses in the field of geotechnical engineering. A overview of SLOPE/W, CrystalBall (combined with a slope stability analysis package), FLAC, @Risk (combined with settlement analysis program) and briefly GoldSim is provided, together with comments on the relative advantages and disadvantages of each when used for probability analyses in geotechnical engineering.

1 INTRODUCTION

A number of tools are currently available to assist geotechnical engineers in performing probability or multiple scenario analyses. This paper presents a brief overview of four currently, and commercially, available software packages for such applications, as follows:

- SLOPE/W, by GEO-SLOPE International Ltd.
- CrystalBall by Decisioneering, Inc. combined with XSlope by the University of Sydney.
- FLAC (*F*ast *L*agrangian *A*nalysis of *C*ontinua), by Itasca.
- @RISK by Palisade, in combination with spreadsheet.
- GoldSim by the GoldSim Consulting Group.

It is important to note that whether you choose to do a probability or sensitivity analysis depends on the quantity and quality of data available. With limited material property information, analysis results would normally be referred to as sensitivity analyses, rather than probability analyses. The information presented in this paper, in terms of available software, is applicable for either probability or sensitivity analyses.

2 SLOPE/W

SLOPE/W by GEO-SLOPE International Ltd is a powerful commercially available stability analysis package commonly used by geotechnical engineers worldwide. The program allows users to choose to undertake a "probabilistic analysis" using a defined number of trials.

For each soil type, basic soil parameters such as unit weight, cohesion and friction angle are assigned values of mean and standard deviation. SLOPE/W performs the stability analysis once and defines the critical failure surface using the mean strength parameters. It then completes a probabilistic analysis on the critical failure surface (mean strength parameters) based on the user-defined standard deviation values

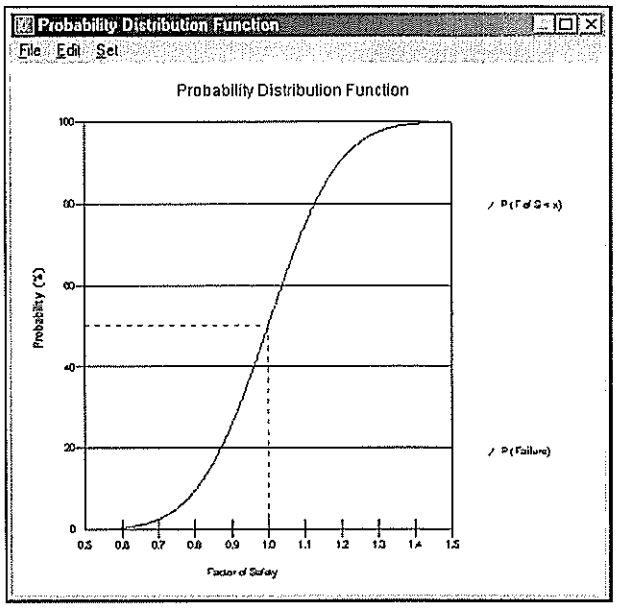

Figure 1 – Example SLOPE/W Output

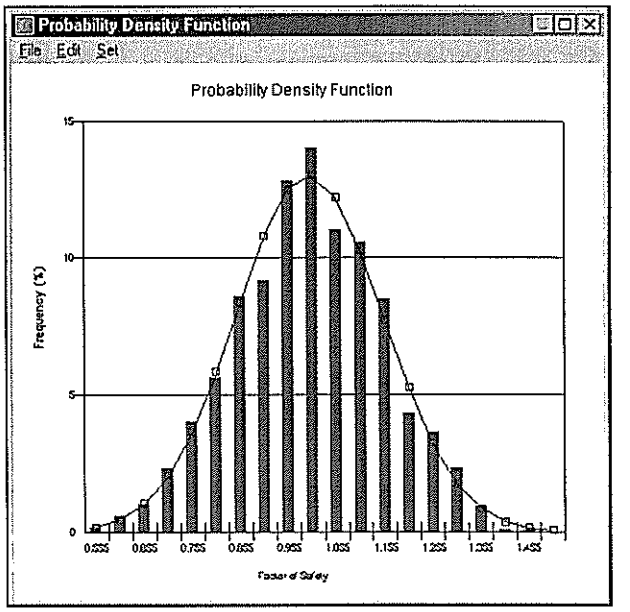

Figure 2 – Example SLOPE/W Output

Standard deviations values may also be applied to line loads and seismic loads.

The program provides charts of probability density function (see Figure 1), and probability distribution function (see Figure 2), which allows the user to identify the probability of obtaining a particular factor of safety value for the critical circle.

Usually, the location of the critical failure surface will vary as soil strength parameters are changed. SLOPE/W would not be appropriate for probability analysis unless the user can confirm that the critical failure surface does not vary significantly across the range of soil strength parameters. This could be done by doing a separate suite of sensitivity analyses, manually varying soil strength parameters to determine range of critical circle locations.

Other limitations include:

- Inability to vary slope geometry.
- Uses only normal distributions for variable parameters.

3 CRYSTALBALL AND XSLOPE

Excel can be used, with an add-in tool, to generate a number of data files which are subsequently used by a slope stability analysis package. A particular example includes the CrystalBall add-in tool for Excel, and XSLOPE. Other stability analysis packages may also be applicable for this use, provided the program can read data files saved as text, comma delimited or tab delimited files generated in Excel.

By macro and CrystalBall, Excel can be programmed to vary the value of any cell in a spreadsheet, and save results to a data file. Values of soil strength may be varied according to any choice of statistical distribution. Co-ordinates at the toe of a slope may be varied within certain limits based on a different statistical distribution. Phreatic surface may be raised, and surface pressures linked to changes in water table. Up to 16 different pre-defined statistical distributions are available in CrystalBall.

Using Excel and CrystalBall, a defined number of unique data files can be generated. The stability analysis package can then run each unique data file to determine the critical failure circle and calculate the minimum factor of safety. Final results can be summarised to provide a range in factor of safety values for the given variations in soil strength, geometry, water table and other variations. A histogram of minimum factor of safety can be generated to easily indicate distribution of values.

Some limitations of using this method of analysis include:

- Most modern stability analysis software packages (ie SLOPE/W) cannot have data files easily accessed, edited or saved through Excel.
- Must write Excel macros to run CystalBall and save data file, and extract all minimum factor of safety value. Must also have stability analysis program that can batch multiple analyses.
- Uses up more memory than SLOPE/W since every analysis is saved.

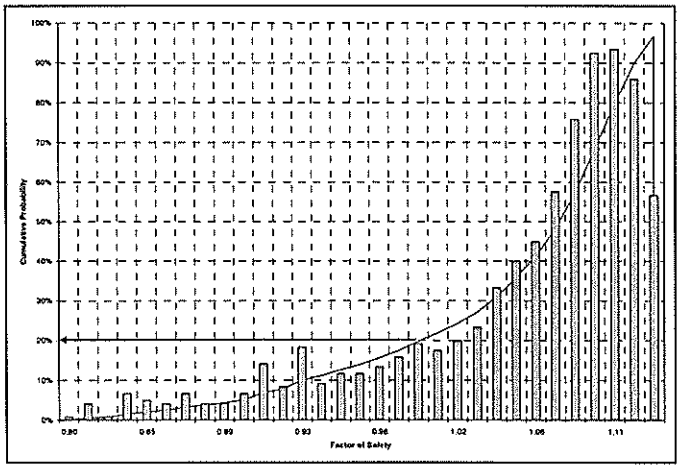

Figure 3 – Example Excel/CrystalBall and XSLOPE Output

Figure 3 presents the results of analysis of 1000 difference critical circles and the probability of obtaining a factor of safety of 1.0 can easily be determined.

4 FLAC (*Fast Lagrangian Analysis of Continua*)

Using FLAC, multiple analyses can be carried out to determine the effect of variations in soil properties on soil/structure interaction.

Often referred to as Monte-Carlo simulations, variable soil strength properties can be assigned to elements within the FLAC grid.

Figure 4 shows the shear modulus values obtained from a number of pressuremeter tests in the same horizon of soil. A line drawn through the lower-bound and upper-bound extent of the data may represent the five percentile and 95 percentile limits of data. Based on this, mean shear modulus and standard deviation can be calculated at any depth.

FLAC has inbuilt random number generators to assist in Monte-Carlo simulations.

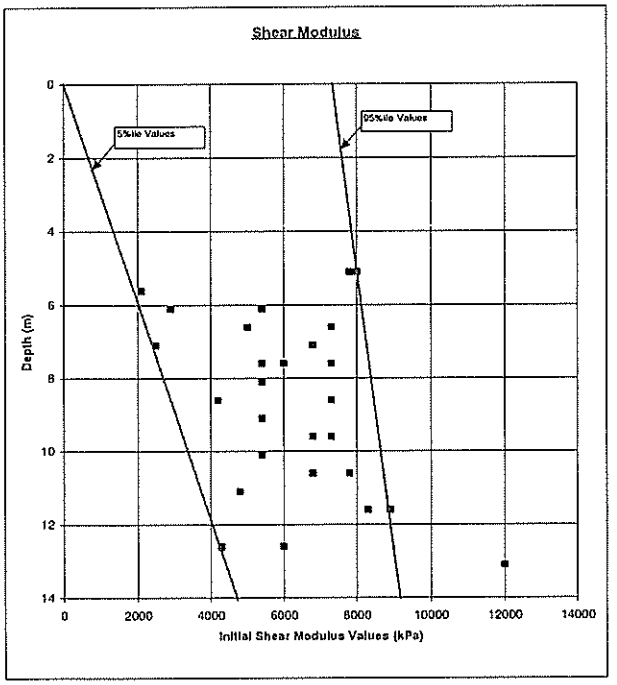

Figure 4 – Example Variation in Soil Strength with Depth

Using the FISH code in FLAC, routines can be written to assign values of shear modulus to the soil, based on the depth of that element, and the mean shear modulus and standard deviation at that depth.

An example FISH code is shown in Figure 5.

```
* This routines creates varying stiffness for each FILL element
in FLAC grid,
* based on predefined mean and SD variables
* FILL_S
def fill_s
loop i (1,izones)
 loop j (25,29)
  fill_sh_mean=9000.0
  fill_sh_SD=1824.0
  random_SD ; random number from normal distribution
  s_mod=fill_sh_mean+fill_sh_SD*num_SD
  p_ratio=0.35
  y_mod=s_mod*2.0*(1.0+p_ratio)
  install ;converts y _mod to s_mod and b_mod
  shear_mod(i,j)=s_mod
  bulk_mod(i,j)=b_mod
  cohesion(i,j)=5.0
  density(i,j)=1.8
  friction(i,j)=25.0
  end_loop
end_loop
end
```

Figure 5 – Example FLAC FISH Code

Other FISH routines need to be defined to save each simulation in a new data file, and the entire FLAC file looped to repeat for each analysis.

Results of an analysis that included 150 unique FLAC simulations are shown Figure 6. In this example, emphasis was placed on assessing the potential effect of variable soil properties on movement of an adjacent structure.

The results were able to demonstrate that, for what appeared to be large variations in soil shear modulus, structure movement did not vary by more than 5 mm.

Some limitations, or disadvantages with using FLAC for multiple analyses are:

- Uses up large amounts of memory to store results of analyses. Example analysis required nearly 70 MB of disk space, uncompressed.
- Analysis takes significant time to complete, depending on complexity of FLAC model and size of grid. Example analysis took about 2 days to complete 150 simulations.
- Required writing of detailed code, which is difficult to debug.

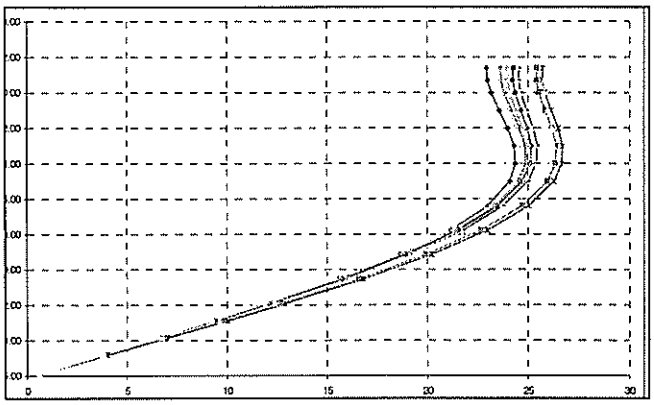

Figure 6 – Example FLAC Monte-Carlo Simulation Output – Structure Horizontal Displacement

Despite its limitations, FLAC is a very powerful tool for performing multiple scenario analyses for geotechnical applications, especially when considering interaction with sensitive structures.

5 @RISK and PCon

A further example of software that can be used to assist in geotechnical engineering applications is the spreadsheet add-in tool @RISK. In combination with spreadsheet-based in-house settlement analysis software (Golder has developed PCon), multiple settlement analyses can be carried out in order to define the probability of obtaining certain values of settlement.

Variable inputs for a settlement analysis may include:

- Compression and re-compression index values for each compressible layer.
- Secondary compression values for both virgin compression and recompression.
- Coefficient of Consolidation; and
- Drainage path length.

Each of these properties can be assigned individual probability distributions.

For design of runways and aprons at the Brisbane International Airport, compression indices were varied using rectangular and triangular distributions, recompression indices were correlated to compression indices, triangular distribution were applied to coefficients of consolidation, and probability distributions applied to either 2-way or 1-way drainage for each compressible soil layer. There are 36 different probability distributions built into @RISK which can be applied to any of the variable parameters.

For each settlement analysis, the required output value must be specified.

After the input and output parameters have been defined, @RISK will recalculate the spreadsheet a defined number of times (maybe 1000 simulations) and present a summary of the results.

Figure 7 presents the results of a settlement analysis at the Brisbane Airport.

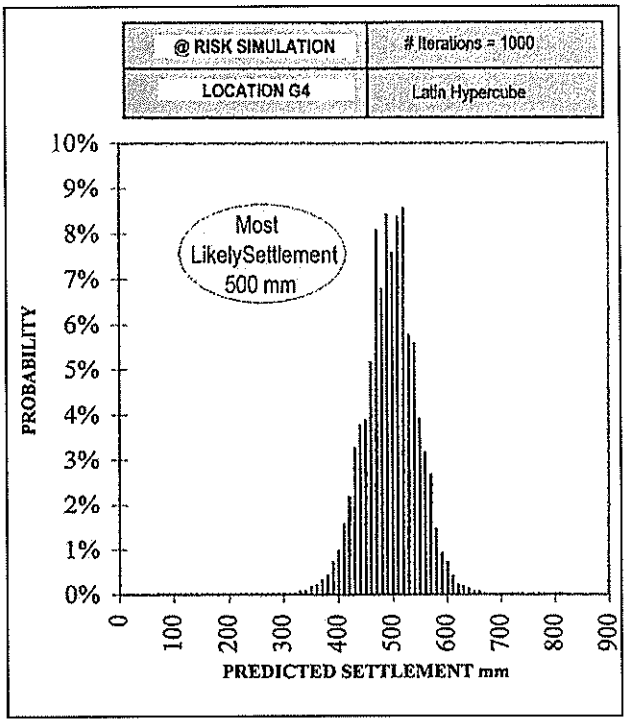

Figure 7 – Example @RISK Output – Predicted Settlement

@RISK functions can be programmed into Excel macros, thereby also allowing @RISK to be used in a similar manner to CystalBall, as described in Section 3 of this paper.

There are few disadvantages to mention in this section, especially when using @RISK for spreadsheet applications. Depending on the magnitude of data and number of input variables, several hours may be required to run a model simulation. If attempting to use @RISK to generate data files for other non-spreadsheet based programs, limitations would be similar to those mentioned in Section 3.

6 GoldSim

GoldSim is a powerful, user-friendly, and highly graphical computer program for carrying out dynamic probabilistic simulations to support management and decision-making in engineering, science and business.

It is flexible platform for visualising and numerically simulating nearly any kind of physical, financial or organisational system. In a sense, GoldSim is like a "visual spreadsheet", that allows you to visually create and manipulate data and equations.

Unlike spreadsheets, however, GoldSim allows you to readily evaluate how systems evolve over time, and predict their future behaviour.

Some typical example applications include:

- Strategic Planning
- Resource Planning and Management
- Water Resources
- Wildlife management
- Environment
- Manufacturing

Geotechnical applications may include:

- Settlement Analysis
- Slope Stability Analysis
- Pile Analysis

GoldSim would be best suited to projects where large numbers of simulations are required. This may reduce the time involved in probability analyses, in comparison to CrystalBall and @RISK applications.

7 REFERENCES

1. Golder Associates Pty Ltd, "Settlement Analysis: Proposed New ITB Brisbane Airport Eagle Farm", December 1992, report 92638149(J).
2. GEO-SLOPE International Ltd "SLOPE/W Version 5 User Manual".

8 COPYRIGHT

Geotechnical Aspects of the Wairau Storage Tank

Kevin Anderson, Geotechnical Engineer, Sinclair Knight Merz Limited, Auckland, New Zealand

The paper discusses the geotechnical design of the Wairau Storage Tank. The tank is a 6,500m^3 buried reinforced concrete structure required to store peak sewage flows to prevent overflow discharges. The regional, local and site geology is outlined. The paper includes the implications of the geology and the required construction methods. The feasibility of the construction of the tank including the various methods of supporting deep excavations is considered. The detailed geotechnical design reviews the procedures undertaken and covers the model development, the geotechnical model and parameters used, the design results, model validation and groundwater inflow. The importance of stage construction in geotechnical modelling is discussed further.

1. INTRODUCTION

Sinclair Knight Merz (SKM) was appointed as principal consultant for the Wastewater Major Improvement Project in Auckland, New Zealand by the North Shore City Council. The NZ$80M project involved extensive upgrading of the wastewater collection system requiring new trunk sewers, pump stations and storage tanks.

SKM provided design criteria development, concept design, programming to meet client capital expenditure, detailed design of the various elements of the scheme, procurement and construction supervision.

The Wairau Storage Tank is a 6,500m^3 buried reinforced concrete structure designed to take peak wet weather flows from the trunk sewer network. This will reduce sewer overflows.

2. GEOLOGY

2.1 Regional Geology

The city of Auckland straddles a narrow isthmus in the North Island of New Zealand. Auckland has a rich and varied geological history. Up to and including the Triassic period the greywacke foundation rocks of the North Island were formed in the New Zealand geosyncline. The area was then subject to uplift and erosion until the Oligocene. During the Miocene era the Waitemata series was deposited. Erosion of the Waitemata occurred during the Pliocene and Pleistocene eras forming deep gullying of the now drowned Waitemata and Manukau rivers and depositing alluvium. Auckland's volcanoes, numbering more than 50, began erupting within the last 100,000 years with Rangitoto rising above the sea only 800 years ago. The Auckland volcanic field is considered to be dormant.

2.2 Local Geology

The site is located in the Wairau Valley on the North Shore of Auckland. The primary geological features of the area are the explosion crater of Lake Pupuke, with associated Pleistocene basaltic lava flows and tuff, Wairau Valley containing Pleistocene and Pliocene alluvial deposits and a higher ridge to the north west formed of the Miocene Waitemata series.

The carbon dating of wood recovered from beneath the Pupuke basalt flows show they are more than 40,000 years old. The lava flows spread over the alluvial flats of Wairau Valley damming the stream. The stream was diverted west and cut a new channel near the site location which was subsequently filled with alluvial deposits.

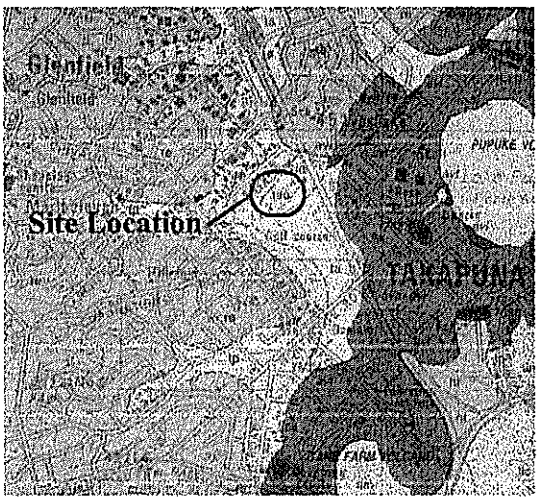

Figure 1 : extract from geological map

2.3 Site Geology

The site is located adjacent to the Takapuna Golf Course near the North Shore Event Centre on an alluvial flat. There are made ground deposits on the site rising above the alluvial plain. A lined open drainage channel is located along one edge of the site. A site specific geotechnical investigation was carried out which comprises 4 No. rotary cored boreholes up to 18m depth and 16 No. cone penetrometer tests (CPT) up to 11m depth. In-situ and laboratory testing was carried out.

The ground conditions comprise 1.5m made ground overlying alluvium to 4.5m to 13.5m depth. The Waitemata series underlies the alluvium. The depth of alluvium varies considerably across the site and was thought to be associated with secondary channels of the diverted Wairau stream. No basaltic lava deposits were found.

The alluvium is Pleistocene Puketoka Alluvium and comprises soft to firm grey pumiceous interbedded silty clay, sandy silt and very loose to loose sand. The standard penetration test 'N' (SPT) varied from 0 to 11, average 4 and the in-situ vane shear strength peak varied from 56 to 183kPa, average 103kPa with a residual of 25 to 75kPa, average 37kPa. The Atterberg limits indicated silts of low to extremely high plasticity, generally intermediate to high. The cone resistance from the CPT results indicated a q_c generally from 0.5 to 2 MPa but with frequent peaks up to 12MPa.

The Waitemata rocks has a distinct weathered zone of 2.5m to 5m comprising grey very to extremely weak sandstone and siltstone with organic laminations sub-horizontal bedding, moderately to completely weathered. The rock was found to be completely weathered to firm clayey silt and loose sand in places. The SPT varied from 10 to >50 and the unconfined compressive strength (UCS) varied from 420 to 1700kPa, average 900kPa.

The unweathered Waitemata is the basement rock and comprises grey weak to extremely weak siltstone and sandstone with sub-horizontal bedding, fresh to slightly weathered. All the SPT values were >50 and the UCS varied from 680 to 6300kPa, average 3550kPa.

The groundwater was monitored with two standpipes. The levels varied between 1m and 1.6m below ground level. The site is subject to occasional flooding.

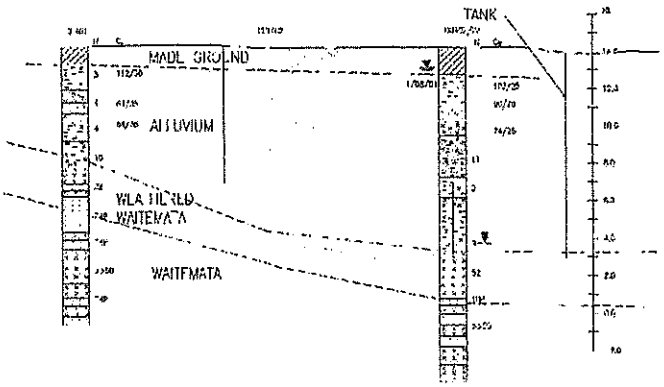

Figure 2 : geological section through tank

3. DESIGN OF RETENTION SYSTEM

3.1 Feasibility

The construction of the tank would require excavation depths of up to 9m. The high groundwater table in combination with sand lenses of high permeability and nearby structures precluded a drained open excavation. An impermeable system was required. The depth of excavation along with the weak alluvial soils would require a greater area than was available for temporary slopes. There was also concern that a contractor would cut temporary slopes too steep in the weak alluvium with unacceptable risk to the project.

Sheet piling was not considered to be feasible due to the difficulty of driving the piles into the Waitemata, which was at or near formation level. Sheet piles would also have required considerable propping to reduce bending moments to acceptable levels. The presence of many props across the excavation would have greatly complicated and hampered construction.

The most appropriate systems for deep excavations below the groundwater table are secant pile walls and diaphragm walls. Contiguous pile walls have a higher risk of permeability due to the gaps between the piles. Soldier pile walls or king post walls are difficult to construct top down and have similar limitations for water tightness.

The construction of deep excavations is still relatively uncommon in New Zealand and the market is such that specialist equipment would probably need to be imported for secant piling and diaphragm walling. Although diaphragm walling has several advantages over secant piling

it is a more specialist technique. Secant piling was chosen over diaphragm walling so as not to restrict the inclusion of local contractors in the tendering. Diaphragm walling would remain an option for contractor proposed alternatives.

3.2 Design

The feasibility design, approved by the client and peer reviewed, had identified secant piling as the preferred retention system. The required outputs of the geotechnical design of the retention system were:-

- depth of embedment;
- structural outputs (bending moment, shear force, deflection) for concrete design of pile;
- propping forces;
- restrictions or limits on construction to be included in specifications.

The finite element computer analysis programme Plaxis Version 7 was used in the design. Plaxis is specifically intended for the analysis of deformation and stability in geotechnical engineering projects. Plaxis allows for advanced soil modelling, stage construction, structural member modelling and is well suited for the analysis of soil – structure interaction.

3.2.1 Model Development

The model development using Plaxis started with simple models and the complexity was gradually built up. Initially the worst case ground conditions were used with the greatest depth of alluvium. A cantilever pile was considered first, but the resulting bending moments and deflections indicated that a very large pile section would be required. A sheet pile option was investigated to confirm that it was not feasible. Deflection and bending moments greatly exceeded that acceptable.

Following the setting up of the basic models, the construction sequencing was introduced. Initially the design area of the tank was considered to be sufficiently large to allow battered slopes inside the tank. This would allow temporary props to be installed before excavating the full extent of the tank whilst maintaining acceptable bending moments. This was considered to be the most suitable approach allowing a large opening in the centre of the tank for working room. The design also allowed flexibility in the contractor's programming and had opportunities for alternatives.

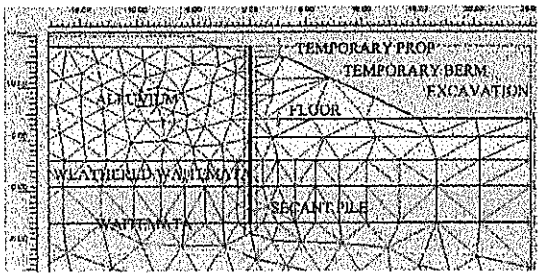

Figure 3 : Plaxis model with temporary berm

At a late stage in the design process the client considered that the cost of the structure was too high and had to be reduced. Additional network modelling also indicated that the scope could be reduced. The pumping station element of the tank was removed and the size of the tank was reduced. The reduced plan dimensions of the tank did not allow the previous design of battered slopes. Therefore the design concept was changed to a top down approach. The new design utilised the roof beams as props for the secant piles. The tension piles required to restrain uplift would be installed at ground level with steel columns above the tank formation. The roof beams would then be installed prior to excavating the tank. Excavation would be complicated by the presence of the columns and beams but should be possible.

The construction sequence is shown in figures 4.1 to 4.6 below.

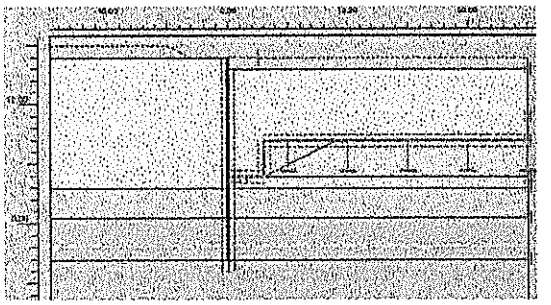

Figure 4.1 : Secant piles installed and 1m excavation

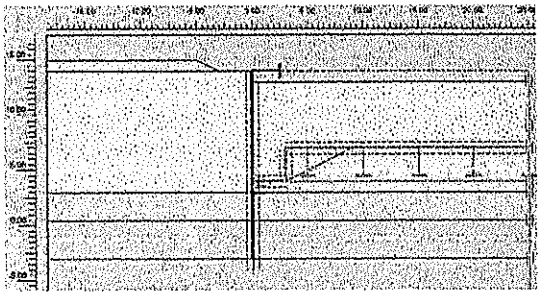

Figure 4.2 : Roof installed

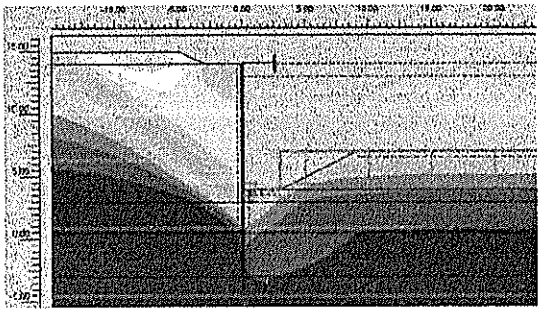

Figure 4.3 : Maximum excavation
(total displacements shown, 56mm maximum)

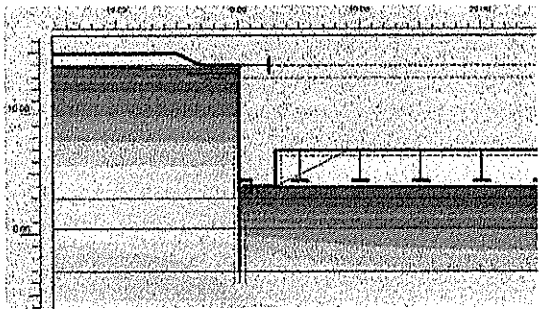

Figure 4.4 : Tank base installed
(pore water pressures shown, steady state groundwater flow)

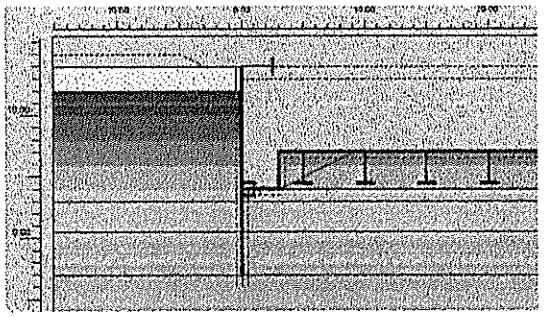

Figure 4.5 : Completed tank
(pore water pressures shown, static groundwater conditions)

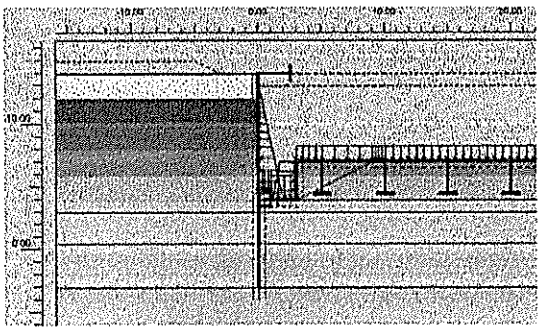

Figure 4.6 : Tank full, operational condition
(pore water pressures shown)

3.2.2 Geotechnical Model

Plaxis allows a variety of soil models to be used. The Waitemata's were modelled using mohr-coulomb. This model requires the following parameters :

- elasticity (E and υ)
- plasticity (φ and c)
- dilatancy (ψ)
- permeability (K) and weight (γ)

The alluvium was modelled using the more advanced model of strain hardening. This model allows the soil stiffness to be more accurately modelled by relating the stiffness to stress. The geotechnical parameters used in the design of the retention system are summarised in the following table.

Para-meter	Units	tp	re(w)	re
γ_{dry}	kN/m^3	14.1	15.7	16.3
γ_{wet}	kN/m^3	18.6	19.6	20.1
k	m/day	1	0.01	0.01
E	MPa	8	60	500
m υ	dimen-sionless	0.5 0.2	n/a 0.15	n/a 0.15
c	kPa	1	10	250
ϕ	degrees	27	33	33
ψ	degrees	0	0	0

notes :-
tp – alluvium
re(w) – weathered Waitemata
re – Waitemata

Table 1 : Summary of geotechnical parameters

3.2.3 Design Results

The design pile length varied from 14m to 17m. The pile length were validated by varying the length for each design case. The length was established by inspecting pile deflection and bending moment profiles to ensure fixity had been achieved. The structural design required maximum bending moments, shear and axial forces and deflections. These results are summarised below.

Design Case	Maximum Bending Moment	Maximum Shear Force	Maximum Pile Deflection
	kNm / m run	kN / m run	mm
Most alluvium	1350	489	33
Intermediate	724	294	16
Least alluvium	453	154	10

Table 2 : Summary of secant pile results

The design loading for the roof and floor were also required for the structural design. The results from the analyses were as follows :

Design Case	Maximum Roof Load kN / m run	Maximum Floor Load kN / m run
Most alluvium	-323 +52	-11 +268
Intermediate	-210	-8 +422
Least alluvium	-154	-3

notes :-
-ve – compressive load
+ve – tensile load

Table 3 : Summary of propping results

3.2.4 Model Validation

A variety of validation and checking analysis runs were carried out. Hand calculations of single propped walls were carried on using the Blum method of fixed earth support (Puller, 1996, pg143). The results were comparable to the Plaxis results. The difference was considered due to the simplicity in the hand calculations in modelling the construction sequence.

Modelling checks were carried out on most of the parameters including soil parameters (angle of internal friction, cohesion etc.), and structural parameters (prop spacing, prop stiffness, concrete parameters, pile length). Additional runs to check the assumptions of the construction sequence were also carried out.

The model was found to be most sensitive to the strength of the alluvium (internal angle of friction, ϕ'). The model also responded to the stiffness of the alluvium to a lesser but significant effect. This was expected and further consideration was given to the parameters used. The stiffness of the concrete was also important to the model. Concrete parameters can be difficult to estimate due to the nature of structural analysis. Structural engineers tend to estimate such parameters conservatively (i.e. low). However, if the true stiffness is higher the structural elements will attract more load.

The other checks such as the prop spacing and stiffness were found to be less influential on the model. Prestressing the props had a significant effect but this option was not considered appropriate when the design was changed to top down construction.

3.2.5 Groundwater Inflow

The total groundwater inflow into the excavated tank was of interest due to the relative proximity (approximately 100m) of several commercial buildings. These buildings were constructed on shallow spread foundations. The presence of sand lenses indicated a risk of a wide zone of influence should the phreatic surface drop significantly at the tank. The effect of dewatering the such sand lenses under the structure was estimated to be 30mm to 100mm settlement.

In additional, the design was intended to maintain groundwater pumping below $5m^3$ per day. This is the limit that Auckland Regional Council will allow without a groundwater removal consent. Obtaining such consents can be an arduous process. The council maintain such strict limits to protect groundwater quality and prevent unexpected damage to property. Such practice is probably wise in locations of high groundwater.

Analysis was carried out modelling a soil zone of appropriate permeability. The standard method of modelling structural elements in Plaxis is to assume they are "impermeable". Plaxis does not consider them impermeable in the calculations, but rather that they are much less permeable than the adjacent soil.

The results of the analysis showed that the secant pile wall and diaphragm wall should reduce groundwater inflow below that required. Contiguous piles were unlikely to meet that requirement. All of these methods had limited influence on the phreatic surface. The influence of a sheet pile wall was found to be considerably greater, influencing the phreatic surface for more than 150m. The inflow under steady state conditions was about 10 times greater than for secant piles, but this flow would be much greater until such steady state conditions were achieved. The analysis showed that sheet piles were not an appropriate solution for the site for groundwater influence alone.

4. DISCUSSION

4.1 Stage Construction

The modelling of the construction sequence was considered to be of critical importance to the design. "Wished in place" is where the structure is installed in a single stage with no intermediate calculation steps. The ground has no opportunity to deform during construction. Ground deformation is of great importance in geotechnical engineering as the strength of the

soil is mobilised at high strains, particularly compared to structures. The non-linear behaviour of soil is also not modelled correctly in "wished in place" models.

In comparing the results of the fully developed construction sequence model with a "wished in place" model it can be seen that certain results are very different. This is particularly the case for the loading on the floor and the roof. In the "wished in place" model the floor is in compression due to the load of the active earth pressures on the retained side of the secant piles and the greater hydrostatic pressures. In the construction model the floor is in tension for the long term condition. This is due to the timing of the placement of the floor. The out of balance hydrostatic pressures are at their greatest prior to the placing of the floor. When the floor is poured the water pressures recover underneath the tank which reduces the out of balance loading. The secant piles try to recover some of their bending but are restrained by the floor, thus creating a tension load.

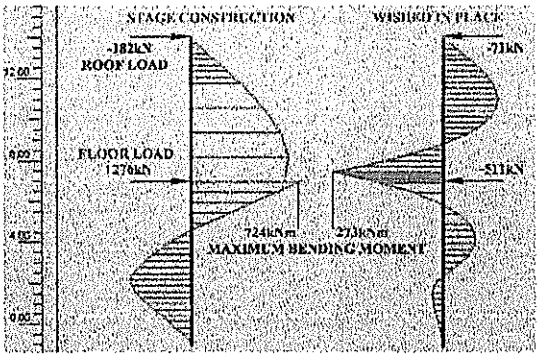

Figure 5 : Comparison of secant pile bending moments and roof and floor loads
(nb. positive load tensile, negative compressive)

Had the design been based on only the wished in place results then the structure may have been subject to problems particularly with cracking between the base and the secant piles. This would have been due to the lack of tensile resistance. Comparison with validating hand calculations should pick up the great difference with the bending moment results. Clearly if the secant piles had been designed to the much lower load then there would have been a considerable risk of a structural failure during construction.

5. CONCLUSIONS

The Wairau Storage Tank is a 6,500m^3 buried reinforced concrete structure required to store peak sewage flows to prevent overflow discharges. The site is located in the Wairau valley in the north of Auckland and is underlain by soft pumiceous alluvium deposits of varying thickness. These overlie the basement Waitemata series.

The soft alluvial deposits in combination with high groundwater will not allow more tradition methods of construction such as temporary battered slopes or sheet piling. Secant piling was preferred over diaphragm walling so as not to restrict local contractors.

The geotechnical design of the structure was assisted by Plaxis, a powerful finite element analysis package specifically design for geo-structural problems. The construction sequence was modelled and found to be of critical importance to the design. The design was changed to top down construction following the review of the overall scheme. The model was validate with a variety of parameter and modelling checks.

The design highlighted the importance of modelling stage construction compared to "wished-in-place" modelling. The non-linear behaviour of soils can result in unexpected results should the stage construction process not be followed.

The results of the geotechnical design have been incorporated into the structural design currently at tender.

6. REFERENCES

SEARLE, E.J., "City of Volcanoes, a geology of Auckland", 1981, Longman Paul

SINCLAIR KNIGHT MERZ LIMITED, "North Shore City Wastewater Network Major Improvement Project PS001 / ST001 Silverfield Geotechnical Investigation Report", September 2001, (not published)

PULLER, M., "Deep excavations : a practical manual", 1996, Thomas Telford

KERMODE, L., "Geology of the Auckland Urban Area, Geological Map 2, scale 1:50,000", 1992, Geological & Nuclear Sciences Limited

A Three-Dimensional Gravity Survey of the Pre-volcanic Topography in Epsom, Auckland

Dev K. Affleck: Pattle Delamore Partners Ltd, P O Box 6136, Wellington, New Zealand

Auckland is a major city built on an active volcanic field, which consists of scoria cones, lava fields, explosion craters and tuff rings. Some of these permeable volcanic deposits constitute a substantial aquifer system within the Auckland isthmus and overlie relatively impermeable Waitemata sediments.

A total of 157 gravity stations were established in the Epsom area on an approximate 200m grid with the objective of determining the thickness of the tuff and basalt overlying the Waitemata sediments. This information was then used to define the palaeotopography underneath the volcanic deposits, which play a controlling part in the complex and divergent groundwater flow regime in the area. The gravity model defined the catchment divide between the ancestral Waitemata and Manukau River systems, which cut deeply into the Waitemata sediments when the sea level was lower during the Pleistocene Ice Ages (100 000 years before present). This buried Waitemata ridge was found to have a northeast orientation through the study area, and an elevation of approximately 70m above sea level.

The gravity method was found to be an effective tool for delineating the extent of basaltic flows and tuffs in the Epsom area. Gravity modelling in this study shows that the palaeotopography is more complex than previously thought.

1 INTRODUCTION

Present-day subsurface drainage basins in the central Auckland area are mostly controlled by buried palaeotopographic ridges of Waitemata sediments. Ancestral valleys restricted the earliest flows, but later flows spread over many of the dividing ridges. The actual position of the ancient catchment divide is therefore significant in determining present day groundwater flows.

The current conceptual model of the pre-volcanic topography in the Epsom area has limitations when compared with physical data. This has implications for understanding the groundwater flow regime in the area. To better understand the shape of the pre-volcanic surface and groundwater flows, a gravity survey was undertaken. Gravity measurements established in the study area (Figure 1) have been used to determine the thickness of the volcanic deposits, which imply the shape of the pre-volcanic surface.

Gravity and magnetic methods have previously been used to successfully model the basalt volcanoes in Auckland and their associated deposits (Rout et al. 1993[1]; Hochstein and Lawton, 1974[2]).

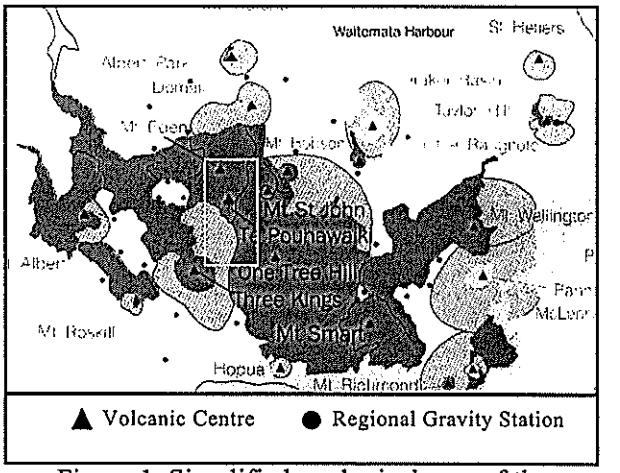

Figure 1. Simplified geological map of the Auckland isthmus (after Kermode, 1992)[3]. Study area shown as white rectangle.

2 GEOLOGICAL SETTING

The basement rock unit in the Auckland region is a thick sequence of Mesozoic greywacke. This is overlain by Miocene Waitemata sediments which consist of alternating sandstones and mudstones up to 1km thick (Ballance, 1974)[4].

The Auckland Volcanic Field comprises about 49 discrete basaltic volcanoes situated within a 20km radius of Auckland City. The volcanoes erupted through, and deposited volcanic materials on, the Waitemata sediments. This volcanic field is

believed to have been active for at least 140 000 years (Wood, 1991)[5] and in that time has produced approximately 4km^3 of eruptive material (Allen and Smith, 1994)[6]. The field is generally considered to be monogenetic, that is, each volcano formed from a single eruption or eruption sequence (Heming and Barnett, 1986)[7]. There is also recent evidence that suggests that more than one volcanic centre was active at the same time (Cassidy et al. 1999)[8].

There are two types of eruption style evident from the Auckland volcanoes. Activity ranges from magmatic (Hawaiian style) to phreatomagmatic (explosive reaction with groundwater), with the eruption style dependent on the water to magma ratio (Wohletz, 1983)[9]. The eruptive style can alternate between magmatic and phreatomagmatic for a particular vent (Cas and Wright, 1987)[10].

The Te Pouhawaiki volcano was a small scoria splatter cone located approximately 600m SSE of the Mt Eden Volcano. It was quarried away in the early part of the 20th century. Searle (1962)[11] referred to this volcano as 'Epsom Avenue'. Kermode (1975)[12] postulated that basalt flows located south of the scoria cone, may have been sourced from a volcano, now completely buried by the Mt Eden lava field.

3 HYDROGEOLOGY

The former Waitemata and Manukau River systems (Searle, 1981)[13] incised deeply into Waitemata sediments during the last Ice Age when sea levels were considerably lower than present day (Figure 2). The last Ice Age ended approximately 6000 years ago and lasted approximately 100 000 years. This created an ancestral catchment divide that passes through the centre of the Auckland isthmus (Figure 2). The exact location of this divide is difficult to determine as the entire area is covered in volcanic deposits. Originally, valleys carved out by the ancestral Waitemata and Manukau River systems would have controlled lava flows from nearby volcanoes. As the valleys filled with volcanic deposits, constraints on the flow directions would have reduced. However, it is considered that today's groundwater flows are still controlled by these pre-volcanic valleys.

Groundwater generally flows readily through the basalt, via rock defects (joints and caverns etc). These rock fracture systems allow rainwater to migrate to the base of the pre-existing valley systems and then be channelled to the sea. Some perching of water tables may occur in zones where individual flows overlap or where interbedded tuff may hinder otherwise relatively free vertical drainage.

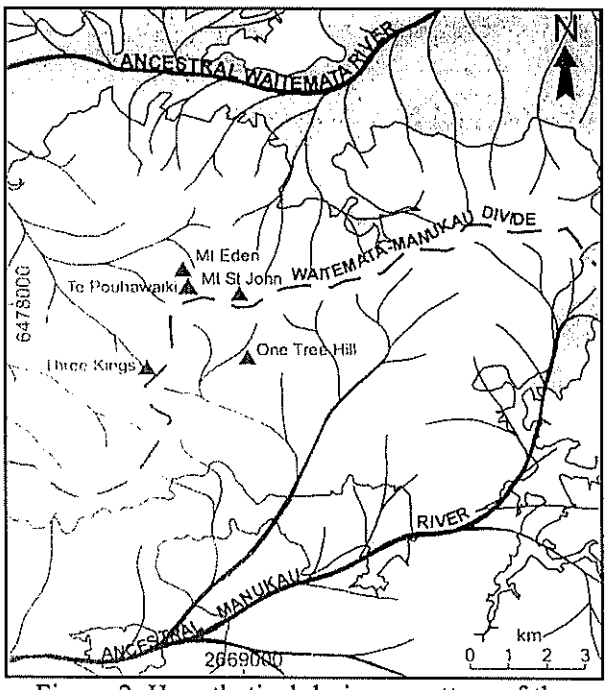

Figure 2. Hypothetical drainage pattern of the Auckland urban area during the Pleistocene superimposed upon the current Auckland coastline (After Kermode, in Searle, 1981)[13].

Existing groundwater data in the Epsom area suggests that drainage occurs within three catchments leading to the west, south and northeast (PDP, 1986)[14]. The stormwater in this catchment is landlocked and has no natural surface outflow. At present, all stormwater in the Epsom area is discharged via soakage systems to ground. In some areas, ground soakage has proven to be difficult because of the presence of tuff.

4 GRAVITY SURVEY

A gravity survey is a subsurface geological investigation that works on the basis that differences in densities of underlying rocks create variations in the Earth's gravitational field, or gravity anomalies.

4.1 Data acquisition and processing

A total of 136 gravity stations were established in the Epsom area on an approximate 200m grid as part of the original investigation (Affleck, 1999)[15]. The preliminary positions were established using a 1:10 000 map of Auckland. In addition, 25 widely spaced gravity stations were established in the surrounding area to define the regional gravity field on Waitemata sediments (Figure 1). A further 21 gravity stations were added in 2001 to cover the entire Epsom catchment. The latitude, longitude and elevation were determined at each

gravity station by using differential GPS. A typical accuracy of ±2cm in elevation was obtained using this method. Gravity data was tied-in to the New Zealand Primary Gravity Network (Reilly, 1972)[16] and corrected using the international gravity formula (1967) and a density of 2.2Mg.m^{-3} (the density of Waitemata sediments (Hochstein and Lawton, 1974[3]; Whiteford and Lumb, 1975[17])). Terrain corrections were calculated out to a radius of 22km from each gravity station using the method of Hammer (1939)[18] for the inner zones (<4.5km radius) and that of Lopez (1989)[19] for the outer zones.

Once the data have been corrected, a Bouguer anomaly map can be produced. (Figure 3). The Bouguer gravity anomaly is dominated by a strong northeast-southwest regional gradient (field), approximately 25μN.kg^{-1}.km^{-1}. This regional field is probably caused by the increasing thickness of Waitemata sediments from the northeast to southwest. Superimposed upon this are a number of smaller variations associated with the volcanic centres.

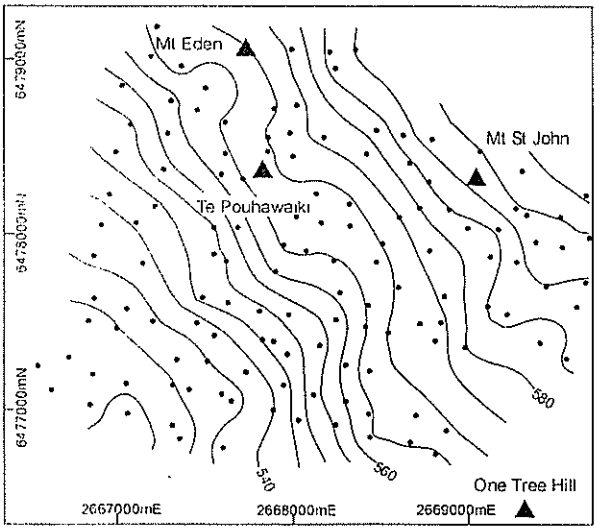

Figure 3. Bouguer gravity anomaly map with a contour internal of 5μN.kg^{-1}. Gravity station locations are shown by dots, volcanoes are shown by triangles (Affleck et al, 2001)[20].

To obtain the residual gravity anomaly (the gravity effect of the structure of interest) the effects of the regional field must first be removed from the Bouguer anomaly map.

The regional field is defined as the combination of all gravity effects in the study area, other than the structure of interest. To determine the regional field, a polynomial surface was fitted to the 25 gravity measurements collected on Waitemata sediments. In this case, a third order polynomial surface was determined to provide the best fit, using the method described by Zeng (1989)[21].

Removal of the regional field produces the residual gravity anomaly shown in Figure 4. The presumed Waitemata ridge is located in the southwest of the study area and extends in a northeast direction toward Mt St John. The top of the ridge is represented by small negative anomalies as it is covered by a thin layer of tuff. The southeast of the study area shows a complex gravity high (up to 15μN.kg^{-1}) indicating thickening lava flows which is consistent with the deepening of the Waitemata surface south of the ancient divide.

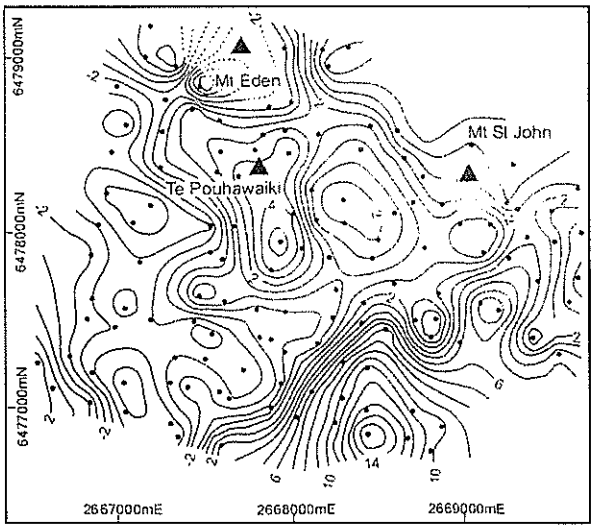

Figure 4. Residual gravity anomaly map (Affleck et al, 2001)[20] derived from Figure 3 by subtraction of the regional field. Symbols are as in Figure 3.

4.2 Gravity modelling

One of the limitations of gravity surveys is that a number of models may fit a measured gravity anomaly. This problem mainly arises when tuff and basalt overlie each other, as they have negative positive density contrasts respectively. A thick layer of tuff overlying a thin layer of basalt would produce the same gravity effect as a model where the tuff were thinner and the basalt non existent. This problem can only be resolved using control data such as borehole logs.

The gravity model was constrained, or calibrated, by information from more than 200 boreholes and other geophysical information (Affleck 1999)[15] in the Epsom area (Figure 5). Borehole data provide control on the depths and thicknesses of the subsurface volcanic deposits. However, most of the boreholes in the study area do not penetrate the full thickness of the volcanics. This limits use of the information to constraining the thickness of the upper layers and to providing an indication of the minimum thickness of the lower lithologic units.

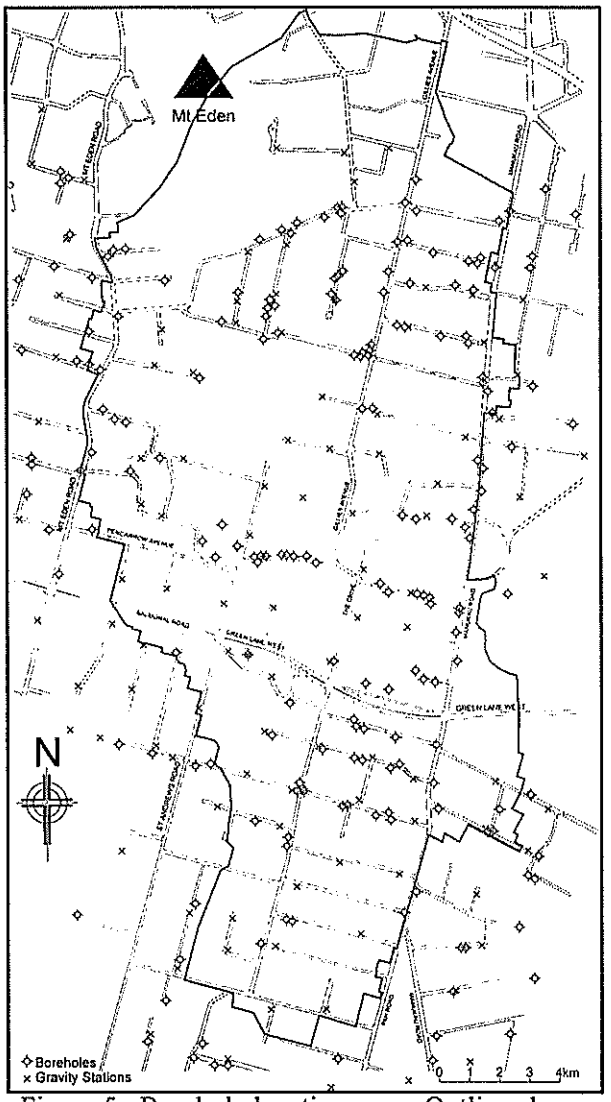

Figure 5. Borehole location map. Outline shows extent of Epsom surface water catchment.

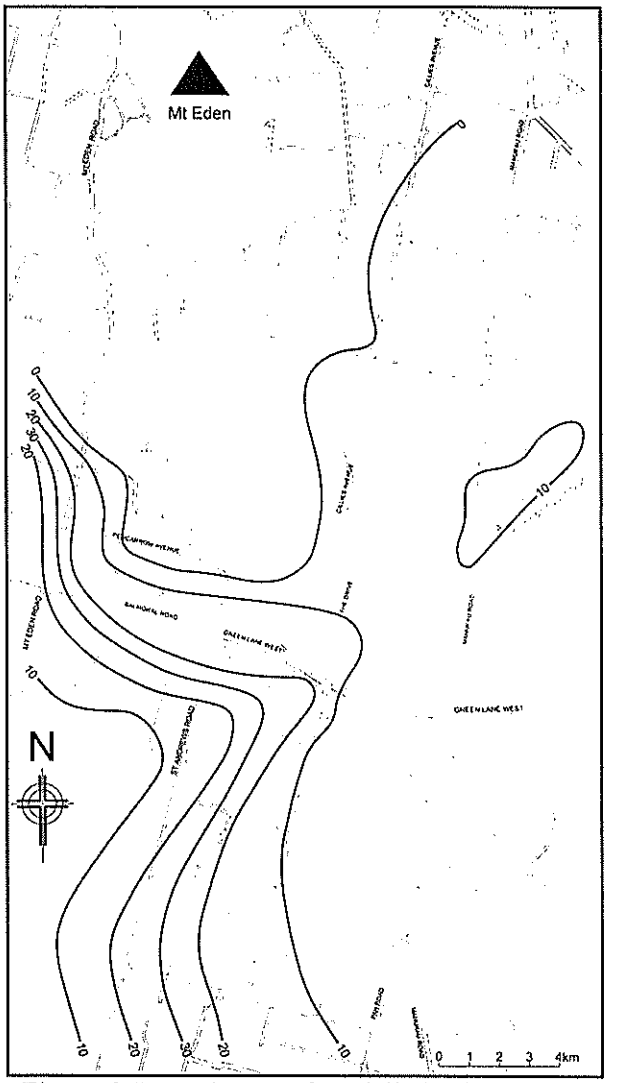

Figure 6: Isopach map of modelled tuff (contour interval 10m)

Borehole information shows that the study area generally consists of layers of tuff overlying basalt lava flows with some areas having no underlying basalt. Each of three main layers was individually modelled using the method developed by Soengokono (1990)[22] which was based on an algorithm developed by Barnett (1976)[23]. The gravity effect of each layer modelled was then calculated and the resulting gravity effects were added together to produce a residual gravity anomaly. The modelled layers comprised, a layer of tuff overlying basalt, a layer of basalt and a layer of tuff overlying Waitemata sediments.. This calculated residual anomaly was then compared with the observed residual anomaly. The root mean square discrepancy between the optimum model and the observed gravity data is $1.2\mu N.kg^{-1}$.

5 GEOLOGICAL INTERPRETATION

Figure 6 shows the variation in the thickness of tuff in the study area derived from the gravity assessment. A thick sequence of tuff overlies Waitemata sediments in the southwest of the study area. This tuff is considered to be derived from the Three Kings and Te Pouhawaiki volcanoes. The tuff thins to the east where it mantles the One Tree Hill basalt. Boreholes that reach the Waitemata sediments in the eastern side of the study area indicate that tuff does not occur in this segment.

The basalt isopach (Figure 7) plan derived from the gravity assessment shows a considerable thickness of basalt (up to 60m thick) in the southeast, thinning to less than 10m in the central and southwestern part of the study area. Basalt has been modelled to a thickness greater than 70m to the north, surrounding the southern side of the Mt Eden Volcano.

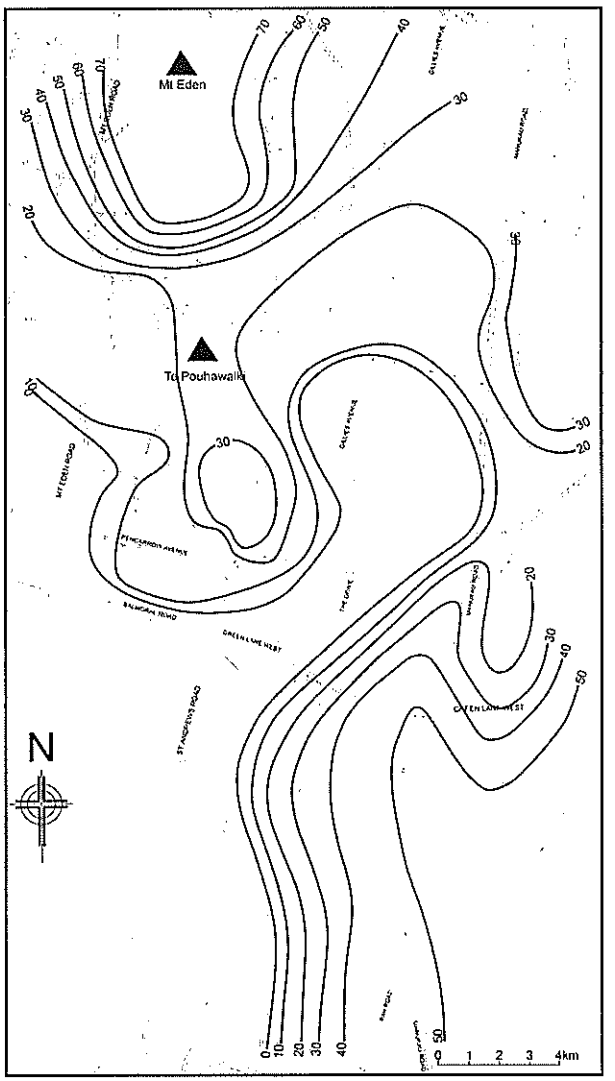

Figure 7: Basalt Isopach Map. The interpreted Te Pouhawaiki Volcano is located in the centre of the figure and the triangle shows the location of the now quarried away scoria cone (contour interval 10m).

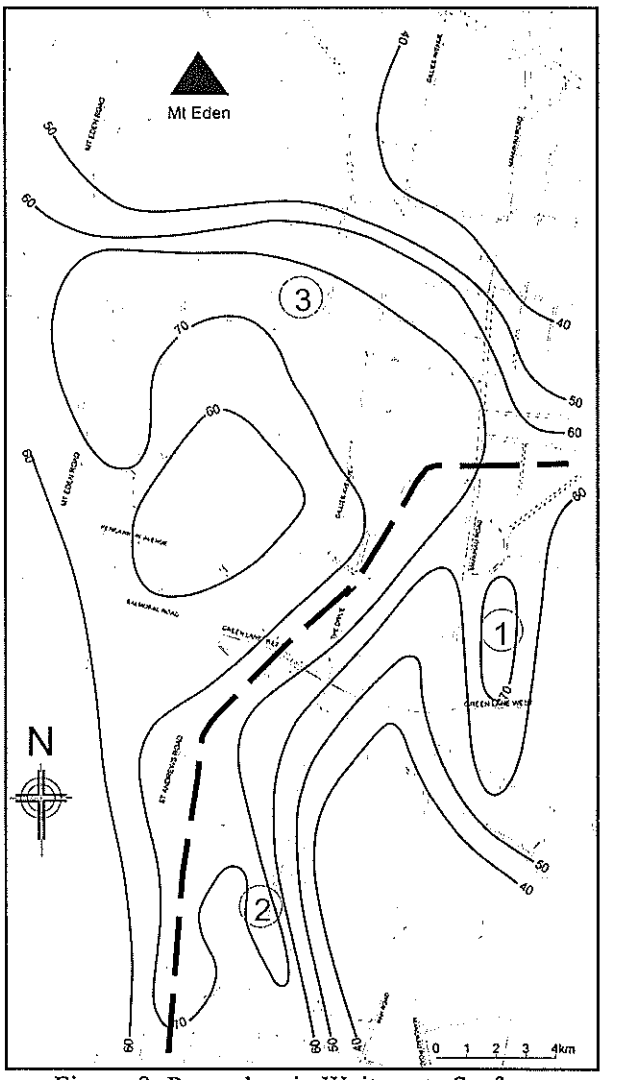

Figure 8: Pre-volcanic Waitemata Surface. Elevations are in metres above present sea level. The main ridge is represented by the dotted line (contour interval 10m). Refer to text for explanation of numbers.

The positive residual anomaly south of the Te Pouhawaiki scoria cone (Figure 8) is modelled as an approximately saucer shaped subsurface body of dense basalt (2.6Mg.m^{-3}), with a diameter of 550m at the surface reducing to 145m at 50m depth. This modelled subsurface body is interpreted as basalt that has filled an explosion crater generated by the interaction of rising magma with groundwater at depth within the Waitemata Group.

The model of the Waitemata surface (Figure 8) shows the Waitemata ridge to be elevated approximately 70m above sea level and have a northeast orientation from the south of the study area toward Mt St John. Smaller north-south trending ridges exist beneath Alexandra Park ① and in the south of the study area ②. Another ridge splits off the main divide in a northwesterly direction ③ toward the base of Mt Eden.

6 CONCLUSIONS

A buried Waitemata ridge was previously known to exist in the Epsom area (Searle, 1981)[10] but its exact location was not well defined. Gravity measurements across the area have provided details of the pre-volcanic Waitemata surface and have defined the ancestral surface water catchment divide as having a north-northeast orientation from the south of the study area toward the Mt St John volcano.

The centre of the complex ridge system is topographically lower and modelling shows it to contain a dense basalt plug from the Te Pouhawaiki volcano. This subsurface basalt

filled depression is almost completely surrounded by Waitemata ridges which implies a locally convergent groundwater flow regime. A thin layer (10-15m thick) of tuff mantles the ridge system around this volcano. Gravity modelling suggests that this volcano is considerably larger than previously thought.

6 ACKNOWLEDGEMENTS

I would like to thank Neil Crampton for his helpful comments, Dianne Rossiter for drawing the figures and Richard Lucy for his assistance in preparing this manuscript.

7 REFERENCES

1. ROUT, D. J.; CASSIDY. J.; LOCKE, C. A.; SMITH, I. E. M. 1993: Geophysical evidence for temporal and structural relationships within the monogenetic basalt volcanoes of the Auckland volcanic field. Journal of Volcanology and Geothermal Research 57: 71-83

2. HOCHSTEIN, M. P.; LAWTON, D.C. 1974: Geophysical measurements over basalt flows in Auckland City. Paper 7(B), Proceedings NELCON 1974, Auckland

3. KERMODE, L.O. 1992: Geology of the Auckland urban area. Scale 1:50 000. Institute of Geological & Nuclear Sciences geological map 2. 1 sheet + 63 p. Lower Hutt, Institute of Geological & Nuclear Sciences.

4. BALLANCE, P.F. 1974: An Inter arc Flysch Basin. Journal of Geology 82: 439-471

5. WOOD, I. 1991: Thermoluminescence dating of the Auckland and Kerikeri basalt fields. Unpublished MSc thesis, lodged in the library, The University of Auckland, Auckland, New Zealand.

6. ALLEN, S. R.; SMITH, I. E. M. 1994: Eruption styles and volcanic hazard in the Auckland Volcanic Field, New Zealand. Geoscience Reports of Shizuoka University 20: 5-14

7. HEMING, R.F.; BARNET, P.R. 1986: The Petrology and Petrochemistry of the Auckland Volcanic Field. In: Smith, I.E.M. (Ed.) Late Cenozoic Volcanism in New Zealand. The Royal Society of New Zealand Bulletin 23: 64-75

8. CASSIDY, J.; LOCKE, C.A.; MILLER, C.A.; ROUT, D.J. 1999: The Auckland Volcanic Field – geophysical evidence for its eruption history. In: Firth, C.R.; McGuire, W.J. (Ed.) Volcanoes in the Quaternary. Geological Society, London, Special Publication 161: 1-10

9. WOHLETZ, K. H. 1983: Mechanisms of hydrovolcanic pyroclast formation: grain size scanning electron microscopy, and experimental studies. Journal of Volcanology and Geothermal Research, 17: 31-63

10. CAS, R. A. F.; WRIGHT, J. V. 1987. Volcanic Successions, Modern and Ancient. Chapman and Hall.

11. SEARLE, E. J. 1962: The volcanoes of Auckland City. New Zealand Journal of Geology and Geophysics 5: 193-227

12. KERMODE, L. O. 1975: Urban geology of Mt Eden Borough, New Zealand. New Zealand Geological Survey unpublished report G17.

13. SEARLE, E.J. 1981. City of Volcanoes: a geology of Auckland (2nd Edition). Auckland, Longman Paul, 195p.

14. PATTLE DELAMORE PARTNERS LTD (PDP LTD) 1986: Eden-Epsom Soakage Studies. Unpublished report for the Auckland City Council.

15. AFFLECK, D.K. 1999: A geophysical delineation of basaltic flows and tuffs in the central Auckland isthmus. Unpublished MSc thesis, lodged in the Library, The University of Auckland, Auckland, New Zealand.

16. REILLY, W.I. 1972: New Zealand gravity map series. New Zealand Journal of Geology and Geophysics 15: 3-15

17. WHITEFORD, P. C.; LUMB, J. T. 1975: A catalogue of physical properties of rocks. DSIR Research Division Reports 106 and 107.

18. HAMMER, S. 1939: Terrain corrections for gravimeter stations. Geophysics 47: 184-194

19. LOPEZ, H. R. B. 1989: Fortran program for automatic terrain corrections of gravity measurements. Computers and Geosciences 16(2): 237-244

20. AFFLECK, D.K.; CASSIDY, J.; LOCKE, C.A. 2001: Te Pouhawaiki Volcano and pre-volcanic topography in central Auckland: volcanological and hydrogeological implications. New Zealand Journal of Geology and Geophysics 44: 313-321

21. ZENG, H. 1989: Estimation of the degree of polynomial fitted to gravity anomalies and its application. Geophysical Prospecting 37: 959-973

22. SOENGOKONO, S. 1990: Geophysical Study of the Western Taupo Volcanic Zone. Unpublished PhD thesis, lodged in the library, The University of Auckland, Auckland, New Zealand.

23. BARNETT, C.T. 1976. Theoretical modelling of the magnetic and gravitational fields of an arbitrarily shaped three-dimensional body. Geophysics 41 (6): 1353-1364

Determination of the Structural Number of Pavements on Volcanic Subgrades

Rosslyn Bailey, GIPENZ, GMICE

Pavements constructed on volcanic soils behave differently to non-volcanic soils and have higher deflections when dynamically loaded. Past relationships between CBR and modulus therefore may not be applicable. Fast non-destructive methods currently being used rely on these relationships and therefore relationship(s) between the CBR and modulus need to be obtained for volcanic soils. The project investigated the various volcanic soils within the North Island and their behaviour. In-situ testing of the volcanic subgrades was conducted using the Falling Weight Deflectonmeter (FWD) test and in-situ CBR together with other standard tests. From the in-situ testing three correlations were identified for volcanic soils, however the third was not well defined. The volcanic soil types represented by the correlations were, clayey, pumiceous and silty/brown ash. To enable the Structural Number of pavements on volcanic soils to be determined, factors were presented, based on the identified relationships and the procedure for determining the Structural Number of pavement from the FWD modulus suggested. Also included were factors that allowed the volcanic relationships to be used in AUSTROADS Pavement Design Guide.

1 INTRODUCTION

Volcanic ash showers have coated large areas of the North Island of New Zealand during the last 100,000years, (1). Past experience has shown that Pavements constructed on volcanic subgrades typically have higher deflections under load than similarly performing pavements constructed on other subgrades. This has created a difficulty in determining the structural strength of these types of pavements based on their deflection response when determined by instruments such as the Falling Weight Deflectonmeter (FWD). The FWD is being used to obtain a measure of the pavement strength for use in pavement deterioration modelling as this is a rapid relatively inexpensive method suitable for network surveys. The anomalous behaviour of volcanic subgrades means the standard methods used for assigning strength based on FWD readings cannot be used.

The concept of describing the strength of a pavement in terms of one number, called the Structural Number (SN), was developed from the AASHO road test published in 1962. The Modified Structural Number (SNC) was developed to incorporate the contribution to the strength from the subgrade. The original definition of the SNC was based on the determination of the California Bearing Ratio (CBR) of the various pavement layers including the subgrade. The CBR test gives an indication of the shear strength of a material. Each pavement layer is then given a weighting based on its strength and thickness. The summation of these factors for each layer and the subgrade gives the SNC. The method for calculating the input into the Modified Structural Number equation can be carried out either directly (CBR) or non-directly, using non-destructive methods.

The in-situ determination of the CBR requires the digging of test pits and thus it is an expensive exercise. In order to obtain a faster and cheaper method the FWD has been used to calculate the modulus of the pavement layers and subgrade and then use a standard relationship between modulus and CBR to assign a strength factor to each layer. The FWD technique therefore relies on the relationship between CBR and modulus.

Research carried out at Central Laboratories, backed by Transfund, Bailey and Patrick (2), developed correlations between the modulus and the shear strength of volcanic soils and how the relationships, should be applied to enable the structural number to be obtained for deterioration modelling and how the findings can be used in pavement design.

2 SOME BACKGROUND ON THE BEHAVIOUR OF VOLCANIC SOILS

2.1 Principle Soil-Forming Centres

The principle centres of soil-forming ash showers in New Zealand are Mt. Egmont, Mt. Ruapehu, Mt. Ngauruhoe, Mt. Tongariro, Mt. Tarawera, and craters near Taupo, Rotorua, and the Bay of Plenty.

Two broad types of ash beds are recognised (3):

1) Intermittent type, in which materials are ejected on numerous occasions over a period of years. The materials are generally andesitic or basaltic and gradually build up a cone around the vent.
2) Paroxysmal type, in which materials are belched out in sudden explosions at long intervals. These materials are generally rhyolitic and are ejected from craters or rifts.

Most volcanic soils are best described as silty clays or clayey silts, despite the fact that they plot well below the Casagrande A-line on the Placticity chart (i.e. are clearly in the silt zone).

Some volcanic ashes have been named to collectively describe the Andesitic tephras which were deposited during the Taranaki eruptions, e.g. Taranaki Brown Ash. Taranaki Brown Ash frequently occurs in thick weak to strongly weathered beds. This weathering process produces a succession of 'clay minerals' with initially allophane being formed, which in time (say 20,000 years) changes to halloysites and finally kaolin. Other groups include the Hamilton ashes and the Taupo pumice. The ashes are given their name from either the locality of the vent or the locality of where the ash is extensively exposed at the surface.

2.2 Engineering Properties of some of the volcanic soils

It has been found from previous studies ((4), (5), (6), (7), (8), (9), (10), (11), (12), (13)) that volcanic soils engineering properties are wide ranging. Some volcanic soils, for example, the brown ashes, tend to be sensitive to remoulding and some volcanic soils can also physically change their properties when remoulded and/or dried; the soil alters its particle size distribution (psd).

It has been reported that the clay mineral 'allophane' and to a lesser extent halloysite are in a large part responsible for the unusual psd changing properties. Allophane contributes to the greasy feel of the soil. The change in the psd occurs due to the effect of the water being expelled from the molecular particle structure by bond-breakdown analogous to the way ice becomes water. The gel-like structure of the clay minerals collapse and form aggregations, which in turn makes the soils 'grity'. These new aggregates are reported to have a relatively high stability.

The sensitivity to remoulding of these soils may be due to the oxidation of iron in the ash. Iron oxide has been reported to form a 'structure' between the particles, which is broken-down when remoulded.

Most undisturbed volcanic soils tend to have high bearing capacities; high pre-consolidation pressures have been measured on undisturbed volcanic ash, accompanied by irregular variations with depth. As no geological evidence as to why these soils have a high over-consolidation ratio it is thought that it is due to the oxidation of iron, as suggested above, forming a type of structure within the soil matrix. Once this pre-consolidation pressure is reached the soils rapidly lose strength and are highly compressible, i.e. the structure has broken-down.

The apparent pre-consolidation pressures can vary markedly. It was reported by Miller (7) that a brown ash material (grey in its reduced state) effectively exhibited no pre-consolidation and was recovered from within a local poorly drained area. Jacquet (5) reported that the pre-consolidation pressure was directly proportional to the shear strength. The strength characteristics of the ash were also reported to vary depending on the degree of weathering, oxidation (drainage conditions) and saturation, (7). Therefore an oxidised ash, with the iron structural matrix developed may be stronger up to the pre-consolidation pressure than an ash in its reduced state.

Pumice soils however tend to be less sensitive to remoulding. This may be due to the kind of deposition and then cementation of the pumice grains. Some pumice soils still exhibit fairly high sensitivities, possibly due to larger amounts of iron present in some areas. Pumice soils also tend to be sandy and contain smaller amounts of the Allophane clay mineral and therefore, after remoulding, any change within the Allophane will be small and less likely to change the overall particle size distribution, compared to such soils as clays.

In general, volcanic materials have been reported as having; a high particle density, due to the presence of heavy minerals; a low dry density due to the high volume of voids, these voids have been found to be discrete internal voids within the particles themselves; the particle shapes are angular, together with the rough microtexure which causes a high shear strength/friction angle; the soils also usually exhibit some cohesion. The natural moisture content of many of the soils, especially the brown ash soils, tends to be high, and in some case have been higher then the Liquid Limit. The Liquid Limit of the soils is also high compared to non-volcanic soils.

Care has to be taken in the interpretation of laboratory test results as it has been found in NZ ashes that four different moisture/density relationships can be obtained, depending on whether a wet or dry soil is the starting point, and whether the same soil is used throughout or a fresh sample is taken for each compaction (5). The clay mineral Allophane may be responsible for these relationships. However for pumice soils their particle size distribution may change under compaction activities due to their soft (low crushing resistance) character and the presence of Allophane.

3 SITE SELECTION AND TESTING

During the review of the existing data, it was found that the test results were wide ranging with overlapping of results making the defining of the volcanic soils difficult. In general a broad grouping of the pumice soils/sands and the brown ashes could be considered reasonable due to their difference in behaviour and engineering properties as discussed above.

Broad groupings of the volcanic soils were chosen so that the selection of the test sites can be conducted simpler. The groupings were; Hamilton ashes, Taranaki ash and Taupo pumice.

Sites were selected so that together with the existing data the results would enable a wide spread of sites within the broad groupings to be obtained and that the testing was not duplicated.

A detailed site inspection ensured that the sites were not located on fill and were representative of the surrounding area. Fifteen sites in total were selected and are detailed below in Table 1 and shown in Figure 1.

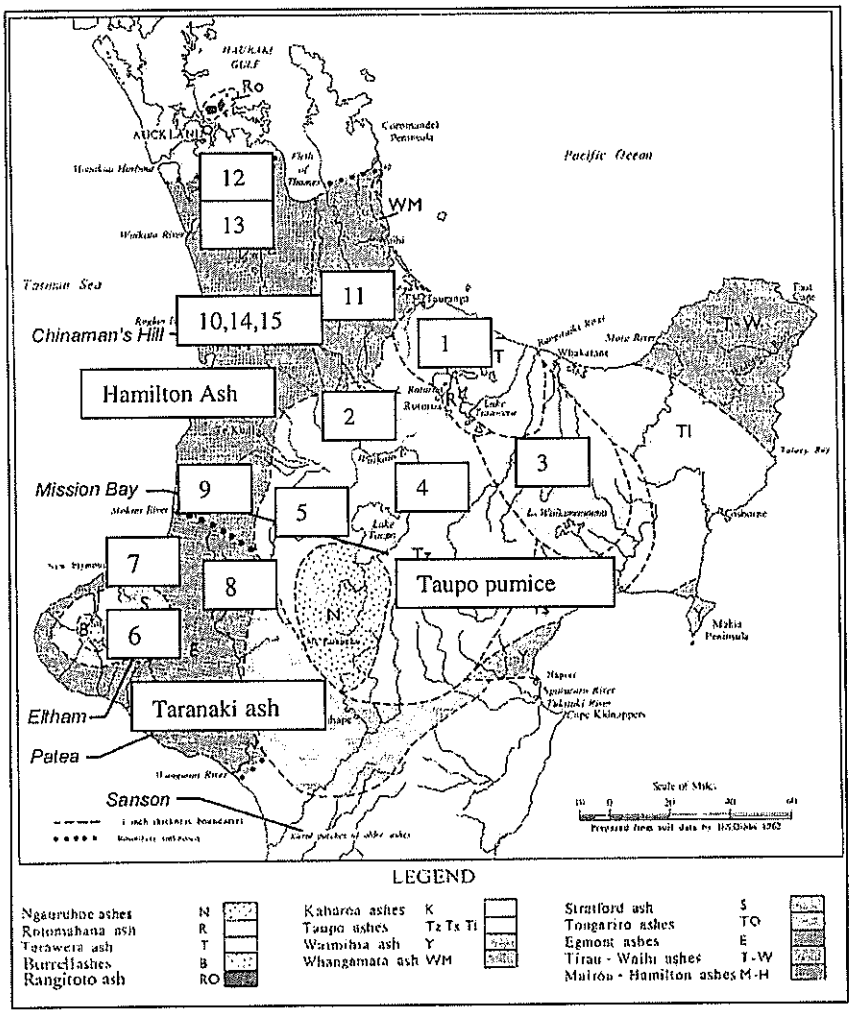

Figure 1 Location of the test sites in volcanic soils (extracted from (1))

Site	Location	Soil Grouping
Site 1.	Okere Falls, Okere Road	Pumiceous
Site 2.	Lichfield, Vospers Road	Pumiceous
Site 3.	Murupara, Golf Road	Pumiceous
Site 4.	Waiotapu, Jay Road	Pumiceous
Site 5.	Bennydale, SH30	Pumiceous
Site 6.	Stratford-Inglewood, Tariki Road	Brown ash
Site 7.	Waitara-Urenui, Upper Epiha Road	Brown ash
Site 8.	Whangamomona, SH43	Brown soil
Site 9.	Pio Pio, Mairoa Road	Hamilton ash (south)
Site 10.	Hamilton-Cambridge, Day Road	Hamilton ash
Site 11.	Te Poi, Stopfords Road	Hamilton ash (east)/pumice
Site 12.	Pukekohe, Coles Road	granular material
Site 13.	Taupiri, Jew Road	Hamilton ash (north, granular)
Site 14.	Te Awamuta, Bowman Road	Non-volcanic
Site 15.	Cambridge, Peake Road	Non-volcanic

Table 1 Sites selected for testing

3.1 Testing

Testing at each site involved; logging two test pits, in-situ CBR tests, dynamic cone penetrometer testing and classification tests. The Allophane content was also determined. FWD testing at the sites was conducted to make an approximation of the pavement layers moduli.

4 RESULTS AND ANALYSIS

The results from the on-site and laboratory testing, and the FWD were analysed and relationships between the CBR and the FWD derived modulus determined for volcanic soils.

4.1 Results

Laboratory Testing

Results from the Allophane testing showed variable amounts of the clay mineral Allophane throughout the sites tested. In general the highest concentrations were found to be located south of Hamilton. Medium levels were obtained near Tauranga and Taranaki. The soils near Taranaki and Tauranga have been historically (5) sensitive to remoulding and able to change their psd, initially reported to be due to the Allophane mineral present however from the testing this may not be the

only reason. As suggested in section 2, the sensitivity may also be due to the break-down of the soil matrix due to the oxidation of iron within the soil.

The detailed test results are included in the Transfund report, Bailey and Patrick (2).

FWD Testing

Transfund report No. 117, (14) describes the procedure for the detailed structural analysis of the pavement from the shape of the deflection bowl. Basically, the outer deflections define the stiffness of the subgrade while the bowl shape close to the loading plate allows analysis of the stiffness of the near-surface layers. A broad bowl with little curvature indicates that the upper layers of the pavement are stiff in relation to the subgrade. A bowl with the same maximum deflection but high curvature around the loading plate indicates that the upper layers are weak in relation to the subgrade.

A back-analysis procedure is generally adopted to find moduli from an observed deflection bowl. Once the pavement profile model is established, a forward-analysis can be carried out to determine the strains for say, a modelled rehabilitation treatment such as overlay.

The back-analysis was conducted using ELMOND (Evaluation of Layer Moduli and Overlay Design) (15).

4.2 FWD Modulus CBR Relationship

It has been documented, (14) that the modulus, CBR relationship may vary by a factor of two. Austroads pavement design for granular roads have suggested using 10 times the CBR for all soils to obtain the vertical anisotropic modulus, and 6.7 times the CBR value for isotropic modulus. The Modified Structural Number is also calculated from the CBR value.

The relationship, ten times the CBR, and thus the pavement design, may be correct for tested CBR values, however the determination of the CBR from the measured in-situ modulus may not be correct, especially for volcanic soils due to their different behaviour as discussed previously.

The results from the in-situ testing and the data from previous studies are shown below in Figure 3.

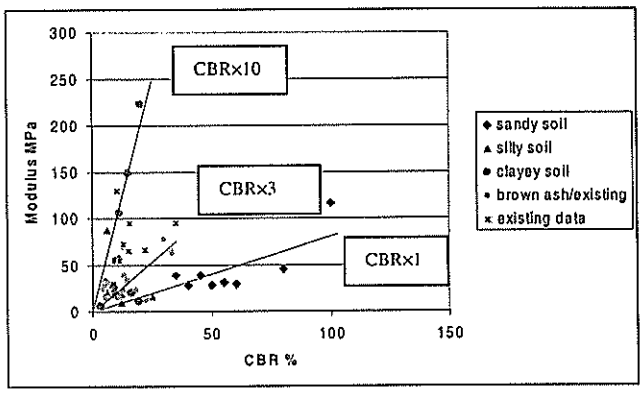

Figure 3 Graph of Isotropic Modulus versus CBR for current data and previous data.

Both the FWD subgrade modulus and in-situ CBR of the subgrade have been plotted. It is apparent that two relationships can be seen, with a possible third in-between.

It was found that, in general, the sandy pumiceous soils lay near the bottom of the graph, with the clayey volcanic materials forming the steeper relationship. A linear regression was carried out and the following correlations found, CBR×10, R^2=0.8307 and CBR×1, R^2=0.7024. The R^2 for the correlation's are reasonable for a network study,

From the graph, the following relationships were drawn:

A: Typically pumice/sandy soils,

Isotropic Modulus = 1× CBR Eqn 1

B: Mixture of Silty soils and Brown ash,

Isotropic Modulus = 3× CBR (However relationship not well defined) Eqn 2

C: Typically includes clayey ash soils,

Isotropic Modulus = 10× CBR Eqn 3

These relationships are very different from each other and may account for the reason for the many discrepancies occur in the testing of volcanic soils.

The Transfund report 128 (9) also recommended a relationship of 3×CBR for brown ashes. A possible reason why this relationship may not be well defined is that when the clayey materials, containing the Allophane mineral, when remoulded they tend to alter their particle size distribution into more like a silt and therefore may lie below the 10×CBR, and therefore obscures the third relationship.

The possible explanation for relationships in Fig 3, may lie in the structure and grain shape of the volcanic soils. Pumice soils tend to be sandy and have sharp angular grains which would indicate and high CBR value however due to their structure, under the FWD loading, the pumice soils exhibit a high elastic deformation and therefore low modulus when back-analysis of the FWD results are carried out. This type of behaviour can be seen in Fig. 3. The clayey soils on the other hand are finer grained and usually exhibit higher water contents, which may lead to lower CBR values and higher modulus values when dynamically loaded by the FWD, this relationship can also be seen in Fig 3. Consequently silty soils tend to lie in-between the two relationships due to them being neither clays or sandy, as would be expected. The brown ash is slightly different in that is shows a low modulus and a low CBR value. This maybe due to the Allophane content, as discussed above and, also, to the in-situ structure of the soils, as pumice, but also the fined grained nature of the soil producing a low CBR. The degree of saturation, an unknown variable in the in-situ CBR test, may affect the results slightly.

The above correlations are not dissimilar to the groups used to select the various site locations for testing, section 3. The pumiceous were mainly sandy soils, and the Hamilton ashes mostly clayey soils. The Taranaki soils however, which were also classified in the test pits as clayey, lay closer to the middle correlation

together with the silty soils. Again, this may be due to the behaviour of Allophane, as suggested above.
The relationships were then used to determine factors for the determination of the CBR from the FWD modulus so that the structural number for pavements could be obtained and also the determination of the vertical modulus from the CBR for use in Austroads pavement design.

5 USING THE RESULTS IN PREDICTION MODELLING & PAVEMENT DESIGN

5.1 Pavement Prediction Modelling Using The SNC

The modified structural number is an indication of the pavement strength and has been adopted in a number of empirically based pavement design and deterioration models of organisations such as AASHTO (16), the Transport and Road Research Laboratory (17) and the World Bank (18).
Structural Numbers can be determined using direct or indirect methods. To determine the SNC using non-destructive methods an indication of the relationship between CBR and modulus needs to be known.
The FWD calculated modulus of the basecourse and subsequent layers can be inputted directly into the structural number equation (Eqn. 4) however the subgrade contribution to the strength of the pavement cannot, as it is based on CBR. Therefore the calculated modulus requires to be converted into CBR value. As discussed above the relationship for volcanic soils is indicated to be different to the standard Modulus=10×CBR usually used for soils. Factors presented below allow the structural number to be determined for volcanic subgrades, based on the relationships indicated in section 4.
The structural number, including the additional variable for subgrade strength, is defined as follows:

$$SNC = (1/25.4)\sum_{i=1}^{n} a_i h_i + SN_{sg} \qquad \text{Eqn 4}$$

where a_i = layer coefficient
h_i = thickness of layer, mm
SN_{sg} = structural number contribution from the subgrade

$$a_i = a_g(E_i/E_g)^{1/3} \qquad \text{Eqn 5}$$

where a_g = layer coefficient of standard materials (AASHTO)
E_i = layer modulus (in this case, from FWD)
E_g = modulus of standard materials (AASHTO)

$$SN_{sg} = -0.85 (\log CBR)^2 + 3.51 (\log CBR) - 1.43 \qquad \text{Eqn 6}$$

Patrick and Dongal (19) also state that care must also be taken when determining the Structural Number on Volcanic subgrades, in that due to the 'bouncy' nature of the soils cracking may be an issue. Patrick and Dongal suggest that a second SNP (SNC for thin pavements) should be derived which may give a better prediction of cracking.

Factors which the isotropic modulus should be divided by to obtain CBR for determination of SNC
From the FWD, in-situ CBR relationship, summarised in section 3, the table below gives a factor which the FWD isotropic modulus should be *divided* by to obtain a value for CBR which can then be inputted into eqn 6.

Volcanic Soil Type	A (pumice)	B (mixture Silty)	C (Clayey)
Factor	1	≅3	10

Table 2 Factor for the determination of CBR for SNC calculations

These factors should only be used for the determination of the SNC, as the isotropic modulus is used.

5.2 Determination Of The Anisotropic And Isotropic Modulus For Input Into Austroads Pavement Design

The AUSTROADS approach to the design of roads uses modulus as the input for calculating the strain in the different pavement layers and assumes a fatigue relationship between subgrade strain and failure.
For the Austroads pavement design on granular pavements; traditionally the anisotropic vertical modulus is calculated from 10×CBR. The isotropic modulus is calculated from 6.7×CBR. If these relationships were used for pavement design on volcanic subgrades, due to the 'bouncy' nature of volcanic soils, a low FWD modulus would result in a low CBR that could lead to the road being over designed. For volcanic soils the following is recommended that the factor in Table 2, be *multiplied* by the CBR to obtain the vertical modulus and isotopic modulus respectively, which can then be inputted into Austroads pavement design.

Volcanic Soil Type	A (pumice)	B (mixture Silty)	C (Clayey)
Factor Vertical Modulus	1.5	≅4.5	15
Factor for Isotropic Modulus	1	≅3	10

Table 3 Factor to be applied to the CBR to determine the Vertical/Isotropic Modulus for input into Austroads pavement design.

Examples, using the above factors to calculate the Structural Number of pavements and in pavement design, are presented in the Transfund report (2).
Another approach would be to develop specific strain fatigue relationships for the different soil types.

6 CONCLUSIONS

The different behaviour of volcanic soils to non-volcanic soils depends largely on the minerals present within the soil.
The engineering properties of volcanic soils are variable due to their amount of weathering, minerals and remoulding. A classification of volcanic soils based on their geological description was presented and

15 sites were selected based on the location of past work. Testing at each site included two test pits with measurements of scala and in-situ CBR. FWD testing was also carried out.

The subgrade modulus, obtained from the FWD tests (via ELMOD), was plotted on a graph with in-situ CBR.

The following relationships were obtained for volcanic soils.

A: Typically pumice/sandy soils, Isotropic Modulus = 1× CBR

B: Mixture of Silty soils and Brown ashes, Isotropic Modulus = 3× CBR (However relationship not well defined)

C: Typically includes clayey ash soils, Isotropic Modulus = 10× CBR

To allow the above relationships to be used in pavement deterioration modelling and pavement design. Factors were presented which related the modulus to CBR for structural number modelling, and CBR to vertical modulus for pavement design, Table 2 and 3.

7 REFERENCES

1. GIBBS, H. S. "Volcanic-ash soils in New Zealand" ,1968. NZ Dept. of Scientific and Industrial Research, Information Series No.65.
2. BAILEY, R. and PATRICK, J.E. "Determination of the structural number of pavements on volcanic subgrades",2001. Transfund New Zealand Research Report 213. 95pp.
3. TAYLOR, N.H. "Soil processes in volcanic ash beds". 1933. NZ Jl. Sci. Technol. 14: 193-202.
4. FULLARTON, "Taranaki Brown Ash as an engineering material".1978. Central Laboratories, Rep. 2-78/2.
5. JACQUET, D. "Bibliography on the physical and engineering properties of volcanic soils in NZ".1987. NZ Soil Bureau Bibliographic, Report 33.
6. JACQUET, D. "Physical and Engineering properties of some volcanic ash materials in NZ".1988. NZ Soil Bureau Report EP28.
7. MILLER, P.J. "The use of Taranaki Brown Ash for Construction Fill". (undated). Central Laboratories Report
8. PARTON, I.M. and OLSEN, A.J. "Compaction properties of Bay of Plenty Volcanic soils". 1980. NZ. 3rd Australia-NZ Conference on Geomechanics, Wellington, Vol. 1.
9. SUTHERLAND, A., DONGAOL, D.M.S., PATRICK, J.E. "Application of Austroads Pavement Design Guide for Wanganui Materials". 1997. Transfund NZ Research Report No 128. 84pp
10. WHITE, T. "Laboratory testing of core samples from Omata tank farm site, North-West Taranaki". 1982. Central Laboratories Report No. 2-82/12
11. PENDER, M.J. "Aspects of the Geotechnical behaviour of some NZ materials". 1996. *NZ* Geomechanics News, No. 52.
12. WESLEY, L.D. and CHAN, S.Y. "The dispersivity of volcanic ash soils".1991. IPENZ Proc. Annual Conference.
13. WESLEY, L.D. "Some lessons from geotechnical engineering in volcanic soils". 1999. Problematic Soils, Rotterdam, ISBN 90 54109971
14. TONKIN and TAYLOR Ltd. "Pavement Deflection Measurement and Interpretation for the Design of Rehabilitation Treatments". 1998. Transfund New Zealand Research Report No. 117.
15. DYNATEST. "ELMOND/ELCON evaluation of layer moduli of pavements". 1989. Journal of Structural Division ASCE SM1: 1-29
16. AASHTO "Guide for the Design of Pavement Structures", American Association of State Highway and Transportation Officials 1986.
17. TRL Road Note 31. "Guide to the Structural Design of Bitumen-Surfaced Road in Tropical and Sub-tropical Countries". 1977. Transport and Road Research Laboratory.
18. PATERSON, W.D.O. "The Highway Design and Maintenance Standards Model (HDM-III), Volume III, Road Deterioration and Maintenance Effects: Models for Planning and Management". 1987. Washington, DC. Transportation Department, World Bank.
19. PATRICK, J.E., DONGAL, D. "Methods for determining Structural Number of New Zealand pavements". 2001 Transfund New Zealand Research Report No. 199. 37 pp.

Importance of Parameters Influencing the Filtration in Embankment Dams.

Sharbaree Biswas[1], and Buddhima Indraratna[2]
[1]PhD student, [2]Professor
Civil Engineering Division, University of Wollongong, NSW, Australia

ABSTRACT

This paper will critically evaluate the importance of the common parameters influencing filtration in embankment dams. As relevant factors cannot be determined directly, various design criteria for safe filters have been developed considering different approaches. Retention ratio, hydraulic gradient, thickness of filter, permeability of filter, cohesion of fine particles, particle shapes are not treated in an equal importance. For example, traditional filter design has involved the retention ratio (i.e. Terzaghi criteria), while filter permeability has been considered as the main design factor by some researchers. The necessity of further study about the effect of filter thickness and hydraulic gradient, and the transport of fine base material through the unsaturated portion of filter will be presented. Experimental data based on large-scale filtration apparatus and high-pressure filtration apparatus tests will be discussed. The change in particle size distribution is taken as a key indicator to assess filtration effectiveness.

1 INTRODUCTION

In geotechnical engineering soil filters are used as barriers to protect the base soils from erosion. If filters are improperly designed, particles from the base soils might erode through them. Progressive accumulation of the particles in filters may lead to build up of excessive pore pressures leading to instability of dams.

Design and performance of granular filters was studied by many researchers (Terzaghi [1], Vaughan and Soares [2], Sherard et al. [3], [4], Indraratna and Vafai [5], Locke [6]). Filters are in general characterized as effective and ineffective, based on whether they can retain the eroded base material and prevent instability of the base material.

2 EFFECT OF FACTORS INFLUENCING FILTRATION

2.1 Particle Size Ratios

Terzaghi [1] was the first to develop granular filter design requirements. He envisaged two requirements, retention ratio, $D_{15F}/d_{85B} \leq$ 4-5 and permeability ratio $D_{15F}/d_{15B} \geq 4$. The Terzaghi [1] requirements describe the important and conflicting grain size relations of a suitable filter. Though the design criteria of Terzaghi [1] are still used for simplified filter design, subsequent research into the behaviour of filters has greatly improved knowledge in this field. The large majority of research has been laboratory based and that has usually led the researcher to recommend an empirical relationship for a stable combination (Sherard and Dunnigan [7]). However, these empirical criteria can only be reliably applied to the range of soils tested. They neither provide an understanding of the mechanisms involved with base soil - filter interaction, nor the time-dependent properties of the filtration process.

In contrast, Vaughan [8] proved that the permeability is the more consistent way of defining filtering power than the arbitrary small size as D_{15}. In the development of the perfect filter concept, he reported that the size of particle retained by a granular filter correlated with its permeability. That relationship enables the design of granular filter to be based on the proportion of the base soil retained, as is done in geotextile filter.

2.2 Hydraulic Gradient

Kassif et al. [9] reported that the critical flow that caused the base soil failure was independent of size of the size of filter. Exit gradient is a function of clay properties and it is independent of the diameter of hole.

USACE [10] explained that the failure of base filter combinations occur at hydraulic gradient below unity and at higher gradients, the susceptibility of piping increases when the filter is subjected to vibrations. A rapid increase in hydraulic gradient has the same effect as vibration. The bridging interface that forms to activate the filter is shown in Figure 1. These soil bridges can be destroyed by vibration or rapid changes in the hydraulic gradient.

As mentioned by Sherard and Dunnigan [11], the Soil Conservation Service (SCS) researchers also concluded that downstream filter would reliably control and seal concentrated leaks, even with excessive hydraulic gradients and flow velocities.

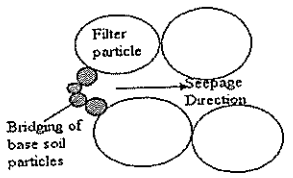

Figure 1. Bridging phenomenon in base-filter interface (after USACE [10]).

Sherard and Dunnigan [11] reported that there is no practical limit on the tolerable hydraulic gradient that can be safely imposed on the impervious earth core, if the water seeping through the earth core material discharges into an adequate filter.

Atmatzidis [12] indicated that the amount of finer particles originally incorporated in the gravel matrix controls the migration distances, duration of the migration process, and the amount of sand migrated. It results in increasing hydraulic gradients. The flow velocity depends directly on the hydraulic gradient and is a considerable factor as they provide the forces that set base material grains in motion.

Locke [6] emphasized that low flow rates may results in sedimentation of particles in the filter voids. Very high flow rates or hydraulic gradient may results in dilation of the filter voids and allow coarser particles to move through the filter.

2.3 Filter Thickness

Silveira [13] summarized that a protective filter (following Terzaghi criteria) of 700 mm thickness will have such a low probability of contamination in its last 300 mm that it may be considered to have no contamination, and if this 300 mm thickness is sufficient from a hydraulic point of view, the filter, in its less favourable portion, can have a thickness of 700 mm.

Schuler and Brauns [14] concluded that filter criteria derived on the basis of filtration tests with fine materials should not be used uncritically for the design of coarse filter, as for fine soils activation of the base/filter interface takes place in a short range of millimetres, while coarse soils need much more space (or base mass loss).

Vafai [15] described that optimum filter thickness depends on the particle geometry and structure as well as hydraulic condition. He recommended further tests where the filter thickness must be varied while keeping the base soil condition the same.

Humes [16] describes methodology of minimum filter thickness that is based on a simulation of the filtration process by washing through analysis. The total possible penetration will be, S= n.s, where n is number of confrontations required to stop a particle with diameter d_b in the interior of the filter of a given void size distribution and is calculated as $n = \log (1-P^*)/\log pv$. P^* is the confidence level fixed for the process and pv is the percentage of voids of the filter equal to or greater than dv, where dv is the internal sphere tangent diameter.

2.4 Cohesion Of Fine Particles

Studies involving cohesive base soils are limited in number and are mostly empirical. Although it was generally maintained that the ratio of sizes of filter and base material particles was an adequate criterion, some doubts were expressed in the studies of Vaughan and Soares [2], and Sherard et al. [4].

USBR [17] has recognized that a soil with fines content has some adhesion between the fines and this would delay or prevent migration under a seepage force and enter into a filter layer. Khor and Woo [18] reported that the needed protective filters are not significantly influenced by the cohesion or plasticity measured by the Aterberg limits.

For cohesive base soil, Burenkova [19] determined a stable rated sphere $D_s = f(D^2_f, a_n, P)$, where, D_s- rated sphere diameter, D_f- diameter of the filter particle, D_0 -

filter pore diameter, a_n - coefficient of filter density and P- load of the tested sample. The rated value ranged between: $D_f > D_s > D_0$ with (a_n) max and $D_f > D_s > D_0$ with (a_n) min.

Vaughan [8] mentioned that the general design criteria are unnecessarily conservative when filtering intact cohesive clay that has inter-particle attractions.

2.5 Particle Shape

Bertram [20] was the first to consider the particle shape on filtration. His investigation revealed that using round shape material for both base and filter, the safe retention ratio is 8.7. Similar results were observed when using both base and filter material as crushed quartz. When a combination was used, the retention ration reduced to 6.5.

Karpoff [21] indicated that the safe ratio was lower for the crushed rock filters than for the sub-rounded filters. Sherard et al. [3] examined that angular particles are as satisfactory as rounded alluvial particles as permeability was not consistently greater than that of the alluvial material with equivalent D_{15}. Khor and Woo (18) reported that crushed rock with angular particles were suitable materials for downstream filter. It is desirable to use well-graded filters containing sufficient quantity of non-cohesive fines of at least 5% by weight passing the 0.15 mm sieve. Spackman [22] showed that filters with rounded particles allow decreased loss of base soil compared with the filters of crushed material with angular particles, when compacted under the same condition.

Indraratna and Vafai [5] adopted a particle shape factor to allow for different particle shapes. Locke [6] then recommended that the shape factor considered by Indraratna and Vafai [5] could be adopted in his model to modify it.

2.6 Permeability Of Filter

Vaughan [8] reported that the size of particle retained by a granular filter correlated with its permeability and that relationship enables the design of granular filter to be based on the proportion of the base soil retained, as is done in geotextile filter. Permeability is a more consistent way of defining filtering power than an arbitrary small size as D_{15}.

2.7 Segregation Of Base Material

Maranha das Neves [23] stated that no visible segregation occurred during transportation of the eroded material, i.e. all the eroded material is transported and there is no preferential movement of fines. On the other hand Vaughan [8] reported segregation during the investigation of the Balderhead Dam.

2.8 The Perfect Filter

Vaughan and Soares [2] circumventing the difficulties associated with the quantitative prediction of colloid-sized floc migration and entrapment, advocated the use of perfect filters with pores fine enough to prevent the penetration of even the finest flocs from the base material.

Vaughan [8] described that the probability of eventual self-healing increases with the proportion of the base soil retained, and the rate and amount of damage should decrease. If a perfect filter is considered unnecessarily conservative, it would be better to design on a proportion of retained particles less than 100% of the base soil, rather than on the results of an empirical test which gives overly conservative filter grain sizes.

2.9 Limitation Of Critical Filter Test

Vaughan [8] reported that the critical filters do not give a consistent proportion of the base soil particles retained. In general, they are less conservative than the perfect filter design, particularly for the sandy clays, which field experience shows to be the most prone to damage. The critical filter tests proposed by Sherard and Dunnigan [7] involve a pre-formed central hole in a base soil subject to downward flow. It does not allow segregation and cannot reproduce the conditions, which may operate in a dam core. The eroding hole is constrained by a plastic cylinder. This prevents the flow path being maintained or re-opened by hydraulic pressure, as may occur in the field.

2.10 Physicochemical Forces

Physicochemical capture is important because progressive accumulation of fine particles in filters over a long period may lead to unacceptable permeability reductions and a build up of excessive pore pressures, leading to instability of geotechnical structures (Rege and Fogler [24]). Initial capture probability:

$$= 4[(\frac{\theta a}{r})^2 - (\frac{\theta a}{r})^3 + (\frac{\theta a}{r})^4]$$

Where, a = radius of particle, r = radius of pore, θ = parameter θ is a lumped parameter that takes into account the effect on deposition of several interparticle forces such as gravitational, inertial, hydrodynamic, electric double layer and van der walls forces.

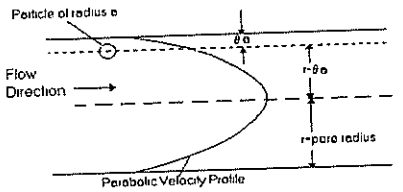

Figure 2. Probability of Particle Capture in a Pore Tube (After Rege and Fogler, [24]).

Reddi and Bonala [25] presented a mathematical model to assess fine particle accumulation in soil filters. The model treated the particle release in base soils and the particle deposition in filters as a combined problem and yielded a closed-form solution for particle deposition in filter material.

Pinheiro et al. [26] presented the forces responsible for parameter, θ as follows: (a) Gravity force (b) Brownian motion or diffusion (c) The Van der Waals force, $F_{vdw} = \pi Hd/12h^2$ in the case of a sphere at a distance h from a plane. H is the Hamaker constant, after Spielman and Cukor [27]. (d) Double layer force when the consolidated media wall is extremely large compared to particles, as $F_{dl} = \varepsilon dke^{-kh}\zeta_p\zeta_m/(2(1+e^{-kh}))$, where ε is the diclectric constant, ζ_p and ζ_m the respective zeta potential of particle and porous medium, and k^{-1} the characteristics thickness of the diffuse layer of charge (Spielman and Cukor, [27]. (e) The hydrodynamic force $F_h = 1.7(3\pi\mu U_h d)$, where U_h is the convective velocity at a distance h from the wall.

Locke [6] developed an analytical model for the cohesive base soil. Concepts such as resistance to erosion, aggregation of cohesive particles, physicochemical capture of particles and concentrated flow through cracks in cohesive soils have been considered in the model.

2.11 Homogeneity Of Filter Material

Schuler and Brauns [14] had mentioned that for granular materials, the non-homogeneity play the most important role in filtration. Coarse base soils are more susceptible to the influence of non- homogeneity as they need much more space for their activation to be implemented. Figure 3 indicates the effect of homogeneity on filtration. Base particles tend to penetrate deep into a non-homogeneous filter, i.e. requiring a greater filter thickness.

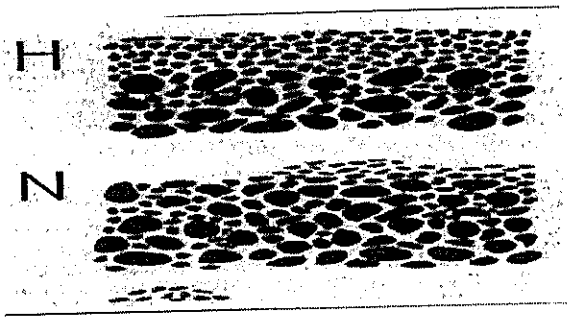

Figure 3. Effect of homogeneity of filter on filtration (H for homogeneous, N for non-homogeneous, after Schuler and Brauns [14]).

2.12 Flow Through Unsaturated Portion Of Filter

From the observation of the escape of air bubbles at some dykes built by Hydro-Quebec, St-Arnaud [28] has suggested that the compression of the free gases within the voids decreases in the direction of the flow. This occurs in accordance with the Boyle's law. Decrease of the compression of gases reduces the value of degree of saturation (S_r) as well as the permeability (k). This reduced permeability induces higher pore pressure compared to the pore pressure with respect to the homogeneous condition. Dissolution of gases (Henry's law) as well as the compression of gases will increase the value of S_r and therefore that of k. Dissolved gases will be carried through the core by the seepage water. After some water pressure decrease, gases will tend to come out of solution in the core itself or in the filter. Some blockage of flow will exist in an impervious zone as long as some free gases are present in it. The S_r-value increases as the air is removed from the pores by the water seeping through the core.

Lafleur et al. [29] confirmed his results and reported that during the construction of the dam and impoundment of the reservoir, an important part of the volume of air

remains trapped within the pores of the core and act according to the method described above.

Fell [30] mentioned that the soil above the phreatic surface in an earthfill core, would remain partially saturated, and have negative (suction) pore pressures. However, it may also be cracked, allowing water to enter from the surface, and develop pore pressures in the crack. The pore pressures in the crack may be quite transient, only responding to rainfall, and dissipating rapidly.

3 RESULTS OF CURRENT STUDY

This section describes some of the experimental results that are currently being carried out in the laboratory. The effects of hydraulic gradient and filter thickness on filtration will be elucidated. Experiments were conducted in the large-scale filtration apparatus and high-pressure filtration apparatus that are described below.

The majority of filter tests performed to determine empirical criteria have been carried out on fine base soils and sand filters. In an embankment dam, it is often necessary to construct multi-layer filters, where a gravel drainage layer is in contact with a sand filter. The normal filtration apparatus is only about 150mm diameter, and is not generally suitable for testing this sand - gravel filter interface. In order to test these materials successfully, a large-scale filter permeameter was built in the laboratory of University of Wollongong. This apparatus is a clear acrylic cylinder, 500mm diameter and 1m high, with steel endplates.

After the self-filtration layer is formed, the erosion rate and the turbidity were not found to be affected much, even with significant increase in hydraulic gradient. Base soil erosion continued to occur after the test has been completed. The large-scale test was conducted for 5 hours, and the total erosion during the test time was measured as 0.6g. A further erosion of 0.5g was recorded while discharging the effluent after the test under zero applied pressure.

With the same filter and base material, tests were conducted in the high-pressure filtration apparatus (Table1). The high-pressure filter equipment is much smaller than the large-scale apparatus. It is made of steel and has a diameter of 155 mm and a height of 245 mm.

In the large-scale test, no vibration was applied to the filter material layers, whereas in the high-pressure test, vibration was applied for 30 seconds to each of the three filter layers subjected to a surcharge pressure of 475 kPa. In the case of large-scale sample, the density of sample was measured as 1611.73 kg/m^3, whereas in the high-pressure test, the density was 1403.32 kg/m^3. With the application of vibration, the material may have become segregated instead of being compacted. Spackman [23] pointed out the need for studying the effect of vibration in the preparation of filter specimens.

Table 1. Test parameters in large-scale and high-pressure apparatus

Test	Base material		Filter material	
	Thickness (cm)	Density (kg/m^3)	Thickness (cm)	Density (kg/m^3)
High-pressure	3.0	1042.98	7.0	1403.32
Large-scale	9.0	1042.98	35.0	1611.73

Retention of base material at different levels of filter is shown in Figures 4-5. These figures show that with the increasing depth of filter from the base-filter interface, the percentage of retention is decreased. Figure 6 shows that the retention of base at 25 cm and towards the end of the filter (35 cm) is negligible as there is no change in the particle size distribution (PSD) with the original PSD of filter. As expected, most base particles are retained in the filter layer just below the interface. Figure 6 shows the comparison of the particle size distribution of the eroded and original base material, that indicates the erosion of the finer material from the base.

Due to the shorter length of filter in the high-pressure test, there was continuous erosion of the base soil with the effluent water. The total erosion was measured as 9.34g and 0.6g in the high-pressure and large-scale test, respectively. This indicates that in order to protect the wash out of the base soil through the filter requires a minimum (optimum) length.

The critical hydraulic gradient (i) measured in the high-pressure and large-scale test was 40.8 (Figure 7). However, the maximum turbidity value was recorded at a smaller hydraulic gradient of 20.4, and not at 40.4 (Figure 8). This maximum turbidity is due to the erosion of the clay fraction of the base material (1.43% of total base). Turbidity was not increased due to the wash out of

the finest particle fraction, but the erosion rate was increased significantly when the hydraulic gradient exceeded 40 (0.08g/lit to 0.17 g/lit) as shown in Figure 8.

Pore pressure transducers were inserted at different levels of the filter. The inlet pressure was measured at 25 cm top of the base filter interface (Figure 9). Pore pressure increased with filter depth because of the increasing resistance to flow by the filter medium. The pressure at 15 cm depth of filter was 6.5 kPa, 10.0 kPa, and 17.5 kPa for the inlet pressure of 2.5 kPa, 6.5 kPa, and 14.0 kPa, respectively. Time dependent increase of pressure in different levels of the filter was not measured, but this would be undertaken in the future.

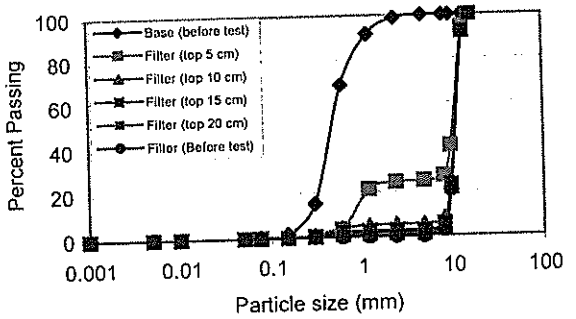

Figure 4. Retention of base particles at various layers of the filter (large scale test).

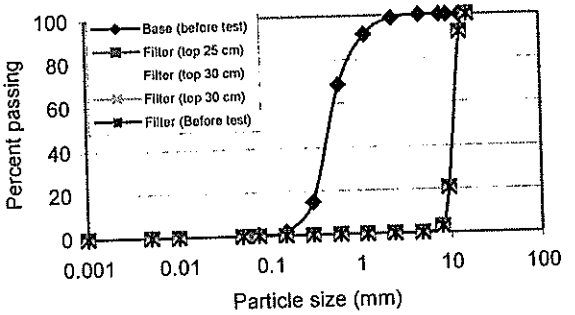

Figure 5. Base particle retention at different layers of filter (large scale test).

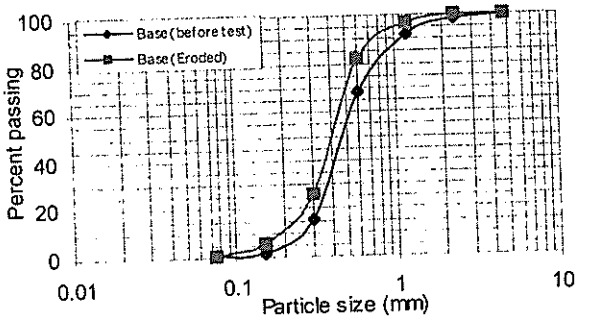

Figure 6. Difference in PSD of original base and the eroded base.

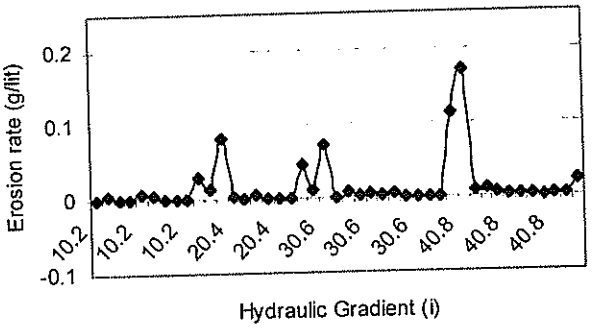

Figure 7. Increase of erosion rate with the increase of hydraulic gradient.

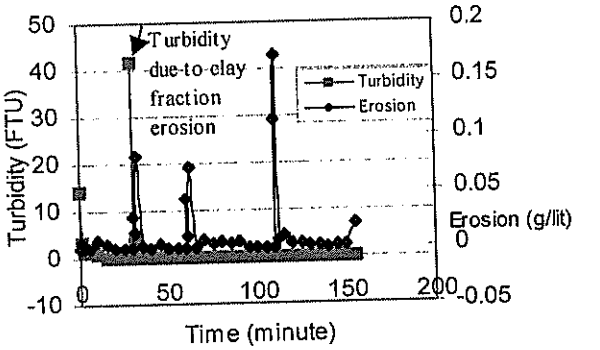

Figure 8. Turbidity and erosion rate of base.

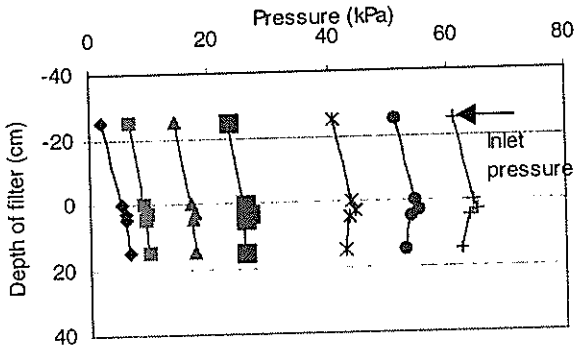

Figure 9. Increase of pore pressure with the increase of filter depth.

4 CONCLUSIONS

The following conclusions can be drawn on the basis of the current study:

- Terzaghi's empirical criteria for the design of granular filters are still used for a given base soil simplified filter design. Continuing research in this field has verified that the Terzaghi criteria are usually very conservative for cohesive soil, and less conservative for internally unstable soil. Therefore time dependent filter design criteria are now becoming more common, based on analytical and numerical modelling (Indraratna and Vafai [5], Locke [6]).
- To make a filter active, initial mobilisation of some coarse base particles is necessary. This facilitates the formation of a self-filtration zone that is capable of preventing further erosion of base soil.
- The thickness of filter is an important factor, as fine base particles penetrate a greater distance into the filter zone before being trapped.

Current filtration study proves that the change in particle size distribution of different filter layers is an indication of the filter becoming effective. The amount of base soil retaining within the filter at increasing depth, is an indication of the required minimum filter depth. Beyond this optimum filter depth, the extent of the base soil retained is insignificant. Effluent turbidity and the mass rate of erosion are important parameters that relate to the critical hydraulic gradient. Pore pressures are generally increased with the increasing depth of the filter medium.

The self-filtration zone is essential in preventing erosion of the base soil. However, laboratory studies show that this self-filtration zone can become unstable at rapid increase in hydraulic gradient. Future studies should focus on the application of hydraulic gradient that is more realistic in the case of real dam situations.

Ongoing research by the authors will consider the effect of vibration on filter density, the effect of homogeneity on filter media, and the time-dependent increase of pore pressure due to the progressive accumulation of base material within the filter. These aspects will also relate to the material stability of the granular filter.

5 ACKNOWLEDGEMENTS

Authors wish to acknowledge the research work by previous postgraduate students of Prof. Indraratna, including Dr F. Vafai, Dr. M. Locke. Additional thanks go to Mr Alan Grant, Bob Rowland, and Ian Laird for their assistance with laboratory work.

6 REFERENCES

[1] Terzaghi, K. "Der Grundbruch an Stauwerken und Seine Verhuntung Forcheimer-Nummer Wasserkr", 17, 1922, pp. 445-449, quoted by Vafai [15].

[2] Vaughan, G. and Soares, H, "Design of filters for clay cores of dams", Journal of Geotechnical Engineering, ASCE, Vol. 108, 1982, pp. 18-31.

[3] Sherard, J., Dunnigan, L., Talbot J, "Basic Properties of Sand and Gravel Filters", Journal of Geotechnical Engineering Division ASCE, Vol 110(GT6), June 1984, pp 684-700.

[4] Sherard, J., Dunnigan, L., Talbot J. "Filters for Silts and Clays", Journal of Geotechnical Engineering, ASCE, Vol. 110(6), June 1984, pp 701-718.

[5] Indraratna, B. and Vafai, F., "Analytical Model for Particle Migration Within base Soil - Filter System", Journal of Geotechnical and Geoenvironmental Engineering, ASCE, Vol. 123 (2), 2000, pp. 100-109.

[6] Locke, M, "Analytical and laboratory modelling of granular filters for embankment dam", PhD thesis, University of Wollongong, NSW, Australia, 2001.

[7] Sherard, J. and Dunnigan L. "Critical Filters for Impervious Soils", Journal of Geotechnical Engineering Division, ASCE, Vol. 115(GT7), July 1989, pp. 927-947.

[8] Vaughan, G. "Filter design for dam cores of clay, a retrospect", Filters and Drainage in Geotechnical and Environmental Engineering, Poland, 2000, pp. 189-196.

[9] Kassif, G., Zaslavsky, D. and Zeitlin, J, "Analysis of Filter Requirements for Compacted Clays", Proc. Sixth Int. Conf. on Soil Mech. and Foundation Eng., Canada, Vol. 2,1965, pp. 495-499.

[10] U.S. Army Corporation of Engineers (USACE), "Dewatering and Groundwater Control for Deep Excavations", Tech. memorandum, No 5-818-5, April, 1971.

[11] Sherard, J.L. and Dunnigan, L. P, "Filters and leakage control in Embankment dams in Seepage and Leakage from dams and impoundments", Proceedings of a symposium sponsored by Geotechnical Engineering Division in conjunction with ASCE National Convention, 1985, pp. 1-30.

[12] Atmatzidis, D. K. "An experimental study of sand migration in Gravel, Groundwater Effects in Geotech. Eng.", Proceedings of the 9th European Conference of soil Mech. and Foundation Eng., 1987, pp. 887-890.

[13] Silveira, A., "An analysis of the problem of washing through in protective filters", Proceedings of 5th Panam Conference on SMFE, Buenos Aires, 3,1965, pp. 160-167.

[14] Schuler, U and Brauns, J., "Behaviour of coarse and well-graded filter", in filters in Geotechnical and Hydraulic Engineering, Germany, 1993, pp. 3-17.

[15] Vafai, F., "Analytical Modelling and Laboratory Studies of Particle Transport in Filter Media", PhD Thesis, 1996, University of Wollongong, NSW, Australia.

[16] Humes, C., "Determination of the thickness of a filter based on washing through analysis", Proceeding of the 3rd International Conference Geofilters in Filters and Drainage in Geotechnical and Environmental Engineering, 2000, pp. 171-174.

[17] U. S. Bureau of Reclamation (USBR), "Design Standards-Embankment Dams", No. 13, Ch 5, 1987.

[18] Khor, C. and Woo H. "Investigation of Crushed Rock Filters for Dam Embankment", Journal of Geotechnical Engineering, ASCE, Vol. 115(3), 1989, pp. 399-412.

[19] Burenkova, V. V., "Protective filters for clayey soils in embankment dams", Filters and Drainage in Geotechnical and Environ. Eng., Balkema, 2000, pp. 167- 170.

[20] Bertram, G. E., "An experimental investigation of protective filters", Publication Grad. School of Engineering, Harvard Pub. no. 267, vol. 6., 1940, pp.

[21] Karpoff, K., "The Use of Laboratory Tests to Develop Design Criteria for Protective Filter", Proc. 58th Annual Meeting, ASTM, 1955, pp. 1183-1198

[22] Spackman, D. "An Investigation into the Effects of Particle Shape in Granular Filter Design" Engineering Honours Thesis, 2000, University of Wollongong, NSW, Australia.

[23] Maranha das Neves E. "Analysis of Crack Erosion in Dam Cores. The Crack Erosion Test", De Mello volume, 1989, pp. 284-298.

[24] Rege, S. and Fogler H., "A Network Model for Deep Bed Filtration of Solid Particles and Emulsion Drops" Journal AIChE, Vol. 34 (11), 1988, pp. 1761-1772.

[25] Reddi, L. and Bonala M, "Analytical Solution for Fine Particle Accumulation in Soil Filters", Journal Geotechnical Engineering Division ASCE, Vol. 123 (12), 1997, pp. 1143-1152.

[26] Pinheiro, I. G., Schmitz, P. and Houi, D., "Particle capture in porous media when physicochemical effects dominate", Journal of Chemical Engineering Science, 1999, Vol. 54(17), pp.3801-3813.

[27] Spielman, L. A. and P. M. Cukor, "Deposition of Non-Brownian Particles under Colloidal Forces", Journal of Colloid Interf Science Vol. 43 (1),1973, pp. 51-.

[28] St-Arnaud, G. "The high pore pressures within embankment dams; an unsaturated soil approach", Canadian Geotechnical Journal, Vol. 32, 1995, pp 892-898.

[29] Lafleur, J., Montes, P., Alicescu, V. and Phoung, N., "Laboratory simulation of filtration through dam cores made of broadly graded moraine", the 3rd Int. Conf. Geofilters, Poland, 2000, pp. 135-144.

[30] Fell, R. "Embankment dams-Some Lessons Learnt, and new Developments, EH Davis Memorial Lecture 1999, Australian Geomechanics, Vol. 35(1), 2000, pp. 5-45.

7 COPYRIGHT

Geotechnical Instrumentation & Monitoring Preload Performance - Stage 3 Expansion Kooragang Coal Terminal, Newcastle, Australia

C Bozinovski BE BSurv MEnvEngSc
Douglas Partners Pty Ltd

Ground improvement to reduce post construction settlements by way of staged preloading was undertaken prior to construction of the 1.4km long coal pad and reclaimer berm at the Kooragang Coal Terminal. Geotechnical instrumentation including settlement monitoring plates, vibrating wire piezometers, inclinometers, earth pressure cells and a deep extensometer were utilised to monitor preload performance which was critical to the staging of construction works. Geotechnical monitoring was successfully utilised in difficult ground conditions to minimise potential delays to construction.

1 INTRODUCTION

The Stage 3 Expansion of the Kooragang Coal Terminal was a $345 million "design and construct" project which boosted the coal exporting capacity of the Port of Newcastle to 89 million tonnes per year.

The Kooragang Coal Terminal, operated by Port Waratah Coal Services Limited, is located at Kooragang Island, in the port of Newcastle, some 160km north of Sydney, NSW, Australia.

Kooragang Island was formed through the extensive reclamation of small islands, shallows and channels and contains deep estuarine sediments which are susceptible to settlement via consolidation and creep.

The site contains the world's largest coal handling operation. Coal is transported primarily by rail from Hunter Valley mines, emptied in the receival (dump) station and conveyed to rail mounted stackers which place coal in designated stockpile areas. Coal is then reclaimed from the stockpiles by bucket wheel reclaimers and transported via conveyors to the shiploaders for export.

Port Waratah Coal Services engaged Bechtel Australia Pty Ltd to undertake the design and construction of the Stage 3 Expansion, which included a third stacking conveyor, rail receival (dump) station, stockpile pad and reclaimer, and shiploading conveyor stream loader.

Due to the presence of deep, soft estuarine sediments, ground improvement by way of staged preloading was undertaken to reduce post construction settlements prior to the construction of the coal pad and reclaimer berm.

This paper discusses the successful implementation and results of geotechnical monitoring associated with preloading for the Stage 3 Expansion works.

2 SITE CHARACTERISATION

An extensive geotechnical investigation program was undertaken to assess site conditions. The site was particularly suited to cone penetration testing (CPT), due to the presence of soft estuarine sediments. The investigation comprised a combination of CPT, piezocone tests, pore pressure dissipation tests, seismic CPT, conventional bore holes and jetted bores, shear vane tests and test pits.

A range of laboratory tests including oedometer, triaxial, permeability, Atterberg, sieve analysis and hydrometer tests were also undertaken to characterize soil conditions.

The interpreted geotechnical soil profile generally comprised the following:

- Unit 1 - filling, mainly sand (up to 5m deep)
- Unit 2 - upper soft to firm clay layer (up to 4m thick)
- Unit 3 - dense to very dense sand (23m to 28m thick)
- Unit 4 - lower stiff estuarine clay (7m to 12m thick)
- Unit 5 - siltstone / sandstone bedrock.

An upper unconfined aquifer was present in Unit 1 fill materials (ie perched). A lower semi-confined aquifer was also present beneath the Unit 2 clays.

The main geotechnical issue at the site was the presence of the upper clay layer with respect to consolidation and creep. The presence of the dual aquifer system also had implications for deep excavation works.

Engineering parameters from CPT data were processed together with the results of laboratory testing to produce continuous profiles of parameters such as shear strength, over consolidation ratio, coefficient of volume change, drained modulus and friction angle. The output can be tailored to present a wide range of interpreted parameters. Data in this format made analysis of settlement / consolidation quick and efficient.

Settlement analysis indicated that settlements of up to 700mm were likely over a 17 year period without ground improvement, for the proposed berm and coal stockpile area. The existing berm and pad facilities at the site had previously experienced up to 400mm settlement over a 5 year period. This magnitude of settlement can result in considerable maintenance costs associated with re-leveling of stacker and reclaimer rails.

The objective of geotechnical design was to design a ground improvement system to limit post construction settlements over a 17 year period to 200mm beneath the reclaimer berm, and 300mm beneath the coal pad.

3 PRELOAD DESIGN

A number of options for ground improvement were considered to limit post construction settlements. Preloading was assessed to be the most feasible and economic option to meet the performance requirements. Settlement analysis indicated that a total preload height of about 9m would be required to achieve the design objectives over a preload period of less than 12 months. The height of preload was also influenced by the availability of preload material, and the staging of construction works.

Stability analysis however indicated that slope failure would occur if the full height of preload was added in a single lift due to the underlying Unit 2 clays. A two stage preload system was therefore designed to address both settlement and stability issues during construction.

The 4m high Stage 1 preload was initially placed and monitored to achieve sufficient strength gain in the upper Unit 2 clays to allow the placement of Stage 2 (additional 5m) without the risk of slope failure.

The requirements for a two stage preload increased the need for accurate and timely monitoring results, in order to ensure that the construction program remained on schedule.

4 PRELOAD MONITORIING

Preload monitoring during construction was required to:

- assess progress of preload settlement.
- determine when Stage 1 preload had achieved appropriate strength gain (confirmed by further CPT testing).
- confirm stability of clay layer during preloading.
- determine when Stage 2 preload could be removed and allow berm construction to continue.

Monitoring of settlement plates, piezometers, inclinometers, extensometer and earth pressure cells were undertaken as discussed below.

4.1 Settlement Monitoring Plates

A total of 45 settlement plates were installed prior to the placement of preload materials. The plates comprised a 500mm square steel base plate with 32mm diameter steel risers, added in sections as the height of preload was

increased. The risers were encased within a protective PVC pipe.

Survey levels were measured on the base plates, and at regular intervals on the steel risers, by the project surveyors.

A typical settlement monitoring plot is presented in Figure 1 below.

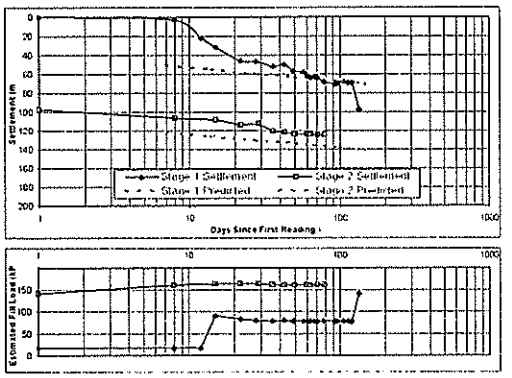

Figure 1: Typical Settlement Plot

The plot shows the recorded settlement compared to the predicted time-settlement behaviour. The lower plot shows the estimated fill load for each stage of loading, based on the recorded fill height and fill unit weight.

4.2 Vibrating Wire Piezometers

A total of 44 vibrating wire piezometers were installed beneath the preload within the upper Unit 2 clay layer to monitor pore water pressures. One piezometer was also installed within the lower Unit 4 clay layer.

Regular piezometer readings were measured, together with settlement plate monitoring, to monitor the dissipation of excess pore pressure and assist in determining when preload could be removed.

A typical piezometer plot is presented in Figure 2 below.

The above plot shows the recorded pore pressure and estimated hydrostatic pressure, with the difference being the excess pore pressure. The estimated fill load and total overburden stress are also plotted.

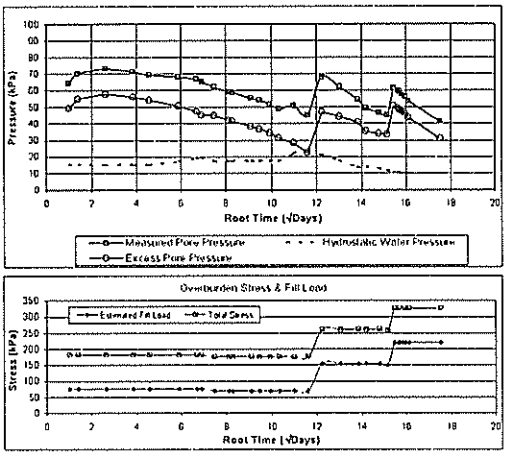

Figure 2: Typical Piezometer Plot

4.3 Inclinometer

A total of 28 inclinometers were installed to a depth of at least 1m below the upper Unit 2 clay strata, adjacent to the toe of the preload, to monitor lateral displacements during the placement of preload.

Regular readings were taken and processed as shown on the typical plot in Figure 3 below.

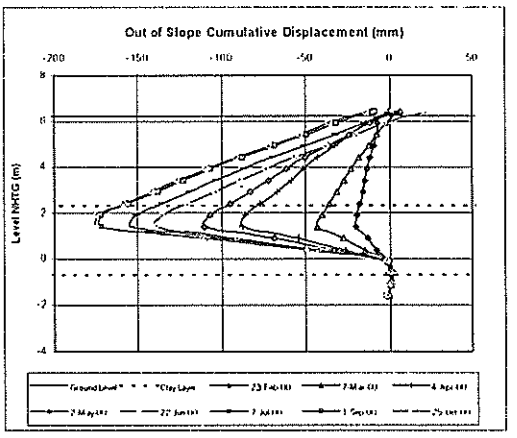

Figure 3: Typical Inclinometer Plot

The above plot shows deflection recorded perpendicular to the slope. The ground level and location of the upper Unit 2 clay later are also shown. The total lateral deformation and rate of deformation was used together with the settlement plate and piezometer monitoring results to confirm the stability of the preload embankment and determine when the Stage 2 preload could be placed.

4.4 Extensometer

An extensometer was installed to bedrock (50m) at one location beneath the preload to measure the contribution of settlement in each layer to the total settlement, and in particular the deep Unit 4 clay layer.

Regular monitoring of the extensometer was undertaken. The settlement associated with each layer was measured. The results indicated that the majority of settlement occurred in the upper Unit 2 clay layer as expected.

4.5 Earth Pressure Cells

A total of four earth pressure cells were installed beneath the preload to confirm the magnitude of the load applied by the preload. Two types of fill material were used as preload: dredged sand (density $\approx$ 18kN/m^3), and Crusher Dust (density $\approx$ 20kN/m^3). The type of fill and the corresponding density were taken into consideration when determining the estimated fill load for settlement, piezometer and extensometer monitoring.

4.6 Cone Penetration Tests (CPT's)

A total of 90 CPT's were carried during preload monitoring to:

- confirm that appropriate strength gain had been achieved in the upper Unit 2 clays after Stage 1 preload (ie ensure that the addition of Stage 2 preload would not induce instability in the preload batter slopes).
- confirm final strength gain in the upper Unit 2 layer after Stage 2 preload, which was required to provide long term stability of the completed coal stockyard.

The results of the CPT's compared favourably with the predicted shear strength gains (ie approximately 30kPa after Stage 1 preload, and approximately 50kPa after Stage 2).

An example of strength gain measured in the upper Unit 2 clay as a result of preloading is presented in Figure 4 below.

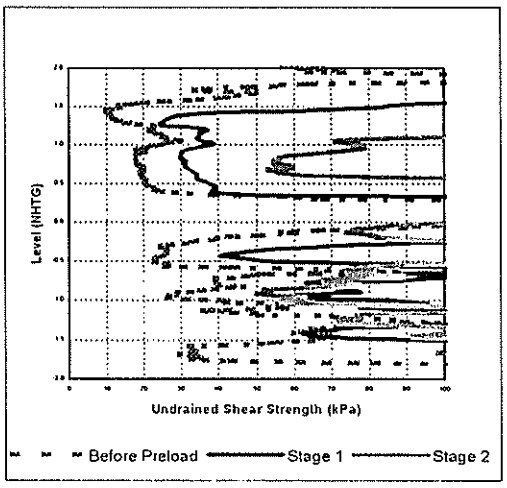

Figure 4: Strength Gain in Unit 2 Clay from Preloading (Ch 1300, Reclaimer Berm)

5 CONCLUSIONS

The monitoring results indicated that the preload generally performed as predicted, with target settlement and strength criteria being met. The success of the project has been attributed to the accurate and timely supply and analysis of monitoring results, together with regular communication and liaison with the project managers, which is considered to be critical for "design and construct" projects.

6 ACKNOWLEDGEMENTS

The author acknowledges the assistance and co-operation from Port Waratah Coal Services Limited (PWCS), and Bechtel Australia Pty Ltd during.

7 REFERENCES

1. DOUGLAS PARTNERS Pty Ltd, "Proposed Coal Stockyard, PWCS Stage 3 Expansion, Kooragang Coal Loader", Project 31100A, April 2000.

2. DOUGLAS PARTNERS Pty Ltd, "Geotechnical Instrumentation Monitoring, PWCS Stage 3 Expansion, Kooragang Coal Loader", Project 31100B, June 2001.

Parametric study of embankments on soft soils using a creep model

Hong Ngoc Bui
Department of Civil Engineering, University of Sydney, Australia.

Summary: A creep model is developed on a phenomenological basis and implemented using a numerical technique of approximation using Laplace transforms and the finite element approach. Direct numerical inversion of the solution is used to obtain the time-dependent solutions. Having introduced time into the soil response in terms of a bulk modulus and shear modulus which can vary with time, these parameters can most simply be derived from a series of one-dimensional consolidation tests or triaxial tests. In this paper, parametric results of the creep model applied to embankments on soft soils will be presented. The results of the time-dependent solutions are compared with the time-independent elastic solutions to aid assessment of soil parameters for predicting the behaviour of the foundation.

1 INTRODUCTION

In the design of embankments on soft soil profiles, creep settlements are one of the most important problems. Hence, a complete geotechnical model for these soft foundations is required to design properly any surface structures as well as to predict their time-dependent settlements.

Different theories have been applied to modeling the foundation response with regard to creep of the soil material. Merchant and Taylor (1) explained that the primary and secondary consolidations occur simultaneously during the consolidation process, and this does not follow the conventional Terzaghi theory. In 1941, Biot (2) presented a mathematical theory of consolidation that considered the soil skeleton to be visco-elastic under general three-dimensional conditions. Some current analyses (Indraratna et al., 3) have employed critical state soil mechanics and adopted the coupled (Biot) consolidation theory to enable predictions of the total settlement of soft soil foundation beneath embankments by incorporating the creep component to the corrected consolidation settlement.

In this paper, a creep model that is based on the visco-elastic theory of materials, is incorporated in a finite element program that employs Fourier transforms and a Laplace transform to include the influence of geometry and time in the solution. The program VSET (Visco-elastic SETtlement analysis), developed by the author (H.Bui, et al., 4) is used to study parameters that influence the design of embankments on soft soils and which may be used for the prediction of foundation settlements.

2 THE CREEP MODEL

A creep model is developed based on visco-elastic consolidation theory and implemented using Laplace transforms, Fourier transforms (for 3D problems) and the finite element approach. During the consolidation process when the load is applied, properties of the soil as represented by bulk modulus (K) and shear modulus (G) will be assumed to vary with time. The time-dependent characteristics of the two parameters are commonly expressed by logarithmic functions or exponential functions with time (Booker and Small, 5). For the case of simple terminating creep settlements, the functions can take the form:

$$\text{and} \qquad \begin{aligned} K(t) &= K_\infty + (K_o - K_\infty)\, e^{-\lambda t} \\ G(t) &= G_\infty + (G_o - G_\infty)\, e^{-\lambda t} \end{aligned} \qquad (1)$$

while for the case of non-terminating creep settlements, the form is:

$$\text{and} \qquad \begin{aligned} K(t) &= K_o + B_K \ln(1 + \alpha_o t) \\ G(t) &= G_o + B_G \ln(1 + \alpha_o t) \end{aligned} \qquad (2)$$

where

K_∞, G_∞ : bulk and shear moduli at very large time
K_o, G_o : initial bulk and shear moduli
λ, α_o : time constants
B_K, B_G : creep rates

The above creep parameters can be derived from conventional oedometer or triaxial tests (H.Bui et al., 4). As long as time-dependent functions for soil properties are defined and applied to the set of equations for numerical analysis of visco-elastic behaviour, the time-dependent deformation of the soil can be predicted. The finite element equations (Booker and Small, 5) can be written for the consolidation of a porous visco-elastic media as:

$$\begin{bmatrix} s\overline{K_E} & -L^T \\ -L & -\dfrac{\Phi}{s} \end{bmatrix} \begin{bmatrix} \bar{\delta} \\ \dot{\bar{q}} \end{bmatrix} = \begin{bmatrix} \bar{f} \\ \bar{0} \end{bmatrix} \qquad (3)$$

where

$\overline{K_E} = \int_V B^T . \overline{D} . B . dV$ element stiffness matrix

$L^T = \int_V d . a^T . dV$ coupling matrix

$\Phi = \frac{1}{\gamma_w} \int_V E^T . k . E . dV$ k : matrix of permeability coefficients for Darcy's law

$\delta^T = (u_1^T, u_2^T, ...)$ displacement vector

$q^T = (p_1^T, p_2^T, ...)$ pore pressure vector

$f^T = (f_1^T, f_2^T, ...)$ force vector

s : Laplace variable and the over bar denotes the Laplace transform.

A FEM program has been developed by the author to carry out the approximate calculations of creep settlement for a 3D problem. The method of analysis involves a combination of the finite element method and mathematical techniques such as the Laplace transform, the Fourier transform and Gaussian integration.

3 TYPICAL CASE OF AN EMBANKMENT

A typical problem for embankment construction on a soft clay foundation is examined and shown in Figure 1.

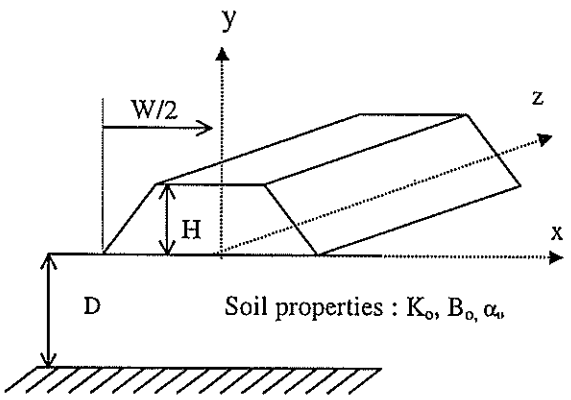

Figure 1. Embankment problem

An embankment that has a height of 4 m, a width of 50 m and a length of 50m is constructed on a soft clay foundation. The embankment material is sand with a unit weight γ of 20 kN/m^3. The embankment will rise to full height in 48 days, hence the rate of construction is 0.0708 m/day. In the general design, the height H and the width W of the embankment are important factors. In particular, the depth D of the soil layer will decide the settlement characteristics of the foundation. Therefore, it is prudent that these factors be normalised to aid in the presentation of the results, and five different values of depth D (4, 8, 16, 25 and 32 m) while a constant value of height H and width W are used in this study.

The soil material beneath the foundation is soft clay and has an initial bulk modulus of 3000 kPa. During the deformation process of the foundation, the Poisson's ratio is assumed to have a constant value of 0.35 and the changes of soil properties with time are expressed by equation 2 where $B_K = 3B_G$ and $K_o = 3G_o$. Values of creep rate B_K and creep coefficient α_o are given in Table 1. A dimensionless influence factor (I) for the vertical displacement is used in this paper, where:

$$I = \frac{S K_o}{\gamma H W} \qquad (5)$$

S: vertical displacement of the foundation
K_o, γ, H, W: chosen constant values of the embankment and the soft clay.

B_K (kPa)	-30	-90	-150
α_o (1/day)	345.6	3.456	0.03456

Table1. Creep parameters

Figure 2 shows the finite element mesh used for a soil layer of 25 m depth and the embankment above (the mesh uses symmetry about the center-line to model the full embankment with a half-mesh). The (exaggerated) deformed mesh of the foundation after 2 years at section z = 0 is also shown in this figure.

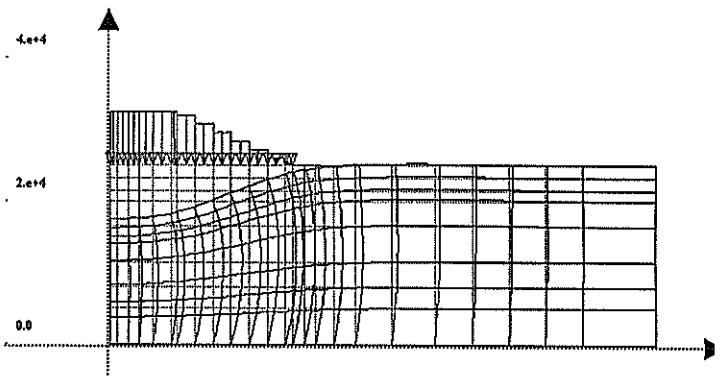

Figure 2. Deformed mesh of the foundation after 2 years

In order to provide verification of this creep model, before using it to study creep parameters, elastic problems are solved using program VSET by using values of creep rate $B_o = 0$ for all five different values of depth D. These results are compared with those obtained by use of elastic theory for uniform load on a square and strip (Poulos and Davis, 6). Figure 3 shows a good agreement between the elastic solutions from VSET with the ones from elastic theory. Because the elastic solutions use a uniform load over the full width of the embankment a larger settlement from the elastic solution compared to that from VSET is expected. It can be seen that at the end of the primary consolidation process, the final settlements of the foundations that are modeled as strip loads acting on

top are larger than those predicted from the square loaded area, as expected.

In consolidation theory, a dimensionless time factor T_v is defined as being directly proportional to the coefficient of consolidation and the time, and inversely proportional to the drainage path (e.g. depth of layer) squared. The elastic settlements due to consolidation processes for five different foundation depths are shown in Figure 4 as a function of time. The responses are represented by the two dimensionless factors T_v and I_e (the dimensionless influence factor for the elastic vertical displacement).

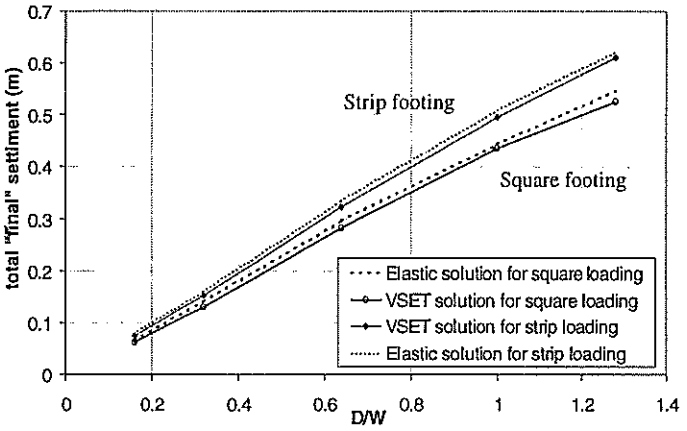

Figure 3. Elastic solutions for square and strip loads

In this figure, the continuous lines are presented for the plane strain cases and the dis-continuous ones are for the square loading. The steepest, early part of each curve is because of the linear loading process occurring during the first 48 days. The depths of the soils have been included in the normalized $T_v = C_v t/D^2$, therefore, the primary consolidation of those foundations ends at nearly the same values of $T_v = 5$.

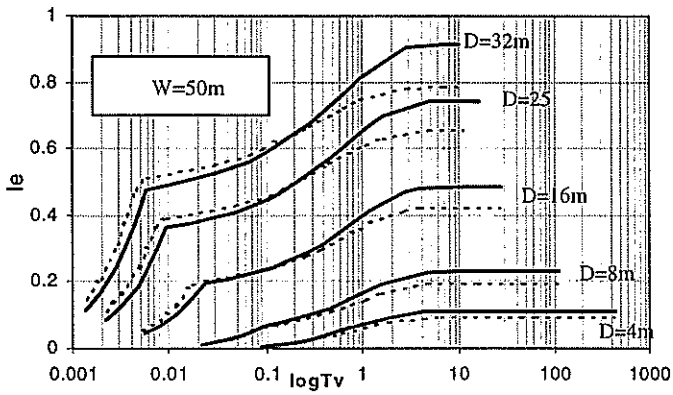

Figure 4. Elastic consolidation settlements of the foundations

While the bulk and shear modulus are constants in the elastic consolidation process, they are functions of time in visco-elastic consolidation theory. In order to examine the influence of creep parameters on the "final" settlement, three different values of B_K and α_o are used as in Table 1 for the five depths of foundation. Figures 5a,b show the ratio of total creep settlements to the elastic settlements versus the nomalised factors of D/W at times of 2 and 20 years. It is clear that the total settlement increases when the creep rate B_K or the time coefficient α_o increases. As well as the settlement due to creep increasing with time, it can be recognized that the creep settlement after 2 years for the foundation of depth 4 m (D/W = 0.16) is lager than the one for the foundation of depth 8 m (D/W = 0.32). This is because those settlements are compared at the same real time, but at different values of T_v, in other words at different of degrees of consolidation. After this time, through out its depth, the shallower foundation has finished consolidation and started creep, while the deeper foundation is still consolidating and not all the soil layer is creeping yet at its final effective stress level. This trend can be found at other times (Figure 5b).

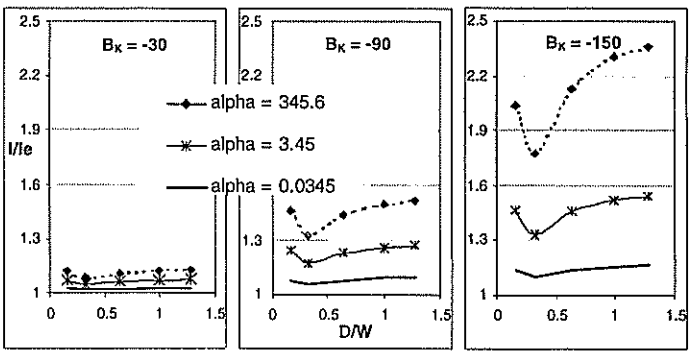

Figure 5a. Influence of B_K and α_o on strip creep settlement after 2 years.

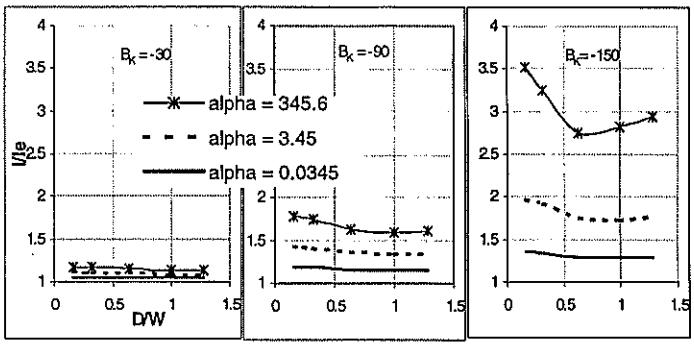

Figure 5b. Influence of B_K and α_o on strip creep settlement after 20 years

In equation 2, the multiplication of α_o*t gives a non-dimensional creep 'time factor'. If it is kept constant with time, then the value of the bulk modulus depends on the creep rate B_K which is equal to zero for elastic problems and differs from zero for the case including creep. Charts with different values of (α_o*t), at particular creep rate B_K, are shown in figures 6a and 6b. From these charts, the dimensionless influence factor for vertical settlement including creep, as well as the elastic settlement, can be determined if the rate B_K, the time t and the ratio D/W are known.

An example of the use of the above charts is given in the following. The foundation has a depth of 16m and the embankment dimensions are the same with the foregoing problem in Figure 1. The material has the creep rate properties B_K = -90 (kPa), α_o= 3.45 (1/day), and C_v = 0.1 (m^2/day). All these values can be defined from triaxial tests. Hence, the settlement of the foundation after 2 years can be estimated by using Figure 6b where:

$$T_v = \frac{C_v * t}{D^2} = \frac{0.1*2*365}{16*16} = 0.286$$

and

$$\alpha_o * t = 3.45*2*365 = 2518$$

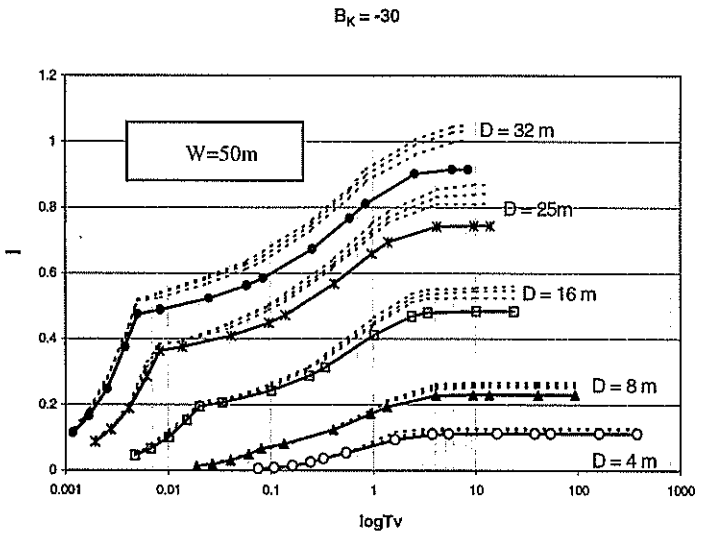

Figure 6a. Influence dimensionless factor I vs time factor T_v for the strip load

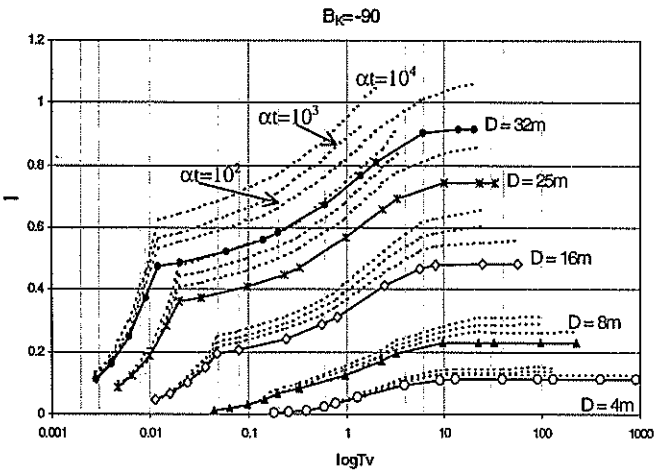

Figure 6b. Dimensionless influence factor I vs time factor T_v for the strip load.

So, the value of the dimensionless influence (I) factor will be approximately 0.34.

From equation 5, the vertical settlement of the foundation at time 2 years is: 0.24 m. This can be checked back with the consolidation settlement curve (Fig.7) which is based on the creep functions for bulk and shear modulus, where B_K = -90 and α_o = 3.45.

If a lot more charts like 6a,b can be created with a lager range for B_K, α_o ... then it would be convenient for quickly estimating settlement for a foundation.

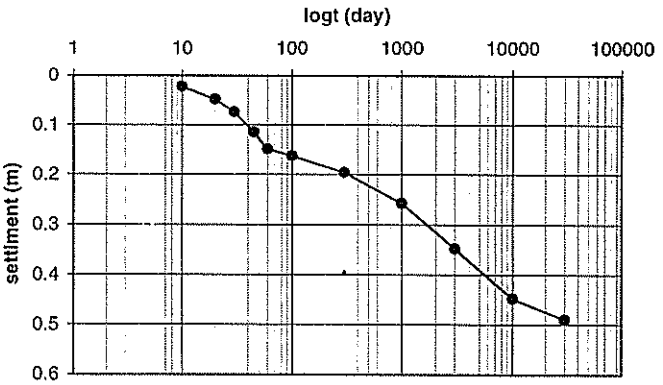

Figure7. Consolidation settlement of the foundation

4 CONCLUSIONS

In this paper, a parametric study using a creep model that is based on visco-elastic consolidation theory is presented. The general problem of an embankment resting on top of a soft clay foundation has been studied. The creep settlement may be found directly at any time by using time-dependent functions of bulk and shear moduli in the finite element program VSET. The creep parameters of those functions may be derived from conventional isotropic and shear tests. The paper has indicated some of the influences of the creep parameters upon the settlement prediction of an embankment. A convenient way to estimate this settlement is by the use of charts such as those presented here. Further study is required on the method of creating the charts and ways to use them effectively to predict (check) creep settlement.

5 REFERENCES

1. TAYLOR, D.W., MERCHANT, W. "A theory of clay consolidation accounting for secondary compressions", Jnl. Math. Phys., 1940, Vol. 19, 167-172.
2. BIOT, M.A, "General theory of three dimensional consolidation", Jnl. Appl. Phys., 1941, Vol. 12, 155-162.
3. INDRARATNA, B., BALASUBRAMANIAM, A.S., SIVANESWARAN, N., "Analysis of settlement and lateral deformation of soft clay foundation beneath two full-scale embankments", Intern. Jnl. For Numerical And Analytical Methods In Geotechnics, 1997, Vol. 21, 599-618.
4. BUI, H.N., SMALL, J.C, HULL, T., "Secondary compression of clays", The 14th Southeast Asian Geotechnical Conference, Dec. 2001, in the press.

5. BOOKER, J.R., SMALL, J.C. "Finite layer analysis of viscoelastic layered materials", Intern. Jnl. For Numerical And Analytical Methods In Geotechnics, 1986, Vol. 10, 415-430.
6. POULOS, H.G., DAVIS, E.H. " Elastic solutions for soil and rock mechanics", John Wiley &Sons, London, 1974.
7. BOOKER, J.R., "One dimensional primary and secondary consolidation of a soil which creeps indefinitely", Research Report R420. School of Civil and Mining Engineering, Univ. of Sydney, Australia.
8. CARTER, J.P., BOOKER, J.R., SMALL, J.C. "The analysis of finite elasto-plastic consolidation", Intern. Jnl. For Numerical And Analytical Methods In Geotechnics, 1979, Vol. 3, 107-129.
9. SINGH, A., MITCHELL, J.K. "General stress-train-time function for soils", Journal of the Soil Mechanics and Foundation Division, Proc. ASCE., 1968, Vol. 94, 21-47.

SLIPS IN ONERAHI CHAOS

Murray Burt : Beca Carter Hollings and Ferner Ltd

A geological formation known Onerahi Chaos Breccia (Northland Allochthon) extends North of Auckland from Silverdale to Kaitaia. The roads within this area are plagued with cut slope failures and underslips caused by creep failure along weak pre-sheared planes within the OC formation. This paper presents a background geological/ geotechnical summary of the OC formation and details recent inclinometer monitoring data at two slip sites on SH16. The inclinometer monitoring indicates that the creep failure at each site was occurring along a shear plane close to the interface between the HW (SPT N=10) and MW (SPT N=35) Onerahi Chaos soil/rock mass. This indicates that creep failure shear planes within OC may be generally located at the interface between the HW and MW material. As the knowledge base of inclinometer monitoring at OC slip sites grows this hypothesis may be proved and therefore in the future it may be possible to reduce the number of costly inclinometer installations at OC slip sites, and accurately identify the slide plane, for remedial design, from SPT strength testing and borehole log information.

1 INTRODUCTION

A geological formation known as Onerahi Chaos Breccia (Northland Allochthon) extends North of Auckland from Silverdale to Kaitaia. Onerahi Chaos (OC) typically forms undulating slopes known for slope instability at shallow angles. The roads within this area are plagued with cut slope failures and underslips caused by slowly creeping slips within the OC formation. Slope instability causes a range of problems from high roughness, poor ride and road width reduction to complete road blockage. Ongoing maintenance to remove debris, fill cracks, smooth and reseal the pavement surface is required at frequent intervals and records indicate annual maintenance costs in the order of $15,000 at each slip site.

This paper presents a background geological/ geotechnical summary of the OC formation and details recent inclinometer monitoring data at two slip sites, which provides valuable insight into understanding characteristic failure mechanisms within OC.

2 ONERAHI CHAOS BRECCIA (NORTHLAND ALLOCHHON)

2.1 Geological Description

Onerahi Chaos Breccia of the Miocene Age (Kear & Waterhouse,1) comprises a chaotic mixture of siliceous shale with lenses of micaeous sandstones and siltstones with rare limestone concretions belonging to the Mangakahia Group and Motatau Group together with large broken rafts of Waitemata Group sediments (Thompson & Schofield,2,3). The rocks are sheared, often to an extreme extent where the differing materials have become intermixed, with many polished slickensided joints throughout the mass. This shearing is now interpreted as occurring during its tectonic emplacement, as the Pacific plate was thrust down beneath the Indian-Australian plate during the Miocene age (Sporli & Kear,4).

Both siliceous and calcareous mudstones/siltstones occur within the Chaos and in places these rocks are thinly interbedded or brecciated (angular fragments of the two types mixed together during tectonic activity). The siliceous mudstones contain sodium montmorillonite and other very high swelling clays, whereas the calcareous mudstones have lesser (but still high) swelling tendencies. The mudstones have low strengths (equivalent to stiff to hard soils, deforming plastically under compressive loads) with low friction on slickensided joint surfaces and shear zones.

Mahurangi Limestone is fine grained, with a significant clay and silt content. It is more brittle than the mudstones and is very closely to extremely closely jointed forming small angular pebble size blocks. Low angle shear zones are common and tend to crush the rock between these zones into a clay/silt pug.

These rocks weather ultimately to a soft to stiff clay to depths of 2 to 10m. The soils are highly impermeable, and have high ground water levels (typically 0 to 3m below the ground surface). The residual soils immediately below this capping layer of clay are often very weak silt with small lumps of less weathered rock (this second very weak layer is often the seat of instability found in OC areas). Creep is common and instability is evident by a connecting profile on the OC slopes.

2.2 Typical Subsurface Profile and Properties

Onerahi Chaos formation typically exhibits a weathered sequence with approximately 3–4m of completely weathered soil strength material at the surface, underlain by 3-4m of highly weathered (HW) residual rock strength material, underlain by moderately weathered (MW) to slightly weathered (SW) weak mudstone or calcareous siltstone rock. Shear zones have been discovered at many locations between the HW and MW material.

Onerahi Chaos materials have highly variable strength properties. The siliceous mudstones have lower effective stress strengths than the calcareous siltstones and limestones, in places these rocks are both mixed together and/or thinly layered. In addition, the material strength is greatly reduced within shear zones. Shearing in the calcareous siltstones and limestones can crush the rock to a wet clay pug in places. The mudstones in contrast are rarely jointed. These joints however have polished slickensided surfaces.

Typical effective stress parameters for Onerahi Chaos have been determined based on measured strength tests, (in-situ shear strengths, triaxial compression tests and UCS tests) and back analyses of surrounding slopes (Tilsley,5).

Table 1 below presents the typical subsurface profile sequence encountered in OC, together with typical engineering properties. (refer also Reference 6 & 7).

Layer	Su (kPa)	SPT N	c' (kPa)	ϕ' (°)
OC CW Residual Soil	30 - 70	11 - 22	2, 5	17
OC CW-HW and shear zones	100 - 140	5 - 50	0	17 - 22
OC MW – SW Mudstone	NA	35-50+	5	28
OC MW-SW Limestone/ Calcareous Siltstone	NA	50+	5	28

Table 1: OC Typical Profile and Properties

Other typical engineering properties for the OC mudstone are listed in Table 2 below (East,6).

Engineering Property	Typical Values
Water Content	15 – 20%
Calcite Content	0 – 25%
Clay Index	7 – 25
Pressuremeter Limit Pressure	0.5 – 3 MPa
Permeability	10^{-7} – 10^{-11} m/s

Table 2 : OC Typical Engineering Properties

2.3 Typical Groundwater Conditions

In Onerahi Chaos formation the ground water levels (GWL) are typically perched, with surface soils close to saturation (GWL typically 1-3m below ground surface). When the rock mass is fractured, ground water levels below the clay crust may be much deeper.

3 SLOPE STABILITY IN ONERAHI CHAOS

3.1 General

Extensive slope movements have been observed in slopes comprised of Onerahi Chaos. These failed slopes typically have gradients of between 5 - 8H:1V (7 – 11°).

Experience with Onerahi Chaos indicates that creep movement occurs along pre sheared bedding planes. These shear planes consist of sheared mudstone clasts suspended in a matrix of soft to firm clay. They contribute significantly to natural slope instability, resulting in movement occurring on slopes as shallow as 7° (8H:1V).

Shear planes in Onerahi Chaos rock can have a dominant direction in local areas. Consequently the orientation of cut slopes in Onerahi Chaos rock with respect to a dominant shear direction can result in stable cuts being steeper or shallower depending on the bedding orientation. These shear planes appear to dominate the slope mass angle of friction.

3.2 Role of Ground Water on Stability

Onerahi Chaos soils are also known to have very low permeability and upper layers are likely to become saturated after periods of rain.

OC often has high piezometric heads likely related to confined water bearing fractures within the rock mass material and the low permeability of the rock mass. Typical rates of permeability for the Onerahi Chaos rock mass range from 10^{-7} to 10^{-11} m/s (East,6).

The slope movements are commonly triggered by saturation of the soils and subsequent failures can be reactivated at flatter slope gradients where soil strengths have been reduced to their residual levels.

4 RECENT INCLINOMETER DATA FROM TWO SLIP SITES ON SH16

4.1 General

As discussed in section 3.1 above, OC is prone to very slow creep failure along weak pre-sheared planes within the soil mass. By installing inclinometers at two slip sites on SH16 we were able to determine the exact level at which creep failure was occurring at each site and gain a better understanding of the typical slip mechanism within OC failures.

4.2 J Farmer Road Slip

J Farmer Road slip is located south of Wellsford on State Highway 16 at RP82/7.1, just south of J Farmer Road. The general topography is rolling, and at the slip site the highway is constructed on a sidling cut and fill. The cut slope above the eastern side of the highway extends up to 3m high with a slope angle of 45°. The fill below the western side of the highway is approximately 2m high with a slope angle of 18° (3H:1V). The natural ground below the embankment

fill slopes down at an angle of 5 – 15° for a distance of 35m to a small stream.

The J Farmer underslip evidenced itself as arcuate cracks that appeared in the pavement surface. These cracks were an ongoing maintenance problem that called for regular pavement resurfacing and the site was described by the RTA 'Truck Ride Survey' as being 'bumpy, undulating, and x-sectional rocking caused and unsafe and uncomfortable ride'.

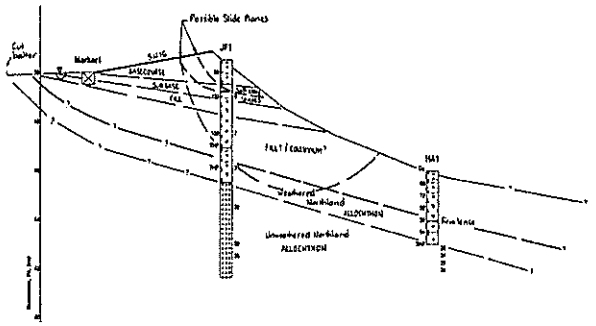

Figure 1 : J Farmer Slip : Geological Cross-Section

4.2.1 Geology

Roadside cuttings and boreholes confirmed that the natural ground at the site was Onerahi Chaos comprising weathered derivatives of grey siliceous shales with pockets of red and green (possible calcareous) shales and fine micaceous sands of the Northland Allochthon.

The lower embankment batter had some terracettes indicating creep had occurred. The slopes below the road were relatively gentle with a hummocky expression and some reed growth. The hummocks indicated that slope movement was occurring in the natural ground. The reeds and the surface ponding indicated waterlogged sub-surface conditions.

Borehole investigation through the center of the slip revealed the following log.

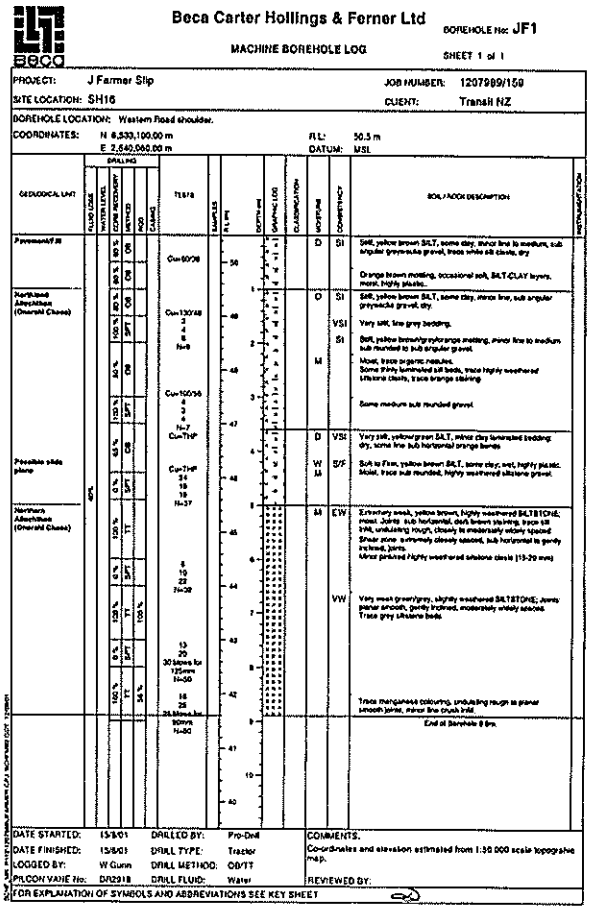

Figure 2: Borehole Log J Farmer Road Slip

4.2.2 Ground Water

At the time of inspection the topsoil either side of the highway was saturated with water standing in puddles within natural depressions. Constant flow was observed in the table drains either side of the highway.

A large volume of seepage was observed to be issuing from the base of the cut slope on the eastern side of the slip site. The table drain on the eastern side of the highway intercepted some of this flow, however a significant volume of water was observed to be seeping through the pavement and flowing out on the western side of the highway.

Two piezometers were installed at the site, one on either side of the highway. Measurement of the water level within the piezometers indicated a groundwater level at the surface on the eastern side of the highway, and at 2.6m below ground level on the western or lower side of the highway.

4.2.3 Inclinometer Monitoring

An inclinometer was installed to a depth of 9m on the western shoulder of the highway, within the centre of the slip mass. Ongoing monitoring of this inclinometer showed defined movement along a shear plane at about 4m below the ground surface. This depth of movement correlated closely to the borelog and soil strength profile as indicated by SPT testing. The inclinometer trace is shown as Figure 3 below.

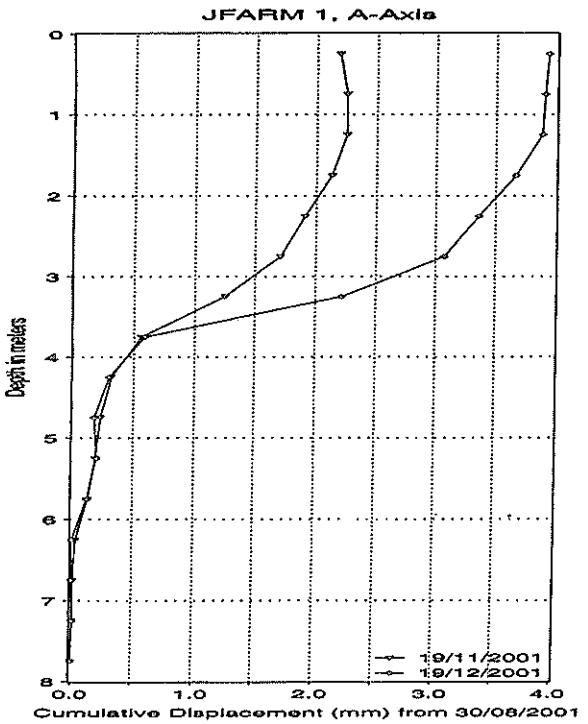

Figure 3 : J Farmer Slip : Inclinometer Trace

4.3 Ingleton Slip

Ingleton slip is located south of Wellsford on State Highway 16 at RP92/6.5, just north of Ingleton Road. The general topography is rolling, and at the slip site the highway traverses a ridge. The highway is constructed on sidling fill on the western side of the ridge. However the top of the embankment is roughly level with the top of the ridge so that the natural ground slopes away on the eastern side of the highway at a slope of 5 – 10°, while the fill below the western side of the highway is approximately 5m high at a slope angle of 30° (1.75H:1V). The natural ground below the embankment fill slopes down at an angle of 5 – 10°.

The Ingleton underslip evidenced itself with pavement cracks visible for a distance of nearly 60m. The cracks were not continuous, with circular cracks at the southern and northern ends of the slip area and mostly planar cracks in the centre of the slip area extending almost across the entire pavement width. These cracks were an ongoing maintenance problem that called for regular pavement resurfacing.

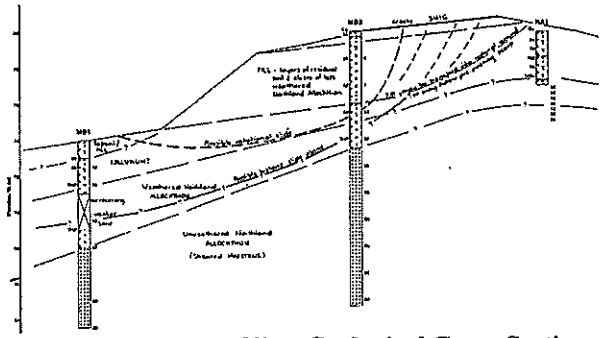

Figure 4 : Ingleton Slip : Geological Cross-Section

4.3.1 Geology

Roadside cuttings and boreholes confirmed that the site geology comprised weathered derivatives of grey siliceous shales intermixed with lenses of calcareous siltstones/fine sandstone of the Northland Allochthon (Onerahi Chaos). These materials were highly sheared with some discrete polished surfaces dipping at steep angles (30-45°).

The slope movement causing the displacement of the highway pavement was in a westward direction down slope. Hummocky ground was visible in the natural ground below the embankment and large mounds were visible some distance downslope of the highway to the stream below, indicating that the slide movement may extend to the stream. The fill embankment itself was steep (1.75H:1V) but showed no signs of internal instability. This indicated that it was sliding on shear planes within the underlying Onerahi Chaos.

Borehole investigation through the center of the slip revealed the following log.

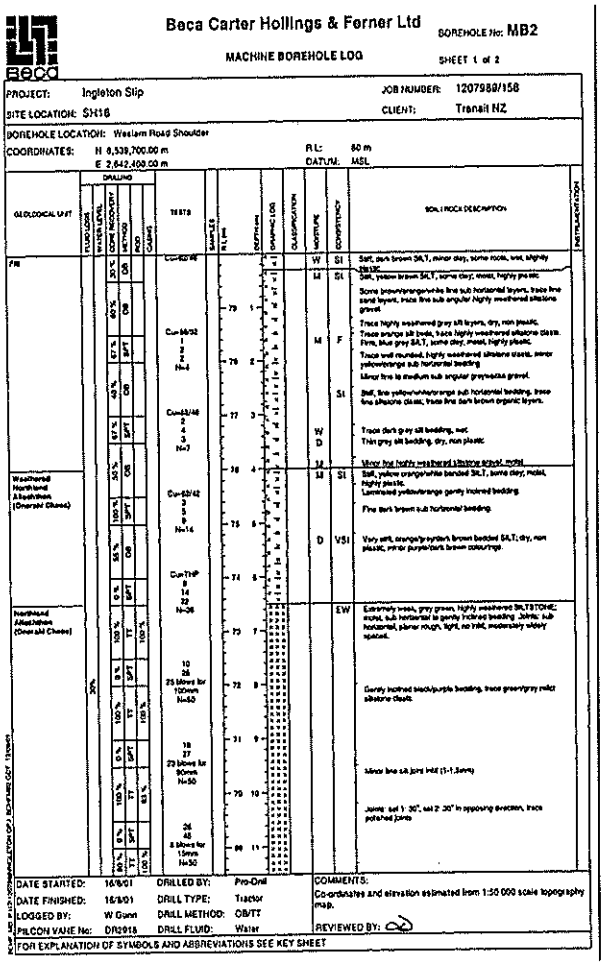

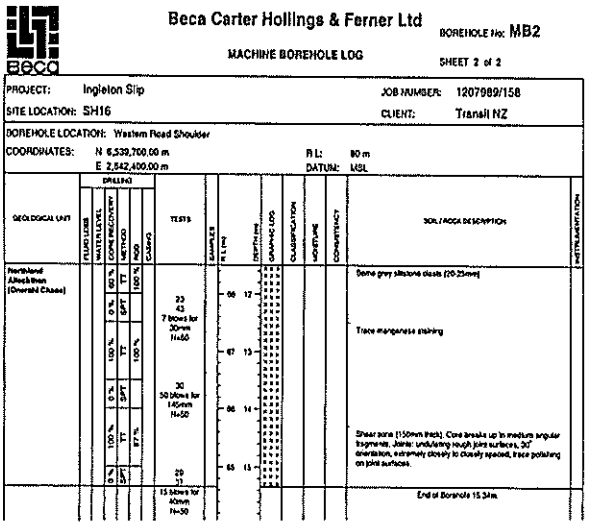

Figure 5: Borehole Log Ingleton Slip

4.3.2 Ground Water

At the time of inspection the topsoil within the paddocks adjacent to the highway was saturated with water standing in puddles within natural depressions. Water had collected in the eastern side drain below the cut batter at the northern end of the slip area. Groundwater was seeping out of the base of the pavement on the western side of the embankment.

Two piezometers were installed at the site, one on either side of the highway. Measurement of the water level in the piezometers indicated a groundwater level 1.6m below the surface on the eastern side of the highway, and 0.1m below the surface at the base of the embankment on the western side of the highway.

4.3.3 Inclinometer Monitoring

An inclinometer was installed to a depth of 15m on the western shoulder of the highway, through the embankment fill and within the centre of the slip mass. Ongoing monitoring of this inclinometer showed defined movement along a shear plane at about 6m below the ground surface. This depth of movement correlated closely to the borelog and soil strength profile as indicated by SPT testing. The inclinometer trace is shown as Figure 6 below.

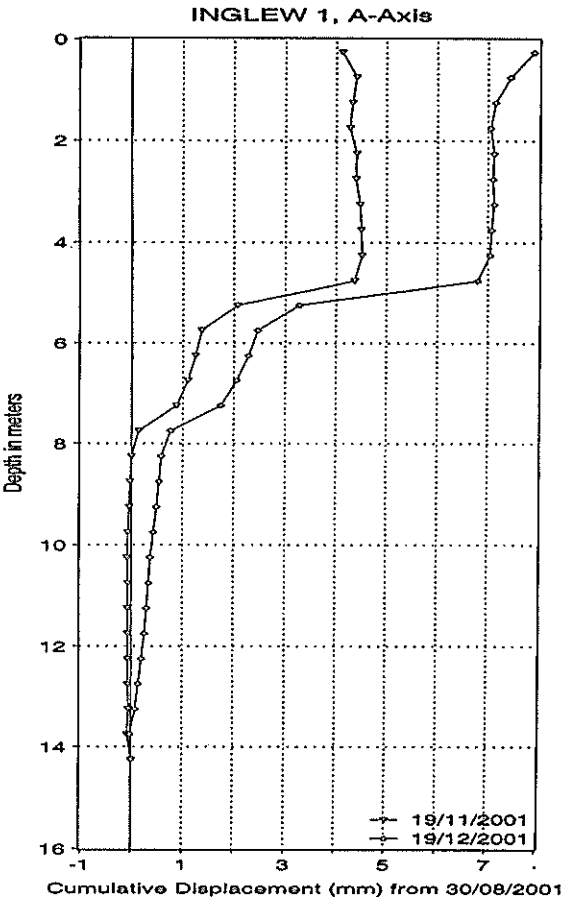

Figure 6 : Ingleton Slip : Inclinometer Trace

5 CONCLUSIONS

OC is prone to very slow creep failure along weak pre-sheared planes within the soil mass. The exact level at which the creep failure is occurring at any particular slip site may be determined by inclinometer monitoring.

Inclinometer monitoring recently carried out at J Farmer Slip and Ingleton Slip on SH16 indicates that the creep failure at each site was occurring along a shear plane close to the interface between the HW (SPT N=10) and MW (SPT N=35) Onerahi Chaos soil/rock mass.

This indicates that creep failure shear planes within OC may be generally located at the interface between the HW and MW material. As the knowledge base of inclinometer monitoring at OC slip sites grows this hypothesis may be proved and therefore in the future it may be possible to reduce the number of costly inclinometer installations at OC slip sites, and still accurately identify the slide plane, for remedial design, from SPT strength testing and borehole log information.

6 REFERENCES

1. KEAR D, WATERHOUSE B C, "Onerahi Chaos-Breccia of Northland", NZ Journal of Geology and Geophysics
2. SPORLI B & KEAR D, "Geology of Northland, accretion, allochthonous and areas at the edge of the NZ micro-continent", 1989, The Royal Society of New Zealand, Bulletin 26.
3. THOMPSON, "Geologic Map of New Zealand 1:250,000 scale, Sheet 2A, Whangarei", 1961, Institute of Geologic and Nuclear Sciences, formerly DSIR.
4. SCHOFIELD J.C, "Geologic Map of New Zealand 1:50,000 scale, Sheet Q10 & R10, Helensville and Whangaparaoa", 1989. Institute of Geologic and Nuclear Sciences, formerly DSIR.
5. EAST G R W, GEORGE A K, 2001, "Roading in Northland Allochthon Terrain – Auckland and Northland, Proceedings NZ Geotechnical Society 2001 Symposium : Engineering In Hazardous Terrain.
6. TILSLEY S C, 1998' "ALPURT Sector B1 – Silverdale to Orewa Geotechnical Report", Beca Carter Hollings and Ferner Ltd.
7. TOAN, D.V, 1980, "Report on Onerahi Chaos Breccia for Rodney District Council", Beca Carter Hollings and Ferner Ltd
8. EAST G R W, "Highway Slip Remedial Measures Within the Auckland/Northland Roading network", Proceedings NZ Geotechnical Society 1998 Symposium : Roading Geotechnics.

CORRELATIONS FOR G_{MAX} FROM THE SEISMIC CONE PENETRATION TEST (SCPT)

Terry Chang

URS Corporation

The cone penetration test (CPT) is one of most widely used and efficient methods for the geotechnical investigation of soil profiles. The cone tip resistance (q_c) and sleeve friction (f_s) values measured during the CPT can be used for soil classification and correlation with geotechnical engineering parameters such as soil strength and modulus.

The seismic cone penetration testing (SCPT) is an extension of the CPT in that geophones are installed inside the cone in order to measure shear (S) waves. Elastic theory can be used to relate the S wave velocity (V_s) to the small strain shear modulus (G_{max}). The SCPT therefore offers a quick and efficient method of estimating the G_{max} profile, which is an essential input for prediction of ground surface motion from earthquakes, and for evaluation of foundations for vibrating equipment.

This paper presents the results of the SCPT carried out at four sites. Possible correlations between the SCPT measurements of q_c and V_s are presented and discussed. Comparison is also made between the SCPT derived G_{max} profiles and the results from load-settlement monitoring of actual foundations. The results indicate that there is a general correlation between q_c and V_s and to a less extent, the correlated G_{max} is able to give rough estimates of the likely foundation settlements

1. INTRODUCTION

The dynamic shear modulus (G_{max} or G_o) is a key parameter for the analysis of soil behaviour in response to dynamic loadings from earthquakes and foundation vibrations. One quick and efficient method of measuring the seismic velocity is via the seismic cone penetration test (SCPT). The SCPT is essentially an extension of the cone penetration test (CPT), with geophones installed inside and behind the cone tip.

This paper presents the results of SCPT carried out at four onshore sites in the southwest of Western Australia (WA). Possible correlations between the SCPT measurements of q_c and V_s are presented and discussed. Comparison is also made between the SCPT derived G_{max} profiles and the results from load-settlement monitoring of actual foundations.

2. SEISMIC CPT PROCEDURES

The cone penetration test (CPT) is one of most widely used and efficient methods for the geotechnical investigation of soil profiles. The most common probe has a diameter of about 36 mm, a cone tip of 10 cm^2 and a friction sleeve area of 150 cm^2 (Campanella and Robertson, 1986). The probe is pressed down into the ground at a penetration rate of 2 cm/sec. The cone tip resistance (q_c) and sleeve friction (f_s) values measured during the conventional CPT can be used for soil classification and correlation with geotechnical engineering parameters such as soil strength and modulus.

The seismic cone penetration testing (SCPT) is an extension of the CPT in that geophones are installed inside the cone penetrometer in order to measure shear (S) waves generated at the ground surface. The CPT is briefly paused to carry out seismic tests at required depth intervals. The shear wave is created by a hammer-blow on a steel-bar pressed against the ground surface by the weight of the drill rig/truck. Individual seismic tests involve the recording of the arrival time of two opposing shear S-waves generated at the ground surface. Each seismic test (trace) is graphically compiled to create a profile of arrival times and is then used to derive a S wave velocity profile with depth. Elastic theory is then used to relate the S wave velocity (V_s) to the small strain shear modulus (G_{max} or G_o) through the following relationship:

$$G_o = G_{max} = \rho V_s^2 \qquad (1)$$

Where:

ρ = bulk density of the soil (kg/m^3)

V_s = shear velocity (m/s)

Figure 1 represents a schematic of how the seismic test is carried out. At a particular depth the CPT probing is momentarily paused and a seismic test is carried out by recording the arrival time of the seismic signal generated via a horizontal blow of an instrumented hammer across a beam on the ground surface.

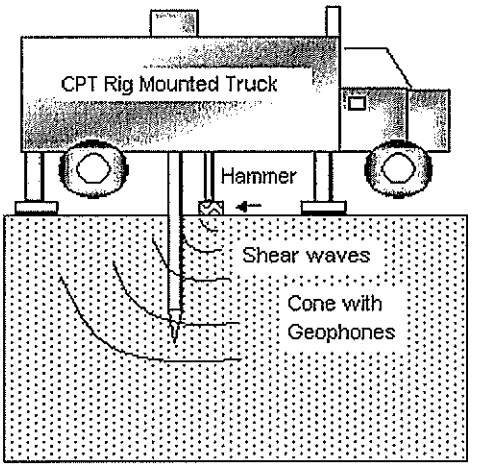

Figure 1: SCPT setup.

3. FIELD DATA

The data for this study were taken from four onshore sites located in the southwest of WA. The soils are typically loose to dense, sand to silty sand. Measured shear velocity values ranged generally from 160 m/s to 500 m/s with cone resistance values ranging from 0.5 MPa to 25 MPa. The shear velocity values are typical values for sands i.e. 100 - 500 m/s (Parasnis, 1997). The cone resistance values are typical of a loose to medium dense sand, with the sand being overconsolidated with respect to existing overburden stress. An example of typical cone resistance and shear wave velocity plot is presented in Figure 2.

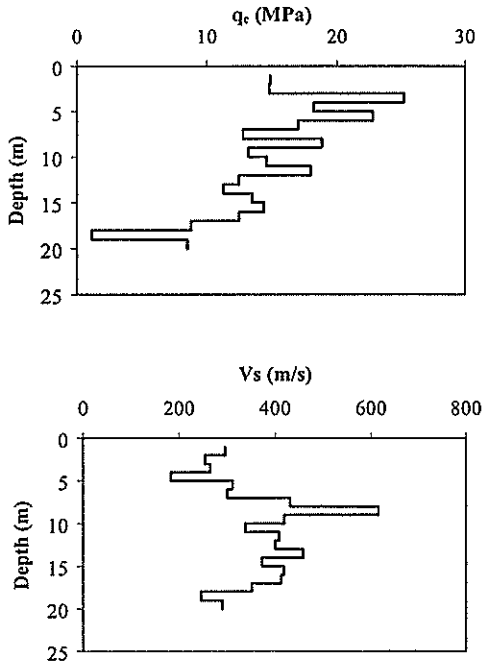

Figure 2: Typical Average Cone Resistance and Shear Wave Velocity Plot.

4. ANALYSIS AND DISCUSSION

4.1 Existing Correlations

Baldi et al (1989) have presented the following correlation between the CPT resistance and shear wave velocity:

$$V_s = 277\, q_c^{0.13}\, \sigma'^{0.27}_{vo} \quad (m/s) \qquad (2)$$

Where q_c = cone resistance (MPa)

σ'_{vo} = vertical effective stress (MPa)

Equation (2) is the correlation presented in the Australian Earthquake Manual as an empirical means of estimating shear velocity from the cone resistance of a soil.

Tanaka and Tanaka (1998) carried out SCPT on three sandy sites in Japan and found that the correlation between the shear velocity and cone resistance follow the same trend and is consistent with that proposed by Baldi et al (1989). Tanaka and Tanaka (1998) also suggested that the correlation is slightly influenced by the over-consolidated ratio.

4.2 Correlation of Measured Data

The measured cone resistance values and inferred soil densities for the four sandy WA sites are correlated with the measured shear wave velocities. This is done by plotting V_s versus q_c and using curve fitting based on the following equation (similar in form to Baldi et al, 1989):

$$V_s = k\, q_c^{a}\, \sigma'^{b}_{vo} \qquad (3)$$

Where k, a and b are constants, although their values are dependent on the given stress and velocity units adopted.

Applying Equation (3) to Equation (1) leads to:

$$G_o = \rho\, V_s^2 = \rho\, k^2\, q_c^{2a}\, \sigma'^{2b}_{vo}$$
$$= C\, q_c^{2a}\, \sigma'^{2b}_{vo} \qquad (4)$$

where $C = \rho\, k^2$

It is noted that if a+b = 0.5 then 2a+2b = 1.0, and it therefore follows that C in Equation (4) will be a dimensionless constant provided that G_o, q_c and σ'_{vo} have the same units of stress.

In order to find the appropriate constants, regression analysis was carried out on the measured shear wave velocities using the Equation (3) for various values of k, a and b. This was done through an iterative process of selecting a combination of the various constants to give the optimum correlation (R^2 value for the calculated and measured V_s). Principally different values of "a" and "b" were assumed, and a best-fit value of "k"

was derived and resulting R^2 value calculated. Some of the results are presented in Figure 3. The curve fitting that gave the highest correlation coefficient (R^2 value) was considered to be optimal. A further condition that a+b = 0.5 was imposed.

On this basis, respective "k", "a" and "b" values of 250, 0.3, and 0.2 were selected as appropriate.

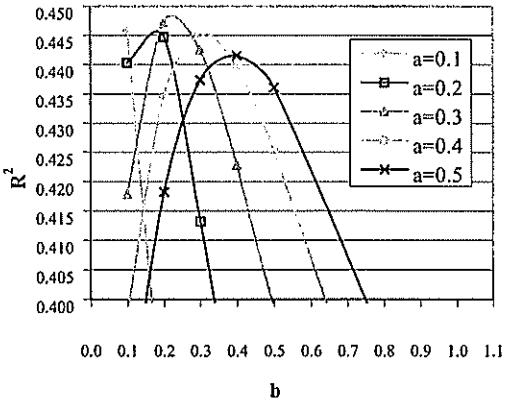

Figure 3: Regression Results (Units: Stress in MPa, Velocity in m/s)

Comparison of calculated and measured velocity values is presented on Figure 4 based on the following optimum correlation:

$$V_s = 250\ q_c^{0.3}\ \sigma'^{0.2}_{vo} \quad \text{(m/s)} \qquad (5)$$

for stress units given in MPa. The results indicate that there is a reasonable correlation between the measured cone resistance and shear velocity. The trend generally follows the relationship proposed by Baldi et al (1989).

As noted previously, Equation (5) has the added advantage that the resulting generalised G_o ($=\rho V_s^2$) expression has G_o cast in the same stress units as q_c and σ'_{vo}.

$$G_o = 125\ q_c^{0.6}\ \sigma'^{0.4}_{vo}$$
$$= C\ q_c^{0.6}\ \sigma'^{0.4}_{vo} \qquad (6)$$

where C = 125, based on $\rho = 2000$ kg/m^3

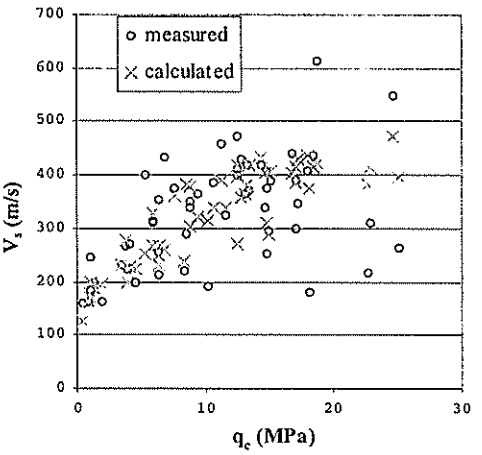

Figure 4: Measured and Calculated Shear Wave Velocities.

4.3 Stress – Strain Curves

Work carried out by Seed et al (1986) showed that the shear modulus ratio for sand, G/G_{max}, reduces as the magnitude of shear strain increases. At shear strains less than 0.001%, G is close to the G_o value. For shear strains greater than 1%, G is less than 10%G_o. The variation of the shear modulus ratio with shear strain is shown on Figure 5.

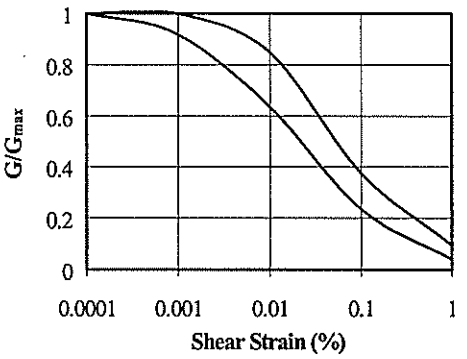

Figure 5: Variation of G/G_{max} With Shear Strain For Sand (after Seed et al., 1986)

4.4 Foundation Settlement Prediction

4.4.1 G Calculation

Figure 5 indicates that the shear modulus (G) value of a soil decreases with increasing strain level. Furthermore, foundation settlement calculation is typically based on "larger strain" static modulus values less than G_o. Massarsch (1999) have shown that the static modulus in sand is about 10 to 20% of the G_o modulus, similar to the work carried out by Seed et al (1986).

Semi-empirical correlations can be used to relate the G_{max} to the static shear modulus (G) via a reduction factor. Massarsch (1999) proposed the following reduction factors at strains of approximately 0.1%:

Soil Description	Reduction Factor
Loose Sand	0.18
Medium Dense Sand	0.15
Dense Sand	0.12

Table I: Modulus reduction factor, after Massarsch (1999).

It is noted in Figure 5 that reduction factors of less than 0.05 are possible. A suitably conservative reduction factor of 0.10 would be considered to be appropriate for typical foundation design.

4.4.2 E Calculation

The Young's modulus for sandy material can be calculated from the static shear modulus by adopting a Poisson's ratio of 0.2 (Bowles 1982):

$$E = 2(1+\upsilon)G = 2.4\ G \qquad (7)$$

These E modulus values can be incorporated into a Terzaghi one dimensional settlement analysis via:

$$m_v = (1+\nu)(1-2\nu)/(1-\nu)E$$
$$\approx 1/E \text{ (for typical } \nu \text{ for sand)} \qquad (8)$$

4.4.3 Settlement Analysis

By applying the reduction factor and equivalent Young's modulus, settlement analysis for shallow foundations at two of the WA sites was carried out. The SCPT performed at these two sites were very close to existing footings at which settlement monitoring had been carried out. For calculation purposes, the reduction factor is conservatively taken to be 0.1.

Actual and SCPT predicted settlements for footings under applied operating loads are presented in Table 2. Also presented on Table 2 is the q_c/bearing pressure ratio, indicating the severity of the loading of the soil profile. The greater this ratio is, the lower is the degree of loading with respect to *in situ* soil strength.

As seen from Table 2, the results indicate that actual settlements for site #1 are close to the values predicted without reduction factor ($G=G_{max}$, small strain response). The actual settlements for site #2, on the other hand, are equal to or greater than the predicted values with reduction factor ($G=10\%G_{max}$, large strain response). It is also evident that site #2 soil profile is more heavily loaded (about double) than site #1.

Site	Foundation Width or Diameter (m)	Bearing Pressure (kPa)	Predicted Settlement (mm)		Actual Settlement (mm)	q_c/Bearing Pressure
			Without Reduction Factor	With Reduction Factor of 0.1		
#1	W =1.8	119	0.9	8.2	0.5	115
		145	1.0	10.0	0.5	95
	W=2.4	136	1.3	12.5	0.5	88
	W=2.9	116	1.3	12.6	0.5	94
#2	D=21	217	7.0	70.0	70-90	49

Table 2: Predicted and Actual Settlements

The accuracy of the predicted settlements seems to be dependent on the choice of the adopted reduction factor as the G/G_{max} ratio is dependent on the level of strain (Figure 5). Further, the range of reduction factors proposed by Massarsch (1999) seem to be inappropriate for these two sites in that no reduction factor is required for site #1, while a reduction factor of <0.1 is required for site #2. This suggests that more data are needed in order to study how the reduction factor relates to foundation load and soil strain level.

5. CONCLUSIONS AND FURTHER WORK

This paper presented the measured shear wave velocity and cone resistance of various sites in the southwest of WA. The results appear to support the proposition that there is generally an empirical correlation between the measured cone resistance and shear wave velocity in sandy soils.

Actual shallow footing settlement was compared with those predicted using the Young's modulus values derived from the calculated G_{max} profiles based on measured q_c profiles. The results indicate the G_{max} profiles appear to give a reasonable prediction of the range of actual footing settlements. The choice of reduction factors relating G_{max} to G is dependent on the strain level and more work is needed in order to study the relationship and its application in settlement analysis.

These observations are based on limited measured data and more field data are required in order to investigate the strength of this trend over a range of soil profiles.

6. ACKNOWLEDGEMENTS

The author like to thank Dr Elio Novello (URS) for his assistance and review of this paper, Brian Edwards (Probedrill) for his technical input, and

Mrs Sharmalie Ranjithkumar for formatting and typing the manuscript.

7. REFERENCES

1. Campanella, R.G., Robertson, P.K., Gillespie, D., Seismic Cone Penetration Test, In: Proceedings of In Situ '86, A Specialty Conference; Use Of In Situ Tests In Geotechnical Engineering, American Society of Civil Engineers, United States, 1986, pp. 116-130.

2. Parasnis, D.S., Principles of Applied Geophysics, Chapman & Hall, England, 1997.

3. Baldi, G., Jamiolkowski, M., Lo Presti, D.C.F., G. and Rix, G.J., Italian Experience In Assessing Shear Wave Velocity From CPT and SPT, Proc. Discussion Session On Influence Of Local Conditions On Seismic Response, 12th. ICSMFE, Rio De Janeiro, 1989, pp. 157-168.

4. Tanaka, H., and Tanaka M., Characterization Of Sandy Soils Using CPT And DMT, Soils and Foundations, Sept. 1998, Vol. 38, No. 3, 55-65.

4. Irvine, M., and Hutchinsion, G., Australian Earthquake Engineering Manual, Techbooks, Australia, 1991.

6. Seed, H. B., Wong, R., T., Idriss, I. M., and Tokimatsu, K., Moduli and Damping Factors for Dynamic Analyses of Cohesive Soils, Journal of Geotechnical Engineering, ASCE, 1986, Vol. 112, No. GT11, pp. 1016-1032.

7. Bowles, J. E., Foundation Analysis And Design, McGraw Hill International Book Company, Japan, 1982.

8. Massarsch, K. R., Deep Compaction Of Granular Soils, Proceedings: International Lecture Series on Geotechnical Engineering and Its Development in the 21st Century, Hangzhou, PR China, January 1999.

Soil and Rock Property Relationships based on Test Results from a Site Investigation in Waitemata Series Material for the Central Motorway Junction Project in Auckland.

By Dean Coutts, Geotechnical Engineer, Sinclair Knight Merz NZ Ltd.

As part of the Scheme Assessment of options for the Central Motorway Junction Project in Auckland, a Site Investigation was carried out consisting of 39 machine boreholes and 9 test pits. The machine boreholes were cored to a depth of between 15m and 50m and the Site Investigation indicated the majority of the site was underlain by Waitemata Series material with some areas of Pleistocene Alluvium. Samples were taken from the boreholes and laboratory tests, including Unconfined Compressive Strength tests and Point Load tests, were carried out. This paper will compare the laboratory test results and SPT test results from the Site Investigation to determine if any relationships can be determined. The results presented are relevant in assessing subsurface soil and rock properties in the Auckland region where extensive detailed Site Investigations may not be possible within the budget limitations of smaller projects.

1 INTRODUCTION

As part of the Central Motorway Junction project in Auckland, Transit New Zealand commissioned Sinclair Knight Merz NZ Ltd to carry out a Scheme Assessment Report to provide options for the improvement of the Central Motorway Junction. The purpose of the project was to develop a masterplan that provides a fully effective and integrated strategy for development of the Strategic Routes in the Central Motorway Junction area, and on the associated Regional Arterial Routes that interface with this area, that will improve the overall efficiency of road transport. The Central Motorway Junction is located at the heart of the Auckland Motorway Network. Configured as a "T" interchange between the Southern/Northern Motorway and the Northwestern Motorway, it also provides a connection to the port from the south. The Central Motorway Junction combines the function of a strategic motorway interchange with local connections to the City street system. The area defined as the Central Motorway Junction is shown in Figure 1 below.

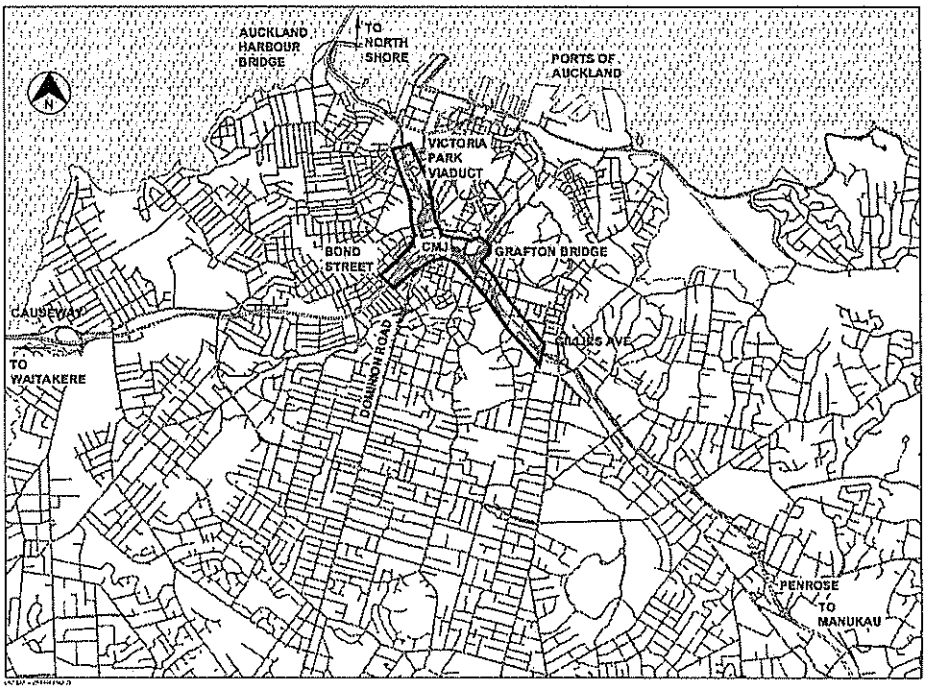

Figure 1: The location of the Central Motorway Junction (CMJ) in Auckland.

The scope of the Scheme Assessment Report included carrying out a preliminary Site Investigation of the Central Motorway Junction area, to determine the ground conditions for the Scheme Assessment design.

2 TOPOGRAPHY

The Central Motorway Junction area encompasses three individual gully systems; Grafton Gully (heading towards the port), Newton Gully/Motions Creek (containing the Northwestern Motorway) and a minor gully to the north (containing the Northern Motorway). The motorway cuts through the dividing ridges (Grafton ridge, Symonds ridge and Karangahape ridge) almost at right angles.

The Central Motorway Junction area has been subjected to considerable modification due to the earthworks placed as part of the construction of the motorway system. Fill was placed in both the Grafton and Newton gullies, and cuttings were created along the ridges. This removed much of the residual and completely weathered Waitemata material, leaving the moderately weathered to unweathered material present at subgrade level. This is the case along the Northwestern Motorway adjacent to the Newton Road overbridge, and possibly also along Ian McKinnon Drive.

3 GEOLOGY

The Central Motorway Junction area is underlain predominantly by Miocene Waitemata Group material which consists of flysch sequences comprising alternating sandstone, siltstone and mudstone layers with subordinate breccia and conglomerate, and rare limestone and quartzose sandstone.

The Waitemata Group is divided into East Coast Bays Formation and the older Paremoremo Formation. The East Coast Bays Formation consists of mudstone, siltstone and graded sandstone with interbeds of Parnell Grit and it is this formation that underlies the Central Motorway Junction area.

The younger sediments occurring in the Central Motorway Junction area are Pleistocene and Recent Alluvium comprising clay, silt, sand and gravel and some organics.

The ridges within the Central Motorway Junction area are predominantly Waitemata Group materials grading from residual soils at the surface to unweathered flysch at depth. Tuff from volcanoes such as the Domain and Mount Eden is found surficially in the area to the south of Grafton Gully on both sides of the motorway. Massive basalt flows from Mount Eden are known to occur south of Grafton Road.

4 SITE INVESTIGATION

The Site Investigation for this project, consisting of 39 machine boreholes and 9 test pits was carried out by Drillwell Exploration NZ Ltd with supervision and logging by staff from Sinclair Knight Merz. The boreholes were drilled to depths of between 15 and 50 metres. Standard penetration tests were carried out generally at 1.5 metre intervals within the fill, alluvium and residual soil and generally at 3 to 6 metre intervals within the Weathered Waitemata Rock. Core was recovered over the full length of each borehole where conditions allowed and the core was wrapped in plastic prior to being transported to Opus International Consultants Ltd Auckland Laboratory for testing. Test carried out included Unconfined Compressive Strength (UCS) tests for residually weathered soils and weathered rocks, and Point Load tests.

5 SUBSURFACE CONDITIONS

Subsurface conditions encountered during the Site Investigation included Fill, Pleistocene Alluvium, Residually Weathered Waitemata soils, Tuff, Weathered Waitemata Rock and Basalt.

Three major areas of fill were identified in the Central Motorway Junction area, between Wellington Street and Hopetoun Street, between Newton Road Bridge and Upper Queen Street, and between Symonds Street and Grafton Road at the head of Grafton Gully. The fill material consisted of uncontrolled fill and engineered fill forming road embankments.

Pleistocene Alluvium material was encountered in various locations including between Hopetoun Street and Union Street, north of the motorway adjacent to Symonds Street, and north of the Northwestern Motorway adjacent to Newton Road. The Alluvium material consisted of light grey to brown grey and orange brown clay and clayey silt with discontinuous layers of dark brown and black organic clay.

Residually Weathered Waitemata soils consisted mainly of pale brownish grey, light brown and light grey silty clay, clayey silt, and silty fine sand. Alternating moderately thick sequences of silt and sand were also encountered.

Volcanic Tuff exists south of the Southern Motorway and St Benedicts Street and Grafton Gully and overlies the Pleistocene Alluvium and Residual Waitemata material. The weathered Tuff is orange brown to light brown and consists of silt with numerous bands of reddish brown sand. The unweathered Tuff comprises sandy silt, fine-grained gravel in a sandy silt matrix and gravelly silty sand, and is light grey, hard and moderately cemented to well cemented.

The Weathered Waitemata Rock underlying the Central Motorway Junction area comprises alternating beds of sandstones, siltstones and mudstones. The Highly and Moderately Weathered Waitemata Rock is generally extremely weak to very weak and the sandstones are poorly cemented.

Pleistocene Basalt flows were encountered to the south of Boston Road and adjacent to the Southern Motorway (derived from the Mount Eden Volcano), and east of Grafton Gully (derived from the Domain Volcano). The Basalt is dark grey, massive, very strong, slightly weathered to unweathered, slightly to highly vesicular and jointed.

6 SPT, UNCONFINED COMPRESSIVE STRENGTH AND POINT LOAD TEST RESULTS AND RELATIONSHIPS

Comparisons have been made between SPT, Unconfined Compressive Strength (UCS) and Point Load test results from the Site Investigation and these relationships are shown in Figures 2 to 8 below. The relationships shown are based on test results from adjacent samples in the boreholes to ensure the results are representative of similar material with similar properties.

Figure 2 shows SPT values versus UCS test results plotted for the Pleistocene Alluvium material. Only six UCS tests were carried out on Alluvium material adjacent to SPT locations. Although a bestfit line has been fitted to the graph, there does not appear to be a significant correlation between the results from the two tests based on this small data set. This is confirmed by the correlation coefficient (a measure of whether Y values on the graph increase with X values) of –0.02. A possible reason for the low correlation is that the SPT test may be unreliable for material in the strength range of Pleistocene Alluvium. Further testing would be required to determine whether a significant relationship could be established.

Figure 3 shows SPT values versus UCS test results for Residual Waitemata material. The bestfit line on the graph has been allowed to intercept the y-axis freely rather than being forced to intercept at the x-axis. This is considered reasonable, as material with low SPT values usually will still have a measurable UCS strength. The relationship suggested by the bestfit line is given by the equation:

$$Y = 1.44 X + 56$$

where X is the SPT value and Y is the corresponding UCS value in kPa. The correlation coefficient of 0.87 indicates a reasonably strong relationship.

The same relationship of SPT and UCS test results is shown for Tuff material in Figure 4. As with Figure 2 for Alluvium material, Figure 4 does not appear to indicate a significant correlation between the results from the two tests based on this data set. The graph appears to indicate that Tuff material may have different relationships for these tests over several discrete ranges, and further testing would be required to determine whether a significant relationship exists.

In Figure 5, there appears to be a stronger relationship between SPT and UCS test results for Waitemata Weathered Rock, which is confirmed by the correlation coefficient of 0.93. The relationship suggested by the bestfit line is given by the equation:

$$Y = 7.5 X$$

where X is the SPT value and Y is the corresponding UCS value in kPa.

A reasonably strong relationship is also shown in Figure 6, a graph of SPT values versus Point Load test results for Waitemata Weathered Rock. The correlation coefficient is 0.77 and the bestfit line suggests a relationship given by the equation:

$$Y = 6 X + 435$$

where X is the SPT value and Y is the corresponding Point Load value, Qu in kPa.

However a strong relationship is not evident when the UCS test results are compared to the Point Load test results for Waitemata Weathered Rock, as indicated by a much lower correlation coefficient of 0.54. This may be due to differences in the respective test procedures, one applying a pressure over the area of the sample and one applying a point load. The variability of the layering of the Waitemata Rock material and the corresponding variations in strength is also likely to be a factor contributing to the low correlation.

There appears to be a reasonable relationship between Point Load and UCS test results for Basalt as shown in Figure 8. The correlation coefficient is 0.78 and the bestfit line suggests a relationship given by the equation:

$$Y = 330 X$$

where X is the Point Load test result, Qu in MPa and Y is the corresponding UCS value in kPa.

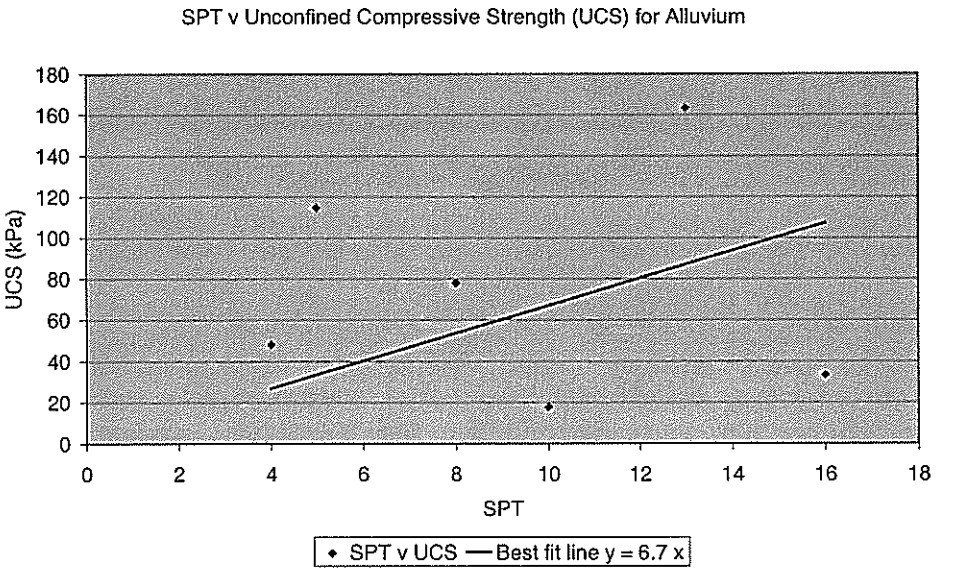

Figure 2: SPT values versus Unconfined Compressive Strength test results for Alluvium material.

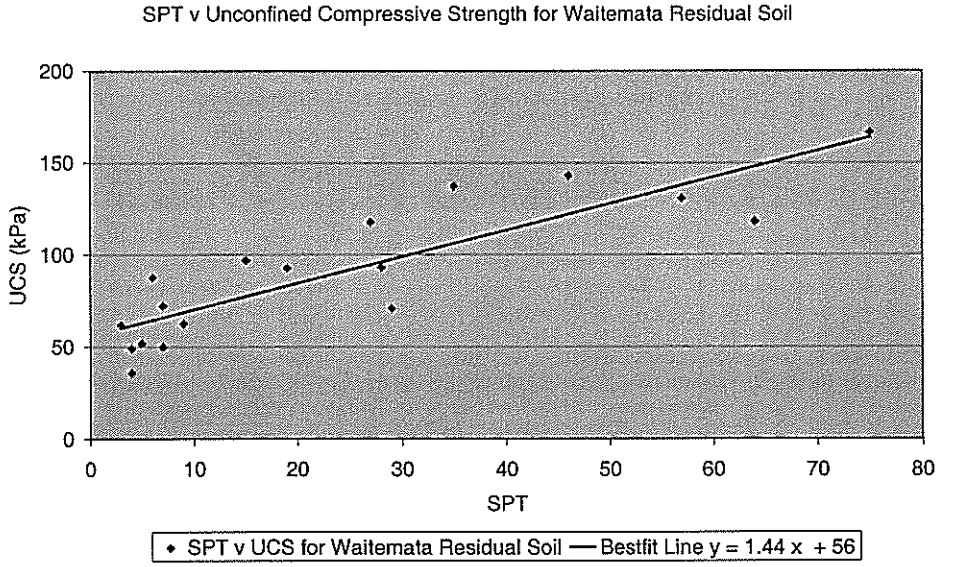

Figure 3: SPT values versus Unconfined Compressive Strength test results for Residual Waitemata material.

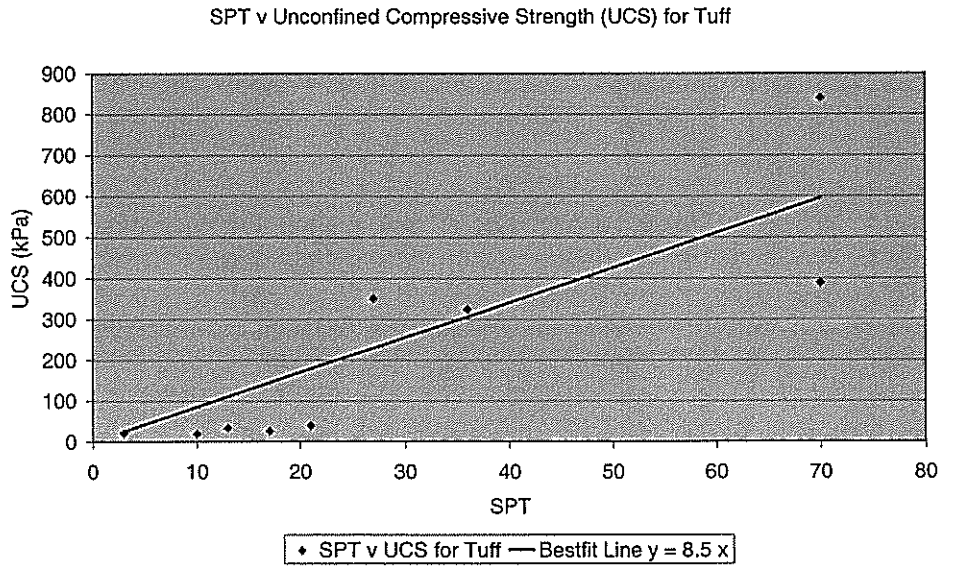

Figure 4: SPT values versus Unconfined Compressive Strength test results for Tuff material.

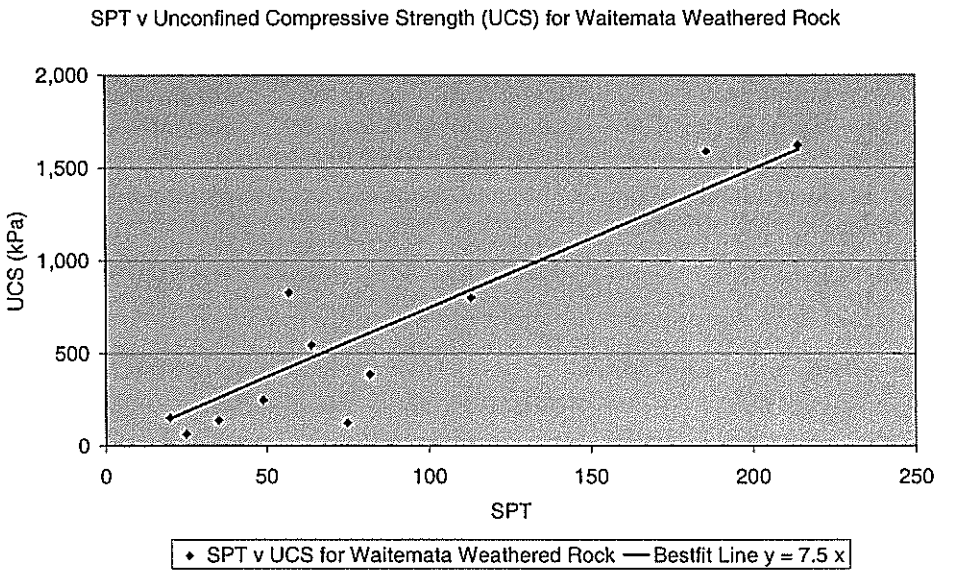

Figure 5: SPT values versus Unconfined Compressive Strength test results for Waitemata Weathered Rock.

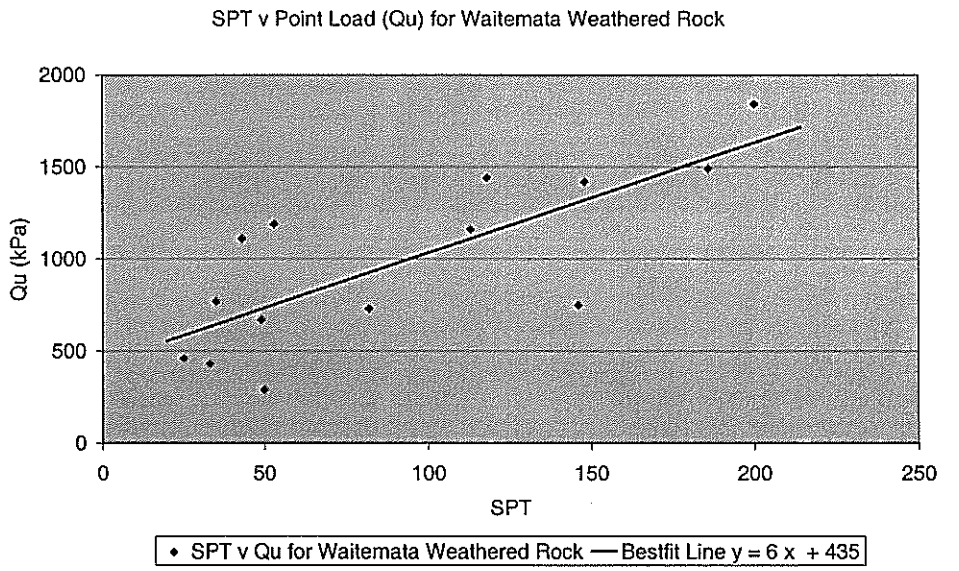

Figure 6: SPT values versus Point Load test results for Waitemata Weathered Rock.

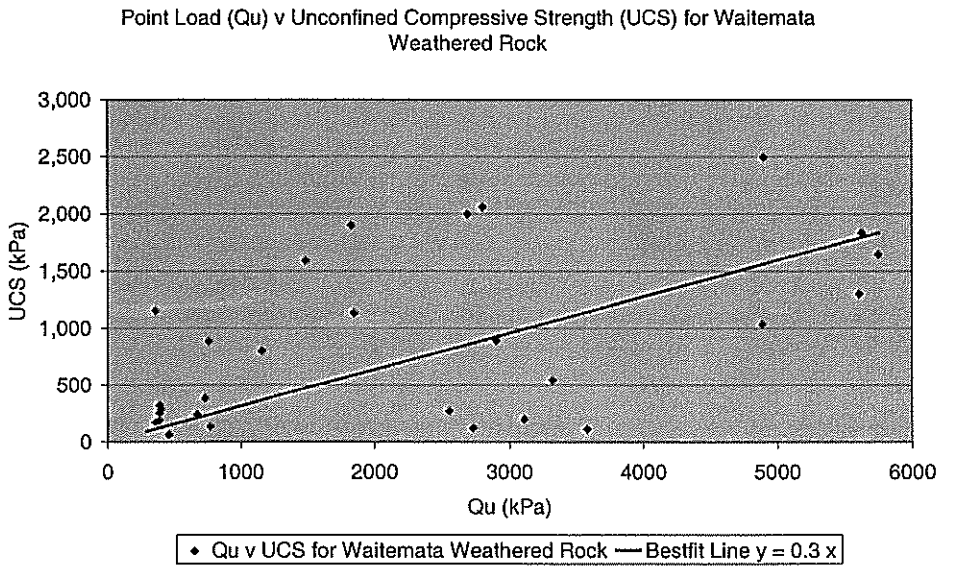

Figure 7: Point Load versus Unconfined Compressive Strength test results for Waitemata Weathered Rock.

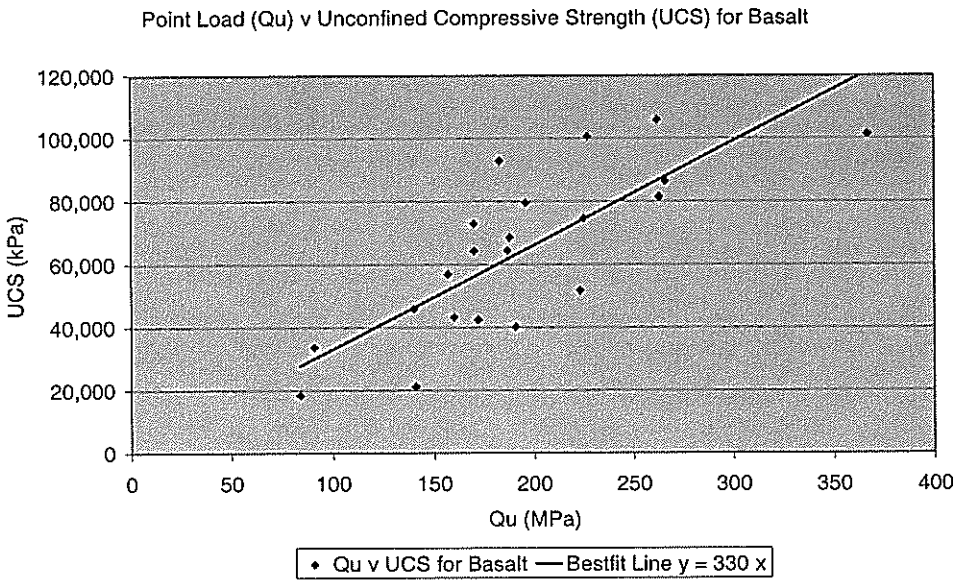

Figure 8: Point Load versus Unconfined Compressive Strength test results for Basalt.

7 CONCLUSIONS

The Site Investigation carried out for the Central Motorway Junction project in Auckland identified areas of Pleistocene Alluvium and Tuff underlain by Miocene Waitemata Group material. Basalt was also identified in the are south of Grafton Road. SPT tests, UCS tests and Point Load tests were carried out on samples from the boreholes and the relationships between these test results were examined. There appears to be a reasonable strong relationship between SPT values and UCS test results for Residual Waitemata material represented by the equation Y = 1.44 X + 56, where X is the SPT value and Y is the corresponding UCS value in kPa. There appears to be a low correlation between SPT values and UCS test results for Alluvium and Tuff material and further testing would be required to determine whether a significant relationship exists.

There also appears to be a strong relationship between SPT values and UCS test results for Waitemata Weathered Rock material represented by the equation Y = 7.5 X, where X is the SPT value and Y is the corresponding UCS value in kPa. The equation Y = 6 X + 435, where X is the SPT value and Y is the corresponding Point Load test value, Qu in kPa appears to provide a good representation of SPT values versus Point Load test values for Waitemata Weathered Rock material. However there does not appear to be a significant relationship between UCS and Point Load test results for Waitemata Weathered Rock material. This may be due to the different test procedures and the variability of the layering of the Waitemata Rock material and the corresponding variations in strength.

A reasonable relationship is evident when comparing the UCS and Point Load test results for Basalt. The relationship is given by the equation Y = 330 X where X is the Point Load test result, Qu in MPa, and Y is the corresponding UCS test value in kPa.

The relationships given above for Residual Waitemata material (SPT vests UCS), Waitemata Weathered Rock material (SPT versus UCS and SPT versus Point Load) and Basalt (Point Load versus UCS) may assist in assessing subsurface soil and rock properties in the Auckland region where extensive Site Investigations may not be possible within the budget limitations of smaller projects.

8 REFERENCES

1. Adhikary, T., "Weathering Profiles and Characteristics of Waitemata Rocks in Auckland Region". NZ Geomechanics News, December 2001, 71 –77.
2. Sinclair Knight Merz, "Interim Geotechnical Report", May 2001.
3. Sinclair Knight Merz, "Stage 2 Geotechnical Report", August 2001.

9 ACKNOWLEDGEMENTS

The author would like to thank his colleagues at Sinclair Knight Merz NZ Ltd for their assistance in summarising the test result data, Sergei Terzagi for reviewing the paper and Sinclair Knight Merz NZ Ltd for permission to publish.

10 COPYRIGHT

Aspects of Low Angle Slope Instability in Tauranga Group Sediments

STEVEN CROOK
Geotechnical Engineer, Meritec Ltd
Auckland, New Zealand

Tauranga Group sediments, comprising highly variable silt, clay and peat, form an important group of soils in Auckland, New Zealand. Two low angle slope failures in these sediments have been examined. In both cases the failed material is inferred to be variably organic silt / clay and backanalysis of first failure gives field strength parameters significantly lower than laboratory derived peak strength values. Possible reasons for this discrepancy are discussed. A number of factors, while significant, appear unable to fully explain the discrepancy. These include porewater pressures, anisotropy of the sample and manipulation of test data. The major contributing factor is concluded to be the susceptibility of these materials to contain difficult to sample very low strength beds. Suggested techniques for recognizing the potential for development of low angle failures include geological appraisal of the wider area, and identification similar organic clays with relatively high c' and low ∅' triaxial parameters.

1 INTRODUCTION

Two low angle slope failures in the Auckland region have been investigated as part of engineering projects. The failures were in soft, mainly cohesive and peaty Tauranga Group sediments and yielded low effective strength parameters on backanalyisis for first failure. In both cases the laboratory peak strength parameters of inferred failure materials are considerably in excess of those determined by backanalysis.

This paper examines possible reasons for the discrepancy between the two sets of parameters. Some techniques for recognition of potential low angle slope failures are suggested.

2 GENERAL GEOLOGY

The Tauranga Group (up to 2 million years old) is a diverse range of low energy fluvial, lacustrine and shallow marine sediments that typically blanket terraces, ridges and the broad elevated topographic surfaces that surround the Waitemata and Manukau Harbours. These sediments comprise clay, silt, sand and peat. Pumiceous silt and sand derived from rhyolitic eruptions in the Taupo Volcanic Zone is also relatively common.

3 FAILURES EXAMINED

Two low angle slope failures are examined in this paper. In each case the topography is relatively flat and inferred failure surfaces dip at low angles, typically less than 7^0. Analysis using conventional limit equilibrium methods and soil strength parameters derived from laboratory triaxial testing, gives factors of safety greater than 2.5 for initial failure on the inferred slip surfaces.

3.1 South Auckland Commercial Facility

This failure occurred on a relatively flat alluvial plain adjacent to a 6m coastal escarpment. The failure surface is inferred within soft to firm, slightly organic clay / silt at a depth of 4m – 6m. The clay / silt immediately overlies white, dense pumiceous sand (ignimbrite). A head scarp has formed up to 50m inland and the total failure area is approximately 0.3 hectares. A cross section through the failure is shown on Figure 1.

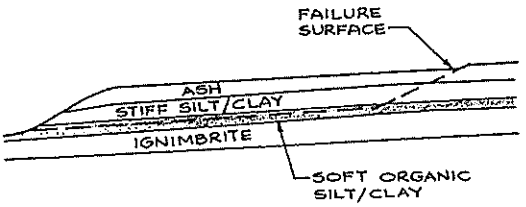

Figure 1: Geotechnical Section South Auckland Commercial Facility

Either side of the failure, the ignimbrite materials are at a higher elevation, indicating that the failure has occurred in materials that infill a former valley.

A 30 year old brick-clad house previously sited entirely within the failure, showed little sign of distress implying that post failure creep of the failed mass has been relatively minor.

3.2 North Auckland Road

The failure is in a low-lying coastal environment and is inferred to have occurred in soft to firm, slightly organic clay / silt at a depth of between about 5m and 8m, dipping at 7^0 towards the coast. The failure encompasses approximately 0.2 hectares and is currently active. The failure is shown in cross section on Figure 2.

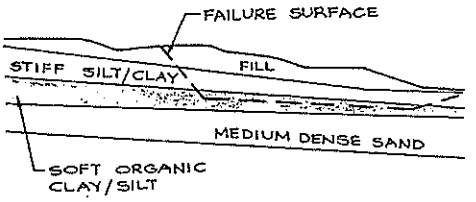

Figure 2 : Geotechnical Section North Auckland Road

It is unknown whether up to 2m of fill materials currently existing over the failure area were placed on failed or unfailed ground. Examination of early aerial photographs however suggests that the stability of the area was at least marginal prior to fill placement.

Attempts to stabilize the failure with bored horizontal drains and toe buttressing have been unsuccessful.

4 FAILURE MATERIAL CHARACTERISTICS

4.1 Material Description

The inferred failure material for both landslides is generally described as soft, black to brown, variably organic Clay and Silt, generally plastic or highly plastic. Typical of the Tauranga Group sediments, the material varies significantly with depth and is interbedded with other materials in gently dipping beds less than about 1m in thickness.

SPT N values typically are in the range of 2 to 6. Undrained shear strength measured by hand vane in pits was interpreted to be generally in the range 30 to 50 kPa.

Plasticity tests confirm that the materials are highly plastic, with plasticity index values as high as 125% recorded, although this may be partially due to organic content.

4.2 Shear Strength

Peak strengths measured in consolidated undrained triaxial tests are given in Table 1.

Table 1. Triaxial (CUP)[1] results.

Case	c'_{peak}	$\varnothing'_{peak}$
Commercial	24 kPa	13^0
Road	16 kPa[2]	13^0

1. CUP – Consolidated undrained with measurement of pore pressure
2. Averaged from two test results

5 BACKANALYSIS

Backanalyses were used to determine the field strength parameters on inferred slip planes under estimated first failure conditions. The Janbu method was selected as being an appropriate limit equilibrium technique. Pore pressure conditions were those observed from standpipe piezometers located on the sites. Table 2 gives results of the backanalyses.

Table 2. Backanalysis results.

Case	Backanalysed slip plane properties (field 'first failure' strengths)			Porewater conditions (observed)
	c'_{field}	$\varnothing'_{field}$	Dip	
Commercial	0[1]	11^0	5^0	GWL 1m below ground
Road	0[1]	11^0	7^0	GWL 2.5m below ground

1. Cohesion taken as 0 kPa for the purposes of this analysis

6 BACKANAYSIS Vs. LABORATORY DERIVED PARAMETERS

The laboratory results were used with observed pore pressures and the inferred slip surfaces, to derive theoretical factors of safety against first failure. Table 3 gives laboratory derived parameters used in the analyses and the factors of safety for first failure.

Table 3. Calculated factors of safety for first failure using laboratory parameters

Case	c'_{peak}	$\varnothing'_{peak}$	FOS for first failure
Commercial	24 kPa	13^0	4.3
Road	16 kPa	13^0	2.5

These results present some interesting questions:

- Why has first failure occurred, given that the calculated factors of safety based on laboratory testing are so high?
- If the stability analyses do not predict failure, what other evidence (if any) is available to aid prediction?

Possible answers to the first question may be broken into two categories:

i) Laboratory test results do not represent the actual field strengths. These are discussed in 6.1 below.

ii) Some other force or mechanism not modeled has acted to initiate failure. This is discussed in 6.2.

Issues relating to the second question are addressed in Section 7.

6.1 Laboratory Test Results not Representative

The discrepancies between laboratory test results and observed field strengths is a subject that is well covered in the literature, although documentation related to New Zealand conditions is somewhat limited. Discussed below are a number of factors associated with sampling, testing, and interpretation of testing that may be relevant to the field examples.

i) Samples taken for testing not representative
If the critical material occurs as a very thin layer, it is probable that it will be missed in the sampling procedure.

With the limited investigation and testing carried out (2 or 3 CUP triaxial tests for each site) in this highly variable material, there is a distinct possibility that the critical material has not been sampled and tested.

ii) Anisotropy
Laboratory strengths may differ from field strengths due to the orientation of the shear plane in the triaxial cell varying from that in the field (Chandler 1987). In these materials, where bedding is approximately parallel to the inferred failure surfaces, this effect may be significant.

iii) Testing and interpretation
Triaxial test results for the two failures were published with the Mohr Coulomb envelopes fitted by least squares regression within a stress range of 50 kPa to 300 kPa. Of the two failures examined, the maximum effective vertical stress at the failure surface was estimated to be in the order of 60 kPa. As shown in Figure 3, the straight-line regression may have overestimated cohesion in the working stress range (Fell, Jeffery 1987). In addition, it is possible that multistage testing carried out for the samples has given lower strengths for final stage samples that have been 'failed' in the previous stages. This may have further overestimated working stress cohesion.

Although the above factors are likely to have contributed to elevated laboratory strength parameters, the overall effect is not expected to be overly significant. This is because the failure surfaces are approximately parallel with the ground surface and are therefore at a uniform effective stress level concurrent with the 50 kPa Mohr Circle. In all cases the 50 kPa Mohrs Circle was reasonably close to the failure envelopes given by the regression analysis.

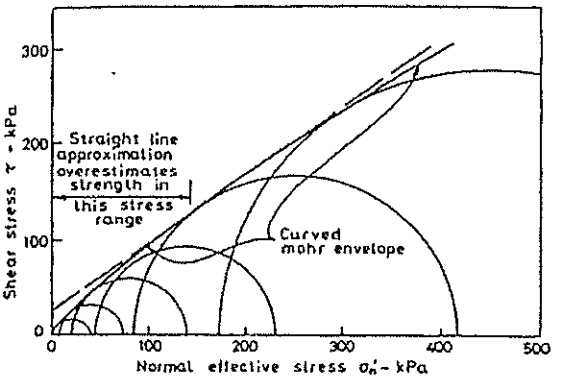

Figure 3 : Effect of least squares regression (from Fell, Jeffery 1987)

6.2 Forces or Mechanisms not Modeled

i) Failure on pre existing planes
A possible mechanism for the development of the slips is that failure occurred along a weakened zone that formed under significantly different topographical and geological conditions, perhaps as a result of tectonic folding or as a part of a completely different landform. This plane of weakness was later exposed when natural erosion processes altered the landform to create conditions for failure on the pre existing surface.

This scenario is possible for both failures examined, however given that the failed materials are shallow and relatively recent in geological terms, it seems unlikely that failure surfaces have been formed by tectonic folding or as a result significantly different topography.

ii) Porewater conditions
There is a possibility that elevated porewater pressures acted to initiate failure. These elevated porewater pressures may have resulted from a particularly prolonged period of heavy rainfall, or from pre existing surface or groundwater regimes, which have been modified by erosion processes or human activity.

Removal of material to expose a permeable layer can result in increased porewater exit gradients at a slope toe as shown in Figure 4 (Lefebvre 1996). This will tend to destabilize the slope toe.

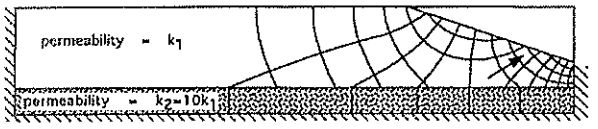

Figure 4 : Effect of exposing permeable layer at base of slope (Lefebvre 1996)

Either porewater case is applicable to the analysed slopes. The commercial facility failure has formed in a buried valley, and elevated porewater pressures could be expected as a result of previously established seepage paths becoming blocked by sedimentation. On excavation of the failure, strong seepage indicative of semi artesian pressures was noted. This was not previously revealed by standpipe piezometers. The topography however is low lying and this, together with the relatively low permeability materials, limits the available head that may be applied to induce theoretical failure.

Both failures have a suitable ground profile for elevated groundwater exit gradients at the toe, however this effect alone would be expected to destabilise the toe area only.

While both of these porewater conditions have probably contributed to initial failure they do not, on their own, provide a sufficient destabilizing force to initiate failure in an analysis that uses laboratory parameters.

iii) Seismic Events

Past seismic events may have initiated the slope failures.

Static analyses were carried to determine the horizontal acceleration required to initiate failure using the laboratory parameters. Horizontal accelerations of 0.6g were required for the commercial facility and 0.25g for the road.

Horizontal accelerations of 0.6g are considered unlikely to have occurred in this region of relatively low sismicity.

iv) Progressive or Retrogressive Failure

This is also a subject well covered in the literature (e.g. Chandler 1984, Fell, Jeffery 1987), although documented New Zealand examples appear rare. Both mechanisms essentially involve initiation of failure somewhere in the slope, commonly at the toe due to high stress concentration or erosion. The failed portion of the slope is sufficiently mobilized to develop softened or residual strength on that part of the failure surface, and to remove support for adjacent intact ground. Failure then progresses to other sections of the slope and in this way full failure can be developed at residual strength.

For this mechanism to apply to the two slips, the failure material would need to be capable of demonstrating a marked difference between peak and residual strengths. Lupini (Lupini, Skinner, Vaughan 1981) suggests that soils with a clay fraction greater than 30% have the potential to demonstrate such behavior. Chandler has shown that high plasticity clays have a tendency to show larger differences between peak and residual strengths, especially where the plasticity index is greater than 40% (Chandler 1984).

Based on the above it is considered that the failure materials examined have the potential to develop a moderate degree of sensitivity.

The potential for progressive / retrogressive failure mechanisms to develop in this material is however unclear and further investigation, testing, and perhaps more involved analyses would need to be carried out to explore this possibility.

7.0 PREDICTION OF FIRST FAILURE

For a practicing geotechnical engineer the design of engineering works in ground affected by past failure can be relatively straight forward: once the failure is identified, backanlysis parameters are used in further design work. The question arises however, as to how the potential for failure can be identified in unfailed ground that otherwise has precursor conditions that could lead to failure.

Both the porewater and earthquake mechanisms can be reasonably predicted and modeled. Correct fitting of the Mohr Coulomb envelope can be readily carried out and anisotropy effects can also be checked, although with greater difficulty.

Problems associated with representative sampling and testing remain. Given the highly variable nature of the Tauranga Group soils, a great deal of sampling and testing would be required to provide assurance that the most critical soils have been tested for any particular project.

This problem highlights the need to implement a range of investigative techniques, in addition to sampling and testing, to ensure confident assessment of stability in unfailed ground.

The following are some suggested techniques for recognizing the potential for low angle slope failures in Tauranga Group materials.

i) Engineering Geological Review, Aerial Mapping and Investigation Outside the Subject Area

An engineering geological review in combination with aerial mapping may help to identify any low angle failures near the subject area. In the event that ground conditions in these failures can be identified, correlation with ground conditions in the

subject area and other areas of unfailed ground may assist in identifying susceptible materials.

In the road project, Meritec were fortunate to have geotechnical information for other nearby areas in both failed and unfailed ground. It appears that the potential for low angle failure is enhanced in these slightly organic plastic clays.

ii) Identification of High c', Low ∅' Materials

In both slides, triaxial test results in the organic clays gave relatively high effective cohesion values and low effective angles of internal friction. Testing for the road project enabled comparison of triaxial parameters for both failed and unfailed ground. The tests with high c', low ∅' results were either in failed ground or in unfailed ground in the immediate vicinity of existing failures.

Although speculative and based on limited data from these two cases, it is possible that for these soft organic clays, high c', low ∅' triaxial test results are indicative of a potential for low angle slope failure.

Furthermore, in both cases the peak ∅' values given by laboratory testing were similar to backanalysed values. Where similar materials are encountered therefore, it may be appropriate to analyse a number of potential low angle failure planes using 'lower bound' parameters. In the first instance these could be estimated by ignoring effective cohesion and adopting the laboratory friction angle. This analytical approach is consistent with current practice.

If such modified parameters give a factor of safety of 1 or greater, design of subsequent works using these parameters may be appropriate.

If the factor of safety is less than 1, then the slope may need to be considered as marginal for the possibility of low angle failure.

iii) Design for no 'Net Destabilising Effect' in Suspect Materials

In suspect areas, design of engineering works in such a way that no net destabilizing force is applied to the subject area may be appropriate.

8.0 CONCLUSIONS

The potential for low angle slope failures in Tauranga Group sediments appears associated with soft slightly organic clay beds in both failures examined. In both cases analysis using laboratory peak strengths gave factors of safety well in excess of 1.

The discrepancy between laboratory peak strengths and backanlysed first failure parameters may be due to a combination of factors, however the sampling of non critical materials appear to be primary. In that regard, thin beds of soft materials are difficult to sample and test. As such beds can be expected in these bedded Tauranga Group sediments, there is a distinct possibility that critical materials are missed in the sampling and testing process.

Techniques for recognizing the potential for the development of low angle failures include geological appraisal of the wider area and identification of organic clays with relatively high effective cohesion intercepts and low effective angles of internal friction under triaxial testing.

This paper is based on very limited data and much further work is needed to establish the validity of opinions expressed here. The author would welcome any comments from other workers who have investigated low angle slope failures in Tauranga Group sediments or similar materials, and perhaps have formed their own views on the failure formation and recognition techniques.

10 REFERENCES

1. CHANDLER, R.J., "Field behavior of clay slopes", 1987, Imperial College course notes.
2. FELL, R., JEFFERY, R.P., "Determination of drained shear strength for slope stability analysis", 1987, Soil Slope Instability and Stabilisation, Proc. of extension course on soil slope instability and stabilisation, 30 Nov – 2 Dec 1987.
3. LEFEBVRE, G., "Soft sensitive clays", 1996, Landslides, investigation and mitigation, U.S. Transportation Research Board special report 247.
4. LUPINI, J.F., SKINNER, A.E., VAUGHAN, P.R., "The drained residual strength of cohesive soils", 1981, Geotechnique 31
5. CHANDLER, R.J., "Recent European experience of landslides in over consolidated clays and soft rocks", 1984, 4th Int. Symp. On Landslides Vol. 1, 61 - 68

Strength – Strain Behaviour of Geosynthetic Reinforced Soils

Craig Davidson
Meritec Ltd
Auckland, New Zealand

This paper compares the strain-mobilised shear resistance of cohesive soils to that of a non-cohesive soil and the implication for construction of Geosynthetic Reinforced Soil (GRS) walls using cohesive fill materials. Results of laboratory tests indicate that cohesive materials are likely to require significantly greater strains to mobilise their peak shear resistance. The increased strain requirement for cohesive soils is likely to result in greater wall deformations than have typically been measured in GRS walls constructed with granular fill material. GRS designers must ensure that ϕ_{design} (the design friction angle selected for the reinforced backfill) is compatible with the reinforcement and that wall deflections are checked under both serviceability and ultimate limit state conditions when using cohesive fill materials. Specific testing of cohesive materials to accurately establish ϕ_{design} is recommended prior to construction of GRS structures where limitations are placed on the allowable magnitude of strain deformation.

1 Introduction

The past 25 years have seen significant advances in the knowledge and understanding of the behaviour of Geosynthetic Reinforced Soil (GRS) structures. However, in common with many aspects of geotechnical engineering, a complete understanding of the behaviour of GRS structures is yet to be achieved.

In New Zealand the majority of engineering problems addressed by the use of GRS structures have involved sites with cohesive soils. Construction of GRS walls at these sites typically involves excavation of an existing slope and construction of a GRS block from imported cohesionless materials. Considerable benefits can therefore be achieved if excavated cohesive materials are re-used in the construction of the GRS block. The potential savings are likely to result in GRS structures being more competitive compared to alternative forms of stabilisation works such as timber pole walls.

This paper considers some of the issues associated with the use of cohesive fill materials in GRS structures with particular focus on the issue of strain deformations. The paper incorporates results of laboratory testing on cohesive soils undertaken as part of my Masters research (Davidson 1999).

2 GRS Theory

The modern science of soil reinforcement was developed by the Frenchman Henri Vidal in the early nineteen sixties. Vidal observed that grains of sand could be arranged at an angle greater than the angle of repose with the aid of pine needles for reinforcement. The discovery, although more by chance than by scientific investigation, had a profound effect in the area of slope stabilisation, and has led to soil reinforcement becoming a commonly used technique throughout the world.

The principal of GRS can be considered analogous to that of reinforced concrete. In the latter case the reinforcement is bonded to the concrete, whereas in the former the reinforcement is 'bonded' to the soil to provide an enhancement in overall strength. Jones (1996) describes the interaction mechanism diagrammatically (Figure 1). The figure shows the individual particles 'tied' together by the reinforcement, producing a form of apparent cohesion.

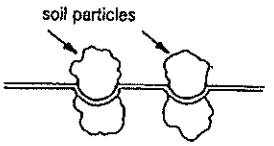

Figure 1 Diagrammatic representation of reinforced soil (after Jones (1996))

The action and function of GRS can be simply understood with reference to Figure 2. If a vertical load is applied to the element, then the element will compress vertically (δ_v), as well as strain laterally (δ_h). If however a layer of reinforcement is added to the soil element, provided there is adequate adhesion or interaction between the reinforcement and the soil, and that the reinforcement is sufficiently stiff, then the soil will be restrained against lateral movement by a force equivalent to the at-rest pressure ($k_o\sigma_v$).

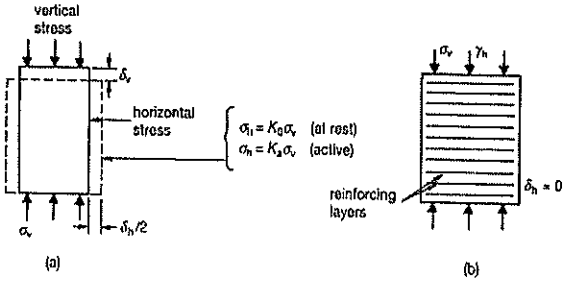

Figure 2 (a) Soil; (b) soil and reinforcement (after Jones (1996)).

For the at-rest pressure state, the stress circle experienced by the reinforced soil is always below the Mohr-Coulomb failure plane (Figure 3). Consequently, failure can only occur within the GRS structure if

either the adhesion between the reinforcement and the soil fails or the reinforcement breaks.

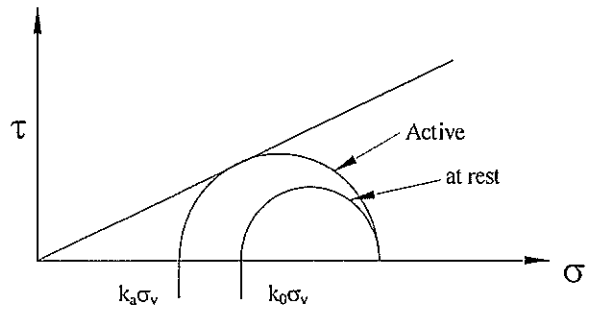

Figure 3 Stress state in soil.

In addition, the overall strength improvement due to the reinforcement depends on the magnitude of the tensile force mobilised in the reinforcement. This is governed by two main mechanisms.

1. The bond between the soil and the reinforcement, developed through frictional shear mechanisms, ultimately limits the force that a strong reinforcement layer can carry.
2. The reinforcement stiffness influences the soil shear deformation required to mobilise the reinforcement force.

The tensile strain in the reinforcement is considered the same as the strain in the adjacent soil due to the interlock ability of the reinforcement with the soil, (Jewell 1996).

Given that the reinforcement and the soil have different stress strain relationships, it is important that consideration be given to the magnitude of the tensile strains that will develop in both the soil and the reinforcement at the point of equilibrium. This ensures that:

1. The equilibrium of the structure can be reached within acceptable deformations;
2. The design values selected for the reinforcement force and the soil shearing resistance can realistically be mobilised together.

According to Jewell (1996) the key factor in GRS design is the relationship at the design loading conditions between the mobilised shearing resistance of the soil (ϕ_{mob}) and the maximum allowable tensile strain (ε_3) in the structure.

The equilibrium of the reinforced soil structure can be investigated by way of a compatibility curve (Jewell 1985), where it is assumed that the tensile strain in the reinforcement is equal to the strain in the soil in the direction of the reinforcement.

A compatibility curve (Figure 4) is produced by considering a structure constructed and held in equilibrium by imaginary external forces. The structure would exhibit zero strain and hence correspond to a situation of at-rest earth pressure in the soil and zero force in the reinforcement. If the imaginary supports were removed, deformation and strains would develop. The required reinforcement force steadily drops to a minimum value corresponding to the peak shear resistance of the soil.

Conversely, the available force provided by the reinforcement steadily increases as the tensile strain develops in the soil and hence in the grid. The rate of increase in the available force is dependent on the stiffness properties of the reinforcement as well as the number of layers that intersect the potential failure surface. Equilibrium is reached when the required and available forces converge.

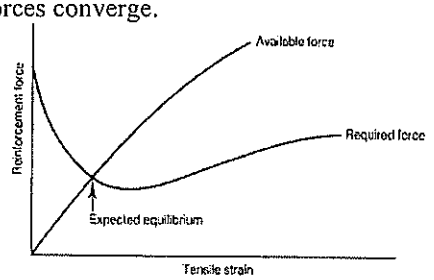

Figure 4 Compatibility curve for determining the equilibrium in reinforced soil (after Jewell (1985))

It is clear therefore that due consideration must be given to the strength/strain properties of the proposed backfill material to ensure that the design friction angle can be mobilised within the allowable strain constraints of the structure.

3 Mobilisation of Soil Strength

Stress paths, in conjunction with the Mohr-Coulomb failure envelope, are typically used to define the *peak strength* parameters of a soil. They do not, however, provide any real information regarding the stress/strain characteristics of a soil, nor do they provide information regarding the available strength parameters of the soil prior to failure.

In order to understand the strength/strain relationship of a soil prior to failure, in particular the strain mobilisation of the c' and ϕ' parameters, an interpretation procedure similar to that used by Schmertmann (1960) was applied to the laboratory test data.

The Cohesion-Friction-Strain technique (CFS) enables measurement of the mobilisation of c' and ϕ' with strain. The procedure is based on the assumption that the Mohr-Coulomb criterion can be applied to stress states prior to failure.

The CFS technique involves a process of linear interpolation of triaxial test data to obtain the p' and q co-ordinates for positions of equal strain. The p' and q co-ordinates are then plotted for the respective strain increments and a linear failure envelope applied to the

results using a least-squares fit. The cohesion intercept and friction angle is calculated from the intercept and gradient of the least squares line.

The technique adopted in the CFS interpretation procedure is illustrated graphically in Figure 5. The figure displays lines of equal lateral strain generated by a process of linear interpolation of the p' and q test data to obtain the appropriate values at the required strain increments. The cohesion intercept and friction angle was then calculated from the intercept and gradient of the line at the various strain increments.

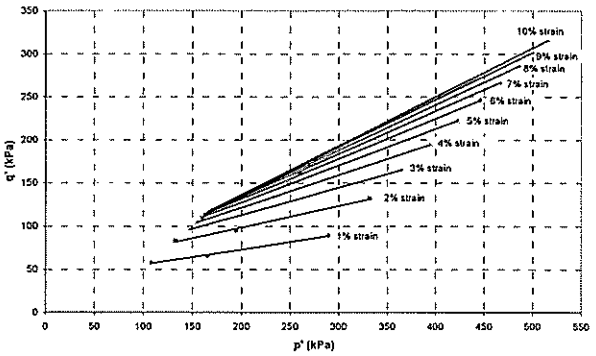

Figure 5 – CFS Interpretation Procedure

The strains denoted on the figure are lateral strains and not the more conventionally plotted axial strains. The use of lateral strain is an attempt to more accurately model the soil deformation behaviour in a GRS structure. Lateral strains for the laboratory tests are defined by:

Lateral strain $$\varepsilon_L = \frac{D_i - D_0}{D_0}$$

Where D_0 = initial diameter of specimen
D_i = adjusted specimen diameter where normal area corrections were applied to the sample.

4 Laboratory Testing Program

4.1 Samples

Four material types were tested during the course of the research (Davidson 1999). Three are from the Auckland urban area and are referred to geologically as Waitamata Group materials. The forth sample, referred to geologically as Taranaki Ash, is from Egmont Village on the slope of Mt Taranaki.

In addition to the four soils, data was obtained from testing carried out on quartz sand by Wesley et al. (1999).

4.2 Scope of Testing

Compaction and classification tests were carried out on the four soils. Based on the results of the compaction test, specimens were prepared at optimum water content and maximum dry density for triaxial testing.

5 RESULTS

5.1 Compaction and Classification Tests

Results of the compaction tests and classification tests are presented in Tables 1 and 2 respectively.

Table 1 Compaction tests

Material	Natural W/C (%)	Optimum W/C (%)	Maximum d.d. (kN/m^3)
Al-Purt	49.5	29.5	1370
Henderson	45.5	32	1392
Shore	26.2	21.7	1585
Taranaki	61.5	49	1027

Table 2 Classification tests

Material	Atterberg Limits		
	LL	PL	PI
Al-Purt	65	32	33
Henderson	84	27	57
Shore	Non - Plastic		
Taranaki	104	60	44

5.2 Triaxial Tests

Results of the triaxial tests for the Al-Purt soil and the Wesley et al (1999) Quartz sand are shown on Figures 6 to 8. The results of the remaining three soils illustrate similar trends.

Figures 6 and 7 show the mobilisation of shear resistance with strain for the Al-Purt and Quartz sand samples respectively. A key feature is the strain required to mobilise the peak strength of the material. At 2% strain (similar to that mobilised in GRS walls), the quartz samples have typically mobilised greater than 80% of their available shear resistance. In contrast, the Al-Purt sample mobilised less than 50% of peak resistance at the corresponding strain level. Likewise at 5% strain, the Quartz sample mobilised greater than 95% of available shear resistance compared to less than 70% for the Al-Purt sample.

Figure 8 illustrates the mobilisation of frictional resistance (ϕ') with strain for the Quartz sand and Al-Purt samples using the CFS interpretation procedure. Of note from the figure is the magnitude of strain required to mobilise the peak friction angle in the respective materials. The Quartz sand sample required less than 2% strain to mobilise over 90% of its peak frictional resistance. In constrast, the Al-Purt sample typically required in excess of 6% strain to mobilise 90% of its peak frictional resistance.

The development of effective cohesion with strain for all materials tested was for the peak effective cohesive strength to be mobilised rapidly (typically <1-2% strain) followed by a steady reduction at post peak strains.

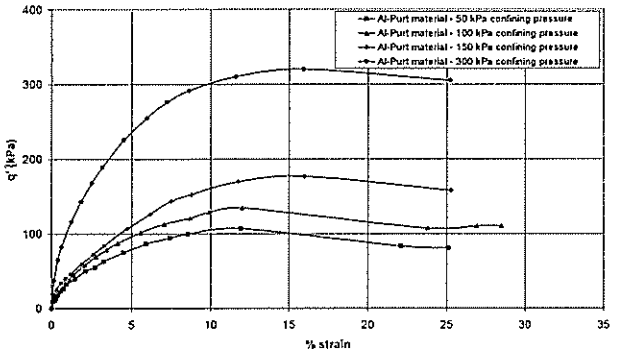

Figure 6 q vs. % Strain (Al-Purt Material)

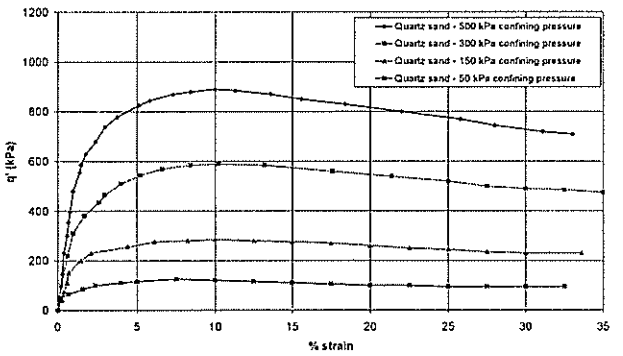

Figure 7 q vs. % Strain (Quartz Material)

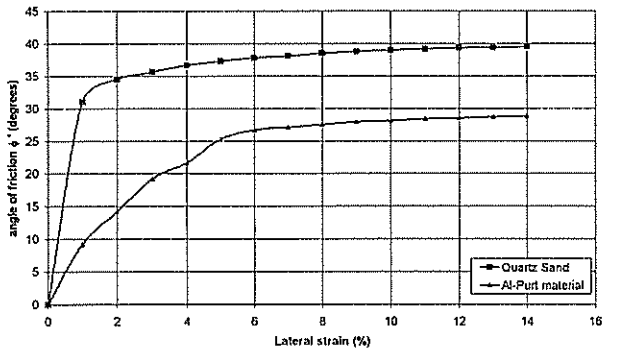

Figure 8 Mobilisation of ϕ' with lateral Strain

6 Discussion

6.1 Strain Compatibility

The triaxial test results highlight that mobilisation of the available shear resistance of the cohesive Al-Purt material is significantly more strain dependant than that of the cohesionless Quartz sand i.e. significantly more strain is required to mobilise the shear resistance in the Al-Purt material than the Quartz sand.

As discussed previously, a fundamental assumption in the design of GRS structures is that strains in reinforcement are equal to strains in the adjacent soil. Yogarajah (1993) reports that the strains generated in the reinforcing elements during the construction phase are typically between 1-2%. Therefore, to ensure strain compatibility between the reinforcement and the soil, the GRS designer must adopt a friction angle that can be mobilised within the range of allowable strains in the GRS structure.

Historically, GRS structures have primarily been constructed with compacted granular materials that generally require small strains to mobilise their peak frictional shear strength. Consequently the safety factors employed in the design process appear to have been sufficient to avoid the need for direct consideration of the strain issue in the design procedure.

This use of granular materials appears to have found its way into the guidelines and recommendations of many codes of practice. For example, BS8006, (1995) requires a cohesionless fill with an effective friction angle greater than 25° and with no more than 15% of the material to be less than 63μm.

With the increasing cost of quality granular fill and construction of reinforced earth structures in areas with limited local rock material, there is increased pressure to use 'poorer quality' cohesive fill materials. This practise has developed to the extent that cohesive fills are now used in the construction of walls in excess of nine metres in height (McClymonts Road, Albany).

The shift towards cohesive materials appears to have occurred without the recognition or understanding that cohesive materials typically display significantly differently strength/strain behaviour compared to cohesionless soils. Invariably little attempt is therefore made in the design process to consider the issue of strain compatibility between the reinforcement and fill material, and little consideration is given to the likely post construction deformations that will occur in the structure.

This issue of likely wall deformations was considered in a paper by Wesley (2001). The paper presented results of a finite element study of a hypothetical wall, 6m high with properties and spacing of geogrid reinforcement typical of many GRS walls. The results, presented in Figure 9 are for a wall with a "soft" facing similar to that of expected from a wall constructed with "Keystone" segmental facing.

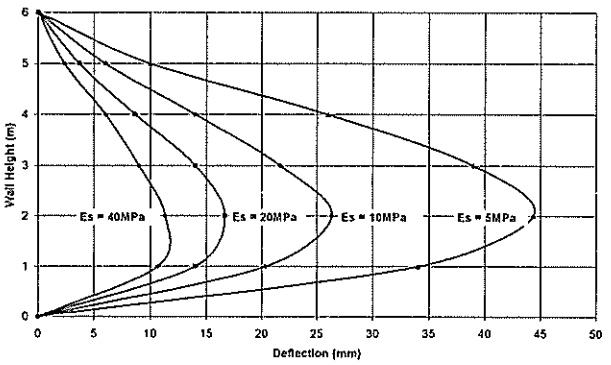

Figure 9 Influence of Soil Modulus on Deflection

The figure illustrates that the magnitude of wall deformation is related in part to the Young's Modulus (E_s) of the backfill material. Young's Modulus at 1% strain for the Al-Purt material (confining stress of 150kPa) is around 5MPa. This compares to around 25MPa for the Quartz sand at the corresponding confinement stress and strain level. Based on the calculated Young's Moduli, the figure illustrates that deformation of a wall constructed with the Al-Purt material is likely to be greater than three times that of a wall constructed with the Quartz sand.

6.2 Construction Pore Pressures

A further issue associated with the use of cohesive fill materials that also appears to be neglected in the design of GRS structures, is the issue of construction pore pressures. Most clays in the North Island have natural water contents considerably higher than their optimum water content. Therefore, unless such materials are dried back sufficiently prior to compaction there is a significant risk of excess pore pressures developing during construction.

It is generally understood that, provided fills are compacted at or below optimum water content, the likelihood of significant pore pressures developing is small. However, no systematic studies have been undertaken to verify this. Consideration should therefore be given to this issue in the design of GRS walls using cohesive fill.

6.3 Effective Cohesion Intercept

The results of the mobilisation of the apparent cohesion intercept with strain indicate that the peak effective cohesion intercept is mobilised rapidly (typically <1-2% strain) followed by a steady reduction at post peak strains.

Cohesive resistance is mobilised rapidly in comparison to the frictional resistance, hence it typically provides the majority of a cohesive soils shear resistance at low strains. It is however generally accepted in the design of GRS structures that the cohesion intercept (c') be ignored. This approach, although somewhat conservative, provides an additional element of security in the design process.

7 CONCLUSIONS

- Results of laboratory testing indicate that cohesive materials require significantly larger strains to mobilise their shear resistance than cohesionless materials. The application of a universal strength reduction factor to cohesive and cohesionless materials alike is not considered appropriate.
- Designers of GRS structures need to ensure that ϕ_{design} (the design friction angle selected for the reinforced backfill) is compatible with the reinforcement.
- Specific testing is recommended when constructing GRS walls with cohesive fill materials to determine the appropriate ϕ_{design}.
- The CFS interpretation procedure appears to provide a suitable method of assessing the frictional resistance of a material at strains prior to failure and therefore provides a suitable means assessing ϕ_{design} for GRS structures.
- Wall deflections should be checked under serviceability and limit state conditions as a matter of course when using cohesive fill materials.
- The potential for generation of construction pore pressures during fill compaction should be considered in the design process.

8 REFERENCES

1. Davidson, D. C. (1999) *'Strength-Strain Behaviour of Reinforced Earth Soils'* Masters Thesis, University of Auckland.
2. Jewell, R.A. (1996) *'Soil Reinforcement with Geotextiles'* Ciria Special Publication 123. Thomas Telford Publishing.
3. Jones, C.J.F.P. (1996). *'Earth Reinforcement and Soil Structures'* Thomas Telford Publishing.
4. Jewell, R.A. (1985). *'Material properties for the design of geotextile reinforced slopes.'* Geotextiles and Geomembranes, Vol. 2 83-109.
5. Schmertmann, J and Osterberg (1960). *'An experimental study of the development of cohesion and friction with axial strain in saturated cohesive soils'*, Proceedings of the Research Conference on Shear Strength of Cohesive Soils, Soil Mechanics and Foundations Division, ASCE, Boulder, Colorado, 643-694.
6. Wesley, L.D., Meyer, V.M., Pranyoto, S., Pender, M.J., Larkin, T.J., Duske, G.C. (1999). *'Engineering properties of a pumice sand'* 8th Australia and New Zealand Conference on Geomechanics, Hobart.
7. Yogarajah, I. (1993). *'Effects if construction procedures on the behaviour of geogrid reinforced soil walls'*, PhD. Thesis, University of Strathclyde, Glasgow, UK, 93-145
8. Wesley, L.D., (2001). *'Issues in the use of clay in reinforced earth construction'* Proceedings Fukuoka Conference.

Centrifuge Modelling of Drag-In Plate Anchors

Sarah Elkhatib
Geomechanics Group
The University of Western Australia

Summary

Research into drag-in plate anchors developed in response to the demand from the offshore industry for anchoring systems capable of withstanding vertical load components. As exploration moves towards deeper waters, catenary systems have become too costly. Taut-leg mooring systems, where anchors are subjected to significant vertical loads, have become more common. Drag-in plate anchors, or Vertically Loaded Anchors (VLAs), were introduced as an alternative to conventional drag anchors. They are capable of withstanding loads at angles as high as 45° to the seabed.

Using the beam geotechnical centrifuge at UWA, the installation and performance of a dimensionally scaled Vryhof Stevmanta anchor were modelled. The results from the testing are presented in this paper and compared to theoretical predictions about anchor behaviour.

1. INTRODUCTION

With the exploration for oil and gas reaching deeper waters, the use of floating production, storage and offloading (FPSO) facilities has increased, identifying a need for high-capacity anchoring systems. Conventional catenary systems have become too costly, and this led to the introduction of taut-wire mooring systems, where anchors are subjected to significant vertical loads. While large drag embedment anchors can have very high holding capacities and offer an economical and simple means of anchoring for a catenary system, their suitability for taut-wire systems remains in question. As a result, drag-in plate anchors, or vertically loaded anchors (VLAs), were introduced about five years ago by anchor manufacturers: the Denla anchor from Bruce Anchors and the Stevmanta anchor from Vryhof Ankers.

VLAs are installed like conventional fluke anchors by pulling up to a target installation load. The loading direction is then changed such that it becomes normal to the fluke, leading to a significant increase in anchor resistance. In this normal loading mode, the anchor acts as an embedded plate. An important factor to consider when designing VLAs is the performance ratio, which is the ratio of pull-out resistance to the installation load. This ratio determines both the necessary size of the anchor and the requirements for the installation vessel.

Using the beam centrifuge at the University of Western Australia (UWA), the installation and performance of a dimensionally scaled Stevmanta anchor were modelled. This paper presents results from a series of centrifuge tests. A discussion about the anchor's performance is provided and the results are compared to theoretical predictions.

2. VRYHOF STEVMANTA

2.1 Description

The Stevmanta (Figure 1) was introduced in 1996 in response to industry demand for an anchor capable of withstanding vertical loads. The traditional rigid shank has been replaced by a system of wires (anchor bridle) connected to a thin plate. An angle adjuster is used to change the loading direction to normal to the plate following installation.

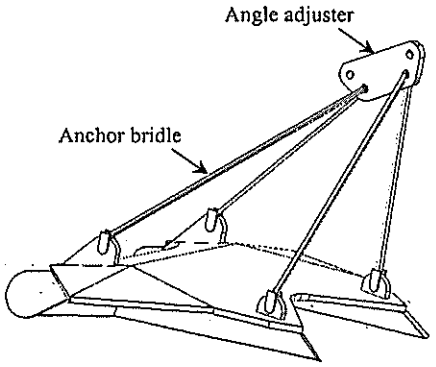

Figure 1: Vryhof Stevmanta

The Stevmanta can be installed using either of the following methods.

Single Line Method (Figure 2)
The anchor is installed using a single line and the angle adjuster is fitted with a calibrated shear pin. During penetration, the load on the anchor increases causing the pin to shear at a pre-determined load, and hence triggering the normal loading mode.

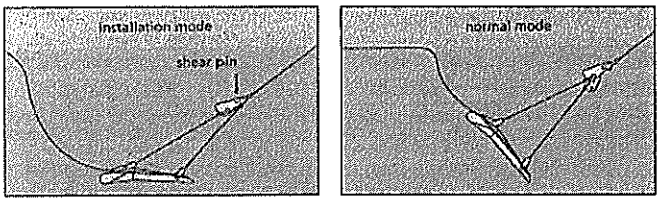

Figure 2: Single line installation method (Vryhof, 1999)

Double Line Method (Figure 3)
Separate lines are used for the installation and normal loading of the anchor. Using this method, the shear pin is not required. The installation line is attached to the front of the angle adjuster creating a suitable fluke-shank angle. Once the required pull-in load is reached, the vertical mode is achieved by pulling the mooring line, which is connected to the rear of the angle adjuster.

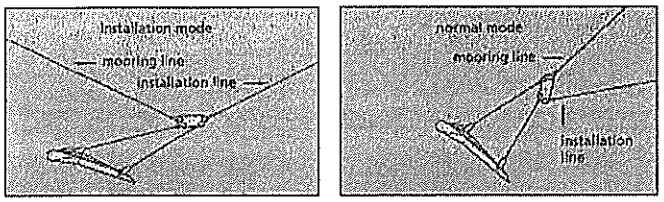

Figure 3: Double line installation method (Vryhof, 1999)

2.2 Field Trials/Applications

Numerous field trials were performed with the Stevmanta. In 1996, tests were carried out in the Gulf of Mexico using 5 m^2 anchors in very soft silty clay. Performance ratios obtained were approximately 2 (Ruinen & Degenkamp, 1999).

In 1997, fifteen tests were performed using 11 m^2 Stevmanta anchors in very soft clay offshore Brazil, and performance ratios were in the range 2 to 3 (Ruinen & Degenkamp, 1999).

Onshore testing on smaller anchors (0.7 m^2 and 1.4 m^2) was carried out in Norway in 1998. Results were influenced negatively due to the presence of a hard top soil layer preventing deep penetration of the anchors. However, ratios obtained ranged from 1.5 to 3 (Dahlberg & Strøm, 1999).

In 1998, the first real application of VLAs was for the P-27 field in the Campos Basin offshore Brazil. Twelve 11 m^2 Stevmanta anchors were installed in very soft clay (Agnevall, 1998).

3. BACKGROUND & THEORY

3.1 Drag Anchor and Chain Theory

Historically, drag anchors were selected using design charts which correlated the anchor weight against holding capacity for general soil types. In the past few years, more sophisticated models have been developed which account for anchor geometry, mooring line characteristics and soil properties (Stewart, 1992; Neubecker & Randolph, 1996; Bransby & O'Neill, 1999)

Neubecker and Randolph (1996) developed a simple method to simulate the performance of a drag anchor. Figure 4 shows the force system adopted in their analysis.

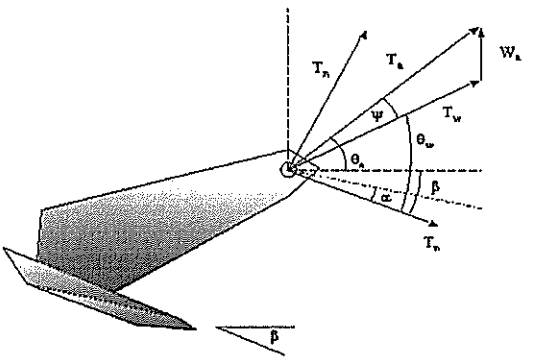

Figure 4: Anchor force system adopted by Neubecker and Randolph (1996)

The force resisting anchor motion, T_p, is defined as:

$$T_p = fA_p N_c s_u \tag{1}$$

where f is the anchor form factor, A_p is the projected area of the anchor onto a plane perpendicular to the fluke, N_c is a bearing capacity factor (taken as 9) and s_u is the undrained shear strength of the soil at the midpoint of the top fluke face.

Temporarily ignoring the anchor self-weight, a soil resistance force normal to the fluke, T_n, must exist for moment equilibrium of the anchor to be maintained. Therefore, the total soil resistance acting on the weightless anchor T_w, which is the resultant of T_p and T_n will form a resultant angle, θ_w, with the top fluke face. It follows that:

$$T_w = \frac{T_p}{\cos\theta_w} \tag{2}$$

The submerged anchor weight, W_a', is then combined with T_w to form the resultant T_a, which is the anchor holding capacity.

The combination of θ_a and T_a must also be compatible with the anchor chain response, where the quantities are linked by the following equation:

$$\frac{T_a \theta_a^2}{2} = DQ \tag{3}$$

where D is the depth to the anchor padeye and Q is the average bearing resistance (per unit length of chain) acting on the chain (Neubecker & Randolph, 1995).

The anchor and chain responses are incorporated into an incremental procedure describing the anchor behaviour. An initial anchor depth and orientation are assumed and the anchor is advanced an incremental horizontal distance. The forces are calculated at each step and a new anchor

orientation is obtained. The anchor is advanced to the new depth and orientation and the process is repeated until the anchor reaches its required depth. This procedure has been shown to give accurate results regarding the anchor's behaviour (O'Neill, 2000).

Whilst this method was developed for drag anchors with a rigid shank, by carefully selecting anchor properties and calculating the appropriate projected area, the method can be applied to the Stevmanta.

Bransby and O'Neill (1999) used plastic limit analysis to analyse the behaviour of a drag anchor. They developed a yield envelope using finite element analysis of the fluke and then used this surface and the plasticity flow rules to determine the anchor's path and orientation. Shank forces were calculated separately using bearing capacity theory. This method achieves the same results as limit equilibrium methods.

3.2 Holding Capacity

When the Stevmanta is in its normal loading mode, it behaves like a plate anchor. The ultimate capacity can be calculated using conventional bearing capacity theory as follows:

$$F = A N_c s_u \tag{4}$$

where A is the area of the anchor, N_C is a bearing capacity factor (Rowe & Davis, 1982; Martin & Randolph, 2001) and s_u is the local undrained shear strength of the soil.

Rowe and Davis (1982) carried out finite element analyses examining the behaviour of anchor plates in clay. Theoretical consideration was given to the effect of anchor embedment depth, overburden pressure and breakaway condition, as well as anchor roughness, thickness and shape. The results are presented in charts which can be used directly for estimating the undrained failure load of anchor plates. They provide good agreement with limit solutions from plasticity theory.

Martin and Randolph (2001) used the method of characteristics for the analysis of buried circular plates in homogeneous soil. For a smooth plate, N_c was found to be 12.42, while for a rough plate, N_c was calculated as 13.11.

4. EXPERIMENTAL MODELLING

4.1 Model Stevmanta

The design of the model anchor was based on a 10 m^2 Vryhof Stevmanta. The model, shown in Figure 5, was fabricated at a scale of 1:100. The anchor plate was made from hardened steel and had a thickness of 0.75 mm and a fluke length of 35 mm. Fishing trace was used to construct the four wires forming the anchor bridle. The lengths of the wires were calculated to give a fluke-shank angle of 60° and the diameters were 0.69 mm. The dry weight of the anchor is approximately 15 g. An angle adjuster was also included to enable normal loading.

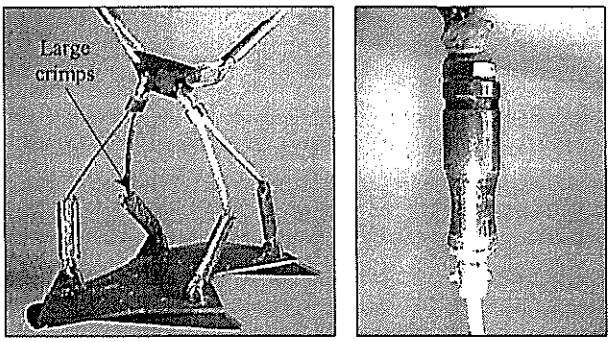

Figure 5: Model Stevmanta and load cell

The double-line method was selected as a more suitable method for installing the anchor due to uncertainties associated with the shear pin failure load. Two anchor chains were used. The chains were constructed by plaiting four strands of 0.6 mm fishing trace, giving an effective width of 1.8 mm. The plaiting technique has been used previously at UWA and was shown to accurately simulate the behaviour of commercially available chain (Neubecker, 1995). Both chains were instrumented with 2 kN load cells to measure installation and pullout forces.

The load cells were fabricated from aluminium and weighed approximately 0.06 N. The load cell, shown in Figure 5, had a length of 30 mm and a diameter of 7 mm. The size of the load cells was significant in comparison to the anchor and so they were placed approximately 120 mm away from the padeye to reduce their influence on the penetration of the anchor. The size and weight of the load cells influences the overall performance of the anchor and this is discussed in more detail in later sections.

4.2 Geotechnical Centrifuge

Centrifuge testing is regarded as one of the most reliable and versatile methods for modelling full scale geotechnical problems. This is due to the stress similitude that is created by the centrifuge modelling. There are also several other advantages. One of these is that the scaling relationship allows miniature models to be created and modelled accurately in the lab without the need for heavy equipment. Centrifuge scaling relationships are presented in Table 1.

Table 1: Centrifuge model scaling relationships

Parameter	Scaling Relationship Prototype/Model
Gravity level	N
Length	N
Mass	N^3
Force	N^2
Stress	1

4.3 Testing Procedure

The testing was carried out in strong boxes designed especially for the centrifuge. The box plan dimensions are 390 mm by 650 mm and the depth is 325 mm.

The aim of the experiment was to carry out the installation and pullout of the anchor in-flight without ramping down in between the two stages. Therefore, two actuators were required to carry out the test: one for the installation line and another for the pullout line.

The testing procedure consisted of a complex system of pulleys. The initial setup is shown in Figure 6a. The anchor is embedded in the clay and the installation line wraps 180° around a pulley at the end of the box. The chain then wraps around another pulley at the base of the actuator and up to a pulley which is driven vertically by the actuator. As the actuator is raised, tension is applied to the installation line, hence embedding the anchor (Figure 6b).

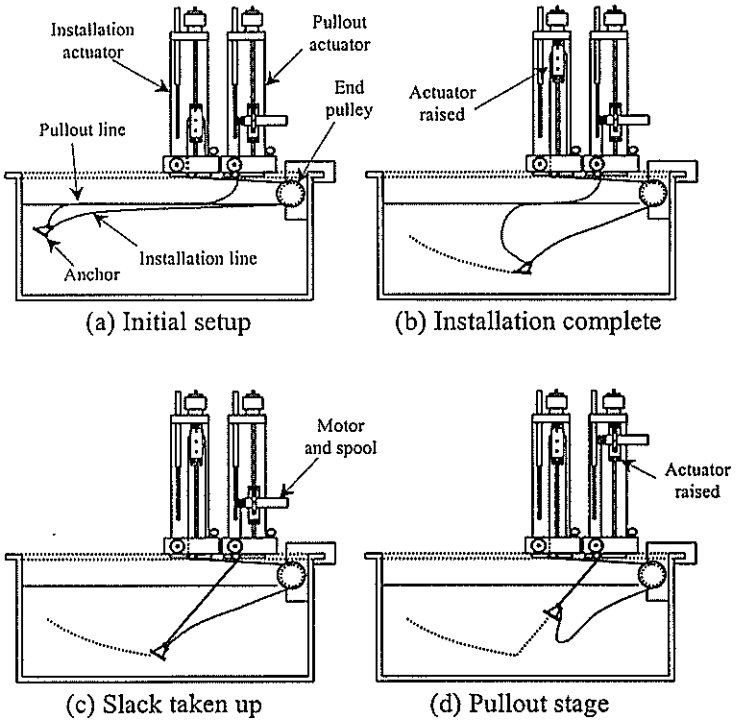

(a) Initial setup (b) Installation complete

(c) Slack taken up (d) Pullout stage

Figure 6: Experimental procedure

The mooring chain is attached to the other actuator. It wraps around a pulley at the base of the actuator and is then attached to a motorised spool. As the anchor is dragged into the soil, the mooring line trails behind (Figure 6b). The slack in the mooring line is taken up by the spool before the pullout is performed (Figure 6c). Following that, the actuator is raised, hence performing the pullout stage of the test (Figure 6d).

A protractor was placed at the base of the pullout actuator to enable measurement of the pullout angle during the test. Also, potassium permanganate crystals were glued to the end of the anchor to trace the path that the anchor travelled.

4.4 Testing Limitations

Due to the limited width of the strong box, only three drags were carried out in each box. This ensures that failure wedges from neighbouring drags do not intersect.

The limited length of the box also prevents a complete drag from being carried out in one stage. The actuator travel distance enables a drag of only 7 fluke lengths and that is not sufficient for the anchor to reach its ultimate embedment depth. After the first stage drag is completed, the anchor is located and pre-embedded at that depth in another drag line for the second stage drag. This procedure is illustrated in Figure 7.

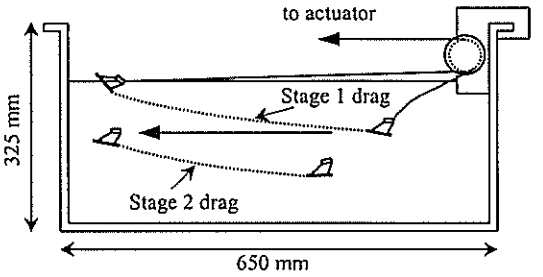

Figure 7: Two stages required for complete drag

4.5 Soil Characterisation

The testing was carried out in normally consolidated kaolin clay at 100g. Commercially available kaolin clay was mixed to a slurry at a water content of 120% (twice the liquid limit). Pore pressure transducers were installed at various depths within the sample to monitor consolidation in the centrifuge. Once the sample had consolidated, soil strength testing was carried out.

Soil characterisation was conducted using a T-bar penetrometer (Stewart & Randolph, 1991). The T-bar penetrometer consists of a cylindrical bar attachment at the end of an instrumented shaft, from which a continuous profile of bearing resistance with depth is obtained. Plasticity solutions are used to derive undrained shear strength from the measured bearing resistance.

Two T-bar tests were carried out prior to the anchor tests and another two following the anchor tests. The T-bars were penetrated at a model rate of 3 mm/s to represent undrained conditions.

5. EXPERIMENTAL RESULTS

5.1 Shear Strength Profiles

The undrained shear strength profiles obtained from the T-bar tests are shown in Figure 8. The sample experienced a slight strength increase during the course of the testing. The average shear strength gradient obtained was 1.1 kPa/m.

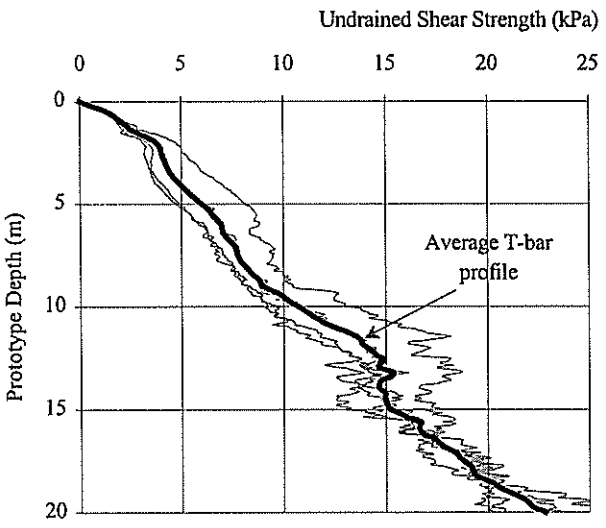

Figure 8: Shear strength profiles

5.2 Installation Loads

Figure 9 shows the installation loads against horizontal drag distance for several tests. The drag tests were performed at a constant model rate of 0.25 mm/s, which results in undrained conditions. One test shows the primary installation and the remaining show secondary installation results appended.

Some problems were encountered with the interpretation of the load cell readings. With the initial installation, the anchor was placed on the clay surface prior to ramp up. As the acceleration level increased, the anchor embedded due to self-weight, exerting a tensile force in the installation chain.

At the start of the drag test, the load cell reading was 690 kN, giving the graph at the top. If the results are offset so that the initial reading is zero, the graph at the bottom is obtained. In reality, the load lies somewhere in between.

With the second stage drags, because the anchor was pre-embedded, it was more stable and hence such an increase in load was not observed. The absolute readings were assumed to be correct and therefore matching the initial results to them was determined to be a reasonable assumption.

With the first stage, a peak in loading is observed at the start of the test followed by a decrease. When the anchor is in a stable orientation, the load increases steadily as the anchor embeds. After a drag distance of 10 fluke lengths, the installation load reached 1250 kN.

At the end of that test, the anchor was located and extracted from the sample, then embedded at the start of the box at that depth for the second stage drag. Subsequent drag tests all had the anchor embedded at a depth of approximately 120 mm (ie 12 m in prototype) to carry out the second stage.

The loads from the remaining drags are also shown in Figure 9. Once again, peaks are observed at the start before the anchor is in a stable orientation. The loads then increase gradually in Tests 3 and 4 as the anchor penetrates deeper into the soil. At the final embedment depth, the installation load reached 1680 kN.

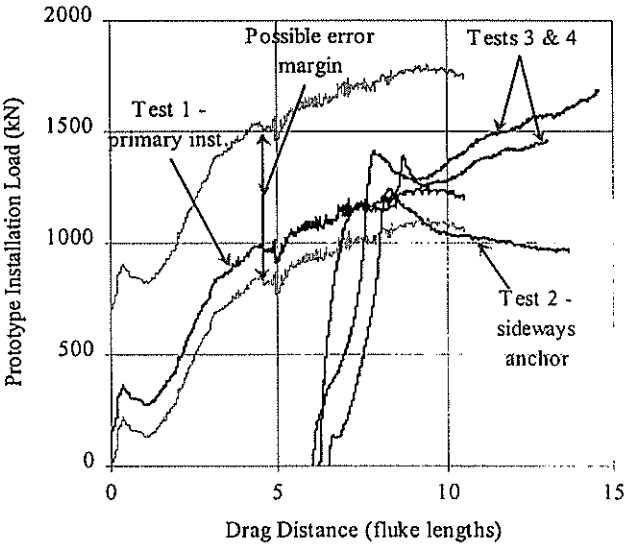

Figure 9: Installation loads

In Test 2, the anchor travelled horizontally towards the edge of the box instead of penetrating deeper into the soil. Since the anchor did not embed deeper, the installation load did not increase as the drag progressed. This situation highlights the importance of ensuring that the anchor is oriented correctly when embedded at the start of the test.

5.3 Pullout Loads

The pullouts were planned to follow immediately after the anchor installation. However, problems were encountered during the testing which prevented this. The pullout chain broke during two of the tests and so the centrifuge was ramped down and the chain repaired temporarily to enable the completion of the tests. A period of reconsolidation was required due to the swelling of the sample during ramp down. The reconsolidation period effectively acted as an unplanned anchor soak. The soaking period was approximately 49 minutes, which is equivalent to approximately 1 year in prototype.

The pullouts were also performed at a model rate of 0.25 mm/s, which ensures undrained conditions during the testing.

Another problem encountered with the interpretation of the results is knowing when exactly the anchor begins to displace in a pullout test. When the slack is taken up using the motorised spool, it is difficult to know when it has all been taken up. As a result, spooling is stopped as soon as the pullout load starts to increase and the actuator is raised. However, there is still some slack in the chain and some of the actuator travel is wasted straightening the chain so that it is normal to the anchor. Since the length spooled was not measured, it was difficult to know when the anchor displacement began. The interpretation of these results is based on the assumption that the anchor displacement begins when the peak load is achieved.

Due to this problem, and the limited actuator travel distance, the pullout tests could not be continued to the clay surface. However, the maximum holding capacity was obtained prior to the completion of the test and so it was sufficient.

The pullout loads are plotted against embedment ratio in Figure 10. The embedment ratio is defined as the ratio of embedment depth to the anchor fluke length of 3.5 m. Tests 1 and 2 did not involve anchor soaking. Test 2 was the anchor which travelled horizontally. Its final embedment depth was shallower than the rest, giving a holding capacity of 1530 kN. Test 1 reached an embedment depth of 16.5 m, resulting in a holding capacity of 2200 kN.

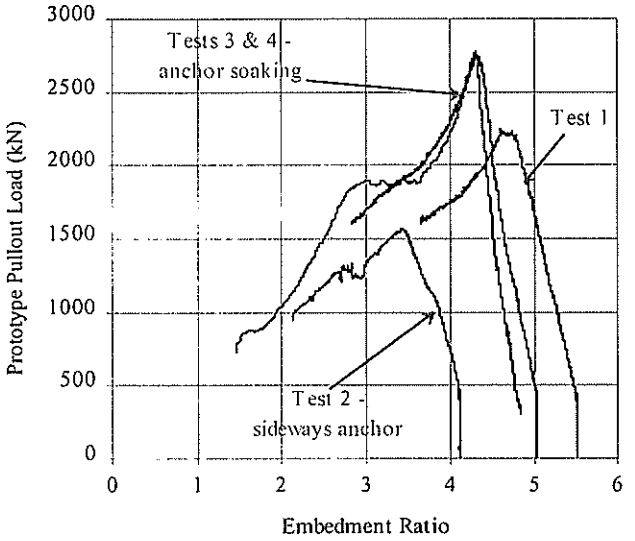

Figure 10: Pullout loads from centrifuge tests

Tests 3 and 4 involved a period of anchor soaking. Anchor soaking allows the clay around the anchor to reconsolidate before the pullout is performed, hence increasing the anchor capacity. This resulted in a 23% increase in holding capacity.

The pullout angles for all the tests ranged between 50° and 60°. This small difference in angle did not seem to influence the pullout capacities.

Visual observations of the clay surface during the test showed that the failure mechanism did not extend to the surface. This type of failure is localised around the anchor and is typically observed for deep anchors.

5.4 Drag/Penetration Path

Upon completion of all the tests in a box, the clay was dissected very carefully to reveal the potassium permanganate traces left by the anchor. These paths were measured to produce a drag/penetration relationship for each test. These provided valuable information which made the analysis of the results much easier.

The ultimate embedment depths were measured enabling a theoretical calculation of the ultimate holding capacity of the anchor. The pullout paths were also observed, enabling the calculation of the pullout angle. Figure 11 shows a section of the clay sample illustrating the anchor drag path. This was the last test performed in the box and so the anchor was kept embedded after the completion of the pullout test. The photo illustrates the limited length of the pullout test due to the problems discussed earlier.

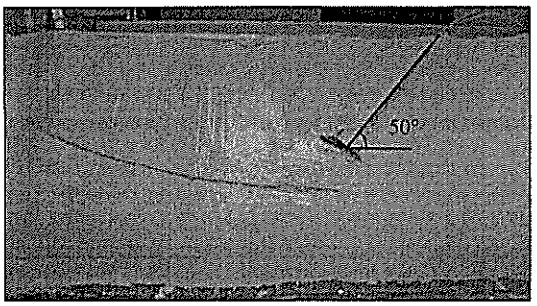

Figure 11: Section of clay sample after completion of test

Figure 12 shows the drag/penetration relationship for the model Stevmanta. The measurements from the first and second stage drags are superimposed to provide a complete path. After a drag of 15 fluke lengths, the anchor embedded 5 fluke lengths. This is compared to the Neubecker-Randolph solution in Figure 12. The results compare well. However, the graph shows how the anchor could have embedded deeper if there was more room in the box for horizontal travel. This would increase the anchor's holding capacity by approximately 16%, but twice the drag distance would be required.

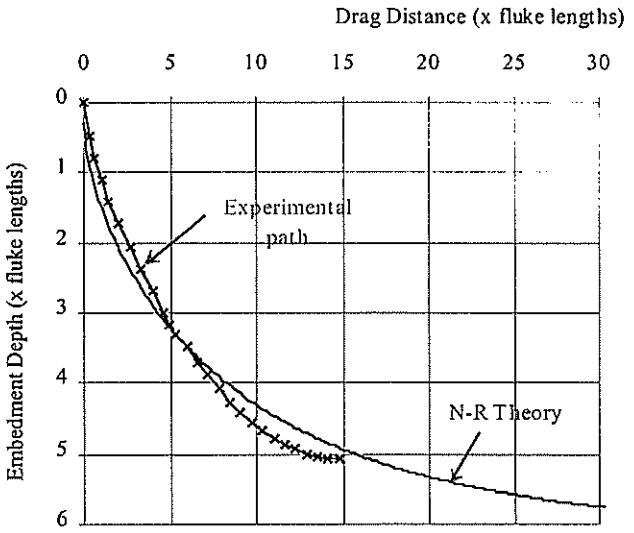

Figure 12: Drag/penetration relationship

5.5 Performance Ratios

Performance ratios obtained from the experimental tests ranged from 1.3 to 1.7. These are lower than ratios obtained by Vryhof in their field trials, which were in the order of 2 to 3. The low ratios can be attributed to a number of factors.

During the installation of the anchor, the large load cells on both the installation and pullout chains, and the crimps on the bridle, create extra bearing resistance contributing to a higher

installation load. Also, the vertical loading component exerted on the anchor as it approaches the end pulley also results in a higher installation load.

6. COMPARISON TO THEORY

6.1 Installation Loads

Figure 13 shows the expected load development from the Neubecker-Randolph method. The projected area used in the analysis incorporated the angle adjuster and the anchor bridle, including the crimps.

The experimental results from the primary installation compare well with the Neubecker-Randolph solution once the anchor becomes stable. Towards the end of the second stage drag, the curves diverge. Higher loads are obtained during the experiment. This can be attributed to the vertical load component exerted on the anchor as it approaches the end pulley.

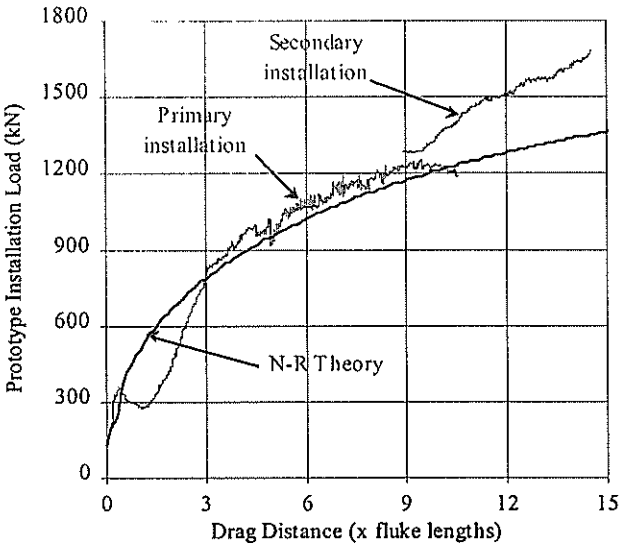

Figure 13: Comparison of installation loads

Not incorporated in the theoretical solution is the effect of the pullout line, which trails behind the anchor during installation. This also creates more resistance, hence increasing the installation load.

6.2 Bearing Capacity Factors

The loads from the pullout tests were converted to bearing capacity factors using Equation 4. The results are shown in Figure 14.

The bearing capacity factors calculated from the pullout tests compared favourably to theoretical solutions. Rowe and Davis (1982) upper bound solutions give a bearing capacity factor of 11.42 and Martin and Randolph (2001) recommend factors of 12.42 for a smooth plate and 13.11 for a rough plate.

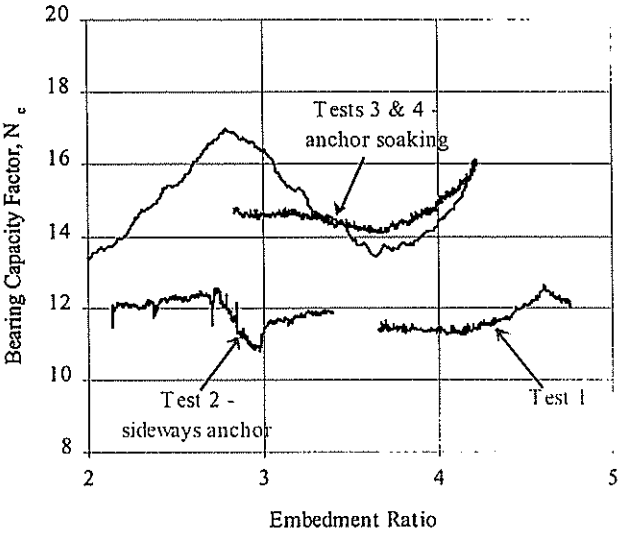

Figure 14: Bearing capacity factors from pullout tests

It should be noted, however, that the above studies were carried out on circular plates and some discrepancies are expected due to the effects of the corners of the anchor.

The bearing capacity factors from the anchor soak tests were higher, averaging about 15.

7. CONCLUSIONS

The performance of a model Stevmanta anchor was modelled in the centrifuge at UWA. Results obtained from the tests did not compare well with the full-scale field tests carried out by Vryhof. Performance ratios obtained were much lower than expected. However, there is still much room for improvement in the testing equipment and procedure and it is anticipated that results will be more promising in future tests.

8. ACKNOWLEDGEMENTS

The author of this paper is supported by an Australian Postgraduate Award. Special acknowledgement is made of the excellent technical support provided by the workshop and centrifuge staff at UWA. The information provided by Vryhof Anchors is also appreciated.

9. REFERENCES

1. Agnevall, T. (1998), Installation and performance of the Petrobras P27 Stevmanta VLA anchors, *2nd Annual Conference on Mooring and Anchoring*, Aberdeen
2. Bransby, M. F. and O'Neill, M. P. (1999), Drag anchor fluke-soil interaction in clays, *NUMOG VII International Symposium on Numerical Models in Geomechanics*, Graz, Austria, Balkema, pp. 489-494
3. Dahlberg, R. and Strøm, P. J. (1999), Unique onshore tests of deepwater drag-in plate anchors, *Proceedings of the 31st Annual Offshore Technology Conference*, Houston, Texas, OTC 10989

4. Martin, C. M and Randolph, M. F. (2001), Application of the lower and upper bound theorems of plasticity to collapse of circular foundations, *Computer Methods and Advances in Geomechanics*, Tuscon, Arizona, 2:1417-1428
5. Neubecker, S. R. (1995), The behaviour of drag anchor and chain systems, PhD Thesis, Department of Civil Engineering, The University of Western Australia
6. Neubecker, S. R. and Randolph, M. F. (1995), Profile and frictional capacity of embedded anchor chains, *Journal of Geotechnical Engineering, ASCE*, Vol. 121, No. 11, pp. 797–803
7. Neubecker, S. R. and Randolph, M. F. (1996), The performance of drag anchor and chain systems in cohesive soil, *Marine Georesources and Geotechnology*, 14, pp. 77–96
8. O'Neill, M. P. (2000), The behaviour of drag anchors in layered soils, PhD Thesis, Department of Civil Engineering, The University of Western Australia
9. Rowe, R. K. and Davis, E. H. (1982), The behaviour of anchor plates in clay, *Geotechnique*, 32, No. 1, pp. 9-23
10. Ruinen, R. and Degenkamp, G (1999), First application of 12 Stevmanta anchors (VLA) in the P27 taut leg mooring system, *Proceedings of Deep Offshore Technology 1999*
11. Stewart, D. P. and Randolph, M. F. (1991), A new site investigation tool for the centrifuge, *Centrifuge '91*, Balkema, pp. 531–538
12. Stewart, W. P (1992), Drag embedment anchor performance prediction in soft soils, Proceedings of the 24th *Annual Offshore Technology Conference*, Houston, Texas, OTC 6970
13. Vryhof Anchors, (1999), Anchor Manual 2000, Krimpen ad Yssel, The Netherlands

Cyclic Loading Effects on the Secondary Consolidation of Clay

Brook Ewers & David Smith, The University of Newcastle, Callaghan NSW, Australia 2308

The Ballina bypass is part of the upgrade of the Pacific Highway between Newcastle and the Queensland border. The bypass consists of a 12km stretch of road over thick deposits of very soft alluvial clay. Thicknesses range between 7m and 25m. An investigation into long-term settlement parameters was undertaken at the University of Newcastle (1), which found the clay exhibited large secondary settlements. Since the primary consolidations are dealt with prior to the roads construction, it is the long-term settlements that govern the effective road design and maintenance considerations. Under low road embankments (less than 3.0m) traffic loads need to be considered as they may have an effect on the long-term deformations of the subsoil. A series of laboratory tests have been undertaken to investigate the effect of cyclic loading on the long-term creep settlements of the soft Ballina clays.

1 INTRODUCTION

The Ballina bypass is part of the upgrade of the Pacific Highway currently being undertaken between Newcastle and the Queensland border. The bypass consists of a 12km stretch of road, over very soft alluvial clay. The long-term settlements of the clays are of great concern to future maintenance cost of the road. A study was undertaken at the University of Newcastle (Ewers and Allman (1)) that found the Ballina clay exhibited significant secondary consolidation. Whilst the coefficient of secondary consolidation is calculated from oedometer tests, it is recognised that embankments experience a dynamic load component from the traffic loads during its service. A series of oedometer tests with a dynamic load component have been carried out to better understand the long-term implications of dynamic load upon creep settlements.

1.1 Background

Bjerrum (2) studied a number of structures that underwent variations in loading. He divided the structures into two groups: (i) those where the load variation was a major component of the total load (examples of these structures are silos and oil tanks) and (ii) those where the load variation was small compared to the total load (an example of this structure is traffic loads on road embankments). What was found was that structures in the first group continued to settle at a constant rate so that settlement and time did not plot as a straight line on a semi-logarithmic graph (which is significantly different to settlement under a static load, such as a standard oedometer test). Bjerrum explained this behaviour by a mechanism of lateral displacements. Indeed a constant rate of displacement in a one-dimensional test is not feasible, as the settlements must converge to some minimum void ratio. Road embankments fit into the second category as the traffic loading is only expected to be small compared to the embankment load. However this does not preclude traffic loading affecting the long-term creep settlements.

Because the settlements during the design life of the embankment are long term, very few case studies are available that demonstrate the effect of the traffic load on creep. However Yamanouchi and Yasuhara (3) presented a case study in Japan where an embankment exhibited an abnormally large settlement and demonstrated that it was likely that the increased rate of settlement was due to traffic loading.

2 SOIL DESCRIPTION

The soft alluvial clays along the Ballina bypass road alignment range in depth from 7 to 25m. In general, the soil profile comprises a thin crust of overconsolidated topsoil, which is underlain by deep deposits of near normally consolidated dark grey alluvial clay, containing shells and traces of silt. The Cumbalum site (located around 2km north of the city centre) comprises around 25m of soft estuarine clay. The physical properties of the soil at the sample location are presented in Table 1.

Depth (m)	w_l (%)	w_p (%)	w (%)	c_u (kPa)
1	35	15	38	20
4	110	35	120	15
8	130	38	115	20
16	100	39	70	35

Table 1: Insitu soil properties

3 TRAFFIC LOADS

The vibrations due to traffic have been recognised as a source of damage to buildings close by major roads (Tynan (4)). When a vibration is generated at the surface of a semi-infinite mass of soil, it is transmitted as body waves (both compression and

shear) and surface waves (known as Rayleigh waves).

Vibrations in a subgrade material may be induced by the interaction between the vehicle's wheels and the road surface. The vibrations that reach the buildings are primarily Rayleigh waves, and since they are transmitted along the surface of the soil, they are not of major concern to this investigation. Nevertheless they warrant mention, as these waves are often felt when standing nearby a road constructed on saturated soil (e.g. as a truck passes by).

There are a number of types of cyclic loading induced by moving traffic. First, there is diurnal variation of vehicles passing on a highway. On a macroscale we would see (in an idealised situation), a slow cyclic load variation with time of day due to the variation of traffic density. Second, if we consider the passing of a T44 truck, then we would see a much higher frequency loading due to the front axle and subsequent axles passing over a given location. Clearly, this frequency of loading will vary with the vehicle speed.

Third, there may be a range of loading frequencies excited due to the interaction of the wheels and the road surface. This mainly depends on the dynamic response of the truck suspension and the roughness of the road (it is noted that this interaction may be analysed by taking a Fourier transform of the road profile and considering resonance with the truck's suspension). Discontinuities in the road surface (e.g. potholes or bumps caused by differential road settlement) may also interact with the tuck's suspension, causing dynamic loadings at a range of frequencies. Fourth, high frequencies may be excited in the tyres of the vehicle as tyres contact (i.e. 'slap') the road surface, creating much of the noise associated with traffic.

Because of the various types of dynamic loading, the frequency and magnitude of the 'traffic load' is hard to define explicitly. Unfortunately, field studies are also rare, and few have attempted to untangle the confounding factors associated with dynamic loading induced by road traffic. However, European countries that use high-speed trains have done extensive studies into the effect of trains on soft ground (Adolfsson et al (5)). Although the studies are mainly concerned with the passing of trains at high speed (200 km/h), there are some important findings that are applicable to traffic loads. Adolfsson et al found that below speeds of 70km/hr track displacements were essentially understandable in terms of an equivalent "static" loading. Measurement of the dynamic pore pressures was not possible, however the cumulative pore pressures monitored over a 12-hour period of heavy traffic showed very little increase (in the order of 1.0kPa at a depth of 3.4m, and 1.4kPa at a depth of 5.9m).

The ground conditions in the study varies slightly compared to those at Ballina, having a crust of organic clay of around 3.0m thick. This accounts for the higher excess pressure at the greater depth although the strains are lower at that depth due to the lower permeability.

3.1 Calculation of Traffic Load

Only the second of the described dynamic load sources will be looked at in this study (i.e. the time taken between the front axle and subsequent axles of a truck (see figure 1)), as this is most easily quantified and has the potential to influence subgrade creep rates. If the truck is travelling at 100km/hr (28m/s) then assuming an axle spacing of 8m, it will take around 0.36 seconds between the axle groups to pass the same reference point, which gives a frequency of the order of 3hz. A simple calculation was made of the stresses beneath a 1.5m thick embankment subject to the rear wheel group of a T44 truck. The loading was taken from the Austroads Bridge Design Code, while the road pavement design is shown in Table 2.

Description	Thickness (m)	E (Mpa)
Asphalt	0.2	2800
Granular	1.3	1400
Layer 1	5.0	4.5
Layer 2	5.0	7.5

Table 2: Road Pavement Design Section

Each wheel was modelled as a circular load of radius 0.1m with a uniform pressure of 750kPa. The stresses where calculated beneath the centre of the rear axle group using a linear elastic finite layer program (FLEA (6)). The analysis predicted a stress of around 2.0 kPa at the ground surface decreasing to around 0.9 kPa at a depth of 5.0m. Multiple close spaced axles would increase this load roughly proportionally to the number of axles.

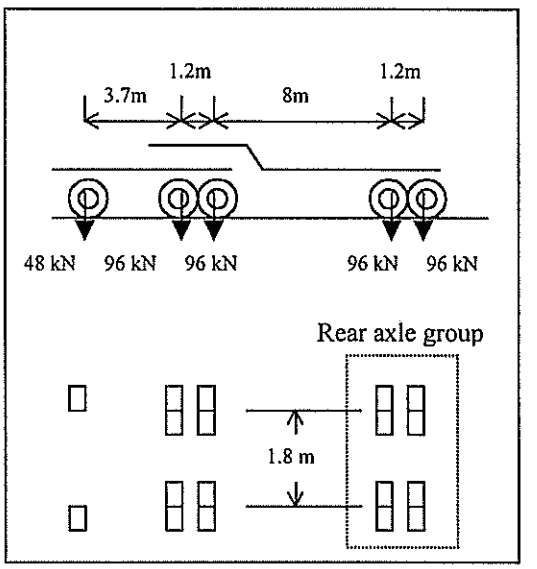

Figure 1: T44 Truck Loading

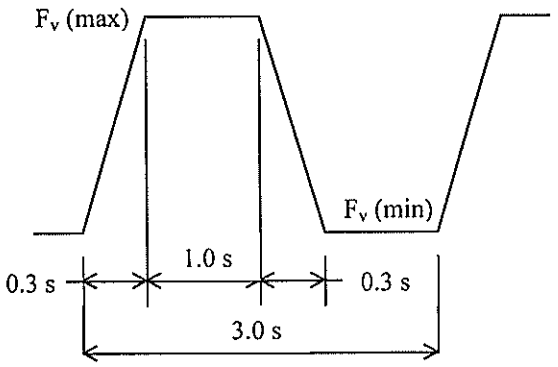

Figure 2 : Depiction of vertical Force

The Australian Standards (7) outline testing methods to determine the resilient modulus and permanent deformation of granular unbound pavement materials, using repeated load triaxial tests. The resilient modulus is defined as the deviator dynamic stress divided by the resilient (recoverable) strain. Determination of the resilient modulus, requires a vertical force waveform as shown in Figure 2. Although this standard is for the evaluation of granular road bases it provides some indication of a plausible traffic model.

4 THE MECHANISM

When clay is subjected to cyclic loading it is common to assume an elastic-plastic deformation model. It is expected that under each load in the cycle there will be elastic (or recoverable strains) and plastic (or irrecoverable) strain. The elastic deformation produces a recoverable change in pore water pressures (recoverable in the sense that excess pore pressures return to zero upon load removal). The plastic strain also produces excess pore water pressures, but these are not recoverable (they remain upon removal of the load). Rapidly cycling pore water pressures will induce vibrations in the clay particles as the pressure wave moves through the particle assembly. The vibrations in the particle assembly will promote irrecoverable particle rearrangement (that is, time dependent plastic deformation (or in other words, creep)). This time dependent particle rearrangement caused by rapidly cycling pore water pressures will result in irrecoverable increases in excess pore water pressure, which in turn will reduce the effective stress in the soil (and so the amount of particle-to-particle contact). This reduction in effective stress in turn will reduce the shear strength of the soil and so promote further particle rearrangement. In other words, if irrecoverable strains generate excess pore pressures faster than the time taken for the pressures to dissipate, then excess pore pressures will build up. If the effective stress reduced to zero, then liquefaction is said to have occurred. However in the case of creep deformation, the time scales involved are usually quite long, giving time for most of the excess pore water pressures to dissipate. While some increase in excess pore pressure may occur (depending on the permeability of the clay and the length of the drainage path), these increases will usually be modest. While they will promote particle rearrangement, they will not cause liquefaction of the soil.

(Wilson and Greenwood (8)) refer to the ratio of static to dynamic deviator stress. Wilson and Greenwood found that for ratios less than 0.37 the strains decreased over time, which resulted in a straight line plot in semi-log time (Bjerrum's 'normal' behaviour). For ratios larger than 0.37 the strains and pore water pressure increase, which indicate the strains are within the plastic region, the rate that the cumulative pore pressures can increace is also a function of the permeability of the clay, the drainage path and the rate that the load is applied.

The clay tested by Wilson and Greenwood was taken from a depth of 12.2m and had moisture content of 25-27%. The sensitivity and high void ratio of the Ballina clay is expected to produce a much lower plastic strain threshold.

8.1 Soil Deformation

While an explanation of soil deformation as a rate dependent process is beyond the scope of this paper. some details are provided here (a detailed explanation can be found in Mitchell (9)). Modelling soil as a rate process considers the clay particles as 'flow units' that require an 'activation energy' to overcome the potential energy barriers that separate equilibrium positions. The application of a shear force will lower the barrier in the direction of the shear force and allow particles to move into new equilibrium positions. Mitchell gives the probability of a given unit becoming thermally activated as,

$$P(\Delta F) = e^{-\Delta F/(nkT)} \qquad (1)$$

Where ΔF is the activation energy per mole, N is Avogadro's number (6.02×10^{23}), k is Boltzmann's constant (1.38×10^{-23} $J°K^{-1}$) and T is the absolute temperature (°K). The effect of the particle vibration is to provide additional energy (i.e. in addition to energy kT) , increasing the probability of overcoming the activation energy ΔF, and so causing permanent particle rearrangement taking place. This theory also explains the higher coefficients of secondary compression at the preconsolidation pressure (see figure 3), as the activation energy ΔF is then minimised (and indeed, is a minimum for all loads, thereby explaining $C\alpha$ being maximised at the preconsolidation pressure). It is plausible that the application of the vibrational load allows for a faster collapsing of the soil structure.

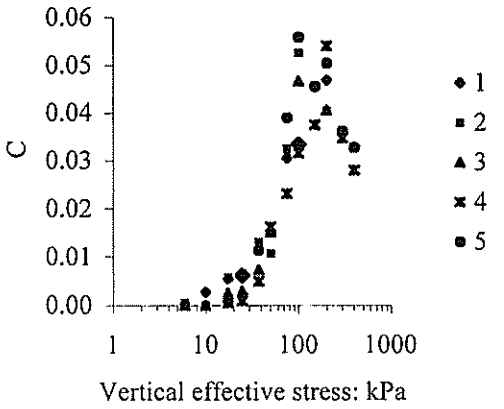

Figure 3: Secondary consolidation versus Effective Stress

6 LABORATORY TESTING

Samples where cut from U75 tubes from a depth of 3.0m. A conventional oedometer apparatus was used for the dynamic load tests. Samples where tested in polished stainless steel rings, 19mm high and 45mm diameter.

A 'mini shaker' was attached to the end of the hanger as shown in Figure 4. The mini shaker has a permanent magnet within a wire coil, so when supplied with a electrical current, the permanent magnet vibrates in sympathy with the induced

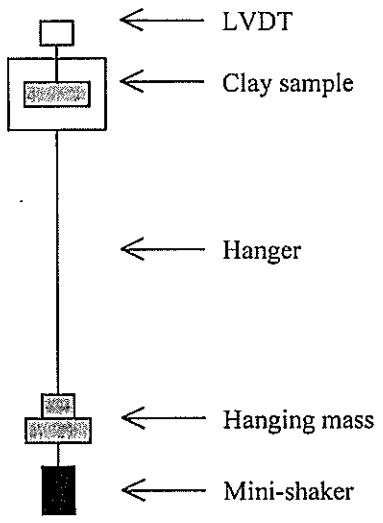

Figure 4: apparatus

magnetic field. It current is controlled by a 'function generator' that can produce square, triangular or sinusoidal waveforms.

6.1 Test Method

The sample was loaded in two increments up to the required initial stress. Time was allowed for completion of primary consolidation. The settlement graph was used to ensure the curve had past the inflection point defining the completion of primary and the beginning of secondary consolidation. The dynamic load component was then applied using the mini shaker. The load applied was a 1.8kPa @ 12Hz sinusoidal wave (due to the technical limitations of the mini-shaker a frequency of 12 Hz).

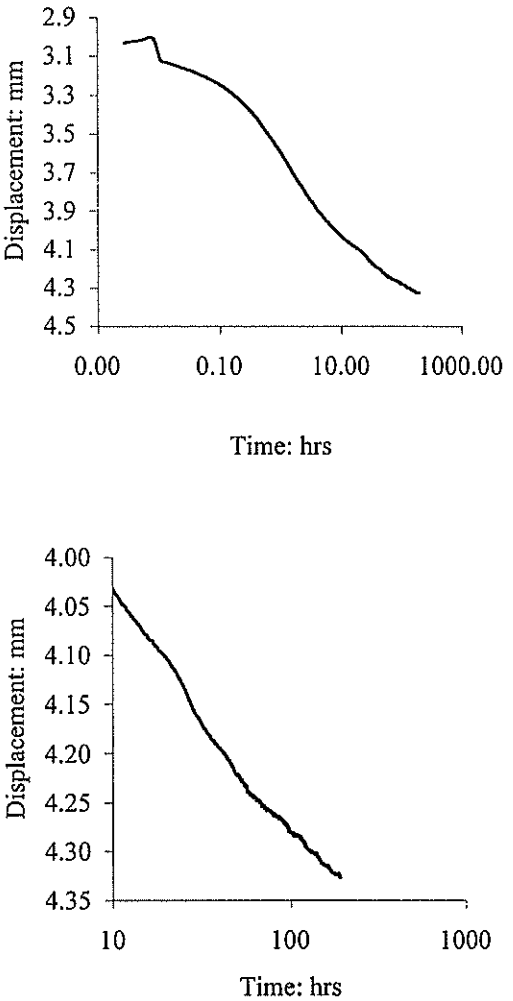

Figure 5: Displacement curve of 50kPa load increment

7 RESULTS

At the time of writing two tests have been completed. Vibrational loading was applied at two load increments, that is, 50kPa and 75kPa. The results so far presented if Figures 3 and 4 below. Each figure shows the complete displacement versus time curve, together with a 'zoomed view' to highlight the change in curve shape following the application of vibration.

Each figure shows an increase in the displacement after the application of the vibrational load, which then gradually decreases with time. The curves show evidence of an immediate response, followed by the

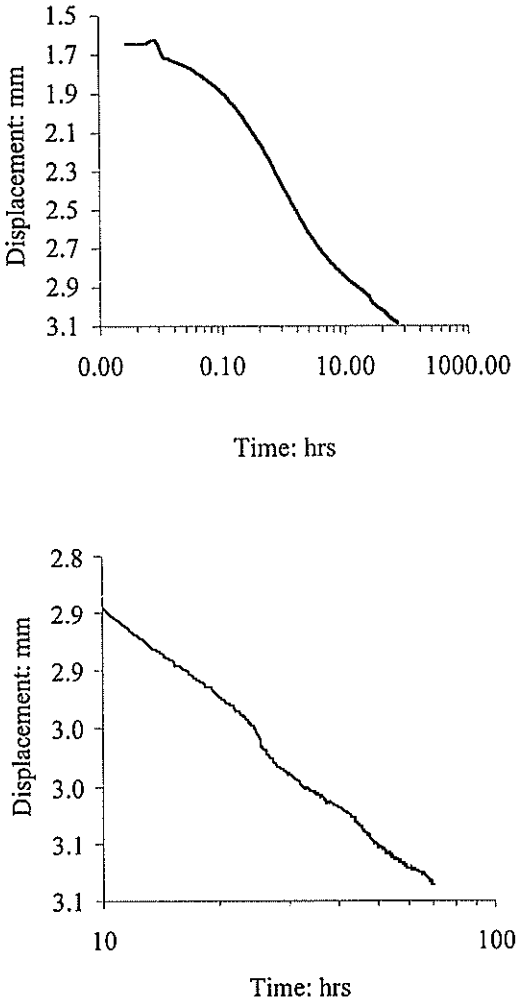

Figure 6: Displacement curve of 75kPa load increment

resumption of a creep curve parallel to the initial curve. So far, the effect of the applied vibration appears to have been minimal. However, there is some evidence of stick-slip behaviour of in the top plate of the oedometer and this requires further investigation before firm conclusions can be drawn.

8 CONCLUSIONS AND RECOMENDATIONS

Due to time restrictions, many further tests in this investigation have not been completed. Testing currently being done looks at the two primary controls on settlement rates: frequency and load ratio. Ewers and Allman found that the coefficient of secondary consolidation was dependent on the effective stress (a summary of results are reproduced in Figure 3). The key feature is that c_α increases past the preconsolidation pressure, and then begins to decrease. This behaviour is thought to be linked to the breakdown of the clay structure. For this reason it is believed that the effect of vibration on the settlement behaviour of the soil will also be dependent on the effective stress relative to the preconsolidation pressure.

9. ACKNOLEDGMENTS

This research has been carried out with the financial support from the RTA, Robert Carr and Associates and the Australian Research Council

1. EWERS, B. & ALLMAN, M. A. Secondary Compression of Soft Clay from Ballina. Proc. GeoEng2000, Melbourne, 2000.

2. BJERRUM, L. Secondary Settlement of Structures Subject to Large Variations in Live Loads. Proc. Symp. Rheology and Soil Mechanics, IUTAM, Grenoble, 1966, pp. 460-471.

3. YAMANOUCHI, T. & YASUHARA, K. Settlement of Clay Subgrades after Opening to Traffic. Proc. 2nd Australia and New Zealand Conf. On Geomechanics, Brisbane, 1975, pp. 115-120.

4. TYNAN, A. E., Ground vibrations Australian Road Research Board Special Report No. 11, 1974

5. ADOLFSSON, K., ANDREASSON, B., BENGTSSON, P. R., AND ZACKRISSON, P. high speed train X2000 on soft organic clay-measurements in Sweden. Proc., 12th Eur. Conf. Soil Mech. Geotech. Engrg., Rotterdam, 1999, Vol. 3, A. A. Balkema, 1713-1718

6. SMALL, J.C., BOOKER, J.R., FLEA, Finite Layer Elastic Analysis, Fortran 3.4, Centre for Geotechnical Research, Civil and Mining Engineering, Sydney University, Sydney

7. AUSTRALIAN STANDARD, AS 1289.6.8.1 – 1995, Soil Strength and Consolidation tests – Determination of the Resilient Modulus and Permanent Deformation of Granular Unbound Pavement Materials.

8. WILSON, N. E., & GREENWOOD, J. R. Pore Pressures and Strains After Repeated Loading of Saturated Clay. Canadian Geotechnical Journal, Vol. 11, No. 269, 1974, pp. 269-277.

9. MITCHELL, J. K., Shearing resistance of soils as a rate process. J. Soil Mech. Fdn Engng Div., Am. Soc. Civ. Engrs 1976,Vol. 90, No. 1, 29-61

Geotechnical Site Characterization using Surface Waves

Sebastiano Foti, COFS, University of Western Australia, Perth

The use of surface wave for characterization purposes in Geotechnical Engineering has recently spread out after the introduction of the SASW test in the middle Eighties. The appeal of surface wave based methods is mainly related to the possibility of obtaining dynamic properties of soil with no need for boreholes and with a certain degree of accuracy.
This paper is mainly devoted to discuss the advantages of multistation techniques for the analysis of surface waves and the effectiveness of these methods. Two case histories are reported, comparing the results with independent borehole seismic tests.
Using a controlled source it is possible to get from multistation measurements an estimate of the damping properties at a site as well as the shear stiffness. The transfer function method allows a simultaneous measurement of experimental dispersion and attenuation curves that are used for a coupled inversion process leading to an estimate of both the stiffness and damping profiles.

1 INTRODUCTION

An accurate evaluation of the soil stiffness at low strains is necessary in Earthquake Geotechnical Engineering and Soil Dynamics for problems like site response analysis and design of vibrating machine foundations. Its evaluation using laboratory tests can be problematic, especially for hard-to-sample materials such as cohesionless soils.

In situ small strain stiffness is often obtained with seismic methods, which are based on wave propagation. Borehole seismic methods such as the cross-hole and the down-hole tests are very accurate but costly and time consuming. Non-invasive surface wave based methods offer an acceptable accurateness without the need for boreholes.

While the cross-hole method and the down-hole method are based on a direct measurement of the velocity of propagation of body waves, surface wave methods are founded on an inversion process aimed at estimating the shear wave velocity profile on the basis of the dispersive behaviour of Rayleigh waves.

Early applications were developed by seismologists for the characterisation of the Earth's crust (Aki and Richards [1]).

On the engineering side, small scale simplified applications were proposed for soil and pavement characterisation using the Steady State Rayleigh method (Jones [2]).

But the wide spread of surface wave methods in geotechnical engineering started from the middle 1980s, when the researchers of the University of Texas at Austin developed the SASW (Spectral Analysis of Surface Waves) method. This method combined a rigorous approach for the inversion process with a strong testing time reduction in the field (Stokoe et al. [3]). In its original configuration the SASW method uses an impact source and a couple of receivers connected to a signal analyser (Stokoe et al. [3]). Such a simple test setup has given a strong impulse for the diffusion of the method, but it has some inherent drawbacks, which are related to the necessity of repeating the test in several different configurations and to some difficulties in data interpretation.

Multistation methods overcome most of these limitations. Multistation detection and analysis of impulsive signals have been successfully applied for soil characterisation on large-scale projects (Gabriels et al. [4], McMechan and Yedlin [5]), but they are not commonly used for geotechnical applications.

In the present paper some applications of multistation surface wave testing are presented.

2 RAYLEIGH WAVES AND SOIL STIFFNESS

Rayleigh waves are generated and propagate along a free surface of a continuous body and the associated motion is confined in a limited skin-depth of the halfspace. The thickness of the superficial stratum involved in the propagation is directly proportional to the wavelength. Hence, assuming that the mechanical parameters of the medium change with depth, the velocity of propagation of a Rayleigh wave is closely related to its wavelength and consequently to its frequency. The relationship between frequency and phase velocity of surface waves is usually named the dispersion curve.

As stated above, the dispersion curve is strongly dependent on the mechanical parameters of the medium the wave is travelling through. Assuming a

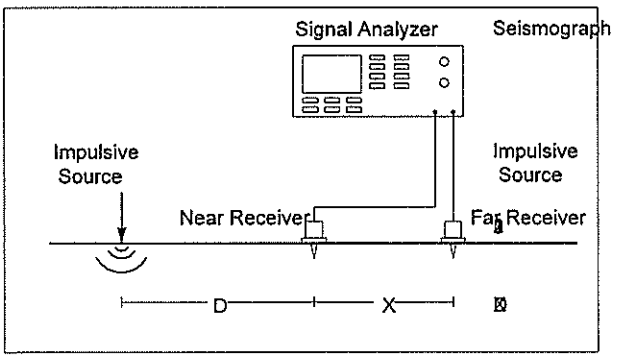

Figure 1 Simple SASW test setup

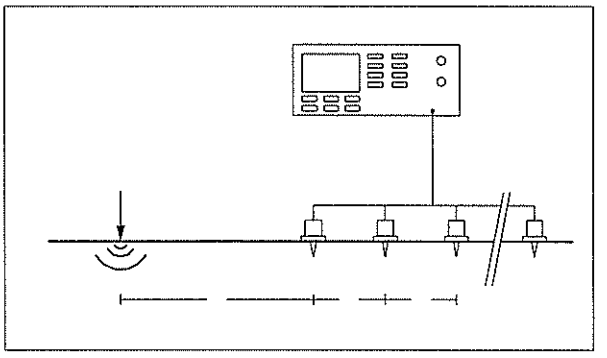

Figure 2 Multistation SASW test setup

given model for the medium, it is possible to estimate the model parameters by knowing the corresponding dispersion curve and solving the associated inverse problem.

Three main steps must be accomplished to characterise a soil deposit using any of the surface wave based methods:

1) field measurements;
2) experimental dispersion curve estimation;
3) solution of the inverse problem to get the stiffness profile.

In field testing the motion associated with surface wave propagation is measured using receivers placed on the ground surface. For soil testing vertical geophones (velocity transducers) having natural frequency in the range 1-5 Hz are usually employed. The testing configuration is dependent on the signal analysis technique that will be used to obtain the dispersion curve. The motion is induced in the ground using a source placed on the free surface, though some techniques based on the measurements of ambient noise (microtremors) have been proposed (Tokimatsu [6], Zywicki and Rix [7]).

Usually an impact source is adopted, e.g. a sledge hammer or a weight drop system depending on the length of the testing array. The use of controlled sources (shaker or vibroseis) acting in a sweep-sine mode can greatly improve the quality of field data, but the testing time increases and such equipment is relatively expensive.

Several techniques for the evaluation of the dispersion curve from field data have been proposed and adopted for surface wave testing in geotechnical engineering. Many of these techniques have been formerly used for seismological or large-scale geophysical applications and then applied to soil characterisation in small-scale projects. In the present paper only the 2-station approach of the SASW test and the multistation approach based on frequency-wavenumber analysis will be considered.

The Spectral Analysis of Surface Wave method is very popular in geotechnical engineering. Two receivers are placed along a straight line starting from the source location and the phase velocity of surface waves is evaluated from the phase difference between the two signals, which have been previously transformed in the frequency domain (Stokoe et al. [3]). The testing configuration is reported in Figure 1. Typically the inter-receiver spacing and the spacing between the source and the first receiver are equal. Because of near-field effects of the source (i.e. interference of body waves), spatial aliasing and attenuation of the signals, a single testing configuration gives information over a narrow frequency range, which is not sufficient for the inversion process. It is therefore necessary to repeat the test using different receiver spacing. The information collected with several testing configurations is finally assembled to obtain the phase velocity of surface waves over a wide spectrum of frequency.

The use of a multistation testing setup (Figure 2) can introduce several advantages in surface wave testing. In this case the motion generated by an impact source is detected simultaneously at several receiver locations and the corresponding signals are analysed as a whole using a double Fourier Transform. It can be shown (Tselentis & Delis [8]) that the dispersion curve can be easily extracted from the location of the spectral maxima in the frequency-wavenumber domain in which the original data are transformed. Using this technique the evaluation of the dispersion curve becomes straightforward and the procedure can be easily automated (Foti [9]). Moreover the need for several testing configurations is strongly reduced with respect to the 2-station procedure of the SASW test and hence the necessary testing and interpretation time decreases.

Once the experimental dispersion curve has been obtained, it is used in an inversion process aimed at estimating the stiffness profile at the site. In this respect it is necessary to choose a framework model and to formulate the mathematical solution of the forward problem, i.e. the implicit relationship between the model parameters and the dispersion curve.

The model adopted for the analysis of surface waves data is constituted by a stack of linear elastic layers over an elastic halfspace. This is a reasonable model for the small strain behaviour of soil deposits, under the condition that no marked lateral variation exists. The geometrical correspondence between the model and the soil deposit is of primary importance for the accurateness of the final results.

Considering that each layer is characterised by 4 parameters (2 elastic parameters, the density and the thickness) except for the underlying halfspace, the thickness of which is not defined, the global number of unknowns for the inversion process would be 4n-1, where n is the number of layers in the model. Typically the number of unknowns is reduced choosing a-priori values for the density and the Poisson ratio of each layer. This procedure is justified by the small influence that such parameters have on the dispersion curve, if compared to the influence of the shear modulus and of the thickness of the layers. It is a standard practice to use as unknown the shear wave velocity instead of the shear modulus.

The forward problem is solved using any of the propagator-matrix formulations proposed for the layered elastic model (Buchen and Ben-Hador [10]). The eigenvalue problem associated to Rayleigh wave propagation is set up assembling the matrices corresponding to each single elastic layer. It can be shown that for each frequency one or more non-trivial solutions exist and they represent the modes of propagation (Aki and Richards [1]). It is important to remark the necessity of considering mode superposition effects for a correct evaluation of the numerical dispersion curve to be compared to the experimental one (Gucunski & Woods [11], Foti et al. [12]).

The inversion process is an iterative procedure based on the comparison between the experimental curve and the numerical dispersion curve corresponding to the profile at the present iteration. The stiffness profile is then gradually changed until convergence is achieved. The simplest way to accomplish this task is by a trial and error procedure in which the operator manually changes the model parameters on the basis of engineering judgement. Automated inversion process have been proposed based on adequate mathematical algorithms and on numerical (Ganji et al. [13]) or analytical (Lai [14]) evaluation of the partial derivatives of the dispersion curves with respect to the model parameters.

A preliminary model must be selected for the first iteration of the inversion process. This task can be accomplished using an approximated procedure for the estimate of the stiffness profiles, as the one based on the relationship between wavelength and depth of soil involved in the propagation (Richart et al. [15]). Obviously additional information about the soil stratigraphy can be of great help at this stage.

Two case histories of soil characterisation using surface waves are presented, comparing the relative results to the ones of seismic borehole methods. In both cases the experimental dispersion curve has been estimated following the multistation procedure based on the use of an impact source and on the analysis in the frequency-wavenumber domain.

The experimental data have been collected using a 24 channel seismic seismograph and 4.5Hz natural frequency vertical geophones. In both cases two different test configurations have been adopted to estimate the experimental dispersion curve over a wide frequency range. For the short array a sledge hammer was used to generate high frequency signals, while for the long array a heavier source (a 130kg weight drop system) was chosen to obtain low frequency waves.

The first site is located in Castelnuovo Garfagnana (Tuscany Region, Central Italy). The local geology is such that at shallow depth alluvial deposits of well-graded gravels, sands and silts of variable thickness underlain by a clayey sand formation are found. Two different testing configurations with inter-receiver spacing of respectively 2m and 1m have been used for the frequency-wavenumber analysis of surface waves. The experimental dispersion curve and the numerical curve relative to the last iteration of the inversion process are reported in Fig. 3-a. The obtained shear wave velocity profile is shown in Fig. 3-b and it is compared to the results of a down-hole test. The results show the presence of very stiff materials, with the underlying clayey sand being even stiffer than the overlying gravelly soil.

The second example is related to a much slower deposit. The results are part of a survey carried out at the Leaning Tower of Pisa site, where the soil deposit is constituted by sandy layers over a uniform thick layer of NC clay starting at about 10m below the ground surface and having thickness of about 11m. The surface wave survey was conducted in this case using geophone spacing of 1m and 2.5m respectively. The shear wave velocity profile obtained from the inversion of the surface wave dispersion curve (Figure 4-a) is compared to the results of a cross-hole test executed not far from the survey location (Figure 4-b). It is important to point out that in this case the thickness of the layers for the inversion process have been chosen according to the stratification information given by a borehole log. Indeed the differences in stiffness between the layers are in this case very small and the inversion process is much more complicated, causing the need for some additional information to constrain the solution.

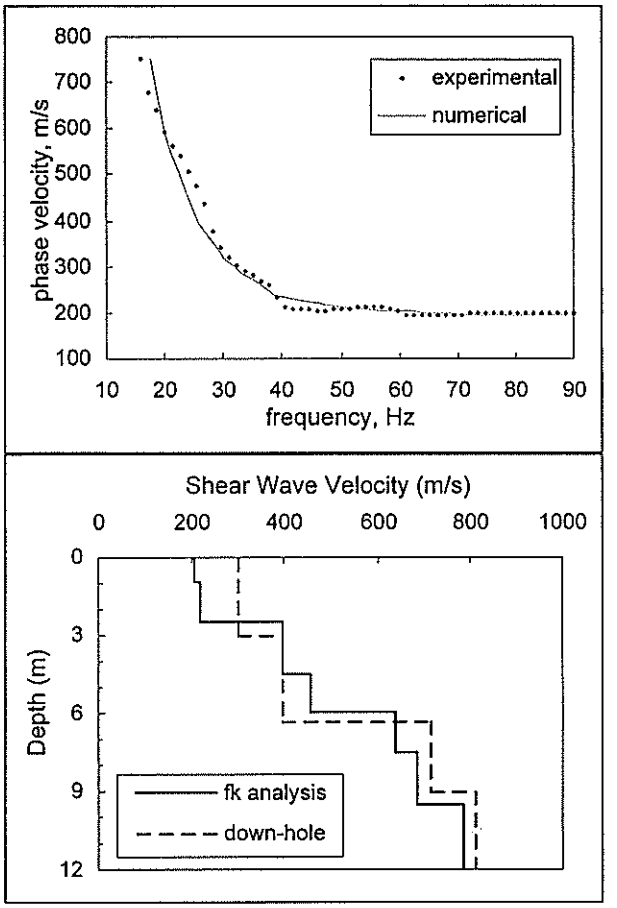

Figure 3 Experimental Results at Castelnuovo G.na (Italy): (a) dispersion curve (b) shear wave velocity profile

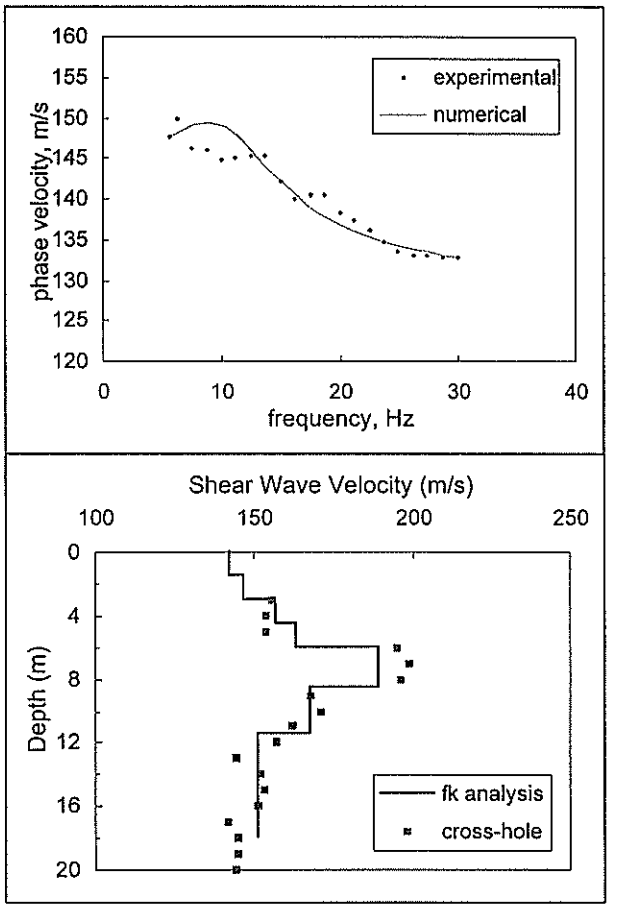

Figure 4 Experimental Results at Castelnuovo G.na (Italy): (a) dispersion curve (b) shear wave velocity profile

3 ADVANCED APPLICATIONS

Some advanced applications of surface wave testing have been proposed in the recent years. In the following the determination of damping ratio profile will be briefly discussed.

As surface waves travel away from the source their amplitude decreases. This decay is due in part to the geometrical spreading of energy over wider wavefronts (geometrical attenuation) and, for the remaining portion, to the internal dissipation in the medium (material attenuation). If the material attenuation is estimated experimentally from field measurement, it is possible to evaluate the damping parameters of the soil deposit by using an inversion process similar to the one used to infer the stiffness profile from the dispersion curve.

The proposed method is based on the following assumptions: a) the soil can be modelled as a layered visco-elastic medium; b) the shear damping ratio is not dependent on frequency. The material attenuation of surface waves can be estimated using a multistation approach based on the measurement of particle motion amplitude at several points on the ground surface at increasing distance from a controlled source (Rix et al. [16]). One of the most delicate aspects is related to the accurate estimate of the geometrical attenuation, which is needed to separate the material attenuation. For a homogenous medium, the geometrical attenuation is inversely proportional to the square root of the distance from the source, but in a layered medium it becomes a non-trivial function of the stiffness profile. For this reason the inversion process is carried out using the profile previously obtained with a classical SASW test (uncoupled procedure).

A coupled simultaneous inversion of both dispersion and attenuation curves is a mathematically better-posed problem, if compared to the uncoupled inversion (Lai [14]). In this view a new multistation scheme for the simultaneous measurement of dispersion and attenuation curves has been proposed, based on the transfer function concept (Rix et al. [17]). The experimental transfer function is obtained measuring the acceleration of a controlled harmonic

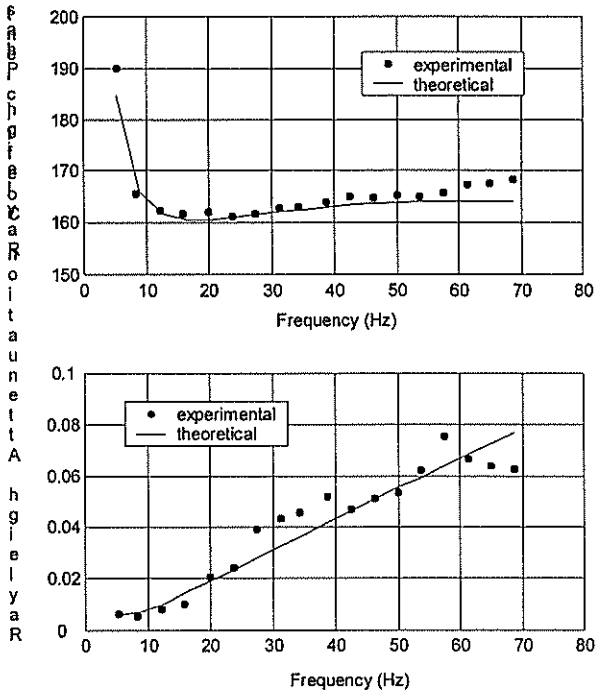

Figure 5 Experimental dispersion and attenuation curves (after Lai et al., 2001)

source and the induced motion at several locations along the ground surface. It is then used for a regression process in the complex number plane to estimate the frequency dependent complex wavenumber, which contain the phase velocity and attenuation information (Figure 5). The inversion of this complex quantity to obtain the stiffness and damping ratio profiles (Figure 6) can be therefore performed simultaneously in a consistent way (Lai et al. [18]).

4 CONCLUSIONS

Advantages of surface wave methods are mainly related to their non-invasive nature. The test is performed from the ground surface, saving time and money for perforation and casing of boreholes. This characteristic is even more valuable for peculiar situations as for example waste disposals in which avoiding boreholes is of primary importance.

Another significant aspect is related to the amount of tested volumes: surface wave tests give a global average estimate over a large testing volume. From this point of view the difference with the local measurement of borehole methods is very marked. Obviously details are missed, but the results well represent the average response of the soil deposit. On

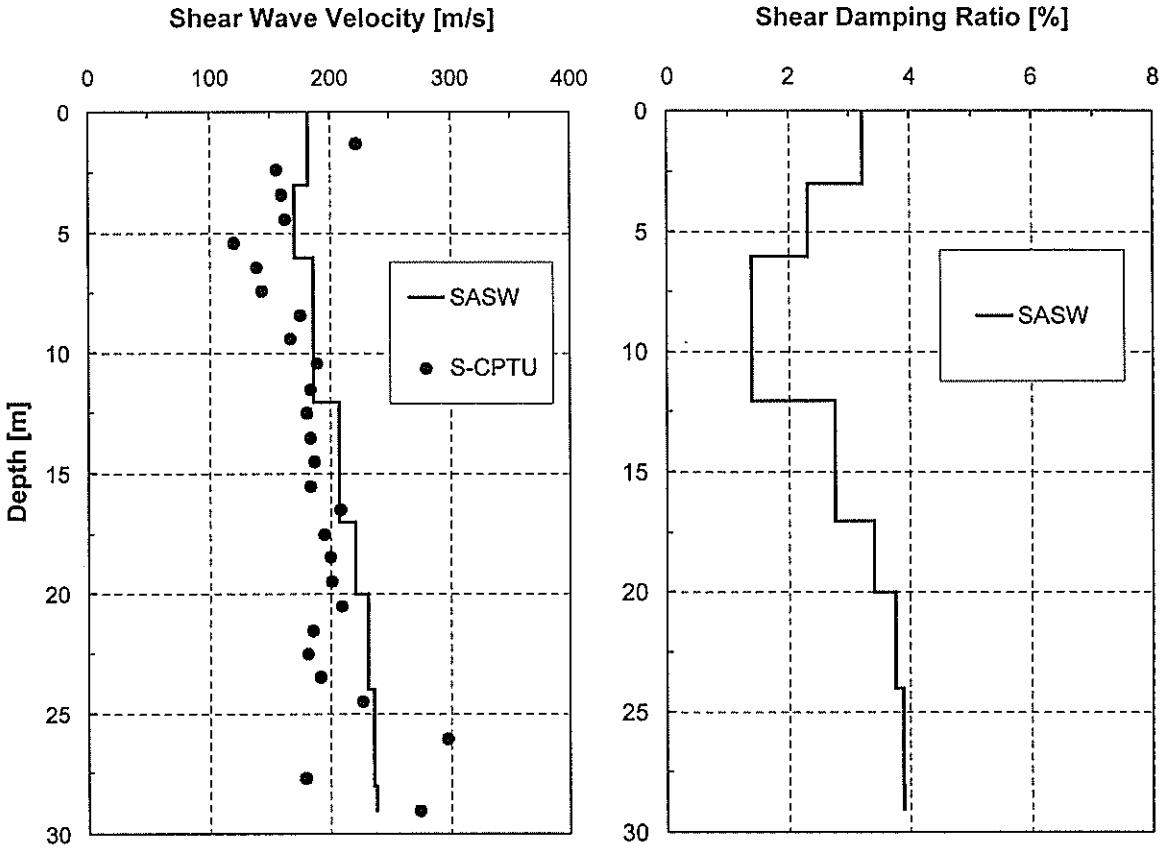

Figure 6 Shear wave velocity and damping ratio profiles (after Lai et al., 2001)

the other side, the resolution of thin layers especially at great depth suffers because of this characteristic of surface wave methods.

Concerning the testing depth, it is important to point out that the survey line should be sufficiently long, if the stiffness profile at great depth has to be estimated. A rule of thumb is that the survey length must be as long as about 3 times the maximum depth of interest. This requirement can be in contrast with the available space for some engineering problems. Moreover massive sources are needed to get good quality signals with long testing arrays, causing an increase of testing time and cost.

The experimental results reported in the present paper show that surface wave methods can be used to get an estimate of soil stiffness and damping ratio with a satisfactory degree of accuracy, as confirmed by the good agreement with borehole seismic results.

5 REFERENCES

1. Aki K., Richards P.G. (1980) "Quantitative seismology: theory and methods - 2 vol.", Freeman, S. Francisco
2. Jones R.B. (1958) "In-situ measurement of the dynamic properties of soil by vibration methods", Geotechnique, vol. 8 (1), pp. 1-21
3. Stokoe K.H. II, Wright S.G., J.A. Bay, J.M. Roesset (1994) "Characterization of geotechnical sites by SASW method", Geophysical Characterization of Sites (ISSMFE TC#10) by R.D. Woods, Oxford & IBH Publ., pp. 15-25
4. Gabriels P., Snieder R., Nolet G. (1987) "In situ measurements of shear-wave velocity in sediments with higher-mode Rayleigh waves", Geophys. Prospect., vol. 35, pp. 187-196
5. McMechan G.A., Yedlin M.J. (1981) "Analysis of dispersive waves by wave field transformation", Geophysics, vol. 46, pp. 869-874
6. Tokimatsu K. (1995) "Geotechnical site characterisation using surface waves", Prooc. 1st Int. Conf. on Earth. Geotechn. Eng., IS-Tokio, pp. 36
7. Zywicki D., Rix G.J. (1999) "Frequency-wavenumber analysis of passive surface waves", Proc. Symp. on the Appl. of Geophysics to Environm. and Eng. Problems, Oakland, pp. 75-84
8. Tselentis G.A., Delis G. (1998) "Rapid assessment of S-wave profiles from the inversion of multichannel surface wave dispersion data", Annali di Geofisica, vol. 41, pp. 1-15
9. Foti S. (2002) "Numerical and experimental comparison between 2-station and multistation methods for spectral analysis of surface waves", RIG (Italian Geotechnical Journal), n.1
10. Buchen P.W., Ben-Hador R. (1996) "Free-mode surface-wave computations", Geophys. J. Int., vol. 124, pp. 869-887
11. Gucunski N., Woods R.D. (1992) "Numerical simulation of SASW test", Soil Dyn. and Earthq. Eng., vol. 11 (4), Elsevier, pp. 213-227
12. Foti S., Lancellotta R., Sambuelli L., Socco L.V. (2000) "Notes on fk analysis of surface waves", Annali di Geofisica, vol. 43, n.6, 1199-1210
13. Ganji V., Gukunski N., Nazarian S. (1998) "Automated inversion procedure for spectral analysis of surface waves", J. Geotech. and Geoenv. Eng., vol. 124, ASCE, pp. 757-770
14. Lai C.G. (1998) "Simultaneous inversion of Rayleigh phase velocity and attenuation for near-surface site characterization", PhD Diss., Georgia Inst. of Techn., Atlanta (Georgia USA)
15. Richart F.E. Jr, Wood R.D., Hall J.R. Jr (1970) "Vibration of soils and foundations", Prentice-Hall, New Jersey
16. Rix G.J., Lai C.G., Wesley Spang A.W. Jr (2000) "In situ measurement of damping ratio using surface waves", J. Geotech. and Geoenvir. Eng., ASCE, vol. 126, pag. 472-480
17. Rix G.J., Lai C.G., Foti S. (2001) "Simultaneous Measurement of Surface Wave Dispersion and Attenuation Curves", Geotech. Testing J., ASTM, Vol. 24, No. 4, pp. 350-358
18. Lai C.G., Rix G.J., Foti S., Roma V. (2001) "Application of Multi-Station Methods to Surface Wave Testing", Proc. 10th Int. Conf. on Soil Dyn. And Earthq. Eng., Philadelfia, USA, October 7-10

Linden Bends - Stage IV, Great Western Highway, Road Widening and Realignment

Tony Gourlay, BE, MIEAust, CPEng, MAGS
Geotechnical Engineer, Arup, Sydney, Australia

Summary Road widening and realignment of the Great Western Highway has been proposed at Linden Bends in the Blue Mountains by the Roads and Traffic Authority of New South Wales (RTA). This forms part of a programme of upgrading of the Great Western Highway to a four-lane highway.

This paper describes the extensive site investigations carried out at two steep vegetated sloping fill embankments at Linden Bends using conventional and specialist drilling equipment. It outlines the development of road widening options considered for each embankment and discusses the analysis and design undertaken for anchored and cantilever bored pile retaining walls, the preferred road widening options. Also presented is the interpretation of the investigation findings, including material strength parameters adopted for detailed design. Geotechnical aspects of the retaining wall design are illustrated and a summary of the analyses is given.

1 INTRODUCTION

In May 2000, the RTA commissioned Arup to carry out detailed geotechnical site investigations, a concept design and the subsequent detailed design and documentation for Stage IV of the road widening and realignment of the Great Western Highway at Linden Bends. The geotechnical investigations were carried out at two steeply sloping fill embankments that forms part of the existing highway– (referred to here as Fill 1 and Fill 2) (see Figure 1).

Following the geotechnical site investigation, road widening options for Fill 1 and Fill 2 were developed with the RTA and concept designs produced for feasibility assessment and costing purposes. Detailed design of the preferred road widening options for Fill 1 and Fill 2 was subsequently carried out.

This paper discusses the investigations, concept designs and detailed design of anchored and cantilevered bored pile retaining wall options for both Fill 1and Fill 2.

2 BACKGROUND

Linden Bends, Stage IV, is located approximately 78km west of Sydney in the Blue Mountains (See Figure 1). The topography of the area is steep, undulating and covered with dense vegetation, rising from Faulconbridge towards Woodford. The original embankments for Fill 1 and Fill 2 have been built in close proximity to the railway lines which run parallel to the existing road alignment. They were constructed with significant cut to fill sections to traverse the original natural steeply sloping gullies.

Historical records indicated it was probable that Fill 1 and Fill 2 had undergone successive widening over the last 80 years. Some of the road embankment construction may have been formed by end tipping rather than by construction in layers.

Due to these topographic conditions, the site was too steep to accommodate conventional fills for the road widening scheme. As such, it would require construction of bridging and/or retaining structures at both Fill 1 and Fill 2.

3 EXISTING EMBANKMENTS

3.1 Fill 1

Fill 1 was approximately 140m long. At the commencement of the geotechnical site investigation, the embankment comprised a single bench approximately 1.5m to 3m below the existing roadway, and about 4m to 7m wide. The upper slope was typically 30° whilst the lower slope was typically 35° to 37° with locally steeper areas.

3.2 Fill 2

Fill 2 was approximately 110m long. At the commencement of the geotechnical site investigation, the embankment comprised a single slope that was typically 32° to 36° with locally steeper areas.

4 GEOLOGY

The geology of the site is typical of the Blue Mountains. It is underlain by Mid-Triassic Hawkesbury Sandstone, described as fine to medium grained sandstone, with occasional minor shale and laminite lenses.

5 SITE INVESTIGATIONS

5.1 Boreholes

5.1.1 Concept Design Phase

A total of 16 boreholes were drilled at Fill 1 and 14 boreholes drilled at Fill 2 in August and September 2000. Boreholes were located on the existing embankments and on the shoulder and verge of the existing westbound carriageway.

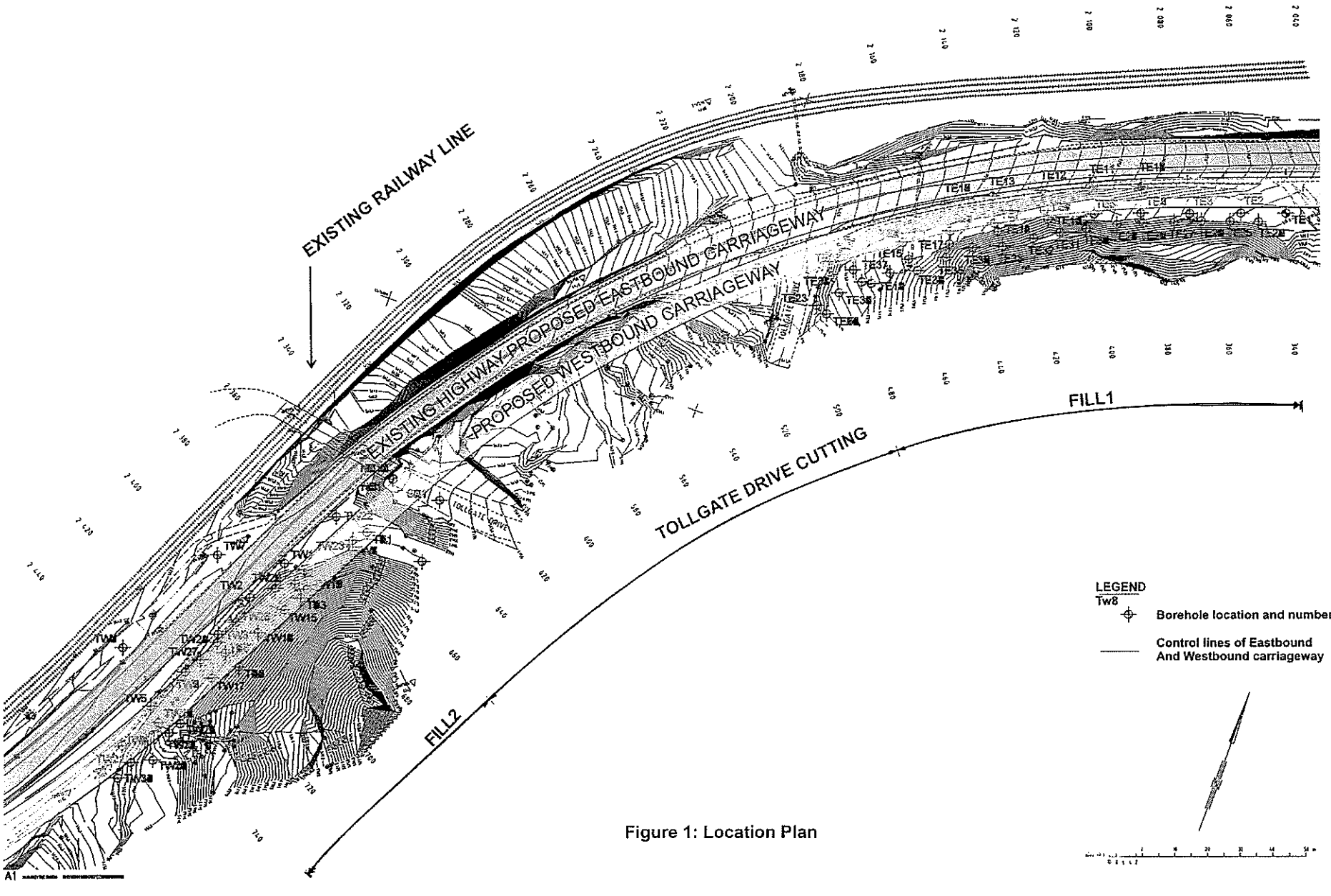

Figure 1: Location Plan

All boreholes were rotary drilled through the fill embankments using auger drilling and wash boring techniques until bedrock was encountered. From bedrock level, rock core samples were recovered using an NMLC size triple tube core barrel. The bedrock was cored to sufficient depth to recover Class II rock. This ensured that the material encountered was in fact bedrock, as opposed to boulders which were occasionally encountered in the fill embankments.

Standard Penetration Tests (SPT) were generally carried out in the overburden soils in the boreholes at approximately 1.5m intervals. Point Load Strength Index Tests were carried out on the rock core samples at approximately 1m intervals. Standpipe piezometers were installed in selected boreholes to monitor groundwater levels in the fill embankments.

Truck-mounted and specialist track-mounted drilling rigs were utilised for the investigations depending on access conditions to each borehole. Avoiding lane closure of the existing highway during the geotechnical investigations was a major requirement of the project. This was achieved using a track-mounted drilling rig positioned on the shoulder or verge of the existing highway without blocking the flow of traffic. While traffic management was still required, lane closure was ultimately avoided. The track-mounted rig was also used for traversing the steep embankments to reach difficult borehole positions unable to be reached by conventional truck-mounted rigs.

5.1.2 Detailed Design Phase

During the detailed design phase, an additional 12 boreholes (5 at Fill 1 and 7 at Fill 2) were drilled by the RTA between May and July 2001. They were drilled in areas where there was a lack of information for detailed design, namely the depth to bedrock along the line of the proposed retention structures. Both truck and track-mounted drilling rigs were used to drill the boreholes. The additional information obtained from these boreholes resulted in some design revisions.

5.1.3 Pretender Phase

The design of the retention structures was based on achieving moment fixity and toe restraint in the bedrock. Therefore, at the completion of the detailed design phase, this design requirement was verified by drilling 26 proof holes (17 at Fill 1 and 9 at Fill 2) beyond the toe of the proposed retention structures. The proof holes were used to determine the depth to rock and check for adverse defects that could affect moment fixity and toe restraint in the bedrock. The additional borehole information resulted in some design revisions. These holes were drilled by the RTA in September 2001using a truck and track-mounted drilling rig.

5.2 Laboratory Testing

Laboratory testing was carried out during the concept and detailed design phase of the investigation and comprised Particle Size Distribution, chemical tests on groundwater samples and Unconfined Compressive Tests (UCS) on rock core samples. The rubble nature of the embankment fill limited the type of testing that could be carried out on this material.

6 INVESTIGATION FINDINGS

6.1 Subsurface Profile

6.1.1 General

The subsurface profile encountered at both Fills 1 and 2 during the concept design phase of the investigation was similar. It generally comprised between 2m to 10m of fill material overlying sandstone bedrock. A thin layer (<1m) of residual soil overlying the bedrock was encountered in 3 boreholes. The depth to bedrock varied over the length of both Fill 1 and Fill 2.

6.1.2 Fill Material

The fill material could be described as ripped or crushed sandstone, generally comprising sand with sandstone gravel, cobbles and boulders. It had a mostly very loose to loose consistency with isolated denser zones. SPT 'N' values recorded in the fill material were generally equal to or less than 10.

6.1.3 Sandstone

The sandstone bedrock is essentially horizontally to sub-horizontally bedded at about 0° to 20°. Generally no adverse jointing or defects were identified in the boreholes however some minor shale layers were encountered. A zone of poorer quality rock was also encountered which could potentially have had an impact on the stability of the proposed retention structures.

At the top of the rock, it could be described as extremely to slightly weathered, extremely low to medium strength with some high strength rock. It could be classified as Class V to Class III sandstone in accordance with Pells et. al. (1).

Generally the strength of the sandstone increased with depth, typically medium strength with the occasional low or high strength section of sandstone. It could be classified as Class III sandstone on average with Class V, IV and Class II zones in accordance with Pells et. al. (1).

6.2 Groundwater Conditions

Standing groundwater levels recorded in the piezometers during and after the scheme design phase of the investigation indicated that in general, the phreatic surface was typically at or just above the top of rock level. Water level readings of between 0.3m to 1.8m above the top of rock level were measured.

6.3 Laboratory Results

6.3.1 Particle Size Distribution

Particle size distribution results confirmed that the fill material was variable, but essentially sandy in nature. The fines content (percent passing the 0.075mm sieve) varied from 6% to 30% which indicates that the fill material has a variable permeability. It is therefore not

entirely free draining although due to the nature of the material, there will be more permeable drainage zones throughout the fill material.

6.3.2 Groundwater Analysis

Groundwater samples extracted from the standpipe piezometers were analysed for chloride ion and sulfate ion concentration, pH and electrical conductivity. The results indicated that the groundwater was slightly acidic to neutral, however in terms of durability of in-ground structures, the subsoil environment was not considered to be aggressive.

6.3.3 Unconfined Compressive Strength (UCS)

The UCS test results confirmed the field assessed rock strengths. Based on a comparison between the UCS results with the point load strength index $Is_{(50)}$ results, the following empirical relationship was appropriate for estimating the UCS of the sandstone:

$$UCS = Is_{(50)} \times 20$$

7 CONCEPT DESIGNS

7.1 General Considerations

At the completion of the concept design phase of the geotechnical site investigation, consultation with the RTA led to the consideration of various road widening and realignment options, with a detailed design completed for the most appropriate option. In developing a suitable option, three main issues were required to be addressed and include:

- budgetary constraints
- avoiding closure of the existing highway during construction
- improving the stability of the existing embankments

Thus the existing highway would form the new eastbound carriageway and the proposed road widening would form the new westbound carriageway.

7.2 Road Widening and Realignment Options - Fill 1

The following road widening and realignment options were considered at Fill 1:

- Reinforced Soil Structure
- Bridging Structure
- Anchored Bored Pile Retaining Wall (Preferred Option)

7.2.1 Reinforced Soil Structure

This option required partial closure of the existing highway or the construction of a temporary sheet pile wall to allow construction to proceed. Partial closure of the highway was not feasible and construction of a temporary sheet pile wall would have been costly and difficult to install in the bouldery fill. This option was therefore abandoned.

7.2.2 Bridging Structure

The construction of a bridge adjacent to the existing highway was rejected on the basis of cost.

7.2.3 Anchored Bored Pile Retaining Wall (Preferred Option)

This option involved the construction of a 120m long anchored bored pile retaining wall along the control line of the proposed westbound carriageway (See Figure 2). The new carriageway would be constructed at approximately the same level as the existing road and the pile wall would therefore support the new carriageway.

The wall itself varied in height (ie from toe of pile to top of wall) from approximately 9m to 20m. It comprised:

- 1200mm diameter bored piles constructed at 1.5m centres and socketed into class IV or better sandstone
- a capping beam constructed on top of the piles
- a single row of rock anchors installed through the capping beam at 3m centres where the height of the retaining wall was less than 15m
- two rows of rock anchors installed through the capping beam at 3m centres where the height of the retaining wall was between 15m and 20m
- a concrete stem wall constructed on top of the capping beam taken to the new road level. The stem wall varied in height from approximately 2m to 5m

This option was selected on the basis of cost, constructability, avoidance of road closure and because it improved the overall stability of the Fill 1 embankment.

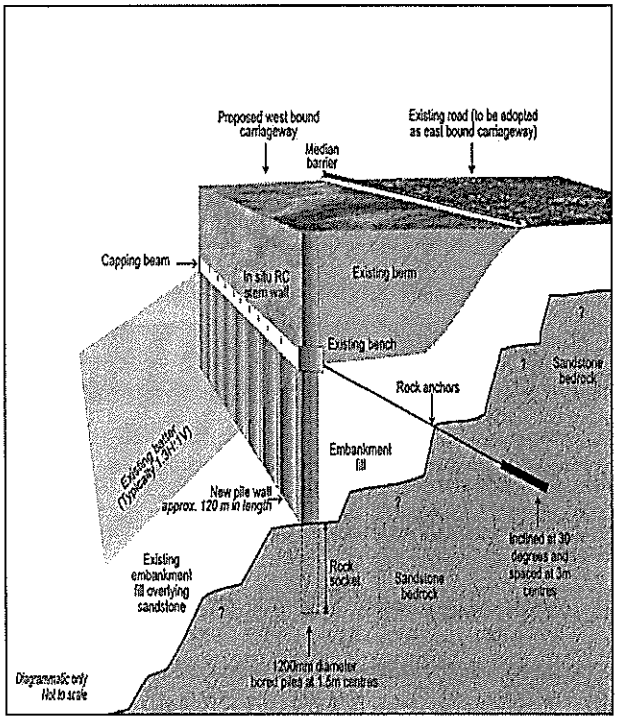

7.3 Road Widening and Realignment Options - Fill 2

The following road widening and realignment options were considered at Fill 2:

- Bridging Structures
- Anchored Bored Pile Retaining Wall
- Combined Bridging Structure & Bored Pile Retaining Walls (Preferred Option)

7.3.1 Bridging Structure

This option involved constructing a bridge for the new westbound carriageway and replacing the existing highway with a bridge to form the new eastbound carriageway. Similar to Fill 1, this option was rejected on the basis of cost.

7.3.2 Anchored Bored Pile Retaining Wall

This was similar to the preferred Fill 1 option. It involved the construction of an anchored bored pile retaining wall along the control line of the westbound carriageway. The new carriageway would be constructed at about the same level as the existing road and the pile wall would therefore support the new carriageway. This option was abandoned due to constructability concerns and the risk of cost overruns.

7.3.3 Combined Bridging Structure & Bored Pile Retaining Walls (Preferred Option)

This option involved supporting the majority of the westbound carriageway on a 3 span, 87m long bridge and the remaining section supported by a 23m long cantilever bored pile retaining wall. A 60m long anchored bored pile wall would support part of the eastbound carriageway, improving the overall stability of the embankment supporting the eastbound carriageway (See Figure 3).

The western bridge abutment was supported on a cantilever bored pile wall designed by Arup and the eastern abutment and bridge structure was designed by the RTA.

The retaining walls varied in height (i.e. from toe of pile to top of wall) from approximately 7.0m to 12.5m. They comprised:

- 900mm diameter bored piles constructed at 1.2m centres and socketed into class IV or better sandstone
- a capping beam constructed on top of the piles
- a single row of rock anchors installed through the capping beam at 2.4m centres for the eastbound carriageway wall (i.e. cantilever wall for the westbound carriageway wall and western bridge abutment)
- a concrete stem wall constructed on top of the capping beam taken to the new road level. The stem wall varied in height from approximately 2m to 4m.

This combination of a bridging structure with bored pile retaining walls was selected on the basis of cost, constructability, avoidance of road closure and because it improved the overall stability of the Fill 2 embankment.

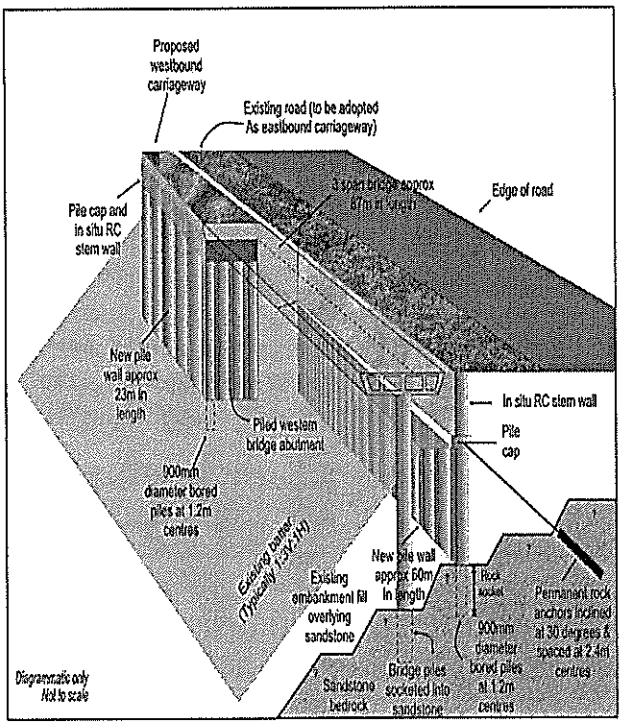

Figure 3: Combined Bridging Structure & Bored Pile Walls (Anchored & Cantilever) – Fill 2

8 DETAILED DESIGN

8.1 Geotechnical Parameters

8.1.1 Characteristic Material Properties

The characteristic material properties (namely shear strength parameters and Young's Modulus) were determined from laboratory and in situ test results, correlation between in situ test results and empirical relationships and from guidance provided in BS8002 (2) and Pells. et. al. (1). The characteristic material properties are presented in Table 1 below.

Material	γ (kN/m^3)	C_u (kPa)	ϕ' (°)	c' (kPa)	E_u (kPa)	E' (kPa)
Existing Fill	19	---	36	0	---	25,000
Sandstone (Class IV)	23	500	---	0	200,000	---

Table 1: Characteristic Material Properties

Effective friction angles adopted for the existing fill material at Fill 1 and Fill 2 correlate well with the batter angles recorded during survey of the embankments. This indicates that the fill batters were placed at an angle close to the effective friction angle of the fill material.

8.1.2 Design Material Properties

Design material properties were derived by multiplying the characteristic material properties by relevant material factors or "strength reduction factors" for serviceability

This indicates that the fill batters were placed at an angle close to the effective friction angle of the fill material.

8.1.2 Design Material Properties

Design material properties were derived by multiplying the characteristic material properties by relevant material factors or "strength reduction factors" for serviceability and ultimate limit states in accordance with Austroads – 1992 (3). The application of material factors provides a factor of safety on the material properties.

For serviceability limit states, a material factor of 1 was applied to the characteristic material properties. These parameters were used to determine serviceability bending moments, shear forces, anchor loads and displacements.

For ultimate limit states various material factors were applied to the characteristic material properties in accordance with Table 3.4.6.3 of Austroads – 1992 (3). These parameters were used to determine ultimate bending moments, shear forces and anchor loads.

8.1.3 Design Groundwater Levels

A maximum groundwater level of 2 m above the top of rock level was adopted for detailed design based on recorded water levels in the piezometers. For both serviceability and ultimate limit states, load factors were applied to the hydrostatic water pressure in accordance with Article 3.4.3.5 of Austroads – 1992 (3).

8.2 Design Loads

8.2.1 Surcharge Loads

For serviceability limit states, construction, traffic and pedestrian surcharges were considered in the design in accordance with Article 2 of Austroads – 1992 (3). For ultimate limit states various material factors were applied to the serviceability surcharge loads in accordance with Table 3.4.3.2 (A) of Austroads – 1992 (3)

8.2.2 Collision Load

For ultimate limit states, a barrier collision load (for a crash barrier located at the top of the retaining walls) was considered in the design and derived in accordance with Article 2.7 of Austroads – 1992 (3).

8.2.3 Earthquake Load

For serviceability and ultimate limit states, an earthquake load associated with an event having a 2000 year return interval was considered in the design in accordance with Article 2.13.3 of Austroads – 1992 (3).

8.3 Retaining Wall Analysis and Design

8.3.1 Geotechnical Analysis

The preferred anchored and cantilever bored pile retaining options at Fill 1 and Fill 2 were designed in accordance Austroads - 1992 (3). The retaining wall analysis was undertaken using FREW from the Oasys Suite of Geotechnical Software. FREW is a finite difference program that models the behaviour of a flexible retaining wall allowing for interaction between the wall and the soil. FREW analyses the various stages of construction and calculates wall bending moments, shear forces, deflections and anchor loads for each construction stage.

8.3.2 Design Philosophy

The bored pile retaining walls were designed on the basis of achieving moment fixity in a class IV or better rock socket. This enabled a more even distribution of bending moments over the length of the pile hence utilising the bending moment capacity of the piles more efficiently. A rock socket of between 2.5m and 3m was typically used.

Toe restraint was required at the base of the wall and for this reason it was important that no adverse slip planes occurred in the rock close to the toe of the wall.

8.3.3 Limit States Design

Limit state design was applied in accordance with Austroads - 1992 (3) and both ultimate and serviceability limit state cases were analysed.

8.3.4 Load Combinations

8.3.4.1 Ultimate Limit States

The following load combinations were analysed for ultimate limit states:

- Permanent Effects + Ultimate Traffic Load + Ultimate Pedestrian Load
- Permanent Effects + Ultimate Collision Load
- Permanent Effects + Earthquake Load

8.3.4.2 Serviceability Limit States

The following load combinations were analysed for serviceability limit states:

- Permanent Effects + Traffic Load + 0.7 x (Pedestrian Load)
- Permanent Effects + Traffic Load + 0.7 x (Earthquake Load)

8.3.5 Construction Sequence

Summarised below is the typical construction sequence adopted for bored pile retaining wall analysis at both Fill 1 and Fill 2.

Stage 1 Install bored piles. Socket into Class IV or better sandstone
Stage 2 Construct capping beam
Stage 3 Install rock anchors through capping beam and stress anchors (this stage excluded for cantilever walls)
Stage 4 Construct stem wall above capping beam to design road surface level (
Stage 5 Backfill behind stem wall to design ground levels including installation of wall drainage
Stage 6 Construct road surface, safety barriers, and pedestrian walkway
Stage 7 Apply long term conditions: wall relaxation and Ko earth pressures behind wall

Stage 8 Raise groundwater level to 2m above top of rock level
Stage 9 Remove passive (fill) support in front of wall
Stage 10 Apply vehicle impact load (ULS only)
Stage 11 Apply earthquake loading

8.3.6 Permanent Rock Anchors

For the permanent rock anchors, minimum design working loads, minimum lock off loads, minimum bond lengths and minimum factors of safety on working loads were specified on the design drawings.

To ensure the adopted rock anchor system for the contract would achieve the design working loads the following tests were specified:

- three proving tests to be carried out on trial anchors prior to construction of the contract anchors for the walls at each embankment
- suitability tests to be carried out on 10% of all contract anchors for the walls at each embankment
- acceptance tests to be carried out on all contract anchors for the walls at each embankment

All tests were to be carried out in accordance with RTA specification R56 (4).

Factors of safety on anchor working loads were specified in accordance with BS8081 - Code of Practice for Ground Anchorages (5) as follows:

- Tendon: FOS =2
- Rock/grout interface: FOS =3
- Grout/tendon or grout/encapsulation interface: FOS = 3

8.4 Results of Analysis

8.4.1 Ultimate Limit States

The results of the analysis generally indicated that for ultimate limit states, permanent effects plus earthquake loading governed the designs. Bending moments and shear forces in the piles were at their greatest for the higher wall sections (i.e. 15m to 20m) with the requirement for 40MPa concrete and up to about 2.5% steel reinforcement.

More typically, the bending moments and shear forces encountered in the piles led to the requirement for 30MPa concrete and between 1.5% to 2.5% steel reinforcement.

8.4.2 Serviceability Limit States

Estimated lateral wall deflections varied depending on the height of wall section analysed and were typically in the order of 10mm to 50mm. The magnitudes of the estimated deflections were considered acceptable for walls of this nature.

Minimum working loads on the permanent rock anchors ranged from 385kN to 1315kN. Minimum lock-off loads varied from 300kN to 450kN.

9 MONITORING REQUIREMENTS

To validate the design assumptions and to monitor the performance of the walls at Fill 1 and Fill 2, inclinometer casing will be installed in the walls so that deflections can be measured during and after construction. Inclinometer casing will be also be installed into the bedrock below pile toe level to monitor the performance of the rock socket which is critical in terms of achieving moment fixity and toe restraint.

10 CONCLUSIONS

Detailed geotechnical site investigations comprising 68 boreholes drilled on steep vegetated embankments and adjacent to the existing highway have been successfully completed without the need for road closure. This was achieved using both conventional and specialised drilling equipment and highlights the value in utilising specialist rigs for sites with difficult or constrained access conditions.

This paper outlined the development of road widening options for both Fill 1 and Fill 2. The preferred road widening options were anchored bored pile walls for Fill 1 and a combined bridging structure and bored pile walls (anchored and cantilever) for Fill 2. In addressing the RTA's selection criteria, these preferred options were adopted on the basis of:

- cost effectiveness in comparison to other options
- constructability in terms of traversing the steep terrain, hence negating the requirement for closure of the existing highway
- improving the stability of the existing embankments by retention

Detailed analysis and design of the preferred retention structures was completed in accordance with Austroads - 1992. Analysis was carried out using the Oasys software FREW. This allowed modelling of moment fixity and toe restraint in the pile sockets, a critical factor in the performance of the retaining structures.

The results of the analysis indicated permanent effects plus earthquake loading governed the designs. Estimated deflections were in the order of 10mm to 50mm and were considered acceptable for walls of this nature.

This project has emphasised the benefit of working closely with a client such as the RTA who was conversant in the various technical aspects of the project. This is valuable in developing sound technical and cost effective solutions to challenging problems such as the road widening and realignment at Linden Bends.

11 ACKNOWLEDGEMENTS

The author wishes to thank the Roads and Traffic Authority of New South Wales for allowing this paper to be published.

12 REFERENCES

1 Pells, PJN, Mostyn, G and Walker, BF, *Foundations on Sandstone and Shale in the Sydney Region*, Australian Geomechanics Journal, No. 33, Part 3, December 1998

2 British Standard, *BS8002 – 1994, Code of Practice for Earth Retaining Structure*

3 *AUSTROADS Bridge Design Code*, 1992, AUSTROADS, Sydney

4 Roads and Traffic Authority, *Specification R56 - Permanent Rock Anchors,* Edition 2, Revision 3, 1999

5 *British Standard, BS8081 – 1989, Code of Practice for Ground Anchorages*

6 Ove Arup & Partners, *Linden Bends Stage IV-Geotechnical Site Investigation Report*, October 2001

7 Ove Arup & Partners, Linden Bends Stage IV-Retaining Options for the Road Widening and Realignment Report, February 2001

Title: Combined Loading of Skirted Foundations

Susan Gourvenec
Centre for Offshore Foundations Systems (COFS), University of Western Australia, Perth, Australia.

In this paper the results of two and three-dimensional finite element analyses of the combined loading of strip and circular skirted foundations on homogenous and non-homogeneous clay are presented. The results are presented in terms of the shape of the failure envelope in vertical, moment and horizontal loading space and compared with data from similar studies where either soil non-homogeneity or three-dimensional geometry was investigated.

1 BACKGROUND

1.1 Bearing capacity of shallow foundations

Much of the existing work relating to failure conditions of shallow foundations pertains to strip footings subjected to predominantly vertical loading resting on homogenous deposits. In the field of offshore engineering, foundations are typically quasi-circular; environmental conditions result in foundations being subjected to substantial lateral and moment forces; and soil shear strengths tend to increase with depth below foundation level.

The conventional bearing capacity equation, originally proposed by Terzaghi[1] (1943), in conjunction with the various modification factors available to take account of load orientation and non-uniform soil conditions (e.g. Brinch-Hansen[2],1970 and Meyerhof[3], 1980) has been shown to be non-conservative for combined loading of strip foundations even in homogeneous clay soils (Ukritchon[4] *et al*, 1998), and its reliability becomes increasingly questionable for circular foundations on non-homogeneous soils subjected to combined loading (Martin[5] and Randolph, 2001).

1.1 Skirted foundations

Skirted foundations are shallow foundations, usually circular, with thin skirts (either a single circumferential skirt or multiple concentric skirts) which penetrate the soil vertically such that there is a bearing area on the seabed with a confined soil plug underneath.

The presence of the skirt alters the behaviour of the foundation significantly compared to the more conventional type of flat or conical shallow foundations, enhancing vertical, horizontal and moment load capacity. Vertical bearing capacity is enhanced as soft surface soils are confined within the skirt and transfer the foundation loads down to harder underlying layers; horizontal load capacity is enhanced due to the embedment of the skirt resisting lateral loads against sliding; and moment load capacity is enhanced due to suctions developed within the skirt during undrained moment loading which resist against uplift.

In soft normally consolidated deposits, typical of many marine sediments, a conventional shallow foundation would have a small bearing capacity and large foundation settlements would occur before significant bearing capacity could be achieved. Skirted foundations provide a desirable alternative to deep foundations as they transfer loads beneath the surface, increase lateral resistance to sliding and provide uplift capacity without the installation complexity and expense of pile driving.

2 FINITE ELEMENT MODEL

2.1 Geometry and material parameters

Finite element analyses of a rigid rough circular footing (of diameter D) founded on the surface of a normally consolidated purely cohesive Tresca soil with both a uniform and a linearly increasing shear strength profile were carried out. The skirt was not modelled in terms of embedment but full adhesion on the foundation/soil interface was assumed enabling tensile forces to be sustained. The material properties used in the analyses are summarised in Table 1. All the analyses were carried out with the finite element program ABAQUS.

Table 1 – Summary of material properties used in finite element analyses

		E kPa	ν	Su kPa
Soil	Homogenous $kD/Su_0=0$	2500	0.5	5
	Non-homogenous $kD/Su_0=2$	2500	0.5	5+z
Foundation		3E10	0.15	-

The shear strength profile is expressed as $Su=Su_0+kz$ where Su_0 is shear strength at the level of the skirt tips, k is the rate of increase of the undrained shear strength with depth and z is the depth below the skirt tips. It is also convenient to express the degree of soil strength non-homogeneity in terms of the non-dimensional factor kD/Su_0 (where D is the width or diameter of the foundation). A non-homogeneity factor $kD/Su_0=2$ was chosen for this study which corresponds to a foundation of diameter D=10m for Su_0=5kPa and k=1kPa/m depth. For a skirted foundation $Su_0=kd$, where d is the skirt depth, such that $kD/Su_0=D/d$, which for the conditions modelled gives d=5m. The magnitude of non-homogeneity factor was chosen as Houlsby[6] and Wroth

(1983) identified this degree of non-homogeneity to result in a shape factor (ζ_s) of approximately unity in terms of vertical bearing capacity.

2.1 Finite element mesh

The finite element mesh is shown in Figure 1. The mesh comprises 3444 second order continuum elements, wedge elements forming the central core of the mesh and hexahedral (brick) elements forming the remaining mesh. Fully integrated wedge elements are mixed with reduced integration brick elements as reduced integration wedge elements are not available in ABAQUS.

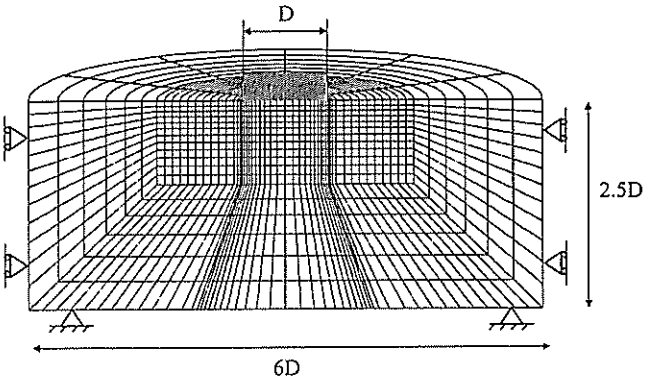

Figure 1 – Finite element mesh

3 ANALYSES

3.1 Side-swipe tests

Side-swipe type displacement probes were used to impose load paths in vertical:horizontal (V:H), vertical:moment (V:M) and horizontal:moment (H:M) load space (Tan[7], 1990). For a side-swipe test in *i:j* space a displacement u_i is imposed from a zero load state until the ultimate load F_{0i} is reached. Further incremental displacement in the *i* direction is then constrained (i.e. $\delta u_i=0$) while a displacement u_j is imposed until the ultimate load F_{0j} is reached. Because elastic stiffness is much greater than plastic stiffness the stress path in the second stage will almost exactly follow the shape of the failure locus as negligible expansion of the failure locus will be required to balance the small elastic deformation.

3.2 Comparative analyses

Plane strain analyses were also carried out to enable comparison of the results of the circular footing with the case of a strip footing. A two-dimensional mesh of the same geometry and discretisation as the front face of the three-dimensional mesh was created, composed of second order reduced integration quadrilateral elements for compatibility with the second order reduced integration hexahedra used in the three-dimensional mesh. Equivalent boundary conditions, soil conditions and analysis procedures were modelled.

4 RESULTS

4.1 Ultimate loads

Table 2 summarises the ultimate vertical load (F_{V0}) calculated in this study along with the available published data of vertical bearing capacity under equivalent conditions. Table 3 presents a similar comparison for the ultimate horizontal load (F_{H0}) and Table 4 presents values of the ultimate moment (F_{M0}) (i.e. at $F_V=0$, $F_H=0$) and the maximum moment (F_{Mmax}). The ultimate loads are presented non-dimensionally by F_{V0}, F_{H0} and F_{M0}, where $F_{V0}=V_0/ASu_0$, $F_{H0}=H_0/ASu_0$ and $F_{M0}=M_0/ADSu_0$.

4.2 Failure envelopes

The failure loci calculated from the finite element analyses are shown in Figures 2a-c along with various published data. The load paths are plotted in non-dimensional load space in terms of F_V, F_H and F_M, where $F_V=V/ASu_0$, $F_H=H/ASu_0$ and $F_M=M/ADSu_0$ respectively The failure loci are symmetrical unless shown otherwise.

5 DISCUSSION

5.1 Vertical bearing capacity

The ultimate bearing capacity under pure vertical load (F_{V0}) for the strip footing on the homogenous soil calculated in the finite element analysis of 5.21 compares well with the exact solution of 5.14 (Prantl[8], 1920; Terzaghi[1], 1943), and for the case of the circular footing on the homogeneous deposit $F_{V0}=5.91$ comparing well with the exact solution of 6.05 (e.g. Shield, 1955[9])

There is no exact solution for the vertical bearing capacity of a strip or circular footing on a non-homogeneous deposit. However plasticity stress characteristic solutions are presented by Davis[10] and Booker (1973) for a strip footing and by Houlsby[6] and Wroth (1983) for both strip and circular foundation geometry and Martin[11] (2001) presents upper bound solutions for circular footings. The results from this study compare well with the published solutions (Table 2).

For the case of the strip footing founded on the non-homogenous deposit it is of interest to compare with the commonly used empirical expression of Peck[12] *et al* (1953), $F_{V0}=Nc_0(1+0.5kD/Su_0)$ which implies an 'equivalent shear strength' (Su_{eq}) equal to the average value of Su over a depth of D below the foundation. The approach gives $F_{V0}=10.28$ which over estimates the finite element solution by over 30%.

All the results are summarised in Table 2.

5.2 Horizontal load capacity

Calculation of the ultimate horizontal load (H_0) for a surface seated foundation is trivial as it will equal the undrained shear strength of the material (Su) with failure occurring as sliding along the seabed at shear stresses in excess of Su. As a result $F_{H0}=1.0$ irrespective of foundation geometry or the degree of soil strength

Table 2 – Ultimate vertical loads

		$kD/Su_0=0$	$kD/Su_0=2$
This study	Strip	5.20	7.71
	Circular	5.91	7.46
Prantl (1920)	Strip	5.14	-
Shield (1955)	Circular	6.05	-
Davis & Booker (1973)	Strip	-	7.65
Houlsby & Wroth (1983)	Strip	-	7.57
	Circular		7.61
Martin (2001)	Circular	-	7.63
Peck *et al* (1953)	Strip	-	10.28

Table 3 – Ultimate horizontal loads

		F_{H0}	
		$kD/Su_0=0$	$kD/Su_0=2$
This study	Strip	1.01	1.02
	Circular	1.03	1.04
Theoretical	Strip	1.0	1.0
	Circular	1.0	1.0

Table 4 – Ultimate and maximum moment loads

		F_{M0}	
		$kD/Su_0=0$	$kD/Su_0=2$
This study	Strip	0.72	1.01
	Circular	0.70	0.94
Theoretical	Strip	0.69	0.96
	Circular	0.67	0.88
		F_{Mmax}	
This study	Strip	0.81 F_H=0.88	1.19 F_H=0.80
	Circular	0.80 F_H=0.84	1.07 F_H=0.74
Ukritchon *et al* (1998)	Strip	0.80 F_H=0.80	
Bransby & Randolph (1998)	Strip	0.89 F_H=0.90	0.89 F_H=0.80
Taiebat & Carter (2000)	Circular	0.89 F_H=0.77	-
Randolph (2001)	Circular	0.78 F_H=0.94	-

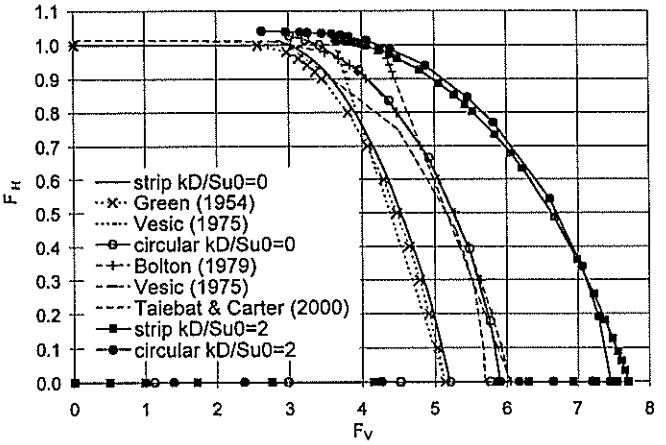

(a)

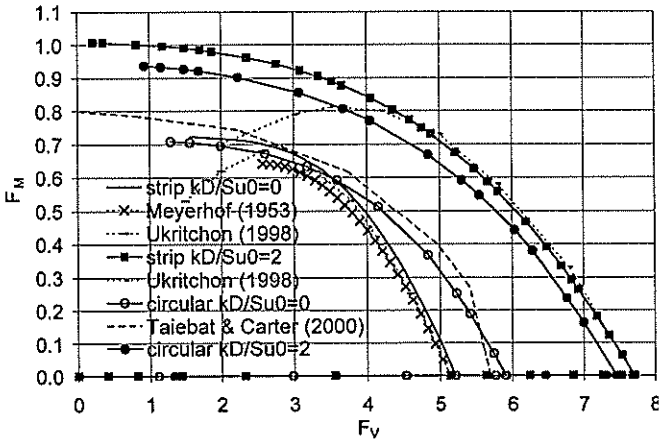

(b)

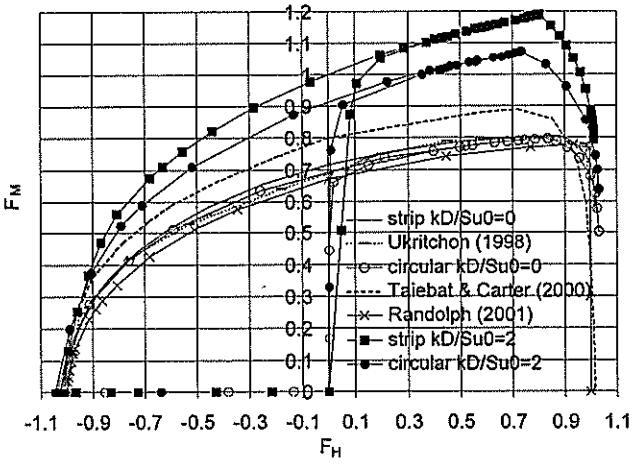

(c)

Figure 2 – Failure loci in (a) V:H loading
(b) V:M loading and (c) H:M loading

non-homogeneity. The finite element results show good agreement with the theoretical solution for lateral load capacity with the calculated results lying in the range $1.01<F_{H0}<1.04$ (Table 3).

5.3 Moment load capacity

Under conditions of pure moment i.e. when V=0 and H=0. failure of a shallow foundation takes place as rotation of a scoop of soil contained beneath the footing and with a centre of rotation a distance f above the centre of the footing. For a strip footing the scoop mechanism can be solved by work balance to provide an exact solution for the ultimate moment load (F_{M0}). For a circular footing geometry a similar solution can be derived by discretisation into an infinite number of infinitesimal strip footings. The solutions can also be extended to conditions of soil non-homogeneity. Comparison of the theoretical solutions with those of the finite element analyses is made in Table 4 and shows good agreement was achieved.

The maximum moment capacity (M_{max}) of a shallow foundation is not mobilised under pure moment loading but at a combination of positive horizontal and moment.

For a strip footing on a homogeneous soil Ukritchon[4] *et al* (1998) present limit (upper and lower bound) solutions and Bransby[13] and Randolph (1998) present results of finite element analyses. For a circular footing on a homogeneous soil Taiebat[14] and Carter (2000) present finite element analysis results. An approximate comparison can also be made for the strip footing on the non-homogenous deposit modelled in this study by interpolating data presented in Bransby[13] and Randolph (1998) at other values of kD/Su_0. For the case of a circular footing on a non-homogeneous soil no published data is available. For all cases results of an upper bound solution (Randolph[15], 2001) based on the conventional Hansen mechanism (Brinch-Hansen[2]) and the kinematic mechanisms reported in Bransby[13] and Randolph (1998) are also presented. The available data is compared in Table 3.

5.4 Vertical and Horizontal (V:H) loading

Figure 2a shows envelopes of failure loads under combined V and H loading from this study and various published sources.

The magnitude of F_{V0} for each of the cases modelled is discussed in Section 5.1. For all the cases modelled for V less than some critical magnitude (approximately $0.5V_0$), H governs failure of the foundation and a pure sliding mechanism is observed, thus the end points of the failure loci shown in Figure 2a correspond to F_{H0}.

For the case of the homogenous deposit an increase in load capacity due to the circular foundation geometry is clearly apparent with a the maximum increase observed when H=0, reducing as H increases until the horizontal failure criterion prevails. The effect of circular foundation geometry on the non-homogeneous deposit appears to be less significant but this is as a result of the loci being constrained at F_{V0}, $F_H=0$ due to the non-homogeneity factor causing a shape factor of 1 (Houlsby[6] and Wroth, 1983) and by the horizontal sliding failure criterion at F_{H0}.

The finite element results of the strip and circular footings on the homogeneous deposit are compared with the exact solutions of Green[16] (1954) for a strip footing and the modified expression proposed by Bolton[17] (1979) for a circular footing and show a good agreement for all combinations of V and H.

The commonly employed expression (proposed by Vesic[18], 1975) using the conventional vertical bearing capacity equation for a strip footing (Prandtl[8], 1920; Terzaghi[1], 1943) modified to account for load inclination is also presented as an indication of its lack of suitability particularly at intermediate values of vertical load.

The failure envelope from a finite element study by Taiebat[14] and Carter (2000) modelling a circular footing resting on a uniform homogenous Tresca soil is also presented for comparison.

5.5 Vertical and Moment (V:M) loading

From Figure 2b it can be seen that for the case of the homogenous deposit the circular geometry enhances the foundation load capacity under combined V and M at high values of V and reduces as the magnitude of M increases. The maximum increase in load capacity occurs under pure V (i.e. $F_M=0$) and reduces until the loci converge at $F_V=3.50$, $F_M=0.60$. For low V the two loci are closely spaced although the curves intersect and the circular footing displays a marginally lower bearing capacity than the strip footing.

This configuration is to be expected as the kinematic mechanisms associated with vertical loading of a strip footing and a circular footing are different: failure of a strip footing taking place predominantly in-plane while failure of a circular footing is essentially axi-symmetric. The kinematic mechanism associated with rotational failure (and sliding) of a strip and circular footing are however similar, occurring in both cases predominantly in-plane.

Further for the case of the non-homogeneous deposit it would be expected that the loci for the strip and circular footings would coincide at the ultimate vertical load (F_{V0}) due to the shape factor (ζ_s) of 1 inferred by $kD/Su_0=2$ (Houlsby[6] and Wroth, 1983) and based on the in-plane deformation mechanisms in rotation it would also be expected that the magnitude of F_{M0} would be similar. The separation between the loci is approximately uniform such that if $F_{V0}^{strip}=F_{V0}^{circle}$ the loci would be coincident.

No exact solution exists to calculate the response of a shallow foundation to combined vertical and moment loading, even for the case of a strip footing on a homogenous deposit. Conventionally the problem is approached using the effective width principle of

Meyerhof[19] (1953). Comparison of the resultant failure loci with that of the finite element analysis clearly illustrates the reduction in moment capacity at low V due to separation of the footing at the interface with the soil in the absence of under-base suctions.

For the case of a strip footing on both homogeneous and non-homogeneous deposits the finite element results can be compared with the limit state analyses presented by Ukritchon[4] *et al* (1998). Zero under-base suction was assumed therefore the loci are expected to be different at low V. For high V however the plasticity solution gives good agreement.

For a circular footing on a non-homogeneous deposit under V:M loading the finite element results from this study can be compared with those presented by Taiebat[14] and Carter (2000). Agreement is good over the most combinations of V and M loads, although the higher value of F_{M0} predicted by Taiebat and Carter causes divergence of the loci at low values of V. No published data exists with which to compare the circular footing on the non-homogeneous deposit.

5.6 Horizontal and Moment (H:M) loading

The failure loci in H:M load space (Figure 2c) show results in both –H:M and H:M load space due to the asymmetry of failure envelope.

For the case of the homogenous deposit the circular foundation geometry appears to have only a minimal effect on the shape of the failure envelope compared to that of the strip footing, the two loci being very closely aligned for all values of H and M. This is a result of the predominantly in-plane kinematic mechanisms associated with sliding and rotational failure of a shallow foundation (as discussed in Section 5.5). The envelope of the strip footing lies marginally outside that of the circular footing in line with the expectation of a slightly higher load capacity under pure M for the strip foundation geometry.

The effect of circular foundation geometry in the non-homogeneous deposit is similar with the failure envelope of the circular footing falling within the failure envelope of the strip footing for all combinations of V and M. However the separation of the loci is more marked compared to the case of the homogeneous deposit affecting both the magnitude of and the value of F_H at M_{max}.

Variation in the shape of the failure loci due to the soil strength non-homogeneity is particularly noticeable post-maximum moment with regard to the degradation of moment capacity.

It is also of interest to note that the intersection of the failure loci at $F_H=0$ is marginally less than M_0 calculated in the V:M side-swipe for all the finite element analyses.

No exact solution exists to calculate the response of a shallow foundation to combined horizontal and moment loading even for the case of a strip footing on a homogenous deposit. However the finite element results of the strip footing on the homogenous deposit can be compared with the limit analyses presented by Ukritchon[4] *et al* (1998) and for a circular footing on a homogeneous deposit with the finite element results of Taiebat[14] and Carter (2000) and the upper bound solution of Randolph[15] (2001). The bound theorem solutions provide a good fit although they become less accurate in the region of the F_{Mmax}, while the results of Taiebat and Carter over predict for nearly the whole range of H and M. There are no data with which to compare the finite element analysis results of the strip or circular footing on the non-homogeneous deposit.

6 CONCLUSIONS

The aim of the work reported in this Paper was to investigate the influence of foundation geometry and soil strength non-homogeneity on bearing capacity under combined loading. Good agreement with available exact solutions (to within 5%) indicated validity of the model. The results confirm:

- Circular foundation geometry increases the ultimate vertical capacity (F_{V0}) and reduces the pure moment capacity (F_{M0}) compared to a strip footing when founded on a homogeneous clay.
- Non-homogeneity increases F_{V0} and F_{M0} of a strip footing.
- A non-homogeneity factor (kD/Su_0) of 2 gives a shape factor (ζ_s) of approximately unity for F_{V0} such that $F_{V0strip}=F_{V0circle}$.
- An increase in F_{M0} of a circular footing compared to a strip footing when founded on a non-homogeneous clay.
- M_{max} of a strip footing increases and the value of H at which it occurs reduces due to non-homogeneity.
- The ultimate lateral load (F_{H0}) for a surface seated footing is unaffected by foundation geometry or non-homogeneity.

The main new findings of the results presented are:

- Applicability of $\zeta_s=1$ to the complete range of combined V:H for $kD/Su_0=2$.
- An increase in gradient of the loci of both the strip and circular footings at intermediate values of H up to H at M_{max} due to non-homogeneity.
- M_{max} and H at M_{max} are only minimally affected by footing geometry on the homogeneous clay but more noticeably affected when founded on the non-homogeneous clay.
- M_{max} of the circular footing founded on the non-homogeneous deposit increases and the value of H at which it occurs reduces compared to the strip footing.

7 FURTHER WORK

The influence of the degree of non-homogeneity under fully combined V:H:M loading and the response to combined H:M loading at non-zero vertical loads on the shape of failure loci for both strip and circular footings are currently being investigated at COFS.

8 ACKNOWLEDGEMENTS

The work described here forms part of the activities of the Special Research Centre for Offshore Foundation Systems, established and supported under the Australian Research Council's Research Centres Program. This support is gratefully acknowledged.

9 REFERENCES

[1] Terzaghi K (1943) *Theoretical soil mechanics* Wiley, New York.

[2] Brinch-Hansen J (1970) "A revised and extended formula for bearing capacity" *Danish Geotechnical Institute Bulletin* No.28, pp 5-11.

[3] Meyerhof GG (1980) "Limit equilibrium plasticity in soil mechanics" *Proc. Application of plasticity and generalised stress-strain in geotechnical engineering* ASCE, pp 7-24.

[4] Ukritchon B, Whittle AJ and Sloan S (1988) "Undrained limit analysis for combined loading of strip footings on clay" *J. Geotech.l and Geoenv. Engng* Vol. 124, No. 3, pp 265-276.

[5] Martin CM and Randolph MF (2001) *"Applications of the lower and upper bound theorems of plasticity to collapse of circular foundations"* Proc. 10th IACMAG Conf., Tucson, Vol. 2, pp 1417-1428.

[6] Houlsby GT and Wroth CP (1983) "Calculation of stresses on shallow penetrometers and footings" *Proc. IUTAM/IUGG* Seabed Mechanics, Newcastle, pp 107-112

[7] Tan FS (1990) *Centrifuge and theoretical modelling of conical footings on sand* PhD Cambridge, UK.

[8] Prantl L (1920) "Eindringungsfestigkeit und festigkeit von schneiden" *Angew. Math. U. Mech* Vol. 1, No.15

[9] Shield RT (1955) "On the plastic flow of metals under conditions of axial symmetry" *Proc. Royal Society London* No. 223, pp 267-287.

[10] Davis EH and Booker JR (1973) "The effect of increasing strength with depth on the bearing capacity of clays" *Geotechnique* Vol. 23, No 4, pp 551-563.

[11] Martin (2001) "Vertical bearing capacity of skirted circular foundations on Tresca soil" *Proc. 15th ICSMGE,* Vol. 1, pp 743-746.

[12] Peck RB, Hansen WE and Thornburn TH (1953) *Foundation Engineering* John Wiley and Sons, p 441.

[13] Bransby MF and Randolph MF (1998) "Combined loading of skirted foundations" *Geotechnique* Vol. 48, No 5, pp 637-655.

[14] Taiebat HA and Carter JP (2000) "Numerical studies of the bearing capacity of shallow foundations on cohesive soil subjected to combined loading" *Geotechnique* Vol. 50, No 4, pp 409-418.

[15] Randolph (2001) Private communication.

[16] Green AP (1954) "The plastic yielding of metal junctions due to combined shear and pressure" *J Mech. Phys. Solids* Vol. 2, No.3, pp 197-211.

[17] Bolton MD (1979) *A guide to soil mechanics* Cambridge University Press.

[18] Vesic AS (1975) "Bearing capacity of shallow foundations" *Foundation Engineering Handbook* Van Nostrand Reinhold, pp 121-147.

[19] Meyerhof GG (1953) "The bearing capacity of foundations under eccentric and inclined loads" *Proc. 3rd ICSMFE* Vol. 1, pp 440-445.

QUARRYING – MODIFIED LAVA FLOW GEOLOGY AND ITS INFLUENCE ON THE EFFECTS OF GROUNDWATER CONTAMINATION

Peter Gringinger: Pattle Delamore Partners Limited, Auckland

A groundwater contamination plume was investigated in a shallow basalt aquifer of the Auckland Volcanic field. Investigations involved the study of geological maps and reports, quarrying operations, installation of groundwater monitoring wells and geophysical surveys. Groundwater and contaminant plume flow is occurring in a thin layer of basalt being directed by a complex paleorelief of shallow valleys and ridges on the fine grained sediments of the Tauranga Group, which underlie the basalt. The basaltic lava flowed over this paleorelief to form a surface basalt layer between 5 and 10 m thick. A Tauranga Group ridge and groundwater flow divide is causing contaminated groundwater to flow away from the site in two directions, following the valleys of the paleorelief. Groundwater flow occurs mainly in the highly permeable zones of vesicular rubbly basalt at the base of the lava flows. Extensive quarrying adjacent to the contaminant plume source area, has removed the basalt lava except for a 1 – 1.5 m thick layer at the base of the flow. The quarried basalt was typically replaced with predominantly fine grained engineered fill comprising silty clay with some gravel. The resulting groundwater flow regime comprises a thin layer of highly permeable basalt, overlain by fine grained confining fill. The thin layer of basalt remains as the primary media for groundwater flow. Contaminants of interest in the plume are volatile organic compounds (VOC's). The potential for these contaminants to pose a human health risk by way of migration from the groundwater up through the vadose zone into indoor air in buildings is being investigated. Backfilling of quarried areas above the contaminant plume with fine grained engineered fill has resulted in a reduction in the potential indoor air human health risk posed by volatile organic compounds in the groundwater, compared with areas not quarried.

1 INTRODUCTION

The site, which has been in operation for more than 30 years, is located on lava flows that are part of the Auckland Volcanic field. Contamination of the basalt aquifer under and away from the site has occurred. The basalt in the site vicinity is an important source for aggregate material. Part of the area adjacent the site was quarried and subsequently landscaped for the redevelopment of the area for light industrial purposes. This development is still taking place with ongoing construction of new industrial buildings.

Extensive investigation of off-site contamination and associated human health and environmental risks is being carried out as part of the resource consenting process.

2 GEOLOGY

2.1 Volcanic Geology

The site is located on a dense, fractured, late Pleistocene basaltic lava flow. The source of the flow is a volcanic complex located approximately 750 m southeast of the site.

The onset of the eruptive phase at the volcanic complex was an explosive eruption, which formed a tuff ring. The second phase of activity was an effusive phase, which included lava outpourings.

The lava field at the site is made up of a series of these outpourings, which flowed westwards from the volcanic center following and infilling existing valleys. The total thickness of the flows is fairly uniform – between 5 and 10 m. Subsurface conditions indicate that the basalt at the site comprises 2-2.5 m of rubbly basalt overlying dense, fractured basalt, and a 1-1.5 m basal layer of rubbly basalt which overlies alluvial sediments.

2.2 Basement Geology

Directly underlying the lava flows are Pleistocene alluvial deposits (Tauranga Group) consisting mostly of silt and clay. These sediments are in turn underlain by Miocene Waitemata Group sand- and siltstones which are the local basement rocks. The total thickness of the alluvial sediments is estimated to be little more than 10m.

Topographic features such as pre-existing valleys, ridges, hills and depressions have influenced the extent and thickness of the lava in the vicinity of the site. A ridge running west to east through the site resulted in both the northward and southward movement of the lava once it reached the site area. Entrenched stream valleys then channeled the lavas as they flowed southwest and to a lesser degree northward away from the site Figure 1).

3 HYDROGEOLOGY

The lava flow sequence is a highly permeable aquifer of limited extent and thickness overlying low permeability Tauranga Group sediments. Hydraulic conductivities of fractured basalt in the Auckland Volcanic Field are in the range of 10^{-5} to 10^{-2} m/sec. The permeability of the underlying sediments has hydraulic conductivities significantly lower (in the range of 10^{-8} to 10^{-6} m/sec).

Groundwater flow originates at the elevated volcanic center to the east of the site and flows west and northwest in the basalt towards the site. An east-west trending groundwater flow divide at the site caused the groundwater to flow both north and southwest away from the site (Figure 2). The groundwater flow follows the pre-existing valleys in the underlying alluvial sediments.

The saturated aquifer thickness in the site vicinity is between 1.5 and 5 m and groundwater level is typically between 2 and 6 m below ground level. Groundwater levels show variable seasonal fluctuations (almost nil to 1.2m) between the winter high and summer low. The groundwater flow gradient varies from 0.01 to 0.03 over the investigation area (Figure 2).

4 QUARRYING

The area surrounding the site has undergone intense quarrying for basalt followed by backfilling operations to restore the land so that it is useable for light industrial development. Quarrying has been carried out over the last 15 – 20 years.

4.1 Quarrying Operations and Restoration

Quarrying typically involved extracting the rock down to approximately 0.5m – 1.5m above the base of the basalt flow. This practice was used to maintain a workable and stable surface for the quarrying operations and machinery. The pre-existing relief affected the thickness of basalt in the vicinity of the site and therefore the level of the bottom of the quarry also varied. This has resulted in varying thickness of fill being placed to restore the land to a suitably consistent level for development.

Quarrying was generally not carried out in a 20m to 30m wide strip of land (buffer zone) adjacent to land (including the site) developed at the time of quarrying (Figure 1).

Quarried areas have been restored by placement of engineered fill to a standard that makes the land suitable for light industrial development. The fill typically comprises a thin layer of topsoil underlain by compacted earthfill (silt or silty clay mixed with some basalt gravel). The filled areas around the site contain at least 1m of earthfill. The actual thickness of earthfill varies, being about 2.5m on average and reaching up to 5 m in some places.

The earthfill is typically underlain by layers of coarser fill including a blinding layer (gravel with some silt/clay) and a rockfill layer (boulders, gravel and some silt/clay, broken concrete, bricks, glass and rubble). In addition, a drainage layer (boulders and gravel) was placed in gullies and creeks.

4.2 Quarrying Influences on Groundwater

Some areas in the vicinity of the site were quarried and subsequently backfilled to below the current groundwater level (Figure 3). In these areas low permeability engineered fill forms a capping aquitard for the thin layer of basalt. Permeable rubbly basalt remains at the base of the flow. This results in a confined or semi-confined situation for the aquifer with the bulk of the groundwater flowing through the thin layer of basalt.

5 GROUNDWATER CONTAMINATION

5.1 General

Contaminants that have seeped into the basalt beneath the site have entered the groundwater and formed plumes of contaminated groundwater. These have subsequently migrated off-site. Contaminants in the plumes include volatile organic compounds (VOC), which comprise the contaminants of interest for environmental and human health risks. Dense non-aqueous phase liquids (DNAPLs, e.g. tricholoroethylene, dichloroethylene, tricholoroethane, etc) and light non-aqueous phase liquids (LNAPLs, e.g. benzene, toluene, ethylbenzene, xylenes, etc) are both present in the contaminant plume. Free phase floating hydrocarbon product (LNAPL) is also present in one area. No free phase sinking product (DNAPL) has so far been found during investigations at the site. Contaminant plumes are migrating to the north and southwest of the site following the general groundwater flow directions already described.

5.2 Investigations

Investigations at the site to date comprise drilling and installation of approximately 30 groundwater monitoring wells, geophysical surveys (ground penetrating radar (GPR) and resistivity profiling), soil gas testing, indoor air and underground services testing and investigations into the quarrying and filling operations. Drilling, GPR, resistivity surveys and quarrying resource information provided useful information on the relief of the base of basalt, thickness and characteristics of the basaltic aquifer and thickness and distribution of engineered fill. Investigations are ongoing.

6 EFFECTS ASSESSMENT

The investigations and assessment work carried out to date has identified offsite areas that overlie actually and possibly contaminated groundwater associated with the site. The same work has identified indoor air inhalation as the principal human health risk potentially associated with the groundwater contamination. The potential indoor air risk is associated with volatilisation of certain

contaminants from the groundwater (e.g. vinyl chloride). Once in gaseous form the contaminants can migrate up through the overlying rock and soil and potentially enter a building through the floor (e.g. via cracks in the concrete floor slab; Figure 4).

Contaminant transport and fate modeling combined with risk modeling has been carried out for the contaminants of interest. This has involved the use of a commercial contaminant transport, fate and risk modeling software package (BP RISC 4). Assessment using the vapor transport model (from groundwater into buildings) showed that indoor air inhalation risk could potentially be present in areas directly southwest of the site. The highest concentrations of some groundwater contaminants were measured in the groundwater in this area. Vapor emissions from dissolved groundwater contaminants are estimated using a one –dimensional steady-state vapor diffusion model. Capillary fringe, vadose zone properties, and building foundation properties are considered in the estimation of gas concentrations in buildings. Other areas around or further away from the site do not appear to pose a risk to human health from indoor air inhalation.

The basaltic aquifer is of low yield (due to limited saturated aquifer thickness), has low water quality and is not used for water supply. Ingestion was therefore excluded as a potential exposure pathway. Surface water sampling at several springs/streams emanating from the edge of lava flows (0.6 to 1km from the site), found water quality consistent with an industrial catchment.

7 INFLUENCE OF QUARRTING ON EFFECTS ASSESSMENT

A critical factor in the evaluation and modeling of contaminant transport and fate from groundwater to indoor air is the aspect of movement of volatile contaminants through the vadose zone above the groundwater table. This is influenced significantly by the distribution of quarried and un-quarried areas (buffer zones) and the type and thickness of engineered fill material placed in the quarried zones.

Very different modeled risk values were obtained for fill and basalt rock due to the distinctly different physical parameters of these materials (e.g. porosity, permeability, moisture content, capillary fringe, etc). Appropriate risk levels and values could be developed for the areas around the site because the extent, type and thickness of fill generally has been determined in the areas of concern.

The result was the identification of zones of elevated risk in areas where no fill is present. A synthetic plastic liner and soil gas extraction system was installed under a warehouse, in one such area being built to mitigate the potential risk.

The engineered fill effectively retards the migration of volatile contaminants in gaseous form up through the vadose zone. The fill also contributes to the degradation (dilution, diffusion, sorption, biodegradation) of the contaminants by slowing their passage through the vadose zone.

Testing of soil gas, various underground services manholes and access ways and indoor air has to date not detected any volatile contaminants in the near surface vadose zone or indoor air related to the groundwater contamination.

8 CONCLUSIONS

Detailed site investigations showed that groundwater and contaminant plume flow is being directed by a complex paleorelief of shallow valleys and ridges on the fine grained sediments of the Tauranga Group, which underlie the basalt. The groundwater flow mainly occurs in the highly permeable zones of vesicular rubbly basalt at the base of the lava flows. Quarrying of basalt and backfilling of quarried areas above the contaminant plume with fine grained engineered fill has resulted in a reduction in the potential indoor air human health risk posed by the volatile organic compounds in the groundwater, compared with areas not quarried.

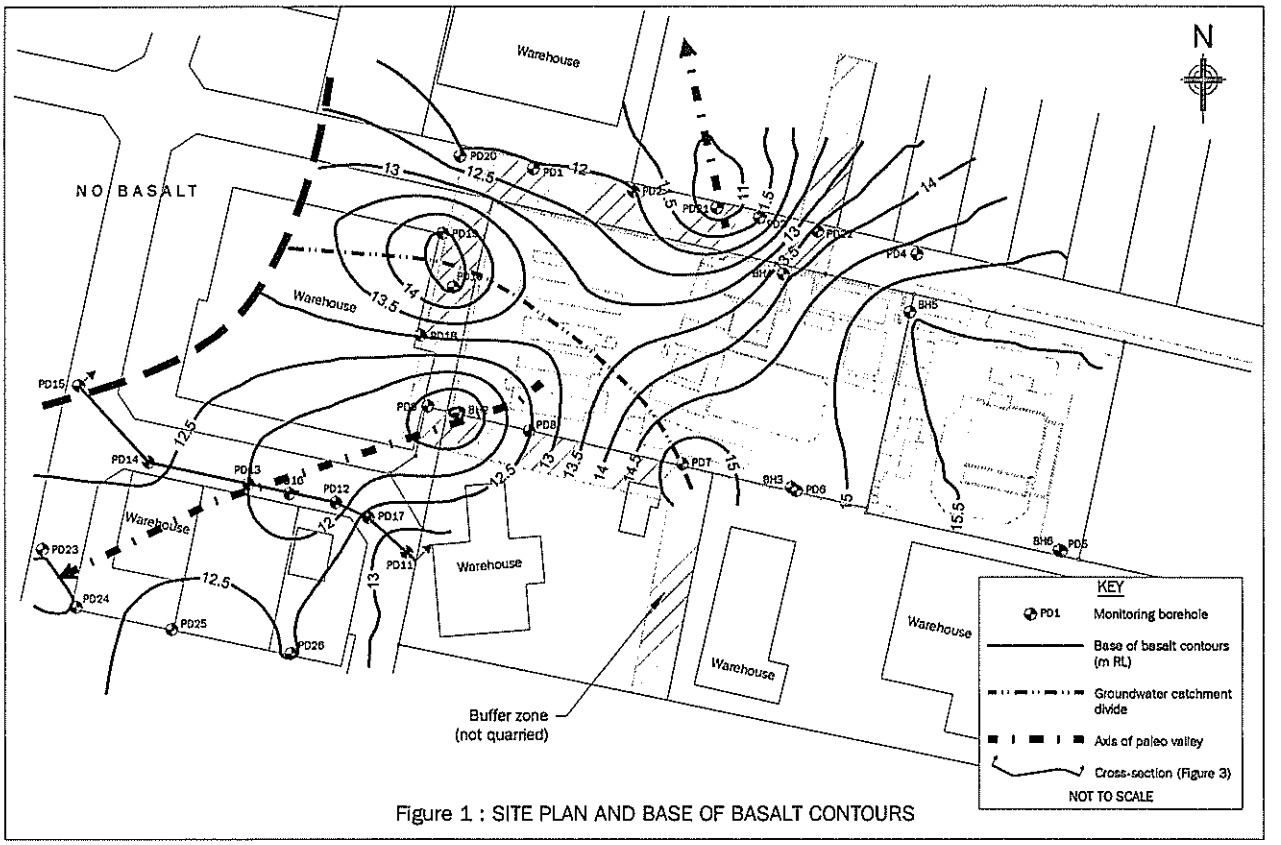

Figure 1 : SITE PLAN AND BASE OF BASALT CONTOURS

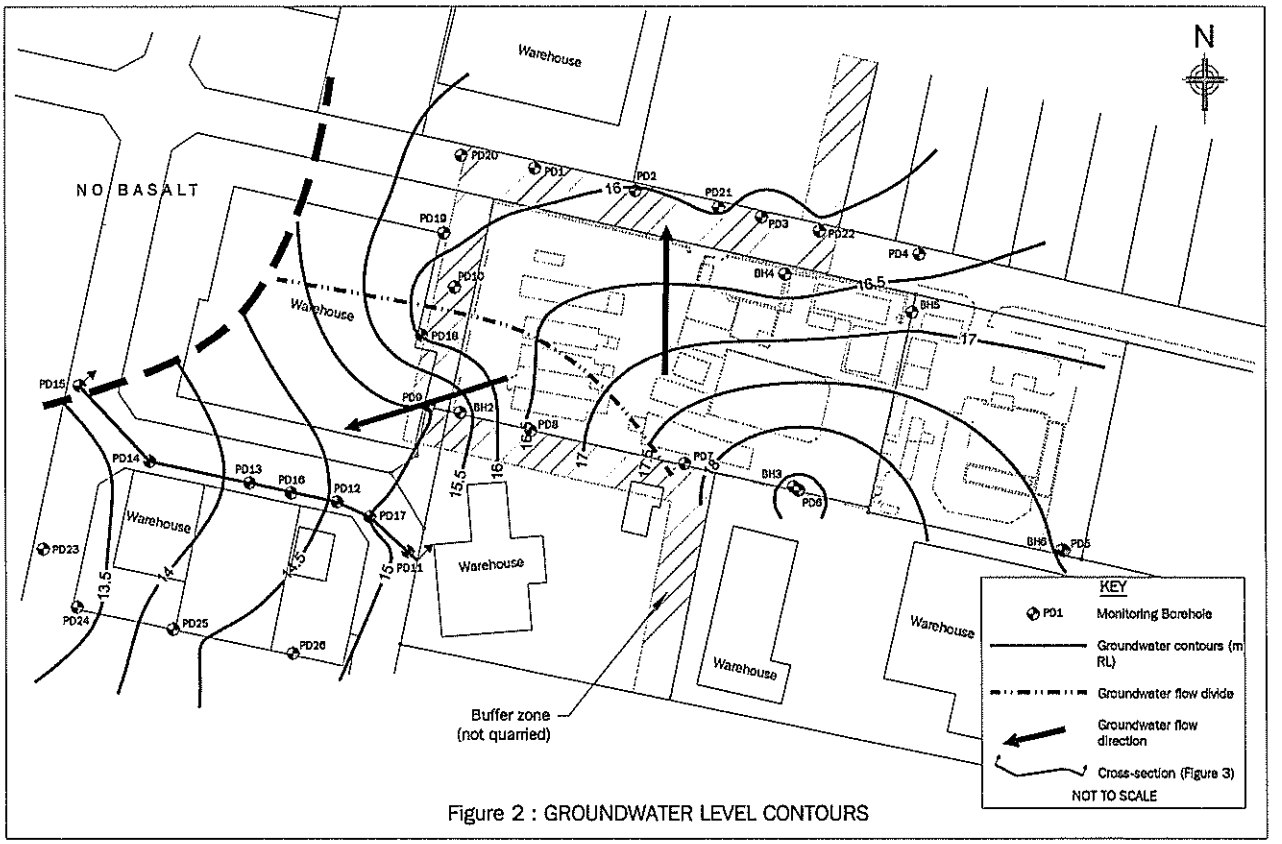

Figure 2 : GROUNDWATER LEVEL CONTOURS

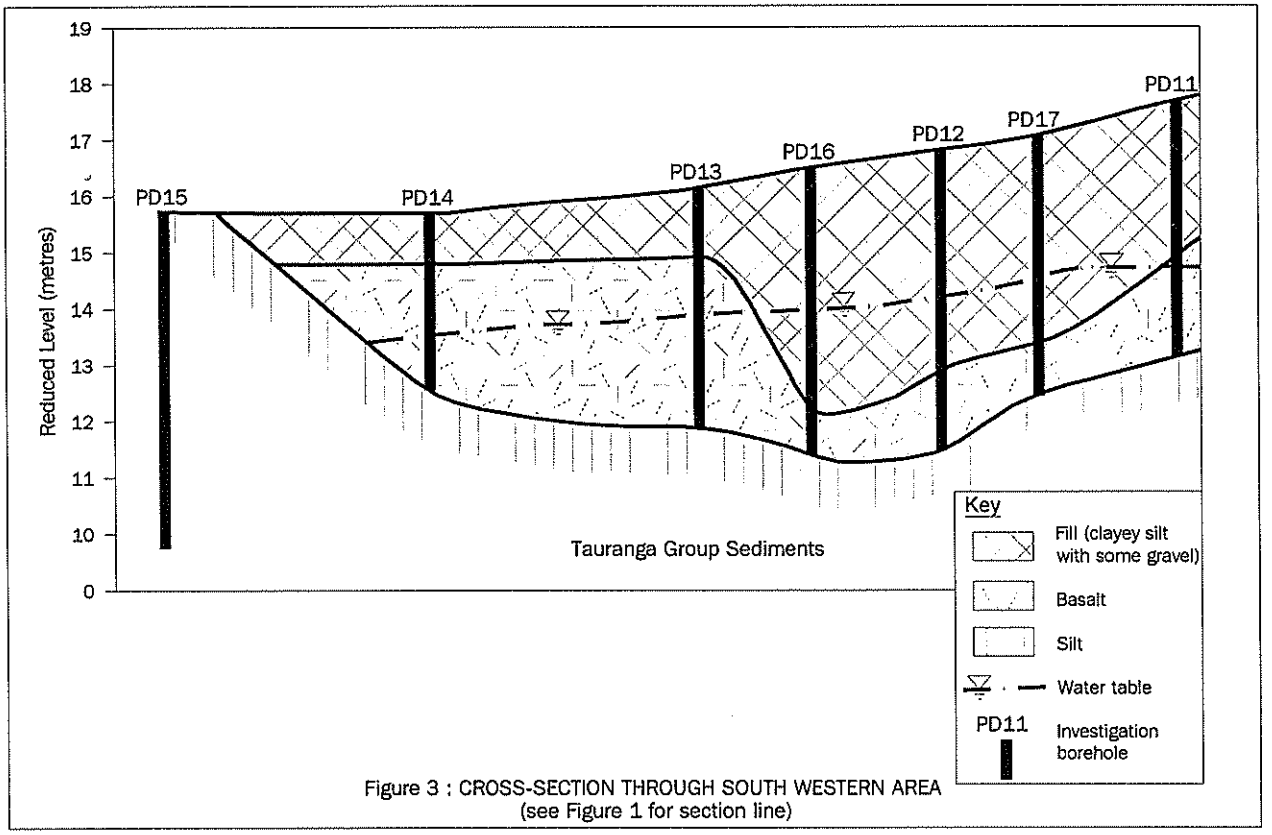

Figure 3 : CROSS-SECTION THROUGH SOUTH WESTERN AREA
(see Figure 1 for section line)

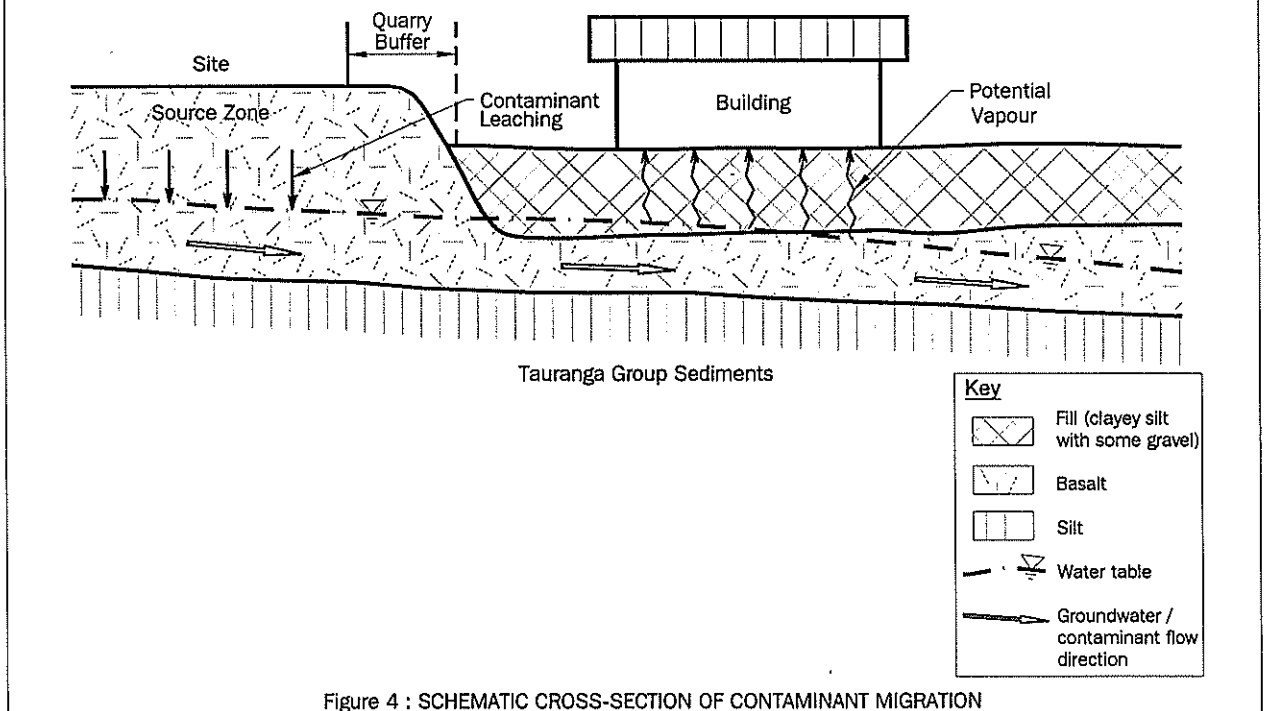

Figure 4 : SCHEMATIC CROSS-SECTION OF CONTAMINANT MIGRATION

Excavation Induced Vibrations In Sydney Sandstones

Gregory A. Hackney, B.E. (Civil) M. Eng. Sci. (Geotechnical)

Senior Geotechnical Engineer, Coffey Geosciences Pty Ltd (Sydney)

Summary: *The risk of damage to nearby structures due to vibrations resulting from rock excavation is becoming an increasingly important issue for development within the Sydney metropolitan area. Vibration levels generated by excavation equipment are measured using specialised equipment, and compared with criteria recommended for particular types of structures to assess if the vibrations are within tolerable levels. Generally, monitoring is carried out under the operating conditions of the excavation equipment at various distances from the vibration source to establish a 'site law'. The 'site law' can be used to provide guidelines on minimum distances between the excavation equipment and adjacent structures to maintain vibrations within acceptable levels. This paper provides guidance on potential vibration levels for various types of excavation equipment and rock classes, which can be used to establish an initial 'site law' prior to site-specific vibration monitoring being undertaken.*

1 INTRODUCTION

The excavation of moderately weathered to fresh sandstone within the Sydney Basin typically requires the use of mechanical excavation equipment due to the relatively high rock substance strength, and infrequent defects within the rock mass. Equipment generally employed for the excavation of such sandstone includes bulldozer mounted rippers; rock hammers and rotary rock grinders mounted on hydraulic excavators; and rock saws. Most typically used in Sydney are rock hammers, due to their portability and relatively high production rates.

A result of the use of mechanical excavation equipment is the generation of ground vibrations, which are of concern with respect to potential damage to structures, and human perception. The magnitude of vibration is a function of the energy at the source, the distance from the source, and the media through which the vibrations propagate[1].

Presented herein are the results of an assessment of vibration levels versus distance from the vibration source for different types and sizes of excavation equipment, within different classes of sandstone. Also presented is an example of the use of the data to establish potential minimum distances between excavation equipment and items at risk to maintain vibrations within acceptable levels.

2 GENERATION AND MEASUREMENT OF VIBRATIONS

Vibrations are generated by the impact of the excavation equipment on the materials being excavated. Wiss[1] demonstrated that vibrations generated from excavation equipment such as rock hammers are pseudo steady state vibrations, in that waves are generated at short enough intervals to approach essentially a steady-state condition. Conversely, vibrations generated from such activities as blasting are considered transient, in that the amplitude of the generated wave is at its peak initially, and dissipates thereafter.

The measurement of ground vibrations is commonly made using small, portable vibration monitoring equipment. Measurements are typically made in terms of a peak particle velocity (PPV in mm/s), which is the resultant particle velocity measured by geophones oriented in three orthogonal directions. Monitoring is routinely carried out on a site-specific basis to establish a 'site law', which is a function of PPV and distance from the vibration source. The 'site law' describes the rate of attenuation of vibrations with increasing distance from the vibration source.

3 GROUND VIBRATION CRITERIA

Many different criteria have been proposed regarding acceptable and unacceptable ground vibration levels for different types of structures. Most of the criteria were developed from within the mining industry in the United States, and specifically related to blasting activities.

The criteria generated for mine blasting activities generally indicate that a limit of about 50 mm/s is considered 'safe' for domestic dwellings in good condition, and a lower limit of between about 10 mm/s and 20 mm/s applicable for structures in poor condition. Several authors have also proposed more detailed criteria including different acceptable levels of vibration for different types of structures. However, as these criteria essentially relate to transient vibrations, their relevance to steady-state or pseudo steady-state vibrations is debatable.

Based on a statistical analysis of the United States Bureau of Mines data, (from which the initial 50 mm/s criteria was developed), Jackson[2] suggested that a peak particle velocity of 5 mm/s may cause architectural damage to structures. The German draft standard (DIN 4150: 1970 draft) also recommended significantly lower limits than those adopted for blasting, with limits ranging from 2 mm/s for historical and ancient buildings, to 4 mm/s for buildings in poor condition, and 8 mm/s for structurally sound buildings. Limits of between 10 mm/s and 40 mm/s were also recommended for industrial buildings.

Little guidance on acceptable ground vibration levels is available for Australian conditions. The Australian Standard on Explosives – Storage, transport and handling, Part 2: Use of explosives (AS 2187.2–1993) provides a recommended upper limit of 10 mm/s for residential structures, and 25 mm/s for industrial buildings. A previous version of AS 2187 also indicated a limit of 2 mm/s for heritage structures.

A publication by the Construction Industry Research and Information Association (CIRIA[3]) also suggested that the acceptance criteria adopted for structures should take account of the natural frequency of the structure and the frequency of vibration. Typically, the natural frequency of low-rise structures is within the range of 10 Hz to 30 Hz. Should vibration frequencies approach the natural frequency of the structure, adopting lower vibration criteria was recommended.

In the author's experience of monitoring and assessing vibrations from excavation equipment, no significant discernable damage to residential structures has been observed while applying vibration limits of the order of those proposed by the German draft standard.

4 ASSESSMENT OF VIBRATIONS FROM EXCAVATION EQUIPMENT

4.2 Hypothesis on Ground Vibrations from Excavation Equipment

The author's hypothesis on ground vibrations from excavation equipment is twofold. Firstly, it is hypothesised that vibrations will attenuate more rapidly in rock of lower strength and with a higher number of defects. Therefore it is expected that higher ground vibrations would be apparent at a particular distance from the source in more competent rock, than in less competent rock. Secondly, it is also hypothesised that larger excavation equipment will produce higher levels of vibration, as they release greater energy during operation.

4.2 Method of Assessment

The assessment of potential ground vibrations from excavation equipment has involved the collation of ground vibration data from various types of equipment, and for various classes of sandstone. Data was sourced from vibration monitoring projects undertaken by Coffey Partners International Pty Ltd and Coffey Geosciences Pty Ltd since 1993. Information on the nature of the material being excavated and the type of machinery being used was recorded, together with the results of the monitoring. The information on the nature of the rock was used to assess a rock classification, in terms of the system proposed by Pells et. al.[4] (1971), which is widely used within the Sydney Basin to assess engineering parameters for sandstones and shales. The system defines classes of rock based on the strength and weathering of the rock substance, and the number of defects. Class I represents the highest class of rock, with high rock strength and few defects. Class V represents the lowest class rock, with low rock strength and frequent defects.

Peak particle velocity (PPV) data for particular classes of rock and types of equipment is plotted against distance from the vibration source, on a log-log scale. Various authors[5] have shown that a linear relationship between peak particle velocity and distance can be produced for data plotted on a log-log scale. This 'site law' relationship can therefore be used to assess likely limits to vibrations.

4.3 Rock Classes

Two basic rock classes have been adopted for the assessment, namely:

- Class I/II Sandstone and,
- Class II/II Sandstone.

Class I/II Sandstone incorporates all sandstone rock classes between Class I and Class II. Similarly, Class II/III Sandstone incorporates all rock classes between Class II/III and Class III. No further differentiation of rock classes was possible due to the nature of the field observations. No data was available for rock classes lower than Class III, as these materials are typically readily excavated by means other than rock hammers or grinders.

4.4 Types of Equipment Incorporated

Equipment for which vibration monitoring was most commonly undertaken are rock breakers mounted on hydraulic excavators. For this assessment, the weight of the rock hammer is the criteria adopted. Rotary rock grinders are also common in areas where rock hammers are unable to be used due to generation of excessive vibrations, and for trimming around site boundaries.

The following types of excavation equipment have been adopted for the assessment:

- Rock hammers between 250 kg and 500 kg weight;
- Rock hammers between 500 kg and 1000 kg weight;
- Rock hammers between 1000 kg and 1500 kg weight;
- Rock hammers above 1500 kg weight; and,
- Rotary Rock Grinders.

5 POTENTIAL VIBRATION LEVELS

The results of the overall 'site law' relationship developed for the Class I/II Sandstone are presented on Figures 1 to 5 below, with upper and lower bound lines for the data. Figure 6 presents a summary of all data for Class I/II Sandstone, with upper bound data lines only. The results of the assessment for the Class II/III Sandstone are presented on Figures 7 to 9, with upper and lower bound lines. Figure 10 presents the data for all types of equipment, for the Class II/III Sandstone, with upper bound lines only.

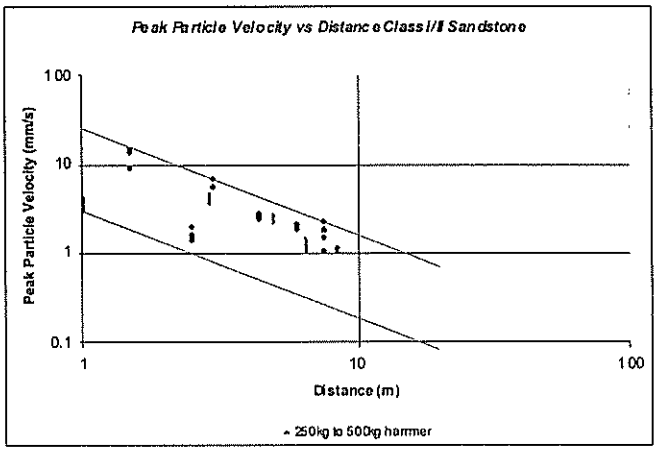

FIGURE 1 – log PPV vs log Distance for 250 kg to 500 kg hammers (Class I/II Sandstone)

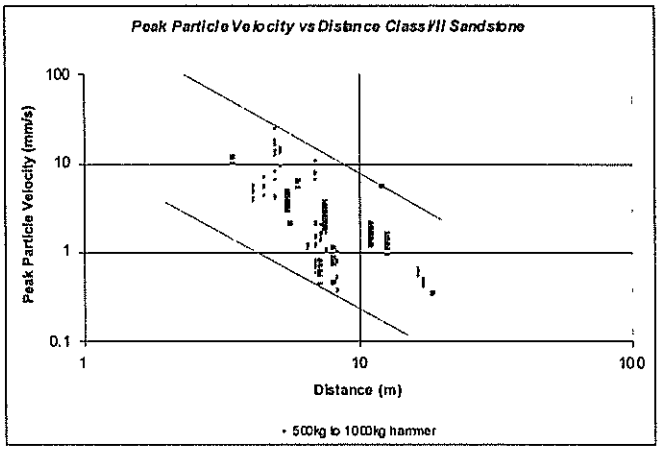

FIGURE 2 – log PPV vs log Distance for 500 kg to 1000 kg hammers (Class I/II Sandstone)

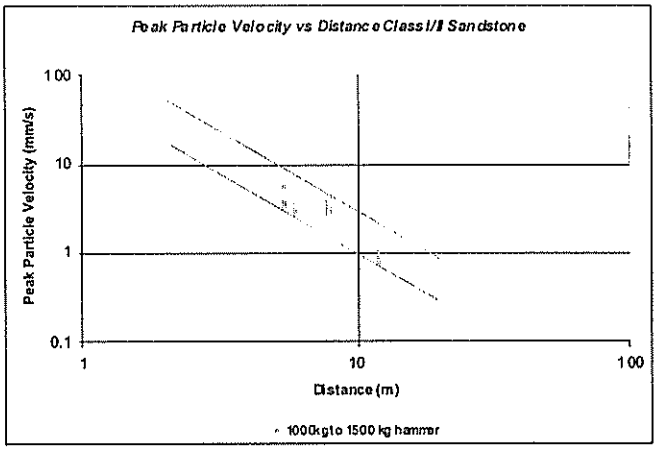

FIGURE 3 – log PPV vs log Distance for 1000 kg to 1500 kg hammers (Class I/II Sandstone)

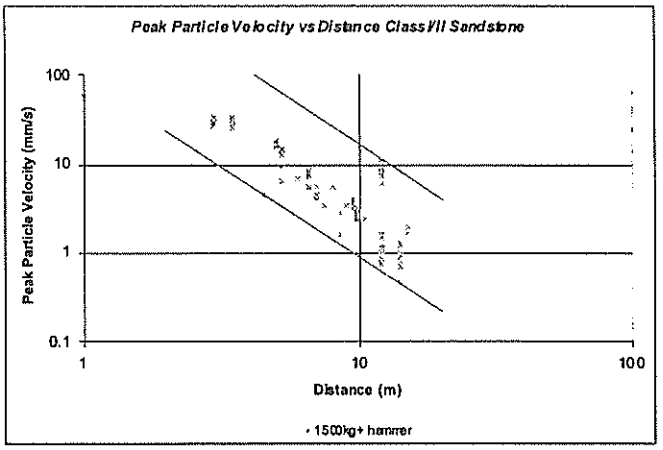

FIGURE 4 – log PPV vs log Distance for 1500 kg + hammers (Class I/II Sandstone)

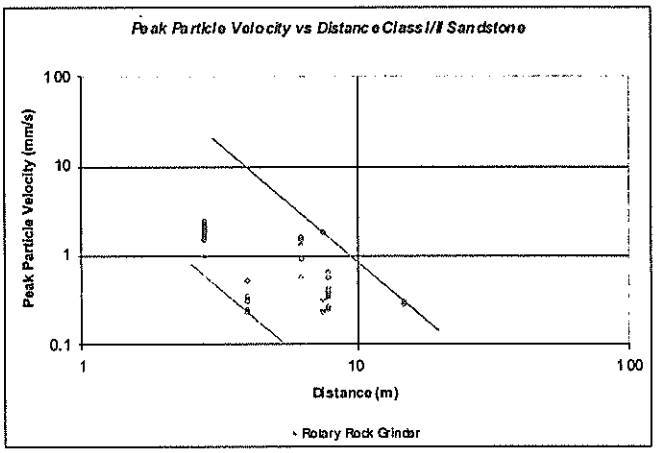

FIGURE 5 – log PPV vs log Distance for 1000 kg to 1500 kg hammers (Class I/II Sandstone)

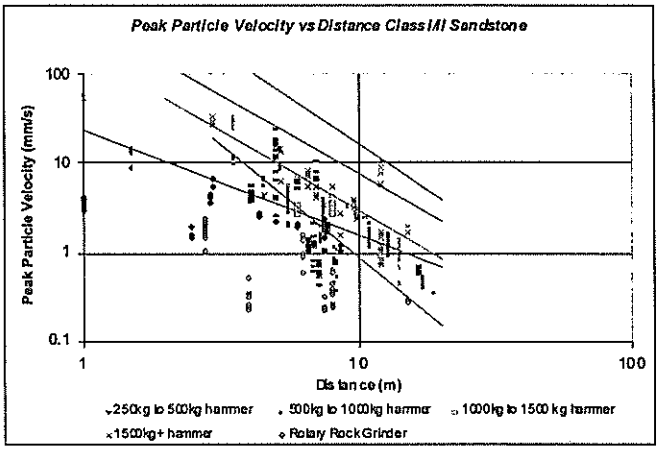

FIGURE 6 – log PPV vs log Distance for All Types of Equipment (Class I/II Sandstone)

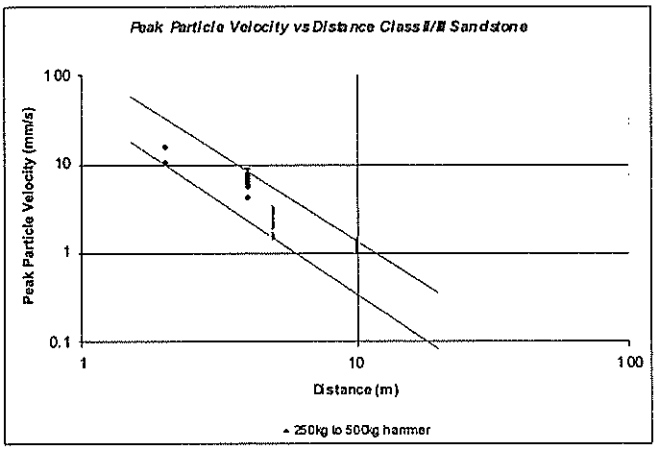

FIGURE 7 – log PPV vs log Distance for 250 kg to 500 kg hammers (Class II/III Sandstone)

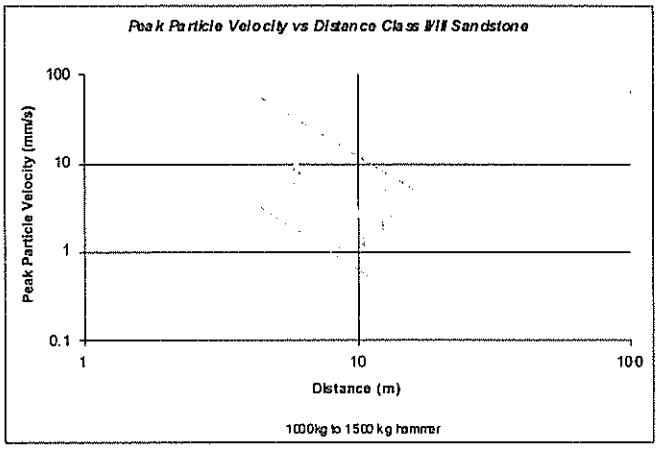

FIGURE 8 – log PPV vs log Distance for 1000 kg to 1500 kg hammers (Class II/III Sandstone)

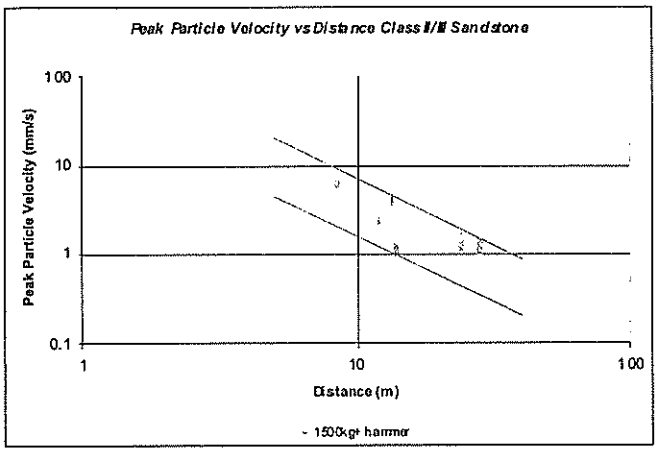

FIGURE 9 – log PPV vs log Distance for 1500 kg + hammers (Class II/III Sandstone)

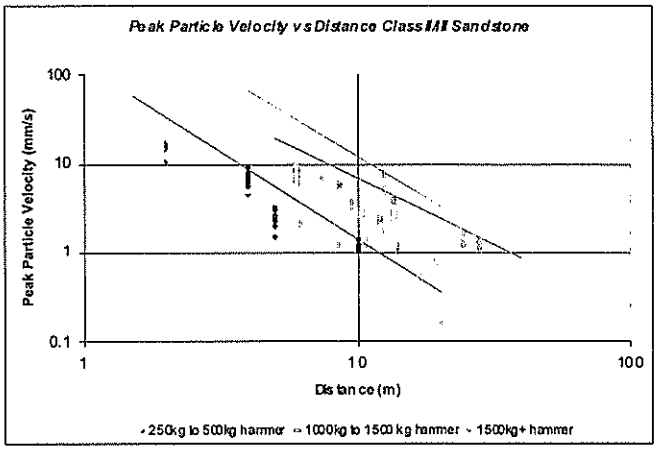

FIGURE 10 – log PPV vs log Distance for All Types of Equipment (Class II/III Sandstone)

The scatter in the data points below the upper bound line in Figures 1 to 10 indicates the need for rigorous on site monitoring during the operation of the excavation equipment. If insufficient monitoring is undertaken, the true upper bound vibration limit may not be properly established, possibly resulting in the designated acceptance criteria being exceeded during the excavation work.

6 DISCUSSION OF RESULTS

6.1 Class I/II Sandstone

The data for the Class I/II Sandstone indicates that with the exception of the 1000kg to 1500 kg hammers, maximum vibration levels increase with increasing equipment size. This tends to confirm the hypothesis that larger equipment will generate a greater level of vibration. It is likely that for the 1000kg to 1500 kg hammers, insufficient data points are available to adequately establish the upper bound.

6.2 Class II/III Sandstone

With the exception of the 1500 kg + hammers, the data from the Class II/III assessment also indicates that ground vibrations increase with increasing size of equipment. As for the 500 kg to 1000 kg size hammers for the Class I/II Sandstone, it is likely that the deviation from this trend for the 1500 kg + hammers in the Class II/III Sandstone assessment is the result of an inadequate number of data points. However, it is noted that the total number of data points for the Class II/III Sandstone is significantly less than for the Class I/II assessment.

No data was available for the 500 kg to 1000 kg rock hammer, or the rotary rock grinder for the Class II/III Sandstone assessment.

7 ASSESSMENT OF POTENTIAL MINIMUM DISTANCE BETWEEN VIBRATION SOURCE AND ITEMS AT RISK

The data shown in Figures 1 to 10 can be used to develop relationships between minimum setback distances for different types and sizes of excavation equipment, and different vibration limit criteria. An assessment of potential minimum setback distances between excavation equipment and items at risk, based on the 'site law' data above has been undertaken for an arbitrary vibration limit of 10 mm/s.

The results of the assessment for the different types of equipment and different rock classes are summarised in Tables 1 and 2.

Table 1: Minimum Distance From Source To Maintain PPV ≤ 10 mm/s (Class I/II Sandstone)

Equipment Type	Minimum Distance for PPV ≤ 10 mm/s
250 kg to 500 kg hammer	2
500 kg to 1000 kg hammer	8.5
1000 kg to 1500 kg hammer	5*
1500 kg + hammer	13
Rotary Rock Grinder	4

Note: * - Result may be biased due to insufficient data points

Table 2: Minimum Distance From Source To Maintain PPV ≤ 10 mm/s (Class II/III Sandstone)

Equipment Type	Minimum Distance for PPV ≤ 10 mm/s
250 kg to 500 kg hammer	3.5
500 kg to 1000 kg hammer	No data
1000 kg to 1500 kg hammer	11
1500 kg + hammer	8*
Rotary Rock Grinder	No data

Note: * - Result may be biased due to insufficient data points

A plot of the data presented in Tables 1 and 2 is shown below in Figure 11. Data considered potentially biased due to insufficient data points has been excluded.

The data shown in Figure 11 indicates a definite trend of increasing ground vibration with increasing weight of equipment, thereby supporting the author's hypothesis.

The data does not indicate any significant difference between potential vibration levels between the I/II and II/III sandstone classes.

To maintain ground vibrations to within a limit of 10 mm/s, larger rock hammers (i.e. 1000kg + in weight) may be used to within about 11 m of particular items at risk. Within this 11 m zone, rock hammers of weights between 500 kg to 1000 kg may be used to within about 8.5 m, and smaller hammers between 250 kg and 500 kg weight to within about 3.5 m. Inside a distance of 3.5 m, other methods such as line drilling and the use of chemical or mechanical splitters, or rock sawing could be adopted.

Although not plotted, data for the rotary rock grinder lies at approximately the same location as for the 250 kg to 500 kg hammers.

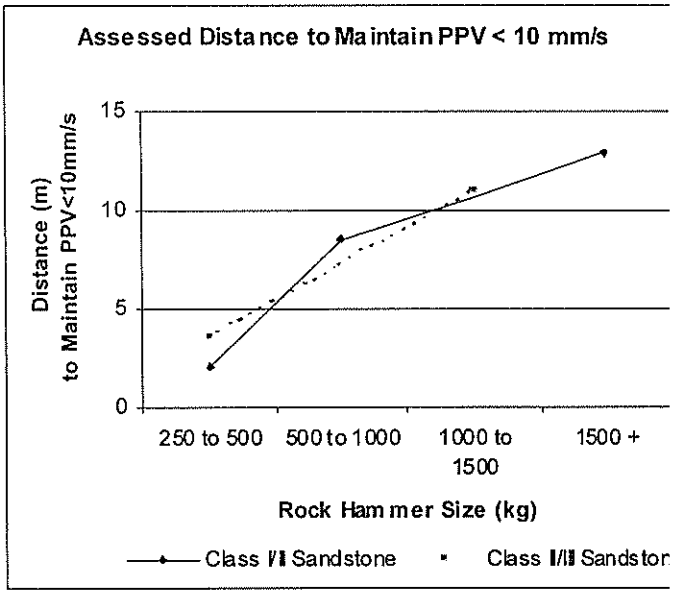

FIGURE 11 – Assessed Minimum Distance to Maintain PPV ≤ 10 mm/s

8 CONCLUSIONS

Based on the analysis of the data undertaken, the following conclusions are drawn:

- The governing criteria for ground vibrations from excavation equipment within Sydney sandstones are the type and size of the excavation equipment.
- No significant variation in the magnitude of ground vibrations is apparent between the various classes of sandstone analysed.
- The overall "site law" relationships developed for different types of excavation equipment and rock classes can be used to provide useful information regarding anticipated minimum setback distances for excavation equipment from items at risk.
- Rigorous site-specific ground vibration monitoring should be carried out at each site to adequately develop a "site law' relationship between distance and PPV.
- Further assessment is required with a more substantial database to assess possible variations in vibration levels with rock class.

- Further assessment of the frequency of vibration from excavation equipment is required to better assess ground vibration acceptance criteria.

9 ACKNOWLEDGMENTS

The author acknowledges Coffey Geosciences Pty Ltd for allowing the use of ground vibration monitoring data, and Mr Peter Volk for providing peer review.

9 REFERENCES

1. Wiss J.F. "Construction Vibrations: State of the Art", *Journal of the Geotechnical Engineering Division Proceedings of the American Society of Civil Engineers, Vol 107, No. GT2,* February 1981.
2. Jackson M.M. "Thresholds of Damage Due to Ground Motion", *Proc. Int. Symp. Wave Prop. Dyn. Props. Earth Mats. New Mexico,* 1967.
3. CIRIA Technical Note 142, Head J.M. and Jardine F.M., "Ground-borne vibrations arising from piling, "*Construction Industry Research and Information Association"*, Westminster, London, 1992.
4. Pells P.J.N. et al. "Design Loading for Foundations on Shale and Sandstone in the Sydney Region", *Aust. Geomech. Jnl. Vol. 8, pp31-39,* 1978.
5. Tynan A.E. "Ground Vibrations, Damaging Effects to Buildings", *Special Report No. 11, Australian Road Research Board,* 1973.

Bearing capacity of a strip footing subjected to an inclined load

Dr M Hjiaj, ARC Research Fellow, Dr A V Lyamin, ARC Research Fellow, Prof S W Sloan
Geotechnical Research Group
Department of Civil, Environmental and Surveying Engineering
The University of Newcastle
University Drive, Callaghan NSW 2308, Australia

Summary. In current practice, the bearing capacity of a strip footing subjected to an inclined load is typically calculated using semi-empirical expressions provided by Meyerhof, Hansen or Vesic. These formulas are based on analysis of the pure vertical capacity of a surface footing resting on weightless soil and, because of their empiricism, often lead to poor estimates of the ultimate load. An attractive alternative to semi-empirical methods for analyzing the stability of geotechnical structures is to use the bound theorems of limit analysis, coupled with the finite element method. A key advantage of this approach is that the exact ultimate load can be bracketed between two values. In this paper, full use of the power of the bound theorems is made to study the bearing capacity of a rigid surface footing subjected to an inclined load. The soil is modeled as cohesive-frictional and its unit weight is taken into account. The inclination angles considered vary between 0° (vertical) to 90° (horizontal). It is shown that, for an inclined load, traditional methods may give non-conservative results.

1 INTRODUCTION

The stability of foundations on soil under inclined loads is a fundamental problem in geotechnical engineering. Indeed, it is particularly important in the oil industry, as offshore foundations are subjected to vertical and horizontal loads as well as moments. Typically, the vertical force stems from the weight of the superstructure (or a part of it), while the horizontal load comes from wind and wave forces. Generally speaking, the case of a foundation subjected to a central vertical load is a gross simplification of what occurs in practice. Even in simple building construction, suspended slab floors generate horizontal forces which are transmitted to the foundation by the load bearing walls. In these cases, however, the horizontal forces are not comparable in magnitude to the vertical ones.

To estimate the ultimate load of a footing subjected to an inclined load, most standards make use of semi-empirical expressions based on the works of Meyerhof, Hansen or Vesic. All these theories have been developed using the principle of superposition introduced by Terzaghi, but are not rigorous from the point of view of continuum mechanics. Given this lack of rigor, it can be expected that they will not provide accurate estimates of the true bearing capacity. To assess these theories and provide more rigorous ultimate loads, we use the limit theorems of classical plasticity. Since analytical solutions to the combined loading problem are very difficult, we adopt powerful discretized versions of these theorems (which employ finite elements) and apply them to calculate numerical upper and lower bounds on the ultimate load. The study is carried out in terms of a dimensionless material parameter, the friction angle and the inclination angle. These quantities are varied to cover most cases of practical interest. An interesting outcome of the study is that the predictions from the classical theories (which are often used in standards) are not always on the safe side. The rest of the paper is organized as follows. Section 2 defines the problem under consideration, describes the governing equations, and introduces the notation used. In section 3, the limit analysis theorems are briefly recalled as well as the mathematical programming problems obtained after discretization. Section 4 discusses some well known semi-empirical expressions that have influenced standards for designing foundations subjected to inclined load. Numerical results are given in section 5 and compared with these theories.

2 GOVERNING EQUATIONS

The present study deals with the ultimate bearing capacity of a single rigid strip footing, resting on a homogenous cohesive-frictional soil of great depth, that is subjected to an inclined load **Q** (Figure1).

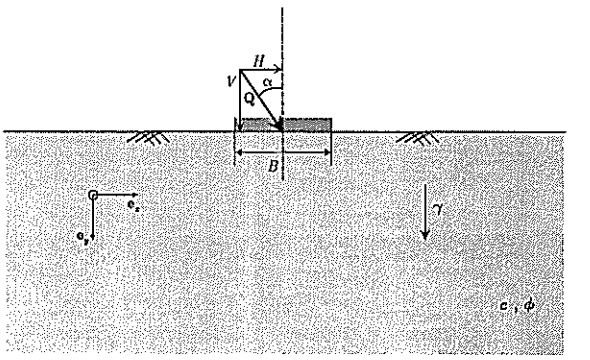

Figure 1: Footing subjected to an inclined load

Further, it is assumed that the footing is rough and the soil is of unit weight γ. The force acting upon

the foundation is centrally inclined at an angle α with respect to the vertical. The cohesive-frictional soil is assumed to be rigid perfectly plastic and modeled by a Mohr-Coulomb yield criterion with cohesion c and friction angle ϕ. The width of the footing is denoted by B and its length L is supposed to be large enough such that a plane strain case will exist in the soil mass supporting the foundation. Practically, plane strain theory will yield fairly good results when $B/L \leq 1/5$ to $1/6$. Under an inclined load, failure can occur either by sliding of the footing along its base or general shear of the underlying soil. If the foundation is rough, sliding will occur within the soil just beneath the footing and not at the interface. The limit load problem consists in finding the limit load multiplier, μ, the stress field, and the velocity field such that governing equations of continuum mechanics are satisfied. For plane strain problems, the kinematics and statics of the continuum are completely specified with in-plane components. Assuming small strains, the governing equations are:

Equilibrium

$$\begin{aligned} &\frac{\partial \sigma_x}{\partial x} + \frac{\partial \tau_{xy}}{\partial y} = 0, \\ &\frac{\partial \tau_{xy}}{\partial x} + \frac{\partial \sigma_y}{\partial y} = \gamma, \end{aligned} \quad \text{in } \Omega \tag{1}$$

$$\begin{aligned} \mu V &= -\int_{-B/2}^{B/2} \sigma_y \, dx = \mu Q \cos\alpha, \\ \mu H &= -\int_{-B/2}^{B/2} \sigma_x \, dx = \mu Q \sin\alpha, \end{aligned} \tag{2}$$

where Ω represents the volume of the half space.

Compatibility

$$\dot{\varepsilon}^p = \nabla_s \mathbf{v} \text{ in } \Omega, \tag{3}$$

$$\mathbf{v} = \mathbf{0} \quad \text{for } \mathbf{x} \in \Omega \text{ far from load}, \tag{4}$$

where $\dot{\varepsilon}^p$ denotes the plastic strain rate vector and ∇_s stands for the symmetric part of the gradient. The relation (4) means that the soil outside the failure surface is rigid.

Behavior

$$\dot{\varepsilon}^p = \dot{\lambda} \frac{\partial f}{\partial \sigma}, \tag{5}$$

$$f(\sigma) \leq 0, \tag{6}$$

where (5) defines an associated flow rule and $f(\sigma)$ the Mohr-Coulomb yield criterion. The normality of the plastic strain to the yield surface is often perceived to be a shortcoming for frictional soils as it predicts excessive dilation upon shear failure. This perception is somewhat pessimistic for geotechnical problems that involve a free surface and an unbounded domain, where non-associated behavior appears to have little effect on the collapse load. This important result is discussed at length by Davis [5] and has been confirmed in a number of independent finite element studies [11].

In the context of limit analysis, a stress is said to be statically admissible (σ^{sa}) if it satisfies the equations of internal equilibrium (1), the boundary conditions for surface tractions (2) and the yield condition (6). A velocity field is said to be kinematically admissible ($\mathbf{v}^{ka}$) if it satisfies the compatibility relations within the domain (3), the kinematic boundary conditions (4), the flow rule (5) and leads to a positive value of the power expended by the external loads. The ultimate load can be bracketed from below/above using the lower/upper bound limit analysis theorems.

Lower Bound Theorem

The lower bound theorem states that the load, determined from a stress field which satisfies equilibrium within the domain and on the boundary and does not violate the yield condition, is not greater than the actual collapse load. The actual limit load is obtained as the supremum:

$$\mu = \sup_{\sigma^{sa}} \mu^s(\sigma). \tag{7}$$

Upper Bound Theorem

The upper bound theorem states that the load (or the load multiplier) determined by equating the external rate of work to the internal rate of dissipation in a kinematically admissible velocity field $\mathbf{v}^{ka}$ is not less than the actual collapse load. As a consequence of the upper bound theorem, the actual load multiplier is the lowest load multiplier:

$$\mu = \inf_{\mathbf{v}^{ka}} \left\{ \int_\Omega \boldsymbol{\sigma} \cdot \dot{\varepsilon}^p(\mathbf{v}) \, d\Omega + \int_\Sigma \mathbf{t} \cdot [\![\mathbf{v}]\!] \, d\Sigma \right\}$$

$$\text{subjected to} \quad \begin{cases} \mathbf{Q} \cdot \mathbf{v}_0 + \gamma \int_\Omega v_y \, d\Omega = 1, \\ \dot{\lambda} \geq 0 \, ; \, f(\sigma) \leq 0 \, ; \, \dot{\lambda} f(\sigma) = 0, \end{cases} \tag{8}$$

where $\mathbf{v}_0$ denotes the velocity of the center of the foundation. An analytical solution that gives the exact load is possible only in a few situations. To harness the power of the limit analysis theorems for design, they are used in a discretized (finite element) form to provide solutions for practical problems. In these formulations, particular attention is paid to conserve the bounding properties. The discrete form of the lower and upper bound is briefly recalled in the next Section.

3 NUMERICAL LIMIT ANALYSIS

The fundamental theorems of limit analysis define convex mathematical programs. After discretiza-

tion, they can be solved by mathematical programming techniques. A full description of the present formulations can be found in [7], [8] and [9].

Discrete formulation of the lower bound

In the lower bound formulation, the stress field is discretized using the finite elements with stress nodal variables:

$$\sigma(\mathbf{x}) = \mathrm{N}_i(\mathbf{x})\,\sigma_i$$

where σ_i is a nodal stress vector and $\mathrm{N}_i(\mathbf{x})$ are shape functions. For a rigorous lower bound, the shape function must be linear to ensure that the yield criterion can be satisfied everywhere by enforcing it only at the nodal points of each element. Linear equality constraints on the nodal stresses arise from the application of equilibrium equations (1) over each element. Equilibrium of the surface tractions emerging on both sides of adjacent triangles should also be enforced. Since the shape functions are linear, this condition is satisfied by only matching traction components at nodal pairs that have the same coordinates and share the same edge. It follows that, unlike the more familiar displacement finite element method, each node is unique to a particular element and several nodes may share the same coordinates. In addition to the above constraints, equilibrium equations on the boundary (2) generate extra linear equalities that have to be added to the previous ones. The nonlinear constraints in the formulation arise from satisfaction of the yield criterion, which is implemented in its native form. To complete the stress field in an unbounded domain, special extension elements are included in the mesh without violating equilibrium, the boundary conditions and the yield criterion. These also generate constraints on the nodal stresses. The presence of statically admissible stress discontinuities between sides of adjacent elements is a key feature of the formulation. Indeed, these discontinuities greatly improve the accuracy of a lower bound solution as they permit the stress field to change rapidly where needed. Figure 2 shows a typical mesh used in lower bound calculations.
The objective function of this nonlinear linear programming problem, which corresponds to the collapse load, is maximized according to:

$$\textit{Maximize}\quad \mathbf{C}^{\mathrm{T}}\boldsymbol{\Sigma}$$

$$\textit{Subject to}\quad \begin{cases} \mathbf{A}\,\boldsymbol{\Sigma} = \mathbf{b} \\ f_i(\sigma) \le 0 \quad i = \{1,\ldots,n\} \end{cases}$$

where $\mathbf{C}$ is a vector of objective function coefficients, $\boldsymbol{\Sigma}$ is a vector of unknowns (nodal stresses), $\mathbf{C}^{\mathrm{T}}\boldsymbol{\Sigma}$ is the collapse load, $\mathbf{A}$ is a matrix of equality constraint coefficients, $\mathbf{b}$ is a vector of coefficients, $f_i(\sigma)$ is the yield function for node i, and n is the number of nodes.

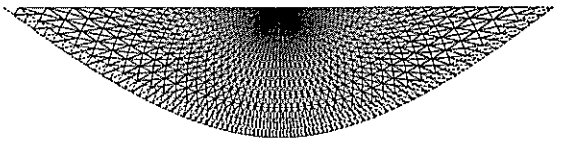

Figure 2: Lower bound mesh

Discrete formulation of the upper bound

The minimum principle (8) is cast in discrete form by expressing the velocity field as function of a finite number of parameters. Plane finite elements based on velocity approximations are employed for this purpose. In each element E $(E = 1,\ldots,N)$ the velocities are expressed as

$$\mathbf{v}(\mathbf{x}) = \mathrm{N}_i(\mathbf{x})\,\mathbf{v}_i$$

where $\mathbf{v}_i$ is a nodal velocity vector and $\mathrm{N}_i(\mathbf{x})$ are shape functions. The linear three-noded triangle is used to model the velocity field. This ensures that the upper bound is strict since the flow rule is satisfied everywhere within each element. Two unknown velocities are associated with each node, and a single plastic multiplier rate plus a constant stress vector are associated with each element. To improve the upper bound calculations and avoid locking that may occur for incompressible materials, Sloan and Kleeman (1995) proposed a new formulation that allows velocity discontinuities along all shared element in the mesh. In their procedure, the direction of shearing is chosen automatically during the minimization process to give the least amount of dissipated power. Figure 3 shows a typical mesh used in upper bound calculations.

Figure 3: Upper bound mesh

To avoid the Kuhn-Tucker constraints, the minimum problem can be transformed into a min-max problem. As a result of this transformation, the plastic multiplier rate does not appear explicitly in the formulation. Once the constraints and the objective function coefficient are assembled, the task of finding a kinematically admissible velocity field, which minimizes the internal power dissipation for a specified set of boundary conditions, may be written as

$$\underset{\boldsymbol{\Sigma}}{\textit{Maximize}}\quad \underset{\mathbf{V},\mathbf{d}}{\textit{Minimize}}\quad \boldsymbol{\Sigma}^{\mathrm{T}}\mathbf{B}\,\mathbf{V} + \mathbf{C}_{\mathrm{u}}^{\mathrm{T}}\mathbf{V} + \mathbf{C}_{\mathrm{d}}^{\mathrm{T}}\mathbf{d}$$

$$\textit{Suject to}\quad \begin{cases} \mathbf{A}_{\mathrm{u}}\mathbf{V} + \mathbf{A}_{\mathrm{d}}\mathbf{d} = \mathbf{b} \\ f_i(\sigma) \le 0 \qquad i = \{1,\ldots,N\} \\ \mathbf{D} \ge \mathbf{0} \end{cases}$$

where $\mathbf{V}$ is a global vector of unknown velocities, $\mathbf{D}$ is a global vector of unknown discontinuity variables, Σ is a global vector of unknown element stresses, $\mathbf{C}_u$ and $\mathbf{C}_d$ are vectors of objective function coefficients for the nodal velocities and discontinuity variables, $\mathbf{A}_u$ and $\mathbf{A}_d$ are matrices of equality constraint coefficients for the nodal velocities and discontinuity variables, $\mathbf{B}$ is a global matrix of compatibility coefficients that operate on the nodal velocities, $\mathbf{b}$ is a vector of coefficients, f_i is the yield function for element i, and E is the number of triangular elements. The objective function $\Sigma^T\mathbf{B}\,\mathbf{V} + \mathbf{C}_u^T\mathbf{V} + \mathbf{C}_d^T\mathbf{d}$ corresponds to the total dissipated power, with the first term giving the dissipation in the continuum, the second term giving the dissipation due to fixed boundary tractions or body forces, and the third term giving the dissipation in the discontinuities.

The discrete formulations of the limit analysis theorems described above are used here to estimate the bearing capacity of a surface footing subjected to an inclined load. The rigorous ultimate load is computed with an error that does not exceed 6%. Before presenting results, we recall below some semi-empirical expressions that are widely used in practice to estimate this ultimate load.

4 BEARING CAPACITY THEORIES FOR INCLINED LOADED STRIP FOOTINGS

During the last fifty years, several bearing capacity theories were proposed for estimating the ultimate bearing capacity of shallow foundations. Most of them rely on the *superposition* principle suggested by Terzaghi (1943), in which contributions to the bearing capacity from the cohesion, the surcharge, and the unit weight are summed. For a strip footing loaded vertically in the plane of symmetry, the ultimate load q_u is represented by the expression

$$q_u = c\,N_c + q\,N_q + \frac{1}{2}\gamma B\,N_\gamma, \qquad (9)$$

where *the bearing capacity factors*, N_c, N_q and N_γ represent the effects due to soil cohesion c, surface loading q, and soil unit weight γ, respectively. The parameters N are all function of the internal friction angle ϕ. Following Terzaghi, other significant developments have been made by Meyerhof (1953), who used the method of limit equilibrium, and by Brinch Hansen (1961) and Vesic (1975), who used the slip-line method. All authors agree on the following expression for N_c and N_q which are due to Prandtl:

$$N_q = e^{\pi\tan\phi}\tan^2\left(\pi/4 + \phi/2\right),$$
$$N_c = \left(N_q - 1\right)\cot\phi.$$

Divergence occurs on the definition of the N_γ factor:

Meyerhof: $\left(N_q - 1\right)\cot(1.4\,\phi)$,

Hansen: $1.5\left(N_q - 1\right)\tan\phi$,

Vesic: $2\left(N_q - 1\right)\tan\phi$.

To take account of the inclination of the load, the original bearing capacity equation for a purely vertical load is often modified using semi-empirical coefficients according to

$$q_u\big|_v = q_u\cos\alpha = c\,N_c\,i_c + q\,N_q\,i_q + \frac{1}{2}\gamma B\,N_\gamma\,i_\gamma, \qquad (10)$$

where i_c, i_q and i_γ are inclination factors defined as follows:

Meyerhof:

$$i_c = i_q = \left(1 - \frac{\alpha^\circ}{90^\circ}\right)^2,$$

$$i_\gamma = \left(1 - \frac{\alpha^\circ}{\phi^\circ}\right)^2;$$

Hansen:

$$i_q = \left(1 - \frac{0.5\,H}{V + B\,L\,c\cot\phi}\right)^{\delta_1},$$

$$i_c = \frac{i_q N_q - 1}{N_q - 1},$$

$$i_\gamma = \left(1 - \frac{0.7\,H}{V + B\,L\,c\cot\phi}\right)^{\delta_2};$$

Vesic:

$$i_q = \left(1 - \frac{H}{V + B\,L\,c\cot\phi}\right)^{m},$$

$$i_c = \frac{i_q N_q - 1}{N_q - 1},$$

$$i_\gamma = \left(1 - \frac{H}{V + B\,L\,c\cot\phi}\right)^{m+1}$$

where $m = (2 + B/L)/(1 + B/L)$.

Remarks:

- The expression of the inclination factor i_γ in Meyerhof's theory is meaningful only for $\alpha < \phi$.
- In his paper, Hansen use 5 for both δ_1 and δ_2.
- The formulation of Vesic uses the shape of the footing in these factors. For a strip footing, the ratio B/L is equal 0.

5 PARAMETRIC STUDY AND DISCUSSION

We now present some new results from the numerical study of the bearing capacity of a surface footing subjected to an inclined load. The study has been carried out using two fundamental dimensionless parameters, the friction angle ϕ and a weight parameter $G = \gamma B/2c$. If G is small the soil behaves essentially as a cohesive weightless medium. If G is large, soil weight rather than cohesion is the principal source of bearing strength. For practical cases one can expect that ϕ lies in the range $0° - 45°$ and G will range from 0 to 3. These limits assume that c ranges from $7\,\text{kN/m}^2$ to $50\,\text{kN/m}^2$, γ ranges from $14\,\text{kN/m}^3$ to $30\,\text{kN/m}^3$, and the footing width ranges from 1m to 10m.

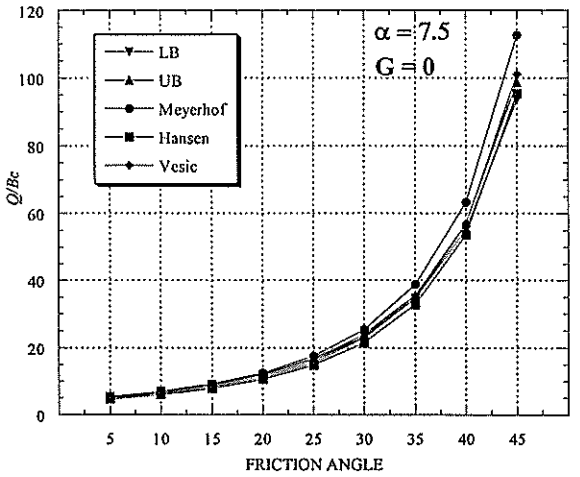

Figure 4

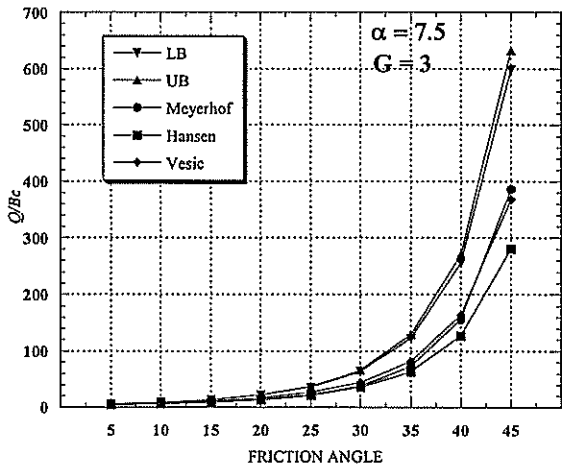

Figure 5

Numerical results are presented for G equal to 0.0 and 3.0 and α equal to 7.5°, 15°, 22.5° and 30°. They are summarized in Figures 4 to 11. As the inclination increases, the vertical component of the ultimate load decreases. For an inclination of 15° with $G = 0$ and $\phi = 45°$, there is a reduction of 50% in the ultimate load.

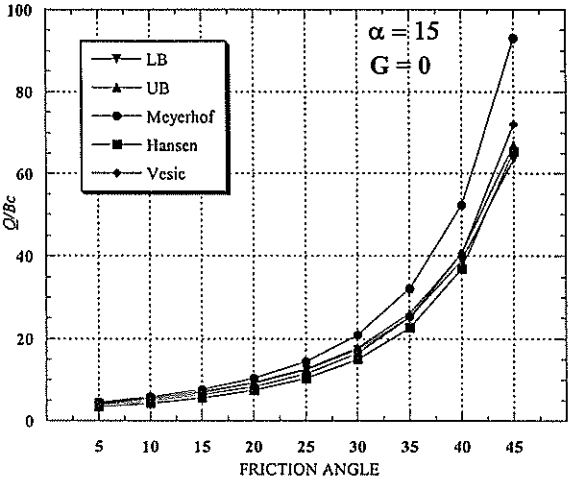

Figure 6

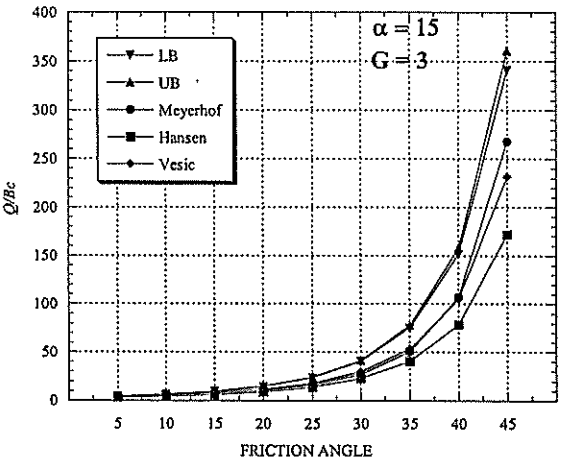

Figure 7

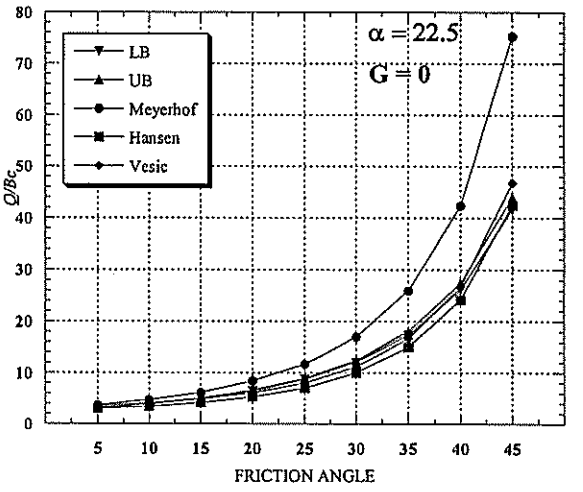

Figure 8

We remark that the results predicted by Meyerhof (1953) are always on the *unsafe* side for a weightless soil. The solutions of Hansen (1970) gives results comparable to those obtained by finite

element limit analysis, and are mostly on the safe side. The differences between the theories are not large for small inclinations, but increase to about 50% for an inclination of 30°.

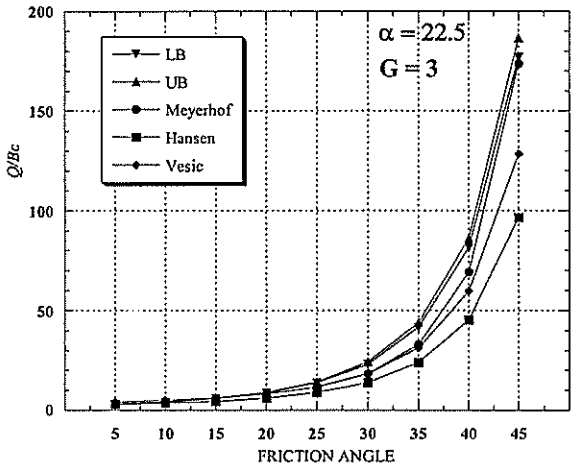

Figure 9

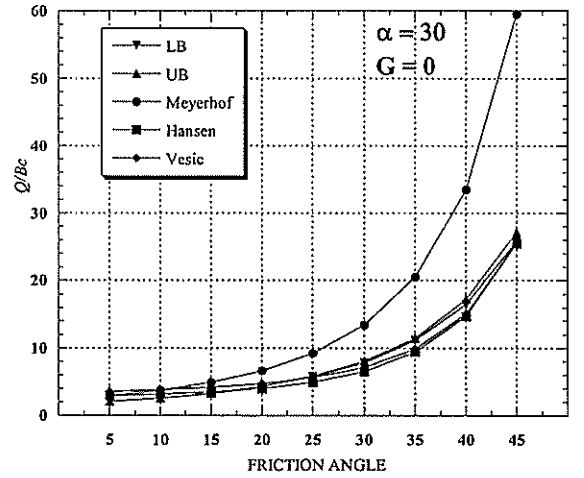

Figure 10

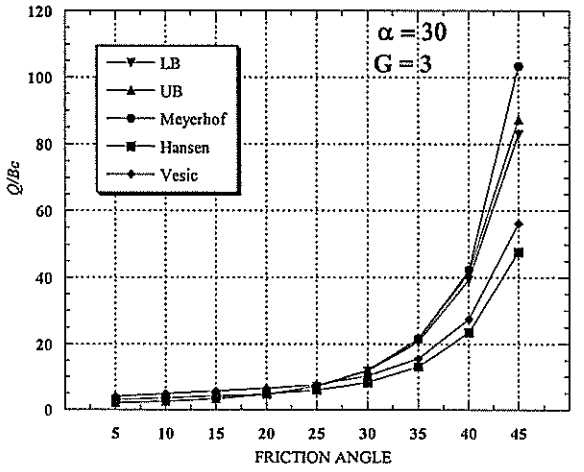

Figure 11

When the unit weight is taken into consideration, the differences between the computed bounds and the other solutions are more pronounced. The Meyerhof (1953) predictions far exceed the finite element upper bounds for some cases with large load inclinations, and are clearly non-conservative.

6 REFERENCES

1. Hansen, J.B, A revised and Extended Formula for Bearing Capacity, Danish Geotechnical Institute, Bulletin No 28, pp. 5-11, 1970.
2. Meyerhof, G. G., The bearing capacity of foundations under eccentric and inclined loads, *Proc. Third Int. Conf. Soil Mech. And Found. Engng*, Zurich, 1953, 1, 440-445.
3. Meyerhof, G. G., Discussion on "Rupture Surfaces in Sand under Oblique Loads." *Journal of the Soil Mechanics and Foundations Division, Proc. Am. Soc. Civil Engrs., n° SM 3* : 1028-15, 1982.
4. Vesic, A., Analysis of ultimate loads of shallow foundations. Journal of Soil Mechanics and Foundations Division, ASCE, 99, SM1, 45-73, 1973.
5. Davis, E. H. 1968. Theories of Plasticity and Failure of Soil Masses. In I. K. Lee (ed.), Soil Mechanics Selected Topics: 341-354. Elsevier: New York.
6. Drucker, D.C., Greenberg, W. & Prager, W. 1952. Extended limit design theorems for continuous media. Quarterly Journal of Applied Mathematics 9: 381-389.
7. Lyamin A. V. 1999. Three-Dimensional Lower Bound Limit Analysis Using Nonlinear Programming, PhD Thesis, University of Newcastle, Australia.
8. Lyamin A. V. & Sloan S. W. 2002. Lower bound limit analysis using nonlinear programming. To appear in International Journal for Numerical Methods in Engineering.
9. Lyamin A. V. & Sloan S. W. 2001. Upper bound limit analysis using linear finite elements and nonlinear programming. International Journal for Numerical and Analytical Methods in Geomechanics, **26**, pp.181-216, 2002.
10. Prandl L. 1920. Über die Härte plastischer Körper. Nachrichten von der Geselschaft der Wissenschaften zu Göttingen, Mathematisch-Physikalische Klasse, **12**:74-85.
11. Sloan, S. W. & Kleeman, P. W. 1995. Upper bound limit analysis with discontinuous velocity fields. Computer Methods in Applied Mechanics and Engineering 127: 293-314.
12. Zienkiewicz, O. C., Humpheson, C. & Lewis, R. W. 1975. Associated and nonassociated viscoplasticity and plasticity in soil mechanics. Géotechnique 25: 671-689.

Assessment of Existing Pile Foundations for Upgrading of Capacity

Sean Holt
Douglas Partners Pty Ltd, Sydney

Summary Recent re-development of large-scale buildings in the Sydney region has called for the assessment of existing pile foundations under the application of proposed higher loads. Douglas Partners has recently been successful in implementing a forensic approach for assessing the as-constructed pile characteristics. Combined with comprehensive site investigation and the adoption of a higher confidence level compared to that of the original design, the assessment of the existing foundation system to support the proposed additional loads has successfully been undertaken. This approach has provided a cost effective way of adding value to existing buildings with the in-place foundation system often adequate for the re-development or upgrade of the building resulting in major cost savings to the project. This paper presents a review of some of the forensic methods adopted, site investigation and design with reference to the above.

1 INTRODUCTION

Douglas Partners have been involved in a number of recent re-developments of large-scale buildings in the Sydney region for which assessment of the existing foundation performance (generally designed in accordance with the former Australian Piling Code AS2159 – 1978, or before) under proposed higher working loads has been warranted.

Prior to the revised Australian Piling Code (AS2159 - 1995) the traditional approach to pile design was to adopt an overall factor of safety for assessment of the geotechnical pile capacity. However the code provided little guidance towards the application of appropriate factors of safety. Consequently, pile design was mostly over conservative. Typical factors of safety in the order of 2.0 to 3.0 (as high as 4.0 on occasions) were traditionally adopted dependant of the level of uncertainty during design and the consequences of failure.

Rock socketed piles were typically designed on the basis of a "working or allowable stress" approach with allowable parameters prescribed on the basis of research in each main population centre. For example, rock socketed pile design in the Sydney region was usually based on the parameters given in Pells et al (1978). The allowable end bearing and shaft adhesion parameters were necessarily conservative given the limited data accumulated on the load-deflection performance of piles within such material.

The current Australian Piling Code (AS2159 - 1995) is based on a limit state approach. This in effect is a partial safety factor approach in which an attempt is made to assign levels of risk to design based on the level of uncertainty in predicting the performance of the piled foundations.

Where re-assessment of existing piles (designed and constructed under the former code) is required to assess performance under proposed higher working loads it can be possible to implement further investigative work to reduce the potential for variation in the geotechnical design process. Also, with over 20 years of accumulated pile load testing data the parameters for design in many rocks have generally increased without compromising performance or safety. This better knowledge of pile-soil interaction and implementation of more reliable and comprehensive site investigation techniques, may facilitate the application of higher design parameters. Hence the designer is in a more informed position and can re-assess the pile with a higher level of confidence, which may result in upgrading of the pile capacity. This approach has brought about significant cost savings with the existing piled foundations used for the upgraded or re-developed building.

This paper discusses the application of forensic methods used for assessing the as-constructed pile characteristics with a view towards upgrading of the existing pile capacity.

The potential of existing foundations is also limited by the structural strength requirements of the as-constructed pile. This paper focuses more on the geotechnical aspects of design. Nonetheless the structural strength should still be assessed with regards to possible upgrading of the pile capacity, as it may be the limiting design criteria.

2 ASSESSING THE AS-CONSTRUCTED PILE CHARACTERISTICS

When trying to determine the as-constructed pile characteristics firstly a background history search should be undertaken. In carrying out this search an attempt should be made to try to identify:

- Pile design, steel reinforcement conditions, etc...
- Pile type, length and method of installation
- Works as executed drawings and/or piling records
- Testing or inspection regime conducted to assess the constructed pile conformance with design
- Relevant geotechnical investigations
- Any other information deemed relevant

All of this can be used to establish a comprehensive model of the as-constructed pile foundation. Where this information can not be obtained, or the information is incomplete (such as missing levels on pile records needed to establish pile toe level) Douglas Partners have adopted a forensic approach to assess the existing pile characteristics through the use of sonic integrity testing (SIT), an established technique routinely used for proof testing of new piles.

Advantages of adopting SIT is that it is a non-destructive test that can quickly and economically be used to assess the structural integrity and length of the pile. This provides the designer with some of the information required to assess the as-constructed condition of the pile.

SIT involves inducing a stress wave in the pile by means of a mallet blow to the head of the pile. The response as this stress wave travels down the pile and reflects back to the head is measured through an accelerometer attached to the pile head. The stress wave reflects off discontinuities in the pile such as significant inclusions or voids, cracks, joints, significant changes in material properties and sharp changes in cross section. The reflections cause movements of the pile head, which are registered by the hand-held accelerometer that is pressed against the pile. A field computer converts the recorded sonic signal into a velocity-time trace. The shape of the recorded sonic signal (reflectogram) provides a qualitative indication of the pile integrity. An example of a typical reflectogram for a sound reinforced concrete pile is given in Figure 2.1. The test does not give any information on the load carrying capacity of the pile.

Typical Reflectogram of a Sound Pile

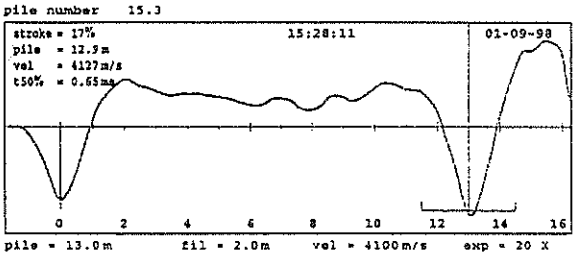

Figure 2.1: Reflectogram of a sound pile

The test requires access to the pile head or to a horizontal landing excavated into the upper pile shaft, so that a hammer blow can be delivered to a plane perpendicular to the pile axis. The pile head or landing must be trimmed back to sound material free of debris, cracks or water and preferably free of impediments such as steel reinforcement.

Once a comprehensive model of the as-constructed pile foundation is established the designer can implement further site investigation techniques to eliminate the geotechnical unknowns in the initial design to more accurately predict the pile performance.

3 SITE INVESTIGATION

For any project the decision as to what level of site investigation and pile testing to carryout is largely an economic one. Hence there is a trade off between potential economies with possible reduction of pile length and the cost of additional site investigation and pile testing to justify a certain confidence level. Where the foundations are existing, additional investigation can be undertaken to assess the potential for upgrading the pile capacity. This additional investigation may also justify an upgrading of the initial design parameters should they have been adopted conservatively based on limited information at the time of design. This can result in significant cost savings for foundations that would otherwise have to be reconstructed, which may be at a premium due to space and operational restrictions imposed by the existing building.

The requirements and methods adopted for site investigation are dependent on the subsurface conditions and also the existing pile system in place. AS2159 Suppl - 1996 provides a commentary on the objectives of site investigation and the suitability of various techniques, hence will not be discussed in detail here. The application of reduction factors in assessing the design geotechnical strength in accordance with AS2159 - 1995 are assessed on the reliability of the test method and confidence level in predicting the appropriate design parameters and subsoil variance across the site. Thus the techniques adopted and frequency are crucial to justify upgrading the existing pile capacity. This is discussed in more detail in the following section.

Restrictions imposed by the existing structure will also influence the selection of investigation techniques. For this reason Douglas Partners have developed portable drilling and cone penetration testing (CPT) capabilities which can operate in restricted areas of low headroom. With continual improvements in investigation equipment and methods (for example, greater hydraulic thrust enabling CPT to advance through bearing layers which it would have previously refuse

on) this portable equipment is able to perform the majority of tasks of it full size equivalent machinary.

4 AUSTRALIAN PILING CODE

4.1 Pile Design Background

The design of pile foundations, like other foundation systems, requires assessment of the following:

- Strength – sufficient margin against the structural and geotechnical failure of the piles subjected to anticipated loading combinations over the design life of the structure.
- Serviceability – foundation movements under the serviceability, or working, loads (without application of reduction factors) are to be within the allowable structural tolerance of the supported structure.
- Durability – the integrity of the piles should be able to withstand wear and deterioration over the design life of the structure. Also the aggressivity of the soil and groundwater may necessitate a sacrificial amount of pile cross-section to accommodate some corrosion.

The former Australian Piling Code (AS2159 - 1978) was based on an overall factor of safety approach for assessment of strength requirements, whilst complying with the other requirements. It was referred to as a "working stress" approach to pile design. Thus, the relationship between the applied load, and the piles ability to resist the subjected loads was expressed in the form:

$$P \leq P_{all} \quad (P_{all} = P_u / FOS) \qquad ...(1)$$

where:

P = Applied Working Load on pile
P_{all} = Allowable pile load
P_u = Ultimate pile resistance
FOS = Factor of safety, typically in the order of 2.0 to 3.0 (as high as 4.0 on occasions), selected by the designer to reflect the level of confidence in design and the consequence of failure.

However the code provided little guidance towards the application of appropriate factors of safety. Consequently, pile design was mostly over conservative.

The recent Australian Piling Code (AS2159 - 1995), superseding the previous code published in 1978, provides a limit state design approach. The code specifies that for geotechnical strength requirements the pile shall be proportioned such that the design strength (i.e. factored down pile strength) is not less than the design action effect (i.e. factored up loads on the pile), or in the form:

$$S^* \leq R^*_g \quad (R^*_g = \phi_g R_{ug}) \qquad ...(2)$$

where:

S^* = Design action effect (i.e. factored up loads where $S^* = U \times S$). In addition to the direct structural loads as specified in AS1170.1 the code specifies that the design must consider the following:
  - Dead loads of pile and pile cap
  - Soil movement, negative friction, expansive soils and earth movements.
  - Handling
  - Installation
  - Any other additional loads and actions that may be applied, e.g. impact, dynamic loading, water pressure and scour.

R^*_g = Design geotechnical strength (factored down pile strength)
ϕ_g = Geotechnical strength reduction factor
R_{ug} = Ultimate geotechnical strength

In effect this is a partial safety factor approach which an attempt is made to assign levels of risk based on the level of investigation and confidence during design. This is reflected by ϕ_g which depends on the level of site investigation and type and number of pile load tests planned. This approach therefore targets risk more appropriately than an overall factor of safety. It should be noted that the ultimate geotechnical strength (R_{ug}) is factored, rather than the individual design parameters to assess both shaft and base components.

The code also requires that foundation movements under serviceability loads (without application of reduction factors) are to be within the allowable structural tolerance of the supported structure so as not to cause loss of serviceability. Durability of the pile over the intended design life should also considered in the design.

4.2 The Application of Strength Reduction Factors to Geotechnical Design

Through comparison of equations 1 and 2, it can be seen that the two equations are equivalent if:

$$FOS = U / \phi_g \qquad ...(3)$$

where:

U = Load factor (used to assess the design action effect i.e. factored up loading).

Typically a load factor of 1.25 is applied to dead loads, 1.5 to live loads with the code suggesting suitable load factors for loads induced by soil movements (not taken into account for geotechnical strength design). If only supplied with the working Load on the pile, or a quick means of checking some designers adopt an average load factor (U) of 1.35.

TABLE 4.1

RANGE OF VALUES FOR GEOTECHNICAL STRENGTH REDUCTION FACTOR ϕ_g

Method of assessment of ultimate geotechnical strength	Range of values of ϕ_g
Static load testing to failure	0.70–0.90
Static proof (not to failure) load testing (NOTE 1)	0.7–0.90
Dynamic load testing to failure supported by signal matching (NOTE 2)	0.65–0.85
Dynamic load testing to failure not supported by signal matching	0.50–0.70
Dynamic proof (not to failure) load testing supported by signal matching (NOTES 1 and 2)	0.65–0.85
Dynamic proof (not to failure) load testing not supported by signal matching (NOTE 1)	0.50–0.70
Static analysis using CPT data	0.45–0.65
Static analysis using SPT data in cohesionless soils	0.40–0.55
Static analysis using laboratory data for cohesive soils	0.45–0.55
Dynamic analysis using wave equation method	0.45–0.55
Dynamic analysis using driving formulae for piles in rock	0.50–0.65
Dynamic analysis using driving formulae for piles in sand	0.45–0.55
Dynamic analysis using driving formulae for piles in clay	Note 2
Measurement during installation of proprietary displacement piles, using well established in-house formulae	0.50–0.65

NOTES:

1 ϕ_g should be applied to the maximum load applied.

2 Signal matching of the recorded data obtained from dynamic load testing should be undertaken on representative test piles using a full wave signal matching process.

3 Caution should be exercised in the sole use of dynamic formulae (e.g. Hiley) for the determination of the ultimate geotechnical strength of piles in clays. In particular, the dynamic measurements will not measure the 'set-up' which occurs after completion of driving. It is preferable that assessment be first made by other methods, with correlation then made with dynamic methods on a site-specific basis if these latter are to be used for site driving control.

4 For cases not covered in Table 4.1, values of ϕ_g should be chosen using the stated values as a guide.

TABLE 4.2

GUIDE FOR ASSESSMENT OF GEOTECHNICAL STRENGTH REDUCTION FACTOR (ϕ_g)

Circumstances in which lower end of range may be appropriate	Circumstances in which upper end of range may be appropriate
Limited site investigation	Comprehensive site investigation
Simple method of calculation	More sophisticated design method
Average geotechnical properties used	Geotechnical properties chosen conservatively
Use of published correlations for design parameters	Use of site-specific correlations for design parameters
Limited construction control	Careful construction control
Less than 3% piles dynamically tested	15% or more piles dynamically tested
Less than 1% piles statically tested	3% or more piles statically tested

AS2159 - 1995 specifies ranges for the adoption of suitable geotechnical reduction factors based on the method of assessing R_{ug} as indicated in Table 4.1 (AS2159 - 1995). Table 4.2 (AS2159 - 1995) gives a guide as to the selection of a specific value within the range. However, this is largely subjective and open to interpretation with different designers having different perceptions on the comprehensiveness of the site investigation.

In effect this is an attempt to assign levels of risk based on the reliability of the test method and confidence level during design. Such that for a relatively inaccurate method of assessing the pile capacity (say limited site investigation with SPT information) a far lower reduction factor (ϕ_g) would be applicable (say 0.45 to 0.55) to that of a more accurate means (such as static load testing of a representative number of piles).

Where the pile foundations have already been constructed and there is a need for additional loading to be supported as part of the proposed re-development of the supported structure there are significant cost savings should the existing pile foundations be able to support these additional loads. With the as-constructed pile characteristics known, comprehensive and reliable site investigation information the designer may be able to justify a higher confidence level to that adopted in the initial design. With the pile capacity being upgraded through application of a higher reduction factor reflecting more confidence in the prediction of the pile performance. It should be noted that there should be compliance with all other design criteria under the code with respects to upgrading of the pile capacity.

By way of example: For a friction pile founded in sand designed under the former code with limited site investigation comprising SPT information, with possible on site correlation using dynamic formulae (e.g. Hiley) a factor of safety of say 3.0 would be appropriate.

If future re-development requires the pile capacity to be reassessed, for this fixed pile length additional investigation could be implemented that may justify a higher level of confidence in predicting the pile performance. If comprehensive static analysis using CPT data were undertaken a reduction factor of 0.65 could be applicable. As shown in equation 3, subject to other limiting design criteria this equates to a factor of safety of some 2.1, significantly lower to that adopted in the initial design. Thus, without taking into account more appropriately assigned design parameters and possible over construction of the pile, this pile could be able to withstand up to some 50% additional load to that of the original design from a geotechnical viewpoint.

5 CONCLUSION

With an increasing number of large-scale buildings being re-developed these days the need for innovative and cost effective solutions for assessing the existing foundation performance under proposed higher working loads is clearly apparent.

In the absence of existing information the implementation of sonic integrity testing provides a quick and economical means of assessing the length, shape and continuity of an existing pile. In addition this technique does not compromise the structural integrity of the existing pile like other methods, such as load testing or concrete coring.

Once the as-constructed foundation characteristics have been determined the designer can then implement more comprehensive and reliable site investigation techniques to more confidently predict the likely performance of the pile. This investigation may enable the application of higher design parameters should the original parameters adopted be conservative. With an increased understanding of the pile performance an informed allocation of risk can be assigned, and may justify the application of higher reduction factors with regards to upgrading the existing pile capacity. Since the as-constructed conditions of the pile are being assessed, if the piles have been over constructed or conservatively designed (based on limited site information) then redesign of the pile can result in an increase in load carrying capacity of the pile.

It is reiterated that the designer must also comply with the structural strength requirements of the current codes, and serviceability criteria in accordance with AS2159 - 1995. Thus, all design criteria must be assessed and the limiting design criteria applied.

The designer may not always be able to upgrade the pile capacity significantly enough to support the additional loads. However through post construction analysis we can assess the areas where the pile is lacking and therefore make a more informed assessment of the most appropriate and cost effective solution to remediate this.

6 CASE STUDY – BULLDOGS LEAGUES CLUB, BELMORE

The re-development of the Canterbury-Bankstown (Bulldogs) Leagues Club in Belmore called for construction of an extra floor level on top of the existing two storey car park structure and hence an assessment of the existing foundations to support this additional loading.

The car park, a reinforced concrete framed structure with floor slabs sloping some 2 to 4%, was constructed

in the early 1980's and is supported on 1000 mm diameter rock socketed bored concrete piers. The bored piers were located centrally under rectangular columns designed with an allowable bearing pressure of 1000 kPa. Steel reinforcement conditions were known from the initial design, however no records existed of the as-constructed pile lengths.

Reference to the Sydney 1:100 000 Geological Series Sheet and previous investigation on the site indicates the site is underlain by residual clays overlying Ashfield Shale belonging to the Winamatta Group. Excavation into the underlying shale was required to construct the lower car park level. Previous site investigation comprised the drilling of test bores using spiral flight augers taken to near refusal in the underlying weaker shale. Core drilling was not undertaken to assess the quality and continuity of the shale, hence limited allowable bearing pressures were allocated for the design of the piles.

Douglas Partners was commissioned to assess the quality of the founding shale for possible upgrading of the allowable bearing pressure to accommodate the additional loads associated with the extra floor.

SIT was carried out on a representative number of existing piles to assess the as-constructed pile lengths. A section of the floor slab was cut out adjacent to the column to access the pile head. SIT was carried out some ten times on each pile for repeatability of results. Based on an adopted stress wave velocity (c) of 3800m/s, consistent with sound concrete of over 10 years age, pile lengths were interpreted from the recorded sonic response to be from 3.0m to 4.8m in length. Higher propagation velocities, of up to 4000m/s, may be possible given the age and strength of the concrete, however this would have had the affect of increasing the pile lengths by some 0.2m on the average. The shorter length bored piers were noted to coincide with areas of additional excavation to construct the grade of the car park and thus are generally founded in more competent shale at depth.

Portable low headroom drilling and CPT equipment was used to define the subsoil profile adjacent to each of the tested piles, with axial point load index testing carried out on the recovered core for assessment of strength characteristics. A summary of the interpreted pile length and subsoil conditions for a given pile is shown in figure 6.1.

The investigation indicated that the bored piers were founded in low to medium strength, fractured to highly fractured shale, or better. Material of this quality is suitable for a Class III classification in accordance with Pells et al (1995), for which an allowable bearing pressure of 2000kPa is considered suitable. In the absence of pile records lower bound shaft adhesion values for the various classes of overlying shale were implemented to account for uncertainties in cleanliness and roughness of the pile shaft.

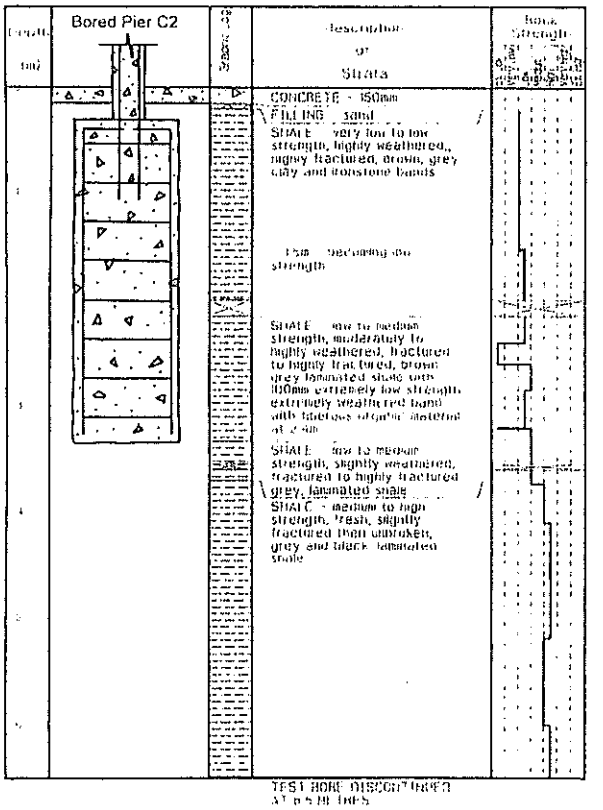

Figure 6.1: Schematic of interpreted pile length along with subsoil conditions for bored pier C2.

With the pile geometry and subsoil properties established assessment of the piles to withstand the additional loads was carried out. Additional settlements associated with the increased loading were anticipated to be only minor (total settlement in the order some 1% of the pile diameter) and within the structural tolerance of the building.

The re-assessment of the bored piers at the Bulldogs Leagues Club allowed additional load to be applied to the founding system with confidence of only minor additional movements being caused. The end resulte in this case was a building owner happy to enjoy an upgraded building with additional storeys, without the extra cost of underpinning, installing extra piles or rebuilding.

7 REFERENCES

1. AS2159 – 1978 "Australian Standard, Piling – Design and Installation", (Superseded)

2. AS2159 - 1995 "Australian Standard, Piling – Design and Installation"

3. AS2159 Suppl – 1996 "AS2159 Supplement 1 – 1996, Piling – Design and Installation - Guidelines", (Supplement to AS2195 – 1995)

4. PELLS, P.J.N et al "Foundations on Shale and Sandstone in the Sydney Region", Australian Geomechanics Journal, 1978, pp 31-39

5. PELLS, P.J.N et al "Foundations on Shale and Sandstone in the Sydney Region", Australian Geomechanics Journal, 1998, pp 17-29

6. POULOS H.G. "The Design of Piles with Particular Reference to the Australian Piling Code", Australian Geomechanics Journal, Dec 1998, pp 25-40

7. DAY R.A. "Geotechnical Design of Piles to AS2159 – 1995", Australian Geomechanics Journal, Dec 1998, pp 76-84

8. TCHEPAK S. "Pile Testing", Australian Geomechanics Society, Symposium on Recent Developments in Piling Practice in Sydney, Aug 1998

Paleoearthquakes and Hazard of the strike-slip Porters Pass fault, Canterbury, New Zealand

Matt Howard
URS New Zealand Ltd, Level 5 Landsborough House, 289 Durham St, Christchurch,
PO Box 4479, NZ. Tel: 64 3 374 8500, Fax 64 3 377 0655, e-mail: matthew_howard@urscorp.com

SUMMARY: The amount of slip/event and the timing of paleoearthquakes are crucial components needed to estimate the earthquake potential of active faults. The measurement of displaced geomorphic markers enabled identification of four to six earthquakes on the Porters Pass fault (PPF), with strike-slip/event ranging between ca 5-7 m. The timing of these earthquakes was constrained by excavating trenches across the fault and radiocarbon-dating preserved organic material. These data suggest that at least four and as many as six earthquakes have occurred in the last 10,000 years. The identification of only one Holocene PPF rupture in the west of the field area indicates the presence of a segment boundary that prevents the propagation of rupture along the full length of the fault during individual earthquakes. This is consistent with displacement data and results in slip rates of 0.3-0.9 mm/yr and 2.9-3.7 mm/yr to the west and east respectively. The combination of geometric, slip rate and timing data has enabled the magnitude of prehistoric earthquakes on the PPF to be estimated at between M6.9 for a 32 km fault rupture from Waimakariri River to Red Lakes, to a maximum of M7.7 that ruptures the entire 100 km length of the Porters Pass-Amberley Fault Zone (PPAFZ).

1. INTRODUCTION

Earthquakes occur mainly in the earth's crust and result in fault slip which may take place repeatedly over millions of years. Most earthquakes occur at or near plate boundaries where they reflect strains induced by jostling of tectonic plates. New Zealand straddles a plate boundary (figure 1) and has experienced many earthquakes since the arrival of Maori people over 800 years ago. Prior to European settlement over 150 years ago, we rely on studies of active-fault traces to provide information on large paleo-earthquakes which ruptured the ground surface.

The Porters Pass fault (PPF) is mainly strike slip and forms an active trace in the eastern foothills of the Southern Alps. The fault is a prominent element of the Porters Pass-Amberley Fault Zone (PPAFZ) which forms a broad zone of active earth deformation c. 100 km long, 60-90 km west and north of Christchurch (1, Cowan). Historically no fault within the PPAFZ is known to have ruptured the ground surface during an earthquake and no large magnitude events have been recorded in this zone. The PPF is clearly defined by a series of discontinuous Holocene active traces from Lake Coleridge north to the Waimakariri River, a distance of c. 40 km. The fault strikes approximately parallel to the plate motion vector resulting in a predominately right lateral strike-slip sense of motion. Scarp height

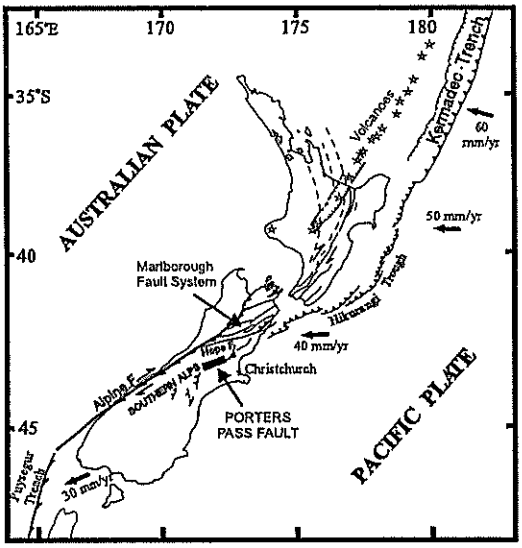

Figure 1: Map of New Zealand's main structural features associated with the obliquely convergent Australia-Pacific plate boundary zone and the location of the Porters Pass fault.

ranges up to 5 m, with both reverse and normal dip slip. The prominence of the fault at the ground surface suggests that it has produced repeated large magnitude earthquakes over the last 10,000 years (i.e. the Holocene) and could contribute significantly to seismic hazard in the Canterbury region. Knowledge of earthquake magnitudes and frequencies on this active fault is therefore important in order to

assess its likely impact on buildings and engineering structures. To better understand paleoseismicity of the PPF a study as part of an M.Sc. thesis was undertaken (2. Howard, see also 3. Nicol).

Prior to this research, three surface-rupturing earthquakes were proposed for the PPF at 500-700 years B.P., 2000-2500 years B.P. and 7500-10,000 years B.P. (4. Burrows, 5. Coyle, 1.,6. Cowan), suggesting recurrence intervals of 1300-5000 years. The timing of these events, however, was based on few data and the timing of paleo-earthquakes was poorly constrained by comparison with paleoseismically important faults elsewhere in New Zealand (e.g. Alpine fault, Hope fault and Wellington fault).

2. REGIONAL TECTONIC SETTING

Earthquakes and active faulting reflect New Zealand's location on the boundary between the Australian and Pacific plates (see figure 1). This plate boundary may have initiated over 40 Ma ago and for the last 10-20 Ma has comprised opposed-dipping subduction systems linked by the Alpine fault (7. Norris et al.). The Alpine Fault forms a strong lineament on satellite images and extends for approximately 400 km northwards from Milford Sound along the western side of the Southern Alps.

To the north along the Hikurangi Margin oceanic crust of the Pacific Plate has been subducted beneath more buoyant Australian continental crust. Convergence increases in obliquity southwards, while the magnitude of the relative plate motion vector decreases southwards from about 53 mm/yr to 37 mm/yr (8, DeMets et al.). Oblique convergence results in both right lateral and reverse fault displacements in the upper plate.

The Puysegur Trench lies southwest of Fiordland where subduction is in the opposite direction to the Hikurangi Margin, with oceanic crust from the Australian Plate passing beneath the oceanic crust of the Pacific Plate.

The Marlborough Fault System (MFS) accommodates the change from east dipping Alpine Fault to west dipping subduction zone of the Hikurangi margin. The MFS covers parts of Marlborough, north Canterbury and offshore northeastern South Island (9. Pettinga and Wise, 1994) and is composed of a number of right-lateral faults that generally strike parallel to the plate vector and splay from the Alpine Fault. The PPF is the southward continuation of the MFS.

3. DISPLACEMENT DETERMINATION

The PPF offsets numerous geomorphic landforms, with predominantly right-lateral strike-slip displacements. These displacements are inferred to have accrued principally during repeated moderate to large magnitude earthquakes, with larger magnitude events generally producing greater fault slip and rupture length (e.g. 10. Wells and Coppersmith). Therefore, by comparison with empirical data from historical earthquakes in Wells and Coppersmith, for example, with data from prehistoric earthquakes, the magnitudes of the latter can be estimated. Documentation and analysis of displacements along the PPF therefore provides a means of estimating the magnitude of prehistoric earthquakes. Displacement data can be combined with timing data to determine recurrence interval/frequency of seismic events.

Displacement of geomorphic features such as abandoned stream channels, ridge crests and flanks, and channel walls were measured at twenty-five sites along the fault. Vertical and horizontal separations of these offset features were obtained using tape measure and EDM topographical surveying equipment. Displacement data were collected using tape measure where linear landscape elements are offset by, and could be correlated across, the fault.

Using an EDM and theodolite, the positions of offset streams and channels were located relative to the steeply dipping fault. In one example near Porters Pass, offset channel axes above and below the fault scarp were projected graphically onto the fault plane which enabled 'piercing points' to be established. It is assumed that prior to faulting these channels coursed approximately parallel to the hill slope, which is normal to fault strike. On another site, west of Porters Pass, topographical surveying provided a basis for matching topography across the fault and estimating the amount of fault displacement by restoring topography to a pre-faulting configuration.

The process of inferring displacement/event from offset markers is based on the premise

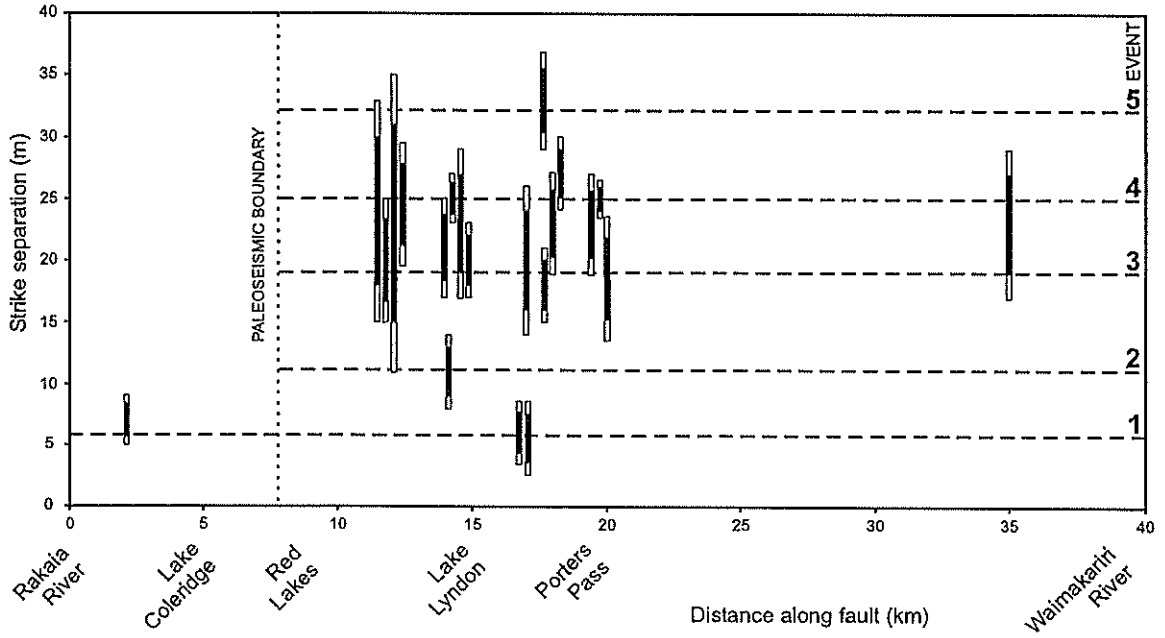

Figure 2: Summary graph of horizontally displaced geomorphic features along the PPF

that all of the offset is coseismic, i.e. that there is no aseismic creep. This assumption is supported for the PPF by the lack of deformation of four penstocks built across the fault almost 90 years ago.

Clustering of horizontal displacements show the cumulative displacements for an estimated 1 to 5 earthquakes (figure 2). These preferred estimates were derived by using the minimum number of slip events necessary to account for the observed strike-slip displacements. The preferred cumulative displacements for 1 to 5 earthquakes are not unique as the overlap in errors on displacement measurements mean that it is sometimes difficult to unequivocally determine the size of individual earthquakes based on this information alone. It would be possible, for example, to introduce an additional event within the accumulated displacement range of 17-28 m.

For the preferred earthquake-slip model five events account for the 33 m with slip/event ranging from 5-7 m. A larger event associated with earthquake 3 is supported by trench data, which indicates a relatively greater seismic event. On average the five earthquakes required to produce a horizontal separation of ~33 m would have been accommodated by ~6.5 m/rupture. Thus given the available data the PPF could be regarded as being broadly characteristic in displacement terms. However, the lack of deformation of glacial deposits south of Lake Coleridge suggests only one paleo-earthquake has ruptured the southwestern end of the fault at the surface since their deposition and so rupture length during individual earthquakes was not constant.

4. TIMING OF EARTHQUAKES

A critical component of this project was to establish the timing and magnitude of past surface rupturing earthquakes on the PPF. These estimates are important for defining the earthquake potential of the fault, which is essential for evaluating the associated seismic hazard. In addition to this, the earthquake history provides key kinematic information about how the fault has grown and how it may be interacting with adjacent structures.

Trenching across active faults to establish the timing of past earthquakes is an important part of paleo-earthquake studies. Radiocarbon dating (^{14}C) of preserved organic material beneath the surface is used to date stratigraphy, which in some cases may be deposited immediately after fault rupture, or may bracket

the timing of formation of fault strands. This provides the most unequivocal means of constraining the timing of prehistoric earthquakes and allows the definition of a window within which the event must have taken place. If possible, trenches are located across sites of preferential accumulation of organic materials (e.g. swamps) whose development is influenced by fault activity, providing the stratigraphic and timing data necessary to constrain the occurrence of rupture events, with a direct link between the fault and stratigraphy.

The timing of paleo-earthquakes on the PPF was constrained using data from five trenches (one of these trenches was part of a previous study) and one hand auger site, with additional information provided by landforms which pre and post-date past earthquakes. Trench locations were identified in the field area where accumulation of organic material adjacent to the fault scarp was considered most likely to have occurred. Three of the four excavated trenches were located on the western part of the PPF near Lake Coleridge, with the remaining trench located at Porters Pass to the east. These data are augmented by information from a previous trench sited within 10 m of trench 1 near Lake Coleridge (11. Wood et al.) and from a road batter at Porters Pass (6. Cowan et al.).

The most unequivocal data was obtained in the trench at Porters Pass where interpretation of data indicates that at least four and as many as six earthquakes have occurred during the Holocene on the PPF. The timing data from the other localities shows that the proposed timing of these events is consistent between the different data sets (figure 3).

Data for events 1, 2 and 4 (event one being the most recent) are from more than one location and have enabled the timing of earthquakes to be constrained in the east of the field area near Porters Pass. From oldest to most recent, preferred ages for fault rupture in years B.P. are 8500 ± 200, 5300 ± 700, 2500 ± 200 and 1000 ± 100. Additional events may have occurred at 6200 ± 500 and 500 ± 100 years B.P. The ambiguous nature of trench 4 data regarding the most recent event horizon, together with the lack of evidence from other

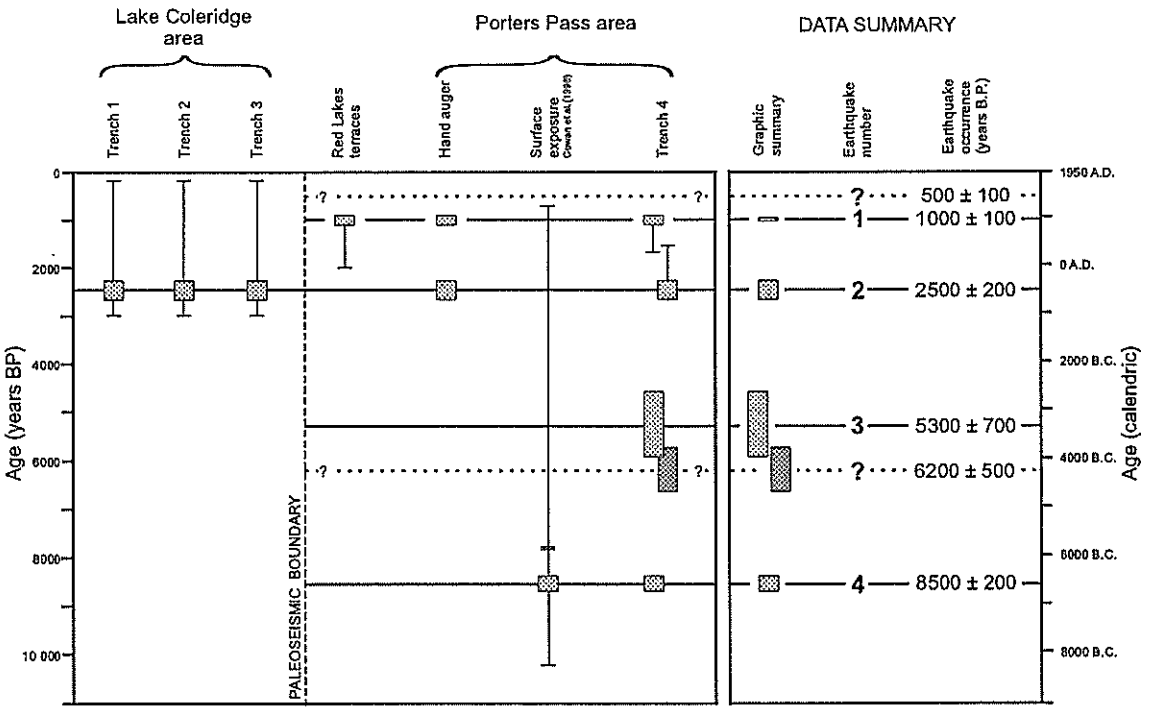

Figure 3: Summary of earthquake timing data along the PPF. Vertical lines indicate possible age range of earthquake event. Preferred ages (shaded boxes) derived by considering all data on table. Horizontal lines show approximate earthquake timing. Question marks denote timing of possible earthquakes.

sites means that this cannot be confirmed. In the west of the field area, near Lake Coleridge, only the 2500 ± 200 event could be identified, supporting the notion that the PPF does not always rupture along its full length. As a result, displacement and timing data give slip rates in the west and east of 0.3-0.9 mm/yr and 2.9-3.7mm/yr respectively.

Recurrence interval is derived by estimating the average time between earthquakes, and ranges from 1700-2500 years in the east and ≥7500 years in the west.

5. HAZARD POSED BY PPF

The hazard posed by the PPF cannot be determined by trenching as this does not provide sufficient data on the magnitude of paleo-earthquakes. Because the PPF has not experienced historic coseismic ruptures, the magnitude of past (pre-historic) earthquakes is most accurately determined by using field data for the single-event displacements and rupture lengths of these events. Estimates of earthquake magnitude rely on the ability to correlate fault geometry with earthquake magnitude and are useful for determining past magnitude of the PPF because they do not rely on historical seismicity.

The moment magnitude scale (12, Kanamori; 13, Hanks and Kanamori) is useful for determining the energy release of an earthquake based upon paleoseismic data. This scale incorporates the seismic moment (Mo) which represents the energy released at the source. Wells and Coppersmith (10) also correlate fault-rupture length and area with magnitude using empirical relationships from a worldwide historical earthquake database. To determine the magnitude of a PPF earthquake, both of these models were used with rupture scenarios that compared a rupture along only part of the PPF (32 km length) compared with a full rupture along this fault and the PPAFZ, a distance of 100 km. A range of average coseismic displacement of 4-8 m was used in order to account for the distribution of displacement data. An average of rupture models with different rupture length scenarios suggests that magnitudes on the PPF would produce a M6.9-7.7 earthquake.

6. CONCLUSIONS

- The PPF is part of the PPAFZ and is an active fault within 60 km of the population centre of Christchurch.
- The horizontal offset of geomorphic features across the PPF were measured using a tape and survey equipment. Clustering of these data suggest that earthquakes on this fault produce 5 – 7 m of displacement.
- Timing of past earthquakes was determined primarily by radiocarbon-dating organic horizons in four trenches excavated across the fault. At least four events in the last 10,000 yrs could be identified on the eastern part of the PPF giving an earthquake recurrence interval of 1700 – 2500 yrs.
- Slip rates on this part of the PPF are as much as 3.7 mm/yr, however the identification of only a single Holocene event on the west of the PPF gives a lower slip rate of 0.9mm/yr. This suggests that the fault is segmented and does not rupture along its full length during an earthquake.
- The expected magnitude on the PPF has been derived using empirical models which rely on fault geometry and movement rates and is between M6.9 and 7.7.
- The fault has the potential to cause significant damage and loss of life in the region.

7. REFERENCES

1. Cowan, H. A., (1992). Structure, seismicity and tectonics of the Porters Pass-Amberley Fault Zone, North Canterbury, New Zealand. Unpublished Ph.D thesis, University of Canterbury, Christchurch, New Zealand.
2. Howard, M. E. (2001). Holocene surface-rupturing earthquakes along the Porters Pass Fault. Unpublished M.Sc. thesis, University of Canterbury, Christchurch, New Zealand.
3. Nicol, A., Howard, M., Campbell, J. and Pettinga, J. (2001). Paleoearthquakes on the Porters Pass Fault. EQC report 2001/97.
4. Burrows, C. J. (1975). A 500-year-old landslide in the Acheron River Valley, Canterbury. New Zealand Journal of Geology and Geophysics. 18; 2, 357-360.
5. Coyle, S. (1988). The Porter's Pass Fault. Unpublished M.Sc thesis, University of Canterbury, Christchurch, New Zealand.
6. Cowan, H., Nicol, A. and Tonkin, P., (1996). A comparison of historical and paleoseismicity in a newly formed fault

zone and a mature fault zone, North Canterbury, New Zealand, Journal of Geophysical Research, 101, 6021-6036.
7. Norris, R. J., Koons, P. O., Cooper, A. F. (1990). The obliquely-convergent plate boundary in the South Island of New Zealand: implications for ancient collision zones. Journal of Structural Geology; 12, 5/6, 715-725.
8. DeMets, C., Gordon, R. G., Argus, D. F., Stein, S. (1994). Effect of recent revisions to the geomagnetic time scale on estimates of current plate motions. Geophysical Research Letters, 21, 2191-2194.
9. Pettinga, J.R. and Wise, D.U. (1994). Paleostress adjacent to the Alpine fault: broader implications, South Island, New Zealand. Journal of Geophysical Research; 99, 2727-2736.
10. Wells, D.L and Coppersmith, K.J. (1994) New empirical relationships among magnitude, rupture length, rupture width, rupture area, and surface displacement. Bulletin of the Seismological Society of America, 84, 4, 974-1002.
11. Wood, P. R., Paterson, B. R. and Howard, G. (1989). An evaluation of foundation geology and seismotectonic hazards of the Lake Coleridge Power Scheme. NZ Geological Survey Contract Report 1989/3.
12. Kanamori, H. (1977). The energy release in great earthquakes. Journal of Geophysical Research; 82, 2981-2987.
13. Hanks, T. C. and Kanamori, H. (1979). A moment magnitude scale. Journal of Geophysical Research; 84, 2348-2350.

ACKNOWLEDGEMENTS

The New Zealand Earthquake Commission (EQC), the Institute of Geological and Nuclear Sciences (GNS) and a University of Canterbury Masters Scholarship have funded research. Assistance to attend conference from EQC and GSNZ are also gratefully acknowledged.

Damage To Embankments Due To Liquefaction And Delayed Effects – A Case Study

Michael E. Jacka – Geotech. Eng., Tonkin & Taylor Ltd; ME Student, Uni. of Canterbury. Christchurch, New Zealand.

Delayed failure due to ground liquefaction is investigated, where failure occurs some minutes or hours after earthquake shaking has ceased. Several historical examples of delayed failure are outlined, as are potential mechanisms proposed in the literature to explain their occurrence. The delayed failure of a bridge approach is chosen as a case study to develop a simple model for analysis of such failures. The software packages Plaxis and Slope/W are used to evaluate the stability of the embankment as excess pore pressures dissipate upwards from the liquefied material into the overlying crust. This analysis shows that the surface crust was strong enough to maintain stability immediately following the earthquake, but after 15 minutes the increase in pore pressure in this layer reduced the available strength to the point where static equilibrium could no longer be maintained.

1 INTRODUCTION

The phenomenon of ground liquefaction has been responsible for a great deal of damage experienced in a large number of earthquakes around the world. The soil strength loss associated with liquefaction can lead to foundation, slope and embankment failures, whilst lateral spreading deformations often cause significant damage to lifelines and other structures. This investigation focuses primarily on the phenomenon of delayed response to liquefaction, where failure or significant deformation occurs some minutes, hours or days after the main earthquake shaking has ceased.

The issue of earthquake damage to embankments is significant both in terms of the cost of repairs and the disruption to services and lifelines. Often embankments are part of essential structures such as roads, railways, bridges, flood-control works and dams. Delayed embankment failure was observed at the Landing Road Bridge, Whakatane, New Zealand, after the 1987 Edgecumbe earthquake. This case study is used to examine how the occurrence of delayed failure could be explained and modelled.

2 HISTORICAL EXAMPLES OF DELAYED LIQUEFACTION FAILURE

In past earthquakes there have been a number of examples of liquefaction failures that have occurred some time after the end of seismic shaking. Three such failures are summarised here, to give a background to the problem of delayed liquefaction failure.

2.1 Lower San Fernando Dam

A near-catastrophic slide failure occurred in the Lower San Fernando Dam as a result of the 1971 San Fernando, California earthquake, as shown in Figure 1. Seed *et al* [1] conclude that liquefaction occurred in a large zone of hydraulic fill at the base of the embankment, upstream of the clay core. The material overlying the liquefied layer broke up and slid as a number of intact blocks, leading to a substantial reduction in the available freeboard. The failure occurred relatively slowly, and did not start until approximately one minute after the earthquake.

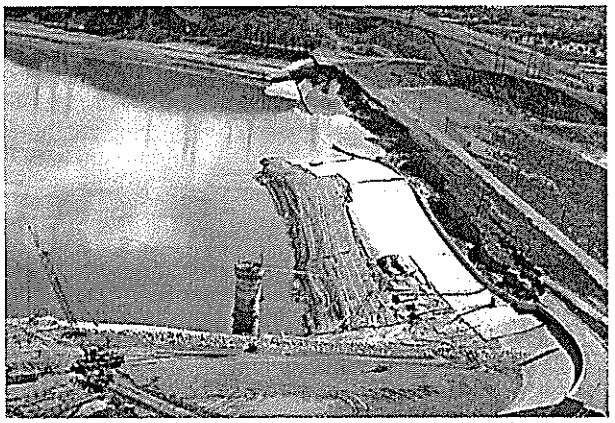

Figure 1 – Damage to the Lower San Fernando Dam. (Steinbrugge Collection, EERC, UC Berkeley)

Castro [2] and Seed *et al.* [1] consider the possible role of pore water migration in the delayed failure. They point out that the upstream toe of the dam was originally a starter dyke for hydraulic filling, and so was compacted to a dense (dilative) state. In this state, the undrained strength is greater than the drained strength. They suggest that as the liquefied material lost strength, the material at the toe was subjected to higher shear stresses, causing a tendency for dilation. If this soil was permeable enough to allow water to be drawn into the voids a volume increase would have occurred, resulting in a stress path reaching the steady state line at a higher void ratio, and thus a lower steady state strength. The one minute delay before failure corresponds to the time required for sufficient drainage to occur to instigate such a loss of strength.

2.2 Mochikoshi Tailings Dam

As a result of the January 1978 earthquake at Izu-Oshima, Japan, two tailings dams at the Mochikoshi

gold mine collapsed. Cross sections of the dams before and after failure are shown in Figure 2.

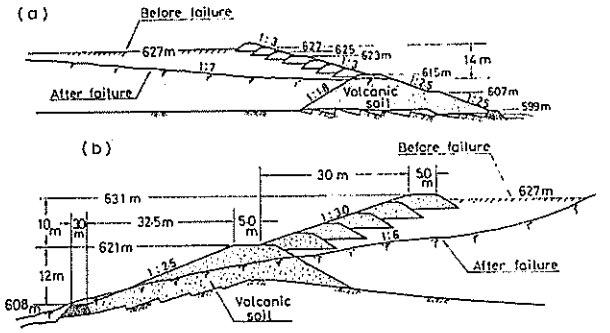

Figure 2 – Mochikoshi Tailings Dam No. 1 (a) and No. 2 (b). (Ishihara, [3])

After about 10 seconds of shaking the crest of Dam No. 1 had settled excessively, and the silty sand tailings material had liquefied. This enabled the tailings to breach the dam and sweep away much of the upper part. Approximately 24 hours after the earthquake Dam No. 2 also failed (Ishihara, [3]). This delayed failure may have been due to gradual upward movement of the phreatic surface, as a result of the liquefaction of the tailings. The subsequent increase in pore pressure in the volcanic silt body of the dam would have reduced the effective stresses, and thus the strength available to resist deformation. Ultimately this reduction in strength was sufficient to allow failure under static driving stresses.

2.3 Prefectural Apartment Buildings, Niigata

As a result of the 1964 earthquake at Niigata, Japan, a number of buildings at the Prefectural apartment complex suffered rotational foundation failure, as shown in Figure 3. Residents of the building reported that this was a very slow and smooth failure.

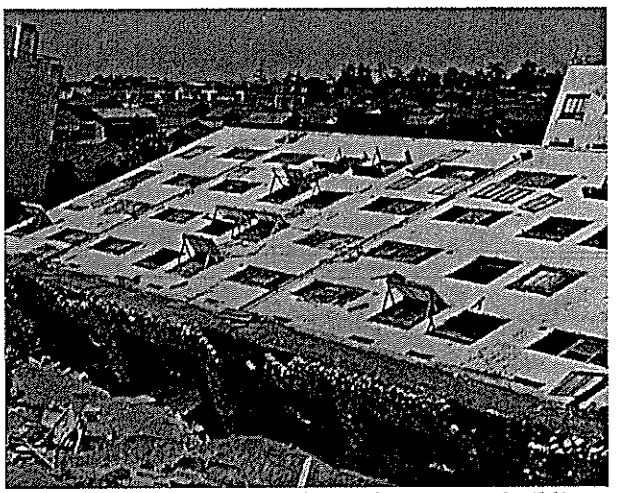

Figure 3 – Overturned prefectural apartment building. (Kawasumi [4])

The absence of any upthrust ground around the building, and the pattern of cracking in the crust suggest that this was not a conventional slip-circle type failure, but rather a case of the building rotating as it sank into the liquefied ground. Failure occurred some minutes after the end of the earthquake (Kawasumi [4]), suggesting that the soil supporting the foundation did not suffer the immediate loss of strength that would be expected if it had liquefied as a direct result of earthquake shaking. It is likely that liquefaction initiated at some depth beneath the building and then gradually moved upwards until it caused the failure of the building's foundations.

3 MECHANISMS OF DELAYED FAILURE

The magnitudes of any deformations which might occur as a result of liquefaction generally depend on the relative magnitudes of the available soil strength and the stresses required to maintain equilibrium. In some cases the immediately available undrained strength of the liquefied and non-liquefied soils may be only just sufficient to ensure stability. In these cases it is possible that any reduction in strength that might occur over time after the earthquake could eventually lead to significant displacements or failure.

3.1 Whitman (1987)

Whitman [5] proposes the two mechanisms for localised strength reduction shown in Figure 4. In the first, a layer of sand is subjected to cyclic straining, causing a tendency for the particles to settle. Thus the upper part of the layer becomes looser while the lower part becomes denser. Although the layer as a whole experiences no volume change, these local changes result in a potential reduction of the steady state strength of the upper part.

The second mechanism shown in Figure 4 occurs as a result of high excess pore pressures in an area of liquefied material. The excess pore pressures are relieved by the outwards and upwards migration of pore pressures and the phreatic surface. This causes the pore pressure in the overlying layer to increase, reducing the effective stress - and thus the strength that the soil can develop by frictional means is reduced.

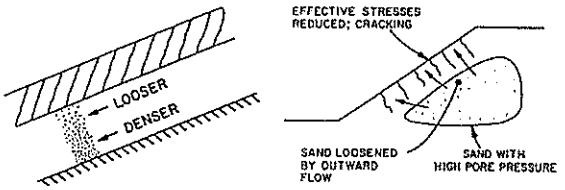

Figure 4 – Void redistribution and pore water migration. (Whitman [5])

3.2 Seed et al. (1975, 1987)

Seed [6] discusses situations where liquefaction develops near the end of earthquake shaking, so failure is driven almost completely by static forces. In these cases he recommends that consideration be given to the effects of gradual pore water redistribution, which may cause failure a considerable time after the end of the earthquake.

As detailed in Section 2.1, Seed *et al.* [1] propose a possible explanation for the one minute delay between the end of earthquake shaking and the failure of the Lower San Fernando Dam. In this case enough drainage may have occurred to allow the dense soil in the embankment toe to dilate to a looser state as it was forced to carry greater forces as a result of the liquefaction of looser material.

3.3 Kutter (1997)

Kutter [7] suggests that migration of pore water can result in a redistribution of void space in a liquefied soil. He argues that a considerable hydraulic gradient is present in a liquefied soil, and that this forces an upwards flow of water. In regions with outwards flow of water a reduction in void ratio is able to occur, while an increase in void ratio can be expected in areas of pore water inflow. This process is often referred to as void redistribution.

Considering that the steady state strength of a soil is strongly related to the void ratio, the process of void redistribution can be expected to reduce the strength of the upper part of a soil profile. Kutter presents a rough calculation using typical parameters to show that in a medium sand sufficient flow could occur to fully soften a 1m zone in approximately 15 minutes. This figure is similar to the delay calculated in the analysis of the Landing Road Bridge site, presented in Section 6.4.

3.4 Scott & Zuckerman (1973)

During their laboratory-based research into sand boils resulting from liquefaction, Scott & Zuckerman [8] witnessed the occurrence of "induced" or "secondary" liquefaction of a coarse-grained dense layer overlying a liquefied material. They observed that from the instant that liquefaction commences soil grains begin to settle out of suspension. Thus at some time after the initiation of liquefaction there exists a layer of re-solidified soil, overlain by a region of soil particles suspended in the pressurised pore fluid. Meanwhile if there exists an overlying non-liquefied layer, it is now left supported only by the soil and water mixture. If this overlying layer is cohesionless then it may begin to unravel at its lower surface. Thus a liquefaction interface moves upwards through the overlying layer.

3.5 Castro (1987)

Castro [2] agrees with the hypothesis of Seed *et al.* [1] presented in Section 2.1, that pore water migration can affect stronger, dilative zones of material. He goes on to recommend that in cases where the soil is permeable enough to allow pore water migration, design for stability should not rely on undrained shear strengths which are greater than drained strengths.

Seed *et al.* [9] agree with this approach, reasoning that the significant tendency for dilation required to provide increased strength tends to localise the zone of shearing. As a result, pore water is able to quickly travel the short distance required to permit volume change to occur, and the high undrained strength can persist only briefly.

4 DELAYED FAILURE OF THE LANDING RD BRIDGE APPROACH EMBANKMENT

Christensen [10] presents an eyewitness report that suggests delayed failure occurred in the northwestern approach embankment of the Landing Rd Bridge as a result of the 1987 Edgecumbe earthquake. Shortly after the earthquake the motorist was able to cross the bridge, however upon returning roughly one hour later the bridge approach was heavily cracked, and differential settlement between the bridge and the abutment had rendered the bridge impassable. Typical damage to the embankment can be seen in Figure 5. The embankment has a maximum height of 3m, and is 23m wide at the base. A generalised soil profile at the site is shown in figure 6.

Figure 5 – Damage to the Landing Rd Bridge approach embankment. (Courtesy of H. Chapman)

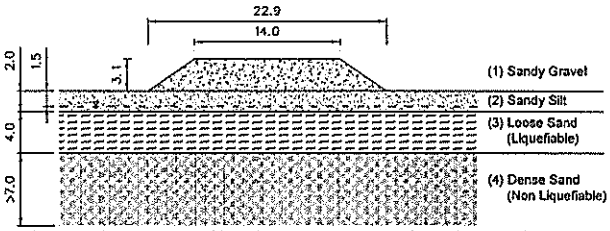

Figure 6 – Generalised geometry and soil profile used for analysis of the Landing Road Bridge approach.

Taking into account the general understanding of possible mechanisms of delayed failure summarised in Section 3, the following hypothesis is proposed to explain the delayed failure at the Landing Rd site:

During the earthquake shaking, liquefaction occurred beneath the embankment in a layer of loose sand, approximately 4m thick (Christensen, 1995). Between the embankment and the liquefied layer was a sandy silt layer roughly 2m thick, which did not liquefy. This study proposes that the strength and thickness of this unliquefied crust was only just sufficient to maintain stability of the embankment during and immediately after the earthquake.

It is hypothesised in this investigation that as time passed after the earthquake, the excess pore pressures in the liquefied material caused pore water to gradually seep upwards into the unliquefied sandy silt. This reduced the strength of the upper layer to the point where the observed moderate displacements were able to occur. Two mechanisms that could possibly be responsible for this strength loss are:

- If the overlying material is considered in terms of its steady state behaviour, then void redistribution could lead to a reduction in the steady state strength.
- If the strength of the overlying material is considered in terms of the Mohr-Coulomb failure criterion, the increase in pore pressure leads to a decrease in effective normal stresses between soil grains. This decreases the frictional resistance and thus the drained strength available to maintain static equilibrium.

It should be noted that it is not suggested that the delay in failure is due to any delay in the occurrence of liquefaction, nor in this case due to any change in the strength of the liquefied material that may occur through time. It is proposed that the delay in failure is simply due to the time taken for void and pore water redistribution to occur sufficiently for the overlying non-liquefied soil to be weakened to the point where failure is possible.

5 ANALYSIS OF THE LANDING RD BRIDGE APPROACH EMBANKMENT

As outlined in Section 4 the northwestern approach embankment of the Landing Road Bridge was damaged by deformations that occurred up to an hour after the earthquake. The primary aim of this analysis is to demonstrate the manner in which migration of excess pore water could cause the observed delayed failure.

Four key stages were considered:

1. Pre-earthquake conditions, with full drained strength for all soils.
2. Immediately post-earthquake stability, considering both zero strength and steady state strength in the liquefied soil.
3. Pore pressure migration, where pore water migration into the upper soil layer is modelled.
4. Stability during pore pressure migration, where the stability is re-analysed under the pore pressure conditions expected at various time intervals after the end of the earthquake.

The investigation made use of two specialist geotechnical software packages - Plaxis and Slope/W. Plaxis is a finite element analysis tool for evaluating deformations and stability of geotechnical structures. This was the primary tool used to model the deformation of the embankment and dissipation of excess pore pressures. Slope/W is a limit equilibrium geotechnical analysis package which uses a variety of slip-circle based methods to provide an estimate of the Factor of Safety against failure (FOS).

Excess pore pressures were introduced into the liquefied layer and the consolidation features of Plaxis used to model the dissipation of excess pore pressures resulting from liquefaction. The initial excess pore pressure to be generated in the sand layer was chosen such that a condition of zero effective stress (*ie.* liquefaction) would occur at the midheight of the layer.

Ideally, a full stability analysis would be carried out at each time step in the pore pressure dissipation calculation. However, the iterative consolidation algorithm used by Plaxis fails to converge as the structure approaches failure, so this option was not feasible. To circumvent this limitation, it was necessary to use a two-step process, firstly calculating the pore pressure distributions at a number of time steps, and then manually introducing these pressures into a conventional stability analysis.

The transition from the material properties and pore pressure conditions immediately after the earthquake (Series 2) to those some time later (Series 4) was implemented using a series of four staged construction steps. These steps represent the pore pressure distributions at 0.5, 4.9, 14.1, and 42.4 minutes after the end of earthquake shaking.

6 ANALYSIS RESULTS

6.1 Pre-Earthquake Conditions

Using Slope/W, factors of safety were determined on three failure surfaces of interest. The predicted critical failure surface for pre-earthquake conditions (FOS = 2.04) reaches down to approximately the midheight of the sandy silt layer. Using a ϕ-c reduction process, Plaxis estimates a critical failure region which is in good agreement with the critical surface proposed by Slope/W, with a similar level of safety (FOS = 1.99).

These results show that the embankment possessed ample stability before the earthquake, and that medium-scale failure of the embankment gravel and the upper part of the sandy silt layer was initially critical. It is encouraging to see that there is good agreement between the results from Plaxis and Slope/W for the critical case.

6.2 Immediate Post-Earthquake Stability

By setting the strength of the liquefied layer to zero we can determine if a strength contribution from the liquefied material is required to maintain static equilibrium. For this condition Slope/W predicts failure on a surface reaching the bottom of the liquefied sand (FOS = 0.72). Plaxis analysis also predicts large displacements. These results suggest that some strength contribution was indeed required from the liquefied material to provide the immediate post-earthquake stability that was observed.

A best-estimate value for the sand's undrained steady state shear strength (c = 11 kPa + 1.3 kPa/m) was determined using a weighted average of various SPT and CPT correlations (Seed & Harder [11]; Stark & Mesri [12]; Robertson [13]). Using this strength, both Slope/W and Plaxis analyses show that embankment stability can be maintained immediately after the earthquake. A sensitivity analysis showed that only small reductions in strength are required to trigger failure, therefore the potential reduction in strength due to pore water migration and void redistribution becomes of great importance.

6.3 Pore Pressure Migration

The results of the pore pressure dissipation analysis are shown in Figure 7. In general, excess pore pressures of up to 10-20 kPa are predicted to occur in the lower part of the surface sandy silt layer approximately 15 to 60 minutes after the end of earthquake shaking.

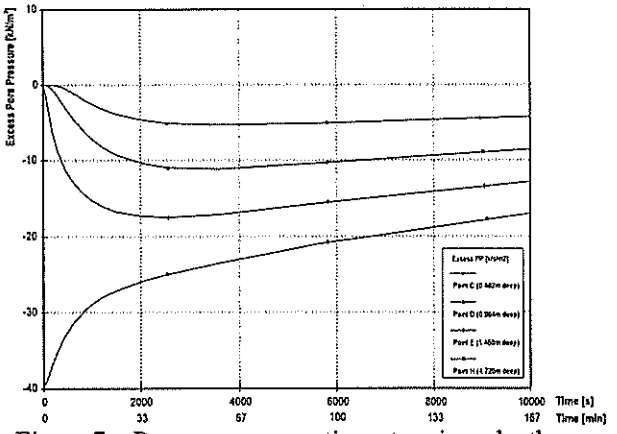

Figure 7 – Pore pressure vs. time at various depths, as calculated by the Plaxis dissipation analysis.

6.4 Stability During Pore Pressure Migration

Slope/W analyses show that the dissipation of excess pore pressures from the liquefied layer reduces the factor of safety against failure by almost 10%, just enough to effect a change from marginally stable to marginally unstable conditions. The upwards movement of the critical failure surface as pore pressures spread confirms that the observed reduction in FOS is due to a reduction in the strength contribution of the surface layer. Based on these results failure or significant deformation of the embankment could be expected to occur roughly 15 minutes after the end of earthquake shaking.

The results of the Plaxis analysis are in good agreement with those from Slope/W. Displacements of approximately 5mm are predicted as the pore pressures are raised to the level corresponding to 4.9 minutes of dissipation, however the embankment retains overall stability. The next calculation phase attempts to raise the pore pressures further, to the level expected 14.1 minutes after the earthquake. Global instability of the embankment develops just before the target pressures are reached, thus Plaxis predicts that failure or significant deformation of the embankment will occur nearly 14 minutes after the end of earthquake shaking.

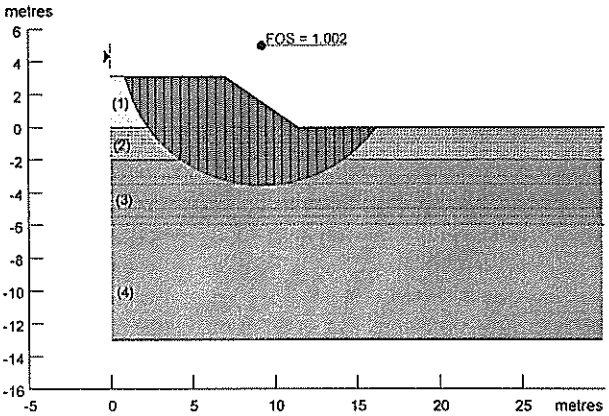

Figure 8 – Slope/W critical failure surface predicting failure after 14 minutes of pore pressure dissipation.

A maximum total displacement in the order of 150mm is predicted up to the point at which the Plaxis calculation is unable to proceed due to the instability. In the 1987 earthquake, large scale collapse of the embankment did not occur, however it was heavily damaged by cracking and subsidence in the order of several hundred millimetres. This suggests that the predicted displacements are of realistic magnitude.

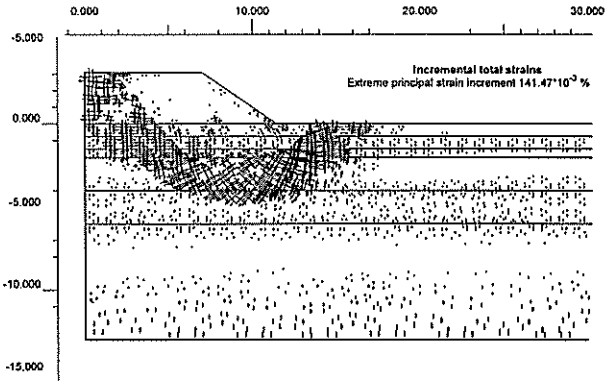

Figure 9 – Plaxis plot of incremental shear strains at failure, after 14 minutes of pore pressure dissipation.

Inspection of the effective stress plot in Figure 10 confirms the role of increased pore pressures in the collapse – with the effective vertical stress approaching zero in the lower part of the surface sandy silt layer.

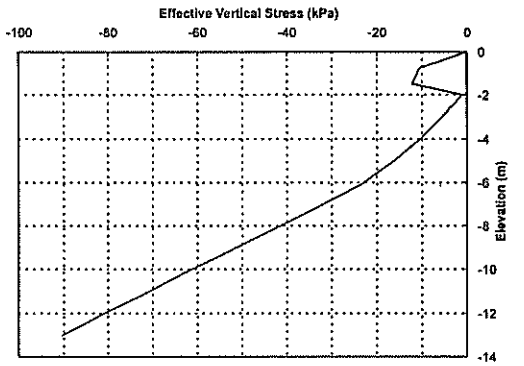

Figure 10 – Plaxis effective vertical stresses at failure.

7 CONCLUSIONS

The analyses summarised in Section 6 support the theory that the embankment would remain marginally stable after the loose sand liquefied, providing that the liquefied material contributes its steady state strength to assist in resisting static driving forces.

Analysis of the dissipation of excess pore pressures from the liquefied layer suggests that the pore pressures in the surface sandy silt layer reached a maximum roughly 45 minutes after the earthquake, with a substantial build up of pressure occurring within the first 15 minutes. In the lower part of the surface layer the resulting total pore pressures would have approached the total overburden stress, leading to a state of near-zero effective stress.

Stability analyses performed using the pore pressure distributions calculated at selected time intervals show that the embankment remains stable up until approximately 15 minutes after the earthquake. At this time the decrease in effective stress in the surface layer is sufficient to reduce the available frictional strength to the point where static equilibrium can no longer be maintained. The predicted 15 minute delay between the end of the earthquake and the appearance of damage is within the upper bound of one hour indicated by an eyewitness account.

Many inter-related theories have been proposed that can be used to explain delayed failures such as observed at the Landing Road Bridge. In general these conceptualise the mechanism as either the gradual redistribution of voids within the soil leading to reduced steady state shear strength, or the movement of pore water reducing effective stresses and thus frictional strengths.

This investigation has shown how a simple model of strength loss can be used in a quantitative framework to assess susceptibility to such secondary failures. This is particularly relevant to the designer in cases where a relatively dense material overlies a potentially liquefiable soil. If the conditions are such that excess pore water from the liquefied material may be readily available to feed a dilative shear zone then it would be unwise to allow post-liquefaction stability to rely on maintaining an undrained strength greater than the drained strength.

REFERENCES

[1] SEED, H.B., *et al.* (1975) The slides in the San Fernando dams during the earthquake of February 9, 1971, *J. of the Geotech. Engrg. Div.*, ASCE, 101(7), 651-688.

[2] CASTRO, G. (1987) On the behaviour of soils during earthquakes. In Cakmak, A.S. ed., *Soil Dyn. and Liquefaction*. Elsevier. 169-204.

[3] ISHIHARA, K. (1984) Post-earthquake failure of a tailings dam due to liquefaction of the pond deposit, *Proc. 1st International Conf. on Earthq. Engrg., Madrid, 1407-1412.*

[4] KAWASUMI, H. ed. (1968) *General Report on the Niigata Earthquake of 1964*, Tokyo Electrical Engrg. College Press.

[5] WHITMAN, R.V. (1987) Liquefaction - the state of knowledge, *Bull. Of NZ Nat. Soc. For Earthq. Engrg.*, 20(3), 145-158.

[6] SEED, H.B. (1987) Design problems in soil liquefaction, *J. of Geotech. Engrg.*, ASCE, 113(8), 827-845.

[7] KUTTER, B.L. (1997) Strength of liquefied soil is not a material constant; liquefaction is a boundary value problem, Pre-workshop written statement, *Shear Strength of Liquefied Soils,* April 17-18 1987, Urbana, Illinois. Online. Available: http://www.conted.uiuc.edu/ci/soil/, 6 March 2001.

[8] SCOTT, R.F., & ZUCKERMAN, K.A. (1973) Sandblows and liquefaction, *The Great Alaskan Earthquake of 1964 - Engineering Volume,* Committee on the Alaska Earthquake, Nat. Academy of Sciences, Washington, D.C., 179-189.

[9] SEED, R.B., *et al.* (2001) *Recent advances in soil liquefaction engineering and seismic site response evaluation.* Paper No. SPL-2, Nat. Inf, Service for Earthq. Engrg., UC Berkeley.

[10] CHRISTENSEN, S.A. (1995) *Liquefaction of cohesionless soils in the March 2, 1987 Edgecumbe earthquake, Bay of Plenty, New Zealand, and other earthquakes.* ME Thesis, Uni. Canterbury, NZ. 373p.

[11] SEED, R.B., & HARDER, L.F. Jr. (1990) SPT-based analysis of cyclic pore pressure generation and undrained residual strength, *Proc. H.B. Seed Memorial Symposium,* May 1990, BiTech Publishing., Vancouver, Vol 2, 351-376.

[12] STRARK, T.D., & MESRI, G. (1992) Undrained shear strength of liquefied sands for stability analysis, *J. of Geotech. Engrg.*, ASCE, 118(11), 1727-1747.

[13] ROBERTSON, P.K. (1999) Estimation of minimum undrained shear strength for flow liquefaction using the CPT, *Proc. 2nd Int. Conf. on Earthq. Geotech. Engrg.*, A.A. Balkema, Vol. 3, 1999, 1021-1028.

ACKNOWLEDGEMENTS

The research summarised in this paper was made possible by the generous financial assistance provided by the New Zealand Returned Services' Association, the New Zealand Society for Earthquake Engineering, Tonkin & Taylor Ltd, and the University of Canterbury. This investigation was supervised by Dr John Berrill, who is thanked for the wealth of experience brought to the project and the invaluable guidance and support he provided.

EARTHQUAKE HAZARD ZONING WITHIN THE CITY OF BRISBANE

Patrick Kidd B App Sc. (Geol.) Cert. Explosive's & Blasting RPGeo, Soil Surveys Engineering Pty Ltd

SUMMARY: The Brisbane City Council area was divided up into different earthquake hazard zones. The zonation was based on the published geological maps and on geotechnical data obtained during site investigations undertaken throughout the city. The Map Info Geographic Information System (GIS) package was utilised to produce a hazard map following the zoning exercise.

Other methodologies of producing earthquake hazard maps were comparatively reviewed during the project.

1.0 INTRODUCTION

Brisbane City Council is one of the largest urban municipal authorities in the world, with an area of 1331.63 square kilometers and a population of approximately 850000. Brisbane is located in the south east corner of Queensland, Australia and is sited on a geology that varies greatly across the city's extent. The various geological units the city is sited upon would react differently under the influence of seismic waves from a significant earthquake.

Records gained from seismographs, that have been installed across South East Queensland within the last fifteen years demonstrate that there is significant seismic activity in the region, regardless of the limited record of earthquakes recorded prior to this point. Figure 1 reproduced from Herrero and Cuthbertson (1995) highlights the earthquakes and their magnitude recorded within the state of Queensland from local seismographs between 1977 and 1994.

2.0 METHODOLOGIES FOR EARTHQUAKE HAZARD MAPPING

Earthquake hazard mapping is a very difficult problem to tackle and numerous approaches have been undertaken. Many of the systems adopted for zoning areas have been based on an assessment of the peak ground acceleration (PGA) on bedrock, that can be expected over a certain time period, and the percentage chance it will be exceeded within that time (Bryant 1991).

This method is based on earthquakes recorded in the past as a guide to the PGA expected in an area. Consequently the more earthquakes recorded in an area, the greater the accuracy of the prediction of the PGA zones.

The PGA maps produced from this approach are designed to be guidelines for structural engineers, to assess the lateral forces a building in a particular area may be subjected to.The Australia Geological Survey Organisation's (AGSO) earthquake hazard map for Australia, which has been reproduced from the Australian Standards Loading Code in Figure 2, is an example of this. Another example of this method is the mapping of continental U.S.A. by Stevens (1988). Husein, Al-Homound and Liang (1995) also produced earthquake hazard maps for Jordan utilising the PGA method, with the provision of additional maps showing the expected Modified Mercalli Intensity over the same area. The Modified Mercalli Intensity Scale is an earthquake rating scale based on the likely damage an earthquake can cause. A copy of the scale is appended.

One difficulty with the PGA method of prediction is that it does not take into account site effects due to ground conditions, other than bedrock being present. Further, if the earthquake record is poorly recorded in a particular area, as it is in much of Australia, an inaccurate perception of the areas at risk could develop. Herrero and Cuthbertson (1995) point out that on the basis of data recorded from recently installed seismographs, the AGSO map shown in Figure 2, which was based on data to 1984, already requires updating.

Some other methods of predicting earthquake hazard zones concentrate on site effects. Site effects are variances in ground conditions across sites, which can produce local variations in the attenuation of seismic waves. Consequently the damage patterns that occur following earthquakes, are often closely related to the differing ground conditions. An example of the amplification

Figure 2. Peak Ground Acceleration Map of Australia

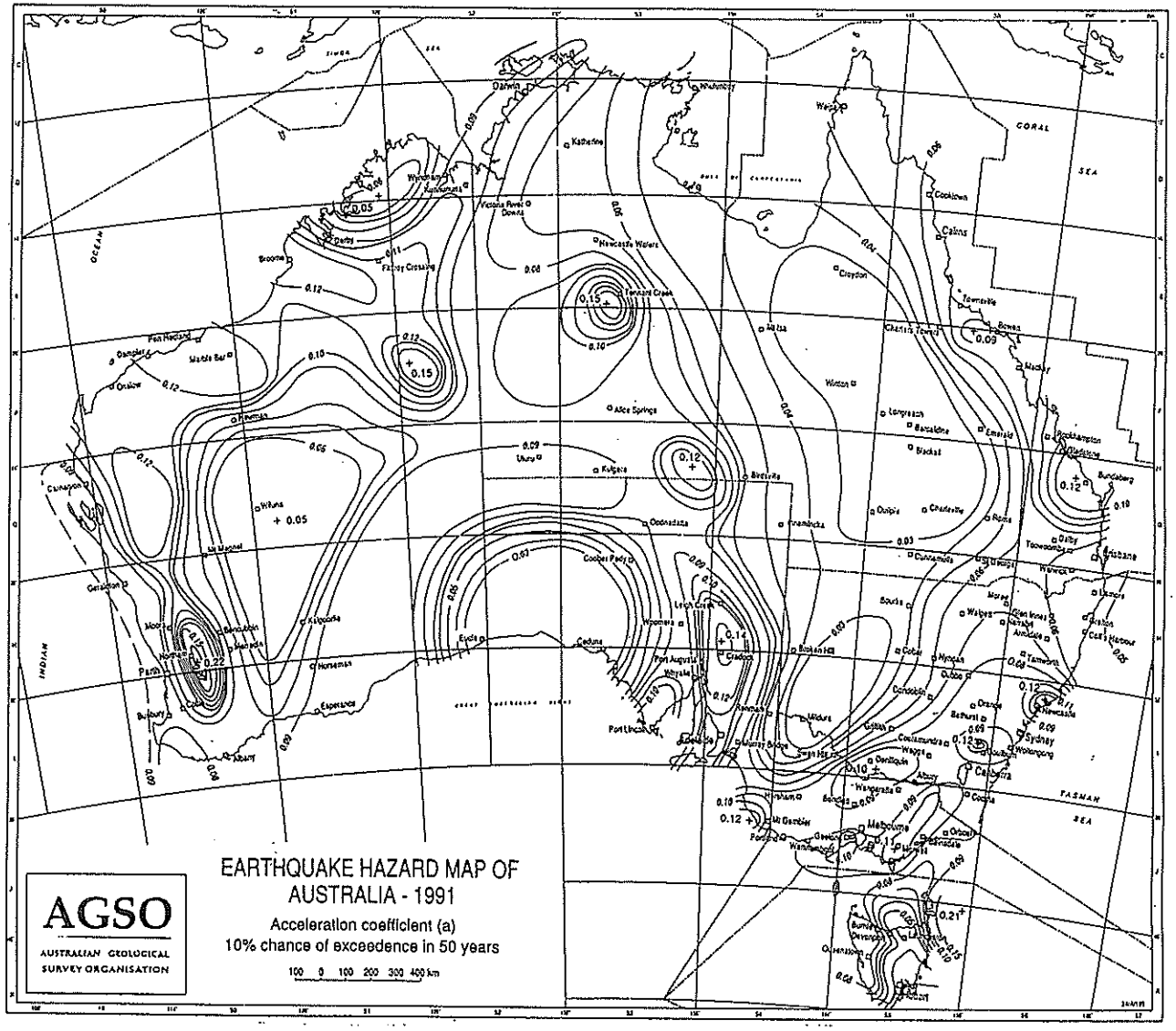

Figure 1. Seismicity Map of Queensland, 1977 to 1994

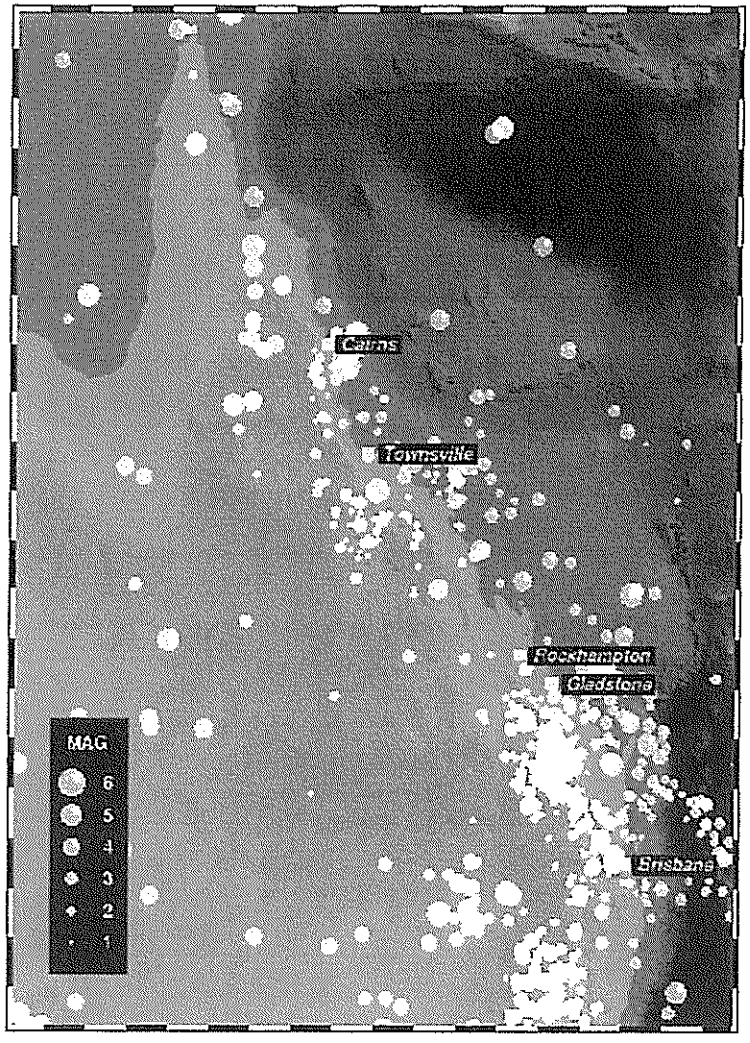

of seismic waves due to site effects was the Mexico City earthquake of 1985. Mexico City is largely built on a former lake bed comprising water charged montmorillionitic clays, which amplified the seismic waves six fold, resulting in enormous damage from a relatively moderate earthquake, as the epicentre was located 350 kilometres away (Bryant 1991).

The 'site factor' method was utilised by Borcherdt *et.al.* (1975) in their production of an expected earthquake intensity map based on the geological conditions present across San Francisco. The production of liquefaction hazard maps by Wills and Hitchcock (1999) and Hitchcock, Loyd and Haydon (1999) for parts of California, utilised a similar method by incorporating geological, borehole and groundwater data into a GIS package to produce the zonation of various levels of risk of liquefaction.

Recent studies such as those undertaken by the RADIUS projects for various cities such as Antofagasta in Chile, Bandung in Indonesia and Addis Abada, Ethiopia, have attempted to combine the two major methods of zonation mentioned above, to produce likely seismic attenuation factors which were then coupled with information on the city's lifelines and existing buildings, in an attempt to predict the overall damage scenarios for expected earthquakes predicted from PGA studies.

3.0 METHODOLOGY ADOPTED

In this study, a zonation was produced using a similar system to that used by Blong and Hunter (1999) in their assessment of probable maximum loss scenarios for various magnitude earthquakes striking Sydney, and that used by Wills and Hitchcock (199) in their production of liquefaction hazard maps. These authors collected available borehole data, geological and soils data and in the case of Wills and Hitchcock's study, topographical and groundwater data. The data was collated within a GIS package, then interpreted to assess the earthquake or liquefaction risks for a particular area; the assessment being based on a predetermined rating system to categorize the risks.

For this zonation various information sources were assessed for their suitability for use as a basis for the planned zonation. The 1:100000 geological maps produced by the Geological Society of Queensland, proved to be the most suitable as they were of a suitable scale and were available in digital format. Other geological maps were available covering the area in both larger and smaller scales but they weren't available digitally. The digital format allowed the information to be used in a GIS package.

Four maps were purchased, then formed into one map of the entire study area in Map Info, the GIS package used. The maps required to cover the Brisbane City Council area were the 1:100000 geological sheets, Brisbane, Beenleigh, Ipswich, Caboolture.

The next consideration was to decide which basal units would be utilised for the zonation. Basal units were required in a digital format to provide boundaries of zoned areas, within the overall boundaries of the study. Both suburbs and census collection districts (CCDs) were considered for use. As demonstrated by Blong and Hunter, the CCDs would have produced a more refined zonation by virtue of their smaller size in respect to urban suburbs. However the CCD data was a less cost effective option and had the disadvantage of requiring significant editing of unnecessary areas. The suburb boundaries were chosen for use, on the basis of the disadvantages of the CCD data.

Once the basal units were acquired the geology and the suburb information were combined and a preliminary assessment of the zonation of each suburb was made, based on the averaged geological conditions within a suburb. The zonation system used was based on a modified version of that utilised in the site factors for general structures from the Australian Loading Standard. The Australian Loading Standard provides methods of assessing the probable site factors for design purposes, based on the soil profile. The majority of the modifications made were taken from Blong and Hunter's zonation system. The modifications used were the inclusion of references to slopes, the age of alluvium and plastic clay soils subject to high shrink and swell. The five zones utilised in the system are outlined below, with zone one being the best and zone five the worst in relation to probable attenuation of seismic waves:

Zone 1 - A profile of rock with a rock strength class of low or better,
- Gentle slopes
- Very shallow soils.

Zone 2 - A profile of extremely low or very low strength rock
- less than 30m of medium dense or dense cohesionless soils or firm or stronger cohesive soils or controlled fill
- Moderate slopes
- Plastic clay soils prone to shrink swell movements

Zone 3 - A soil profile with more than 30m of medium dense or denser cohesionless soils or firm or stronger cohesive soils or controlled fill.
- Steep slopes
- Consolidated old alluvium
- Less than 6m of loose or looser cohesionless soils or soft or softer cohesive soil or uncontrolled fill.

Zone 4 - Shallow recent alluvium,
- 6 to 12m of loose or looser cohesive soils or soft or softer cohesive soils or uncontrolled fill.

Zone 5 - Deep recent alluvium
- 12m or greater depths of loose or looser cohesionless soils or soft or softer cohesive soils or uncontrolled filling.

*The Australian Standard for Geotechnical Site Investigations AS1726-1993 provides explanations of terms used in the zones above.

The preliminary zonation given to each of the 186 suburbs was based on what geological units were present within the boundaries of each suburb and substantial local information of the geological units, topography and major rock outcrops throughout the city. Due to the averaged nature of the zonation within a particular suburb, the basis of categorisation undertaken was as shown in the following table.

Table 1. The Categorisation Criteria

Zone	% of Profile Types	Other Factors
Zone 1	100% very shallow soils overlying rock	
Zone 2	100% to 60% residual soils overlying relatively shallow rock less than 40% alluvium	If 100% residual soils dependent on the depth to rock and slope. Generally less than 30% alluvium unless very shallow
Zone 3	70% to 40% residual soils and 30% to 75% young alluvium, up to 100% old alluvium	Dependent on age and density of alluvium
Zone 4	75% to 100% moderately deep alluvium	Dependent on density and depth of alluvium
Zone 5	100% deep alluvium	Dependent on density and depth of alluvium

For example, approximately 80% of the inner city suburb of Kangaroo Point is located on very shallow soils overlying low or better strength rock, with the remainder being located on alluvium, therefore the suburb was rated as zone 2. If all of Kangaroo Point were located on very shallow soils overlying low or better strength rock a rating of zone 1 would have applied.

Following the preliminary rating of all the suburbs, a reassessment of all the ratings was made utilising the information gathered during geotechnical investigations carried out on 92 sites spread across the city. The geotechnical information reviewed included 557 test bores, 75 cone penetrometer tests and 86 test pits. The geotechnical data correlated well with the proposed ratings generated from the geological maps.

The geotechnical information was used to recalibrate the assessments made from the geological data. It was particularly useful in definitively categorising suburbs, which were on the border between two zones and for the higher zones (3 to 5), where actual depths of soils present were required for the zonation.

After the zonation was completed a map of all the suburbs was generated utilising Map Info, showing the different ratings, this map is attached to the report as Figure 3. A map showing the location of the suburbs within Brisbane City has also been attached in Figure 4. A list of the hazard ratings for each suburb is appended.

4.0 LESSONS LEARNT DURING THE EXERCISE

If the author or others were to repeat the zonation exercise for other areas the following points are worth noting:

•It would be possible to undertake the zonation without the geotechnical data. However the zonation produced would be less accurate than if significant geotechnical

Figure 3. Earthquake Hazard Zones within the City of Brisbane

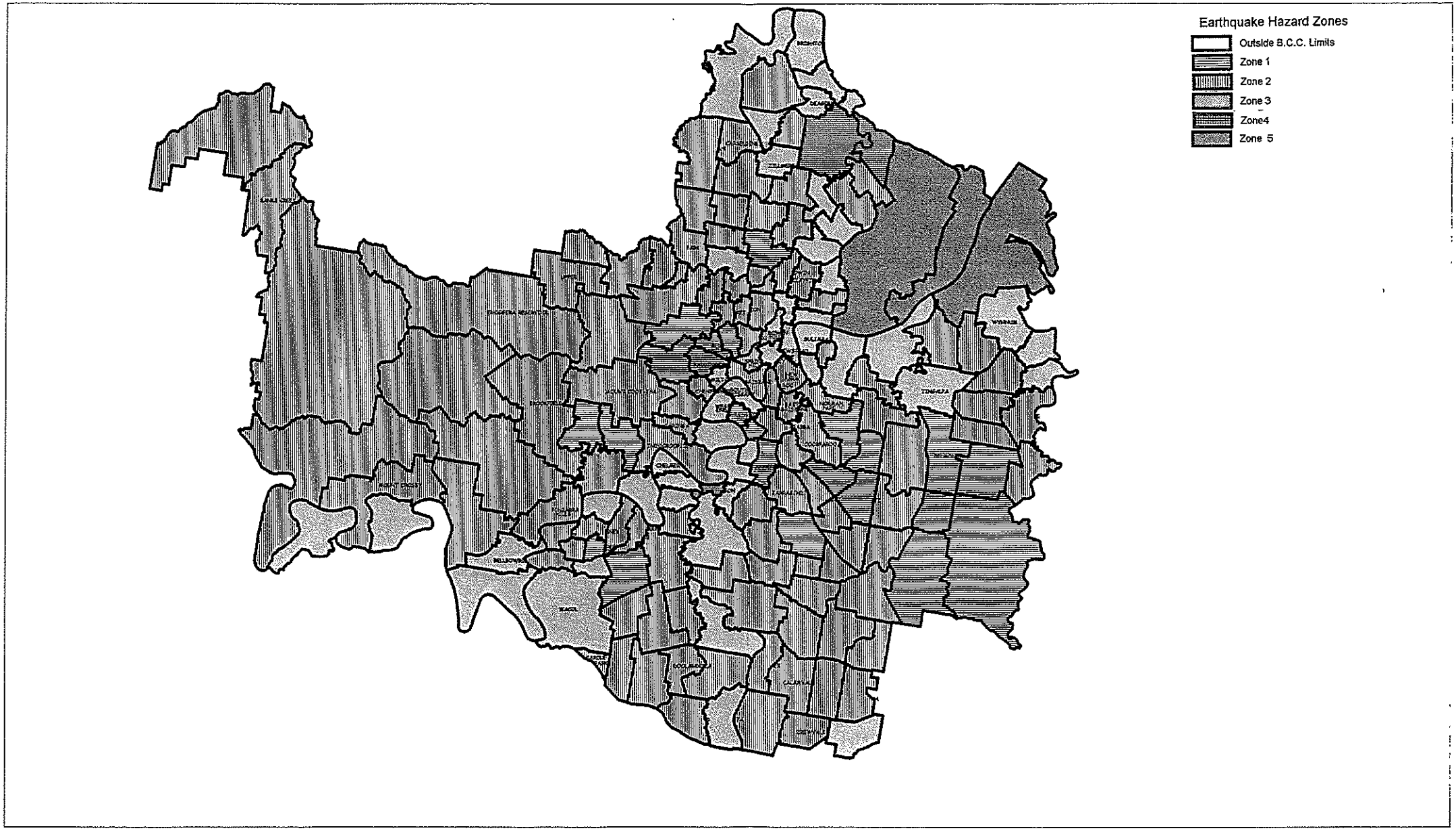

Figure 4. Suburb Locations within the City of Brisbane

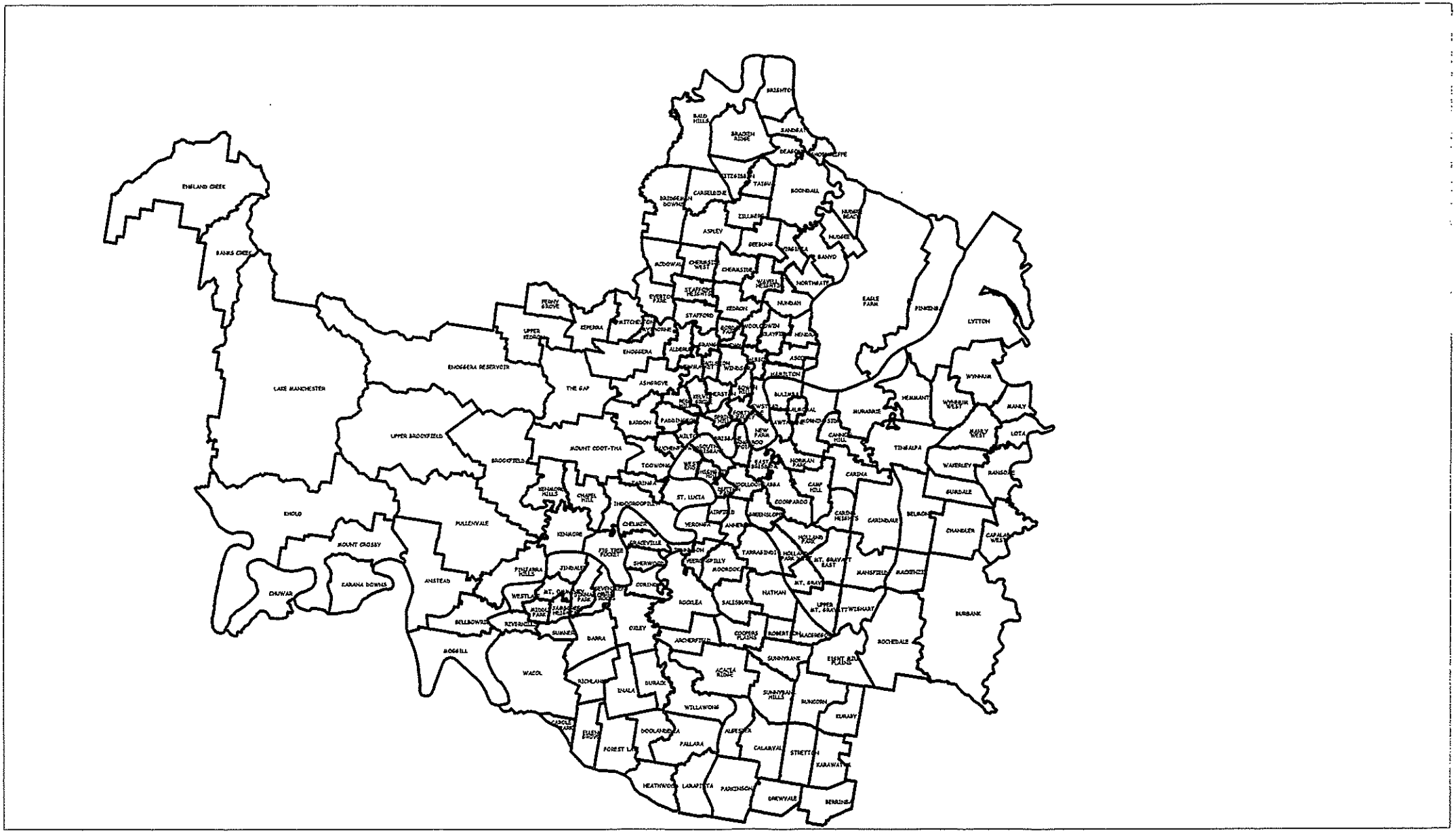

information were available, as it would prove to be particularly problematic for the zones requiring depths of material, because geological maps do not show depths of alluvium.

•Ideally the basal units for a zonation would be smaller than the suburbs utilised in this study, as the smaller units would allow a less averaged approach to an area's zonation.

• Ideally the basal map would be able to be coloured.

•Digital geological maps are not the only possible source of information required to undertake a similar study. If the basal units can be printed onto a map of equal scale to hard copy geological maps, overlaying would be a possible method of assessing the zonation.

•When utilising adjoining geological maps either digital or hard copy, the edges often do not join together well. Therefore the information around the edges of maps should be viewed with some caution and alternative information should be sought to clarify the geology in these areas.

•The incorporation of topographical information and groundwater levels may improve the zonation method.

•The greater the authors local geological/geotechnical knowledge is of an area being mapped, the lesser the need is for additional information other than the geological map.

5.0 ACKNOWLEDGEMENTS

The author would like to thank Soil Surveys Engineering Pty Ltd and Douglas Partners Pty Ltd for making their considerable databases available for the review of geotechnical data collected from across the city.

6.0 REFERENCES

Australian Standard, Minimum Design Loads on Structures, Part 4: Earthquake Loads AS1170.4 and Supplement, p5-9, 15-24, 1993.

Bell, F.G., Engineering Geology, Blackwell Scientific Publications, Melbourne, 1993.

Bevin, J., Seismic Microzoning of the Ground Shaking Hazard from Soil Geotechnical Properties, Gisbourne, New Zealand, Proceedings Fourth Australia New Zealand Young Geotechnical Professionals Conference, House and Watson (Ed's) February 2000.

Blong, R and Hunter, L., Earthquake PML Household Buildings, Sydney II, Greg Feister, 1997.

Borchedrt, R.D., Joyner, W.B., Warrick, R.E. And Gibbs, J.F., Response of Local Geologic Units to Ground Shaking, Evaluating Earthquake Hazards in the Los Angeles Region an Earth Science Perspective. Us Govt. Printing Office, Washington. United States Geological Survey Professional Paper 1360: p93-99.

Bryant, E., Natural Hazards, Cambridge University Press, Hong Kong, 1991.

Cooke, R.U. And Doorkamp, J.C., Geomorphology in Environmental Management, A New Introduction, Second Edition, Oxford University Press, New York, 1990.

Cranfield, L.C., Schwarzbock, C. And Day R.W. Geology of the Ipswich and Brisbane 1:250000 Sheet Areas, Geological Survey of Queensland, 1976.

Cuthbertson, R., Queensland Seismically, shake2.earthsciences.up.edu.au, 1995.

Foley, D., McKenzie, G.D. And Utgard, R.O., Investigations in Environmental Geology, Second Edition, Prentice Hall, New Jersey, 1999.

Geological Surveys of Queensland (Ed), Brisbane, Beenleigh, Caboolture and Ipswich 1:100000 series Geological maps.

Herrero, A and Cutherbertson, R. Seismic Hazard in Queensland. Snake2.earthsciences.uq.edu.au, 1995

Hitchcock, S.C., Loyd, R.C. And Haydon, W.D., Mapping Liquefaction Hazards in Simi Valley, Ventura County, California, Environmental and Engineering Geosciences, P 441-458, Vol. V, No. 4 Winter 1999.

Husein, A.I., Al-Homund, A.S. And Liang, R.Y., Seismic Hazard Mapping of Jordan, Quarterly Journal of Engineering Geology, p75-81, 28, 1995.

International Decade For Natural Disaster Reduction (IDNDR) Secretariat of United Nations and the City of Addis Ababa, RADIUS Program (Earthquake Damage Assessment). Addis Ababa, full Case Study, Working Groups Nov. 1998.

Latchet, C., Hatzfeld, D., Pierre-Yves, B, Theodulidis, N., Papaioannou, C and Savvaidis, A, Site Effects and Microzonation in the City of Thessaloniki (Greece) comparison of different approaches, Bulletin of the Seismological Society of America, p1692-1703, Vol. 86, December, 1996.

Purbani, H. And Pribadi, K.S., RADIUS Project, Bandung Indonesia, Second Semi-Annual Report, August 1998 to February 1999 Tapia, P, Pereira, M and Carvajal, M, RADIUS Project, Atofagasta, Chile, Second Semi-annual Report, August 1998 to February 1999.

Wills, CJ and Hitchcock, C.S., Late Quaternary Sedimetation and Liquefaction Hazard in the San Fernando Valley, Los Angeles County, California. Environmental and Engineering Geoscience, p419-439, Vol. V, No. 4, Winter 1999.

ASSESSING BRINE LEAKAGE AT A SOLAR SALT WORKS: AN ENGINEERING GEOLOGICAL APPROACH.

Cameron Lines.
Engineering Geologist, Pells Sullivan Meynink Pty Ltd

SUMMARY

This paper outlines how an Engineering Geological approach may be used to successfully solve geotechnical or environmental problems. In the case study presented this approach was used to assess potential brine leakage from a solar salt works onto neighbouring farmland.

Lake Grassmere is situated inland from Clifford Bay in Marlborough on the northeast coast of the South Island, New Zealand. In the Lower Grassmere Valley Miocene/Pliocene Awatere Group mudstones, with thin interbedded sandstones and conglomerates, are overlain by flat lying post Pliocene sediments upon which the Dominion Salt Ltd (DSL) solar salt works have been constructed. Deep Storage Pond Three (DS3) was constructed 1965-66.

The objective of this study was to evaluate whether fully saturated brine was leaking from DS3 through the sub-surface to neighbouring farmland and if so to establish the cause and extent of leakage.

Investigations comprised drilling and excavation of test pits, laboratory testing, geophysical investigation, ground water chemistry and monitoring, and an evaluation of the relationship between dryland salinity processes and the evolution of the Lower Grassmere Valley during the Holocene.

The holistic approach used to evaluate the problem resulted in the confident interpretation of a brine plume extending from the DS3 embankment covering an area of ~18,000 m^2 with a maximum extent of ~90 m from the storage pond. Salinity problems beyond this area are interpreted to be due to natural dryland salinity problems associated with uplifted marine sediments.

1 INTRODUCTION

Lake Grassmere is located on the northeast coast of the South Island of New Zealand. It is situated inland from Clifford Bay, approximately 288 km from Christchurch and 34 km from Blenheim (Figure 1). State Highway 1 between Picton and Christchurch is located approximately 1 km to the west of the saltworks and the north-south main trunk railway line passes along the western boundary of the Main Lake (Figure 2).

Prior to construction of the salt works, Lake Grassmere was a seasonal lake, which filled with water during the winter months (when evaporation is low) as it received runoff from the Grassmere Valley to the southwest of the lake. Water accumulated from runoff over winter would then evaporate during summer leaving a parched area of ground of little use for farming.

The solar salt works at Lake Grassmere were constructed in 1943 by Dominion Salt Ltd (DSL).

Initial construction of the salt works included intake and outlet structures to Clifford Bay and construction of embankments to create the concentrating ponds and crystallising ponds.

Four deep storage ponds were constructed in the late 1950's and early to mid 1960's so excess brine could be stored over winter to facilitate an earlier start to the salt making season. Deep Storage Pond Three (DS3) was constructed 1965-66.

In recent times, there has been an ongoing claim by a local farmer that the operation of DS3 adjacent to his land has been the cause of the infertility of his soils and subsequent damage to his pasture and crops. The farmer claimed that the area affected by brine leakage is ~12 ha between the storage pond, the DSL plant access road and State Highway One (Figure 2).

The primary objective of this study was to determine whether or not DS3 was leaking, and if so, to establish the cause and extent of leakage.

This was achieved using a holistic approach of integrating a broad spectrum of investigative measures, resulting in the formulation of a geological framework on which the leakage assessment could be based.

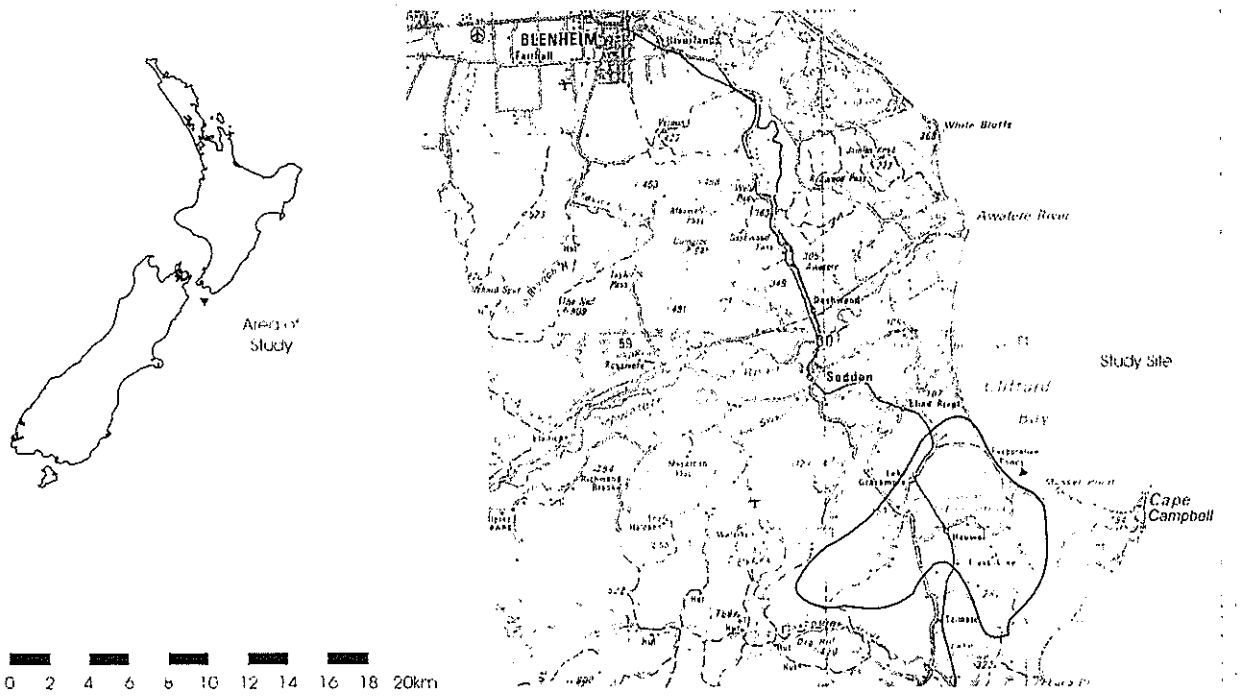

Figure 1: Location Map

2 METHODOLOGY

The Lake Grassmere study was essentially completed in two phases. The first involved direct investigation of DS3 to generate some initial data allowing the scope and possible extent of the problem to be understood more fully. This phase comprised:

- Drilling and logging of 8 cored boreholes in the vicinity of DS3,
- Installation of 10 piezometers (2 additional non-cored boreholes were drilled),
- Excavation of 18 test pits,
- Collection of single groundwater samples from test pits and multiple samples from boreholes over a six week period,
- Electromagnetic (EM) surveys,
- Ground penetrating radar surveys, and
- Surficial engineering geological mapping.

After the initial study phase was completed and summarised a second phase of study was undertaken to develop an evolutionary model for the Lower Grassmere Valley post-Pliocene. It was considered this model would have significant implications for the DS3 investigation in terms of soil salinity, physical hydrology and groundwater chemistry. Work during this phase included:

- Continued groundwater chemistry and water level monitoring,
- Drilling of a further 10 cored boreholes in the greater Lake Grassmere area,
- Further geophysical investigation at other areas of the lake shore,
- Grain size analyses of soil samples from core,
- Regional geological mapping,
- Radiocarbon dating of shell and wood material, and
- Palaeoecological analyses of Recent fossils.

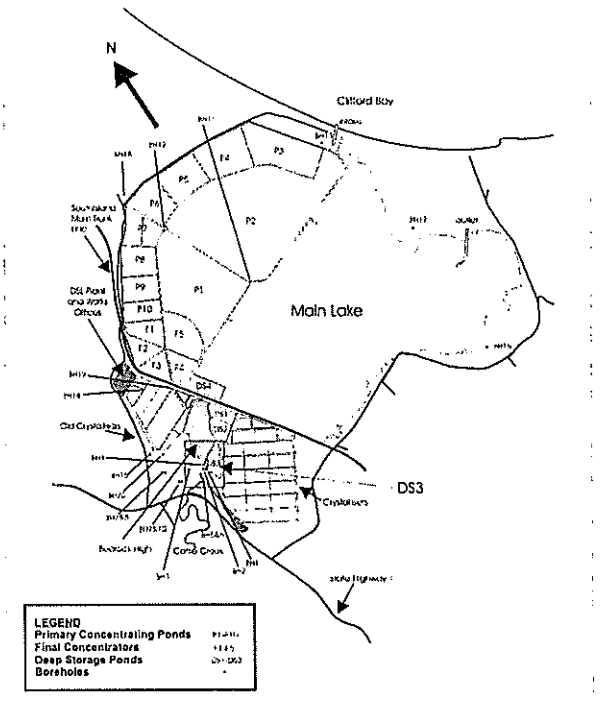

Figure 2: Detailed Location plan of the Solar Salt works at Lake Grassmere

3 REGIONAL SETTING

3.1 Geology

The majority of Grassmere Valley is composed of the Miocene/Pliocene Awatere Group sediments. Pleistocene glacial outwash gravels, fan gravels and silts occur further up the catchment as do minor elements of the Torlesse Greywacke and Amuri Limestone.

The Lower Starborough Mudstone member of the Awatere Group outcrops on all landward sides of Lake Grassmere, with a lone block evident protruding from within the salt works; this mudstone is projected to underlie Lake Grassmere; Roberts and Wilson (1).

The Lower Starborough Mudstone is dominated by a massive silty mudstone with thin concretionary sandstone beds in places. This mudstone is considered "basement" rock for the purposes of this study.

Limited previous research has been conducted on the post-Pliocene sediments which infill the Lower Grassmere Valley. These were examined during the course of this study.

3.2 Structural Framework

Lake Grassmere is situated within the Marlborough fault system (MFS, Figure 3), a zone of intense earth deformation, which transfers movement from subduction of oceanic lithosphere along the Hikurangi Margin of the East Coast, North Island to oblique, transpressive strike-slip along the Alpine fault in the South Island; Field et al (2).

Tectonic activity is primarily transpressive strike-slip movement along the four major faults that comprise the MFS, namely the Wairau, Awatere, Clarence and Hope faults.

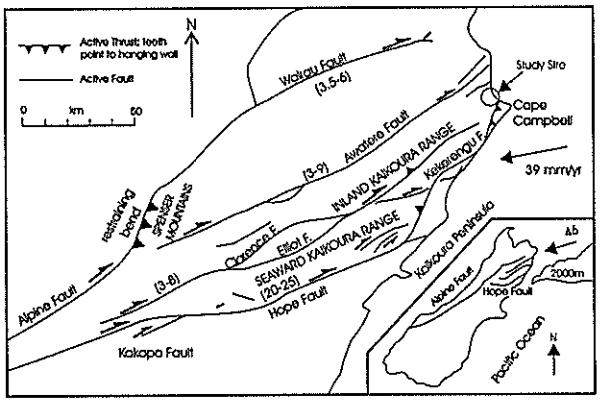

Figure 3: Summary Map of the Marlborough Fault System after van Dissen and Yeats (3).

Lake Grassmere is located between tectonically controlled ranges of hills to the south and north, and is bounded on three sides by structural elements of the MFS, namely the Awatere, London Hill and Haldon Hills/Flaxbourne faults (Figure 4). Ota et al (4) suggested that the lower Grassmere Valley may have been uplifted by up to ~1 m in the Late Holocene.

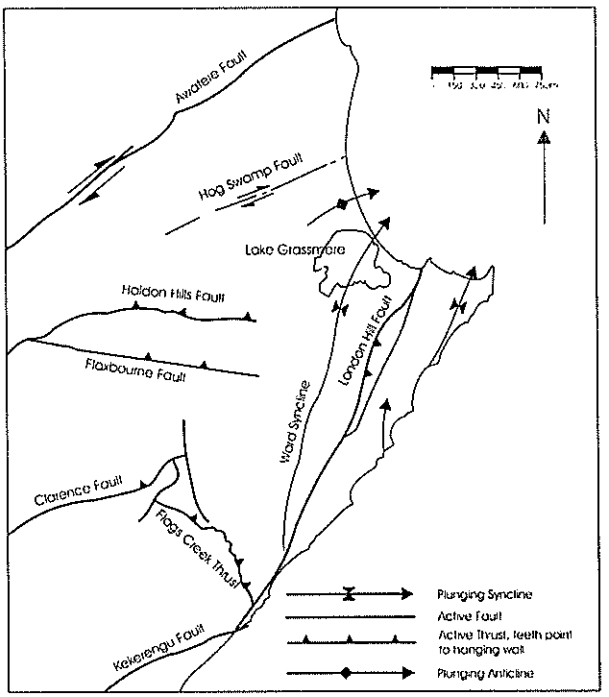

Figure 4: Location of Lake Grassmere to Structural Elements of the Marlborough Fault System, after Little and Jones (5).

4 EVOLUTION OF THE GRASSMERE BASIN

Prior to ~10,000 years BP the Grassmere Valley is interpreted to have been a northeast-southwest trending valley with a 1.5-2 m thickness of reworked glacial outwash gravel and local fan gravel being built out of the valley towards the ocean. These gravels overlie the bedrock Starborough Formation siltstone and are present in the bottom of boreholes 7, 9, and 20.

Marine sedimentation in the Grassmere Basin is interpreted to have begun approximately 8800 years BP, during post-glacial sea-level rise and is based on radiocarbon dates and back calculation of sedimentation rates calculated between known radiocarbon dates at various depths. Sea-level rise is interpreted to have continued until ~6500 years BP inundating all of the current extent of Lake Grassmere; Gibb (6). Geomorphic and geological mapping indicates that marine transgression may have extended as far as 2km up tributary valleys.

Paleo-environmental analysis of both macro-fossils and micro-fossils indicate that estuarine conditions were initiated within the lower valley initially followed by shallow marine conditions with estuarine conditions near the margins and deeper water at the present coastline as sea-level reached its maximum ~6500 years BP.

Rapid sea-level rise and subsequent suspension of inundated soils and weathering of loose, weak rock is inferred to be the cause of the rapid sedimentation rates calculated from radiocarbon dates at known depth intervals.

Once sea level was established at approximately its current level around 6500 years BP, the highest beach ridges currently positioned to the north and south of Lake Grassmere began to form. The nature of the beach ridges suggests that no beach bar existed and the shores of the valley mouth were open to the ocean; Ota et al (4). At this point water depths in the mouth of the embayment were likely to have been approximately 15 m.

Large quantities of organic material below approximately -3.2 m RL in boreholes at the mouth of the present day Grassmere Valley, and the presence of marginal marine, brackish water and fresh water microfossils suggest an estuarine environment with significant fresh water influences. This estuary is interpreted to have deepened towards the coast (indicated by the presence of marginal marine, enclosed harbour and inner shelf microfossils) becoming a shallow marine environment.

Sedimentation infilled the basin between approximately 8800 years BP and 4400 years BP based on a radiocarbon date of 4870±170 years BP, at 2.6 m above sea level (within 0.4m of the surface) in a test pit near the present day mouth of the Grassmere Valley. During this time, rapid sedimentation is interpreted to have filled the marginal estuaries forming extensive inter-tidal mud and sand flats, colonised by the estuarine bivalves *Austrovenus stuchburyi*, and *Mactra ovata*.

It is interpreted that continued reworking and transport of gravels in the upper Grassmere Valley resulted in interfingering of thin layers of gravel within the estuarine sediments during deposition at the margins of the embayment. This is visible in several slightly incised stream channels in the lower valley.

Based on radiocarbon dates and sedimentation rates, an uplift event of between 1-1.5 m is interpreted to have occurred around 4400 years BP, which halted further sedimentation around the margins of the embayment, and uplifted the oldest set of beach ridges visible to the north and south of the Lake. This substantially reduced the extent of the embayment forming shallow estuarine conditions just east of the present location of State Highway 1, evidenced by paleo-shorelines present in this area.

Between ~4400 years BP and ~2000 years BP sedimentation continued within the estuary forming the younger beach ridges to the north and south of Lake Grassmere. From approximately 2800 years BP the barrier bar began to form; Ota et al (4).

At approximately 2000 years BP a second uplift event of between 0.5-1.0 m is interpreted to have occurred, which uplifted the second set of beach ridges and most of Lake Grassmere to its present position. A small shallow inter-tidal inlet was formed protected by the barrier bar, which was almost complete by this time. The shoreline of Clifford Bay on the south side of the inlet is interpreted to have been located near BH17.

Estimates of uplift are based on correlation of dated samples with Holocene sea level at the time of deposition to determine minimum uplift values. The timing of uplift correlates reasonably well with events at ~4200 years BP and 2000 years BP on the Awatere fault recognised by Knuepfer (7), in which the southeast side was up thrown by ~ 2.5 m and ~ 0.5 m respectively. At ~1800 years BP the barrier bar completely enclosed Lake Grassmere; Ota et al (3), cutting off the inlet and forming the conditions seen at the present day in Lake Grassmere.

Since 1800 years BP, rainwater and stream flow is interpreted to have filled the stranded estuary and a seasonal lake developed at the lowest point of the catchment. The flushing effect of this rainfall on uplifted marine sediments over the last 1800 years is interpreted to have been extremely limited because evaporation exceeds precipitation on average for 11 months of the year. Furthermore, the shallow water table facilitates concentration of salt in topsoil by evaporation and the relatively low permeabilities of the in-situ marine and estuarine silts limit transport of fresh water. Naturally occurring saline groundwater is interpreted to have been concentrated in Lake Grassmere and adjoining land since the last uplift event ~2000 years BP.

5 DS3 INVESTIGATIONS

5.1 DS3 Construction and Operation

DS3 has been in use by DSL since 1967. Fully saturated brine (approximately 300 g/l NaCl) is pumped from the concentrating ponds after the harvest period (March) into deep storage. DS3 is typically filled over the course of a few weeks and held at full supply level for most of winter. Full supply level is approximately 3.6m RL, approximately 1m higher than surrounding farmland.

The pond was constructed as a cut and fill type operation, where fine sandy silts from the base of the pond were excavated and compacted to form the embankment walls. No clay or membrane lining was built. The base of the pond is approximately 1m RL, approximately 1m lower than the surrounding farmland.

During construction Cattle Creek/Grassmere Stream had to be diverted from its original course and now runs parallel to the southwest wall of DS3.

5.2 Units Identified

The units identified within the sub-surface are as follows:

- An effectively impermeable bedrock consisting of a grey siltstone, at a depth of approx. 1-10 m throughout the area between the salt works and State Highway 1,
- Fluvial gravel layers of approximately 1-1.5 m thickness sourced from the glacial gravels in the upper Grassmere Valley,
- Unweathered shallow marine/estuarine silts with some fine sand with zones of large quantities of organic material and sparse shell layers in the top 1-2 meters, and
- Estuarine/inter-tidal mud flat silts and fine sands, with showing limonite staining, with no organic material but abundant shell material both disseminated and in discontinuous layers.

5.3 Piezometric Data

Piezometric data indicates when DS3 is full there is a 2m hydraulic head differential resulting in a hydraulic gradient sloping back into the neighbouring property; groundwater levels are highest in the embankment wall and reduce with increasing distance to the NW.

Piezometric levels are variable throughout the suite of piezometers installed around DS3; this was interpreted to be due to perched water tables on shallow bedrock (BH4), the effect of elevated fluid levels in DS3 (BH1, 2, 4) and the effect of tapping into semi-confined gravel layers in the base of boreholes 7 and 9. Boreholes 3, 9, and 10 are considered to indicate the natural level of the water table in the area out towards the DSL access road. Boreholes 5 and 6 may be draining towards the low point created by Cattle Creek since its diversion.

5.4 Shell Layers

Test pit and borehole investigations showed a number of shell beds within the unconsolidated sediments around DS3. These were most prominent in the area just northwest of the northern wall of the embankment where beds up to 380 mm thick were found. These layers did not typically show lateral continuity between test pits and boreholes.

The shell layers found in test pits 1, 2, 5 and 7, and remnants in boreholes 1 and 2, suggest that at least one and perhaps a succession of abandoned channels, which drained through intertidal mud flats, now lie beneath the embankment wall at its northern extent. These shell layers have been interpreted as the primary mechanism by which leakage is occurring from DS3, as they provide a higher permeability conduit for brine leakage to escape from DS3. They also increase the bulk permeability of the in-situ sediments in the neighbouring paddocks, speeding the propagation of the brine contamination plume.

Thicknesses of individual shell layers are between 10-400 mm, but lateral dimensions of these are difficult to quantify given their discontinuous extent in the boreholes and test pits logged. Rather it is possible to define a zone of shell rich layers which extends at least 100 m to the west towards borehole 5 and ~100 m to the NW towards test pit 18 (though extremely thin and silt bound here). This shell rich zone is most evident in the top 3m of soils.

5.5 Water Chemistry

Water chemistry data from boreholes near DS3 are presented in Table 1.

Table 1
Average Salt Content (NaCl) in Piezometers

Borehole	Distance from BH1	Average NaCl (g/l)
BH1	0.0 m	188
BH2	28 m	83
BH3	182 m	51
BH4	55 m	127
BH5	107 m	37
BH6	110 m	56
BH7	579 m	7
BH8	575 m	17
BH9	374 m	4
BH10	370 m	4
DS3 Brine		305
Seawater		27

These results can be broken into three categories:

- Very high salinity >80 g/l NaCl (boreholes 1, 2, 4);
- High salinity approximately 20 to 50 g/l NaCl (boreholes 3, 5, and 6); and
- Brackish-fresh <20 g/l NaCl, (boreholes 7-10).

Its is evident the very high salinity readings are brine influenced, given the proximity of the boreholes in question to DS3 and the very high salinity values recorded. Equally, the brackish to fresh samples from boreholes 7-10 are probably not directly influenced by DS3 leakage. The remaining boreholes (3, 5 and 7) show salinities exceeding that of seawater. These require further discussion.

5.6 Geophysical Data

The electromagnetic survey delineated a highly conductive plume extending out to a maximum distance of 90 m from the embankment wall (Figure 5). This was based on a background conductivity value of 200mS/m derived from noticeable breaks in conductivity vs distance charts (Figure 6). Data was used from both DS3 and from land adjacent to the south side of the main lake (an area removed from the very high salinity concentrating ponds).

The results from the radar surveys substantiate the results of electromagnetic surveys. The lateral extent of attenuated radar signal (typical of highly conductive sub-surface units) matched up very well with the plume delineated by the electromagnetic survey, strengthening the case for a plume of this size.

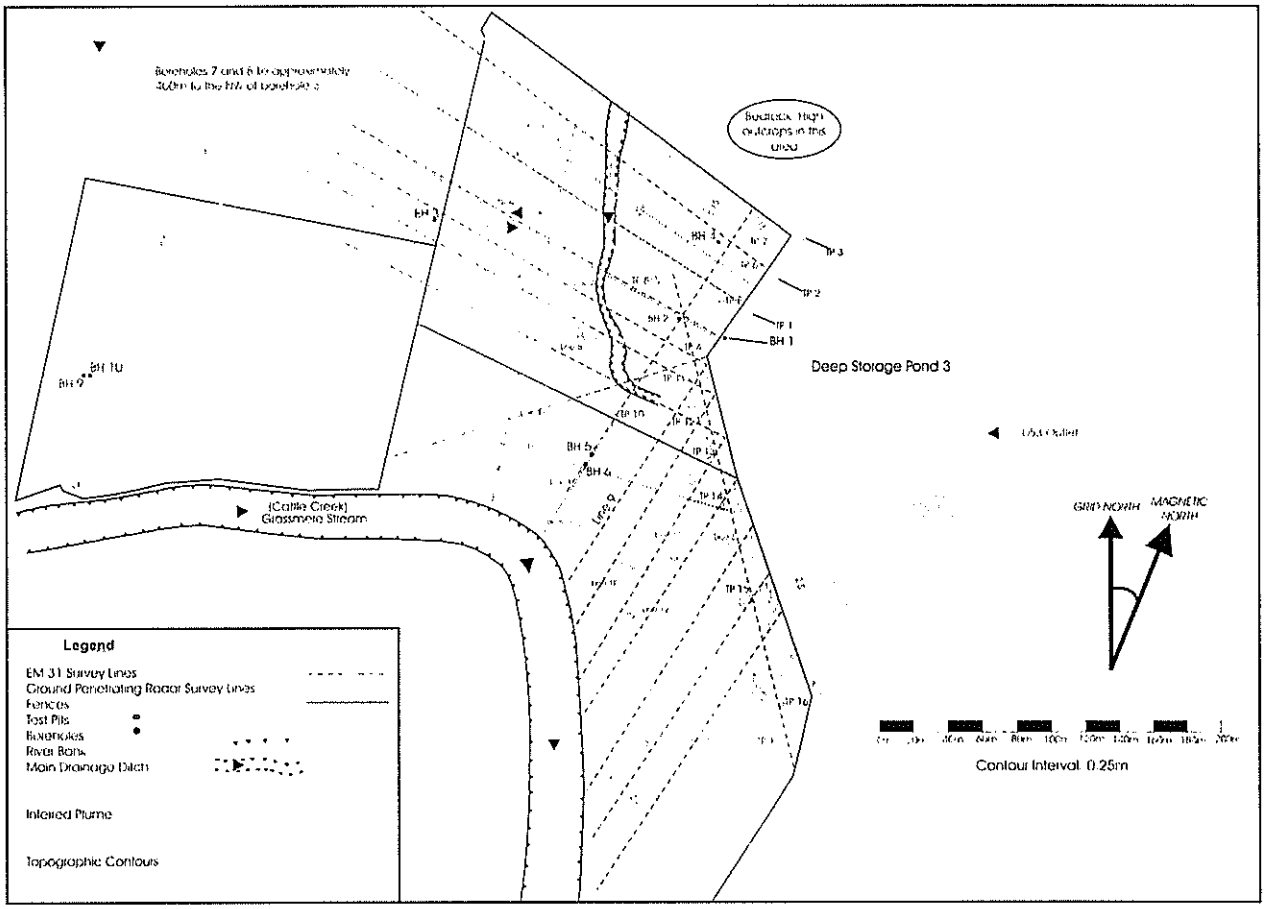

Figure 5: Location plan of Investigations Surrounding Deep Storage Pond Three and the Inferred Extent of the Brine Plume.

5.7 Engineering Geological Model and Causes of High Salinity

The following Engineering Geological model (refer Figure 7) was developed for the area surrounding DS3.

- The operating level of DS3 is of sufficient height to generate a hydraulic head of some 2 m compared to the groundwater in the adjoining property. When at full supply level, this head difference creates a hydraulic gradient back into the adjoining property.
- Brine appears to be leaking out of the embankment though the shell layers identified though these shell layers do not form a continuous higher permeability layer and are silt and clay bound at their furthermost extent, limiting the extent of brine influence.
- Propagation of brine through the sediments in the adjoining property is through the shell layers, which though discontinuous, increase the bulk permeability of the marine sediments allowing more rapid fluid transfer over short distances.
- The fluvial gravels identified in the base of boreholes 7-10 are a source of fresh water recharge to the system but given their distance from DS3 and the sub-surface permeabilities (~10^{-8} m/s) these fresh water recharge zones will not be able to effectively dilute high salinity groundwater found closer to DS3.
- Bedrock is considered effectively impermeable due to a fracture spacing >1 m and no open joints found in borehole core or in surficial outcrop. Bedrock topography limits the extent of brine leakage where shallow (~1 m depth) bedrock is encountered.

Evidence gathered from geophysical and sub-surface investigations appear to limit the primary extent of brine infiltration to within 90 m of the embankment. This plume is likely to have a marginal fringe, probably of the order of tens of metres.

The development of an evolutionary model for the Grassmere Valley in the Holocene has shown that two uplift events of fully saturated marine sediments have occurred at 4400 years BP and 2000 years BP. Furthermore, the shallow estuary formed by the latter event was cut off from the ocean at approximately 1800 years BP. Since this time evaporation and concentration of saline surface water and groundwater

is interpreted to have occurred resulting in the natural development of high salinity groundwater.

Based on the evolutionary model, salinity of groundwater in boreholes outside of the defined plume is considered to be due primarily to evaporation of saline lake waters. These high salinity values are similar to naturally occurring saline groundwater reported by Chambers (8) at a seasonal lake very similar to Lake Grassmere in the Spencer Gulf of South Australia.

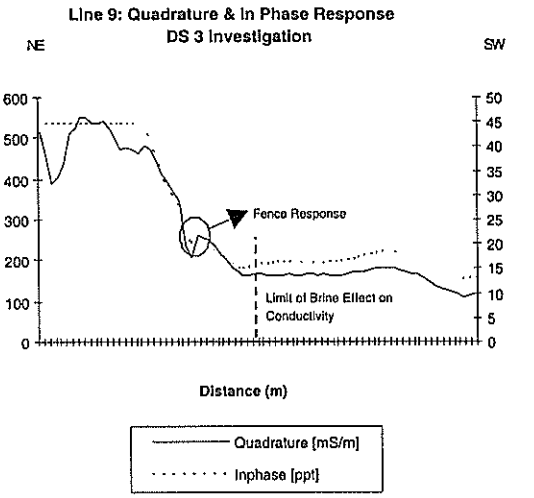

Figure 6: Bulk conductivity vs Distance Plots for Electromagnetic Survey Line 9.

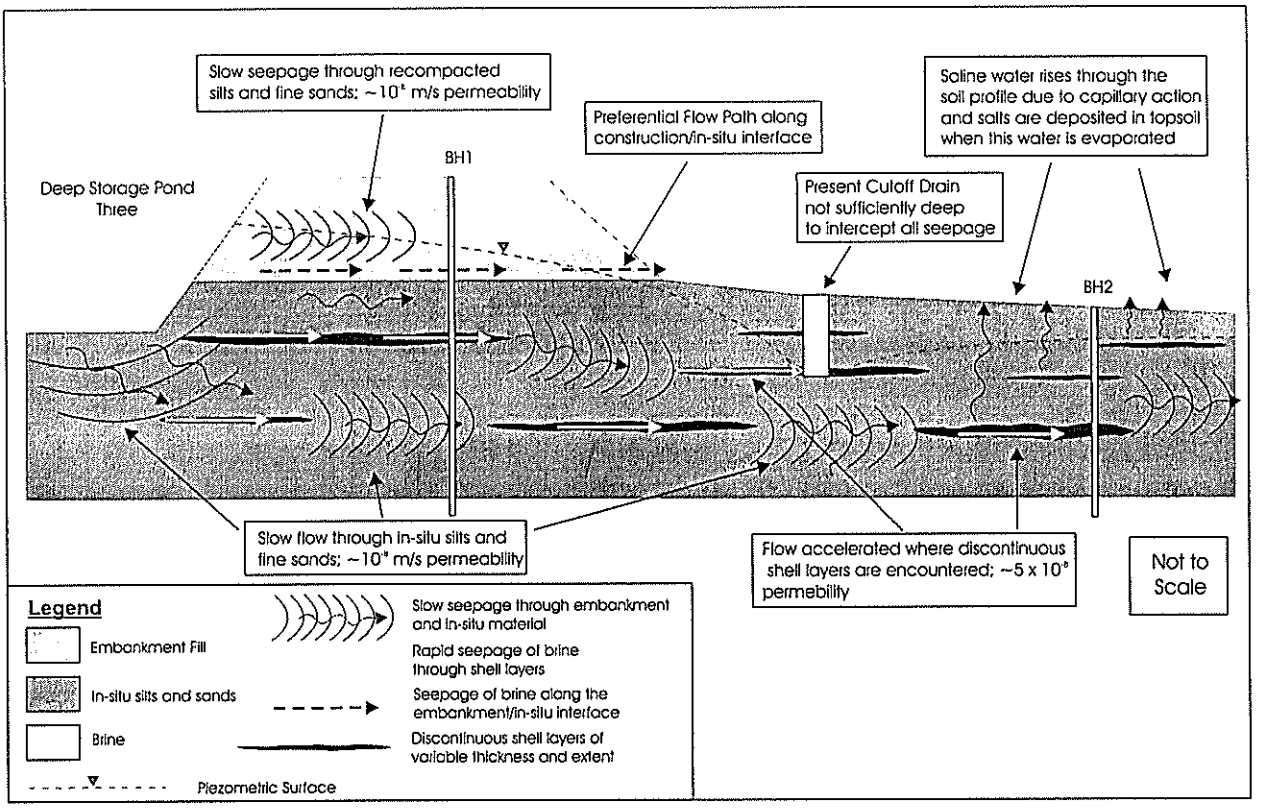

Figure 7: Engineering Geological Model for Brine Leakage from Deep Storage Pond Three.

6 SUMMARY AND CONCLUSIONS

The objective of this study was to determine whether DS3 was leaking and if so to establish the cause and extent of leakage.

The assessment showed that DS3 was leaking primarily through discontinuous shell layers present both below the constructed embankment and within the in-situ soils of the neighbouring property. The brine plume has been interpreted as extending out to a maximum distance of 90 m from the embankment wall.

High salinity levels outside this brine plume are considered to be primarily due to evaporation of naturally occurring saline waters, originating from uplifted fully saturate marine and estuarine sediments that underlie the site.

Lastly, it is important to recognise that the approach of using every available piece of geological data to fully understand the geological model has been crucial to the success of this study.

ACKNOWLEDGEMENTS

The author wishes to thank Dominion Salt Ltd for their permission to publish this case study and Mr Mark Eggers for constructive suggestions during the writing of the paper.

REFERENCES

1. Roberts, A. P., Wilson, G. S., 1992, Stratigraphy of the Awatere Group, Marlborough, New Zealand. *Journal of the Royal Society of New Zealand.* v: 22, p. 187-204.

2. Field, B. D., Uruski, C. I., and others., 1997, *Cretaceous-Cenozoic geology and petroleum systems of the East Coast region, New Zealand.* Geological monograph 19, Institute of Geological and Nuclear Sciences, Lower Hutt.

3. van Dissen, R,. Yeats, R.S., 1991, Hope fault, Jordan thrust and uplift of the seaward Kaikoura Range, New Zealand. *Geology.* v: 19, p. 393-396.

4. Ota, Y., Brown, L. J., Berryman, K. J., Fujimori, T., Miyauchi, T., 1995, Vertical tectonic movement in northeastern Marlborough: stratigraphic, radiocarbon, and paleoecological data from Holocene estuaries. *New Zealand journal of geology and geophysics.* v: 38, p. 269-282.

5. Little, T.A., Jones, A., 1998, Distribution and mechanism of Neogene to present-day vertical axis rotations, Pacific-Australia plate boundary zone, South Island, New Zealand. *Journal of geophysical research.* v: 102 B9, p20447-20468.

6. Gibb, J. G., 1986, A New Zealand regional Holocene eustatic sea-level curve and its application to determination of vertical tectonic movements. *Royal Society of New Zealand Bulletin* v: 24. p. 377-395.

7. Knuepfer, P. L. K. 1992, Temporal variations in latest Quaternary slip across the Australian-Pacific plate boundary, northeastern South Island, New Zealand. *Tectonics.* v: 11, p. 449-464.

8. Chambers, L. A., Ferguson, J., Burne, R. V., 1990, Controls and effects of continental brine formation in a supratidal ephemeral lake in the semi-arid enviroment of Spencer Gulf, South Australia. *Australian journal of earth sciences.* v: 37, p. 71-84.

Makara Road Carriageway Realignment, Case Study

Chris Lyons, Geotechncial Engineer, Tonkin & Taylor Ltd.

The realignment of Makara Road carriageway proved to be a testing and rewarding project due to its technical, managerial and site specific challenges. The project progressed from an initial investigation of a failing retaining wall into a realignment of 200m of carriageway incorporating the design of bulk earthworks, palisade wall construction and carriageway reconstruction. The client's request for urgency in completing the works resulted in separation of the project works into three contracts with tight managerial constraints. Added to this were site specific challenges such as a narrow carriageway, clay lined rock defects and the presence of Telecom's north-south island link fibre optic cable behind the failing retaining wall.

1. INTRODUCTION

In December 2000 subsidence and cracking was observed in the Makara Road carriageway. Tonkin & Taylor were engaged by Wellington City Council (WCC) to investigate the cause of the deformation and were later asked to provide design and contract supervision for the remedial works.

Following a preliminary site visit, we considered the edge of the carriageway was potentially unstable and had a high risk of failure. Traffic was isolated immediately from behind the wall for the extent of cracking. A detailed stability assessment of the wall was performed.

This paper looks at the work involved in the project from the initial investigation, through the proposed carriageway realignment design and the design and construction of the earthworks, retaining wall and carriageway formation contracts. The various technical, managerial and site specific issues affecting each stage of the works are covered, providing an overview of the project.

2. MAKARA ROAD RAILWAY IRON WALL

Makara Road is located to the west of Wellington City and mainly serves the rural community of Makara, Makara Beach and one of Wellington's main cemeteries. The road has typically been formed as a sidling cut to fill road, typically 6m wide with tight radius corners and steep embankment slopes. Average traffic flows over Makara Road are in the order of 2,000 vehicles per day including funeral processions, school busses, boat trailers and large trucks.

At the site the road is formed on a steep slope (approximately 40^0). The northern or downslope edge of the carriageway was supported by a retaining wall, retaining approximately 1.75m height. The southern side of the carriageway has been excavated into greywacke rock slope cut batters up to 8m in height.

The retaining wall consisted of timber lagging spanning between driven railway irons. Each railway iron was tied back by a steel cable to a second row of driven railway irons buried beneath the carriageway. The railway irons were driven to the underlying rock approximately 5.0m below the outer edge of the carriageway. The railway irons were spaced at approximately 1.8m. No as built records could be found for the existing wall.

The observed carriageway cracking and deformation occurred along approximately 50m length behind the existing wall. Individual cracks up to 12mm wide, with total lateral displacements in the order of 25mm had formed behind the retaining wall. The wall visibly deflected under the weight of passing trucks and railway irons had rotated up to 10^o outward. Additional subsidence had occurred at the western end of the wall where groundwater flows had internally eroded carriageway sub-base layers resulting in settlement of the carriageway and formation of a tomo beneath the carriageway edge.

3. RETAINING WALL INVESTIGATION

The investigation objectives were to determine;

- Subsurface conditions
- Cause of wall failure
- Stability of the retaining wall
- Remedial options and construction cost estimates

The site investigation consisted of;

- Two machine augered boreholes to 4.9m depth with standard penetration tests (SPT)
- 4 cone penetration tests (CPT) to 5.2m depth
- 5 Scala penetration test up to 7.7m depth

The site investigation indicated the outer edge of the carriageway was most likely formed from loose fill underlain by colluvium. The surface of underlying highly weathered greywacke rock was falling steeply (approximately 40°) to the north, consistent with the surrounding topography.

A pre-investigation services check revealed that Telecom New Zealand's multi-million dollar fibre optic cable, providing the primary tele-communication links to the South Island was buried approximately 500mm behind the existing failing wall, significantly increasing the consequence of wall failure.

The most effective option for stabilising the carriageway was considered to be construction of a concrete palisade wall with ground anchors. The estimated construction cost for this work was $180,000.

4. REALIGNMENT UPGRADE DESIGN

Given the cost to provide slope stabilisation remedial works to the carriageway, WCC decided to upgrade the length of road to a 100-year design standard. This would involve widening the carriageway and straightening some tight corners. The proposed remedial works consisted of bulk earthwork excavation for the new carriageway alignment, construction of a concrete palisade retaining wall and carriageway regrading, formation and sealing.

The proposed works were separated into three contracts allowing;

- Streamlined programming due to building and resource consent requirements for different aspects of the works.
- 3 specialist contractors to undertake different aspects of the works with minimal overlap.
- Earlier finalisation of design for contract works
- Reduced time for contract and tender documentation preparation
- Reduced contract tendering periods

The three aspects were;

- Bulk earthworks
- Retaining wall construction
- Formation grading and carriageway sealing.

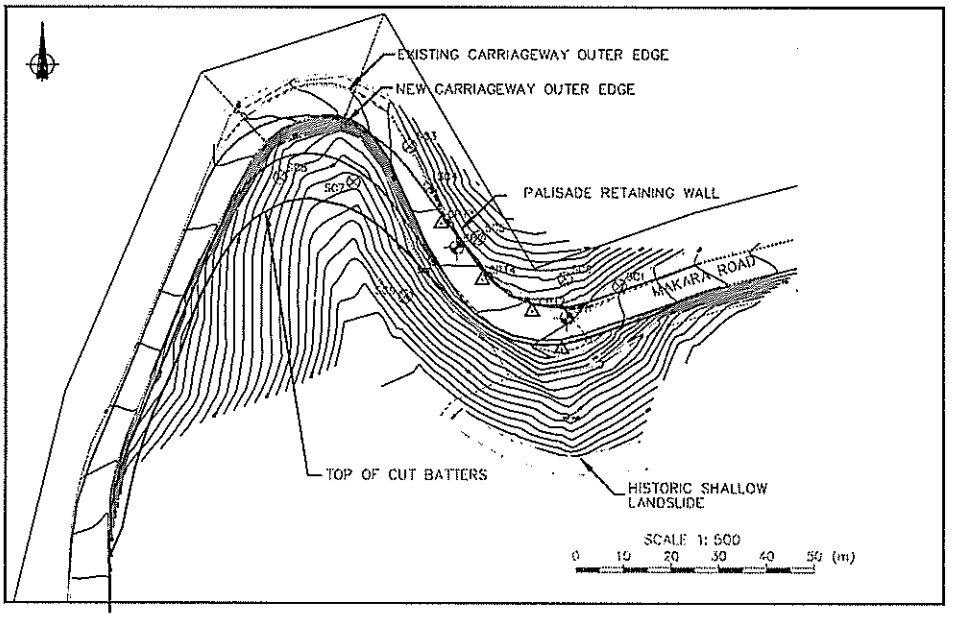

Figure 1. Existing contour plan with investigation test locations and the proposed carriageway alignment.

A specialist sub consultant carried out the geometric design of the new carriageway alignment.

5. EARTHWORKS CONTRACT

The earthworks contract primarily consisted of the excavation, transportation and compaction of approximately 3,700m^3 of rock material. This contract also included minor stormwater works. Some of the more complex issues related to the construction were the organisation of securing land for the new carriageway alignment, locating and designing a cost effective fill disposal site and traffic management for the very narrow carriageway.

Batter cut designs were added to a three dimensional survey and carriageway alignment model allowing cross-sections to be generated. Earthworks volumes and areas were calculated from the 3 dimensional model. Figure 1 shows the carriageway realignment. The inside edge of the new alignment moved up to 8m into the slope.

Subsoil drains and a concrete dish channel were designed along the toe of the cut batters to intercept surface stormwater and subsurface flows from the cut faces.

5.1 Batter Slope Design

Batter slope recommendations were based upon Geological mapping and stability assessment of the existing cut faces. The main bedding of the rock was dipping to the east, into the existing rock face with only a few minor adverse joint sets likely to daylight and affect batter stability. Several areas of weaker rock and colluvium were noted and batters designed accordingly. The existing batter slopes were sitting at approximately 1H:5V with no significant slips or defects. Batters were recommended to be cut from typically 1H:2V to 1H:4V, with 12m maximum height and a bench at 6m height. The calculated volume of earthworks to be excavated was 3,700m^3. The finished cut batters were hydroseeded to minimise erosion of the cut surface and also to improve the appearance of the cut batters.

Approximately 3750m^2 of the plan area of the excavation works (75%) was located in private property. Once the carriageway alignment and cut batter design had been finalised, the Council could confirm negotiations to purchase the property required.

5.2 Fill Buttress Embankment

Another challenge was to find a cost-effective way to dispose of the 3,700m^3 of excavated material. The solution was to use the excess material to stabilise a nearby (3km) subsiding carriageway formed on a loose earth embankment. The existing embankment was 5m high, formed with a 45° slope. A previous investigation had recommended a fill buttress to stabilise the embankment.

The design, consenting and neighbouring property agreements for the formation of the buttress provided additional tasks prior to tendering the first contract. The area below the existing embankment (approximately 400m^2) was relatively flat, bounded by South Makara Road and Makara Stream. An assessment of environmental effects for consents was required including some limited flood modelling of Makara Stream. The property was owned by a local farming station and Wellington City Council agreed to do small civil works on the station to compensate for placing fill on the station. An agreement was negotiated and was finally confirmed during tendering. The contract was awarded within a week of tenders closing.

5.3 Traffic Management

When the Contractor (John Ray Ltd) commenced excavation, traffic control was difficult. Excavation commenced at the crest of the existing cut faces with a 20 tonne excavator loading trucks every 5minutes. Traffic flow was controlled with stop-go signs and/or traffic lights. Problems were anticipated from parking a truck on the inside corner of a 6.0m wide carriageway, being loaded from an excavator 3m above, while traffic had to pass within the remaining carriageway width. During excavation and loading from the top batter both lanes had to be closed periodically due to falling debris.

Once the excavation works had cleared a 25m^2 working platform at road level for truck loading, traffic was generally controlled via a single lane give way system.

5.4 Rock Defect Failure

2 weeks after completion of the cut batters, a slip occurred on a planar clay lined defect after a period of prolonged rainfall. Approximately $12m^3$ of material fell from the lower bench face onto the dish channel at the toe of the slope. The defect plane dipped at approximately 50° and was orientated at approximately 45° to the cut face. The estimated friction angle of the plane was 20°. A geological inspection of the cut batters and comparison with the logging of the original cut face 8m away indicated the defect plane had dipped 15 – 20° steeper than its orientation at the logged face.

The defect was assessed with a stereo-net to determine a suitable cut slope to prevent further fall-outs. Calculation indicated that a 53° batter would alleviate the risk of further failures on the defect plane. Although flattening the slope to 45° would have further reduced the risk of additional fall-outs, this would have involved a significant amount of excavation. The client opted to cut the batter at 53°, accepting that further small scale failures could be expected. The boundary at the top of the batter was repositioned to accommodate possible future failures, which would be dealt with as they occurred.

6. PALISADE WALL CONSTRUCTION

The contract for the palisade wall started at the completion of the bulk earthworks, and consisted of concrete piles (up to 600mm dia.) with 350kN anchors retaining up to 6.7m of loose fill and colluvium. The protection and relaying of the Telecom fibre optic cable behind the new wall was a crucial part of the wall design and construction sequencing.

6.1 Palisade Wall Concept Design

A palisade wall was considered the most suitable option for the site due to several factors:

- No significant excavation into the existing narrow carriageway was required, allowing one lane of Makara Road to remain open during construction.
- Piles could found in the rock several metres below the existing carriageway providing a stable foundation.
- The wall could be built in front of the existing railway iron wall, providing stability throughout construction and minimising disturbance to the Telecom fibre optic cable.
- The depth to and steeply dipping surface of underlying bedrock restricted the use of gravity type structures.

Following construction of the new wall, the existing railway irons were trimmed to 150mm above the top of the existing tie-backs and the existing timber lagging was removed. A 250mm gap was left between the new and existing walls for drainage material and new ducting for the fibre optic cable.

6.2 Palisade Wall Design

The palisade wall consisted of concrete piles and capping beam with ground anchors and timber lagging supporting 6.5m of fill and carriageway (Figure 2). A 500mm x 500mm concrete capping beam ran along the wall, 2m below the proposed carriageway level. 500mm and 600mm dia. piles up to 6.2m long extended down from the capping beam into the highly weathered greywacke rock. Concrete columns extended 1.6m up from the capping beam to carriageway level with timber lagging.

Ground anchors up to 8m long were drilled through the fill and colluvium and embedded 5m into the greywacke rock. Anchors consisted of 32mm dia. high tensile strength Reid bars centrally placed in 150mm dia. anchor holes and injected with grout. Once the grout had reached sufficient strength the anchors were tested to 320kN and locked off at 200kN.

6.3 Telecom Fibre Optic Cable

The protection of the Telecom fibre optic cable was significant in the design and construction of the new retaining wall. Wellington City Council, Telecom NZ Ltd and Tonkin & Taylor Ltd wanted to minimise the disturbance to the multi-million dollar cable to avoid potential damage. The cable carried the majority of internet and telecommunications traffic between the North and South Islands so cable failure would have been highly disruptive.

The cable was approximately 37mm in dia. inside a 100mm dia. protective ducting. The understanding was that the cable could tolerate minor deformation and elongation.

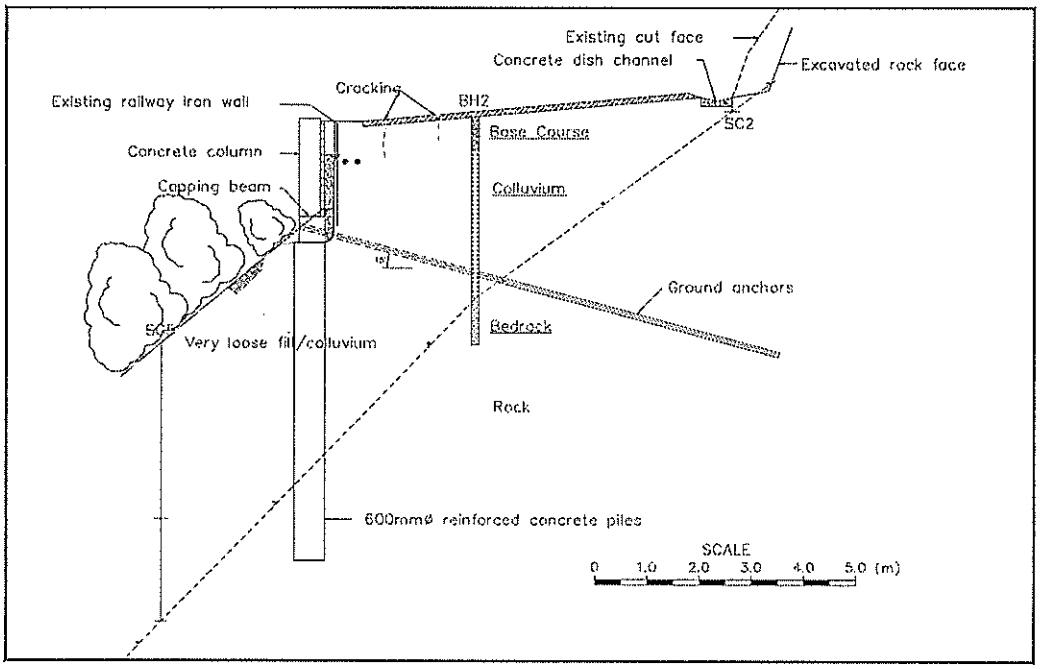

Figure 2. Typical retaining wall detail with concrete piles, capping beam and columns.

Due to a reduction in carriageway levels, the existing cover above the cable would have been reduced from 600mm to 100mm in places so sections of the cable required relaying. By constructing the palisade wall in front of the existing wall and then relaying the cable behind the new wall, the cable could remain protected for the majority of the palisade wall construction.

While drilling piles for the palisade wall, significant cracking and fallouts occurred in the carriageway directly below the fibre optic cable at the western end of the wall construction, where the new wall extended past the existing railway iron wall. During drilling of the final piles with a 20ton excavator, vibrations caused cracks in the carriageway to grow from 10mm wide to 40 mm wide. This was noted and all heavy plant was immediately moved away. If the temporary excavation for the capping beam had failed it was likely the fibre optic cable would have experienced some degree of damage. To reduce the immediate potential of failure three steps were taken;

- Excavation of the cracked carriageway above the fibre optic cable, leaving the cable half exposed at the ground surface. This reduced the surcharge load on the material beneath the cable and allowed the cable to hang free in the event of failure rather than being dragged down.
- A small bund (75mm high) was formed with cold mix around the extent of the major cracking to divert surface water from the cracks.
- The existing site fencing was shifted an additional metre into the carriageway to reduce any potential surcharge loading and vibration effects from heavy traffic.

Further rainfall the next day resulted in two small fallouts in the unsupported temporary excavation leaving the fibre optic cable unsupported along a length of several metres. In consultation with the Contractor (Pendleton Corporation) it was decided to provide additional support to the unsupported excavation in the form of reinforcing bars driven into the excavation and a thin facing of sprayed concrete. No other significant deformation or fallouts occurred in the temporary excavation for the duration of the contract.

Once the capping beam and columns had been formed and partially back-filled, 100m length of the fibre optic cable was exposed, lifted and relayed behind the new wall by Alstom (Telecom's cabling contractor).

7. CARRIAGEWAY REGRADING

The carriageway formation works involved adjusting finished carriageway levels by up to 600mm and moving the carriageway sideways for the formation of basecourse and sub-base layers.

Pavement layers varied between founding on highly weathered rock and loose fill/colluvium material. Areas of unsuitable material were locally excavated and replaced including a significant section in the vicinity of the existing tomo which had internally eroded existing carriageway sub-grade layers.

8. CONCLUSIONS AND LESSONS LEARNED

The realignment and stabilisation of Makara Road is an interesting case study due to the applications of various elements of civil and geotechnical engineering in a situation with significant pressure for prompt results and challenging site characteristics.

Throughout the duration of the project a variety of engineering skills were used including;.

- Geotechnical investigation and risk assessment of the existing railway iron wall
- Slope stability analysis and earth embankment design
- Geological logging and stereo-nets analysis.
- Stormwater control and flood regime modelling
- Palisade wall design retaining 6.7m of loose fill and colluvium with concrete piles and high strength ground anchors
- Geometric pavement design and assessment of sub-grade material suitability.
- Onsite crack monitoring, traffic management and implementation of temporary stability measures.

Managerial pressures on the contract included;

- Pressure to provide prompt, cost effective solutions.
- Separating the works into three contracts to minimise consenting, tendering and design periods and optimising construction costs.
- Sequential design of contract works while construction on previous phases was only partially complete requiring consistent, accurate, complete and flexible designs.
- Supervising and liaising with three separate Contractors on one site.

Site specific challenges complicating the contract works were;

- Complex traffic management
- Telecom's fibre optic cable requiring solutions to protect our client and successfully deal with the cable in a safe realistic manner.
- Liaising with property owners and providing solutions that suited their needs.

The variety of engineering, managerial and site specific challenges made the project interesting and rewarding to work on

Mechanically Stabilised Embankment Construction Te Awa Recreational Reserve Pedestrian Access

David J Morton (BSc MSc (Tech) Hons)
Mark T Mitchell Ltd - Consulting Geotechnical Engineers

Waikato District Council required the construction of a pedestrian access formation extending 20 metres in elevation from an alluvial pumice-dominated terrace formation down to the Waikato Rivers edge. Soil and slope conditions were indicative of a marginally stable escarpment formation, which was confirmed by specific slope stability analyses. Access requirements and a limited budget narrowed construction design options considerably. A multi-level Mechanically Stabilised Embankment (MSE) retaining option was chosen for the site due to its relatively low-cost and flexible nature but most importantly for its construction practicalities. Construction challenges necessitated a review of slope failure mechanisms and subsequent construction procedures. Utilisation of the tensile strength characteristics of the MSE construction units (geogrids) provided a stable construction platform that allowed the contractor to complete the access formation to the client's requirements with an aesthetic 'green' design finish blending the formation in with the surrounding recreational reserve environment.

1 INTRODUCTION

Mark T Mitchell Ltd, Consulting Geotechnical and Environmental Engineers were commissioned by Waikato District Council in April 2001 to design and inspect the construction of a pedestrian access formation extending from an elevated terrace formation down to the Waikato Rivers edge located 20 metres below.

The access formation was considered a necessity by Waikato District Council to provide a readily accessible recreational reserve facility within an exclusive rural-residential development area where high annual rate charges have been imposed.

Development of a design concept for the project was particularly challenging due to the presence of a steep-faced escarpment in combination with significant depths of very loose granular (pumice) soils. The escarpment was marginally stable and susceptible to erosion.

The recreational reserve is to contain aesthitically landscaped gardens and lawn areas together with a jetty extending out into the Waikato River. In time, the reserve will form an integral part of the Waikato District Councils planned rivers edge pedestrian walkway.

The access formation was to be of a sufficient slope gradient to permit wheel chair access (maximum 1:8) and of a suitable width to allow the passage of a ride-on lawnmower for maintenance of the lower reserve area.

Council also advised that the utilisation of available low-skill labour (ie, task force green workers) was desirable if possible in the construction of the access formation.

2 GEOLOGICAL SETTING

The subject site is situated between two developed rural-residential properties on Te Awa Road, itself located approximately 10 kilometres to the south of Hamilton City within the rural settlement of Tamahere.

2.1 Regional Geology

The regional topography is dominated by the presence of a gently undulating alluvial terrace formation, which within the Tamahere District, is elevated 30 to 40 metres above the general Waikato River level. The alluvial deposit is termed the Hinuera Geological Formation, forming the infill deposit of the Hamilton Basin.

Published geological information by Kear and Schofield (1) identifies the Hinuera Formation as consisting of mainly rhyolitic, current bedded sands and gravels interbedded with peats and pumiceous silts and sands. Hinuera sediments originate from the central North Island Region after the Waikato River broke into the Hamilton Basin resulting in deposition of an alluvial fan.

Two main periods of sedimentation have been identified, the first dating slightly more than 20,000 years ago with the second between 12,000 and 16,000 years ago, Schofield (2). Following the main period of deposition, the Waikato River and tributaries have become more channeled having cut down into the Hinuera sediments.

Aggradation then followed during more recent volcanic activity within the Taupo Volcanic Zone some 1,800 years ago, Kear and Schofield (1). The resulting Taupo Pumice Alluvium is commonly encountered within the

Waikato Basin being restricted in distribution to alongside the margins of the present river course.

Fluctuating perched water tables are common within the Hinuera deposits during the wetter winter months where fine-grained silt lenses are present.

2.2 Local Geology

Along the margins of the entrenched Waikato River channel, the regional terrace formation steps down successively in a series of near-level benches.

The benches were formed following the main period of Hinuera deposition, where the Waikato River became more channelled and began eroding into the Hinuera deposits lowering the level of the river. Each successive lowering of the river level is represented by a single bench or terrace formation, which continued downcutting through the Taupo Pumice Alluvium sediments.

The benches are separated by natural escarpments that vary in gradient from 26 degrees (1:2) to 45 degrees (1:1) to the horizontal. The gradients encountered being dependent on soil lithologies, historical groundwater fluctuations and vegetation cover.

The project site is situated over one of these natural escarpment formations.

3 GLOBAL STABILITY CONSIDERATIONS

3.1 Slope Configuration

The pedestrian access required traversing down a steep river escarpment separating two successive alluvial terrace formations. Slope gradients are inclined at gradients of between 26 (1:2) and 38 (1:1.3) degrees to the horizontal.

Typical cross sections surveyed through the escarpment are presented in Figure 1.

The cross sections show the terrace to be elevated above the adjacent Waikato River level (as measured on 6 December 2001) by some 20 metres. A further narrow terrace level, elevated between 5 and 6 metres above the measured river elevation, buttresses the upper steep escarpment, representing the most recent of alluvial deposition associated with the river course.

3.2 Soil Conditions

Initial geotechnical investigations revealed the presence of fine to medium-grained sands and pumiceous sands extending to depths of between 2.0 and 2.5 metres below the original ground slope surface. Scala Penetrometer probes identified these soils as being classified as very loose to loose, Read et al (3).

Below that depth, a distinct transition in soil fabric and density was observed with the underlying materials consisting of fine to coarse-grained sands and pumice gravels typical of the Taupo Pumice Alluvium. These soils were classified as being medium dense to dense to beyond 4.0-metres depth.

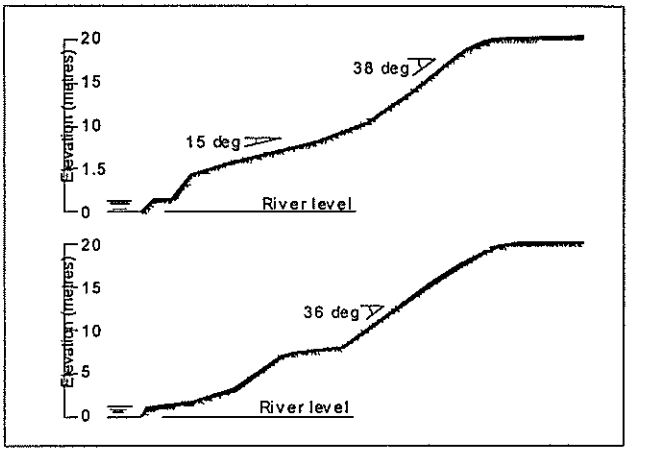

Figure 1: Typical Escarpment Cross Sections

These soil conditions were found to be typical of the full escarpment height with no observable silt lenses being present. Accordingly, groundwater elevations remain depressed at the regional water table level, which responds to nearby river level fluctuations.

3.3 Review of Slope Performance

Evidence of relatively large-scale relic slope movements was identified at the subject site and adjacent properties in the form of old slip scarps. However, with the exception of the situation where man-induced disturbance has occurred, the continuation of such events in more recent times (during static conditions) is not evident in the general region.

The majority of the larger-scale land instability scarps were therefore considered having developed at times of initial groundwater stabilisation in response to falling river levels, or alternatively in conjunction with historical ground shaking events associated with tectonic activity.

Over the steeper slope gradients, the ground surface was observed to be notably hummocky being indicative of continuing downslope soil creep and shallow-seated slide movements within the near surface soil layers. That observation was consistent with the loose near-surface soil conditions encountered.

3.4 Adoption of Soil Design Parameters

Based on the observed performance of the present site slopes together with a review of slope configurations and near-surface soil densities, these materials were considered being in only a marginal state of stability under both static and seismic design conditions.

The vegetative cover that has dominated the slopes over recent times was considered the only mechanism enabling the present slope gradients to be maintained.

The observed shallow sliding failure mechanisms were typical of cohesionless soils. Accordingly, a stability analysis model that was developed for the site assigned zero cohesion for a shallow surface layer. Present levels of slope failure activity at the site determined that the existing safety factor was slightly less than 1.0 for that simulated process.

More deep-seated failure patterns were observed as being rare in recent times (under static and depressed groundwater conditions). The potential for penetration of failure arcs below the more dense sand and gravel layers was therefore considered low requiring the adoption of high design parameters for the more dense soils.

The following soil parameters were adopted for the initial stability analyses:

Soil Layer 1:	Cohesion (c)	0 kPa
	Angle of friction (ϕ)	33°
	Unit weight (γ)	17 kN/m^3
Soil Layer 2:	Cohesion (c)	2 kPa
	Angle of friction (ϕ)	35°
	Unit weight (γ)	17 kN/m^3

3.5 Review of Stability Model Analysis

Verification of the soil design parameters that were adopted was carried out by comparing the practicality of results obtained in relation to observed slope failure mechanisms described above.

Analyses were conducted using the 'Macstars' software package, which adopts the Limit Equilibrium (Bishop) Method of Slices analysis technique.

Results of a number of failure arcs (simulated through the critical slope area) obtained from the analyses are illustrated in Figure 2.

The results obtained were considered representative of on-site conditions with the soil design parameters therefore considered representative.

In simulating a seismic horizontal acceleration effect, resulting slope failure arc factors of safety reduced to around 70 % of the static values (between 0.67 and 1.02).

Extreme flood level data obtained for the Waikato River indicated that the critical steeper slopes were not at threat of toe inundation and associated stability reduction.

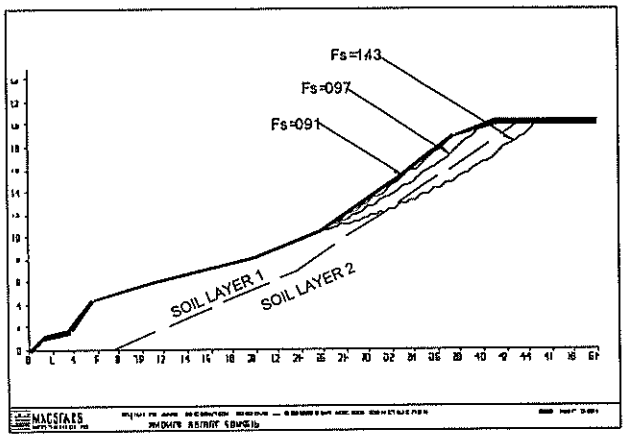

Figure 2: Critical Slope Stability Safety Factors (Static Case)

4 CONSIDERATION OF DESIGN OPTIONS

A number of design options were considered for the site taking into account soil and slope restrictions in conjunction with client requirements. Each of the options considered are described below with a review of preliminary alternative design considerations presented in Figure 3.

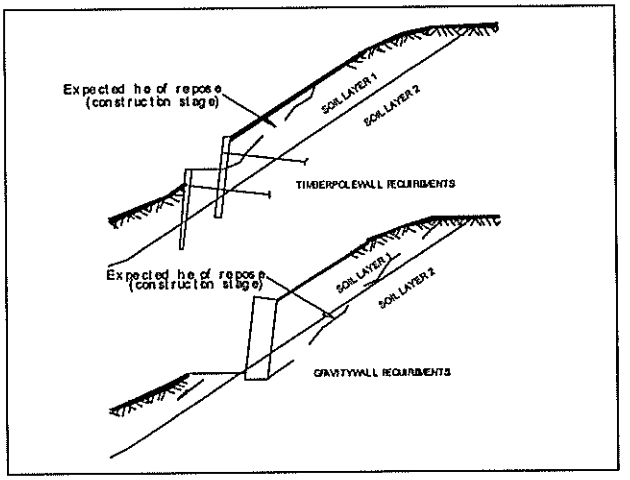

Figure 3: Design Restrictions

4.1 Gravity Wall

The adoption of a gravity wall structure, such as gabion baskets or crib walls relies on relatively high soil bearing capacity due to their limited base areas.

That requirement would necessitate a single large excavation that intercepted the dense sand and gravel soils at depth. However, the soil and slope characteristics at the site introduced construction difficulties for that option due to expected large construction-induced slide failures and costly backfilling operations.

The single gravity wall option satisfies only upslope stability considerations. Settlement and continued sliding of soils located below the outer edge of the access formation is still likely to continue without the installation of further reinforcement in that area.

Additionally, steep slope gradients behind the wall required the adoption of large retaining members at relatively high cost.

4.2 Timber Pole Wall

The geotechnical and environmental restrictions at the site lead to the consideration of a dual timber wall system that would provide a reduction in excavation depths and the magnitude of potential construction-related slope failures.

However, the mobile nature of the near-surface soils would have required excessive foundation and pole lengths to provide adequate bearing capacity. Additionally, the lack of any lateral soil resistance against a cantilever pole wall would require extensive horizontal anchorage support.

The cost for construction of a dual timber retaining wall system to meet these objectives was considered, in relative terms, excessive for the project.

4.3 Concrete Block Wall

Steel-reinforced (cantilever) concrete retaining construction provides high bearing pressure at the foundation toe where excavation depths are shallow and the ground unstable. The design option would therefore require foundation burial depth and associated larger excavation heights.

Costs associated with concrete wall construction to the required height plus the additional steep slope gradients behind the wall also rendered this design option particularly expensive.

4.4 Mechanically Stabilised Embankment (MSE)

A Mechanically Stabilised Embankment (MSE) or Geosynthetic-Reinforced Soil (GRS) retaining structure was also considered for the site.

This design option provides a flexible structure that is more tolerant of small ground movements or settlements than other rigid structures. Additionally, the structure contains a large base surface area over which to distribute loads to the supporting soil and provide resistance against lateral movement.

The construction materials are relatively cheap and easy to handle with the geometry of the retaining structure able to be manipulated to suit the site conditions.

5 DESIGN SELECTION

5.1 Design Justification

Geotechnical and environmental site restrictions required the adoption of a multi-level retaining option to minimise excavation depths and associated construction-related slope instability.

Mechanically Stabilised Embankments (MSE) were chosen for the site due to their relatively low-cost and flexible nature allowing the more widespread distribution of foundation loads. MSE construction was also considered superior for its construction practicalities and ability to utilise low-skill labour, such as task force green workers.

The escarpment over which the access formation was to be constructed was determined to be in a critical state of stability. The prevention of global slope movements by the access formation construction under seismic conditions was considered lying beyond the scope of the project. A key aspect of the design was to therefore provide some form of compromise between construction practicalities and slope reinforcement. The flexible nature of MSE construction was considered being more tolerant of potential ground movements than other 'hard' design options.

The 'soft' engineering solution or 'green' design finish provided by MSE construction was considered by the client as an added bonus due to its location.

5.2 Technology History

In terms of earth retaining, MSE technology is a comparatively new technique with its numerous benefits resulting in its application becoming increasingly more widespread throughout the world.

Reinforced earth was first studied by Lee et al. (4) in 1973 using metallic strips and then applied to geotextile and later geogrid materials. The publication of an American national guideline in 1991 (AASHTO Bridge Design Specifications) quickly resulted in more widespread design use, Schaefer (5).

In New Zealand, software packages originating from various offshore sources have been provided by local supply representatives and have been in use for a number of years. More recently, a set of preliminary design guidelines was provided within a Transfund commissioned Review and Discussion paper (Transfund NZ Research Report No. 123), released in 1998. Further work in 1999-2000 resulted in the preparation of draft comprehensive guidelines for design and construction of GRS structures (Transfund NZ Research Report No 194).

5.3 Technology Review

All soils have some form of compressive and tensile strength characteristic, which is related to their fabric and density/shear strength. However, most soil materials provide very little or no resistance to tensile stress.

The mechanical properties of a reinforced soil mass are dramatically improved by the placement of a tensile-resistant material (geogrid) parallel to the principal stress direction.

The improved tensile properties of the reinforced soil mass are a result of the interaction between the soil and the reinforcement material.

The requirements of each reinforcement layer are determined by lateral earth pressure theory with the most common method adopting the tie-back wedge analysis. That method assumes an active wedge of soil located outside a line drawn at $45° + \phi/2$ from the toe of the embankment.

The length and spacing of each reinforcement layer, to provide adequate shear resistance against the active wedge failing, is calculated in terms of pullout resistance and direct shear resistance.

The dynamic performance of MSE generally exceeds that of conventional retaining walls due largely to their flexible nature. Murashev (6) reports that studies of numerous MSE structures were carried out following the Kobe earthquake with no significant damage reported.

6 INTERNAL STABILITY CONSIDERATIONS

The internal stability requirements of the MSE walls were obtained using the software package TENAX Slope 3.02 – Reinforced soil slope design program.

The software package stipulates the required geogrid lengths and spacings based on a set of design parameters specified by the user. The input parameters include information on the MSE configuration, soil and pore water pressures, surcharge loading and numerous design safety factors.

It is not the intention of this paper to go into great detail explaining the justification of safety factors adopted and other design input parameters. For a more thorough discussion of these aspects, reference should be made to the preliminary New Zealand design guideline document prepared by Murashev, 1998(6).

Analysis of the programs generated outputs determined that the required reinforcement lengths were dependent on the effective height of the structure and soil friction angle. The spacing of the reinforcement layers was largely determined by the active earth pressure coefficient (Ka) specified by the user. For this project, Ka values were high due to the steeply inclined slope gradient behind the stabilised embankment.

A review of seismic design requirements was carried out in accordance with the AASHTO (USA) design method, which is outlined by Murashev(6).

7 EXTERNAL STABILITY CONSIDERATIONS

The following failure modes were checked as part of the external stability analysis:

a. Forward sliding
b. Overturning
c. Bearing Capacity
d. Deep seated failure

The potential for forward sliding of the stabilised earth mass is determined by the length of the reinforcement layers and forms part of the design software analysis.

It follows that the potential for overturning of the reinforced block is very low due to its geometry and flexibility. Simulating slope stability failure arcs from the reinforced block toe verifies that assumption.

Bearing capacity requirements are significantly reduced for MSE construction due to the distribution of loads provided by the geogrid base layer and flexible nature of the structure. However, it is noted that a compacted metal base was stipulated in the design due to the particularly loose nature of the soils underlying the structure.

The potential for deep-seated failure implications is discussed more fully in Section 3 of this paper. The scope of the project did not warrant the consideration of preventing global instability of the natural escarpment by

MSE construction. However, it was important that the present level of instability was not jeopardised by removing lower slope toe buttress support or conversely increasing upper slope mobilising earth mass to the embankment. Subsequently, net mass changes (in cross section area) were avoided.

The resulting access design details that were adopted for its construction, taking into account internal and external design considerations are presented in Figure 4.

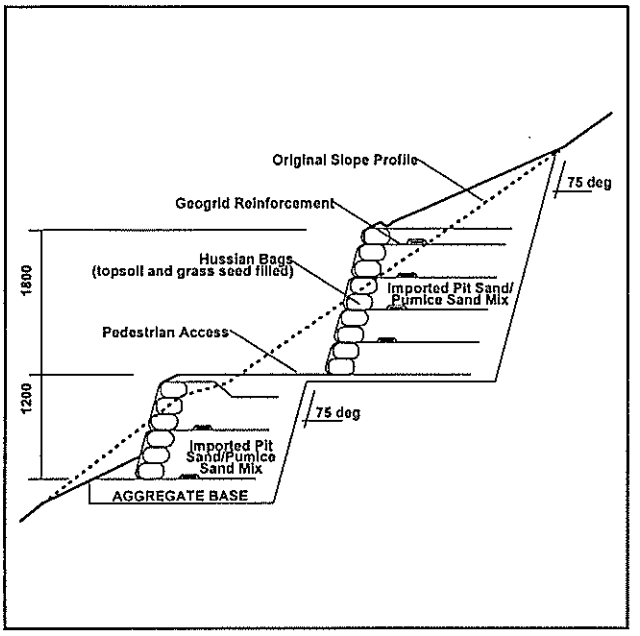

Figure 4: Construction Design Details

The design utilises a wrap-around face detail, which is formed from the placement of hussian bags filled with a topsoil, sand and grass seed mixture. The purpose of the bags was to provide temporary formwork for construction of the embankment and to provide a medium in which the final grassed face could become established.

The hussian bags will deteriorate with time, which necessitates the placement of an erosion control mat inside the wrapped geogrid facing to prevent soil spilling out of the embankment face in the future.

8 CONSTRUCTION IMPLICATIONS

The contract documentation was issued on 13 June 2001, outlining material and procedure specifications.

The recommended procedure adopted a two-stage construction sequence. The purpose being to reduce excavation depths and the magnitude of expected construction-induced slope instability, as deduced from slope stability analyses.

The use of large self-supporting slope shoring measures was considered impractical due to access difficulties and confined working spaces. An alternative shoring method for the small cut faces (less than 2.5 metres) was suggested using waratah-anchored sheets of plywood.

An on-site pre-construction meeting was held between the client, contractor and designer in August 2001 to discuss the recommended construction sequence.

8.1 Construction Challenges

It was anticipated at the design stage that an initial access track be cut into the slope to allow bobcat machinery to service the lower slope area for spoil relocation.

However, excavations into the steeper escarpment slopes resulted in upslope ground failures following the mechanisms identified by previous slope stability analyses. An illustration of a typical failure is presented in Figure 5.

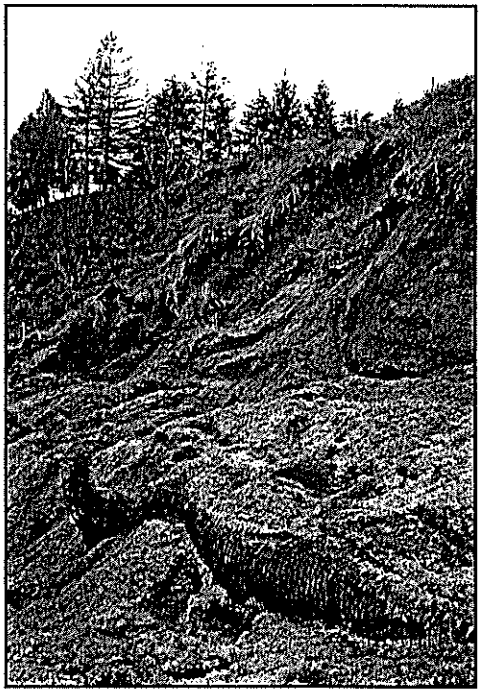

Figure 5: Typical Construction-Induced Slide Failure

Evidence of further sliding failures being generated immediately downslope of the working platform as a result of point loading created by earthworks machinery were also noted. The potential for that failure mechanism in conjunction with upslope ground movements resulted in the construction being abandoned.

In addition to the obvious construction difficulties created by soils cascading across the working platform, these failures were of a sufficient magnitude to cause safety concerns to the contractor.

One of the larger failures resulted in the temporary machinery access construction being reconsidered with a review of the MSE construction sequence carried out to determine a safe and practical methodology.

8.2 Construction Solutions

The construction sequence was further fine tuned by the designers with a site meeting held to demonstrate its applicability.

The process involved the progressive stepped construction of the lower wall in short 4.0-metre sections, being equivalent to the reach of a small 2-tonne excavator.

The first section was constructed to the initial geogrid wrap height only (ie. 600mm) and a minimum of 200mm of granular backfill placed over the wrapped geogrid length to create a stable working platform. The excavator was then positioned over the partially completed wall and the next section excavated to the design depth. The efficiency of the geogrid reinforcement to withstand high point loads was highlighted with no observable deformation at the wall face observed during this procedure.

The process was repeated along the wall alignment with a high rate of efficiency achieved. The resulting stepped construction procedure is illustrated in Figure 6.

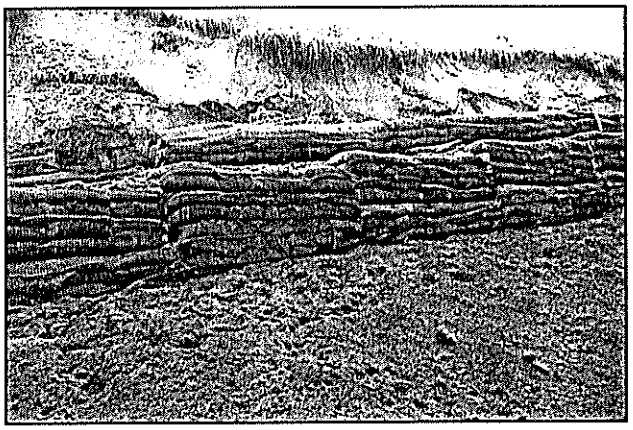

Figure 6: Stepped Construction of Lower MSE

Once the stable platform had been created, the upper wall construction progressed in short time with the access formation completed in mid September 2001.

Vegetation establishment was rapid and is illustrated in Figure 7, taken some 3 months following construction.

Figure 7: Final MSE Construction showing Vegetation Establishment

9 CONCLUSIONS

Challenging geotechnical and environmental site restrictions combined with low budgetary requirements and adoption of low-skill labour introduced a particularly limited scope for design and construction of a pedestrian access formation.

Following a review of possible alternatives, MSE construction was chosen as the only practical construction solution that met both geotechnical and client demands.

Detailed external stability analyses adopting a simplified slope stability model were carried out. Results of those studies determined that complete stabilisation of the marginally stable escarpment by MSE construction (for seismic-induced deep-seated failure mechanism) was not warranted by the scope of the project. Construction was therefore designed to meet all other stability and construction requirements and avoid any net mass alternations to the original slope.

Commencement of construction activities encountered significant difficulties in the form of construction-induced slide failures of the original marginally stable escarpment formation. Threats to worker safety resulted in the construction project being abandoned for a time pending discussions with the project designers to overcome construction difficulties.

Construction solutions involved a progressive stepped construction sequence that utilised the tensile strength characteristics of the MSE construction units (geogrids) to provide a stable working platform.

As a result of the adopted construction sequence, it was considered that the use of geogrids was the only possible construction technique available. The MSE construction turned out to be even more cost effective than initially expected due to it utilisation in both the construction phase and as a final mechanical reinforcement material.

The pedestrian access formation was completed on budget to geotechnical, environmental and client requirements.

10 REFERENCES

1. KEAR, DAVID and SCHOFIELD, J.C., "Geological Map of New Zealand Sheet N65 – Hamilton", Department of Scientific and Industrial Research, 1965).

2. SCHOFIELD, J.C., "The Hinuera Formation and Associated Quaternary Events", N.Z. J. Geol. Geophys. 8: 772-791, 1965.

3. READ, P.J., MILLAR, P.J., LUXFORD, N.S. and OLSEN, A.J., "Guidelines for the Field Description of Soils and Rocks in Engineering Use", New Zealand Geomechanics Society, November 1998.

4. LEE, K.L., ADAMS, B.D. and VAGNERON, J.M.J., "Reinforced Earth Retaining Walls", J Soil Mech Fdtn Eng Div, ASCE, No. SM10: 745-764, 1973.

5. SCHAFER, V.R., "Ground Improvement; Ground Reinforcement; Ground Treatment Developments 1987-1997", American Society of Civil Engineers, Geotechnical Special Publication No. 69, July 1997.

6. MURASHEV, A.K., "Design & Construction of Geosynthetic-Reinforced Soil Structures in New Zealand: Review and Discussion Paper", Transfund New Zealand Research Report No. 123. 110pp.

The Influence of Clay Infill on the Shear Behaviour of a Rock Mass

Mathias Nagy[1] and Buddhima Indraratna[2]
[1]PhD Student, [2]Professor
Faculty of Engineering, University of Wollongong, NSW, Australia

It has become well known in the field of rock mechanics that a rock mass can fail in many different circumstances under varying load conditions, whether near the surface of the Earth or deeper underground. The failure of a rock mass generally involves mechanical slip, which is governed primarily by the shear strength of the joints within a rock mass. Research conducted by members of the University of Wollongong upon the influence of clay infill on bolted and unbolted joint shear strength has extended the current knowledge of rock mass behaviour. The results of the research are reported upon here and have been extended to include the preliminary findings of current research being conducted into the influence of pore pressure upon the shear behaviour of an infilled rock joint.

1 INTRODUCTION

The correct evaluation of the shear strength of rock joints plays an important role in the design of rock-socketed piles, excavations in rock (such as tunnelling and mining) and the stability analysis of rock slopes. Its evaluation is far from a perfect science due to the difficulty of understanding all the complex variables that affect a mass of rock in its natural state. This difficulty increases rapidly as a greater volume of rock mass is being considered.

The difficulty in understanding the behaviour of a rock mass arises when one realises that a rock mass is not a simple elastic material, but rather a heterogeneous, deformable, discontinuous material that exists naturally in a pre-existing anisotropic stress field. Its properties can vary widely, depending upon the type of rock material(s) and degree of jointing within the rock mass. This wide variation of properties can occur broadly over a region of the same rock type (e.g. within a region of contact metamorphic rock) or instantaneously between regions of two different rock types (e.g. across a bedding plane).

A discontinuous rock mass is often broken up by a regular set of *joints*, which rarely changes the volume of the rock mass but will reduce the rock mass strength overall. As a rock joint has significantly lower shear strength than the rock material itself (in most cases), its shear strength will often govern many of the failure mechanisms of the rock mass. Thus the shear strength of a rock joint is of obvious practical interest and can be investigated in the laboratory.

From the literature over the last several decades, the relevant experimental variables that have been ascertained for this type of investigation are summarised as follows:

- Joints: artificial or natural
- Joint surface: planar or rough (i.e. is the surface profile flat or irregular)
- Testing conditions: constant normal load (CNL) or constant normal stiffness (CNS)
- Infill: present or not present

Natural joints, by their nature, have unpredictable and random properties such as surface profile and infill degree and type. Artificial joints are produced in the laboratory so that parameters such as surface profile and infill can be controlled. The disadvantage of using artificial joints is that the effectiveness of the sample to model a real joint is reduced, as it becomes an idealised representation of a rock joint that is unlikely to occur in nature. The advantage of the artificial joint is that the results obtained from these controlled experiments form the basis of empirical equations that are used to model the experimental joint behaviour and will hopefully extend to the behaviour of a natural rock joint as well.

The joint surface profile is an important consideration since it is now known that the increasing roughness and unevenness of a joint contributes toward increased joint shear strength as a result of interlocking *asperities*. Asperities are the facial features of opposing rock faces and their mechanical behaviour is determined by the rock material properties. In the event of the shear motion of a rock joint, it is the rock asperities that directly govern the shear behaviour. If the asperities are hard and resilient, or soft but under low confinement, the opposing asperities will eventually ride over each other when displaced in shear, often requiring the deformation or dilation of the asperities and the host rock mass to accommodate the motion. If normal confinement does not allow for dilation and the

asperities begin to fail (i.e., shear off at the base) under shear, the asperities' frictional contribution will have been lost and will further contribute to the loss of shear strength of the joint by becoming infill.

If the entire volume of the rock is displaced above the joint, the shear motion could be said to be operating under Constant Normal Load (CNL) conditions. If the rock mass is required to deform to accommodate the riding asperities, then the shear motion could be said to be operating under Constant Normal Stiffness (CNS) conditions. The importance of these testing conditions is discussed in the next section.

2 CNL AND CNS TESTING CONDITIONS

In much of the literature investigating the shear behaviour of a rock mass, testing has been conducted under conditions of *Constant Normal Load* (or *CNL*). An important characteristic of the experiments conducted at the University of Wollongong has been the use of *Constant Normal Stiffness* (*CNS*), rather than Constant Normal Load, testing conditions.

CNL, as its name suggests, represents a testing regime where the load applied normally to a sample is maintained at a constant value. This has been found to be representative of:

- a "smooth", planar rock surface that is moderately constrained;
- a rough, planar rock surface that is so tightly constrained that the influence of roughness is minimal as the asperities shear away almost immediately;
- a smooth or rough, non-planar joint surface in which the upper surface is unconstrained and free to move upward and thus follow the undulations of the surface contact without deformation.

In testing of rough, natural and artificial rock joints under moderate (normal) confinement, research has shown that CNL significantly underestimates the resulting shear strength, making it inaccurate for practical purposes (Goodman [1]). On the other hand, CNS has proven itself to be a most accurate analytical technique in these circumstances (Indraratna [2]).

CNS testing is representative of many realistic engineering situations in which a rock mass' joints have rough surfaces and exists in a state of moderate normal confinement. In these circumstances, the shear motion of a joint surface requires normal dilation to occur as a result of the resistance of interfering asperities. As this normal dilation involves deformation of the host rock mass, this deformation will be resisted and result in an increase in the normal load applied to the joint. The change in normal load is proportional to the normal stiffness (K) of the joint and is calculated by (Lee and Harrison [3]):

$$\Delta N = K dy \qquad (1)$$

where:

ΔN	Change in normal load (N)
K	normal stiffness of the rock fracture (kN/mm)
dy	dilation (compression) of asperity (mm)

Normal stiffness has also been defined in the literature as the inverse of compliance (Herdocia [4]). Compliance has the unit mm/MPa making these stiffness units MPa/mm. Thus, the equation to calculate normal stress, σ_n, in terms of stress per unit dilation (i.e. "stress stiffness") becomes:

$$\sigma_n = \sigma_{no} + k\delta_v \qquad (2)$$

where,

σ_n	normal stress after dilation δ_v (MPa)
σ_{no}	initial normal stress (MPa)
k	normal stiffness (MPa/mm)
δ_v	dilation (mm)

The actual significance of the differing units of K and k may require further investigation, but at least it can be said that the versatility of stiffness allows for a CNS and CNL analysis of a rock mass to use either force quantities or stress quantities in its calculations.

3 EXPERIMENTAL BACKGROUND

Initial research into infilled joint behaviour at the University of Wollongong was conducted by Asadul Haque [5] and extended to include rock bolts by Ashitava Dey [6]. In both cases, the CNS shear box designed and built at UoW was used (Figure 1). The shear box applies the horizontal shear force via a hydraulic ram to a maximum of 120 kN and can apply a rate of displacement between 0.35 and 1.70 mm/min. The normal force is applied via a load cell to a maximum of 180 kN, through a spring system that delivers a simulated stiffness of 8.5kN/mm. This stiffness was found to be representative of the natural stiffness of coal measure rocks in the Illawarra region of New South Wales.

The unbolted, unfilled (i.e. clean) and infilled joint tests conducted by Haque [5] will be discussed first. A comprehensive series of tests under both CNL and CNS conditions were conducted on natural tension joints (obtained from Brazilian tests), natural field joints and artificial plaster joints made in the laboratory. The artificial joint material used

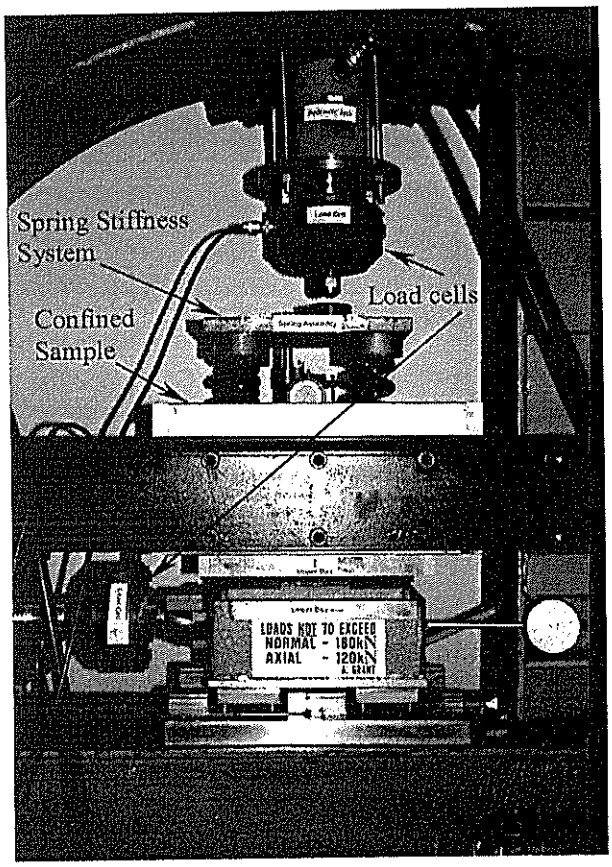

Figure 1. Main components of the CNS equipment

was a cured gypsum plaster, with the physical properties of uniaxial compressive strength σ_c = 11 – 13 MPa and Young's modulus E = 1.9 – 2.3 GPa. The tests were conducted on sawtooth samples of varying asperity heights, 2.5 mm, 5.0 mm and 7.5 mm, coinciding with individual asperity angles of i = 9.5°, 18.5° and 26.5° respectively.

The CNL tests were conducted without infill; the CNS tests were conducted both clean and with infilled clay layers of varying thickness. The material used for the infill clay was commercial bentonite, with the physical properties of water content w = 12.5% and peak friction angle ϕ_b = 35.5°, a similar value to the clays used in the literature (Phien-wej et. al. [7] and Suorineni and Tsidzi [8]). The complete series of tests is described as a flowchart in Figure 2. Note the number in the brackets is the number of individual tests conducted in each series.

In the literature, the shear displacement rate had been found to considerably affect soft joints under CNL conditions. Thus, a varying shear displacement rate was applied to unfilled joints under CNS to see if a similar influence was found. This investigation became the first series of experiments (Series I), conducted on artificial sawtooth joints (i = 18.5°). While not relevant to this investigation, it was found that the peak shear strength did rise significantly for a small increase in the shear displacement rate. Aside from this series, the remaining experiments were conducted at a constant shear displacement rate of 0.50 mm/min.

Varying the applied initial normal stress was the main impetus for the individual tests in a series, so that a strength envelope could be ascertained for clean and infilled joints. The initial normal stress in each test ranged between 0.56 MPa to 2.69 MPa for the clean tests and 0.16 MPa to 1.10 MPa for the infilled tests. Under the infilled CNS conditions, the variation in infill thickness was also accommodated to determine its influence on shear strength at each variation of initial normal stress.

Dey [6] extended this line of research by investigating (amongst other things) the impact of clay infill upon the shear strength of bolted artificial joints under CNS conditions. Again a cured plaster was used as the joint material, with the physical properties of uniaxial compressive strength σ_c = 18 – 22 MPa, tensile strength σ_t = 6.0 MPa and Young's modulus E = 7.3 GPa.

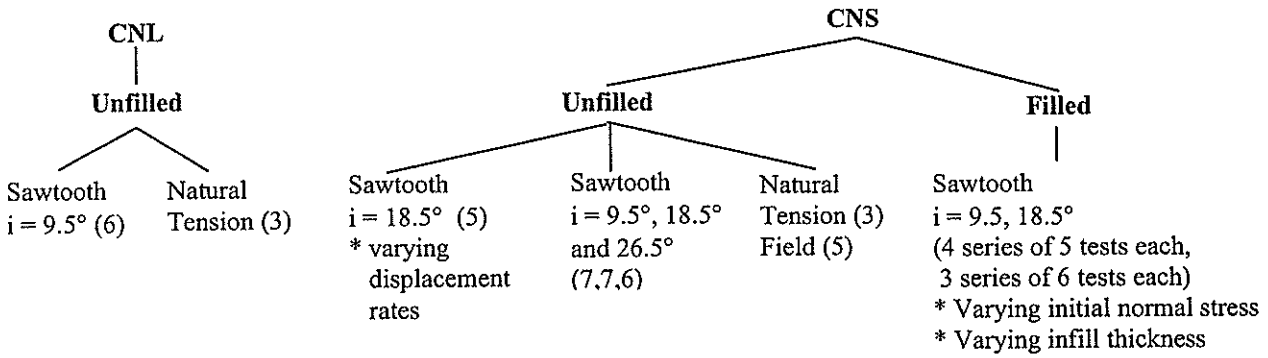

Figure 2. Summary of experiments conducted by Haque [5]

For use in the bolted tests, the properties of the hardened resin after three hours were σ_c = 76.5 MPa, σ_t = 13.5 MPa and E = 11.7 GPa. The tests were conducted on sawtooth samples using an asperity height of 5.0 mm, coinciding with an asperity angle of i = 18.5°. Both bolted and unbolted samples were tested for the purpose of comparison.

The experiments were conducted in two parts. Firstly, a series of tests were conducted on 'clean' and infilled non-bolted joints at an initial normal stress level ranging between 0.13 MPa and 3.25 MPa, respectively. Subsequently, another series of clean and infilled bolted joints were tested at the same initial normal stress level. The purpose of these two series of tests was firstly to determine the effect of the bolt on the shear strength of the joint and secondly to determine the strength envelope of clean and infilled, bolted and non-bolted joints.

The applied normal stress was limited to a maximum of 3.25 MPa due to the capacity of the CNS equipment. A constant strain rate of 0.5 mm/min was maintained for all the shear tests conducted. The stiffness of the system was again 8.5 kN/mm, obtained from the spring assembly located between the normal load cell and the top of the sample (Figure 1). In all cases, the mode of failure was observed after dismantling the apparatus after the test. The joint profile was mapped if warranted.

The filled tests used a thickness of the infill clay that increased incrementally from 1.5 mm to 7.5 mm in four steps, providing an infill thickness to asperity height ratio (t/a) of 0.3, 0.5, 1 and 1.5, respectively. Ordinary bricklaying clay was used as the infill material, as it is widely available and its composition can be varied depending on the testing requirements.

4 RESULTS AND DISCUSSION

The most relevant results of the experiments of Haque (Figures 3-6) and Dey (Figures 7-8) are presented here and overleaf.

Figure 3 is probably one of the most useful and interesting of all the graphs. It identifies the t/a critical ratio, t/a_{crit}, at which point the shear strength of the joint is no longer affected by interfering asperities, but rather is influenced by the clay layer alone.

Prior to a t/a of 1 or less, a horizontal displacement of around 10 mm is required to achieve peak shear strength. At this point asperities will begin to shear *or* the asperities will have reached their maximum normal dilation and begin to travel down the opposing asperity face, relieving normal stress and requiring less shear stress for the same shear displacement to occur.

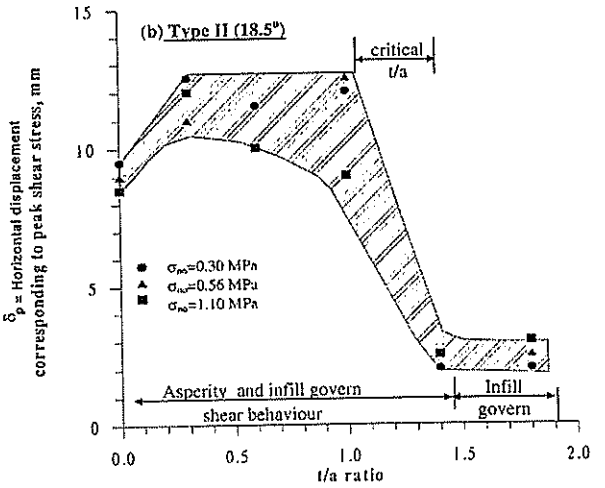

Figure 3. Horizontal displacement corresponding to peak shear stress vs. t/a ratio (Haque [5])

Above a t/a ratio of around 1.0, asperities stop interacting and the entire joint face begins to slide on the clay layer alone. Because riding of the asperities on a thicker clay layer occurs easy and quickly, achieving minimum shear strength at t/a ratios greater than t/a_{crit} will occur almost instantaneously, as identified in figure 3. "Infill govern" identifies the point at which the asperities no longer interact and the work of the system occurs entirely along a shear plane within the clay layer.

Whether an asperity shears or dilates will depend upon the strength and deformability of the host rock mass. In our case, our samples can be comparatively defined as a "soft" joint and will begin shearing at moderate levels of normal stress. It is quite possible that the clay layer in an in-situ joint is quite deformable, particularly in the presence of water, resulting in temporary joint shear strength even lower than the shear strength determined under these experimental conditions. Nonetheless, considering the small width of many joint sets found insitu, the research is still applicable to many practical engineering situations. At small joint widths, the clay itself does not need to be "mobilised" and is assumed to resist normal and shear forces almost immediately.

Both experiments were conducted with the artificial joint samples being laterally confined. The lateral confinement minimised the impact of free clay deformation, resulting in only minor losses at the ends of the sample, but not at the side. Free clay deformation was therefore kept to a minimum and was possibly only an influence in the experiments using the thicker clay layers.

The possible influence of free clay deformation can be noted in Figure 4, where an infill thickness of t = 9 mm always resulted in reducing (rather than increasing) normal shear stress as the test progressed. This would require negative dilation across the entire joint face, which could only occur as a result of a reduced volume (or thickness) of

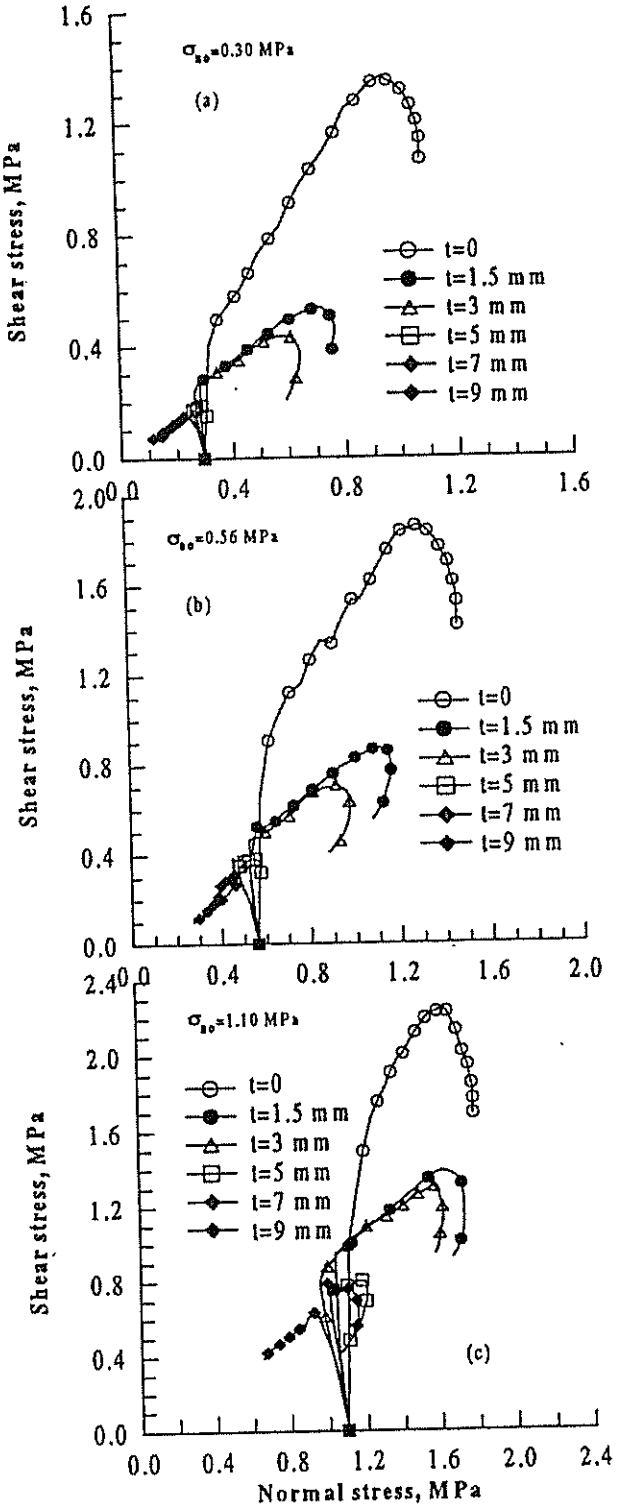

Figure 4. Shear stress vs. normal stress at varying infill thicknesses, for three levels of initial normal stress (Haque [5])

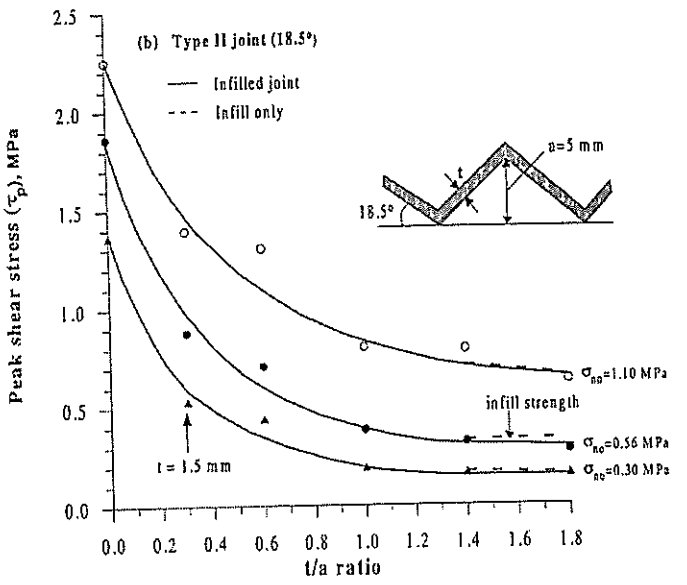

Figure 5. Peak shear stress vs. t/a ratio (Haque [5])

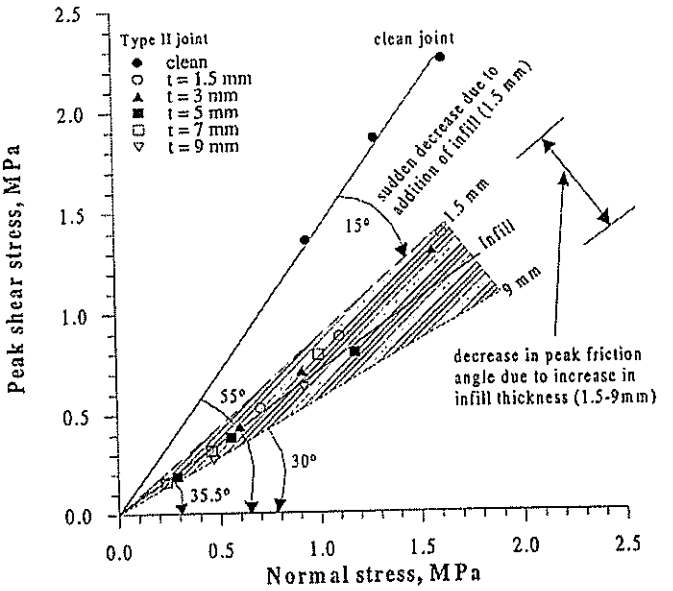

Figure 6. Infill influence on the joint friction angle (Haque [5])

the clay layer. This may also suggest that the t/a_{crit} value is lower than the experimentally determined 1.4, because relatively speaking, if the clay thickness is reducing as a result of significant volume losses at the edge of the system, then t/a would drop below the initial 1.4 as a result. Yet there is still no interaction of asperities as the normal stress continues to reduce, suggesting there is 'room to move' for the asperities and they still do not interact at the lower t/a value. Thus, while experimentally t/a_{crit} is known to be 1.4, the reasoning above may suggest that its true value is actually lower. It is a pity more experiments were

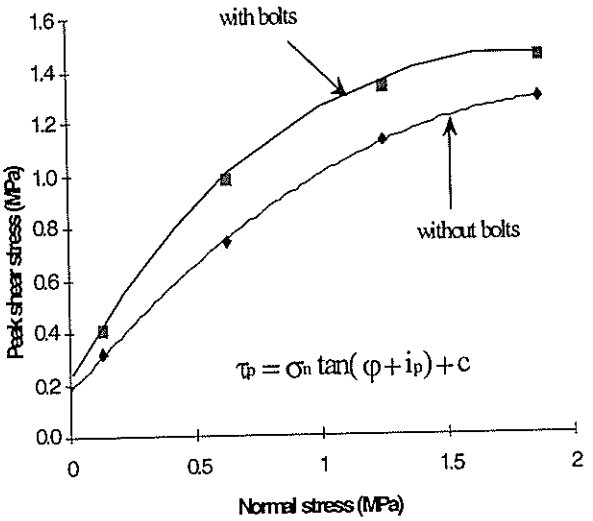

Figure 7: Shear strength envelopes of bolted and non-bolted joints at 2.5 mm infill. (Dey [6])

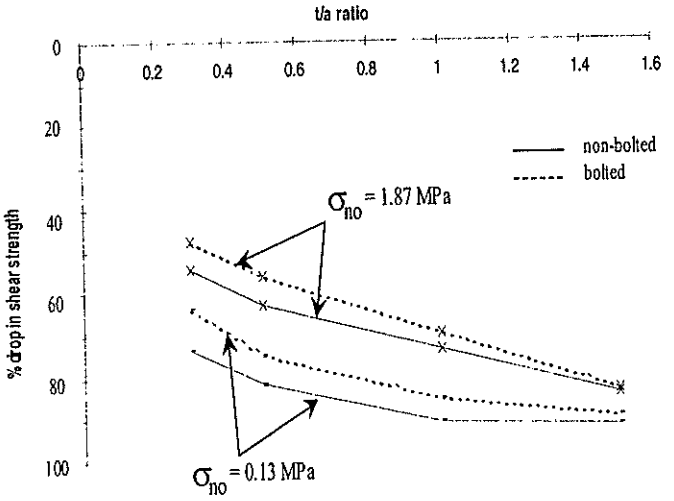

Figure 8: Variation of % drop in peak shear strength with infill thickness. (Dey [6])

not conducted on infill thicknesses that fell between 1.0 and 1.4.

Aside from the interesting normal stress behaviour shown at high infill thickness, Figure 4 also shows the reducing peak shear strength of the joint as infill thickness increases for a given initial normal stress level. Note that the shape of each infill curve remains similar across the three initial normal stress levels (Figures 4a, 4b and 4c). Finally, Figure 4 shows the expected trend of higher normal stress requiring greater shear strength to move the same horizontal displacement.

A steady drop in peak shear strength as the infill thickness increases is again seen in Figure 5. This is further reflected in Figure 8, which shows a similar trend for both bolted and unbolted artificial joints at two different initial normal stress levels. It is also interesting to note in Figure 8 that the influence of the bolt reduces at the higher normal stress level as the infill thickness increases.

Figure 6 identifies the influence of infill as an immediate drop in shear strength. The basic friction angle of the clean joint is ϕ_b = 55°, but under the influence of only 1.5 mm of clay infill, the basic friction angle of the joint becomes ϕ_b = 40°, which represents a substantial drop in joint shear strength of $\Delta\phi_b$ = 15°. At a thickness of t = 9 mm, it can be seen that the peak friction angle is lower than the basic friction angle of the clay infill itself, again suggesting that volume reduction rather than failure along a shear plane is occurring at this point.

Figure 7 from Dey [6] shows the strength envelope of a bolted and unbolted joint at an infill of 2.5 mm.

The contribution of a bolt to the system showed a similar curve but with a moderate increase in shear strength, as would be expected. Interestingly, Dey's data show a curvilinear strength envelope, while the standard relationship stated in the diagram is actually a linear one.

In the field, the graph with probably the most practical application is Figure 5. In fact, Haque [5] developed a hyperbolic relationship to model the reduction in peak shear strength as a result of infill in the joint, as follows:

$$\frac{\Delta\tau}{\sigma_{no}} = \frac{t/a}{\alpha(t/a)+\beta} \qquad (3)$$

The LHS of the equation is known as the *Normalised Strength Drop* and α and β are experimentally derived constants based on initial normal strength and surface roughness.

The shear strength of a infilled joint under CNS conditions can now be estimated using the following equation, if one knows the t/a ratio, the (initial) normal stress and unfilled shear strength of the joint:

$$\tau_{infilled} = \tau_{unfilled} - \Delta\tau \qquad (4)$$

This allows for the shear strength of a rock joint of any infill thickness to be determined.

5 CURRENT AND FUTURE RESEARCH

The influence of groundwater in a rock mass has received fair investigation in the literature, but little

has been written in relation to the influence of pore pressure upon the shear behaviour of a rock joint. The only literature of minor relevance the authors are aware of is in relation to the shear behaviour of a wetted rock joint, found in Hassani & Scoble [9], which states that a wetted rock joint has its basic angle of friction reduced by 5% - 10%.

Within the clay infill, the *pore pressure* is an essential mechanical parameter. Many analytical techniques of soil mechanics are based on effective stresses (Terzaghi [10]), or:

$$\sigma' = \sigma - u \qquad (5)$$

where,

σ'	effective stress (MPa)
σ	overall stress acting upon soil skeleton (MPa)
u	pore pressure (MPa)

The application of the effective stress concept to rock mechanics is, unfortunately, not as simple as in soil mechanics. A soil is composed of discrete particles with a significant space around them. Water can fill these spaces, often under pressure, so that the impact of the normal stress applied to the overall soil skeleton is reduced.

In rock mechanics, though, the flow rate of water through the rock material is often several orders of magnitude lower than the flow rate of water around the individual rock blocks that comprise the rock mass system. Therefore, the majority of water flow in a rock mass will occur through the rock joints and other discontinuities. This makes the development of a global effective stress model for a rock mass, integrating joint and matrix pore pressure, much more difficult to achieve.

While the influence of pore pressure within a rock joint has been (slightly) investigated in the literature, the influence of pore pressure on the shear behaviour of a rock joint/rock mass has not (as far as the author is aware), motivating the current research in this area at the University of Wollongong. Preliminary research has monitored the pore pressure within a sliding rock joint infilled with saturated clay. The results have indicated that pore pressure does build up initially as the clay consolidates in shear, but rapidly dissipates, eliminating its influence very quickly.

This rapid loss of pore pressure influence may be a result of voids opening up in the clay as it is being sheared, which may allow water to flow away from the contact region. This will result in less water (and therefore less pore pressure) within the contact area of the joint faces. Alternatively, the rapid dissipation of pore pressure may be the result of water being absorbed into the porous rock joint material itself, assisted by the high normal pressure the joint is being subject to. Finally, the results may simply be experimental error, as the pore pressure transducers were not designed for the environment they were applied to.

It is hoped that the pore pressure influence on the shear behaviour of a rock joint may be investigated successfully with our equipment after further modification and design, or through the use of new equipment if necessary. The authors are relying on the intimate and confined nature of water in clay to achieve this. The moisture content of the clay, from saturated to unsaturated conditions, may provide conditions conducive to pore pressure measurement, although the difficulty of measuring pore pressure in this environment has produced only internally consistent pore pressure results so far. Further investigation is hoped to result in a further detailed study of this area.

6 CONCLUSIONS

Where present in the joint(s) of a rock mass, infill will significantly reduce the shear strength of the joint(s), resulting in the reduced stability of the entire rock mass. Infill reduces the effectiveness of a rock bolt; it also changes analysis (of bolted or unbolted rock mass) from CNS to CNL conditions due to the single, smooth failure plane occurring in the clay after shear displacement. The normal stress change gets progressively smaller as the infill thickness increases, to the point where peak shear strength is at its lowest value and is achieved at the lowest shear displacement.

The ratio t/a is obtained by dividing the thickness of the clay layer by the mean asperity height and can be used to determine the current shear strength drop by a hyperbolic relationship (Equation 3). A t/a ratio greater than t/a_{crit}, which has been experimentally determined to lie between 1.0 and 1.4, is the point at which the shear strength of the joint is at its lowest value for any subsequent shear displacement. The friction angle ϕ of the joint at this point is likely to be that of the infill material. Thus a simple test to determine the friction angle of a sample of infill can be used to obtain the important parameter of the minimum peak shear strength of the joint system. The maximum shear strength of the joint system is obtained from a CNS shear test of a clean natural joint.

The influence of pore pressure in the infilled joint system may result in an initial 'impulse' of reduced shear strength. Over any significant displacement, though, the basic friction angle of the joint will rapidly increase back to that of the infill material itself as the system becomes dominated by the shear characteristics of the clay. Preliminary investigations tentatively suggest that pore pressure

will only have a significant impact on the shear behaviour of a rock joint over a very small shear displacement. Further experimental investigation is required to verify this contention.

7 ACKNOWLEDGEMENTS

The authors would like to thank the technical staff of the University of Wollongong (particularly Alan Grant) for their assistance in laboratory work, Dr. Haque and Dr. Dey for their previous PhD studies and data and the undergraduate student Matthew Brady for his work and assistance in pore pressure experimentation.

8 REFERENCES

1. Goodman, R. E., "Methods of Geological Engineering", West Publishing Company, 1976, 472p.
2. Indraratna, B. and Haque, A., "Shear Behaviour of Rock Joints", A. A. Balkema Publisher, Rotterdam, 2000, p. 17
3. Lee, S. D. and J. P. Harrison, Hydro-mechanical behaviour of a rock mass, Proc. 38th U.S. Rock Mechanics Symp., 2001, pp. 807-813.
4. Herdocia, A., Direct shear tests of artificial rock joints, Proc. Int. Symp. On Fundamentals of Rock Joints, 1985, pp. 123-132.
5. Haque, A., "Shear Behaviour of Soft Rock Joints Under Constant Normal Stiffness", PhD Thesis, University of Wollongong, 1999, 272 p.
6. Dey, A., "Shear Behaviour of Fully Grouted Bolts Under Constant Normal Stiffness Condition", PhD Thesis, University of Wollongong, 2000, 274 p.
7. Phien-wej, N., U.B. Shrestha, and G. Rantucci, Effect of infill thickness on shear behaviour of rock joints, *Rock Joints* (Barton & Stephansson eds.), A. A. Balkema Publisher, Rotterdam, 1990, pp. 289-294.
8. Suorineni, F. T. and Tsidzi, K. E. N., Geomechanical characteristics of a pulverised infilling material of a shear zone, *Rock Joints* (Barton & Stephansson, eds.), A. A. Balkema Publisher, Rotterdam, 1990, pp. 317-321.
9. Hassani, F. P. and Scoble, M. J., Frictional mechanisms and properties of rock discontinuities, Proc. Int. Symp. On Fundamentals of Rock Joints, 1985, pp. 185-196.
10. Terzaghi, K., "Theoretical Soil Mechanics", John Wiley, New York, 1963.

9 COPYRIGHT

A Piled Raft Foundation to Mitigate Liquefaction Induced Settlement of a Pipeline

Wataru Okada, Sinclair Knight Merz Ltd. (NZ)

This paper presents a case study of use of a piled raft foundation to prevent liquefaction induced settlement from causing damage to a continuous steel pipeline in a potentially liquefiable area. A power development is currently under construction in a reclaimed land near Dhaka, Bangladesh. The project site comprise a 7 m layer of reclamation fill underlain by inter-layered micaceous alluviums. Extensive ground investigations indicated that there was a potential for liquefaction of the in-situ alluvial sand and silt during strong ground motion. The cooling water discharge pipeline was to be constructed in an area where the potential for liquefaction had been identified. A piled raft foundation was the chosen method of mitigating adverse effects of the liquefaction-induced settlement. The methodology of liquefaction analysis and design of the piled raft foundation is presented in this paper.

1 INTRODUCTION

O'Rourke and Liu (1999) [1] provide accounts of some of the past earthquakes where liquefaction-induced ground deformation caused hundreds of breaks in various piping systems. Such damage to pipelines may result in an enormous economic loss to the society. For example, the trans-Ecuadorian pipeline was the largest single pipeline loss in history. It cost US$ 850 million in lost sales and reconstruction (O'Rourke and Liu, 1999, [1]).

In Bangladesh, a 450 MW combined cycle power plant is currently under construction in a reclaimed land. Ground investigations have identified a potential for soil liquefaction in the in situ alluvium unit underlying the reclamation fill. The main plant structure area had been improved by sand compaction piling so that the factor of safety against liquefaction is sufficiently high for the design earthquake of magnitude 6.

The cooling water discharge pipeline, in which cooling water is transported to the outfall structure in the nearby river, was to be constructed outside the improved ground. If this cooling water discharge pipeline incurs any substantial damage during an earthquake, the generation capacity of the power plant will be severely reduced, and this would result in huge sales loss. Moreover, reconstruction of the 3080 mm diameter pipeline, which is approximately 800 m in length, would be quite costly. Therefore some of mitigation measures was required to protect the cooling water discharge pipeline during the design earthquake. Following careful consideration of various techniques commonly used to mitigate liquefaction potential, it was decided that a piled foundation would provide the most cost effective and innovative design solution.

2 PROJECT SITE

The power development site is located adjacent to Meghna River, 20 km south of Dhaka, Bangladesh. Figure 1 shows the regional map of Bangladesh. Dhaka and Meghna River are shown in the centre of the figure.

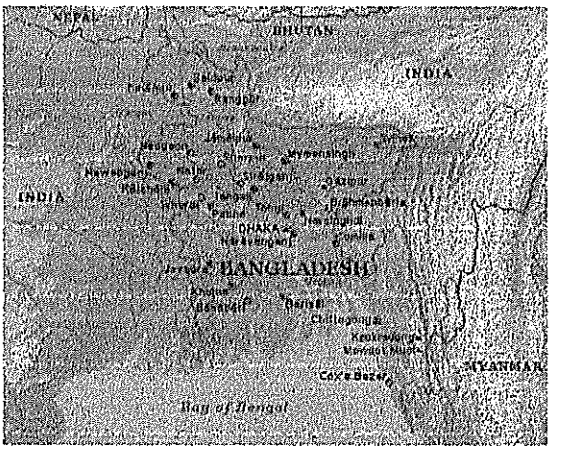

Figure 1: Regional Map (Stroop *et al.*, 2001 [2])

3 LOCAL GEOLOGY

The geology of Bangladesh consists primarily of Pleistocene to Holocene aged deltaic alluvial sediments, of thickness of about 180 m in the north-west and thickening to the south-east where the project site is located (Mollah, 1995) [3]. The sediments consist of an alternating sequence of sands and silts, the recent sediments

being predominantly flat bedded. Much of the sediments contain abundant quartz grains and a minor to moderate mica content. The minerals owe their origin to the predominantly schistose and quartzose rocks of the Himalayas. The upper sediments tend to be loose and normally consolidated, and together with the frequent occurrence of high groundwater level present a potential for liquefaction during earthquake ground motion. Large liquefaction events have occurred in the region in the recent past. (Sickling and Stroop, 2001) [4].

4 SITE CONDITIONS

4.1 Subsurface Conditions

The project site comprises a reclaimed land constructed on the in-situ alluviums. The reclamation fill, which has an approximately uniform thickness of 7 m across the site, consists of fine sand dredged from the adjacent Meghna River. Beneath the reclamation fill, there are inter-layers of fine to medium sand and silty sand. These alluviums become denser with increasing depth. The in-situ soils are characterized by a relatively high mica content. Recent ground investigations suggest that the mica content is as high as 5-10% on average. A potential for liquefaction has been identified in the inter-layered sand and silty sand between 7 m and 15 m below ground level, or in terms of the local Public Works Datum (PWD) +1 to –7 m. The top of the reclamation is PWD +8m. The subsurface conditions of the project site are summarised in the table below.

Geological Unit	Depth m PWD	Description
Reclamation Fill	+7.8 to +6.5	Medium dense, fine to medium sand, minor silt
	+6.5 to +2.0	Becomes very loose to loose
Top soil?/ Alluvium	+2.0 to 0.0	Soft silt, occasional loose silty sand, trace organic material
Alluvium	0.0 to -7.0	Loose to medium dense silty sand
	-7.0 to -20.0	Becomes medium dense
Older Alluvium	-20.0 to -29.0	Medium dense to dense silty sand
	-29.0 to -32.0	Firm to stiff, clayey silt

Table 1: Subsurface soil strata

4.2 Groundwater

Large seasonal fluctuations of the groundwater occur as the adjacent Meghna River level varies throughout the year. In 2000, the mean river level was approximately PWD +3 m.

5 LIQUEFACTION ASSESSMENT

The seismicity of Bangladesh is moderate to strong (Sickling and Stroop, 2001 [4]). For the purpose of liquefaction assessment of the site, a design earthquake of Richter scale magnitude 6 with a peak horizontal and vertical ground acceleration of 0.15g was specified by the client. The factor of safety against liquefaction was assessed from the CPT correlation method proposed by Seed and Idriss (1982) [5] and Youd and Idriss. (1997) [6]. Four CPT's were undertaken in the vicinity of the cooling water discharge pipeline. All of these CPT data were interpreted in the liquefaction assessment.

Figure 2 shows a plot of the correlated factors of safety versus depth obtained from the vicinity of the cooling water discharge pipeline.

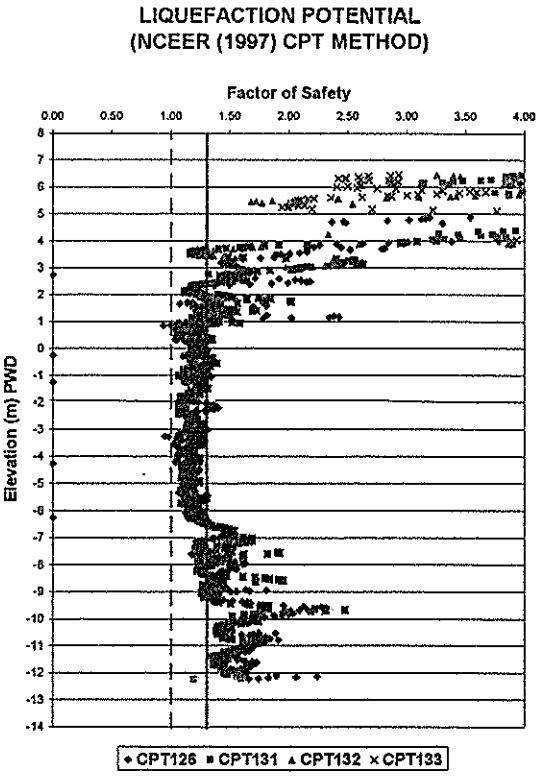

Figure 2: Factor of Safety versus Elevation

As can be seen in Figure 2, the factor of safety is relatively high in the reclamation fill material, which has probably been heavily compacted in the course of construction. Nonetheless, the factor of safety is as low as unity between PWD 1 m and –7 m. The client specified the required factor of safety of 1.3, which is slightly higher than 1.25 recommended in Eurocode8 [7]. Some

form of mitigation was required for the zone where the factor of safety against liquefaction was below 1.3.

6 MITIGATION METHODS

Various methods of mitigating liquefaction potential are now available. Port and Harbour Research Institute (1997) [8] provides examples of liquefaction mitigation techniques that are commonly used worldwide. However, due to limited availability of material and equipment in Bangladesh, sand compaction piling, surcharging and piled foundations were the only feasible options. In particular, sand compaction piling was considered to be a feasible option since it had been used successfully to improve the main plant structure foundation. Unfortunately the sand compaction piling rigs broke down before they became available to improve the ground for the cooling water discharge pipeline. It was uneconomical to mobilise another rig and therefore the sand compaction piling option was abandoned. Surcharging was considered to be ineffective for the cooling water discharge pipeline because of the limited space available for surcharge material to be placed. Therefore it was decided that a piled raft foundation would be constructed to support the pipeline in the event of soil liquefaction.

7 PILED RAFT FOUNDATION

7.1 Estimated Pile Capacity

It was desirable to construct the piled raft foundation using the most economical and readily available material. In this project, excess precast RC piles, which were also used in the foundation of the main plant structure, were available in a large quantity. Pile driving rigs with the hammer weight and stroke optimised for this type of piles were mobilised from the main plant structure site. Photographs of the RC piles and pile driving rigs are shown in Figures 3 and 4. Therefore the primary objective of the design of the piled raft foundation for the cooling water discharge pipeline was to determine the optimum founding level and arrangement of the available RC piles based on the existing information on the site conditions. This was followed by detail design of the raft to provide the required stiffness for the given pile arrangement to limit deflection and strain in the pipeline.

The precast RC piles were 400 mm square piles, and come in 6 m and 12 m segments. 12 m single segment piles were used for all of the foundation piles to avoid splicing, thus saving construction time. Furthermore, the recent ground investigation data indicated that 12 m long piles would be founded in a relatively competent layer.

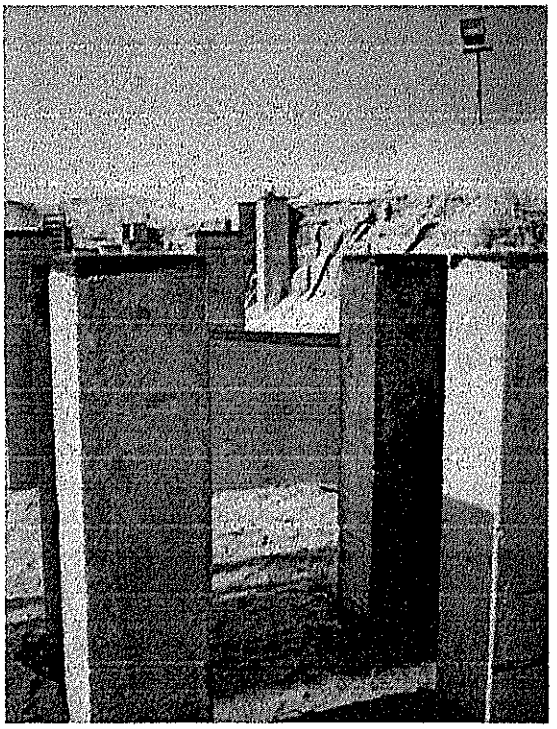

Figure 3: 400 mm Square RC Piles

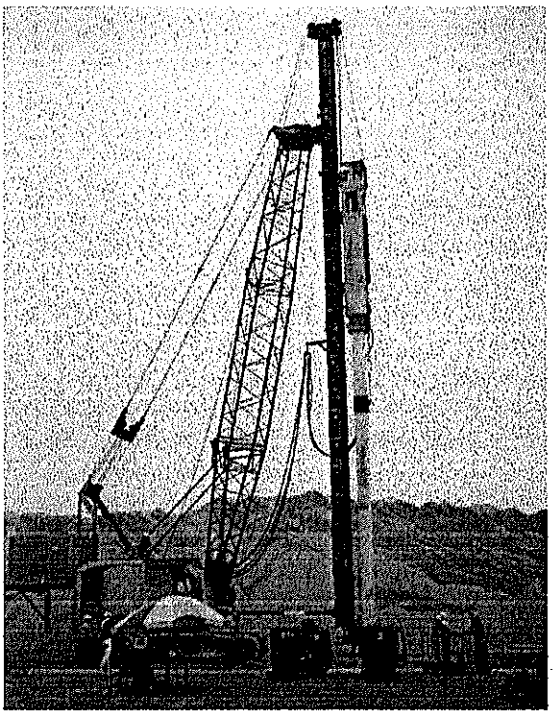

Figure 4: Pile Driving Rig, Twinwood V100D

The capacity of these 12 m RC piles was calculated based on the CPT data obtained in the vicinity of the cooling water discharge pipeline. The pile capacity was calculated using the CPT correlation method proposed by Laboratoire Central des Ponts et Chaussees (LCPC) as referenced by Coduto (1994) [9]. The LCPC's CPT correlation method calculates the end

bearing and skin friction of a pile as follows:

LCPC CPT correlation method (ref. Coduto, 1994 [9])

The end bearing capacity of a pile is given by:

$$Q_c = q_{ca} k_c A_b \quad (1)$$

where Q_c = end bearing capacity of a pile

q_{ca} = equivalent cone bearing resistance at pile tip, taken as the average q_c value from 1.5 diameter above to 1.5 diameter below the pile tip

k_c = cone end bearing factor

= 0.375 for piles driven in sands

A_b = end bearing area of a pile

The skin friction of a pile is computed as follows:

$$Q_s = q_s A_s \quad (2)$$

where Q_s = skin friction of a pile

q_s = shaft resistance correlated from q_c

A_s = shaft area of a pile

The pile capacity calculated using the above method has been factored and allowance has been made for a small loss of skin friction during soil liquefaction. This factored design load capacity is presented in the table below, and comparison is made to the factored design load capacity calculated based on the widely used static method and Mayerhof's SPT correlation method as shown below:

Static method (ref. Tomlinson, 1994, [10])

$$Q_p = N_q \sigma'_{vo} A_b + \frac{1}{2} K_s \sigma'_{vo} \tan\delta A_s \quad (3)$$

Mayerhof's SPT method (ref Bowles, 1995, [11])

$$Q_p = A_b \cdot 40N \cdot \left(\frac{L_b}{B}\right) + 2NA_s \quad (4)$$

where

$$40N \cdot \left(\frac{L_b}{B}\right) \leq 400$$

Method	Factored Design Load Capacity
CPT	580 kN
Static	710 kN
SPT	630 kN

Table 2: Calculated Capacities for 12 m Piles

The CPT correlation method was accepted as the design pile capacity because it results in a slightly conservative pile capacity compared to the other two methods but is not overly conservative. It should also be noted that the CPT's were scattered evenly alongside the cooling water discharge pipeline, and hence the CPT readings were considered to provide a realistic representation of the in situ soil conditions.

Next the spacing of these piles was determined so that the capacity of each pile would be sufficient to carry the anticipated axial load during possible soil liquefaction. The transverse view of the pipeline and piled foundation is shown in Figure 5.

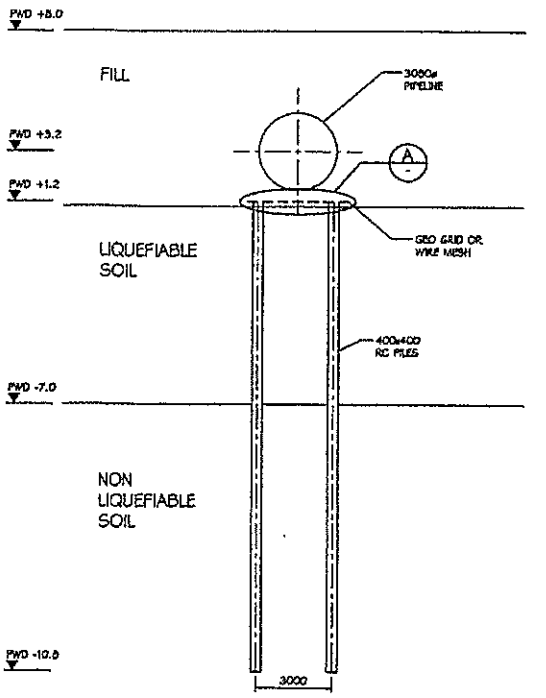

Figure 5: Piled Raft Foundation (not to scale)

7.2 Finite Element Analysis

Following the calculation of the required pile arrangement, the next step was to analyse the response of the piled raft foundation system to the loss of bearing capacity in the liquefiable alluvium layer. The piled raft foundation was analysed using PLAXIS Version 7.2, which is a two-dimensional finite element code developed

specially for analysis of geo-materials. The results of the two dimensional analysis were verified with the 3D beta module of PLAXIS.

PLAXIS is capable of modelling staged construction phases which not only allow for step by step construction of the pipeline, but also allow the soil parameters to be changed during each calculation phase. Therefore it is possible to simulate a possible liquefaction event by introducing a phase where the strength of the liquefiable alluvium layer is manually reduced to account for the loss of strength during liquefaction. The displacement, stress and strain of the pipeline and pile raft foundation were calculated in the following stages.

1) Initial state ie. pre-construction state
2) Excavation and construction of piles and raft
3) Backfilling
4) Filling the pipeline with water
5) Liquefaction

The primary advantage of the staged construction phase feature is that incremental stress-strain changes in the soils before and after construction activities, and the stress path history of the soils prior to the liquefaction event are fully accounted for.

The residual shear strength and stiffness of the liquefied soil has been estimated from the experimental data reported by Ishihara (1996) [12].

The model output generated by PLAXIS is shown below. Figure 6 shows a colour contour plot of the stresses in the pipeline model expected to occur during the liquefaction.

The inspection of the model output of the calculated stresses indicated that the maximum axial force that would act in the foundation piles during the potential liquefaction would be no more than 440 kN. This is approximately 80% of the design load capacity of the 12 m piles, which is 580 kN.

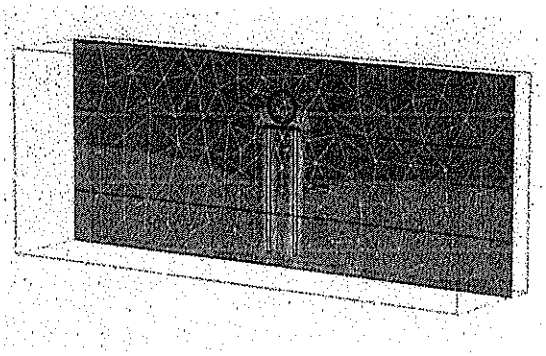

Figure 6: Mean Effective Stress during Potential Liquefaction (Max. Stress 1770 kN/m^2)

7.3 Pipeline Failure Criteria

The most common failure modes of steel continuous pipelines are tensile rupture and local buckling due to axial compression. O'Rourke and Liu (1999) [1] have proposed the following failure criteria for the two major failure modes:

Tensile rupture: $\varepsilon_{cr} > 4\%$
Local buckling: $0.15\ t/R < \varepsilon_c < 0.20\ t/R$

Where: ε_{cr} = critical pipe strain
t = pipe wall thickness
R = pipe radius.

The diameter and wall thickness of the cooling water discharge pipeline are 3.08 m and 0.016 m, respectively. The critical pipe strain for local buckling of the pipeline is therefore 0.16% - 0.21%. In Figure 7, the calculated displacement in the pipeline for the potential liquefaction event is shown. The pipe strain was calculated from this displacement plot.

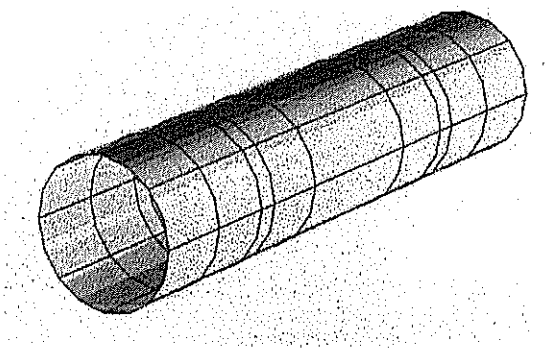

Figure 7: Pipeline Displacement during Potential Liquefaction (Max. Displacement 13 mm)

The maximum compressive and tensile strains in the pipeline calculated via the finite element analysis are:

Maximum tensile strain 0.003%
Maximum compressive strain 0.01%

These strains are well below the critical values calculated in accordance with O'Rourke and Liu's failure criteria. The finite element analysis has therefore demonstrated that the piled raft foundation system will provide sufficient support and restraint against the deformation of the pipeline even if the underlying alluvium layer liquefies during strong ground motion provided the raft has adequate stiffness.

7.4 The Raft Reinforcement

The finite element analysis of the pipeline has also determined the tensile strength of the raft reinforcement required to limit the deformation and strain of the pipeline within the tolerable range. The analysis of the cooling water discharge pipeline suggests that the required tensile strength of the raft reinforcement is about 20 kN/m for the given pile arrangement. Even lower strength geosynthetics commonly available in the industry satisfy this requirement.

8 DISCUSSION OF DESIGN METHODS

The piled raft foundation was designed using a combination of analytical methods and PLAXIS, a finite element code for analysis of soils and rocks.

The design load capacity of the foundation piles was estimated via the LCPC CPT correlation method, and the calculated design load capacity was compared and verified with the conventional static and SPT correlation method. In-situ test correlation methods may provide more accurate estimates of the pile axial capacity for a reclaimed land in micaceous soil. This is because the effects of the high mica content and highly modified stress states in the reclamation fill are reflected in the CPT readings to some extent. Such characteristics may affect the accuracy of the conventional static method.

The finite element analysis by PLAXIS proved to be a powerful tool for the design of the piled raft foundation. PLAXIS is capable of 3D modeling of pipelines with its built-in tunnel elements. Furthermore special interface elements accommodate high concentrations of strain expected to occur around the pipe element. The program computed the pipe strain and deformation with a minimal computer time, taking full accounts of the three dimensional effects of the problem.

9 CONCLUSIONS

A case study of the mitigation of liquefaction-induced damage to a steel continuous pipeline constructed in a potentially liquefiable ground has been presented. A piled raft foundation was the chosen method of mitigating such damage because various factors including site constraint, machinery breakdown and mobilization cost made conventional ground improvement techniques unfeasible.

The finite element analysis of the piled raft foundation demonstrated that it would effectively limit the deformation and strain of the pipeline within the tolerable limits even if the underlying alluvium layer liquefies during strong ground motion.

It is concluded that piled raft foundations provide a simple, cost effective design solution to a pipeline in potentially liquefiable ground. It is possible to design particularly economical piled raft foundations if pile material and piling machinery can be reused and remobilized from a nearby site, as is the case for many power developments.

10 ACKNOWLEDGEMENTS

The author wishes to thank our client Hyundai Engineering and Construction Co. (HDEC) and AES, the plant developer for their permission to publish this paper. Special thanks go to Mr. K.Y. Jeong (Project Control Manager), Mr. D.H. Kim (Project Manager), Mr. D.S. Choi (Civil Manager) and Mr. O.D. Kwon (Assistant Civil Manager) of HDEC, and Peter Fox (Construction Manager) of AES for their continual support on and off site. Mr. S. Terzaghi, who reviewed the early draft of this paper, is gratefully acknowledged for his inspiring and constructive comments.

11 REFERENCES

1. O'ROURKE, M. J., LIU, X., Response of buried pipelines subject to earthquake effects, MCEER, 1999, 2-3, 59-62.
2. STROOP, R., SICKLING, J., MURRAY, G., "Geotechnical design for the Meghnaghat 450MW Combined Cycle Power Plant, Bangladesh", Proc. of Int. Eng. and Construction Symposium, 2001.
3. MOLLAH, M. A., "Liquefaction of the alluvial soils of Bangladesh" Proc. 3rd Int. Conf. on Recent Advances in Earthquake Eng. & Soil Dynamics, Vol 1, 1995.
4. SICKLING, J., STROOP, R., "Case history: Sand compaction piling to reduce liquefaction potential, Bangladesh", Proc. of NZ Geotech. Society 2001 Symposium, 2001, 281-282.
5. SEED, H. B., IDRISS, I. M., "Ground motions and soil liquefaction during earthquakes", Earthquake Engineering Research Institute, 1982, 134
6. YOUD, T. L., IDRISS, I. M., Proceedings of the NCEER workshop on evaluation of liquefaction resistance of soils, NCEER, 1997
7. EUROCODE8, Design provisions for earthquake resistance of structures, European Committee for Standardisation, 1994
8. PORT AND HARBOUR RESEARCH INSTITUTE, Handbook on liquefaction remediation of reclaimed land, A. A. Balkelma, 1997.
9. CODUTO, D. P., Foundation design – Principles and practices, Prentice Hall, 1994, 392-399.
10. TOMLINSON, M. J., Pile design and

construction practice, Chapman and Hall, 1994, 114-119.
11. BOWELS, J. E., Foundation analysis and design, McGraw Hill, 1996, 897.
12. ISHIHARA, K., Soil behaviour in earthquake geotechnics, Oxford University Press, 1996, 274

Slope Failure in a Complex Volcanic Terrain Opito Bay, Kuaotunu, Coromandel Peninsula

Steven Price – Riley Consultants Ltd, Auckland

The Ohinau Drive slope failure has occurred at the northern base of the volcanic Tahanga Hill, Opito Bay. The failure has affected a recent subdivision on Ohinau Drive situated immediately adjacent to the hill.

The slide is a complex, variable depth failure encompassing several differing geological units. It extends a distance of 170m from headscarp to toe with an estimated maximum width of 130m. It comprises both shallow seated and deep seated failure mechanisms to a maximum depth of approximately 20m.

In the winter of 1996 slope instability was recognised following development of a headscarp and ongoing disturbance to kerbing and manholes.

Investigations undertaken revealed complex geological conditions generally comprising hydro-thermally altered andesite partially overlain by basaltic debris and weathered basalt lava. Artesian water pressures were encountered within the andesite. The investigation results indicate that both a deep seated failure through the underlying andesite and a shallow seated movement involving the basalt debris were recently active.

A geotechnical model was constructed along 2 cross sections with computer aided stability analyses undertaken. Target groundwater levels were determined to achieve a satisfactory Factor of Safety to allow future subdivision development. Drainage installation and monitoring is yet to be established following liaison with Council.

1 INTRODUCTION

The Ohinau Drive slide is located at Opito Bay in the eastern extent of Kuaotunu Peninsula, north eastern Coromandel Peninsula. (Figure 1) The slope failure has developed largely beneath vacant lots of a recent subdivision extending southward into a Pine plantation covering Tahanga Hill (Figure 2).

Earthworks were undertaken in the late 1980's removing up to 5.0m from an existing ridge line at the base of Tahanga Hill for the purposes of forming Ohinau Drive and the subdivision.

In 1996 significant ground movement occurred and a headscarp developed above the southern end of Ohinau Drive. Ground heave was also noted north of Ohinau Drive, with damage to services including the road, footpaths and stormwater reticulation. Lot boundary pegs placed in 1993 have suffered lateral movement

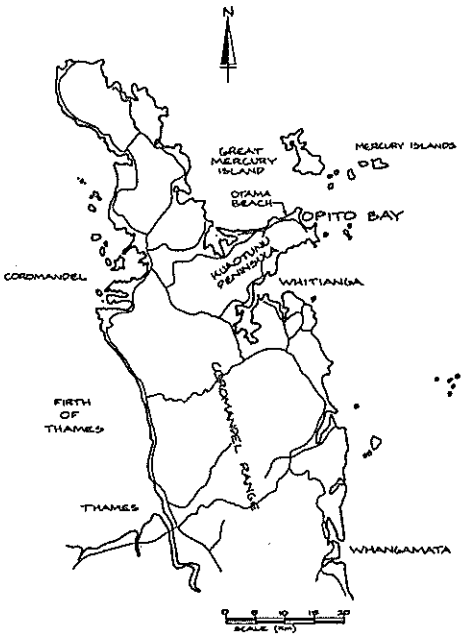

Figure 1 – Locality Plan

by up to 0.5m during the last 8 years. No further development has proceeded within the affected area since 1996. Thames Coromandel District Council has imposed a section 36(2) encumbrance on all titles within the affected area.

Section 36(2) of the Building Act 1991 allows territorial authorities to issue building consents on properties subject to subsidence provided the building work will not accelerate, worsen or result in subsidence. Such an encumbrance typically detrimentally affects the property value and insurance cover.

2 LANDSLIDE INVESTIGATION

Whilst a complete definition of the lateral extent, depth and interfaces between the various units has not been determined, a geological/geotechnical model was developed with a reasonable degree of confidence.

Two phases of investigation were undertaken. An initial investigation in 1997 was performed by Worley Consultants Ltd (WCL)[1]. The second stage of investigation was undertaken by Riley Consultants Ltd (RCL)[2] in 2000.

The initial RCL investigation comprised a review of existing information including borehole logs, piezometer and land survey monitoring records. From this a preliminary subsurface investigation programme was planned. During the investigation the location of boreholes and test pits were altered as the exploration continued.

A total of 5 machine boreholes, 4 hand auger boreholes and 5 test pits were drilled and excavated over these two phases of investigation conducted by WCL and RCL.

A walkover appraisal and review of pre-earthworks topographical plans was also undertaken.

No subsurface investigation was undertaken adjacent to the headscarp as permission from the neighbouring land owners was not forthcoming.

The objective of the investigations was to assess the subsurface conditions and identify possible failure surface(s).

3 GEOLOGY AND SUBSURFACE CONDITIONS

The geology of the general area has been described by Skinner[3] and in more recent times Hawthorn[4]. The area generally consists of the basaltic Tahanga Hill surrounded by a mixture of basalt lava/plugs and thick andesite lava deposits.

Geology of the area investigated was found to be more complex than shown on available geological plans with several materials encountered north of the basaltic Tahanga Hill (Figure 3). In stratigraphic (chronographic) order the following units were encountered:

Fill

Encountered adjacent to the eastern gully. Inferred to be remnants of a stockpile created during earthworks. Typically firm to very stiff silt with topsoil layers.

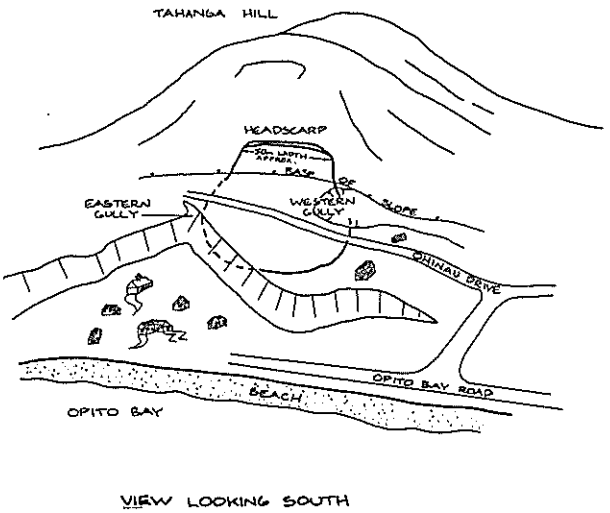

Figure 2 – Perspective View

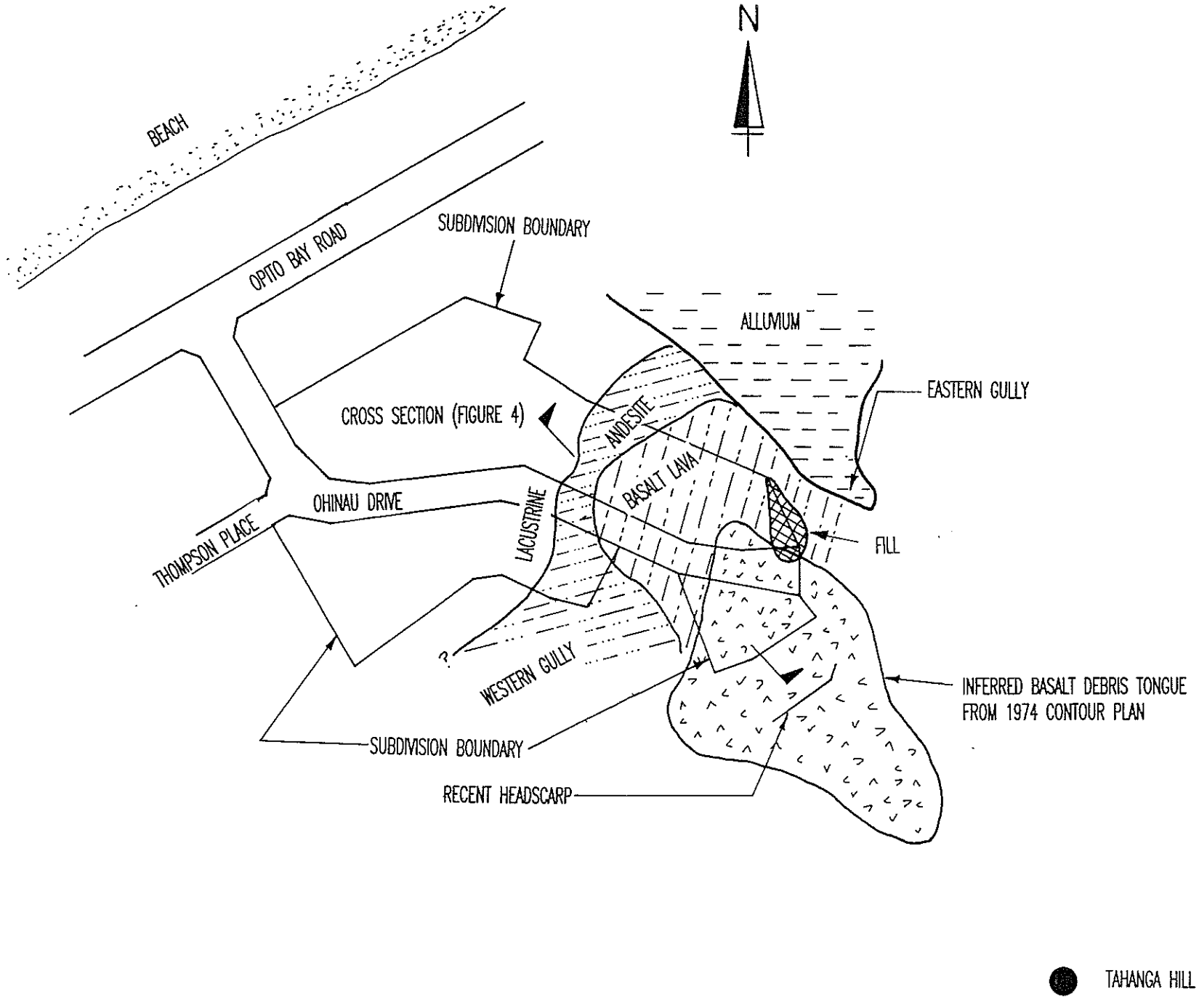

FIGURE 3 - *GEOLOGICAL PLAN OF OHINAU DRIVE AREA*

Alluvium
Firm to very stiff clay and silt, found beneath the fill within the eastern gully.

Surface Debris
Consisting of basalt gravels, cobbles and boulders in a silt/clay matrix. Encountered at the northern base of Tahanga Hill and interpreted to extend beneath the adjacent Ohinau Drive. This material was encountered to a depth of nearly 11.0m.

Weathered Basalt
Highly weathered products of basalt lava, very stiff to hard inferred to be filling an ancient palaeovalley.

Lacustrine Deposits
Stiff silts and clays encountered forming a "buttress" at the landslide toe. These deposits included minor quantities of coarse quartz/flint and rounded mudstone.

Hydrothermally Altered Andesite
Underlying the basalt and outcropping north of Ohinau Drive, the andesite was typically of stiff to very stiff consistency.

Andesite
Basement rock inferred to underlie the entire subdivision. This is hydrothermally altered and whilst typically of very weak rock strength, is sheared and of soil strength in places. Artesian water pressures were encountered in this material in 1997.

Failure Planes
Failure surfaces are often not easily detected in recovered core however a distinct failure surface was encountered in drillhole R1 at the base of the basaltic debris where it contacts the underlying andesite consisting of a striated slickenslide. A failure surface was also observed in a test pit excavated in the toe heave zone, with movement of highly weathered hydrothermally altered andesite over lacustrine deposits.

4 LANDSLIDE CHARACTERISTICS

4.1 Geomorphology

Topography near Ohinau Drive is dominated by the 212m elevation basaltic peak and associated lava flows. A concave depression is evident on the steep sided slopes with a hummocky landscape below. A review of the topographical plan from 1974 (prior to earthworks) indicates a large "tongue" of material below (north) of this concave depression and the most recent scarp. This "tongue" feature has been obliterated by recent earthworks.

North of Ohinau Drive consists a flat to gentle graded area created by earthworks where up to 5.0m was cut from a pre-existing ridge line. A heave zone of approximately 150mm height is evident in this area.

4.2 Failure Surface

From the earlier study by Worley Consultants Ltd it was postulated that either of two failure mechanisms could exist: a) a shallow failure surface involving movement of the surface debris, b) a deep failure through the underlying andesite. However, a failure along either one of the surfaces alone was not entirely consistent with the surficial expressions of movement (eg deflection of boundary pegs, location of tension cracks etc). Despite this inconsistency the combination of borehole information and surface observations did not indicate any plausible alternative failure scenarios.

Accordingly it is concluded that the movement was attributed to one or a combination of the following two basic failure mechanisms.

- **Surface Debris Failure**
  Reactivation of ancient slip debris moving over the underlying andesite. This failure explains relatively large boundary peg movements (in the order of 0.5m) in Lots adjacent to Tahanga Hill and the development of a tension crack in the basaltic material at the base of Tahanga Hill. However, this failure mechanism does not explain the andesite toe heave north of Ohinau Drive or movement at the andesite western gully base.

- **Andesite Failure**
  Deep failure within the andesite along shear zones or clay seams as identified in cores. This failure mechanism is thought to have been active in winter of 1996 and is consistent with toe heave.

  Both failure surfaces are shown on Figure 4.

4.3 Recent Movement and Groundwater

The 1996 mass movement appears to have been strongly influenced by highly localised artesian groundwater pressures in combination with subdivision earthworks that removed approximately 5.0m of earth from the toe area. Two boreholes drilled into the andesite in 1997 encountered artesian water pressures, although 3 others did not. It is inferred that the location of such water pressures is dependant upon defects within the andesite. Water levels within the surface debris were also found to be high (within 2.5m of ground surface during winter months, probably at or close to ground surface at the time of failure).

5 DRAINAGE

A single horizontal bored drain was installed in mid 1997 with an outlet in the eastern incised gully. The 65m long bored drain targeted the zone of andesite artesian water pressure located centrally below the landslide mass. The effect of this drain was a substantial reduction in groundwater levels; approximately 1.7m and 8.7m within the surface debris and andesite respectively. However, the effect was localized to the central area and other areas showed no significant drops in water level that can be directly attributed to the bored drain.

Since the installation of the drain no discernable ground movement has occurred.

6 STABILITY ANALYSES

A series of computer assisted stability analyses were undertaken for both failure surfaces. Effective stress strength parameters were determined from back analysis of the existing slope movement and considered judgment of soil characteristics. Effective stress strength parameters assumed for the failure plane within the andesite were c'=2kPa and Ø'=15°

The analyses indicate that groundwater pressures within the underlying andesite are critical to the slope stability.

It was determined that lowering sub-basal (andesite) groundwater levels to between 5m and 7m below ground surface will achieve a the Factor of Safety between 1.4 and 1.5. As often occurs with large scale failures, such as through the andesite, relatively large changes to groundwater levels are required to achieve significant changes in the Factor of Safety.

Within the shallow basaltic debris an assessed FOS exceeding 1.5 can be achieved by lowering groundwater levels below 4.0m from ground surface.

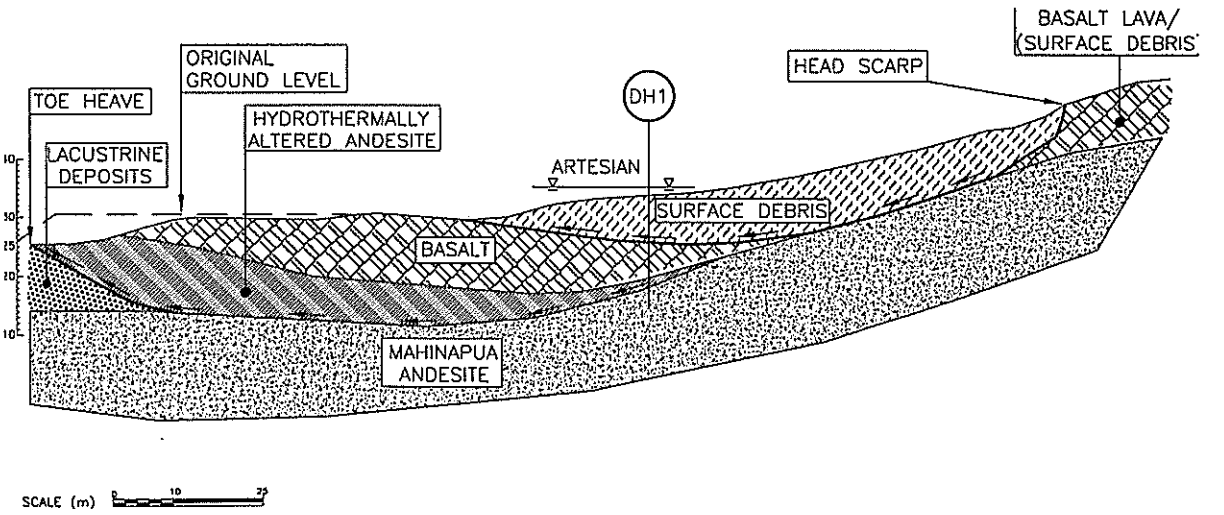

Figure 4 – Geological Cross Section of Ohinau Drive Failure

7 FUTURE DEVELOPMENT

It is proposed to install counterfort (buttress) drains within the surface debris to minimize the risk of saturation and achieve a Factor of Safety in excess of 1.5.

Large diameter bored drains are the preferred drainage method for the andesite drilled from the slope toe. Achieving a Factor of Safety in excess of 1.5 for the underlying andesite is considered impractical given the slope gradients and depth of drawndown required. A Factor of Safety of 1.4 is the recommended objective. With no dwellings with the main movement area, nor immediately adjacent, any settlement caused by drainage is considered unlikely to affect existing structures.

Alternative methods of stabilization have been considered, such as toe buttressing. However, these are generally impractical and/or provide insignificant improvements in the Factor of Safety.

It is proposed to assess the effectiveness of the bored drains by monitoring of piezometers for a period of at least 2 years following the installation of bored drains. If groundwater levels are found to be satisfactorily low, such that an acceptable Factor of Safety is achieved, then it would be considered appropriate for development to be able to occur without a section 36(2) encumbrance.

Maintenance of the piezometers and bored drains could be carried out by a body corporate.

8 CONCLUSION

A large, deep seated failure within complex volcanic terrain has affected a recent subdivision in Ohinau Drive, Opito Bay. Investigation of the movement indicates possible multiple failure mechanisms following heavy rain and removal of toe weight.

Stability analyses indicate that satisfactory Factors of Safety can be achieved by subsurface groundwater drainage. It is proposed to install a combination of counterfort and bored drains.

Acknowledgements

I wish to acknowledge Cawdor Properties for allowing this paper to be prepared. I also wish to thank Ian Grierson of Harrison Grierson for his assistance during the investigation and assessment. Thank you to the staff of Riley Consultants who assisted with the study and preparation of this document.

References

1. WORLEY CONSULTANTS LTD & HARRISON GRIERSON CONSULTANTS LTD, "Ohinau Drive, Opito Bay, Investigation of Slope Instability", 1997, Ref: 19-147-02.

2. RILEY CONSULTANTS LTD, "Revised Geotechnical Investigation & Stability Assessment, Ohinau Drive, Opito Bay", 2001, Ref: 00122-E.

3. SKINNER, D.N.B, "Sheet N40 and Pts N35, N36, N39 Northern Coromandel, Geological Map of NZ, DSIR, Wellington, NZ", 1976.

4. HAWTHORN BM, "Volcanic Geology of the Opito Bay Region, Northern Coromandel Peninsula", MSc Thesis, University of Waikato, 1996.

The Seepage Modelling of Cosseys Dam Upgrade.

Sandip Ranchhod, URS New Zealand Limited, Auckland, New Zealand.

Located in the Hunua Ranges to the south of Auckland, Cosseys Dam is a water supply dam constructed as a zoned earth embankment. The dam is currently being upgraded to modern design standards due to incompatibility of the core and underdrain materials. Seepage modelling of the dam provided information on how pore pressures and flow regimes throughout the dam would react during construction of the remedial works. Oblique two-dimensional analysis methods were used to model seepage through the dam's three-dimensional principle seepage line. The resultant phreatic surface predictions could then be imported into corresponding stability models and predicted flow velocities used to calculated the risk of internal piping. During initial construction stages, the predicted seepage pressures and flows within the structure have proved to be within threshold levels.

Introduction

Cosseys Dam is a 41m high zoned-earthfill dam located in the Hunua Ranges South of Auckland. The reservoir, at full supply level contains 14 million cubic meters of water, covering a surface area of 119 hectares with a contributing catchment area of 2,200 hectares. Construction was completed in 1954 with the official opening in 1955.

"Cosseys Dam Upgrade Feasibility – Embankment Stability", (URS, October 2000) confirmed an underdrain material incompatibility. Two key events, signalled by rapid rises in piezometric pressures, provided evidence of erosion of the core which had lead to a blockage in the underdrain. Following the second key event in 1994, a depressurisation well (Well A) was installed upstream of the underdrain blockage, to relieve the elevated pore pressures in the core.

Following the study of remedial options Watercare Service Ltd, (the dam owner) engaged URS New Zealand Limited to progress the detailed design of the preferred option. The chosen option required excavation of the downstream shoulder, and replacement of the existing underdrain with an engineered underdrain and filter blanket extending over the downstream face of the core and across the abutments.

The works are to take place over two earthworks seasons. Stage 1 (2001/2002) provides a filter layer to the downstream toe of the dam as an interim protection against piping until the excavation of the shoulder allows placement of filter against the core (Stage 2) of the works can be completed in the following season (2002/2003).

The following sections describe the seepage analyses required to assess the stability and piping risk of the proposed construction works.

General Observations of Seepage Regime

The earth embankment was built over a narrow gully with ridges intruding from the left and right abutments giving rise to a streambed that meanders beneath the embankment (Figure 1). The meandering underdrain and intruding abutments create significant three-dimensional seepage effects.

Chemical analysis of the underdrain flows supported the three-dimensional nature of the seepage. Analysis showed that approximately 30% of the underdrain seepage originated from the abutments, with the remainder seeping through the earth embankment.

Section M follows the underdrain and represents the principal seepage flow in recognition of the 3-dimensional nature of the abutment geometry.

A dewatering pump has been installed upstream of the blockage to depressurise the underdrain and overlying core. The pump has been removing water from the underdrain at a rate of 60 litres/min.

A number of multilevel piezometers have been installed in the embankment and provide data on the pressure distribution within the embankment. A review of the data was undertaken to assess the reliability of the piezometers. This data was used to calibrate the principle seepage section.

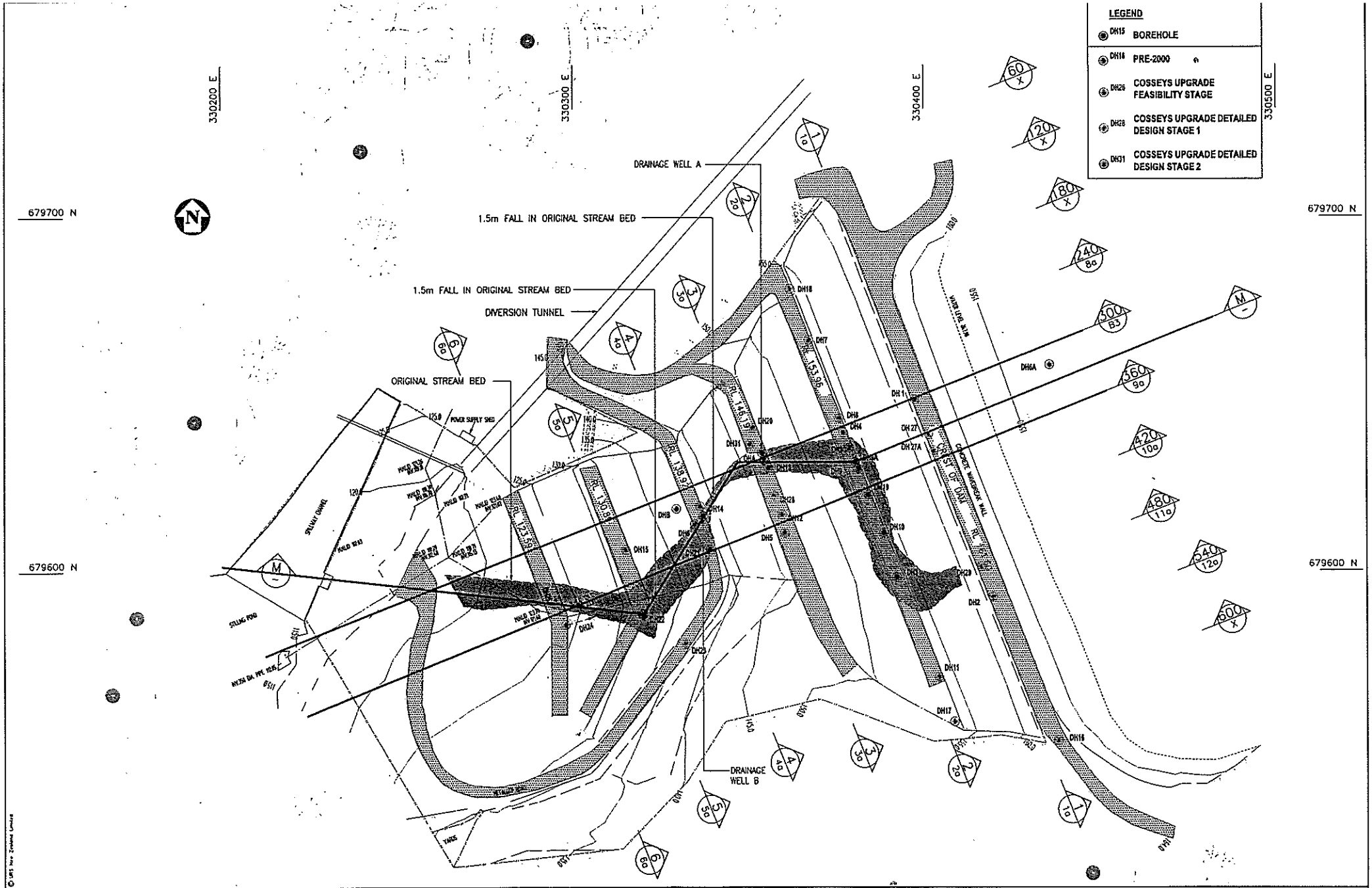

REV	DESCRIPTION OF REVISION	BY	CHK	DATE
B	FINAL ISSUE	STT		10/9/01
A	ISSUE FOR REVIEW	JAWD		

waterCare services limited

URS Woodward Clyde Dames & Moore

URS New Zealand Limited
Bank Direct Centre
13-15 College Hill
P.O. Box 821
Auckland
New Zealand
Ph 0-9-355 1300
Fax 0-9-355 1333

CAD FILE NAME: U:\PROJCAD\46537\016\Design Report + Misc\ws016r009.dwg
TAB: Layout1
XREF FILES:
SCALES: 1:500 (A1) 1:1000 (A3)
ORIGINAL SIZE: A1
DESIGNED:
DRAWN: JAWD
CHECKED:
PROJECT MANAGER:
DATE: 28 Aug 01

COSSEYS DAM UPGRADE & REMEDIAL WORKS

BOREHOLE LOCATIONS

WATERCARE DRAWING No.

STATUS: FINAL
REVISION: B

DRAWING NUMBER: FIGURE D-1

Seepage Modelling

The objectives of the seepage analysis included:

- Predicting hydraulic pressures within the dam for various dewatering and excavation scenarios. This information was required to assess construction slope stability.
- Predicting hydraulic velocities within the dam for various underdrain dewatering and unblocking scenarios. Unblocking the underdrain could expose the core to high seepage gradients and initiate internal erosion at the boundary of the underdrain and core.
- Predicting underdrain flows during construction.

SEEP/W is a finite element software package that simulates the flow and pore water distribution within porous media. The program simulates both saturated and unsaturated flow, under steady-state or transient conditions. It is ideally suited to analysing flow of water through the variably saturated embankment under conditions of changing reservoir levels.

The general approach to constructing a model and running a simulation is summarised as:

1. Creation of a two-dimensional grid to represent the embankment;
2. Assignment of material properties and boundary conditions;
3. Simulation under current steady-state conditions;
4. Comparison of the predicted phreatic surface with the observed behaviour from the dam piezometers;
5. If necessary, adjustment of material properties, within acceptable limits, then re-running the model until an acceptable match to the observed water levels is attained (calibration);
6. Simulate future conditions by changing the boundary conditions (reservoir drawdown, excavation);

Model Development

Figure 2 shows the grid for Section M. The model includes discrete zones of the core, transition shoulder and underdrain. The multiple zones provide the flexibility to simulate varying excavation profiles by switching off zones in succession and re-initiating the next run with the heads from the previous run. The underdrain is modelled as a thin zone of permeable material with a low permeability zone representing the blockage within the underdrain. The dewatering pump at Well A, used to depressurise underdrain, is modelled as a discrete flux.

The sections at Sta.300ft and Sta.360ft, either side of Section M were used to model the stability. This required translating head files from SEEP/W through to the SLOPE/W files.

The transfer of head files to SLOPE/W models requires a true two-dimensional section with coordinate grids compatible with the stability models. Figure 1 shows how the underdrain moves oblique to Sections Sta.300ft and Sta.360ft at various places. Water therefore flows in/out of these sections at those places. The translation of the seepage patterns from Section M to Sections Sta.300ft and Sta.360ft was achieved by transferring head-functions from the Section M underdrain nodes across to the corresponding underdrain nodes at Sections Sta.300ft and Sta.360ft. The pressure head-functions at these nodes are achieved in the model by generating flux at that node simulating the oblique component of the flow in/out of the section. So, in section M, the seepage flows generate the head pressures, but in Sections Sta.300ft and Sta.360ft, the head pressures generate the seepage flows.

Pump tests confirmed that the underdrain was free-flowing downstream and upstream of the blockage. This absence of large pressure gradients along the free-flowing portions of underdrain allowed a transfer of head functions from one section to another.

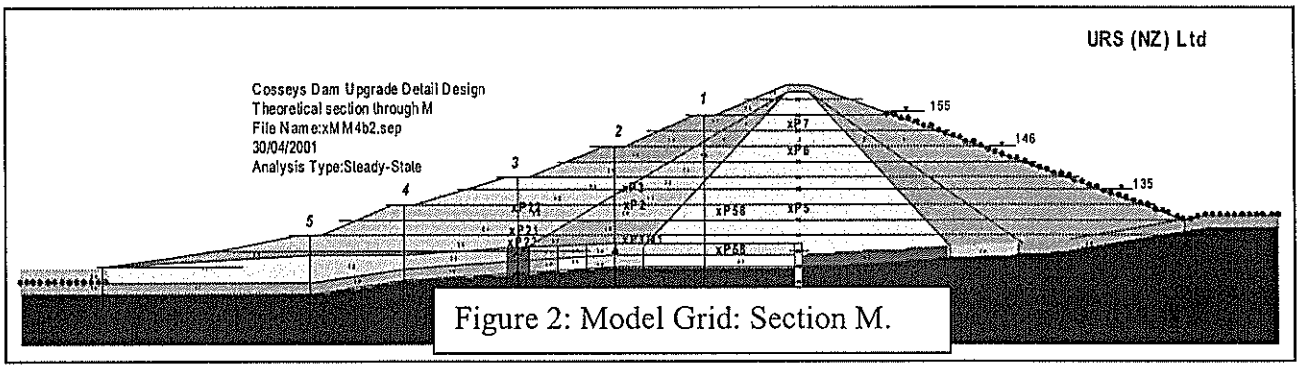

Figure 2: Model Grid: Section M.

Material Parameters

The material parameters required for analysis were:

- Hydraulic Conductivity (permeability)
- Anisotropy
- Storativity (effective void ratio)

Table 1 provides the range of hydraulic conductivity values and anisotropy applied for the zone materials.

Table 1: Hydraulic Conductivity Values

	Saturated Hydraulic Conductivity (m/s)	**Anisotropy k_v/k_h**	**Saturated Storativity**
Core	$1x\ 10^{-8}$ to $1x\ 10^{-6}$	0.2 to 1	0.35 to 0.38
Transition	$1x\ 10^{-8}$ to $5x\ 10^{-6}$	0.2 to 1	0.21 to 0.25
Shoulder	$5x\ 10^{-8}$ to $5x\ 10^{-5}$	0.2 to 1	0.21 to 0.25
Drain	$1x\ 10^{-4}$	1	0.35
Greywacke	$1x\ 10^{-7}$ to $1x\ 10^{-5}$	1	0.35
Cutoff	$1x\ 10^{-7}$ to $2.5x\ 10^{-6}$	1	0.35

The material parameters shown above were estimated from investigation borelogs, laboratory permeability tests and piezometer falling head tests. The above values represent the reasonable range of parameters available for each material in order to achieve calibration.

Boundary Conditions

Boundary conditions included:

- A projected reservoir draw-down rate (Figures 3a & 3b.)
- Varying pumping rates at well A
- Storm inflows to the reservoir

Head/time functions were used on the upstream face of the dam for the transient analyses simulating reservoir drawdown from 155m RL to 150m RL (Stage 1) and then to 135m RL (Stage 2). Drawdown to 150m RL was commenced at month 3 and finished at month 10. The reservoir was held constant at 150m RL until month 16 then drawn down to 135m RL by month 18.

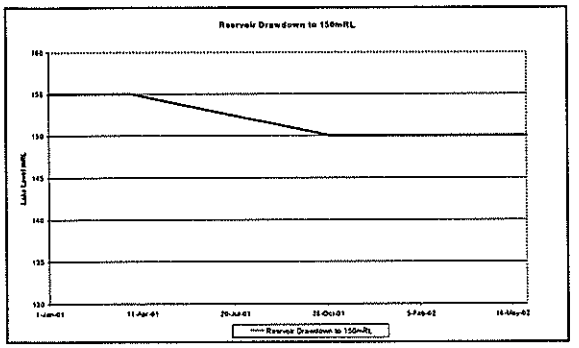

Figure 3a: Stage 1 Drawdown Schedule

Well A pump rates were modelled as a node with a negative flux simulating water outflow.

Storm inflows were modelled as rapid rises in the reservoir level in the same manner as described for reservoir drawdown.

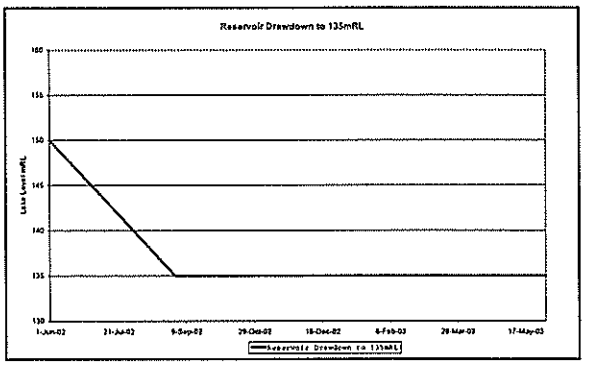

Figure 3b: Stage 2 Drawdown Schedule

Model Calibration

Calibration was achieved by varying zone permeabilities within the range of the reasonable material parameters shown in Table 1 until close correlation with the observed phreatic surface and head distribution was achieved. Calibration to the observed pressure heads only establishes acceptable ratios of zone hydraulic conductivities. Absolute values of hydraulic conductivity require calibration to the observed flowrates exiting the underdrain. The steady state heads were found to be within 7 to 15% of those measured in the piezometers whilst the modelled flow through the embankment was $130m^3/d$ compared to $100m^3/d$ as estimated from earlier chemical analysis of the seepage water.

The calibration provides a reasonable match to the observed seepage regime with material parameters within acceptable limits.

Sensitivity

A series of sensitivity runs were carried out by:

- Varying grid size to improve phreatic surface shape.
- Changing storativty functions.
- Changing hydraulic conductivity functions and anisotropy.

The sensitivity analyses showed that the models were most sensitive to varying hydraulic conductivity functions and anisotropy. But the dual calibration to both heads and flows limits the range of hydraulic

conductivities and provides confidence that the models are representative.

Seepage Predictions

The main objective of the seepage analysis was to provide seepage flows for different construction and dewatering scenarios, hydraulic velocities and predictions of pore pressures. There were scenarios modelled for different pumping, reservoir lowering, excavation profiles, and internal pore pressure constraints. The results below are summaries of proposed remediation option.

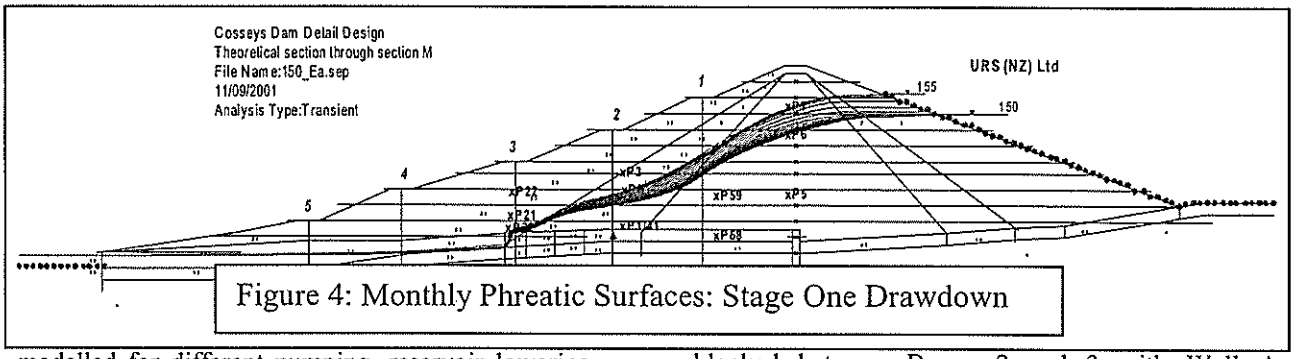

Figure 4: Monthly Phreatic Surfaces: Stage One Drawdown

Drawdown Scenario – Stage 1

The proposed work for Stage 1 includes lowering the reservoir to 150m RL to allow completion of embankment toe filter works. A reservoir level of 150m RL is then maintained through to Stage 2.

Figure 4 shows the monthly reservoir level and phreatic surface changes during the period of drawdown for stage 1.

Note that:

- The underdrain remains blocked between Berms 2 and 3; forcing the seepage through the transition zone.
- Well A pumping continues at the current rate (60 l/m);
- The underdrain downstream of the blockage remains free flowing.

The model reveals that at the projected rate of reservoir drawdown there is no excess pore pressure within the core.

Drawdown Scenario – Stage 2

The seepage predictions of Stage 2 drawdown profile begins where the Stage 1 drawdown profile ends. The reservoir is drawn down from 150m RL to 135m RL in six months and held at 135m RL.

During the stage 2 drawdown the underdrain remains blocked between Berms 2 and 3 with Well A continuing to pump at the current rate. The underdrain downstream of the blockage is free flowing.

Following the reservoir level reaching 135m RL, the blockage is removed and pumping is stopped. This allows the underdrain to flow freely along its full length.

Figure 5 shows the monthly reservoir levels and phreatic surface profiles during the lake draw down and the Stage 2 construction period.

Note that:

- Excess pore pressures are unlikely to dissipate within the drawdown timeframe.
- Following excavation of the underdrain blockage, the presence of a free flowing underdrain beneath Berm 1 will allow depressurisation of the core over much of the dam width and enhance core stability.
- During unblocking of the underdrain, seepage velocities along the interface of core and existing underdrain, where the risk of piping is greatest, are reduced by about 65% from the current situation of reservoir level and rate of pumping.

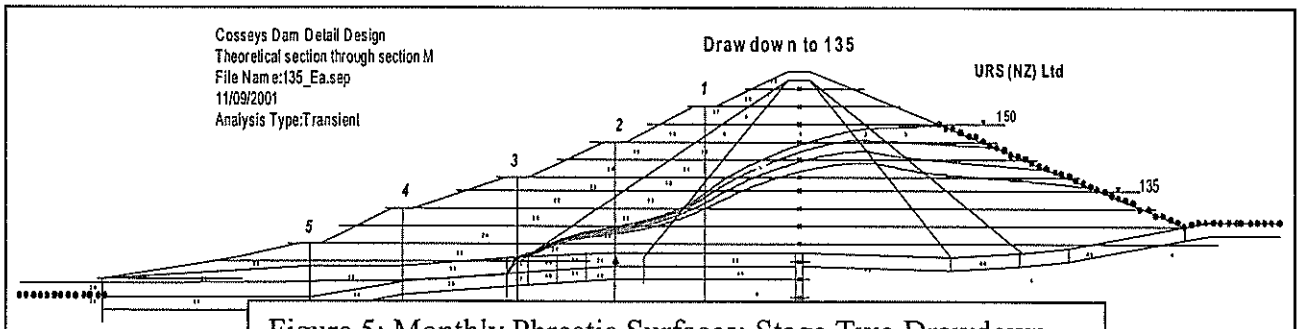

Figure 5: Monthly Phreatic Surfaces: Stage Two Drawdown

Summary

An oblique two-dimensional analysis was used to model seepage through the dam's three-dimensional principle seepage line. The principle seepage line, Section M, was calibrated to material parameters and observed seepage behaviour. Boundary conditions (head functions) defined from Section M were then transposed onto true two-dimensional sections (Sta.300ft and Sta.360ft) as required for stability analysis.

At the time of writing, the seepage pressures with the reservoir at Stage 1 target level of RL 150m are tracking slightly lower than predicted. Threshold levels of pore pressures have been achieved in readiness for the stage 1 excavation works.

References

Cosseys Dam Upgrade Feasibility Study – Embankment Stability. Prepared for Watercare Services Ltd by URS New Zealand Ltd, October 2000

Mechanism Controlling the Cyclic Strength of Cemented Soil

Shambhu S. Sharma

Centre for Offshore Foundation Systems (COFS)

The University of Western Australia

Summary The mechanism controlling the cyclic behaviour of cemented soil is investigated. It is observed that the cyclic response of cemented soil is strongly linked to the mechanism observed in static tests. The cyclic behaviour of cemented soil can be explained using the maximum stress ratio η_{max} and the Critical State Line (CSL) obtained from the corresponding monotonic tests. Examination of the experimental results obtained from cemented sand showed that there is a general trend of increasing pore water pressure with progressive cycles until the stress-state reaches the η_{max} line obtained from a monotonic test. Further straining beyond η_{max} line causes generation or dissipation of pore pressure, depending on the relative position of the stress-state with respect to the CSL in stress (q - p′) space. The stress space can, thus, be sub-divided into two main sub-spaces, depending on the pore pressure response during cyclic loading, which can be used to explain the fatigue behaviour of cemented soil.

1. INTRODUCTION

The behaviour of cemented calcareous soils subjected to cyclic loading is of considerable importance in the design of offshore structures. Most of the current design practices in geotechnical engineering are based on strength criteria, where monotonic shear strength is considered as one of the most important design parameters. However, in designing structures subjected to cyclic loading due to waves, wind or earthquakes, it is very important to consider the cyclic shear strength, since the consideration of only monotonic shear strength could overestimate the stability.

Several approaches have been reported in the literature to determine the cyclic shear strength of soils. Most of these approaches are based on the hypothesis that monotonic loading tests define a boundary surface for the corresponding cyclic behaviour and, hence, can be used in evaluating the cyclic shear strength (Alarcon-Guzman *et al.*, 1988). Although there is general agreement that there exits a boundary surface defined by the monotonic tests, which can be used in defining the cyclic behaviour, there are differences in how the boundary surface is defined. Mohamad and Dobry (1986) considered the steady state line as a boundary surface in defining the cyclic shear strength, while Sladen *et al.* (1985) considered that the peak strength envelope defines a boundary for cyclic flow failure. On the other hand, Hyde and Ward (1995) recommended that the dry side of the State Boundary Surface (SBS), often named the Hvorslev surface, defines the boundary for stability of cyclic effective stress. Most of these findings are, however, based on experimental results obtained from uncemented granular materials, and there are still some uncertainties in using these findings to cemented calcareous soils.

Despite the extensive research on calcareous soils in recent years, there have been very limited systematic studies on the cyclic behaviour of cemented calcareous soils (Airey and Fahey, 1991; Hyodo *et al.*, 1996). In an attempt to study the cyclic behaviour of cemented soils, artificially cemented samples prepared using the CIPS (Calcite Insitu Precipitation Systems) technique were tested extensively, under triaxial conditions with different levels of stress combination and consolidation history.

In this paper, the characteristic phenomenon that controls the undrained cyclic triaxial behaviour of cemented soil will be analysed. Experimental results obtained from laboratory testing will be used to examine what defines the boundary surface for the cyclic stress path, and how it is linked to the corresponding monotonic behaviour. An attempt will also be made to explain the cyclic fatigue behaviour of cemented soil based on the experimental results.

2. MATERIAL USED

The soil used in this study is a reconstituted fine-grained offshore calcareous soil recovered from the seabed near the vicinity of the Goodwyn 'A' gas platform. Figure 1 shows the grading curve of the soil, which shows that the soil is a fine to medium silty sand, with fines content (< 0.075 mm) of about 37%. Table 1 summaries some of the physical properties of the soil. Details of the soil can be found in Ismail (2000).

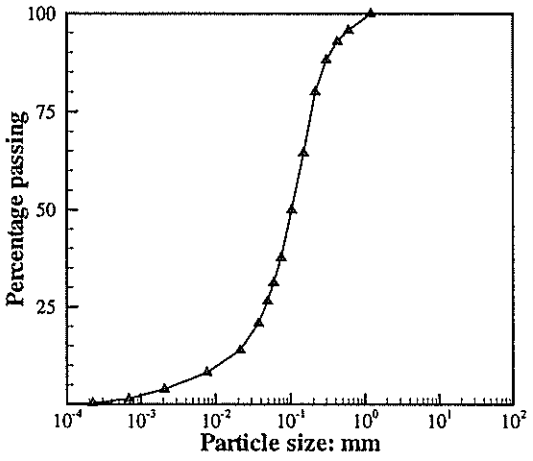

Figure 1 Particle size distribution

Table 1 physical properties of soil

G_s	D_{60}	D_{10}	Carbonate %	e_{max}	e_{min}
2.72	0.13	0.133	94	2.317	1.266

A proprietary chemical cementation system called CIPS (Calcite In-situ Precipitation System) developed by the CSIRO is used in this study for artificial cementation. In the CIPS technique, cementation is achieved by flushing a mixture of two solutions through the soil sample resulting in precipitation of calcite on the surface of the soil grains, and this imparts cohesive strength due to bonding at particle contacts (Kucharski *et al.* 1996; Ismail, 2000).

3. EXPERIMENTAL PROCEDURE

3.1 Sample preparation

The sample preparation technique described by Ismail (2000) was used in this study to prepare artificially cemented samples for triaxial testing. This technique consisted of pluviating the dry soil inside a rubber membrane stretched inside a mould. The preselected density was achieved by tapping the mould with a plastic hammer. The sample was then loaded with a seating pressure. Carbon dioxide gas was flushed through the sample from bottom to top followed by flushing of water. The mixture of the CIPS solution was then flushed through the sample. A minimum of 15 kPa effective pressure was always maintained between the seating pressure and flushing pressure to avoid heave of the sample during the flushing process. The sample was left to cure for 24 hours. The same procedures were repeated for the next flush of CIPS, whenever multiple flushes of CIPS is needed. An interval of 24 hours was always maintained between each successive flush of the CIPS solution. After the last flush, the sample was left to cure for another 24 hours before testing.

3.2 Triaxial tests

Triaxial tests were carried out using a computer controlled triaxial machine designed and fabricated at The University of Western Australia. Axial load and displacement were measured using a load cell and an external potentiometer respectively. Internal submersible LVDTs were also used to measure the local strains. The LVDTs were fixed to the sample using four minute aluminium footings implanted into the sample by gluing them inside the rubber membrane prior to sample preparation (Ismail *et al,* 2000). The arrangement used to fix the LVDTs is shown in Figure 2. This arrangement avoids possible errors due to the relative slippage between the rubber membrane and the sample surface, which could jeopardise the accuracy of results (Tatsuoka & Kohata, 1995). This measuring system can resolve axial strain down to about 0.00001.

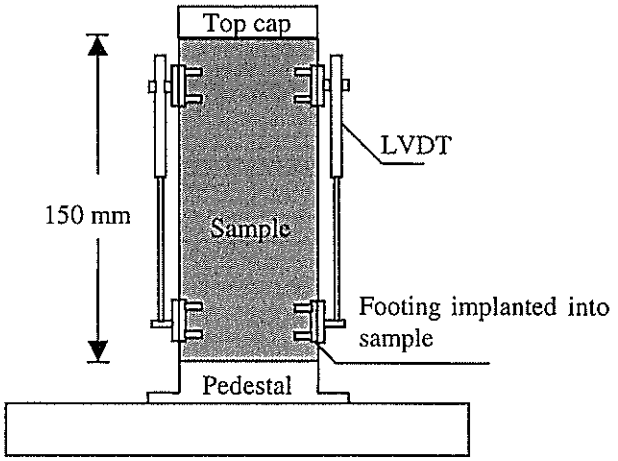

Figure 2 Schematic diagram of the set-up of a sample in the triaxial with internal LVDTs (Figure not in scale)

4. TEST RESULTS

4. 1 Unconfined compressive strength (UCS)

To quantify the effect of cementation due to precipitation of calcite, UCS test was performed on cemented samples. Many researchers reported that the strength of cemented samples reduced with the increase in the degree of saturation (Cook, 1999). To avoid this problem and to obtain consistent results, cemented samples were saturated inside the triaxial cell before testing. For this study only one level of cementation was selected with UCS of 0.5 MPa. This was achieved by using two flushes of the CIPS solution with calcite concentration of 0.15 t/m^3. The resulting cement/soil ratio of cemented samples was 0.17. The final dry density of all the cemented samples was 1.17 ± 0.05 t/m^3.

4.2 Monotonic shearing response

Results of undrained triaxial tests performed on isotropically consolidated cemented samples under confining pressures (p'_o) from 50 to 1000 kPa are shown in Fig 3. During undrained shearing at low confining pressure (50 kPa and 200 kPa), the pore pressure increases first until the deviator stress approaches the maximum value. This is followed by a

decreasing pore pressure and brittle yielding with strain-softening response. Samples consolidated to a higher confining pressure also showed the strain softening response after peak deviator stress; however, with increasing pore pressure. It can be observed that the peak deviator stress varies with (p'_o). For the samples tested at values of p'_o (at 50 to 600 kPa), the increase in (p'_o) increases the peak strength significantly. However, the change in the peak strength for the samples tested at 1000 kPa compared with those tested at 600 kPa is relatively small. This is believed to be due to some degradation of the cementation bond after consolidating the sample to the higher stress level.

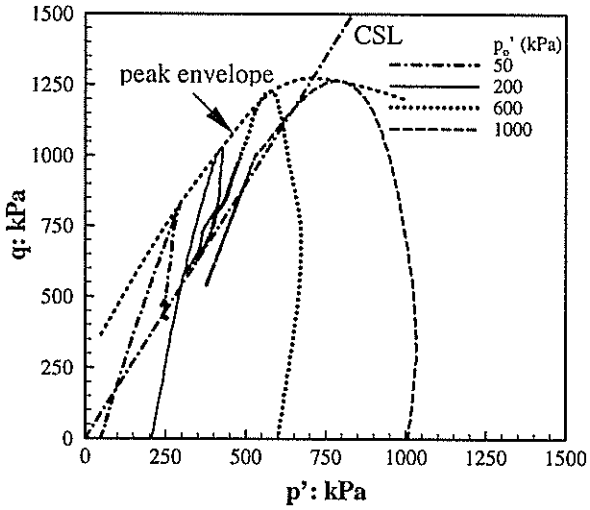

Figure 3 Effective stress paths for cemented soil

Since the peak deviator stress is followed by strain softening response in all the samples, the peak stress can be considered as a failure stress. Hence, the line passing through the peak deviator stress points could be used to define the peak envelope. The peak envelope of these samples is also superimposed on Figure 3.

Scrutiny of the effective stress paths reveals that cemented samples reach different maximum stress ratios, η_{max} for different initial consolidation pressures (p'_o). The η_{max} decreases with increasing (p'_o), and at (p'_o) = 1000 kPa, η_{max} is almost equal to the slope of the CSL (M). For the test results shown in Figure 3, η_{max} corresponds to the peak deviator stress. However differences could also be observed (Ismail, 2000).

To examine the effect of anisotropic consolidation, cemented samples were consolidated anisotropically to different Ko values (points a and b in Fig 4), maintaining the same mean effective consolidation pressure, (p'_o) of 200 kPa as shown in Figure 4. The value of 200 kPa was chosen to avoid degradation of the cementation resulting from consolidation to higher mean effective stresses. The stress paths of these samples during undrained shearing, after the anisotropic consolidation, are very similar to those obtained from isotropically consolidated samples. However, with increasing initial deviator stress during consolidation, there is a trend of decreasing peak deviator stress with increasing η_{max}.

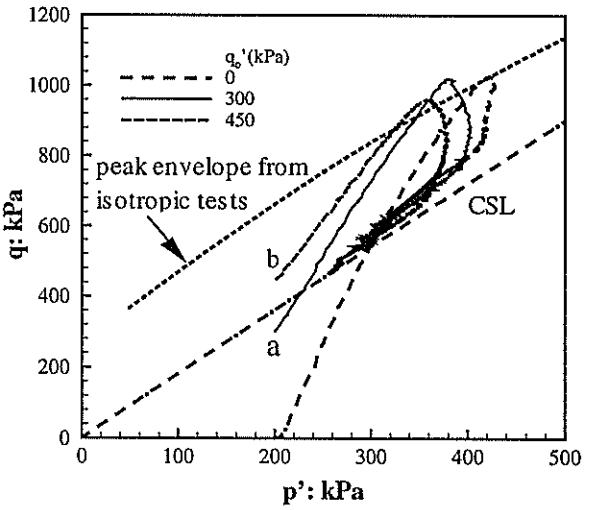

Figure 4 Monotonic effective stress paths for anisotropically consolidated cemented soil

4.3 Cyclic shearing response

A large number of cyclic triaxial tests with different initial conditions were performed in this study. Typical results obtained from these tests are shown in Figures 5 and 6. These tests can be classified into three main groups, based on the testing conditions: (i) one-way tests with $q_{mean} = q_{cyc}$; (ii) one-way tests with $q_{mean} > q_{cyc}$; and (iii) two-way tests with stress reversal, $q_{mean} < q_{cyc}$. Both the stress paths and the associated stress–strain curves are shown in Figures 5 and 6. However, the stress path corresponding to only selected number of cycles are shown for the sake of clarity. Superimposed on the plots of stress paths are peak envelope, η_{max} and CSL obtained from the corresponding monotonic tests.

Three extreme kinds of failure patterns were observed in the samples tested in this series. The first is liquefaction or cyclic mobility, where the stress path reaches zero (or close to zero) effective stress during cyclic loading, and failure of the samples takes place due to the development of large cyclic axial strain (Figure 5b and 6b). In the second case, where the samples were subjected to one-way cyclic loading, the failure of the sample takes place due to accumulation of large residual strain instead of cyclic strain (Figure 5a, 6a and 5c, 6c). In the third case, failure is due to combined accumulation of residual strain and large cyclic strain (Figure 5d and 6d).

Further investigation of the test results shows that the effective stress path moves towards the origin due to accumulation of pore pressure during undrained cyclic loading until it touches the η_{max} line obtained form the corresponding monotonic test. Further straining causes either development of large cyclic strain with rapid development of pore pressure or rapid accumulation of residual strain with increasing or decreasing pore

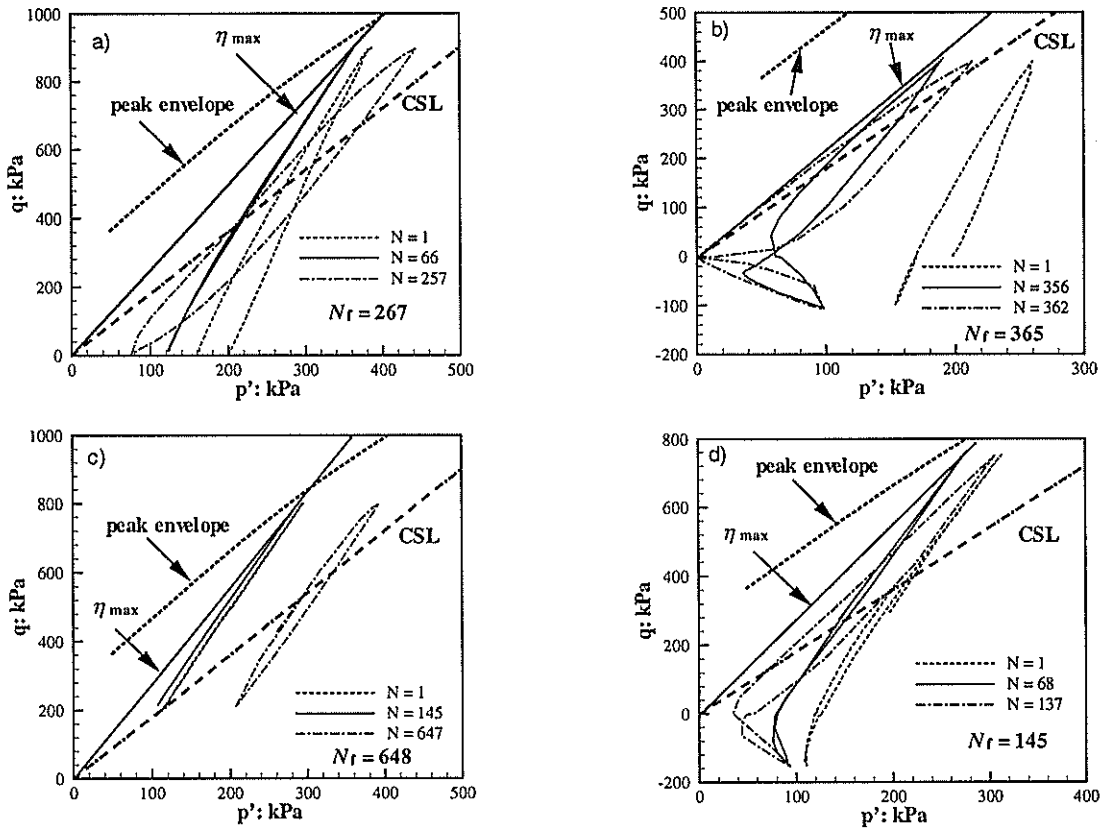

Figure 5 Typical stress paths for cemented samples observed in cyclic triaxial tests

pressure, depending on the level of applied cyclic and mean deviator stress as well as the location of the stress-state in the stress space.

The previous discussion means that for all tested samples in this series, there is initial accumulation of positive pore pressure until the stress path touches the η_{max} line obtained from monotonic test. However, the differences in the response among the different samples lie in the response after straining of the sample beyond the η_{max} line.

The response can be categorised into two typical stress paths based on the response of residual pore pressure after the sample reaches the state of η_{max} during cyclic loading. In the first type, the accumulation of residual pore pressure or cyclic liquefaction can be observed. This type of response is shown in Figure 5a, 5b and 5d. On the other hand, the second type shows that dissipation of residual pore pressure after the stress-state touches the η_{max} line as shown in Figure 5c.

These responses are very typical for all the cemented Goodwyn samples tested in this study irrespective of the confining pressure, consolidation history or whether the cyclic regime incorporates one-way or two-way loading.

4.4 Cyclic fatigue theory for cemented sand

Among the three envelopes-the failure envelope, the η_{max} line and the CSL, obtained from the monotonic tests- it is observed that both the η_{max} line and the CSL control the orientation of the effective stress path during cyclic loading. Therefor the apparent analogy between cyclic and monotonic loading tests could be made using the η_{max} line and the CSL. The observed phenomena during cyclic loading of cemented sand can be represented by the schematic diagram shown in Figure 7.

For the one-way tests, after the stress-state reaches the η_{max} line, accumulation or dissipation of pore pressure during cyclic loading takes place depending on the relative position of the stress-state with respect to the CSL. If the initial (at the end of the consolidation stage) stress-state (q - p' space) during cyclic loading lies below the CSL (eg. point X in Fig 7a), positive pore water pressure would develop. However, if the initial stress-state during cyclic loading lies above the CSL (eg. point Y in Fig 7c), the pore water pressure would dissipate with successive cycles after the η_{max} line is reached.

For the two-way tests, failure is dominated by liquefaction-related phenomena. The response in two-way tests is similar to one-way tests until the stress-state reaches the η_{max} line, either in extension or in compression. If the stress path reaches the η_{max} line in extension first, rapid generation of pore pressure, and hence the development of large cyclic strain, takes place, and failure occurs. This phenomenon is called cyclic liquefaction (Figure 7b). On the other hand, if the stress path reaches the η_{max} line in the compression side first, failure is due to the combination of large

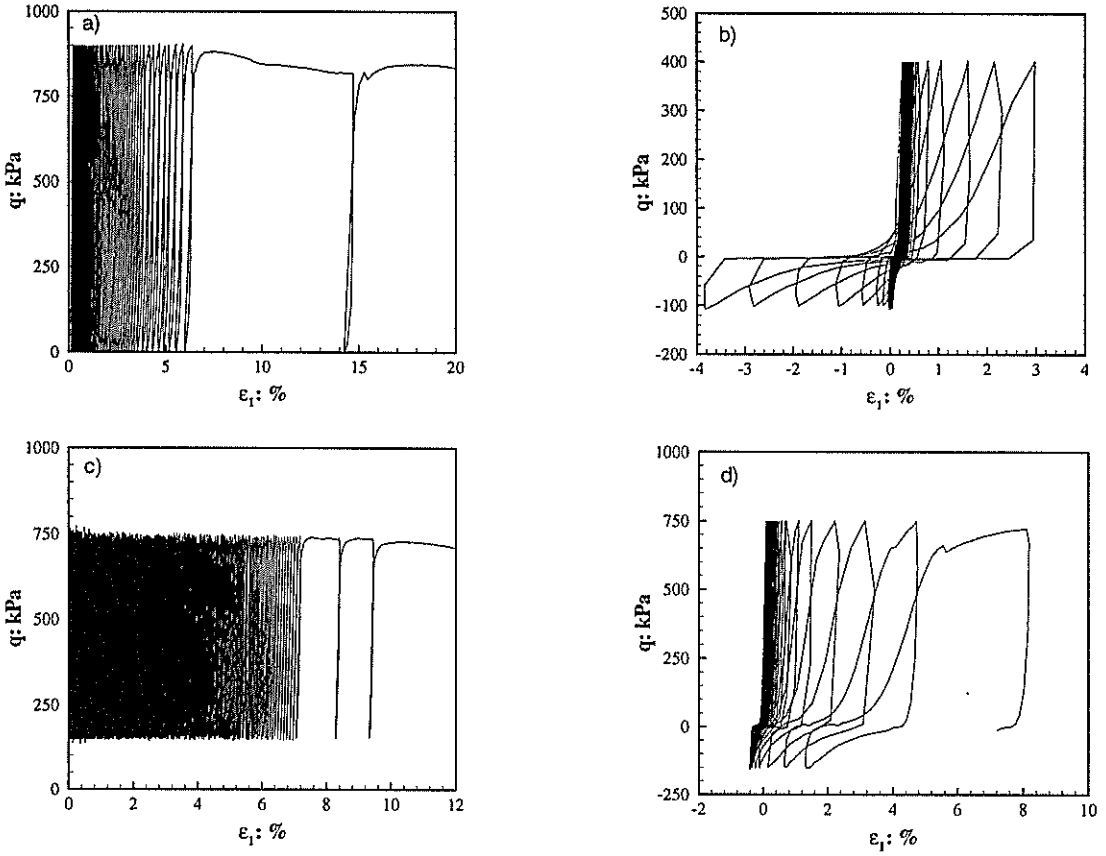

Figure 6 Typical stress strain curves for cemented samples observed in cyclic triaxial tests

residual strain and large cyclic strain. In this condition, the generation or dissipation of pore pressure depends on the relative position of the stress-state during cyclic loading with respect to the CSL as discussed before.

The schematic representation presented in this diagram is similar to the one presented by Ibsen (1998). However, the difference lies on the considerations of the boundary. Ibsen (1998) considered the characteristics state, a state where $\delta\varepsilon_v/\delta\varepsilon_1 = 0$, as the boundary that controls the cyclic behaviour of uncemented sand. Whereas for the cemented sand tested under undrained conditions, the η_{max} line obtained from monotonic test serves as a boundary for cyclic tests. This suggests that, provided the boundary is defined properly, the behaviour of cemented and uncemented soils can be explained within the same framework.

Only undrained cyclic triaxial tests were performed in this study. No effort has been made to define the behaviour during drained cyclic loading. However, it is believed that a proper normalisation scheme (most probably the one proposed by Cuccovillo and Coop, 1999) should be able to link the behaviour proposed during undrained tests with that in drained cyclic tests.

5. SUMMARY AND CONCLUSIONS

This paper has investigated the behaviour of cemented sand under undrained cyclic loading. It has been found that, the response in cyclic loading is similar to that observed during monotonic loading. It is found that the cyclic response can be explained using the η_{max} line and CSL obtained from the corresponding monotonic tests.

A similar response, in terms of generation of positive pore pressure, is observed for all the samples tested under cyclic loading, irrespective of confining pressure and consolidation history. The generation of positive pore pressure continues until the stress path during cyclic loading touches the η_{max} line obtained from the corresponding monotonic tests. However, differences in response in terms of pore pressure and the associated failure condition are observed with further straining after the samples reach the state of η_{max}. The stress space (q - p′ space) during cyclic loading can be divided into two sub-spaces. In the first, cyclic loading will generate positive pore pressure if the initial stress-state was located below the CSL. In the second, negative pore pressure would develop if the initial stress-state lies above the CSL.

6. ACKNOWLEDGEMENTS

The work presented in this paper forms part of the research activities of the Centre for Offshore Foundation Systems (COFS), established and supported under the Australian Research Council's Research Centres Program. The author is supported by an International Postgraduate Research Scholarship (IPRS) and a Geomechanics group Studentship. This support is gratefully acknowledged. The collaboration of Dr Edward Kucharski and Bob Middleton from Lithic Technology (who provided the CIPS solution) is also appreciated.

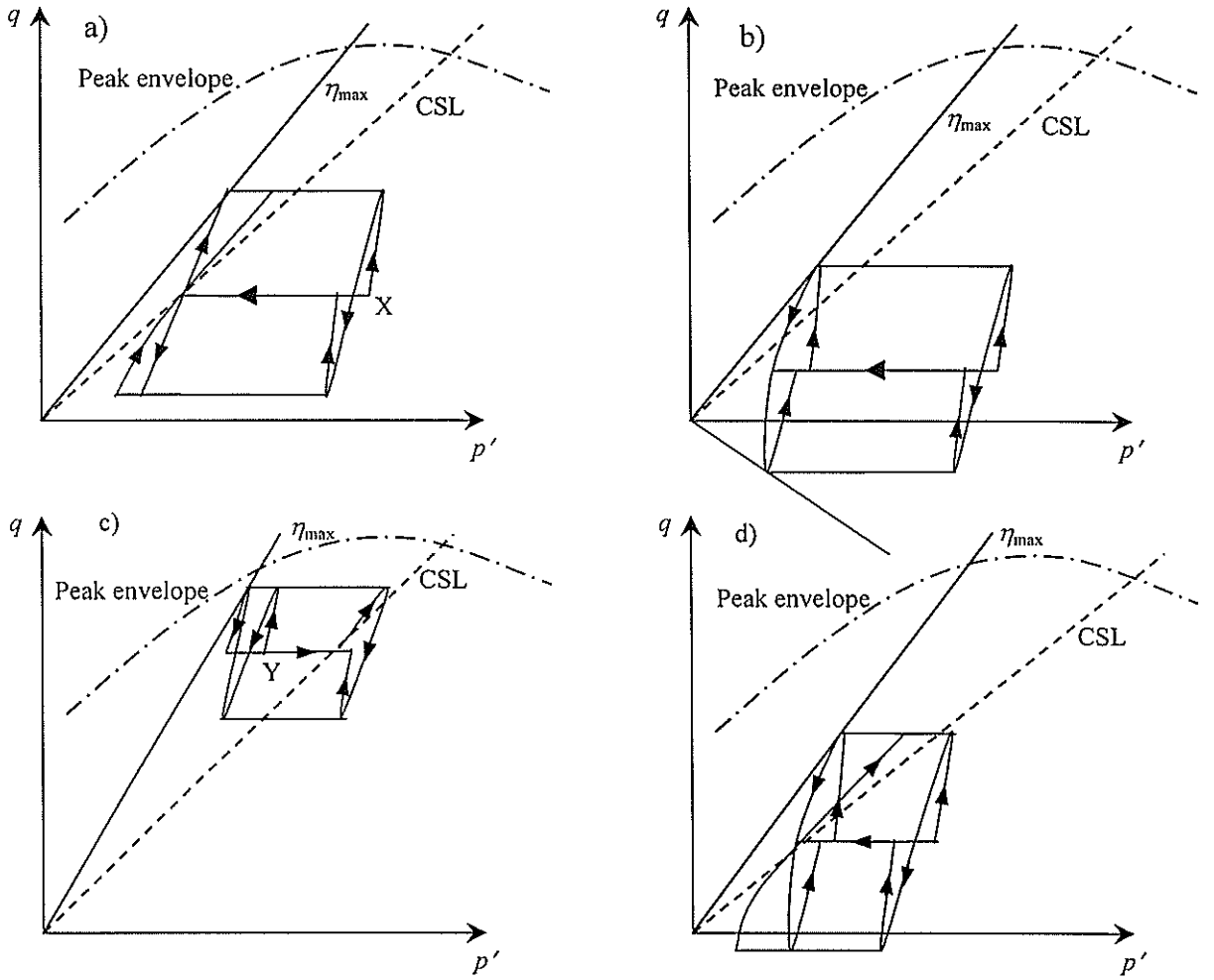

Figure 7 Schematic diagram explaining the fatigue theory of cemented sand

7. REFERENCES

1. Alarcon-Guzman, A., Leonards, G. A. & Chameau, J. L. (1988), "Undrained monotonic and cyclic strength of sands", Journal of Geotechnical Engineering, ASCE **114**, No. 10, 1089-1109.

2. Mohamad, R. & Dobry, R. (1986), "Undrained monotonic and cyclic triaxial strength of sand", Journal of Geotechnical Engineering, ASCE **112**, No. 10, 941-958.

3. Sladen, J. A. D'Hollander, R. D. & Krahn, J. (1985), "The liquefaction of sands, a Collapse Surface approach", Canadian Geotechnical Journal, **22**, 564-578.

4. Hyde, A. F. L. & Ward, S.J. (1985), "A pore pressure and stability model for a silty Clay under repeated loading", Géotechnique, **35**, No. 2, 113-125.

5. Airey, D.W. & Fahey, M. (1991), "Cyclic response of calcareous soil from the North-West Shelf of Australia", Géotechnique, **41**, No. 1, 101-121.

6. Hyodo, M., Hyde, A.F.L., & Aramaki, N. (1998), "Liquefaction of crushable soils", Géotechnique, **48**, No. 4, 527-54.

7. Kucharski, E., Price, G., Li, H., & Joer H. A. (1996), "Engineering properties of CIPS cemented calcareous sand", Proc. of the 30th Int'l Geological Congress, China, 92-97.

8. Ismail, M. A. (2000), "Strength and deformation behaviour of calcite-cemented calcareous soils", PhD Thesis, The University of Western Australia.

9. Ismail, M. A., Sharma, S. S. & Randolph, M. F. (2000), "Small and large strain behaviour of a calcareous soil lithified by different cements", GeoEng 2000, Melbourne.

10. Tatsuoka, F. & Kohata, Y. (1995), "Stiffness of hard soils and soft rocks in engineering applications", Prefailure Deformation of geomaterials, **2**, Shibuya, Mitachi & Miura (eds), 947-1063, Balkema, Rotterdam.

11. Cook, A. W. (1999), "The rate of drying out of calcarenite", Proc. of the 2nd Int'l Conf. on Calcareous Sediments, Bahrain **1**, 229-231.

12. Ibsen, L. B. (1998), "The mechanism controlling the static liquefaction and cyclic strength of sand", Physics and mechanisms of soil liquefaction, Lade & Yamamuro (eds), Balkema, Rotterdam, 29-39.

13. Cuccovillo, T. and Coop, M.R., 1999, "On the mechanics of Structured Sands", Géotechnique, **49**, No. 6, 741-760

Geotechnical Properties and Geothermal Instability Hazards of Kuirau Park, Rotorua

M.A. Slako & W.M. Prebble, Department of Geology, University of Auckland

SUMMARY

Kuirau Park lies above the exploited Rotorua Geothermal Field. Due to recent increased thermal activity, a study of thermal features and geotechnical properties was carried out. The stratigraphy consisits of a permeable and impermeable, faulted sedimentary sequence, which overlies the fractured and faulted Rotorua Rhyloite aquifer and Mamaku Ignimbrite. Faults penetrate the strata to allow thermal fluids to discharge at the surface in the form of acid-sulfate and alkali-chloride pools, barren ground and hydrothermal eruptions. Fifty thermal features within the park were monitored over six months for temperature, pH and visible activity. The results show a trend back towards an earlier condition of the geothermal field. Hydrothermal eruptions within Kuirau Park are hazardous. The nature of the January 26th eruption of feature 721 was studied. The eruption trigger was most probably from a slight increase in temperature beneath Kuirau Park.

1. INTRODUCTION

1.1 Geography

The Rotorua Geothermal Field (RGF) lies at the southern end of Lake Rotorua, within the Rotorua Caldera. Rotorua City lies within the RGF, and the study area, Kuirau Park is located north-west of the city centre (Figure 1). Kuirau Park extends south from Ohinemutu and west of Hospital Hill (Pukeroa) covering an area approximately 1 km^2.

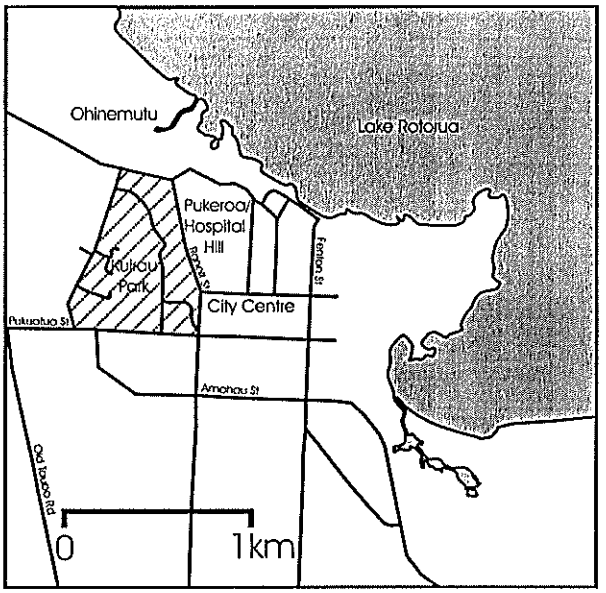

Figure 1: Rotorua City and location of Kuirau Park

Kuirau Park is low lying and sits only slightly above Lake Rotorua. It is an area of swampy alluvial ground.

1.2 Regional and Local Setting

The RGF is situated in the north-western part of the Taupo Volcanic Zone (TVZ), Central North Island, New Zealand (Figure 2). The TVZ extends north-east from the Tongariro Volcanic district to White Island (Simmons, Browne and Brathwaite [1],1992).

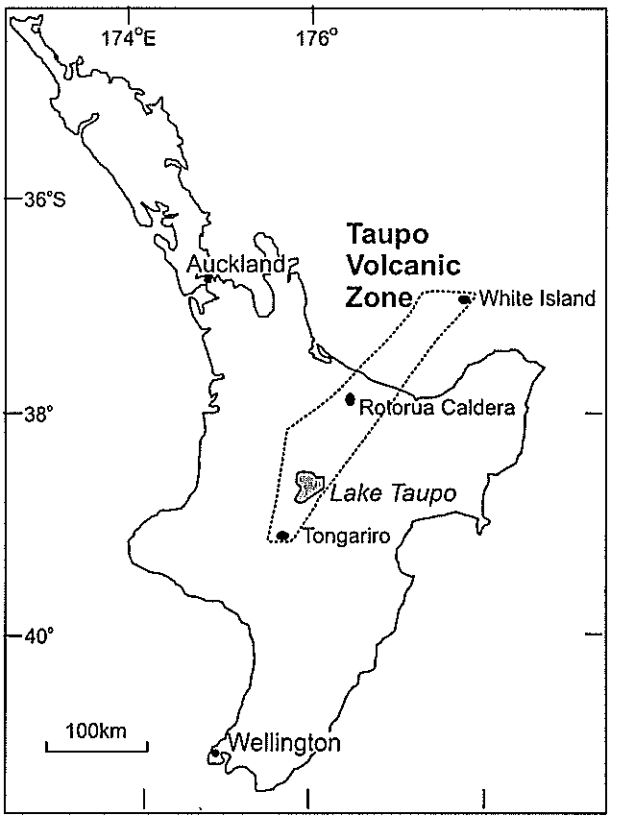

Figure 2: Rotorua Caldera, TVZ, North Island, New Zealand (adapted from (Shane [2],2000))

The RGF is one of over 20 geothermal fields in the TVZ. It covers an area of approximately 12km^2 towards the southern margin of the Rotorua Caldera Basin. It is the only exploited geothermal field in the world where a management scheme has later been emplaced to restrict exploitation and enhance surface expression (Wood [3],1992).

1.3 Purpose of Study

Concerns were raised in the mid 1970s about the 'quieting' and possible extinction of Rotorua's geysers and hot springs. In 1986, the New Zealand Government initiated the closure of all government

owned bores in Rotorua City and all geothermal wells within a 1.5 km radius of Pohutu Geyser at Whakarewarewa (Scott and Cody [4],2000). The aim of the shut down was to restore pressure and water levels in the geothermal aquifer. The closure of private bores and the re-injection of commercially abstracted fluid back into the aquifer has seen Rotorua's geothermal field respond and move back towards its previous condition.

Over the last 12 months there has been much interest in events at Kuirau Park, in particular the hydrothermal eruption from feature '721' in the north-eastern part of the park. This eruption ejected mud and debris up to 100 m towards a nearby street and left a 15 m wide crater. In addition, the basketball courts at the southern end of Kuirau Park have been subsiding and buckling and hot water pools have appeared around the edges of the playing surface. Numerous thermal features within the park have increased in activity, bubbling to higher levels and more intensely in recent times.

In February 2001, Environment Bay of Plenty (EnvBOP) decided the situation in Kuirau Park needed to be monitored and assessed. Previously, there was no regular monitoring of geothermal activity in Kuirau Park. The intention of this study is to determine what is happening to geothermal activity, to assess the stratigraphy beneath the park including the distribution of sinter deposits and to examine the geotechnical properties of the materials present. The research also aims to study the deposits, dynamics, possible causes and triggers of the hydrothermal eruption of feature 721.

2. ROCK AND SOIL MASSES

2.1 Stratigraphy

Most of what is known about the stratigraphy of the Rotorua Geothermal Field has been ascertained from drill logs of geothermal wells. Most drillholes in the RGF are less than 200 m deep, so little is known about the geology of the deep geothermal reservoir. The units encountered are:

Mamaku Ignimbrite

The lowest unit penetrated, Mamaku Ignimbrite, lies at a depth below 200 m (Figure 3). The ignimbrite was laid down as a sheet during the formation of the Rotorua Caldera, 230,000 years ago (Shane, Black and Westgate [5],1994). Poorly consolidated pumiceous Mamaku tuff overlies welded ignimbrite (Wood [6],1985). The soft tuff is either an erosional deposit derived from the Mamaku Ignimbrite or an unwelded ash flow member of the same formation.

Mamaku Ignimbrite is described from cores as a pink pumice-lapilli crystal vitric tuff (Wood [6],1985). In drill cuttings the ignimbrite and soft tuff are indistinguishable. In some wells the soft tuff is absent and impermeable organic-rich sediments directly overly fractured ignimbrite. This indicates erosion occurred prior to lake transgression in these areas.

Rotorua (Haparangi) Rhyolite

Rotorua's multiple rhyolite domes may all be part of

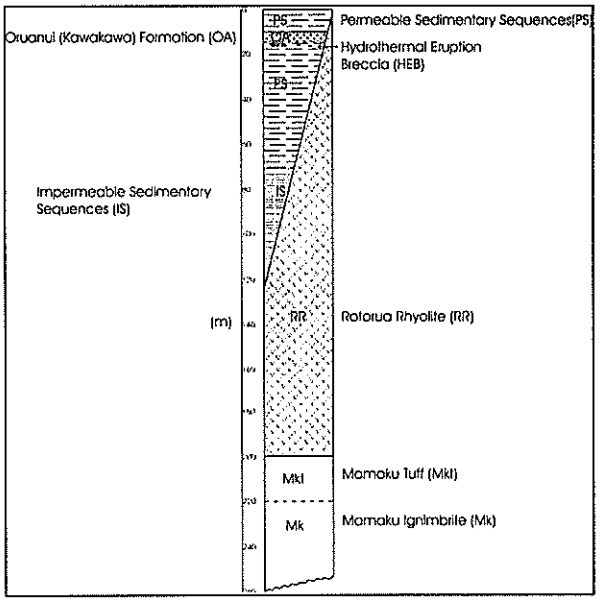

Figure 3: Stratigraphic column of lithology beneath Kuirau Park

the same extensive rhyolite volcano complex which followed formation of the Rotorua Caldera. The domes are thought to represent the extrusion of copious amounts of rhyolitic magma from the Mamaku Ignimbrite eruption vents (Wood [3],1992). Pukeroa (Hospital Hill) on the eastern side of Kuirau Park is one of these domes (Figure 1).

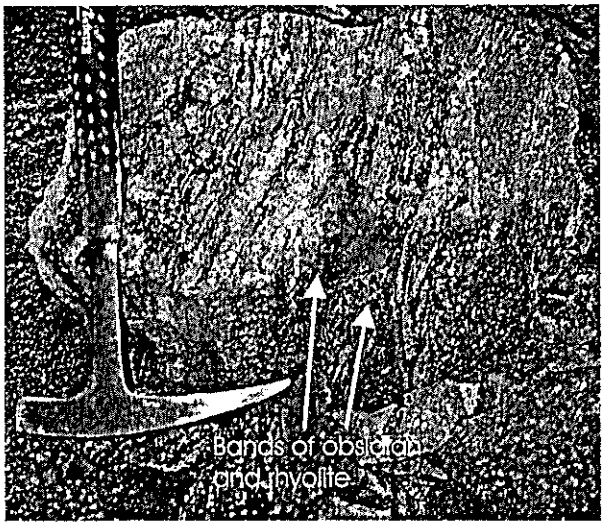

Figure 4: Rotorua Rhyolite at Ngongotaha Quarry ~10 km north of Rotorua City

Most geothermal boreholes in the city area have penetrated the Rotorua Rhyolite. The lava outcrops on the eastern side of Pukeroa dome. A cap of silicified, coarse rhyolite breccias make up the top 40 metres of the dome (Wood [6],1985). The rhyolite is described as light grey, moderately soft, sugary, slightly vesicular crystalline rock (Thompson [7],1974) and is illustrated in Figure 4. Rotorua Rhyolite typically grades down through a series of mantling skins. First perlitic glass, then obsidian with more spherulites, to a grey

spherulitic lithic rhyolite that forms the bulk of the domes. The thickness of the rhyolite under the city is unknown, as no boreholes have penetrated its base (Wood [3],1992). Beneath Kuirau Park the rhyolite extends down approximately 200 metres before the Mamaku Ignimbrite begins.

Sedimentary Sequences
The sedimentary sequences within the Rotorua Caldera basin cannot be correlated across the entire RGF. A number of stratigraphic units result from different phases of localised deposition and volcanic activity. The deposits have accumulated in a varied and changeable environment at the caldera margin. Problems of poor sampling from drillholes and sharp lateral and vertical variability preclude the establishment of a type sequence of strata (Wood [3],1992)

The impermeable sediment layers are essentially muddy sands and silts (I.S., Figure 3). The thickness of the muds ranges from 20 to 190 m throughout the Rotorua basin. The change from impermeable to permeable sediments is diachronous and dependent on local conditions (Wood [6],1985). The range of sediment types is wide. The overlying permeable sediments are mostly porous gravels, sands and pumiceous tephras.

2.2 Geotechnical Properties

Mamaku Ignimbrite
The Mamaku Ignimbrite acts as an aquifer beneath Rotorua City (Figure 5). The tuff and ignimbrite units are hydrogeologically distinct (Wood [6],1985). The tuff is more porous than the massive ignimbrite which is however, vertically jointed . As depth increases, the ignimbrite becomes harder and fractures are more numerous (Thompson [7],1974). In outcrops outside the RGF, Mamaku Ignimbrite shows a fracture frequency of 0.5 – 1 joints per metre (Wood [6],1985).

The welded ignimbrite is moderately strong (R3) and is also permeable (NZGS [8],1988). Hot fluids penetrate the pumiceous groundmass, and the rock exhibits pervasive hydrothermal alteration (Wood [6],1985).

Rotorua (Haparangi) Rhyolite
The rhyolite lava is the production aquifer for most boreholes in the commercial district and southern suburbs of Rotorua City (Wood [3],1992). Hot water rises into the Rotorua rhyolite and flows laterally through the exploited extent of the aquifer.

The outer cap of rubbly, pumiceous rhyolite is permeable and weakly fractured but mainly impermeable rock lies beneath. The permeability of the rhyolite appears to decrease with depth (Wood [6],1985). Rock strength is R2 – R3, which is weak to moderately strong (NZGS [8],1988).

Sedimentary Sequences
Individual beds within the lower sedimentary layers may be moderately permeable. Layers of tuff, gravels and coarse sands have limited lateral extent and are

Lithology	Description	Permeability	Strength	Weathering	Defects/Fractures	Water
Permeable Sedimentary Sequences PS	Layered sequences of primary and redeposited volcanic tephras, alluvium and lacustrine sediments. Pumice gravels, diatomatic muds, peat beds and vitric tuffs.	Highly porous gravels, sands and permeable pumiceous layers.	S1-S2	Sensitive tan-white pumiceous sands; liquefy when shaken and remould.		Aquifer - pumice sands are very wet in places.
Oruanui Ash OA	Greenish grey fall member. Accretionary lapilli up to 2cm diam.	Defects indicating some permeability.	S6	Slightly weathered.	Pyrite filled veins within blocks.	Water movement through veins, indicated by pyritic infillings.
Hydrothermal Eruption Breccia HEB	Hydrothermal Eruption Breccia. Very poorly sorted, polymict texture.	Impermeable fabric, fracture permeability uncertain.	R2	Altered, matrix is two different colours.	Uncertain, probably fractured.	?
Impermeable Sedimentary Sequences IS	Muddy sands and silts, deposited mainly in between the formation of Mamaku Ignimbrite and Rotorua Rhyolite.	Aquitard - impermeable muds. Also individual, discrete porous beds, but with limited lateral extent.	?	?	Complex fault pattern associated with caldera margins. Some silicification, reducing permeability.	Aquitard - faults channel fluids through impermeable sediments.
Rotorua Rhyolite RR	Glassy and lithoidal rhyolite of early dome building stages.	Good fracture permeability. Permeability decreases with depth.	R2-R3	Brecciated cap, ~40m thick.	Outer cap of rubbly pumiceous rhyolite. Weakly fractured impermeable rock beneath this.	Aquifer - hot water rises into rhyolite and flows laterally through exploited extent of the Rotorua Rhyolite aquifer.
Mamaku Ignimbrite 230,000 Mk Mk tuff Mk	Pale pink to grey Ignimbrite containing plagioclase and minor quartz. Poorly welded. Tuff - poorly consolidated, soft, pumiceous tuff - either erosional deposit or unwelded ashflow member.	Tuff - more porous than ignimbrite. Ignimbrite - good fracture permeability, but may have been affected by hydrothermal alt. and self-sealing.	R3	Pervasive hydrothermal alteration.	Fracture frequency of 0.5 - 1 joint/metre veins in outcrops outside RGF.	Aquifer

Figure 5: Geotechnical legend showing properties of materials (refer also to Figure 3)

occluded by low-permeability muddy sands and silts. Silicification of some of these sediments has also reduced permeability.

In Kuirau Park the uppermost sediments are mainly permeable pumice sands. These are very wet and act as an aquifer. Samples taken near the surface show some sensitivity. They are pinkish tan and liquefy when disturbed. Soil strength is classified as S1 – S2 (NZGS [8],1988).

3. FAULT STRUCTURE

The Kuirau Fault is inferred to occur along the eastern side of Kuirau Park and the thermal features within the park are fed from the Pukeroa dome rhyolite aquifer which is cut by this fault (Figure 6). The impermeable mudstones overlying the rhyolite act as aquitards. Where the layers have been faulted, fluids are probably channelled through the aquitard (Wood [6],1985).

The Kuirua Fault is inferred from geomorphic and geothermal evidence. Ranolf Street forms the eastern boundary of Kuirau Park. East of the street, the topography rises steeply to Pukeroa Dome and this indicates a probable fault trace.

The thermal features in Kuirau Park are aligned in two main directions (Figure 6). One lineament trends NNW – SSE. The other, splays off this and trends NW – SE. The coincidence of surface thermal activity, high bore temperatures, and rhyolite surface morphology in Kuirau Park further imply a concealed fault trace. The Kuirau Fault is thought to control the locations of thermal features at the surface.

4. THERMAL SURFACE EXPRESSION

In New Zealand geothermal systems the principal fluid type is characterised by near neutral pH chloride waters with variable CO_2 contents (Hedenquist [9],1986). The surface thermal expression in Kuirau Park is represented by a range of different features:

1) Acid-Sulfate; forms from steam heated waters. Rising thermal water fractionates into vapour (steam plus gas) and liquid phases. If the vapour condenses into groundwater, then the H_2S present can be oxidised to sulfate, forming steam-heated acid-sulfate waters. These fluids are surficial (Hedenquist [9],1986). Acid-sulfate water occurs at the surface as mud pools, with kaolin, alunite and native sulfur.

2) Alkali-Chloride; from the deep, high-temperature upflow. It discharges from boiling springs which deposit sinter.

3) Areas of barren ground; these are areas of bare ground due to high ground temperatures with no vegetation. Salts are often deposited on their surface.

Nearly two thirds of thermal features in Kuirau Park are acid-sulfate. The areas near Tarewa Road, around Whakaterekohukohu, Soda Spring and Kuirau Lake tend to be more alkali-chloride in nature (Figure 6). The Toot and Whistle area, areas north-east of Timaru

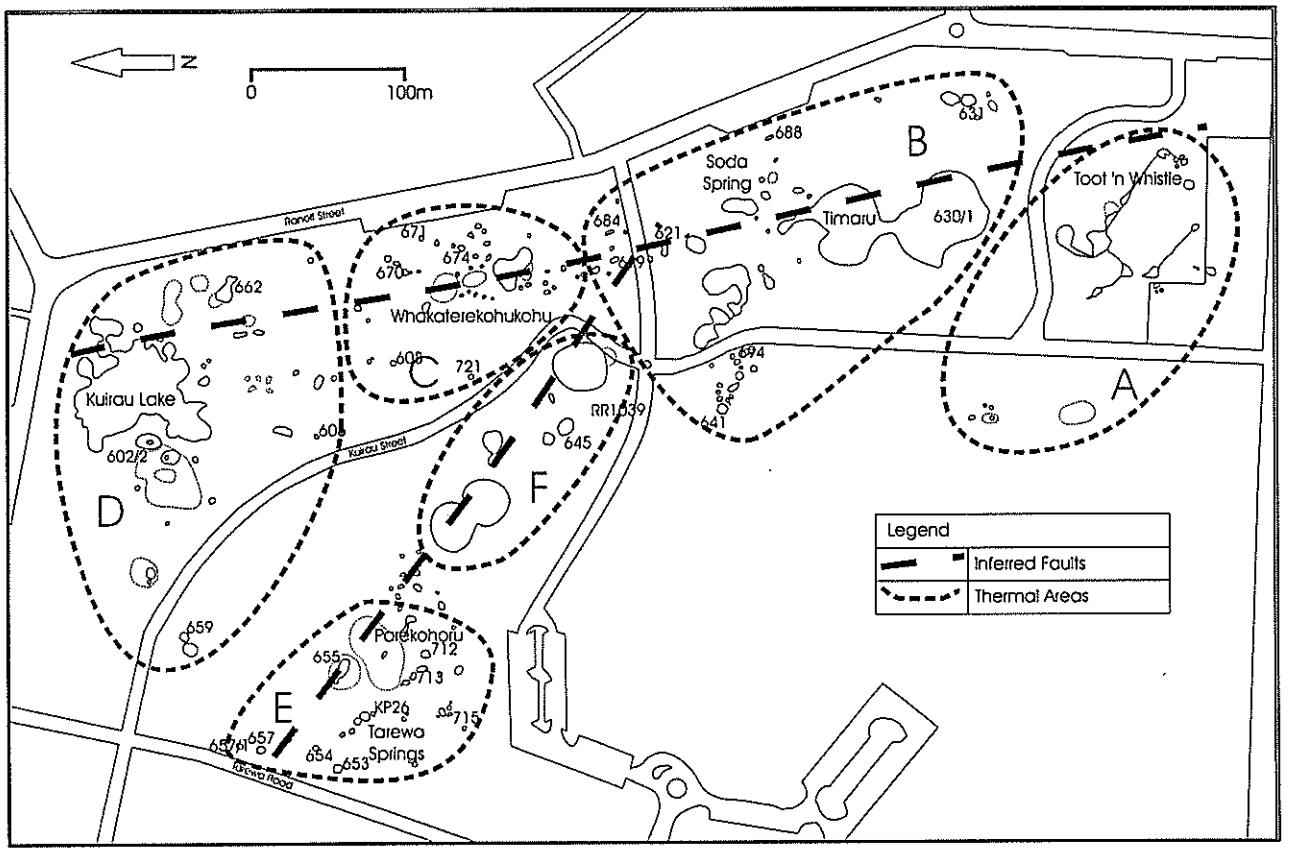

Figure 6: Map of Kuirau Park showing features, faults and thermal areas

Lake, and west of Whakaterekohukohu distribution are more acid-sulfate.

5. METHODOLOGY OF MEASUREMENTS

The initial study of thermal features within Kuirau Park involved cataloguing 175 features. A program was then carried out over the next 6 months monitoring 50 selected features distributed throughout the park. These features were chosen according to their distribution and type in order to obtain a representative pattern of activity across the area.

The surveys were carried out between February and November of 2001. Size, shape, physical characteristics, surrounding deposits and the condition of vegetation adjacent to the features were mapped. Temperature, pH, water levels, ebullition height, gases, and smell were measured and recorded.

For consistency, a sketch of each feature was made and sample locations were recorded. A Comark, Evolution N9001 thermometer was used with a resolution of 0.1 and precision of + or – 0.1°C. A MeterLab PHM202 pH meter was used, with a resolution of 0.01 pH units and precision of + or - 0.01 pH units.

6. RESULTS

The features were divided into 6 areas (A – F), (Figure 6) and grouped to look for any spatial and temporal trends.

Seven features were monitored in area A. A general gradual increase in both temperature and pH was seen over the 6 months. Some features appeared to cool from May to June, and others did so from June to August.

Area B is north of Area A. Ten features were monitored within this area. A dip in temperature over the May-June period was evident in nearly all of its (619 and 684, 641) (Figure 7). Some features may have peaked in temperature in July, making the May-June dip look more extreme (631, 621, 641). Feature 688, however, showed a rise in temperature from May to June. Feature 694 (west of Kuirau street) recorded relatively stable temperatures until October when it experienced a sharp increase, heating over 10 degrees.

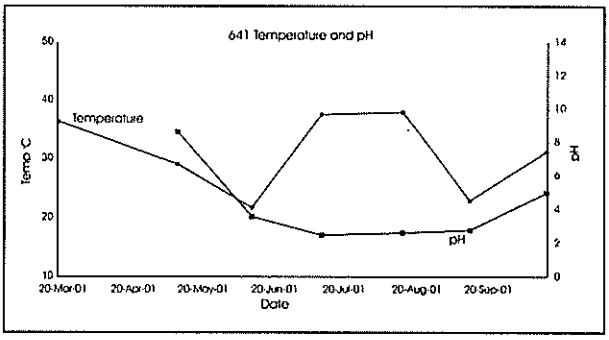

Figure 7: Temperature and pH changes for Feature 641

Area C lies around the Jaycee's monument, west of Ranolf Street. This area also includes the site of the January 26th hydrothermal eruption (Feature 721) and the area of the park where the deepest derived thermal fluid is discharged at the surface. Eight thermal features were monitored here. The May-June cooling that is evident in Area B is not so apparent in Area C. Temperatures appear to have increased in the months of June-July and features 721 and 670 both show this. Features 608 and 671 showed gradual heating over 6 months (Figure 8). Feature 674 cooled in September.

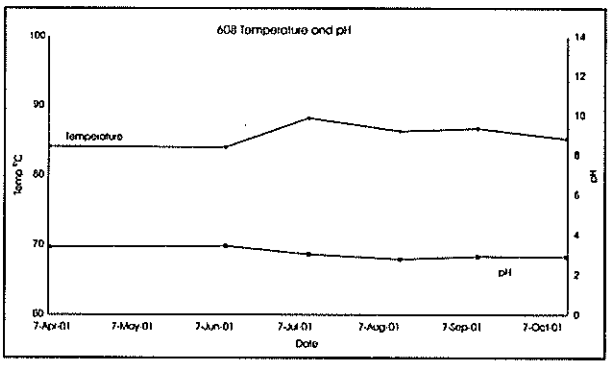

Figure 8: Temperature and pH changes for Feature 608

Area D incorporates the northern end of Kuirau Park including Kuirau Lake, and many small nearby features. Seven geothermal features were monitored. Four cooled over May to June (659, 662, 606, 602/2). Kuirau Lake cooled over July to August, but the temperature then increased in September. The pH of surface fluid remained very constant at all the features monitored in Area D over the 6 month period.

Area E covers the western region of Kuirau Park, adjacent to the Tarewa Road marae. Eleven more alkaline features were monitored in this area. Six cooled from May to June (KP26, 657, 654, 657/1, 653, 655). Three others showed a gradual increase in

surface temperature over 6 months (712, 713). The Mayors Mouth (715), however, experienced a gradual decrease in temperature consistently over the 6 month period. Once again, pH levels remained relatively constant across all the monitored features.

Area F covers the remaining features west of Kuirau Street. This includes the area of a bore RR1039 blow-out in October as well as feature 645 which was very active in April. Three features were monitored in this area. The pH again remained relatively constant. Following the very vigorous boiling and bubbling of 645 in April, this feature gradually cooled. Its temperature dropped 30° over 6 months but its pH remained constant. The other 2 features in the area experienced a slight cooling over July to August.

Overall, 40% of the features monitored experienced an increase in temperature over 6 months. 25% of features remained the same temperature, whilst 25% cooled, and 10% fluctuated showing no apparent trend.

7. HYDROTHERMAL ERUPTION HAZARD

A hydrothermal eruption is an eruption ejecting at least some solid material and whose energy derives solely from heat loss and phase changes in a convecting hot water or steam-dominated hydrothermal system (Browne and Lawless [10],2001).

In historic times, explosive hydrothermal eruptions have occurred throughout Rotorua City. These events appear to correlate with large-scale disturbances of the RGF (Scott and Cody [4],2000).

7.1 Sequence of Events

On January 26th, 2001 the largest hydrothermal eruption since 1966 occurred within Kuirau Park. During the morning of the 26th, acid-sulfate spring 721 (see Figure 9) was noticed by ground staff as it flowed across Kuirau Street to the west. About 3.30pm the spring erupted and a tourist jumped for cover into shrubbery on the west side of Kuirau Street. The eruption lasted for approximately 15 minutes. Mud and blocks were ejected about 100 metres into the air and over 120 metres east towards Ranolf Street.

7.2 Description of Deposits

Five eruption deposits can be recognized within the debris:

1) Hydrothermal mud from the crater
2) Ballistic block bed
3) Dark-grey wide spread mud spatter
4) Light-grey more directional mud spatter
5) An aerosol component

The wind at the time of the eruption was to the north-west. Black mud from the crater overflowed out towards Kuirau Street.

The next stage involved the effusive eruption of dark-grey mud and ballistic blocks to the east. These were ejected at low angles covered a fan shaped area of 65° east of the crater. Following this was the effusive eruption of light-grey, more directional mud spatter and ballistics. Materials were again ejected at low angles, but in a narrower band, approximately 25° wide.

Ballistic blocks were present beneath, within and on top of all phases of mud spatter. This indicates ballistics were ejected in all stages of the eruption. Some ballistics had sheltered zones on their leeward

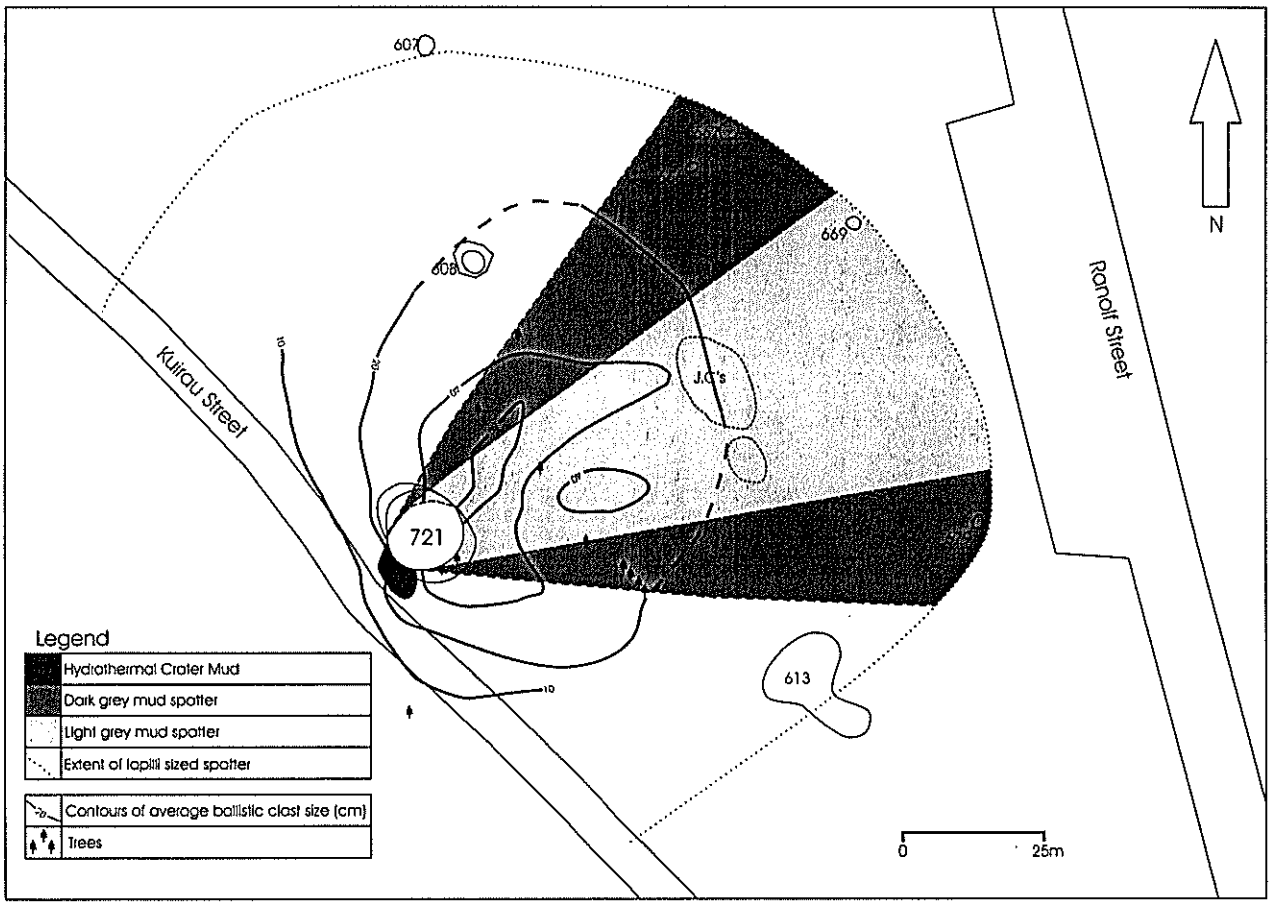

Figure 9: Deposits of 721 hydrothermal eruption on January 26th 2001

sides where no mud was deposited. The last phase of the eruption seems to have included a 'rain' of small lapilli and block sized clasts that impacted across the mud surface producing a pitted 'orange-peel' effect.

7.3 Possible Triggers

Thermal fluid in the aquifer beneath Kuirau Park is very close to boiling. As depth and pressures increase, the boiling temperature of water increases (Figure 10). Hydrothermal eruptions occur when the vapour pressure of geothermal fluids exceeds the hydrostatic boiling pressure for a given temperature (Wohletz and Heiken [11],1992).

Figure 10 shows the Pressure-Temperature curve for pure water. When dissolved gases such as CO_2 and H_2S are also present in the water, its boiling temperatures are reduced.

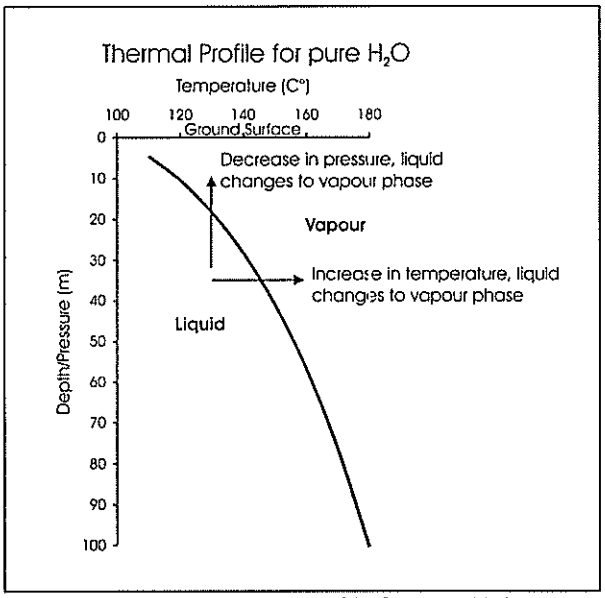

Figure 10: Thermal profile for pure H_2O

When thermal fluid boils it turns from liquid into vapour. The vapour expands greatly and occupies a much greater volume than the liquid, driving and sustaining the eruption.. As fluid temperatures beneath Kuirau Park are very near to boiling, it would take only a small increase in temperature to induce boiling, and the transition of liquid into vapour.

Approximately one week prior to the hydrothermal eruption of feature 721, a swarm of earthquakes occurred beneath Lake Rotorua. One possibility is that the seismic disturbance may have allowed gases (mainly CO_2) to enter thermal water beneath Kuirau Park. If this occurred, boiling temperatures would have suddenly been reduced. A temperature increase may, however, have occurred, independently of any gas input, or pressure decrease by a change in 'plumbing'.

8. DISCUSSION

It has been suggested that rainfall and air temperature are a large contributing factor to the temperature and pH levels of thermal features in Kuirau Park. However, if this were the case then no features would show stable trends throughout the seasons. Whilst many features have fluctuated, with increasing or decreasing temperature and pHs, some remained constant. Therefore we can draw the conclusion that the amount of rainfall and air temperature do not significantly contribute to temperature and pH variations.

Over the monitored six months, pH levels remained relatively constant. There was a dip in temperature in many features over May to June, but overall 40% of thermal features experienced an increase in temperature.

The hydrothermal eruption of feature 721 in January, 2001 most probably did not result from a build-up in pressure beneath a cap rock. It is more likely to have been triggered by a small increase in water temperature of thermal fluid beneath the park.

9. CONCLUSIONS

Kuirau Park is currently experiencing increased thermal activity. This could be a result of private bore closures and re-injection of commercially abstracted fluid back into Rotorua's geothermal aquifer. The aquifer has begun to revert back towards its pre-exploitation condition. This response is reflected in the hydrothermal eruptions and the changes in temperature and activity of thermal features in the park during 2001.

10. REFERENCES

1. Simmons, S.F., P.R.L. Browne, and R.L. Brathwaite, eds. "Active and Extinct Hydrothermal Systems of the North Island, New Zealand". Guidebook Series of the Society of Economic Geologists, ed. T.B. Thompson. Vol. 15. 1992: Fort Collins, CO.
2. Shane, P., "Tephrochronology: a New Zealand case study.". Earth Science Reviews, 2000. 49: p. 223-259.
3. Wood, C.P., "Geology of the Rotorua Geothermal Field". Geothermics, 1992. 21(1/2): p. 25-41.
4. Scott, B.J. and A.D. Cody, "Response of the Rotorua geothermal system to exploitation and varying management regimes". Geothermics, 2000. 29: p. 573-592.
5. Shane, P.A.R., T. Black, and J. Westgate, "Isothermal plateau fission-track age for a paleomagnetic excursion in the Mamaku Ignimbrite, New Zealand, and implications for late Quaternary stratigraphy". Geophysical Research Letters, August 1994. 21(16): p. 1695-1698.
6. Wood, C.P., "Geology of the Rotorua Geothermal Field", in The Rotorua Geothermal Field: Technical Report of the Geothermal Monitoring Programme 1982-1985. 1985, New Zealand Geological Survey, Rotorua; DSIR: Rotorua. p. 275-286.

7. Thompson, B.N., "Geology of the Rotorua Geothermal District", in Geothermal Resources Survey, Rotorua Geothermal District 1974, DSIR, Editor. 1974, DSIR New Zealand.
8. NZGS, "New Zealand Geomechanics Society Guidelines for the Field Description of Soils and Rocks in Engineering Use". 1988.
9. Hedenquist, J.W., "Geothermal Systems in the Taupo Volcanic Zone: Their Characteristics and Relation to Volcanism and Mineralisation". Royal Society of New Zealand Bulletin, 1986. 23: p. 134-168.
10. Browne, P.R.L. and J.V. Lawless, "Characteristics of hydrothermal eruptions, with examples from New Zealand and elsewhere". Earth-Science Reviews, 2001. 52: p. 299-331.
11. Wohletz, K. and G. Heiken, "Volcanology and Geothermal Energy", ed. J.H. Heiken. 1992, Berkley and Los Angeles: University of California Press.

Predicting Long-Term Seepage and Runoff from Tailings Storage Facilities to Facilitate Cost-Effective and Timely Closure and Lease Surrender.

D. J. Stolberg, BE (Hons), MEngSc, GradIEAust, and D. J. Williams, BE (Hons I), PhD, MIEAust
Department of Civil Engineering, The University of Queensland, Brisbane, Australia

ABSTRACT: Tailings Storage Facilities (TSFs) remain in existence long after closure. Accordingly, it is paramount that the mine operator, or owner, takes appropriate measures to ensure the long-term safety and environmental performance of both the stored tailings and the containment embankments, with all ancillary structures. Each of these components is generally considered during the TSF design phase, by means of tailings and water management plans, and the meeting of all the structural/geotechnical criteria for facility construction. However, what is often neglected during the design phase (which may be ongoing during the life of the facility) is due consideration for post-mining rehabilitation and appropriate land-use.

In order to properly assess and recommend appropriate rehabilitation measures for the agreed post-mining land-use, a complete understanding of the long-term mechanisms of tailings and water behaviour must be understood. Seepage and runoff mechanisms are key issues, with erosion and subsequent sediment release also of significant importance. Fully understanding these site specific mechanisms will facilitate the accurate prediction of seepage, runoff, and sediment volumes being transported off site, enabling the operator/owner to properly assess the potential long-term risk to the surrounding environment, and to optimise these processes accordingly by means of an appropriate long-term cover system.

This paper introduces a research project being conducted at The University of Queensland, Australia, entitled "Predicting Long-term Seepage and Runoff from Tailings Storage Facilities to Facilitate Cost-effective and Timely Closure and Lease Surrender". This project aims to develop a methodology for the development of site specific solutions to mitigate the environmental risk of impacts from TSF seepage and runoff in the long term. It also aims to develop site specific alternative rehabilitation strategies for different mine operations, which were selected because of their longer-term future, their geographical spread, covering a range of climatic settings, and to encompass a range of commodities and waste types.

1 INTRODUCTION

Never has there been more need or pressure from governments, communities and industry for responsible, sustainable mining development. This means successful mine site rehabilitation, a field that has historically been dominated by agricultural science. However, geomechanics has a major and important role to play in this field and in recent years has had increasing input as a result. The important application of geomechanics in mine site rehabilitation work essentially comprises the following:

- Slope stability analysis and settlement prediction of waste rock dumps, spoil piles and tailings.
- Understanding and controlling the engineering of tailings following their deposition and on rehabilitation, including both short-term and long-term behaviour, which are very important to facilitating cost-effective and timely closure and lease surrender of a mined area. The key mechanisms describing the behaviour of TSFs are beaching and hydraulic sorting of particles, sedimentation, consolidation, desiccation, seepage and runoff.

Of the engineering mechanisms presented above, the two most fundamental processes are seepage and runoff, as they drive the long-term performance of a TSF and the selection of the rehabilitation strategy. Consequently, the main focus of the current research project is to better understand these two mechanisms and to make a holistic assessment of the best cover/ rehabilitation solutions for minimising the adverse affects of both mechanisms, for a number of test mine sites.

The recommended cover and rehabilitation solutions are likely to differ vastly from the standard of practice at most mine sites. Typically, cover systems are designed to promote runoff, as a means of minimising seepage through the tailings. This approach has generally led to large-scale erosion and consequent loss of potentially contaminating tailings to the surrounding environment, and in some cases to nearby ephemeral streams and waterways. Instead, a cover system similar to that portrayed by Figure 1 ("Store and Release" cover) would provide a solution that "stores" wet season rainfall, thereby facilitating successful revegetation; but also minimises both seepage and runoff by encouraging evapotranspiration during the dry season.

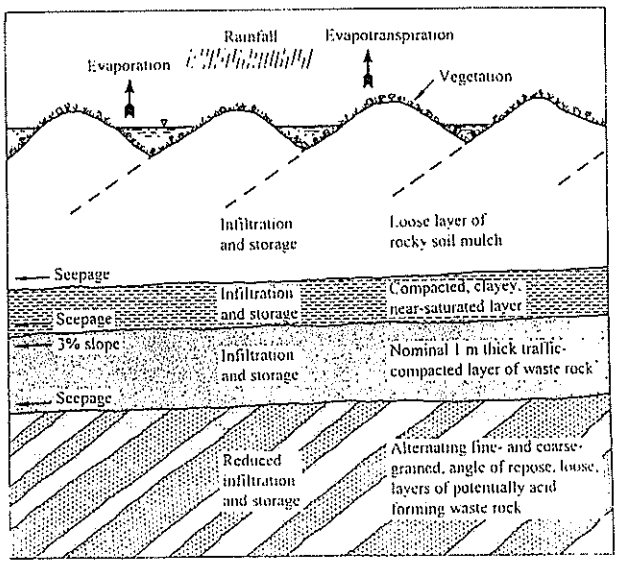

Figure 1: "Store and Release" cover system (Williams [1])

2 FUNDAMENTAL ISSUES - LONG-TERM SEEPAGE AND RUNOFF

Only recently have mining companies recognised that to obtain approval for the closure and surrender of waste rock dumps and tailings storage facilities, the owner must be able to demonstrate that after closure there will be no health or safety risk to the public and no unacceptable environmental impact. Geotechnical engineering principles have much to offer in achieving these mine site rehabilitation aims. Research in this area is still in its infancy compared with other areas in the field of geotechnical engineering. Hence the extensive research currently being conducted in this area.

Dealing initially with the issue of rainfall runoff, civil engineering hydraulic diversion works such as tunnels, buried culverts, or channels are frequently built so that water can by-pass a tailings deposit without damage. However, diversion works are not the complete answer, for two specific reasons:

- While these works may function properly during construction and operation of the tailings storage facility, if they are maintained clean and in proper working condition for the passage of water, there are several case histories of failures of such diversions, which have caused overtopping and breaching of tailings storages and near failures leading to drastic consequences (Blight et al [2]).
- Runoff from the tailings catchment itself is substantial and has to be dealt with no matter what the state of the exterior diversion works.

At closure of a mine site, tailings stored in above-ground facilities can still contain a significant volume of entrained water. If long-term management measures are not put in place, the resulting hydraulic gradient may drive potentially contaminating seepage from the tailings storage facility into the receiving environment. This may persist for many years and uncontrolled or unmanaged seepage may cause vegetation deaths or the contamination of stock or potable near-surface groundwater resources (Williams [3]).

In addition to the above, another problem area exists where hypersaline water has been used for processing, and the runoff from the exposed tailings surface may also become hyper-saline. Concentrated runoff may cause uncontrolled erosion, which may result in hypersaline tailings being released into the environment (Williams [3]). It is therefore very important that present research be utilised, and further research be undertaken in order to improve our understanding and the predictive capability of long-term seepage and runoff processes, and improved operational and closure practices to mitigate health, safety and environmental risks associated with the closure of TSFs.

3 PROJECT METHODOLOGY

On the basis of the research work completed to date, and in light of the foregoing discussion, the project methodology presented below has been adopted in order to achieve the research objectives.

1. Literature review, including the assessment of current and emerging cover technologies and other remedial measures to mitigate the adverse effects emanating from long-term seepage and runoff from TSFs.
2. Supplementary material characterisation. Various field investigations have already been conducted at each of the test sites, with the development of correlations between shear strength and moisture content (refer to the example plot for the tailings at Mount Keith Nickel Operation (MKO) - Figure 2). Extensive laboratory testing has commenced and will continue throughout the course of the project in collaboration with further sampling of various tailings over time.

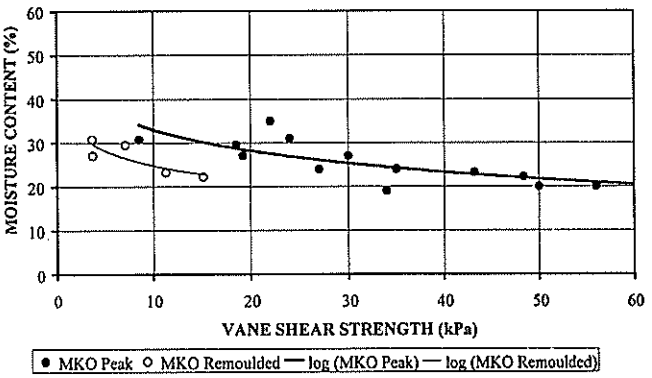

Figure 2: MKO vane shear strength versus moisture content

3. Field investigations, including the study of seepage drivers (entrained tailings water and seepage pathways), and runoff drivers (tailings and wall erodibility by water and wind, tailings hardpan development, natural salt crusting, and beaching and hydraulic sorting of tailings).

4. Column testing. The column test apparatus comprises a 2 m high 300 mm diameter Perspex cylinder to be filled with whole tailings in layers. The column testing will be conducted in association with the field trials and seepage driver studies, and will be a means of assessing the relationship between soil suction and moisture content. The column testing will also be a means of assessing the effects of changing the boundary conditions of a TSF (and will be cross-checked against the results of field trials, which are restricted in number and sophistication due to time and cost limitations).
5. Ongoing sampling and testing. This phase will mainly constitute the regular measurement of moisture contents and the phreatic surface at each of the test sites, in order to assess how the moisture profiles change with time (before, after and during wet seasons). Relationships will be developed, linking moisture content with various boundary conditions such as matric and osmotic suction, as well as shear strength (important for cover design), thereby painting the long-term big picture in terms of measured moisture content profiles. Figure 3 presents a plot of moisture content versus total suction for the tailings at Mount Keith Nickel Mine. The data for this plot were determined during a recent visit to MKO to assess the success of a cover trial on TSF 1.

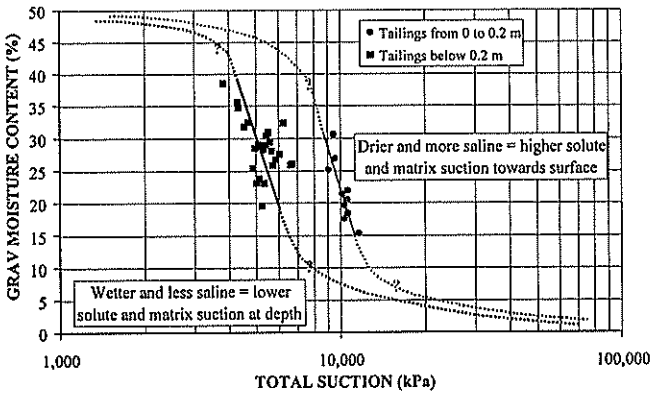

Figure 3: Summary of total suction and gravimetric moisture content data for shallow and deep tailings in Cell 2 of TSF 1 at MKO (including diagrammatic extrapolations of full SWCCs).

6. Field trials in order to assess the range of potential boundary conditions and their resulting effects. The field trials will include assessing the impact of closing down decants and tailings seepage recovery bores at the various TSFs, the impact of desiccation and surface ponding on the tailings, as well as erosion studies (refer to Section 3.1), and various cover trials. The results of the seepage/ cover trials will be used to calibrate the seepage models, once they are developed.
7. Analysis of seepage and runoff, and subsequently, closure options, flowing from the available site data and the results of the field trials, and including "back-of-the-envelope", 1-D, 2-D and 3-D approaches. The seepage models will be run over the long-term once they are calibrated using the column testing and field studies/trials, and erosion will be linearly extrapolated so that a long-term assessment may be made (as discussed further in Section 3.1).
8. Risk assessment and cost-benefit analyses of long-term performance, at both qualitative and semi-quantitative levels. This phase of the study will draw on the results of the analyses (that is, the calculated risks associated with each closure option at each site, based on the calculated seepage and sediment paths and volumes) and link them with cost and practicality. It is at this point that the broader applications of this research will also be presented, linking the general outcomes and project methodology to various other mine sites and conditions. Emanating from the risk assessment and cost-effectiveness analyses may be various recommendations on cover type, thickness, and geometry, as well as vegetation and underdrainage requirements.

The recommended rehabilitation strategies will be site specific, but ultimately some general findings will apply to all of the study sites (that is, general guidelines and the study methodology used). For example, under net evaporative conditions, such as those occurring in the Kalgoorlie region, it should be possible to demonstrate at all sites that ongoing seepage will generally not be sustained post-closure. In this case, it may be possible to retain all incident rainfall on the top surface of the TSF, whether or not it is covered, with no seepage impact.

The general guidelines and the study methodology developed as part of this project will facilitate the application of the research findings to different sites and environments (that is, humid as well as arid/semi-arid). A holistic solution to carrying out long-term seepage and runoff analysis of disused TSFs, and presenting rehabilitation techniques that minimise adverse effects resulting from these mechanisms, will be presented.

The successful completion of the study will ultimately facilitate a reduction in the financial liability assigned to TSFs, ensuring that the management of TSFs is placed on an equal footing with mining and processing, which currently enjoy far better defined objectives and costs.

3.1 Predicting Long-Term Erosion of TSF Slopes

The prediction of soil erosion by the action of water, which in the case of mine slopes is the predominant means of sediment loss, has until now been based largely on the Universal Soil Loss Equation (USLE) and its variations. This equation was derived from data collected from flat agricultural land in the United States of America (Williams [4]).

TSF slopes are quite unlike the agricultural slopes on which the predictive tools for erosion by water were based (that is, they are relatively steep, and the materials used to construct the walls generally incorporate waste rock materials, which are often

unsuitable as a growing medium). Unlike the wealth of data available from agricultural slopes, there are a scarcity of data from mine slopes. Further, nearly all of the work that has been done to assess these parameters has been conducted using rainfall simulation techniques, with information gained under natural rainfall conditions essentially non-existent (McIntosh and Barnhisel [5]). However it is important to note that simulation is necessarily required for the assessment of long-term climatic conditions (Riley and East [6]).

With agriculturally based methods deemed inappropriate for use in assessing the erosion of mine slopes, other means of estimating the expected rates of erosion have evolved. Correlations with the strength of the soil/rock surface, the slope length, slope angle, and so on, have been investigated, but with limited success. Blight [7] found that there is weak correlation between the shear strength of the materials and the rate of erosion, as well as the length of the slope.

It has been shown that certain parameters (such as the particle size distribution, slope steepness and length, etc) may greatly affect the rate of erosion of a mine slope, but this is not well defined, and is by no means general. Accordingly, an approach to erosion measurement and prediction that can directly measure erosion loss with time is the only means of successfully calibrating an erosion model for the long-term prediction of erosion loss as a result of rainfall runoff. The method adopted employs high resolution digital stereo photography and is an extension of the stereo-photogrammetric techniques, initially adapted by CSIRO for the geological assessment of rock masses, to the measurement of erosion to support modelling and management of mine site rehabilitation.

The erosion study to date has focussed on the most pronounced erosion gullies, which were observed in the outer slopes of disused TSFs that had been capped to shed rainfall runoff to the outer wall, resulting from rainfall runoff ponding against low points along the outer wall and overtopping the wall.

The stereo-photos of the erosion gullies were processed using CSIRO's computer program 3D MAPPER to produce three-dimensional images, from which x, y, z - co-ordinates were derived. The co-ordinates were then imported into the commercial contouring and three-dimensional surface mapping computer program SURFER to enable estimates to be made of the total amount of erosion that the gullies have experienced. A simplistic chart representing this methodology is presented as Figure 4.

Figure 5 presents one of the corrected images (that is, the original digital image with distortion removed), and the SURFER wireframe plot produced from the 3D MAPPER data points, for TSF 1 at Leinster Nickel Operation (LNO). The wireframe plot is used to estimate the total erosion loss from the gully and subsequent stereo-photos from the same baseline will be used to determine the erosion loss for subsequent defined rainfall events.

The digital stereo-photogrammetric techniques applied to the study of rainfall runoff-induced erosion of TSFs are independent of unsuitable agriculturally-based methods and are also applicable to the study of the erosion of waste rock dump slopes and the degradation over time of disused open pit slopes.

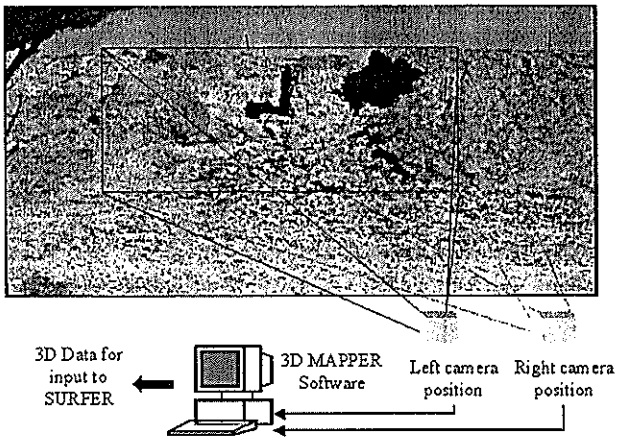

Figure 4: Erosion measurement and monitoring using photogrammetry

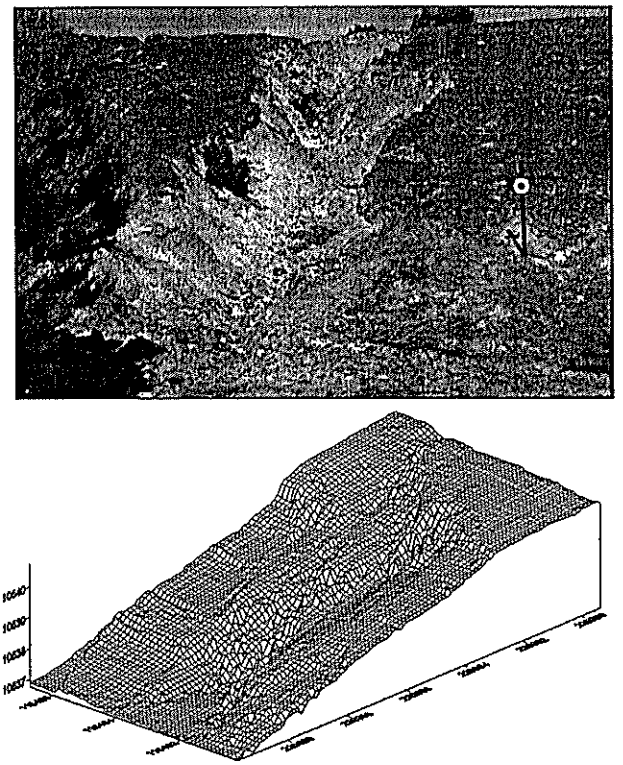

Figure 5: LNO TSF 1 corrected left-hand image and SURFER wireframe plot

4 CONCLUSION

This project aims to develop a methodology for the development of site specific solutions to mitigate the environmental risk of impacts from TSF seepage and runoff in the long term. It also aims to develop site specific alternative rehabilitation strategies for different mine operations, which were selected because of their longer-term future, their geographical spread within the arid Kalgoorlie region of Western Australia, and to

encompass both nickel and gold operations (that is, variable waste characteristics).

While the solutions are site specific, understanding the complex mechanisms involved is both universal and innovative. More importantly, the methodologies developed for predicting long-term seepage, runoff and erosion/sediment release, and subsequently developing alternative rehabilitation technologies, can be applied to mining operations worldwide, facilitating cost-effective and timely mine closure and lease surrender.

The research is expected to show as a general outcome that cover systems for TSFs in arid regions should be designed to promote water storage and evapotranspiration rather than runoff and subsequent sediment deposition, in order to minimise disturbance to the surrounding environment and thereby also minimise health risks to surrounding communities. This in fact contests the current state of practice in TSF rehabilitation, which aims to promote runoff as a means of minimising seepage through the tailings. This approach has generally led to large-scale erosion and consequent loss of potentially contaminating tailings to the surrounding environment, and in some cases nearby streams and waterways. If a cover system can be designed to effectively control the rate of seepage, and evapotranspiration potential can also be maximised, then a holistic solution to the problem will ensue.

5 REFERENCES

1. Williams, D.J. (2000). *Predicting Long-Term Seepage and Runoff from Tailings Storage Facilities to Facilitate Cost-Effective and Timely Closure and Lease Surrender – Proposed Study Scope*. Department of Civil Engineering, Faculty of Engineering Physical Sciences and Architecture, University of Queensland, Brisbane, Australia. July 2000.
2. Blight, G. E., J. H. Troncoso, et al. (2000). *Issues in the Geotechnics of Mining Wastes and Tailings.* GeoEng 2000, Melbourne, Victoria, Australia.
3. Williams, D. J. (2001). *Mine Waste Management & Landform Design.* Department of Civil Engineering, Faculty of Engineering Physical Sciences and Architecture, University of Queensland, Brisbane, Australia.
4. Williams, D.J. (2000). *Extension of Agricultural-Based Erosion Prediction to Steep Mine Waste Slopes.* Proceedings of 5th International Symposium on Environmental Geotechnology and Global Sustainable Development, Belo Horizonte, 17-23 August 2000. 16pp.
5. McIntosh, J.E., and Barnhisel, R I (1993). *Erodibility and Sediment Yield by Natural Rainfall from Reconstructed Mine Soils.* Soil Science. Volume 156, No. 2, pp. 118-126. Williams and Wilkins, USA.
6. Riley, S.J., and East, T.J. (1990). *Investigation of the Erosional Stability of Waste Rock Dumps Under Simulated Rainfall.* Supervising Scientist for the Alligator Rivers Region. Technical Memorandum 31. Australian Government Publishing Service, Canberra.
7. Blight, G.E. (1989). *Erosion Losses From the Surfaces of Gold-tailings Dams.* Journal of the South African Institute of Mining and Metallurgy, Volume 89, No. 1, January 1989, pp. 23-29.

Design and Construction Monitoring of a Landfill Containment Bund on Soft Marine Sediments

Tony Wallis, BE (Hons), MIPENZ, R.Eng.

Senior Geotechnical Engineer, Beca Carter Hollings & Ferner Ltd

This paper describes the design concept and construction monitoring of a 900m long rock bund founded on soft marine deposits to form a new seawall retaining a landfill for 1.6 million cubic metres of dewatered sludge. Design of the bund is largely controlled by stability against a sliding/rotational slip failure through the underlying soft marine clay deposit. The bund was constructed in stages to allow time for the marine deposits to increase in strength before adding the next lift of bund material. The strength gain was predicted during design and was monitored during construction by in situ testing with a large shear vane. Settlement plates were installed and monitored by precise levelling. Four vibrating wire piezometers were installed to monitor the generation of excess pore water pressure with application of bund construction loading and dissipation of excess pore water pressures with time. The results of shear vane tests, settlement monitoring and piezometer monitoring are presented and discussed. The correlation between the time for settlement as shown by the settlement plot and dissipation of excess pore water pressure is discussed.

1 INTRODUCTION

"Project Manukau" is the upgrading of Auckland's wastewater treatment plant at Mangere. The project has three main purposes – to increase the capacity, to increase the effluent quality and to remove the four oxidation ponds in order to return the pond area to the Manukau Harbour. The latter of these involves the removal of accumulated sludge from the base of the oxidation ponds, partial dewatering of the sludge, and deposition of it in a landfill constructed in one corner of the ponds.

This paper describes the design concept and construction monitoring of a 900m long rock bund constructed on soft marine deposits to form a new seawall retaining the landfill.

2 PROJECT DESCRIPTION

The treatment plant oxidation ponds were built in the 1960s by enclosing an intertidal mudflat area of around 500 hectares in the Manukau Harbour. The treatment plant upgrade project required a new landfill to be built in the eastern corner of Pond No.2. Prior to commencement of the sludge dewatering, the geotechnical properties of the sludge were not known but its behaviour was expected to resemble a "jelly", ie. very low strength and slightly viscous.

The sludge was dewatered in centrifuges from a solids content of around 8% to 20% by weight, resulting in a material with density slightly greater than water and shear strength estimated to be around 1kPa.

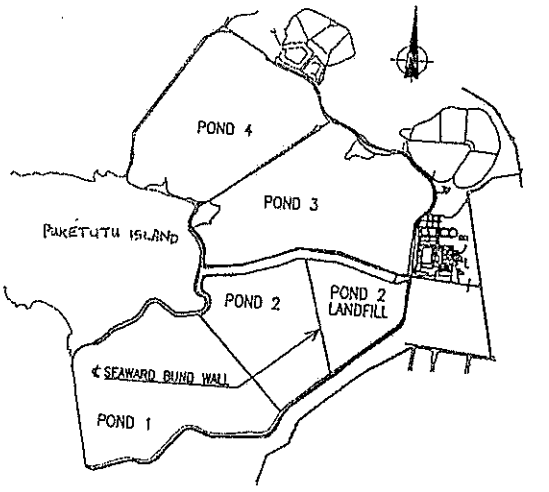

Figure 1 – Site Plan

The landfill design was based on an assumed angle of repose of the sludge of 1 vertical to 120 horizontal. From the estimated four million cubic metres of dewatered sludge, it was determined that the landfill was required to cover an area of around 50 hectares. A new 900m long bund was required, to 3.6m height

above seabed level (approximately at mean sea level) which would become a seawall exposed to the Manukau Harbour upon removal of the oxidation pond bunds.

The seabed generally comprised soft clay, which was not traffickable by machinery. Sludge placement was achieved by construction of an inclined conveyor founded on driven piles, and aligned in the centre of the landfill. Sludge could be dropped off the conveyor at variable positions allowing it to flow outwards towards the edge containment bunds.

3 GEOLOGY AND SOIL PROFILE

The surficial geology at the treatment plant site includes recent marine sediments, Tauranga Group alluvium and volcanics comprising ash, tuff and basalt. The bund design and construction was controlled largely by the recently deposited marine sediments, which consisted of soft clayey silt up to 5m thick. This was underlain by the Tauranga Group alluvium comprising stiff peats, silts and clays and sand layers.

Early site investigations had comprised a few boreholes drilled from a barge, which were followed by large shear vane tests to measure the in situ strength of the soft clayey silts.

Later stages of investigation were undertaken through a rock fill starter bund and consisted of more machine boreholes, several cone penetrometer tests (CPT) and further large shear vane tests.

The continuous soil profile record of the CPTs was found to provide a useful guide of the stratigraphy, such as identification of thin sand layers. While it readily identified the thickness of the soft marine muds, the sensitivity was considered insufficient to provide a design value for shear strength. A shear vane of 100 x 50mm was used to more accurately measure the shear strength.

From the shear vane tests, the marine mud was found to be close to normally consolidated with a shear strength profile of around 4 kPa at the seabed, increasing by around 2 kPa for every metre depth.

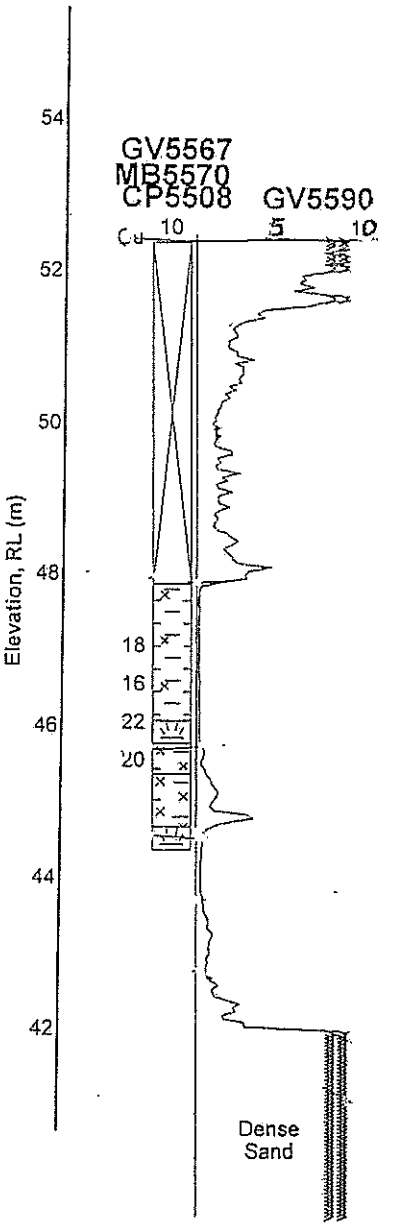

Figure 2 – Soil Profile

4 BUND DESIGN

The bund design cross-section depended largely on stability against a rotational slip failure through the underlying soft marine deposits. Other design criteria were permeability for sludge and leachate containment and armouring for wave protection. Stability was assessed using computer software for calculating factors of safety for circular and non-circular slip surfaces.

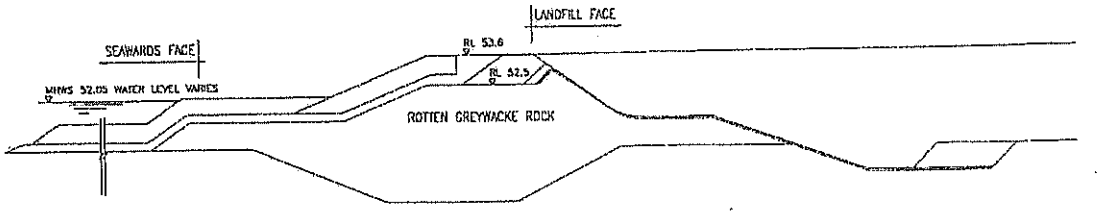

Figure 3 – Bund Cross Section

The construction stages were analysed using total stress soil parameters since stability would be critical immediately upon loading.

It was found that for the bund to be constructed to full height in a single operation, the depth of undercut of soft clay and/or overall slope angle required would be excessive. Instead, the design called for staged construction since it was considered that the soft marine mud would increase in strength with consolidation due to the partial bund loading.

The mechanism understood to occur is as follows. The marine sediments have a certain initial undrained shear strength and is in an at-rest effective stress state, ie. the pore pressure equals the head due to the pond level, which is constant. Immediately upon placement of bund fill, the undrained shear strength stays the same but the pore water pressure rises. As the clayey silts have low permeabilities, the excess pore water pressure dissipates gradually. As the water is expelled from the pores, the soil particles press together resulting in consolidation and increase in the undrained shear strength.

The increase in strength was predicted by considering the effective stress that would be applied and the design required further shear vane testing to verify that the required strength gain had been achieved. The staged construction with lengthy holding periods was possible due to a 2.5 year construction period over which dredging would occur.

Figure 3 shows the final bund cross-section.

5 BUND CONSTRUCTION

Preliminary bund design called for a two metre deep undercut of the seabed mud and construction of a starter bund by placing rock fill to 0.5m above pond water level, which was typically 2.0m above the seabed level. An excavator working off a barge completed the undercut and the starter bund was advanced by end tipping rock just above water level. The bund core comprised "rotten greywacke", a highly weathered quarry waste product.

The actual margin of stability was found to be close to that predicted in the design, as indicated by slumping that occurred during construction. Slumping occurred where material was stockpiled on the bund crest about 1m higher than allowed for in the design.

The landfill construction required dewatering of the landfill area, so the bund's initial work was to resist instability into the dewatered landfill area. Seepage due to the 2m head difference was not excessive and where significant flow did occur, it was reduced by placing mud on the outer face.

An HDPE liner was placed on the inside face of the bund for leachate containment.

It was found that the sludge dried to a cake to a depth of a 200 to 300mm and a firm, cohesive fill material could be made by drying the sludge in windrows. The dried sludge could then be placed in layers by tracking with an excavator. Such a layer was placed on the inside face of the bund to form a buffer against the much weaker sludge. This dried sludge provided toe buttressing for the bund and allowed some construction trafficking.

An excavator working from the bund crest placed rock armour on the outside face of the bund under water. The excavator was equipped with reach and depth readout equipment to assist with placement of material to the correct lines and levels under water.

6 INTRUMENTATION

Instrumentation of the bund comprised settlement plates and three types of piezometer, namely vibrating wire, pneumatic and standpipes.

Settlement needed to be measured primarily in order to predict with increasing accuracy the remaining settlement so that the target crest

level could be met. An accurate prediction was required because excess fill would be undesirable both from a material quantity/cost perspective and because any excess in fill height had an adverse effect on stability. Conversely, if greater settlement than estimated occurred, additional filling would be required a later date to maintain the required seawall crest height.

Monitoring the settlement plates provided the sum of the settlement of all underlying layers at the time of the reading. While the underlying layers settle at different rates due to different thicknesses and permeabilities, the plot of settlement against time or log time would allow extrapolation in order to estimate the long term settlement.

Settlement plates were installed on the base of the undercut and rock fill carefully placed around the rods while under water. Success in protecting settlement rods from construction traffic was less than total, but enough settlement plates survived to provide data for the entire construction period.

Piezometers were installed in the soft clay layer to monitor the excess pore water pressure developed under the bund loading. The results were not expected to be used in stability analyses since total stress parameters were used in the design. However, the dissipation of excess pore water pressure provided a measure of the degree of consolidation and therefore the time for settlement could be predicted.

Both pneumatic and vibrating wire type piezometers were installed to provide cross checking of data and backup in case of their failure. The vibrating wire piezometers were selected with a response range to suit the maximum expected pore pressure. The lowest pressure range piezometer was selected since the accuracy was quoted as a percentage of the maximum pressure. The accuracy was quoted as ±0.5% of the 170 kPa range, ie. ±87mm of water head and the resolution as 0.025% of the 170 kPa range, ie. ±4.3mm of water head. The former of these specifications provides an indication of the absolute measurement of pressure, while the latter indicates the repeatability of the results.

The pneumatic piezometers and readout unit were found to be unable to provide sufficiently accurate readings to be useful in measuring a few metres of excess pore pressure.

Standpipe piezometers were installed and screened within the bund core (relatively permeable material) in order to give the static ground water level in the bund, ie. the piezometric level to which the excess pore pressure in the underlying clay layers would eventually dissipate.

7 MONITORING RESULTS

a) Shear Vane Results

In March 2001, around 2.5 years after the initial bund loading, the strength of the clay immediately beneath the bund was found to have increased. The trend line inferred from the scatter of results was 23 kPa, which was constant with depth. This equates to a strength gain of 15 kPa at 2m depth and 11 kPa at 4m depth below seabed. The applied load was around 75 kPa.

The greater strength gain at shallower depth can be explained by the higher degree of consolidation due to the shorter drainage path nearer the base of the bund.

b) Settlement Results

Figure 4 shows the settlement versus time plot for a typical settlement plate. The initial loading of around 40 kPa resulted in around 400mm of settlement, the rate of which became minimal by about February 2000, some 18 months after commencement of construction. The rate of settlement then increased again with more load application. The latter stages of loading were the order of another 40 kPa, with additional settlement approaching 250mm recorded to date.

c) Piezometer Results

Figure 5 shows the piezometric level for a typical vibrating wire piezometer along with the adjacent standpipe. In order to relate the pressure level to the construction levels, the elevation of the piezometric surface is plotted, ie. as a reduced level in meters to the same datum as the bund construction (note that the site datum is RL50m at mean sea level).

The plot clearly shows the response of pore water pressure to the each of the applied loading steps, followed by dissipation. Between May and September 2000, the pore pressure increased by about 1.3m or 13 kPa, while at the same time dissipation of around 7 kPa occurred (estimated from inspection of the plot), ie. a

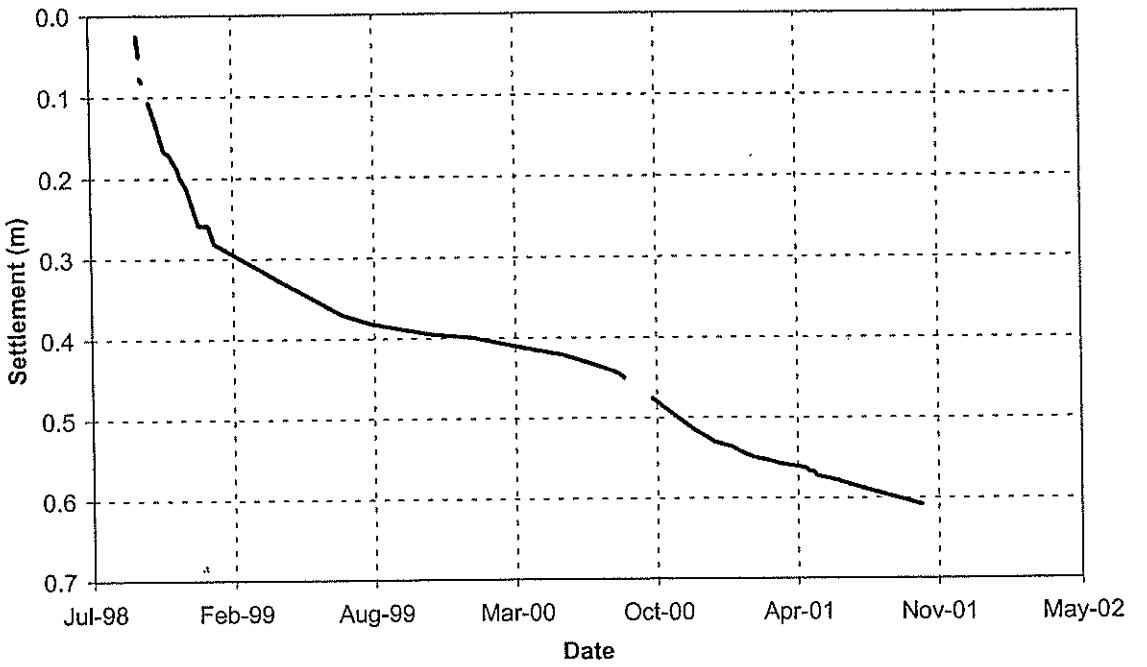

Figure 4 – Settlement Monitoring Results

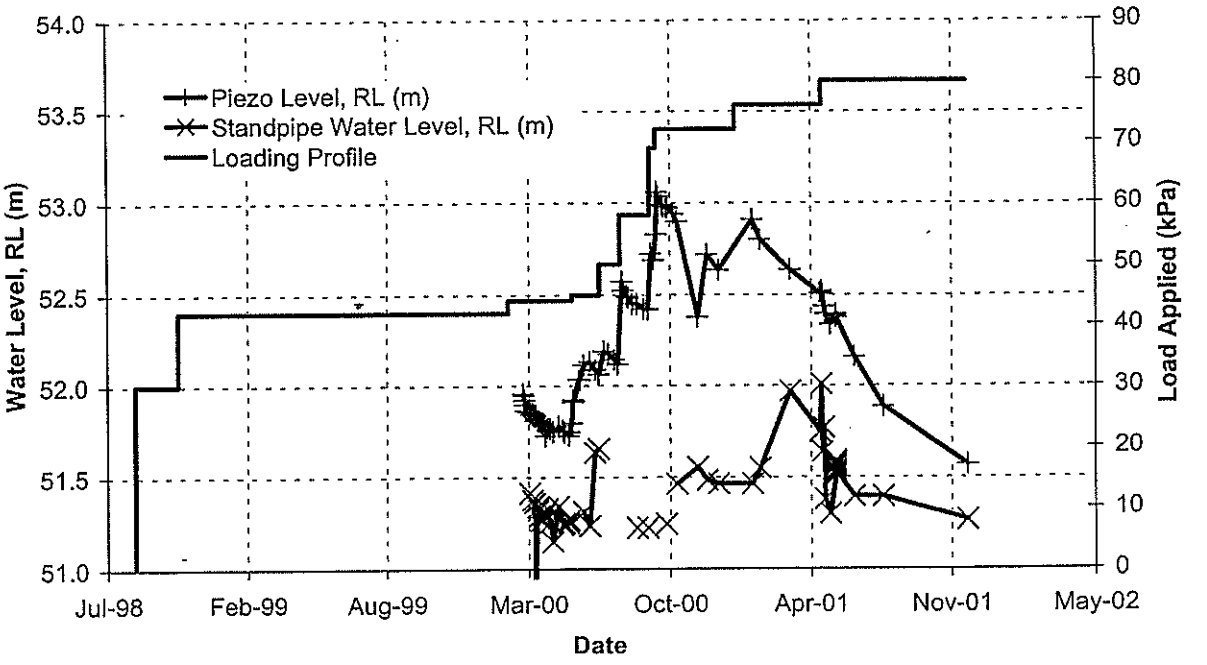

Figure 5 – Applied Load and Piezometric Level

total of 20 kPa pore pressure increase in response to about 26 kPa of applied load.

The importance of timely instrument readings can be seen from the piezometer plot. For example, there is a rise in pore pressure between 8 December 2000 and 25 January 2001, but sparse data over this period means that the date of the increase and the peak level to which the pressure rose cannot be determined. The break coincides with the Christmas break. Clearly, readings were needed immediately before and immediately after any load placement to collect the most useful information.

If load had been applied in a single stage, or if more complete dissipation had occurred between loading stages, it would be possible to assess the "degree of consolidation" for that loading stage. The coefficient of consolidation, c_v, could therefore be calculated, and hence more accurate estimates of time for settlement. In the case described above, the multiple loading stages overlapped and interpretation could not be as accurate.

8 SUMMARY

A landfill containment bund has been designed comprising rock fill placed under water onto soft marine sediments to a height of 3.6m above the seabed. Staged construction was required with holding periods to allow time for consolidation and strength gain of the soft clay. Construction was successfully completed when breaching of the outer seawall exposed the bund to tide and waves about 18 months after commencement.

Construction monitoring instrumentation comprised settlement plates, vibrating wire piezometers and standpipes. In addition, shear vane testing was undertaken to verify the predicted strength gains. The vibrating wire piezometers were found to produce accurate, reliable results over an 18 month construction period in a coastal environment. The pore pressure and settlement monitoring programme has proved valuable in assessing the bund performance compared with the design requirements, in particular the time for settlement.

9 ACKNOWLEDGEMENTS

The author wishes to thank Watercare Services Ltd and Manukau Wastewater Services Ltd for the permission to publish this paper. Thanks is also given to Dr D V Toan and Dr D P Carter for guidance during the project and for review of this paper.

10 COPYRIGHT

Development of Efficient, High Moment Capacity Foundations

Dr Phil Watson and Dr Derek Pennington
Arup Geotechnics, 11 Harvest Tce, West Perth WA 6005 AUSTRALIA

Summary Arup Geotechnics (Perth) recently provided geotechnical services for the former One.Tel Network Rollout in Perth, Western Australia. Activities carried out for this project included desk studies, site investigations and foundation design for 44 greenfield sites, and provision of construction supervision services for the 11 sites eventually constructed. This paper outlines the design and development issues associated with the novel foundation alternative implemented for the project.

1 INTRODUCTION

Throughout 2000, Arup Geotechnics (Perth) provided geotechnical services for the former One.Tel Network Rollout in Perth, Western Australia. Geotechnics worked as part of a larger infrastructure team, providing project management, civil and structural services to the project.

The One.Tel Network Rollout involved establishing a communications network across the Perth metropolitan area. In many instances, base stations comprising an array of telecommunications antennae were established on existing buildings and towers. However, numerous greenfield sites needed to be developed, comprising monopole structures to support the antennae. An example of a constructed One.Tel monopole is shown in Figure 1.

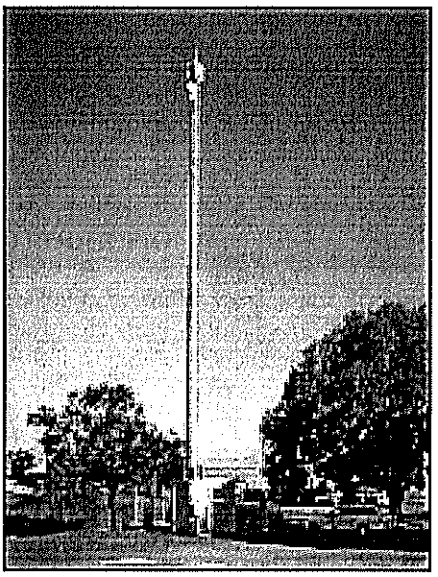

Figure 1 Telecommunications monopole

The heights of these poles are typically in the range 25-35 m above ground level, although 40 m high support structures were also required at several locations. In these instances lattice structures were usually specified, although the novel high moment foundation solution was also adapted for 40 m high monopoles.

This paper outlines the design and development issues associated with the foundation solution used for the monopole structures.

1.1 Historical Foundation Solution

The One.Tel Network Rollout is one of several network rollouts that has been undertaken across Australia over the last few years. Given the proliferation of these projects, and the associated large number of required monopole structures, it was not surprising that a 'standard' foundation solution has generally been adopted as the basis for all foundation requirements across the country.

This 'standard' foundation comprises a mass concrete foundation, generally 5-6 m square and 1.5 m deep. In addition, maximum allowable bearing pressures are typically limited to 120 kPa. This type of foundation solution was again proposed for the One.Tel project in Perth. However, it was subsequently shown that this foundation type was unable to meet the client requirements for the project, and was also not the most cost efficient foundation available.

1.2 Client Requirements

There were a number of constraints provided by the client that affected the choice of foundation solution. These included:

- Speed of construction. As noted above, several network rollouts were being completed simultaneously, and there was likely to be a significant competitive advantage to the telecommunications carrier whose network was operational first.
- Total project cost was a factor in the strongly competitive telecommunications industry. Evidence for strong competition evidenced in One.Tel no longer operating in Australia.
- Standardisation was one of the main client requirements, in part linked to optimising construction time and cost.
- Greenfield lease areas were fixed at 4.5 m x 8 m. The width of monopole foundations was thus limited by the width of the lease area, and the expected zone of

'disturbance' around the foundations (such as from passive failure of the material in front of the footing).

Added to these requirements were issues relating to variable (and challenging) ground conditions, extreme loading conditions, and strict deflection criteria. These requirements all contributed to the motivation to develop a novel foundation solution.

2 GEOTECHNICAL SITE INVESTIGATIONS / GROUND CONDITIONS

Arup Geotechnics (Perth) was originally commissioned to carry out desk studies, site investigations and foundation design for only two sites. This was extended to 44 greenfield sites. In addition, Arup provided construction supervision services for the foundations of the 11 greenfield sites eventually constructed.

2.1 Geotechnical Site Investigations

The geotechnical site investigations for the green field sites consisted of a desk study and insitu investigation. Both were carried out with a significant cost driver. The desk study generally comprised:

- A review of geotechnical information held in the Arup site investigation database;
- A review of 1:50 000 Environmental Geology Series maps for the Perth metropolitan area;
- Summarising anticipated ground conditions, including depth to ground water.

The site investigation typically comprised:

- Recovery of hand auger samples to a depth of about 2 m for description of the near surface soils, and laboratory testing if appropriate;
- At least one Electric Friction Cone Penetrometer Test (EFCPT) to refusal. As will be discussed in later sections knowledge of soils to roughly 15 m below ground level was required for the design of ground anchors.
- Where stiff clays were encountered, the EFCPT could not always penetrate sufficiently into the substratum due to friction. In these cases a Mechanical Cone Penetrometer Test (MCPT) was carried out.
- Probe holes were dipped to determine the depth to the water table. If required, a standpipe piezometer was installed, enabling the depth to the water table to be monitored over time.

All EFCPT testing was performed using the cone penetrometer truck shown in Figure 2, and was completed to Australian Standard 1289.F5.1[1]. Interpretation of soil types and material properties was generally based on correlations in Lunne et al (1997)[2], with additional reference to local correlations.

In most cases the ECPT testing was completed within one hour of arrival on site, with a total cost of around $500 AUD. The short time on site resulted in relatively low total site investigation costs, while the EFCPT results themselves gave the required confidence in soil conditions to enable novel foundation solutions to be investigated.

The proposed greenfield sites varied in nature across the metropolitan area. Sites varied from those relatively clear of obstructions, to others located in sand dunes along the coastal strip, within scrub areas along the foothills of the Darling scarp, or behind existing buildings. Examples of the greenfield sites investigated are shown in Figure 2.

(a) Rear of industrial complex, Balcatta

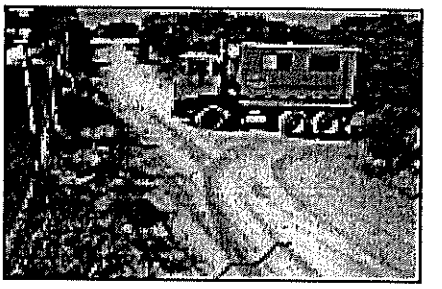

(b) Sand dunes at Campbell Military Barracks, Swanbourne

(c) Mt Whaleback Golf Course, Lynwood

Figure 2 Typical greenfield sites

2.2 Variable Ground Conditions

As expected, ground conditions encountered at the 44 greenfield sites varied significantly. Soils included:

- Very loose to very dense sand;
- Stiff to hard clays;
- Lightly to heavily weathered limestone;
- Peat.

Examples of EFCPT profiles measured at different sites are shown in Figure 3. Given the client preference for a standard foundation design for all sites, the foundation solution was developed to be sufficiently robust to be easily adopted at significantly different soil types.

The depth of the water table was also highly variable at the sites examined, ranging from depths of less than 1 m below ground level to sites where water was not encountered at all. This also has implications for foundation design, as well as introducing construction problems in those cases where the water table was above foundation level.

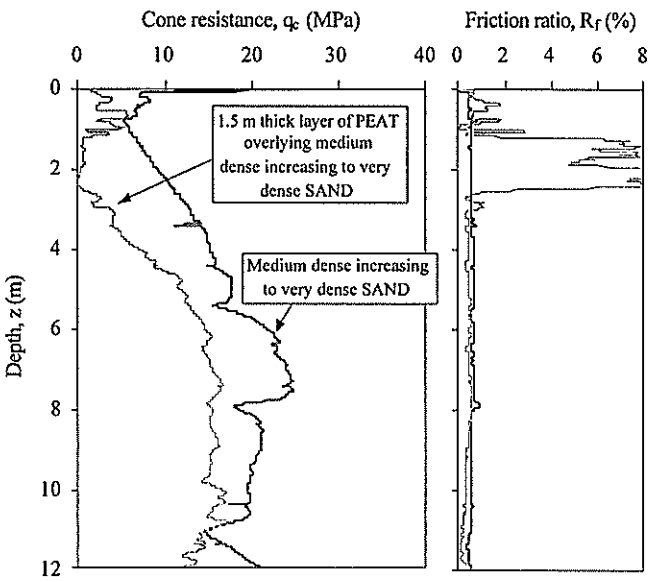

(a) Peat, sand

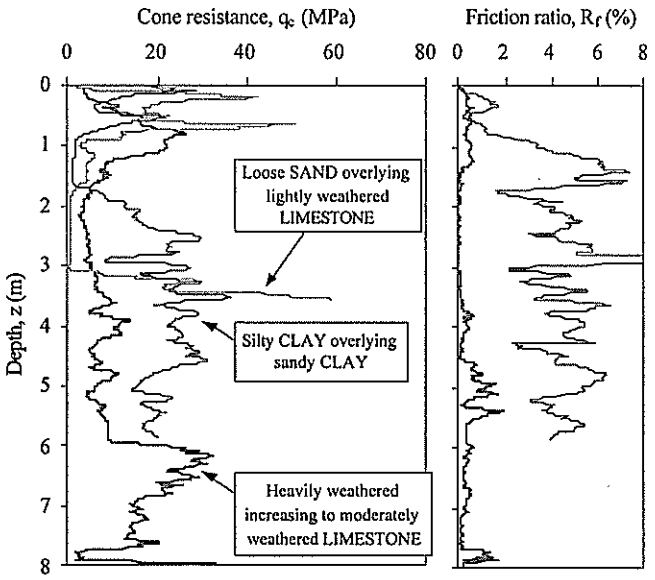

(b) Lightly to heavily weathered limestone, clay

Figure 3 Examples of the variable ground conditions

3 LOAD CASES / DEFLECTION CRITERIA

Perth is one of the windiest capital cities in the world, resulting in relatively large design lateral loads on the monopole structures. The combination of these loads with the long lever arm of the lateral load above ground level resulted in extreme overturning moments being applied to the monopole foundation.

Table 1 shows the ultimate and serviceability loading conditions (at ground level) for the different monopole heights. From the table, it can be shown that (excluding the weight of the foundation), the moment induced eccentricity is in the range 19.7-23.3 m for the ultimate load cases.

	Monopole height (m)			
	20	25	30	35
Ultimate loads				
• Base moment (kNm)	532	789	976	1292
• Base Shear (kN)	38	46	47	54
• Axial load (kN)	27	34	42	65
Serviceability loads				
• Base moment (kNm)	355	526	651	861
• Base Shear (kN)	25	31	31	36
• Axial load (kN)	22	27	34	52

Table 1 Design ultimate and serviceability loads

In addition to the load cases, serviceability deflection criteria needed to be observed. This was to ensure the telecommunications antennae remain within 'line of sight' of other base stations during service. The serviceability criteria for the monopoles are as follows:

- deflection at the mast head of less than 300mm
- rotation of less than 0.5°

It was significant that 88% of the rotation permitted at the top of the monopole was due to deflection of the monopole, and hence the foundation was required to be effectively rigid.

4 FOUNDATION OPTIONS

There are a number of foundation options available for monopole structures, including the traditional mass concrete solution discussed above. Issues which were considered in adopting a foundation solution included the following:

- Design loading condition;
- Type and state of soils underlying the site;
- Depth to groundwater (and requirements for dewatering);
- Space available for construction (note limited lease area);
- Construction programme;
- Construction cost.

Standard piled solutions, although an efficient means of resisting lateral and overturning moment, were excluded as the cost of mobilising a piling rig to each site was considered prohibitive.

The solutions considered were:

- Monolithic pad foundations (traditional solution);
- Caisson foundation (or stubby pile);
- Hybrid foundation.

This section outlines these options, and the relative advantages / disadvantages of each. Initial foundation sizing and preliminary analysis was based on the soil conditions observed at the first two sites investigated.

4.1 Monolithic Pad Foundation

A typical monolithic pad foundation is illustrated in Figure 4. The size shown is the typical range in base sizes for the different monopole heights and loading conditions.

Lateral capacity is generated through passive resistance, and overturning moment generally governs the foundation design. Bearing capacity was determined using the Brinch Hansen approach described in Tomlinson (1986)[3].

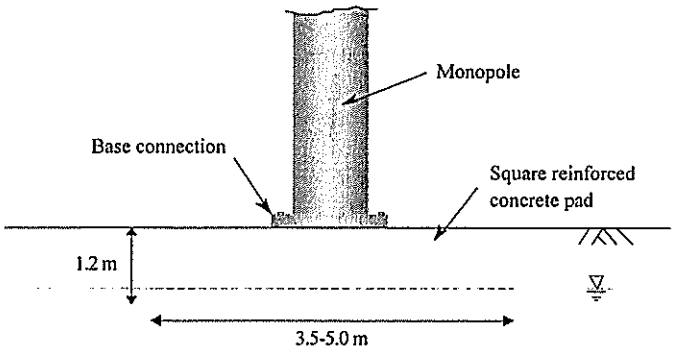

Figure 4 Typical monolithic pad foundation

Advantages:
- Ease of construction, using traditional practices;
- Industry acceptance.

Disadvantages:
- Construction times are relatively long and cost was consequently high;
- Most monopoles had heights in the range 25-30 m, with corresponding base widths in the range 4-4.5 m. with generally exceeds the agreed lease areas (4.5 x 8m).

4.2 Caisson Foundation (Stubby Pile)

Caisson foundations (or stubby piles) for the monopoles consist of vertical columns of reinforced concrete in the range 1-1.5m diameter, and length 5 to 8m in depth. It is frequently not economical to construct these "large diameter" piles in Perth conditions (typically sand with water table relatively near the surface) using traditional bored piling equipment, since the mobilisation to site for a single pile outweighs the savings in materials. To save on mobilisation costs, hand dug piled caissons have previously been constructed in Perth.

Figure 5 shows a typical caisson foundation, for a 30 m monopole. Preliminary analysis was performed using the approach of Broms, as detailed in Tomlinson (1994)[4]. As the pile is essentially an end bearing pile, no shaft friction was assumed.

Advantages:
- Efficient use of foundation materials;
- Limited construction space required (satisfies small lease area);
- Relatively quick construction (except hand dug caissons);
- Hand dug caissons likely to be significantly cheaper than those constructed using bored piling equipment.

Disadvantages:
- There is limited availability of suitable equipment in Perth to construct these foundations;
- Risk of hole collapse, with potential for considerable construction delays;
- Where the watertable is high, construction would have to be carried either within casing, or in conjunction with dewatering (expensive).

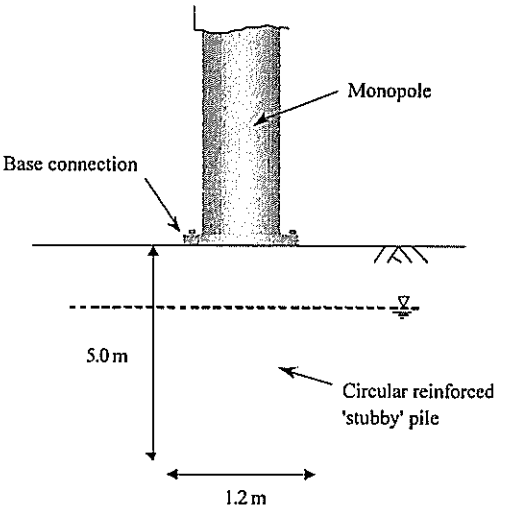

Figure 5 Typical caisson foundation

4.3 Hybrid Foundation

The foundation solution developed, comprised a square pad footing, with tension anchorages at each of the corners, as shown schematically in Figure 6. A number of options are available to provide the tension anchorages. These include screw piles, tension piles, ground anchors and stress bar anchors. In the current study, ground anchors were adopted as the preferred solution. The ground anchor capacity and foundation sizes shown in Figure 6 are optimised for the range of monopole heights and loading conditions.

Analysis of these foundations is discussed in more detail in Section 5.0.

Advantages:
- Reduced construction time and cost;
- Limited construction space required (satisfies the limited lease area);
- Efficient materials use compared with the monolithic pad foundations.

Disadvantages:
- Novel concept, requiring additional engineering to increase confidence in its use;
- Requires slightly deeper site investigation. However, once mobilised to site, it is relatively cheap to probe using the CPT to the required depth.

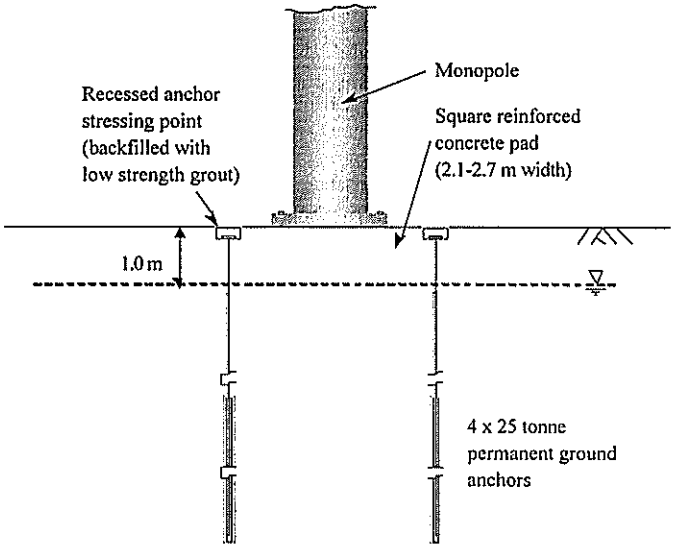

Figure 6 Hybrid foundation using ground anchors

4.4 Comparison of Foundation Options

A comparative study of the above options was carried out. Projected total cost and base size were investigated for each monopole height, using a generic soil profile typical of that encountered in the Perth metropolitan area. Analysis of the caisson solution assumed construction using bored piling equipment.

Figure 7 shows the results obtained. Based on this, the hybrid foundation was selected as the preferred foundation.

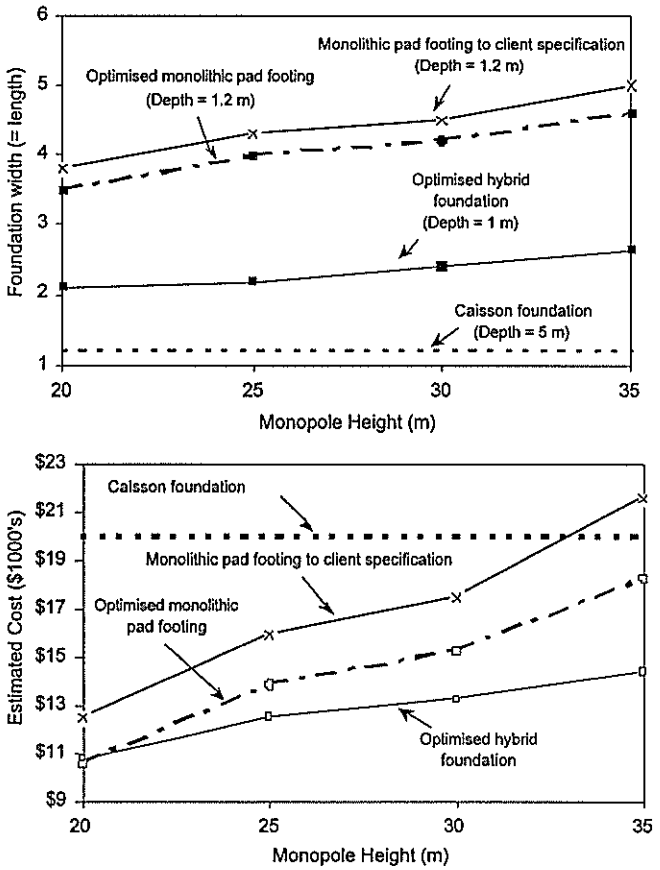

Figure 7 Comparison of foundation options

5 ANALYSIS OF HYBRID FOUNDATION

Performance of hybrid foundations is governed by the detailed design of both the pad foundation, and the anchorages. The design of the tensioned anchor pad foundations was performed to examine:

- Bearing capacity under ultimate loading conditions.
- Foundation displacement under service loading conditions.

An analysis method similar to that developed for piled raft foundations was developed, with consideration given to the following aspects of design:

- Traditional bearing capacity of the pad using the Brinch Hansen approach described in Tomlinson (1986)[3];
- The distribution of contact stress on the soil - foundation;
- Flexibility of the ground anchors, primarily from changes in the anchor free length, and subsequent changes in anchor tension;
- Differential settlement (and rotation) of the footing, calculated using *Oasys* VDISP settlement prediction software, and comparison with deflection criteria;
- Lateral resistance derived from passive soil capacity.

The approach adopted, comprising an Excel spreadsheet run interactively with displacement prediction software, enabled the capacity of the hybrid foundations to be determined, and the foundations optimised.

6 CONSTRUCTION SEQUENCE AND ISSUES

The hybrid foundations were constructed as follows:

- Excavate and construct pad foundation;
- If required, undertake near surface ground improvement (such as the removal of peat and replacement with clean sand);
- Backfill around foundation, using lean mix concrete to increase passive capacity as required;
- Drill ground anchor bores to required depth through preinstalled guide holes in the pad footings;
- Install ground anchors and grout fixed/free length as required;
- After grout achieves strength, perform anchor acceptance tests, and finally lock off at predetermined anchor prestress (after certification by the engineer);
- Backfill anchor recess with low strength grout to enable anchor prestress to be checked if required.

Figure 8 shows the track driven, hydraulic rig used to install the ground anchors, while Figure 9 shows an installed ground anchor prior to prestressing and locking off. Construction of the ground anchors was typically completed within one day.

To achieve standardisation of foundation solutions, two different foundation options were ultimately developed as used for all greenfield sites:

- A 2.7 m x 2.7 m x 1.0 m foundation with 4 x 25 tonne capacity ground anchors;
- A 3.2 m x 3.2 m x 1.0 m foundation with 4 x 25 tonne capacity ground anchors;

The first of these was used for sites with good ground conditions and monopoles up to 30 m in height, while the

larger foundation was used in difficult ground conditions or for 35 m monopoles.

Note that the foundation could be optimised to reduce the pad weight to less than 10 tonnes, enabling the pad to be precast and trucked to site. This would reduce construction times further and improve quality by avoiding insitu concrete. However, this was not done on this project.

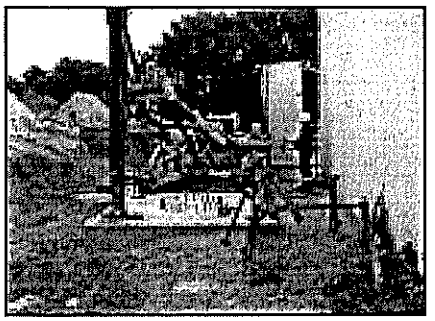

Figure 8 Ground anchor installation rig

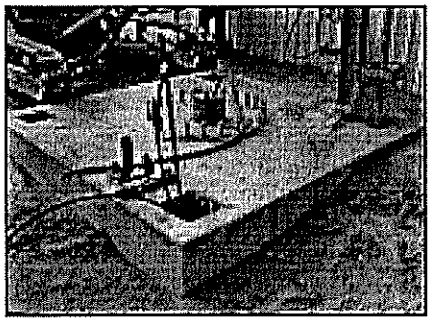

Figure 9 Installed ground anchor

As mentioned, ground conditions varied considerably across the metropolitan area. An advantage of ground anchors is the flexibility of the procedure in different ground conditions. Figure 10 shows the range of drilling bits used for different ground conditions. In addition, the anchor holes could either be constructed fully cased or open hole, depending on encountered soil and ground water conditions.

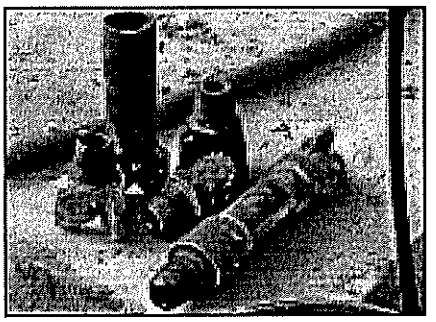

Figure 10 Range of drilling bits for different ground conditions

Design and construction of the ground anchors was performed to British Standard 8081[5] for permanent anchors. Significant consideration was therefore given to quality control and corrosion protection.

6.1 Monitoring of Anchor Prestressing and Back-Analysis

As noted above, tight deflection criteria were specified for the monopoles. This was considered in the analysis. However, estimation of ground stiffness based on EFCPT data is somewhat questionable, and so a programme of monitoring pad footing settlement using anchor prestressing was carried out.

In each case the displacement observed during prestress trials of the anchors (each to 1.5 times the required 25 tonne anchor capacity) was monitored. It was hoped to use the information to develop a local correlation of soil stiffness and EFCPT results. Figure 11 illustrates the anchor stressing and monitoring operation.

The results indicated that the soil stiffness determined based on the EFCPT results was conservative, with far higher stiffness observed insitu. However local correlations could not be clearly defined for the range of materials.

Figure 11 Anchor prestressing

7 VARIATIONS TO 'STANDARD' DESIGN

During the project, two variations to the standard hybrid foundation were developed.

7.1 Anchored Pile Foundation

At several sites, the ground conditions were observed to comprise very loose sand overlying limestone. The surface of the limestone was typically characterised by pinnacles, with depth to limestone varying up to several metres over short distances. This is illustrated in Figure 12, showing EFCPT profiles within a 1 m radius.

This soil profile creates a range of problems for surface foundations, including:

- The loose surficial sand is likely to be susceptible to high compression under the action of cyclic loads, as occurs under wind loading;
- The depth to the limestone (up to 7 m) is too deep for ground improvement techniques to be cost effective;
- The limestone pinnacles will likely result in significant differential settlement, giving rise to unacceptably high rotation of the monopole.

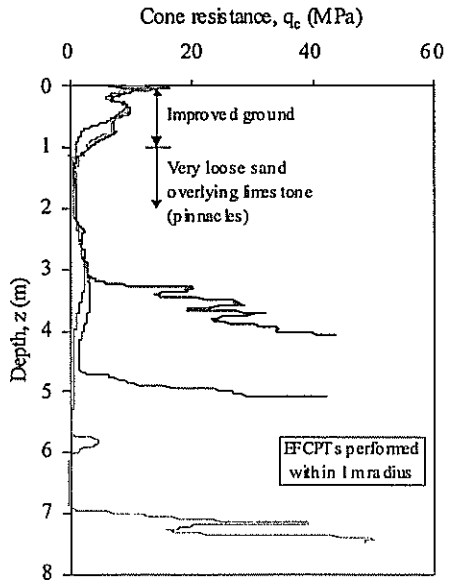

Figure 12 EFCPT profiles showing very loose sand over limestone at variable depth.

The solution adopted for these soil types was an anchored pile solution, comprising end bearing piles founding on the limestone formation and tension anchors embedded into the limestone. The foundation is shown in Figure 13.

The anchored pile foundation system is designed to resist the applied foundation loads as follows:

- Passive resistance in the dense to very dense material above the foundation level is mobilised to resist the applied lateral load;
- The anchor piles withstand the applied overturning moment and vertical loads due to wind loading through a combination of end bearing and anchor shaft friction.

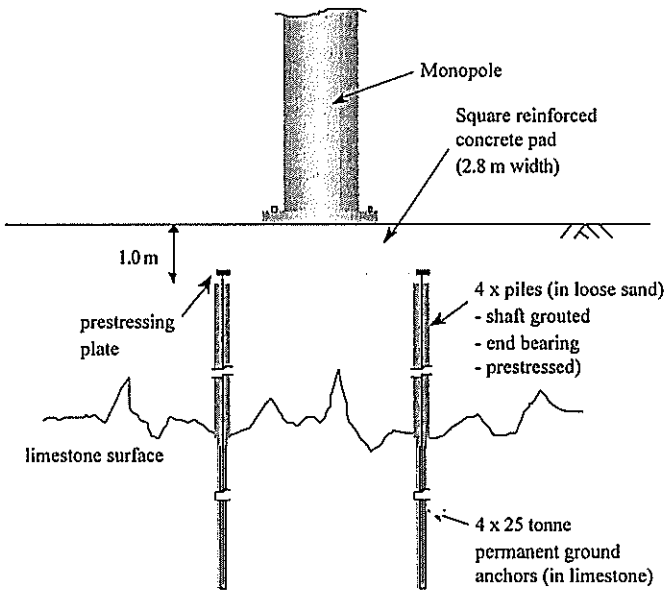

Figure 13 Anchored pile foundation

Features of the anchored pile solution include:

- Reinforcement for the pile is provided by the casing used to drill through the loose surface sand;
- The piles are shaft grouted after installation as restraint against buckling;
- The piles and ground anchors are proof tested independently prior to final grouting (by stressing against each other), to ensure sufficient pile end bearing and anchor tension capacity;
- The anchors apply permanent prestress to the piles, such that they remain in compression even under ultimate monopole loading.

These foundations were ultimately recommended for four out of the 44 greenfield sites.

7.2 Screw Pile Foundation

Toward the end of the project, a Brisbane competitor was invited to submit an alternative foundation design. The solution proposed was similar to the anchored pile solution (with comparable pad footing dimension), although the tension capacity was provided from four screw piles installed in the corners of the pad.

During construction numerous problems were encountered with the installation of the screw piles. Arup were requested to remedy the installation problems, and although the piles were eventually installed successfully, it was evident that the ground anchor option was the most efficient solution.

8 FUTURE DEVELOPMENTS

Since completing the One.Tel Network Rollout in Perth, Arup Geotechnics have been considering the use of anchored pad foundations for other projects. Examples of other projects where hybrid foundations have been proposed include:

Onshore Projects

- Crane footings where there is insufficient space for large spread footings;
- Specialist projects, such as a recently completed winch testing facility in Perth.

Offshore Projects

- Replacement for solid ballast in loadout jetties and other offshore structures. In these cases solid ballast (usually haematite) is placed in expensive and time consuming offshore operations. Installation of high capacity, permanent ground anchors may be more cost effective. In addition, on decommissioning ground anchors can easily be de-stressed and cut below mudline level. This is far simpler (and less expensive) than the operation required to remove solid ballast.

Although not appropriate for all situations, it is expected that these foundations will be increasingly used in the future.

9 CONCLUSIONS

This paper has described the geotechnical services provided by Arup Geotechnics (Perth) for the One.Tel Network Rollout in Perth, Western Australia. Activities carried out for this project included desk studies, site investigations and foundation design for 44 greenfield sites, and provision of construction supervision services for the 11 sites eventually constructed. The focus of this paper has been the development of the novel foundation alternative recommended for the project.

Speed of construction and total cost were major factors in the foundation design, and standardisation was a high client

priority. Compounding the challenges facing the foundation designer were:

- Highly variable ground condition across the metropolitan area. Ground conditions generally ranged from very weak limestone, to loose to medium dense sands and stiff clays.
- High water tables and costs associated with mobilising large diameter casing precluded piled foundations as an alternative.
- The leased sites were small (4.5 m x 8 m) in comparison with the size of typically used gravity base foundations (typically > 5 m square).
- Moment loads on the 20-35 m high monopoles are extreme, particularly when compared with a very strict rotational tolerance. Total rotation permitted at the top of the mast was 0.5 degrees, of which the monopole deflection accounted for 88%.

The foundation solution adopted was an anchored prestressed pad foundation. Optimised foundation dimensions ranged from 2.1 m to 2.7 m square depending on the monopole height, with four 25 tonne vertical permanent anchors installed to supply the required prestressing. In keeping with the clients requirement for standardisation, two base sizes were finally selected to be used at all sites, depending on the nature of the ground conditions and the monopole height.

Design of these foundations was performed using an Excel spreadsheet run interactively with displacement prediction software. Settlements were monitored during anchor prestressing, and back analysed to refine knowledge of the local ground conditions.

Following the success of the hybrid foundation on this project, Arup Geotechnics (Perth) have considered their use on a number of onshore and offshore projects. It is expected that use of these foundations will increase as confidence increases in their performance.

10 REFERENCES

1. Australian Standard AS 1289.F5.1 - 1977 Determination of the Static cone penetration resistance of a Soil - Field Test using a cone of a friction cone Penetrometer.
2. Lunne, T, Robertson PK, and Powell JJM (1997) Cone Penetration Testing in Geotechnical Practice, Blackie Academic and Professional.
3. Tomlinson, MJ (1986) Foundation Design and Construction, 5th Edition, Longman Scientific and Technical, Singapore.
4. Tomlinson, MJ (1994). Pile Design and Construction Practice, 4th Edition, E & FN Spon, London.
5. BS 8081 : 1989. British Standard Code of Practice for Ground Anchorages.

Lateral Spreading Assessment of Petrochemical Tanks Founded on Reclaimed Wellington Waterfront

Hadley Wick, Tonkin & Taylor Ltd

Lateral spreading of reclaimed waterfront land during strong seismic shaking has been observed in past earthquakes. This paper summarises a geotechnical study to found two petrochemical tanks on Wellington's waterfront. The study was carried out at a feasibility stage to assess the performance of the site during seismic shaking and provide remedial options to mitigate rupturing of the tanks during a design earthquake with 0.5g peak ground acceleration.

The stability of the site was assessed using a limit equilibrium analysis and displacements due to lateral spreading were calculated using a Newmark block analysis. A stability assessment was carried out for both the existing site conditions and following the proposed ground improvement through the use of gravel columns.

1 INTRODUCTION

In the late 1800's through to the middle of the 1900's dredgings were pumped from the harbour and other fill end tipped to reclaim land along Wellington's waterfront.

A site recently assessed at a feasibility stage involved the placement of two large petrochemical tanks near Wellington's waterfront on land reclaimed between 1924 and 1932. Due to the challenging geotechnical aspects of the site and the feasibility stage of the project simple methods were needed to assess the viability of the development.

The site comprised reclaimed fill 15m thick at the waterfront edge decreasing to 13m thick 42m inland at the back of the site. Holocene marine sediments underlie the reclamation fill, which is further underlain by Pleistocene alluvial gravels.

A 16m high, mass concrete wall, with a 7m wide base retains the fill. The current ground surface is approximately flat and the natural underlying alluvial and marine sediments slope towards the waterfront at approximately 4 degrees.

The proposed tanks are up to 24m in diameter and 11m high. Surrounding the tanks are bund walls, designed to contain the contents of a tank in the event of a tank rupturing.

Site constraints meant the tanks had to be within 12m of the waterfront edge.

1.1 Liquefaction

Shaking of the ground during an earthquake can cause layers of loose sand to try to reach a denser particle configuration by decreasing in volume. To decrease in volume the sand particles must move closer together, decreasing the void spaces between them. If the sand is saturated and fine enough to inhibit the flow of pore water out of the voids then the pore pressures will rise. If the shaking is severe enough the pore pressures can approach the initial effective stress in the soil. As the total stress of the soil must remain constant, the effective stress will decrease and approach zero. At this stage the pore pressure has reached the confining pressure of the soil (Taylor (1)), and its strength is greatly reduced.

Liquefaction of a soil is primarily, but not exclusively, related to loose, saturated fine to medium sands. Housner and committee (2) suggest any saturated granular soil has the potential to increase in pore pressure if the shaking is of sufficient intensity and duration. Liquefaction has been seen in non-plastic silts and at the other end of the range in gravels. However, for soil other than loose saturated sands, the potential to liquefy decreases as grain size moves out of the sand range.

Reclamation fill is often prone to liquefaction. Extensive liquefaction was seen in reclamation in the 1964 Niigata and the 1995 Kobe earthquakes (Yoshida et al. (3)). Reclamation fill along reclaimed waterfront is often pumped hydraulic sand and weak silts. The fill is typically allowed to settle out through water

causing layering of the deposit through sedimentation. Consequently reclamation fill is often loose and layers of clean sands are often present.

1.2 Lateral Spreading

Lateral spreading, also referred to as cyclic mobility, involves the displacement of large blocks of soil towards a free surface. These blocks will slide along layers of liquefied soil where the shearing resistance will be reduced to residual strengths.

Consider the free body of a soil mass adjacent to a free surface, such as a waterfront edge.

As shown in Figure 1, source Berrill (4), the liquefied soil exerts a pressure of ρgz on the left-hand side of the body, where ρ is the bulk density, g is the acceleration due to gravity and z is the depth measured below the water table. On the right hand side the water in the sea exerts a pressure $\rho_w gz$ in the opposite direction, where ρ_w is the density of water. As the bulk density is greater than the density of water the block of soil will be driven towards the free surface by the out of balance force.

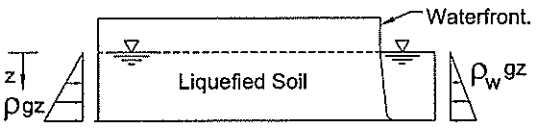

Figure 1: Free body diagram of a liquefied soil mass, adjacent to a sea waterfront.

The out of balance force and the lateral motions experienced by the soil block during an earthquake cause the soil mass to "shuffle" towards the free surface in incremental displacements.

Lateral spreading will typically occur on mild slopes or even plane land as observed by Yoshida et al. (3) following the 1995 Kobe earthquake.

2 METHODOLOGY

2.1 Site model

The model primarily consisted of the cross section shown in Figure 2. The cross section was compiled from survey data, Cone penetrometer tests (CPTs), boreholes, Standard penetration tests (SPTs) and historical drawings from the construction of the seawalls.

An important component of the model was predicting the behaviour of the seawall during strong seismic shaking. The wharf and other structures were assumed to provide little resistance to the stability of the wall.

A simple static stress analysis of the wall showed it was expected to fail by sliding or toppling in a 0.2g peak ground acceleration (PGA). Hence at levels of shaking greater than PGA = 0.2g it is assumed the wall will provide no contribution to the stability of the soil mass.

In assessing the stability of the seawall we analysed both the case where the wall is founded on the alluvial gravels and the case where it is founded on the marine sediments. This was of importance as the shearing resistance along the base of the seawall is considerably greater for alluvial gravels than marine sediments. The historical seawall drawings did not provide information on the founding conditions.

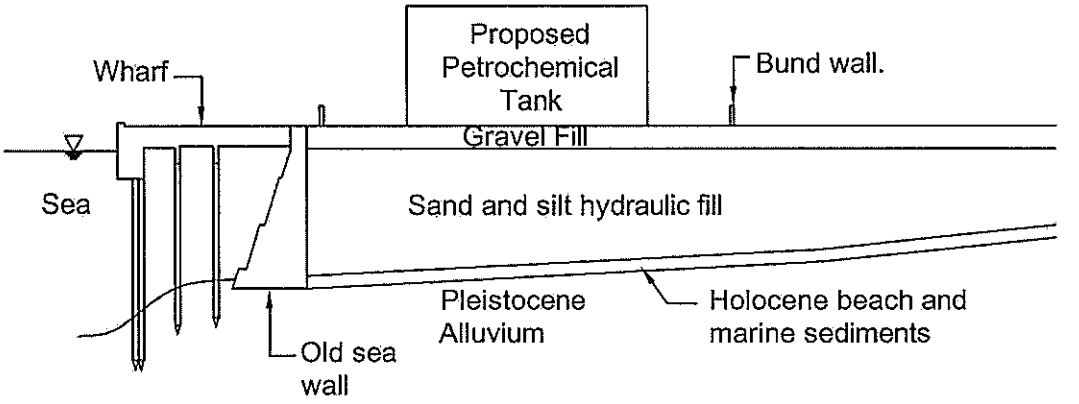

Figure 2: Cross section of the proposed petrochemical tank location

If the project moved beyond the feasibility stage coring of the seawall to assess the founding material is likely to be beneficial.

Following possible toppling of the seawall it is expected the low cohesive fill will fail back incrementally, in a "scalloping" behaviour. The incremental failures would progress inwards until the front face is approximately at the angle of friction of the fill. Larger soil blocks extending further back from the wall would shuffle forward due to lateral spreading.

2.2 Seismic Loading

Under the Dangerous Goods Regulations 1985, the tanks are to be designed for a 450-year return period. A 450-year return period could impose accelerations of up to 0.5g.

At this loading the tanks are able to be non-operational following the shaking, however they would need to maintain their integrity.

The location of the Wellington fault relative to the site was also of concern as initial assessments suggested the fault lies very close, if not below, the site. However, work by the Institute of Geological and Nuclear Sciences suggests the fault does not pass directly below the site but it is within 100 metres.

2.3 Seismic History

The most intense shaking felt by the reclamation at this site was during the two Masterton earthquakes in June and August 1942. These earthquakes were approximately magnitude 7 and were felt as a Modified Mercalli Intensity of MM7 near the site. An MM7 intensity suggests a ground acceleration of the order of 0.1g. There were reports of sand boils being observed in areas of Wellington's waterfront following these earthquakes indicating the occurrence of local liquefaction.

2.4 Soil Properties

Soil conditions were evaluated from past work in the area and then later re-evaluated on the completion of boreholes, SPT and CPT tests at the site. The assumed subsurface soil profile and corresponding measured SPT N values are shown in Table 1.

Table 1: Subsurface soil conditions

Layer Description	Thickness (m)	SPT N value (range, average)
Gravel Fill	2.0 - 2.2	9 – 15, 12
Sand hydraulic fill	4.8 – 6.8	5 – 19, 11
Silt hydraulic fill	2.4 – 4.0	1 – 5, 3
Holocene beach and marine sediments	1.0 – 2.8	13 – 14, 14
Pleistocene alluvium	-	23 – 60, 44

Based on the available data we expect the onset of localised liquefaction of the sandy hydraulic fill at a PGA of 0.1g to 0.2g. The extent of liquefaction will increase with the intensity of shaking. It is also likely that the weak silty hydraulic fill may be prone displacements under cyclic loading. Residual strengths were therefore assigned to the silty and the sandy hydraulic fill at PGA>0.2g. The residual strengths were calculated from SPT correlations.

2.5 Yield Accelerations

Newmark's method was used to calculate displacements, which require yield acceleration of the block of soil being assessed. A pseudo-static analysis was used. Where the yield acceleration is the horizontal earthquake acceleration required to bring the factor of safety to 1.0.

A limit equilibrium approach, considering the free body of a soil block such as is shown in Figure 3, was used to calculate yield accelerations.

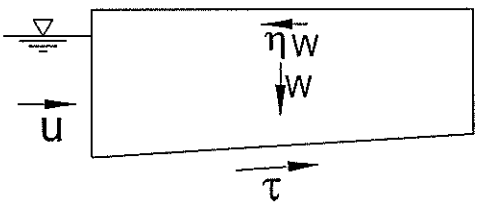

Figure 3: Free body of a soil mass.

The surcharge of the tanks were ignored when considering the free body diagrams of failure blocks, as the tanks will be piled.

2.6 Displacements

Newmark (5) suggested a relationship giving the expected displacement as a function of the yield acceleration coefficient and the maximum acceleration coefficient of the ground-motion time-history. Further work was then done by Ambraseys and Menu (6) for earthquakes in the magnitude range 6.6 to 7.3. Ambraseys and Menu's relationship was adopted for this analysis.

Newmark developed his analysis by assuming that during strong seismic shaking, once ground failure is initiated, displacements will develop if the seismic forces exceed the yield resistance. Then movement would continue until the seismic forces are removed or reversed.

Using calculated yield accelerations displacements were calculated at various critical distances beneath the tanks and bund walls.

As well as providing information for design, calculating expected displacements following strong shaking is often beneficial in helping the client appreciate the likely effects of an earthquake.

2.7 Mitigation

During assessment of possible remedial works techniques were used which were applicable to a feasibility stage for a medium sized project such as this. More detailed investigations would likely make use of finite element dynamic modelling.

The remedial option considered to be the most cost-effective was a combination of piles and ground improvement by the use of gravel columns

The extent of gravel columns likely to be required are columns on a 2m grid beneath the tanks, extending 5m to each side of the tanks and extending to the seawall in front of the tanks.

The extent of the gravel columns beyond the tanks was estimated using the zone of improvement suggested by Iai et al. and Kramar (7). It is suggested the ground improvement should be performed within a zone defined by a 30 to 45° line as shown in Figure 4, sourced from Kramer (7).

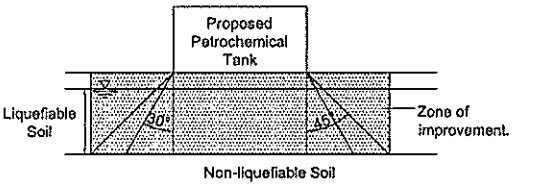

Figure 4: Suggested extent of improvement for liquefiable soil.

The gravel columns would have 3 main benefits:

- provide drainage and therefore mitigate pore pressure build-up;
- increase shear strengths along shear planes;
- densify existing soil during construction.

Increasing the shear strength will have the effect of decreasing the extent of a wedge failure directly behind the wall in the possible event of the seawall toppling. A limit-equilibrium analysis, based on friction angles, suggests the wedge failure would extend 15m back from the wall for the improved ground case compared with 20m for the unimproved ground case. This suggests the tanks could be undermined by approximately 3 metres, even with the ground improvements. The undermining of the tanks could be accommodated in the design of the piles. In estimating the undermining of the tanks we have made the conservative assumption that the strength contribution from the piles is ignored.

Piles would be driven between the gravel columns beneath the footprint of the tanks. The piles are likely to comprise concrete piles embedded into the underlying alluvial gravels.

Retrofitting of the seawall to be able to cope with a PGA=0.5 was also assessed. However this option is unlikely to be cost effective due to the extent of work required and increased costs of working below the water level.

Dynamic compaction techniques through the use of a falling weight were not considered viable at the site due to the close proximity of the seawall and the significant depth to liquefiable layers.

The shear strength of gravel columns was modelled by the use of average strength parameters. That is, the strength of the improved ground was the average shearing resistance a failure surface would experience in the improved ground. This simplified technique allowed direct comparison between

the pre-ground improvement and the post-ground improvement modelling.

3 SUMMARY

Wellington's reclaimed waterfront provides many challenges to the geotechnical engineer due to the region's earthquake activity and potentially liquefiable soils.

A further challenge of this project was to provide cost-effective investigation and analysis methods, where the client requested solutions that were appropriate for the feasibility stage.

The importance of a good site model must be stressed. The site model addresses how the slope may potentially fail and what impact surrounding structures will have.

In this paper I have summarised a number of simple techniques we have used in determining the stability of the reclaimed land with respect to lateral spreading. However care is needed in using the techniques and an appreciation of these analysis and its limits is important.

4 REFERENCES

1. TAYLOR, P.W., Liquefaction, Notes for a Seminar Engineering and Seismology and Fundamentals for Seismic Design of Earth Structures, Departments of Extension Studies and Civil Engineering, University of Canterbury, 1978.

2. HOUSNER, G.W. & COMMITTEE, Liquefaction of Soils During Earthquakes, National Academy Press, 1985.

3. YOSHIDA, M., MIYAJIMA, M., KITAURA, M., Characteristics of Liquefied Ground Flow at Plane Reclaimed Land During the 1995 Kobe Earthquakes, 2000.

4. BERRILL, J.B., Seismic Liquefaction and Lifelines; Risk and Realities, Centre for Advanced Engineering, University of Canterbury, 1997.

5. NEWMARK, N.M., Effects of Earthquakes on Dams and Embankments, Geotechnique 15, 1965, 139-160.

6. AMBRASEYS, N.M., MENU, J.M., Earthquake-Induced Ground Displacements, Earthquake Engineering and Structural Dynamics, 1988, Vol. 16, 985-1006.

7. KRAMER, S.L., Geotechnical Earthquake Engineering, Prentice Hall Inc., 1996, 514-515.

Management of Creep Settlement in Dumped Rockfill by Surcharging

J.C. Willey, Dams/Geotechnical Engineer, Gutteridge Haskins & Davey Pty Ltd, Brisbane
A. Litwinowicz, Manager – Geotechnical & Dams, Gutteridge Haskins & Davey Pty Ltd, Brisbane

Post-construction creep settlement of rockfill dam embankments is managed by provision of a longitudinal camber, ie constructing over-height. This is impractical for port facilities and similar structures where other components, such as rail and road access, terminal areas, cranes and associated services often must be in place soon after completion of the embankment and minimal post-construction settlements are important for trouble-free operation. Surcharging of dumped rockfill has the potential to reduce post-construction settlements by a) creating an additional elasto-plastic settlement due to the placement of the surcharge fill; b) increasing the rate of settlement during the surcharging period; and c) reducing the settlement rate or delaying creep settlement after removal of the surcharge load. The literature is generally silent on the benefits and methods of predicting the performance of surcharging of rockfills. A model has been developed for predicting the effects of surcharging for improvement of settlement performance.

1 INTRODUCTION

Marine facilities such as ports are constructed in difficult conditions and often have stringent post-construction settlement requirements in filled areas. Dumped rockfill is commonly used as a construction material where placement under water is required. Minimal post-construction settlement is difficult to achieve when poorer quality rockfill is the only economically viable construction material. Surcharging of rockfill embankments and reclamations can be a potentially cost-effective technique for minimising post-construction settlements. The mechanism of creep is discussed and a model for prediction of surcharging behaviour is proposed.

2 CREEP SETTLEMENT OF ROCKFILL

2.1 General

The mechanism of post-construction settlement of rockfill is largely due to creep effects caused by compression and/or deterioration of particle-to-particle contacts and particle re-arrangement. Other factors which may affect the magnitude of settlement include rockfill gradation, saturation, sluicing and wet-dry cycles. Chemical effects due to the mineralogy of the rock and composition of the immersing liquid also play a role as does the fabric permeability.

Sowers et al (Ref 1) analysed settlements of completed rockfill embankment dams and determined that the settlement during the first 10 years after construction is 0.25% to 1% of the embankment height. These assessments also indicated that the amount of settlement appeared to be independent of the embankment height and rockfill characteristics, but highly dependent on the construction method. Rockfill settlement can be approximated as a linear relationship on a semi-log plot of settlement versus log time. Settlement, S, of an embankment of height, H, between times, t_1 and t_2, is given by the following equation:

$$S = \alpha.H.\log\frac{t_2}{t_1}$$

The creep factor, α, expressed as a percentage, is taken as a constant which represents the rate of settlement in log time or settlement decay in real time. Values of α, quoted by Sowers range from 0.2% for well-compacted sluiced schist to greater than 1% for limestone placed by dumping and limited sluicing.

Penman (Ref 2) noted that large settlements occurred during the construction of rockfill embankment dams with additional settlement as the reservoir filled. Penman quoted Terzaghi who suggested that the additional settlement upon filling was due to a reduction in the material strength on saturation. From values quoted in Penman, the wet strength can be as low as 47% of the dry strength for a dense quartz-mica schist. In reference to Sowers' findings, Penman concluded that the value of α increases with increasing time, but that assuming a constant value will give an adequate indication of the settlement.

The many papers reviewed generally presented very little data on rockfill grading or its effect. However, Matheson (Ref 3) indicated that well-graded materials settle less than single sized materials due to the reduced point stresses at the particle contacts and less freedom for particle rearrangement.

2.2 Stress-Dependency of Creep Settlement

In reviewing the more common and comprehensive reference papers on rockfill settlement, it became evident there is a paucity of data on surcharging. Most of the data is derived from the observed settlement of rockfill dams which traditionally are constructed with a longitudinal camber to allow for post construction settlement, but are generally not surcharged during construction.

Based on the data from dams one is generally led to believe that creep settlements are largely independent of stress level and the creep factor, α, is independent of

fill height. In a sense this is supported by the data which generally shows that there is no clear correlation between dam height (and hence stress level) and α. This is not a surprising conclusion from this data since:

- the many factors affecting creep and the range of creep values for similar rock quality tend to give low confidence in the accuracy of α; and
- the literature reviewed does not differentiate between different section heights within each dam from which data was obtained.

As mentioned previously, it is generally acknowledged that creep in rockfill is largely due to degradation or decay of stressed rock-rock contacts over time. Factors affecting this include initial wetting, rockfill compaction and rockfill grading. It is reasonable to expect that increasing stress levels would also result in accelerated deterioration of rock-to-rock contacts. In the case of rockfill surcharging, this would result in the building-in of settlement during construction with the intent of reducing post-construction settlements.

Charles (Ref 4) discussed two well-compacted rockfill dams (Scammonden Dam in west Yorkshire and Llyn Brianne Dam in central Wales) where the creep factor, α, was clearly proportional to the stress level. Scammonden Dam, completed in 1969, is 73 m high with an upstream sloping clay core and heavily compacted sandstone and mudstone shoulders. Llyn Brianne Dam, completed in 1971, is 90 m high with a wide central clay core and heavily compacted mudstone shoulders.

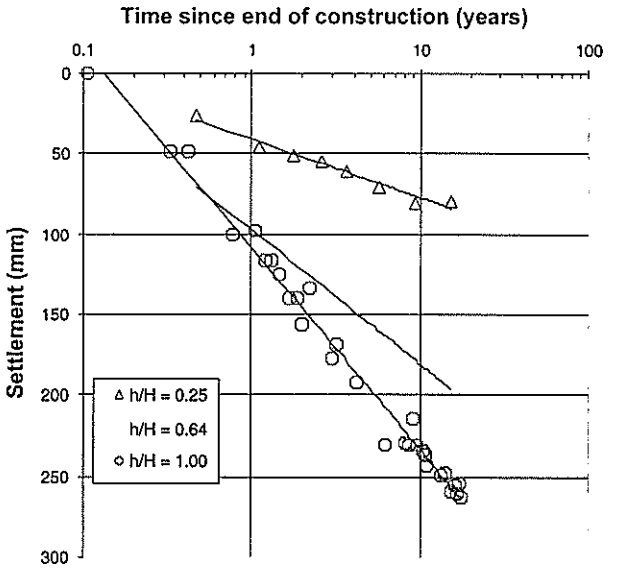

Figure 1: Settlement histories of various section heights for Scammonden Dam (after Ref 4), where h/H is the ratio of the section height to the maximum embankment height

Settlement histories are shown in Figure 1 for three different heights in Scammonden Dam. At these locations the section heights, denoted by h, are 73 m (maximum section), 47 m (0.64 relative height) and 18 m (0.25 relative height).

Plots of α indicating the stress dependent nature of creep for Scammonden and Llyn Brianne Dams are shown in Figures 2 and 3.

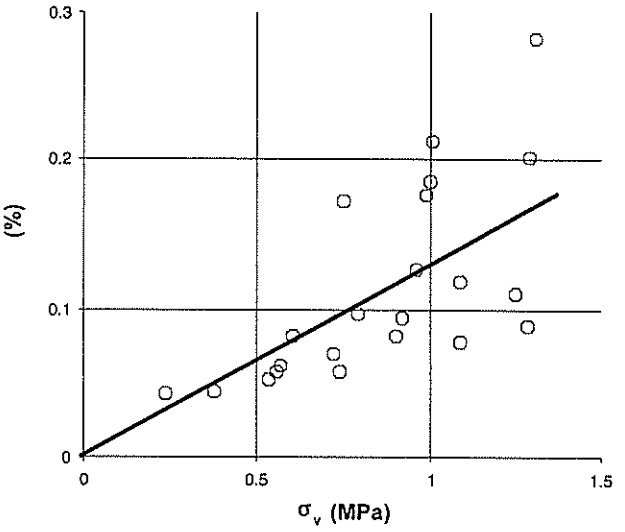

Figure 2: Creep factor, α vs stress level for Scammonden Dam (after Ref 4)

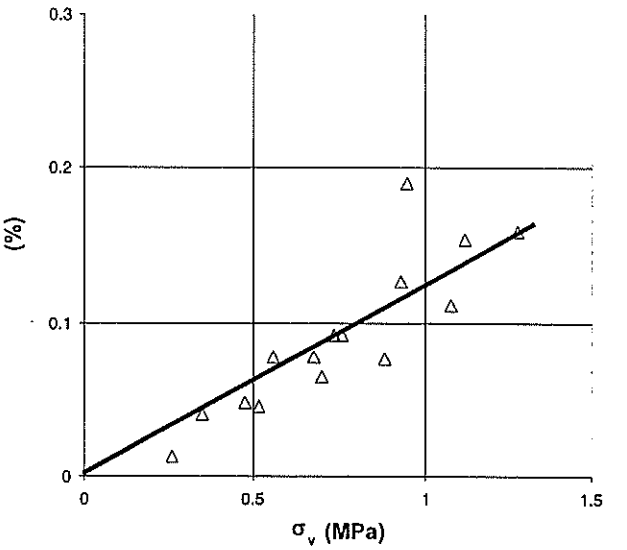

Figure 3: Creep factor, α vs stress level for Llyn Brianne Dam (after Ref 4)

As shown in Figures 2 and 3 the relationship between α and stress level can be represented by a linear approximation. For these two dams, the relationship between α (in %) and stress level, σ_v (in MPa) is as follows for σ_v up to 1.3 MPa. It does not appear to be defined in the paper whether this is in terms of effective or total stress, but it is thought to be effective stress.

$$\alpha = 0.12 \text{ to } 0.13\ \sigma_v$$

2.3 Effect of Material Grading on Creep Rate

Matheson stated that well-graded materials settle less than single-sized materials and this was also reinforced by Charles. Charles presented relationships between α and stress level for three dams – Scammonden and Llyn Brianne Dams both constructed of rockfill and Megget Dam constructed of a more broadly-graded sandy gravel fill. Although this material is not specifically a rockfill, the mechanism of settlement is similar in that the broader grading leads to greater particle interaction and a reduction in contact stresses. The relationships for Scammonden and Llyn Brianne Dams and Megget Dam are:

Scammonden/Llyn Brianne Dams:

$$\alpha = 0.12 \text{ to } 0.13\ \sigma_v$$

Megget Dam: $\alpha = 0.04\ \sigma_v$

This is some confirmation that the creep rate is lower for more broadly graded materials probably due to the reduction in point stresses between the particles.

2.4 Creep after Removal of Surcharge

Mesri and Godlewski (Ref 5) proposed a general model for creep as a function of the state of compressibility known as the C_α/C_c approach. They showed that C_α is directly proportional to compressibility and the ratio is approximately constant throughout the complete stress range from overconsolidated to normally consolidated. Whilst this mainly held for clays, it was also shown to apply to a wide range of materials including soft sensitive clays, highly plastic compacted clay shales and granular materials (Ref 6). Low compressibility following removal surcharge would result in low creep rates. There is no reason to believe that this would not also apply to rockfill.

Charles presented laboratory consolidation data for poorly compacted sandstone rockfill (Figure 4) which showed minimal rebound during unloading and a substantially higher reload stiffness than for the initial loading. This is confirmation that building-in settlements with surcharge has a positive effect (at least for short-term loadings) and creep following surcharge removal would be substantially decreased if not negligible.

Mesri and Feng (Ref 7) presented a model for rebound and delayed creep following the removal of surcharge. The authors are not aware of any proven model for the post-surcharge performance of rockfill but, as for soils, it would be reasonable to expect that removal of surcharge would result in a decreased rate of settlement consistent with reduced compressibility.

In the absence of more definitive data, the Mesri and Feng model of creep (related to the state of compressibility and hence minimal creep post-surcharge until the original creep curve is reached) has a sound basis and is most likely representative of the behaviour of rockfills. When considering the physical mechanisms at play during rockfill creep, it would be expected that overstressing with a surcharge would create accelerated degradation at particle contacts and hence settlement and creep rate would substantially reduce on unloading, consistent with the approaches above and the laboratory testing of Charles.

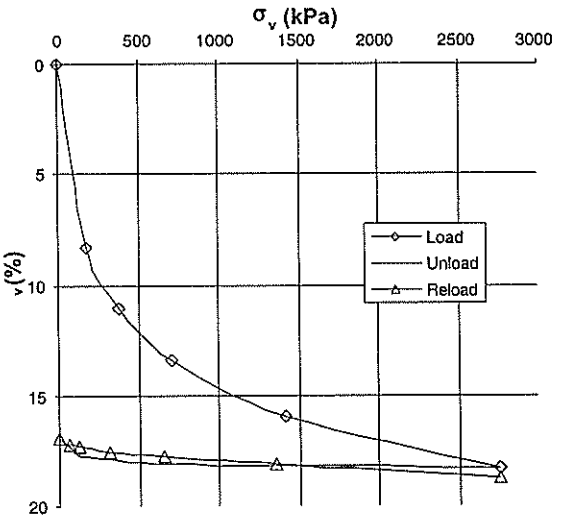

Figure 4: Laboratory consolidation test on poorly compacted sandstone rockfill (after Ref 4)

3 SURCHARGING OF ROCKFILL EMBANKMENTS

3.1 Proposed Model for Prediction of Surcharge Effects

Whilst there is little direct evidence in the literature of the benefits of surcharging dumped rockfills, there is a sufficient basis to suggest that it will have a positive effect and, provided that stability is satisfactory, there are no perceived negative impacts. If a finer rockfill or one prone to breakdown was utilised, surcharging would also assist in accelerating primary consolidation if it were to occur.

The model proposed for assessing the benefits of surcharging is schematically depicted in Figure 5. The settlement considered here is the settlement at point "X" at the top of the final embankment section.

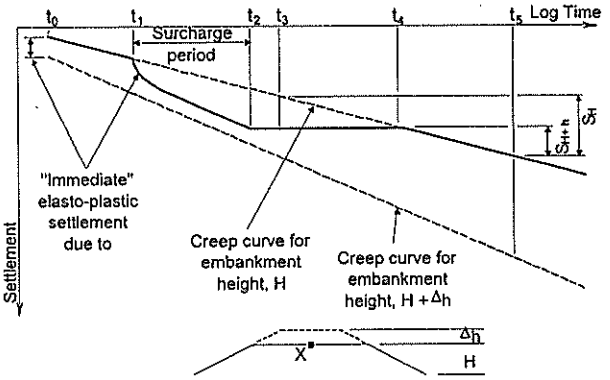

Figure 5: Sketch of model proposed for assessment of surcharge

Application of the surcharge (additional height of Δh) at time, t_1, causes a largely irreversible "immediate" elasto-plastic settlement followed by creep at a higher rate due to the increased stress caused by the surcharge. The creep curve during the surcharging period is parallel to the dotted line, which represents the creep curve for an embankment height of $H+\Delta h$. The surcharge is left in place for the period from t_1 to t_2. Time t_3 represents the project handover and the commencement of the maintenance period. At time t_5, the end of the design life, the post-construction settlements for the unsurcharged and surcharged embankments are represented by S_H and $S_{H+\Delta h}$, respectively.

In this model, it is assumed that creep is linear in log time, there is minimal rebound on removal of the surcharge and there is negligible settlement until the settlement curve reaches the original creep curve at a later time. These assumptions are discussed further.

3.2 "Immediate" Settlement upon Application of Surcharge

As illustrated in Figure 5, the settlement which occurs after application of the surcharge load consists of both an immediate (elasto-plastic) and a creep component. The immediate component of the settlement, S_I, for a given surcharge, $\Delta\sigma$, can be estimated from the following formula where E is the deformation modulus.

$$S_I = \frac{\Delta\sigma.H}{E}$$

3.3 Creep during the Surcharge Period

Creep settlement of a surcharged embankment occurs at a greater rate than for an unsurcharged embankment due to the stress-dependency of the creep rate. As indicated by Charles, the relationship between creep rate and stress level is approximately linear. Therefore, for a surcharge of Δh on an embankment of height H, the creep rate during surcharging is $(H+\Delta h)/H$ times the pre-surcharge creep rate.

3.4 Creep after Removal of the Surcharge

As discussed previously in Section 2.4, the approach of Mesri and Feng has been adopted and the following elements have been considered:

- immediate (elasto-plastic) rebound on unloading;
- secondary (creep) rebound that flattens out in time; and
- re-establishment of the original creep rate considered to occur, for the purposes here, at the time at which the equivalent settlement would have occurred without surcharging.

To simplify the procedure, immediate rebound and rebound creep have been ignored and the settlement is considered static until creep recommences. In the absence of any more definitive data, it is assumed that creep recommences at the time at which the equivalent settlement would have occurred without surcharge (time t_4 in Figure 5). This time estimate can only be improved with specific data on rockfill. Some data exists for clays, but none is likely to exist for rockfill. However, the assumption has some basis since one would not expect the creep rate at a given state of decay (or settlement) to be widely different to that for the non-surcharged embankment at the same height. This leads to the conclusion that post-surcharge settlement (when coupled with rebound and rebound creep) should be in effect negligible until the original curve is reached.

4 EXAMPLE OF ROCKFILL EMBANKMENT SURCHARGING

This example will demonstrate how surcharging would be beneficial if low quality dumped rockfill were the only economically available source of material. Consider a 20 m high embankment specified to be constructed of high quality dense rockfill with an estimated creep rate, α of 0.3%. The settlement history of this material is shown in Figure 6, assuming the handover time and the commencement of the maintenance period is 120 days after construction and the end of the maintenance period is 10 years hence. The only available rockfill is of lower quality with an estimated α of 0.8%. The settlement history of this material is also shown in Figure 6. Post-construction settlements are predicted to be 90 mm and 240 mm, respectively.

The post-construction settlement (taken as the settlement which takes place after handover) of the high quality rockfill (90 mm) sets the post-construction settlement criterion for the surcharged low quality rockfill embankment. This can be achieved using the lower quality rockfill by adjusting the height of the surcharge and/or the length of time it is left in place.

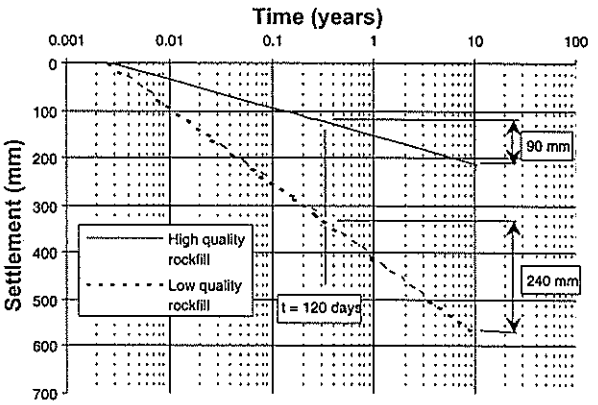

Figure 6: Comparison of settlement behaviour of high and low quality rockfill

A surcharge height of 2 m is proposed to match the post-construction performance of the high quality rockfill and ensure embankment stability. By applying Charles' finding that the relationship between stress level and α is linear, the addition of a 2 m surcharge to a 20 m high embankment will result in a 10% increase in α to approximately 0.9%.

For simplicity, the "immediate" elasto-plastic settlement is assumed to take place instantaneously upon application of the surcharge. Assuming the rockfill has a unit weight and deformation modulus of 20 kN/m_ and 10MPa, the immediate settlement would be 80 mm. The surcharge is placed approximately 1 month after the end of construction and left in place for sufficient time to reduce the post-construction settlement.

The required surcharging period to meet the settlement criteria is determined from Figure 7.

This process indicates that the post-construction settlement performance of a low quality dumped rockfill embankment can be improved to match that of a high quality rockfill embankment through the application of a surcharge. In this case, the post-construction settlement can be reduced from 240 mm to 90 mm by applying a 2 m surcharge for approximately 8 months. A similar reduction could be achieved by applying a greater surcharge for a shorter period provided that stability of the bund was not compromised.

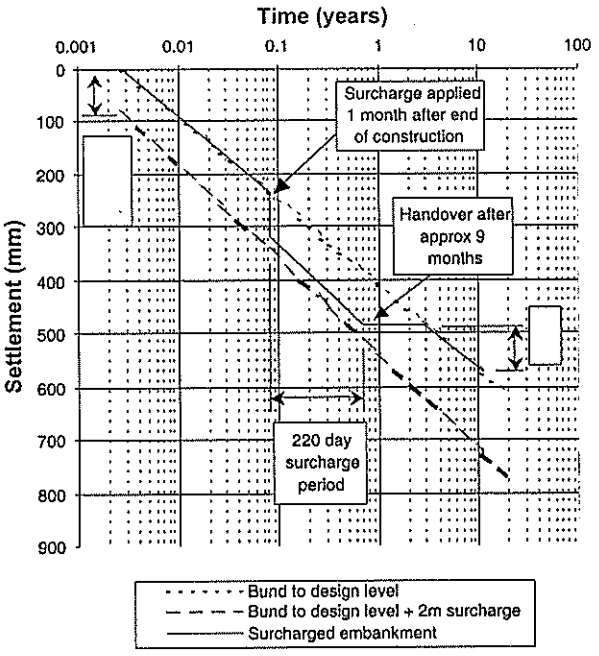

Figure 7: Example for determining required surcharge period for a given surcharge height

5 SUMMARY

Creep settlement is a phenomenon which affects all rockfill structures to varying extents, depending on factors such as method of placement, material quality and grading, and saturation. The basic mechanisms causing creep and the limited published data strongly indicate that creep rate is also dependent on stress level. This is beneficial when considering the effects of surcharging to improve post-construction performance. There is a dearth of information in the literature either on methods of prediction or actual performance of surcharging rockfills. The model developed and proposed for prediction of surcharge effects is consistent with normally accepted engineering principles, the physical nature of creep development and is supported by the various published data presented in this paper. There is strong evidence that performance of rockfill structures can be improved through surcharging. The authors are currently involved in several projects where surcharging of rockfill is showing early signs of confirming the approach proposed.

6 REFERENCES

1. SOWERS, G.F., WILLIAMS, R.C. & WALLACE, T.S., "Compressibility of broken rock and settlement of rockfills" in Proceedings of 6th International Conference on Soil Mechanics and Foundation Engineering, 1965, pp 561-565.

2. PENMAN, A.D.M., "Rockfill" in Building Research Station Current Paper 15/71, Building Research Establishment, Watford, 1971, pp 1-10.

3. MATHESON, G.M., "Relationship between compacted rockfill density and gradation" in Journal of Geotechnical Engineering, December 1986, pp 1119-1124.

4. CHARLES, J.A., "Chapter 5 – Laboratory compression tests and the deformation of rockfill structures" in Advances in Rockfill Structures, Kluwer Academic Publishers, Dordrecht, 1991, pp 73-96.

5. MESRI, G. & GODLEWSKI, P.M., "Time- and Stress-Compressibility Inter-relationship" in Journal of the Geotechnical Engineering Division, ASCE, May 1977, pp 417-430.

6. MESRI, G. & CASTRO, A., "C_α/C_c Concept and K_o during Secondary Compression" in Journal of Geotechnical Engineering, March 1987, pp230-247.

7. MESRI, G. & FENG, T.W., "Surcharging to Reduce Secondary Settlements" in Proceedings of International Conference on Geotechnical Engineering for Coastal Development, Yokohama, 1991, pp 359-364.

Piled Embankment Response via Simplified Methods

Sii Chung Wong
Department of Civil Engineering, University of Sydney, Australia.

Summary: The application of piles in embankment construction has been widely adopted, especially in Southeast Asia and Scandinavian nations. However, piled embankments are often designed based on empirical methods. The three-dimensional nature of the piled embankment system requires it to be analysed as a three-dimensional problem. In this paper, a three-dimensional finite difference analysis (FLAC3D) has been used to study some characteristics of piled embankment behaviour. A simplified approach has also been used to predict the piled embankment response, and compared to the FLAC3D analysis. The two approaches showed reasonable agreement, with the simplified approach able to solve the problem more rapidly than FLAC3D. It therefore appears to hold promise as a convenient tool for analysing and designing piled embankments.

1 INTRODUCTION

In the design of high performance roads, highways, trunk roads and airport runways over soft soil profiles, it is often essential to provide an elevated platform often via an embankment. Conventional methods of embankment construction such as pre-loading are usually associated with long "waiting" periods for consolidation. Subsequently, the use of piles in embankment construction provides an attractive alternative especially in the growing "fast-track" construction environment. The use of piles in embankment constructions has been documented by Eide (1), Holmberg (2), Tan et al. (3), and Ruenkrairergsa (4).

This present study is aimed at examining some response characteristics of piled embankment systems via a full three-dimensional analysis, and then assessing the potential for simplified methods of analysis to be used in design. Consideration is given to ground settlement, and underlying pile axial loads.

2 HYPOTHETICAL PROBLEMS

The hypothetical piled embankment problem devised in this study considers two different types of basal reinforcement, namely, individual pile caps overlain by a geo-grid net; and a lightly reinforced continuous slab. A piled embankment with individual pile caps only was not considered in this study as this type of construction tends not to perform satisfactorily, especially with large embankment pressure as detailed by Wong and Poulos (5).

The analysis involves three stages of construction with embankment heights, H_e at 3m, 6m, and 10m (see Figure 1). The standard properties adopted for each material are detailed in Figure 1 and also tabulated in Table 1. All properties in the hypothetical problems remained constant throughout this study except for the properties and the geometry of different basal reinforcements used. The cases examined are typical of conditions in some parts of Malaysia.

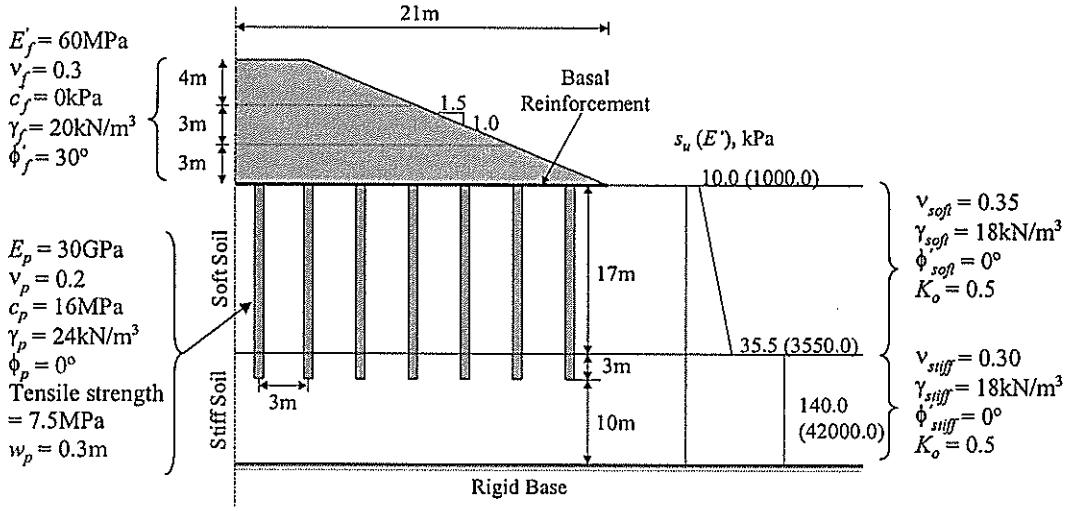

Note:

- E' represents Young's modulus, ν' represents the Poisson's ratio, c' represents the drained cohesive strength, s_u represents the undrained cohesive strength, γ represents the unit weight, ϕ' represents the internal angle of friction, and w_p represents the width of piles.
- Subscripts on each parameter represent the respective materials referred in the diagram.

Figure 1: Standard hypothetical piled embankment problem

Table 1: Material properties for embankment basal reinforcements

Material	Parameters	Value
Pile caps and reinforced concrete slab.	Young's modulus	30 GPa
	Poisson's ratio	0.2
	Density	24 kN/m^3
	Cohesive strength,	16 MPa*
	Tensile strength	5.7 MPa*
	Angle of friction	0°
	Slab and cap thickness	0.4 m
	Cap width (square)	0.6 m
Geo-grid.	Young's modulus	3 GPa
	Cross sectional area	0.005 m^2/m
	Exposed perimeter	2 m/m
	Max. axial tension	1.2 GN/m

Note:
Assuming concrete compressive strength, f'_c, is 32 MPa reinforced with 0.35% of steel.

3 MODELING OF PILED EMBANKMENT

3.1 FLAC3D Modeling

In the modelling of a piled-embankment via the three-dimensional finite difference program FLAC3D by Itasca (6), polyhedral grids of solid elements were used to represent the soil medium, the underlying piles and the embankment fill. The piled-embankment system was modelled as a unit of piled-embankment shown in Figure 2. Only one half-width of the piled-embankment system was modelled to reduce the computing resources and the required computational time.

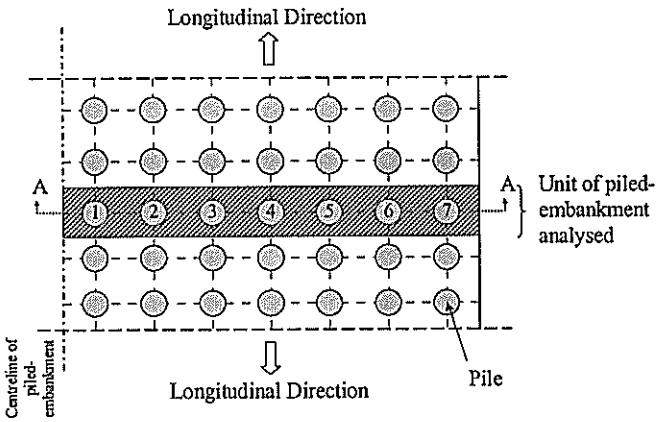

Figure 2: A unit of piled embankment used in FLAC3D modelling

Individual pile caps and continuous concrete slabs were both modelled as polyhedral grids of solid elements. Pile caps and concrete slabs were all analysed as a Mohr-Coulomb material, in which the structural strengths were represented by specified cohesive and tensile strengths. The cohesive strength was taken to be half of the concrete compressive strength, ignoring the contribution from steel bars, while the tensile strength of these structures was derived from the corresponding stress at extreme fibres at ultimate bending moment capacity.

Geo-grid reinforcement was modelled via one-dimensional linear elastic perfectly plastic cable elements in FLAC3D. The use of cable elements to represent geo-grid reinforcement was also employed by several authors, for example, Russell and Pierpoint (7), and Kempton et al. (8). The interface between the geo-grid and the soil medium was modelled via elastic springs, hence requiring the spring stiffness as input. Slip between geo-grid and soil medium was allowed by specifying a cohesive strength and internal angle of friction. In this study, both cohesive strength and internal angle of friction were assumed equal to the undrained strength and internal angle of friction of the surrounding soil medium, respectively.

Ideally, the interface (spring) stiffness should be obtained from a pullout test. However, in the absence of such test data, the interface stiffness used in this study was estimated from equation (1), which was originally derived by Randolph (9) for a pile foundation.

$$k_s = 1.6G \qquad (1)$$

where, G is the shear modulus of the geo-grid.

3.2 Simplified Methods

The simplified method of analysis adopted in this study is based on a piled raft analysis via the programs GARP and PIRAF developed by Poulos (10), and Ta and Small (11) respectively. GARP employs a simplified form of soil-structure analysis of plate elements with piles represented as interacting springs and the underlying soil represented as a layered elastic medium. Non-linear behaviour of soil is partially considered by limiting the contact pressure between the raft and the underlying soil to the bearing capacity of the underlying soil. GARP also allows for non-linear pile behaviour by limiting the pile head load to the ultimate pile capacity. Uplift of raft elements is allowed by limiting the uplift capacity of raft elements, which is usually small in magnitude.

PIRAF utilises a modified finite layer method to represent the soil medium with piles treated as a series of cylindrical elements. The surface raft is analysed as elastic thin plate elements. Unlike GARP, PIRAF is only capable of analysing linear elastic systems.

Inevitably, the use of a simplified method requires assumptions in the modeling and analysis of the piled embankment systems. The following are the assumptions adopted in this present study for the analysis conducted via the simplified methods:

- The embankment fill is represented by "active" vertical pressure imposed on raft elements.
- The piles are subjected to vertical loads only.
- The soil medium behaves as a series of purely elastic layers.

4 COMPARISONS BETWEEN FLAC3D AND SIMPLIFIED METHODS

In predicting piled embankment response with a continuous slab via the simplified method, GARP5 (finite difference "raft" elements); GARP6 (finite element "raft" elements); and PIRAF were used. For the piled embankment with pile caps and geo-grid (flexible mat), GARP6 and PIRAF were used, as GARP5 was unable to cater for non-uniform stiffness of the raft.

4.1 Piled Embankment with a Continuous Slab

Figure 3 shows the settlement distribution obtained from FLAC3D and the simplified methods of analysis across section A-A (see Figure 2) for H_e = 3m. There is reasonable agreement between FLAC3D and the simplified approaches. Generally, PIRAF (linear elastic analysis) slightly underestimates (<10%) the settlement predicted by FLAC3D towards the centreline of the embankment, while GARP5 and GARP6 slightly overestimate the settlement (by <7%). The figure also shows that all three simplified methods underestimate the settlement towards the embankment toe (side slope) compared to FLAC3D. This could be due to representing the embankment fill as a purely vertical pressure and only considered the underlying piles to be vertically loaded, whereby both assumptions could lead to less restraint of edge lifting. However, such predictions by the simplified methods will lead to conservative predictions of differential settlement.

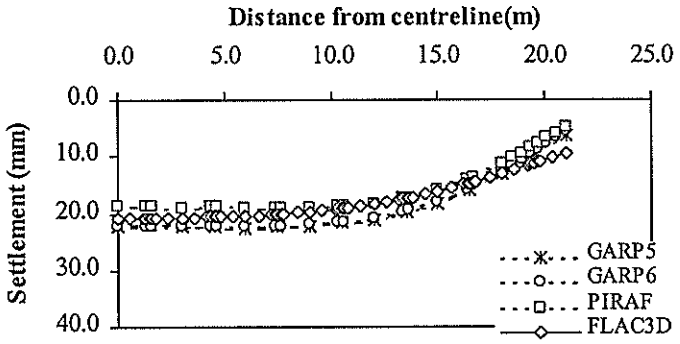

Figure 3: Comparison of settlement profile at ground level (H_e = 3m with continuous slab)

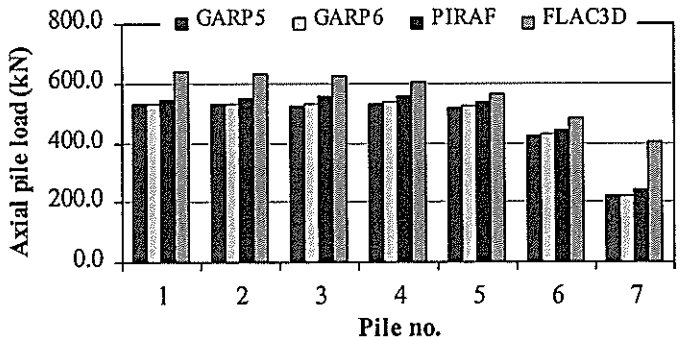

Figure 4: Comparison of pile axial load distribution (H_e = 3m with continuous slab)

Figure 4 shows pile load distributions predicted via FLAC3D and the simplified methods. The simplified methods, showed reasonable agreement with FLAC3D in predicting the pile axial load, although they predicted a slightly lower pile axial load than FLAC3D for Pile 1 to Pile 6 (by about 7% to 17%). Pile 7 shows the least favourable agreement in pile axial load predicted.

The comparison of the maximum settlement predicted via various methods of analysis with embankment height is shown in Figure 5. A reasonable agreement between FLAC3D and the simplified method of analysis is demonstrated for H_e up to 6m. With H_e at 10m, PIRAF showed the smallest maximum settlement, as it was an elastic analysis, while GARP5 and GARP6 predicted a larger maximum settlement than FLAC3D. Overestimation by GARP5 and GARP6 at H_e equal to 10m could be contributed to the neglect of the embankment fill stiffness in the analysis. The additional fill stiffness could encourage better distribution of embankment pressure to the underlying piles. The additional fill stiffness can be approximately considered via the thickness of "raft" elements. Equivalent "raft" thickness can be estimated by adopting a "reinforced concrete slab design" analogy, whereby a "composite" slab, consisting of a continuous slab and embankment fill, is formed, with the former acting as a tensile component while the latter acting as a compressive component. Such an approach has been adopted in GARP6 and from Figure 5, the results show a relatively good correspondence to FLAC3D.

The approximate computing time taken for this piled embankment configuration by various methods of analysis is tabulated in Table 2. The simplified methods of analysis, especially GARP5 and GARP6, were substantially quicker than the FLAC3D analysis.

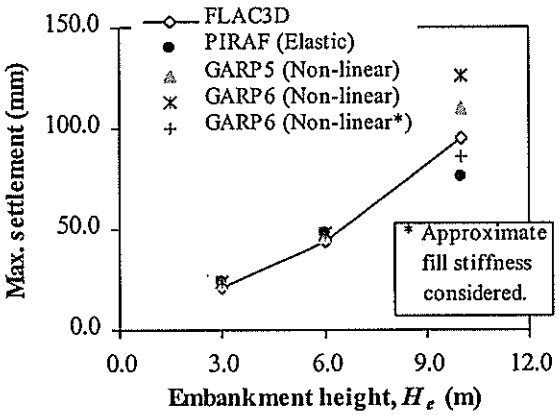

Figure 5: Maximum ground settlement with embankment height, *He* (continuous slab)

4.2 Piled Embankment with Pile Caps and Geo-grid Reinforcement

In the simplified method, the individual pile caps were represented as discrete "raft" elements, while the geo-grid reinforcement net was represented as "raft" elements with small bending stiffness.

Table 2: Approximate computing time of different methods of analysis (H_e = 3m)

Method of analysis	Approximate computing time (mins.)	
	Continuous slab	Pile caps & geo-grid
FLAC3D	3408	3512
PIRAF	116	116
GARP5	3	-
GARP6	17	17

Piled embankments with a combination of pile caps and geo-grid can be modeled by having a raft with non-uniform stiffness. The appropriate raft thickness to represent the geo-grid net can be estimated from the following steps:

- Determine the thickness of the "virtual" composite slab by providing identical axial stiffness (EA) between the geo-grid net and the embankment fill for a unit length of the system. The embankment fill is considered as a compressive component and the geo-grid net as a tensile component.
- Depth of the rectangular compressive stress block developed in the embankment fill is assumed to be equal to 2/3 of the overall "virtual" slab thickness.
- With the known dimensions of the rectangular compressive stress block and the geo-grid net, the bending stiffness of the composite slab, $E_{v.slab} \cdot I_{v.slab}$, can be obtained. Subsequently, the equivalent raft thickness can be obtained via $E_{v.slab} \cdot I_{v.slab} = E_{raft} \cdot I_{raft}$, where $E_{raft} \cdot I_{raft}$ represents the bending stiffness of "raft" elements used in the analysis.

It is shown in Figure 6 that the simplified method of analysis is in reasonable agreement to the FLAC3D analysis in predicting the settlement profile of the piled embankment with a flexible mat. However, the simplified methods underestimate the settlement towards the embankment toe compared to the FLAC3D predictions. A reasonably good agreement between FLAC3D and the simplified methods in predicting the distribution of pile axial load is shown in Figure 7, with marginal underestimation (<7%) for Pile 1 to Pile 6 (see Figure 2). The simplified methods predict a significantly lower pile axial load for the edge pile (Pile 7) than FLAC3D (about half).

Figure 8 shows comparisons of maximum ground settlement with embankment height predicted by various methods of analysis. Elastic analysis via the simplified methods significantly underestimates the maximum ground settlement. The non-linear GARP6 analysis predicted a lower maximum settlement than FLAC3D (by about 15%) for H_e at 10m. Stiffer response exhibited by GARP6 is presumably due to the soil medium being assumed to behave as a linear elastic material in GARP6, whereby progressive development of plastic zones in the soil medium is allowed in FLAC3D. Once again, it was found that the simplified methods were able to provide substantial time saving in the analysis compared to FLAC3D (see Table 2).

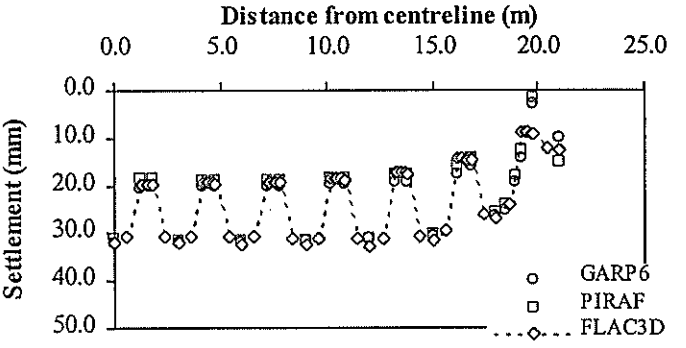

Figure 6: Comparison of settlement profile at ground level (H_e = 3m with flexible mat)

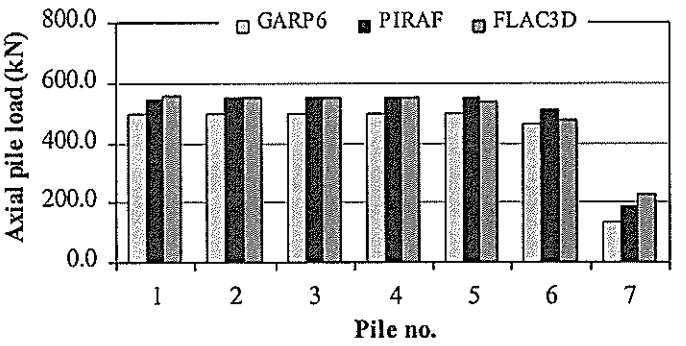

Figure 7: Comparison of pile axial load distribution (H_e = 3m with flexible mat)

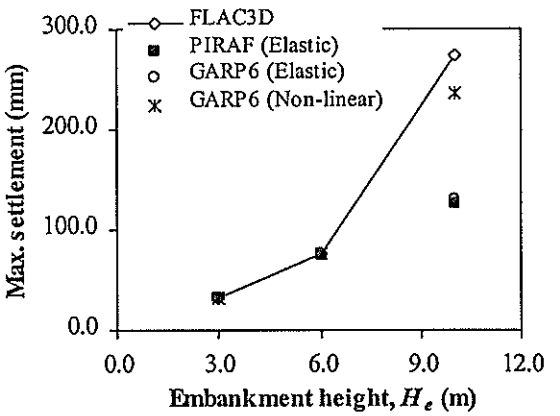

Figure 8: Maximum ground settlement with embankment height, *He* (with flexible mat)

5 CONCLUSIONS

In this study, comparisons have been made between FLAC3D and three simplified methods of analysis based on a piled raft analysis of a piled embankment. By making appropriate allowances for the effects of the embankment fill stiffness and geo-grid reinforcement modelling, the simplified methods of analysis showed reasonably good agreement to FLAC3D in predicting ground settlement and pile axial load. Although the use of the simplified methods requires some engineering judgement, they show promise as tools to be used to predict behaviour of piled embankment

systems rapidly, and for providing a more efficient and convenient design tool than FLAC3D.

6 ACKNOWLEDGEMENT

The work presented in this paper forms part of a project on "The use of piles in construction of pavements and embankments" which is financially supported by The Australian Research Council. It was carried out by the author under the supervision and the guidance of Professor H.G. Poulos during his Ph.D. candidature at The University of Sydney. The author gratefully acknowledges Prof. H.G. Poulos and Assoc. Prof. J.C. Small for proof reading this paper.

7 REFERENCES

1. EIDE, O. "Geotechnical problems with soft Bangkok Clay on the Nakhon Sawan Highway Project", Publication No. 78, Norwegian Geotechnical Institute, 1968, 9p.
2. HOLMBERG, S. "Bridge approaches on soft clay supported by embankment piles", Geotechnical Engineering 10(1), 1978, 77-89.
3. TAN, S.B., TAN, S.L., YANG, K.S. & CHIN, Y.K. "Soil improvement methods in Singapore", 3rd Intern. Geotech. Seminar on Soil Improvement Methods, Singapore, 27-29 Nov. 1985, 249-272.
4. RUENKRAIRENGSA, T. "Recent Ground Improvement Works for Highways in Thailand", 13th Southeast Asian Geotechnical Conference, Taipei, Taiwan R.O.C., 16-20 Nov. 1998, 17-43.
5. WONG, S.C. & POULOS, H.G. "Performance of various piled embankment systems", 5th Intern. Conf. On Deep Foundation Practice incorporating Piletalk, Singapore, 4-6 April 2001, 395-402.
6. ITASCA CONSULTING GROUP, INC. "FLAC3D (Version 2.0) User's Manual", 1997.
7. RUSSELL, D. & PIERPOINT, N.D., "An assessment of design methods for piled embankments", Ground Engineering, Nov. 1997, 39-44.
8. KEMPTON, G., RUSSELL, D., PIERPOINT, N.D. & JONES, C.J.F.P. "Two- and three-dimensional numerical analysis of the performance of piled embankment", 6th Intern. Conf. On Geosynthetics, 1998, 767-772.
9. RANDOLPH, M.F. "Short course notes on Engineering of Piled Foundations", Kuala Lumpur, 1992.
10. POULOS, H.G. "An approximate numerical analysis of pile-raft interaction", Intern. Journal for Numerical and Analytical Methods in Geomechanics 18(2), 1994, 73-92.
11. TA, L.D. & SMALL, J.C. "Analysis of piled raft systems in layered soil", Intern. Journal for Numerical and Analytical Methods in Geomechanics 20(1), 1996, 57-72.

SH6 Nevis Bluff Rockfall and Risk Assessment, Central Otago, New Zealand

PR Woodmansey : Principal Geotechnical Engineer, Opus International Consultants Ltd

SUMMARY

The Nevis Bluff rockfall was a failure of several thousand cubic metres of schist debris onto State Highway 6 in Central Otago, New Zealand. It occurred in September 2000 over a length of approximately 100m of highway. The rocks narrowly missed traffic on the highway. A motorist travelling towards Queenstown climbed out of her car and ran in haste as rocks fell down around her. It was nothing short of chance that no one was killed. This was the second time that such a failure had occurred from the bluff in the last 25 years (previous failure of similar magnitude was in 1975).

SH6 is the main arterial route to Queenstown, the adventure tourist capital of the world. Transit New Zealand and Opus International Consultants Ltd managed the emergency response and clean up.

The bluff is approximately 140m high and mountainous rising much higher away from the active face. The rock face typically stands at a slope angle 70°.

This paper describes the failure mechanism, geotechnical and risk assessment and the long-term options for security of the route for the highway.

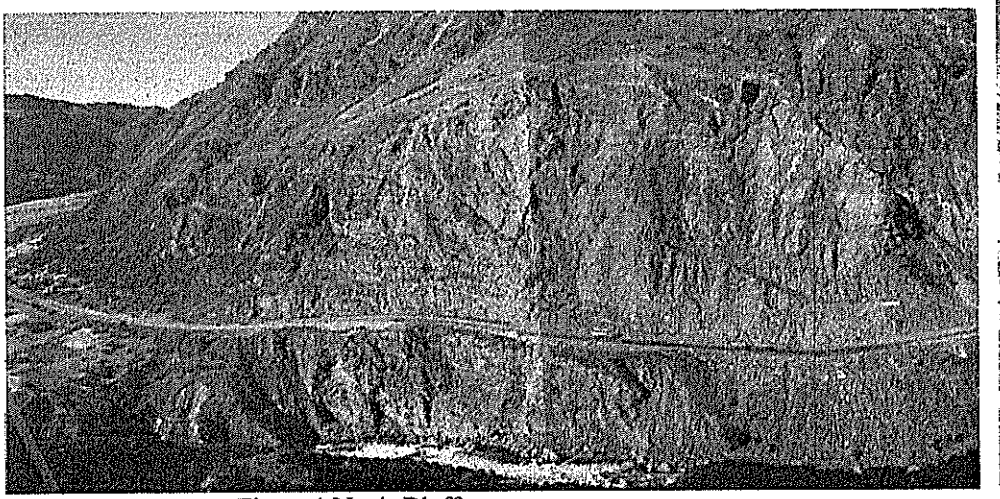

Figure 1 Nevis Bluff

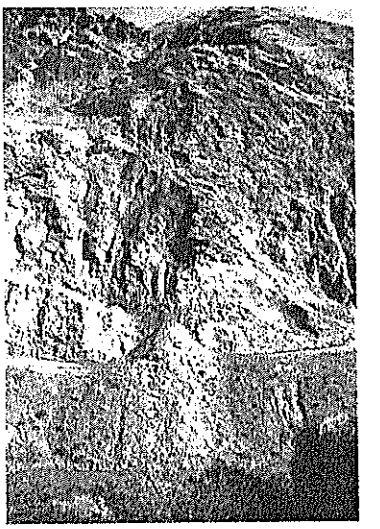

Figure 2 September 2000 Rockfall

SITE LOCATION

The site is located on SH6 near Queenstown. In this location the highway runs on a 20m wide platform between the bluff face and the Kawarau River. The highway is approximately 50m above the River. Below the highway the ground plunges steeply down into the gorge formed by the Kawarau River which is quite often a raging torrent.

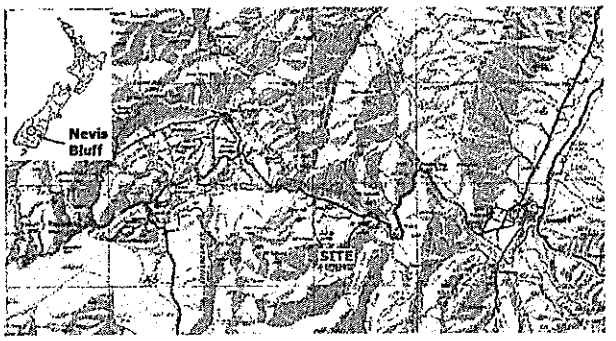

Figure 3: Site Location

GEOLOGY

The site is located within the Aspiring lithologic association of the Torlesse Terrane of the Otago Schist. This is largely quartzofeldspathic schist with two conformable bands of Greenschist.

Locally the schistocity dips into the face at 35°-45°. In general the different rock unit boundaries are conformable with the schistocity. Shear zones including the major (25m wide) zone forming the western margin of the Bluff and a further major shear, which follows the river at the base of the ridge. A further major shear up to 2m wide extends upslope from eastern end of the bluff. A number of other narrower shear zones have been mapped as traversing the face ranging in thickness form 75 to 200mm wide.

Mapping of Joints has disclosed up to four prominent joint sets in two domains. These generally are steeply dipping and subdivide the face into a series of "columns".

The combination of the complexity of the rock units, the schistocity, shear zones and joint orientations has a major impact on the stability of the Nevis Bluff as discussed later.

At the top of the bluff area is a remnant channel running sub parallel to the slope, which is in filled with, subangular to subrounded Sandy Gravels. The Upper Terrace comprises Fan gravels which overly and grade onto the channel fill. Prominent colluvial deposits blanket the less steep slopes of the bluff area and the surrounding slopes. These comprise poorly sorted angular schist blocks ranging from gravel size to large boulders in a sandy silt matrix. Large Boulders have accumulated at the base of the slopes.

The Kawarau River is actively down cutting at this point and the slopes are being continually undermined with considerable scour during floods. The Underlying geology is not exposed but is thought to consist of rocks similar to those exposed at the Nevis Bluff.

ROCKFALL FAILURE MECHANISM

The failure of the rock face at the Nevis Bluff is now reasonably well understood. The failures are due to stress relief of the face. Historically this has been caused by activities such as cutting the base of the slope for the highway construction or through geological processes such as the active down cutting of the Kawarau River.

What appears to happen is that a bulging out of the face precedes failure with the opening of fresh cracks sub-parallel to the face. This does not correspond to any simple mode of failure. The slope fails by a combination of the crest of the slope rotating about the toe. The failure resembles flexural toppling where continuous columns break in flexure as they slide along schistocity surfaces. Flexural cracking is then responsible for propagating the plane along which sliding occurs.

The middle areas of the slab starts to shatter while the upper and (particularly) the lower portions remain somewhat intact, Figure 3. As the rotation outward proceeds, the mass becomes concentrated into the lower slab and it commences to "punch into" the lower quartz rich schist. Penetration by displacement of schistocity of up to 150mm has been observed on the face below some of the intact slabs. Fresh cracking is observed in the slab above the toe and blocks start to become detached in the lowermost toe region, Figure 5.

As movement continues the column remains hung up on asperities developed as the back failure plane as defined by the joint sets which step in and out along the schistocity that dips into the slope at about 40°. These asperities commence to fail through a combination of stress concentration and some weathering.

With continued movement the centre of the column rotates outwards, a shear plane develops along a plane of schistocity and the upper part of the column falls.

The centre fractured mass then falls behind the descending upper portion and "kicks out" the lower slab, Figure 6, resulting in devastating collapse.

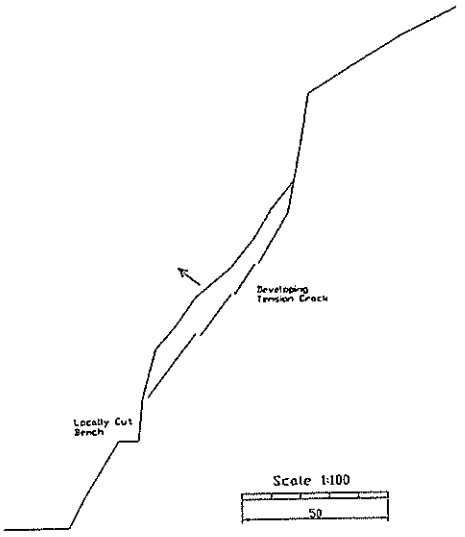

Figure 4 : Tension Crack Development

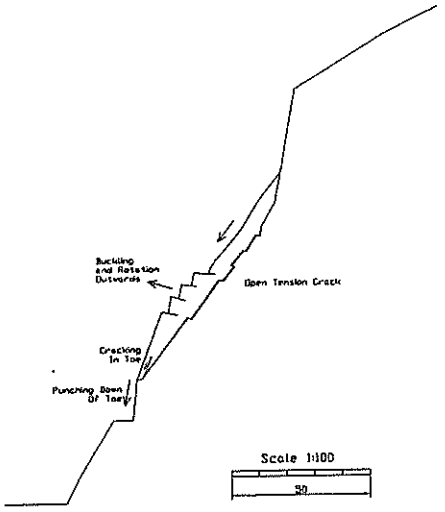

Figure 5 : Buckling and Rotation

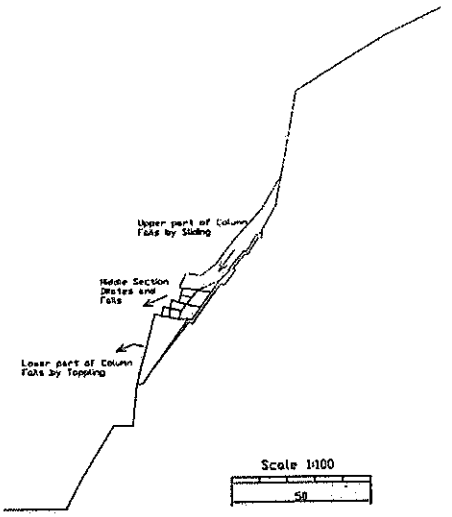

Figure 6 : Failure by sliding and toppling

The toe of the September 2000 failure was located above the road corresponding to the top of the highway cut batter slope of 1972. A column of rock some 60m height fell leaving the adjacent upper columns "hung up" in a precarious position on the slope. It became readily apparent that the mass of rock was resting on a number of significant asperities.

RISK OF FUTURE ROCKFALL

The bluff has been continually monitored since last September 2000. We have identified 5 more column features on the face which are starting to show signs of incipient collapse. We are not however, able to predict time to collapse. What we can say is that failure of at least one of them is expected within the next 5 years.

We presented the problem to TNZ in a risk framework so that the threat to the highway could be evaluated and funds apportioned appropriately.

RISK ASSESSMENT

In assessing the risks in the area we carried out both a quantitative and qualitative analysis.

The purpose of the risk assessment was to determine the likelihood and consequence of a rockfall of any size at the site.

Historically there have been around 12 small ($1m^3$) rockfalls per year at the Nevis Bluff and two very large ones measuring several thousand cubic metres of material.

This year, 2001 we have implemented a Slope Check monitoring system, which includes pro-

active maintenance by removing potentially hazardous material from the face as emergency work. We have had only one small rockfall this year as a result.

There still however remains the risk of a major collapse, and we expect another to occur within the next 3-5 years.

The number of vehicles using the highway below the bluff is AADT 2300veh/day, which pass through a rockfall hazard area of approximately 200m.

The risk analysis we adopted was the one based on the principles presented by Bunce and Cruden 1997 following the Argillite Cut rockfall death in British Columbia. It is a probability type assessment, which uses binomial theorem. The full derivations are presented in their paper.

The calculations are not presented here but a summary of the results is shown in Table 1. Risk calculations of this kind are meaningless unless they are compared with other civil engineering construction project risks.

In the absence of any New Zealand standard, we used the ANCOLD criteria, Figure 6, which is one of the most widely recognised in this field and presents acceptable risk for dam failures. It has been adopted by the Australian Geomechanics Society, and is the used by the Geotechnical Engineering Office for assessing rockfall hazards in Hong Kong.

Table 1: Summary of rockfall risk compared to ANCOLD criteria

Risk Event	Annual Probability of fatality	ANCOLD criteria	Acceptability
Small/ intermediate rockfall impacts moving vehicle	2×10^{-3}	10^{-4}	**Unacceptable**
Large rockfall impacts moving vehicle	3.4×10^{-4}	10^{-4}	Acceptable
Large scale rockfall impacts stopped vehicle	1.8×10^{-5}	10^{-4}	Acceptable
Vehicle impacts fallen rock or has accident because of fallen rock	5×10^{-3}	10^{-4}	**Unacceptable**

The calculations show that two of the risks fall into the 'Unacceptable' zone. The graph also shows other risk criteria used around the world by way of comparison.

We also carried out a qualitative assessment adapting principles of NZS 4360: 1999 Risk Management, and the summary of this is presented in Table 2. The definitions of likelihood and consequence were taken from the standard.

Table 2: Qualitative Risk Assessment to NZS 4360 : 1999 Risk Management

Hazard	Likelihood	Consequence	RISK
Small falling rock impacts vehicle	Rare	Major	**High**
Driver swerves out of control to avoid small falling rock	Rare	Moderate	Medium
Driver hits small fallen rock	Likely	Moderate	**High**
Driver swerves out of control to avoid small fallen rock	Likely	Major	**Extreme**
Major rock falls require road closure for repairs	Moderate	Moderate	**High**
Major rock fall impacts vehicle/vehicles	Moderate	Catastrophic	**Extreme**

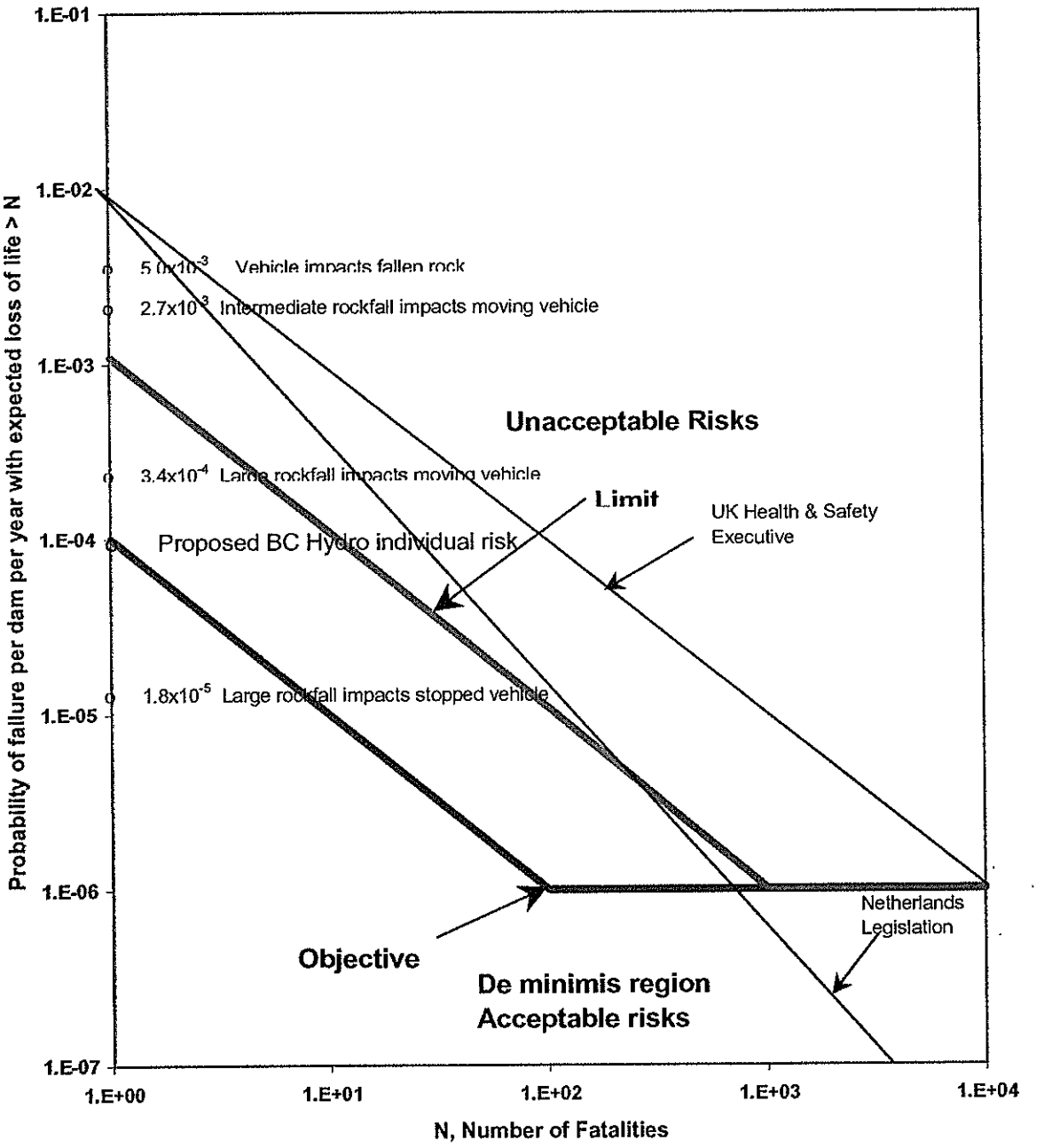

Figure 6 Risks compared with ANCOLD amended interim social criteria

At this stage the two assessments are quite separate. They show that the risks on the face are 'Unacceptable' and 'Extreme'.

There appears a need to further develop the New Standard to include quantitative assessment particularly for rockfall or landslide hazard assessment. This could be based on the work already done.

One of the other difficulties we have found is deciding on appropriate criteria. The ANCOLD criteria is quite clear in terms of what is acceptable and what is not. But this criteria is for dam construction and not for rockfall, and especially not for rockfall in Central Otago.

We should perhaps be talking about what is tolerable by the public rather than what is acceptable to society irrespective of the situation. For example, we are all well aware of the hazards in driving on the roads but whatever the statistics show, it is likely that we would always regard the risks as tolerable even if they were not actually classified as acceptable.

RISK REDUCTION

The purpose of Risk Reduction is to reduce either the likelihood of an occurrence or its consequences. In this case to either reduce the likelihood of rock falls (engineering works on the face) or reduce the consequence of a fall (realign or protect the road).

We looked at every conceivable option to reduce the risk at the bluff. Options included removing more material from the face (Face Clean Up), rock shed, half bridge, benching the face, tunnel, road realignment and even a viaduct.

The major problem we faced was that all the options to reduce the risks were very expensive. Rough Order Construction costs ranged from $3m (removing specific hazards from the face) to $27m (viaduct). Some of the options, even after construction, still carried residual risk. The main problem is that it would be very difficult to install any kind of structure capable of withstanding the force of impact such as was seen during the September 2000 rockfall. A great deal of material would have to be removed from the face prior to constuction, further increasing the costs.

TNZ use the BCR (Benefits Costs Ratio) system to justify projects. We calculated a maximum BCR of 0.7. A robust BCR of at least 4 is normally required to justify a project and so on this basis the project could not proceed. The problems were high construction cost and low accident rates due to rockfalls at present, even though the consequences were unacceptable.

We were also unable to state categorically that the situation was an emergency and so our justification for the project had to therefore become one of Preventative Maintenance. This is a separate budget TNZ have for funding projects. The Preventative Maintenance budget is limited annually and projects such as this one can quite quickly soak up a large proportion of the nation wide current allocation.

The BCR method proved to be inappropriate for projects of this kind, so we had to approach the matter from a cost versus risk perspective. The lowest cost option (and lowest present value option) which could be justified on a risk basis but would require a program of ongoing maintenance for the next 25 years was the 'Do Minimum', limited face clean up.

DO MINIMUM (FACE CLEAN UP)

The 'Do Minimum' option is one, which relates to the minimum level of expenditure required to maintain the link. To satisfy this requirement, we considered it necessary to carry out a face clean up operation. This would involve removing from the face, features (hazardous columns of material) which could collapse onto the highway within the next 3-5 years. The ROC for the option was $3m. The work is programmed to start during the year 2002 and is likely to be spread over a 3 year period to minimise disruption to the highway with the features being brought down in order of risk priority.

CONCLUSIONS

We presented the hazards at the Nevis Bluff to TNZ in a risk based framework, which included the recommendation that TNZ adopt a risk management approach to decision making and not one based on B/C ratio.

Our recommendation was that the Do minimum option, "Face Clean Up", which includes removing selected features from the bluff face, be fully implemented. This would involve physical works carried out in three stages at an estimated cost of $3m as Preventative Maintenance over the next three years with prioritisation of the features to be removed.

We have raised the need to include quantitative risk assessment especially for rockfalls and landslides into a New Zealand standard, perhaps based on the work which has been done in this field elsewhere.

It maybe necessary to set the guidelines on tolerable risk for such events rather than acceptable when compared with other construction activities.

REFERENCES

1. BUNCE CM, CRUDEN DM, MORGENSTERN NR (1997) "Assessment of the Hazard from Rockfall on a Highway", Canadian Geotechnical Journal, No. 34: Pages 344-356.

2. Australian Geomechanics Society, Sub-Committee on Landslide Risk Management. *Landslide Risk Management Concepts and Guidelines.* New Zealand Geotechnical Society Geomechanics News, Issue 60, December 2000

3. NZS 4360: 1999 Risk Management.

4. Opus International Consultants Ltd (2001) Nevis Bluff Options Report No. 864.

5. Opus International Consultants Ltd (2001) Nevis Bluff Scoping Report No.927.

6. Opus International Consultants Ltd (2001) Nevis Bluff Slope Check Manual